

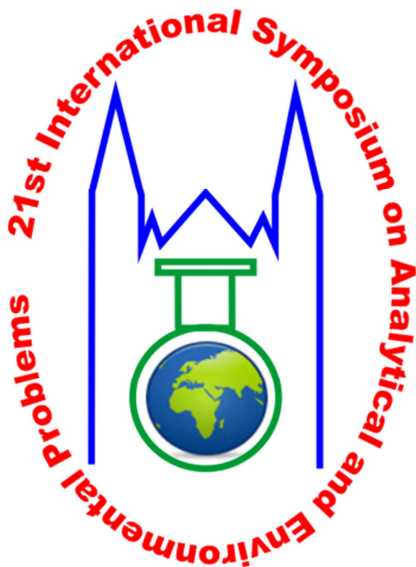


***PROCEEDINGS OF THE***

***21<sup>st</sup> International Symposium***  
***on Analytical and Environmental Problems***

*September 28, 2015*

**University of Szeged, Department of Inorganic and  
Analytical Chemistry**



***Szeged***  
***Hungary***

**Edited by:**  
Tünde Alapi  
István Ilisz

**Publisher:**  
University of Szeged, Department of Inorganic and Analytical  
Chemistry, H-6720 Szeged, Dóm tér 7, Hungary

**ISBN 978-963-306-411-5**

**2015.**  
**Szeged, Hungary**

***The 21<sup>st</sup> International Symposium  
on Analytical and Environmental Problems***

**Organized by:**

SZAB Kémiai Szakbizottság Analitikai és Környezetvédelmi Munkabizottsága

**Supporting Organizations**

*University of Szeged, Department of Inorganic and Analytical Chemistry  
Hungarian Academy of Sciences*

**Symposium Chairman:**

*István Ilisz, PhD*

**Honorary Chairman:**

*Zoltán Galbács, PhD*

**Organizing Committee:**

*István Ilisz, PhD*

*associate professor*

*University of Szeged Department of Inorganic and Analytical Chemistry*

*ilisz@chem.u-szeged.hu*

*Zoltán Galbács, PhD*

*honorary professor*

*University of Szeged Department of Inorganic and Analytical Chemistry*

*zgalbacs@chem.u-szeged.hu*

*Tünde Alapi, PhD*

*assistant professor*

*University of Szeged Department of Inorganic and Analytical Chemistry*

*alapi@chem.u-szeged.hu*

## **Lecture Proceedings**



## **The Perception of Social Responsibility among Students in Higher Education**

**László Berényi**

*Institute of Management Science, University of Miskolc, H-3515 Miskolc-Egyetemváros,  
Hungary*

*e-mail: szvblaci@uni-miskolc.hu*

### **Abstract**

Professional solutions, including management systems and tool set presumes a certain level of knowledge about the topic. Sustainable development can be interpreted in many ways, an engineer or an economist will emphasise different aspects. Furthermore, personal aspects and non-professional opinions must be considered because these will influence both consumer choice and business strategy. The paper analysis the difference of opinions about sustainable development and CSR between bachelor and master level students. It can be concluded that the bachelor students have a more hopeful opinion but differences are not significant in each factor.

### **Introduction**

Personal and professional opinions about a product, service, process or organisation may be basically different from each other. The knowledge level of customers is limited and influenced by e.g. advertisement, news, and opinion of friends. Professional knowledge may be available at the product developers, producers and dealers. An interesting challenge comes from the fact that the corporation owners and decision makers may be in the absence of the relevant knowledge elements.

In order to be able to solve the global problems the reasoning above is particularly true. Exploring the personal elements of thinking is useful because it allows to develop both tool set of professional support and the educational efforts.

### **Experimental**

The reports about the limit to growth has forecasted a global social and ecological disaster if the present consuming habits were continued [1] [2]. The proposals were rejected but it has begun finding the way out. The concept of sustainable development [3] and CSR (corporate social responsibility) [4] are to highlight as complex managing perspectives. The idea of true responsibility [5] freshens the pursuits.

These concepts and the tool set behind them is continuously developed, differentiation may disappear in personal thinking:

- The ecological, social and economical pillars of sustainable development have an equal importance, but in practice the economic one covers both the limit of feasibility of necessary actions and escape from the responsibility.
- The concept of CSR is earlier than sustainable development [6], however its popularity is due to the limits of sustainability. CSR introduces ecological and social issues as clearly subordinated ones to business goals.
- True responsibility refines the challenges and possibilities. A truly responsible corporation follows the basic principles of minimising transportation, maximal justice in decision making, avoid of economism, and producing sustainable products.

The empirical results presented in this paper does not seeks the practical differences of the theoretical models. The paper focuses on the comprehensive personal opinions of some

selected factors of a wider research. There is a comparison between the subsamples of bachelor and master students, the analysis tries to explore whether the opinions differs significantly between them or not.

The research on the characteristics of the future management generation has been launched at the Institute of Management Science, University of Miskolc in 2013. The main goal is to give an overview about the personal opinions, knowledge and attitudes of higher education students who will give the next generation of corporate decision makers of corporations.

The research sample covers respondents of the University of Miskolc in the data collection period of autumn, 2014. The sample includes 269 respondents, 221 bachelor and 48 master students. The analysis uses the independent samples t-test, calculated with the support of the SPSS software. The results are not representative because the respondents are from the same university and limited mainly to economical students and some mechanical engineering and environmental engineering students.

## Results and discussion

### Components of sustainability

The survey asked to evaluate the importance of some issues related to sustainable development on a 1..6 scale. The results may show a bias in opinions, each factor is evaluated rather important than not, but relative comparison is allowed and useful. The overall picture signs that social and environmental issues are more important than technological and economic issues for the respondents.

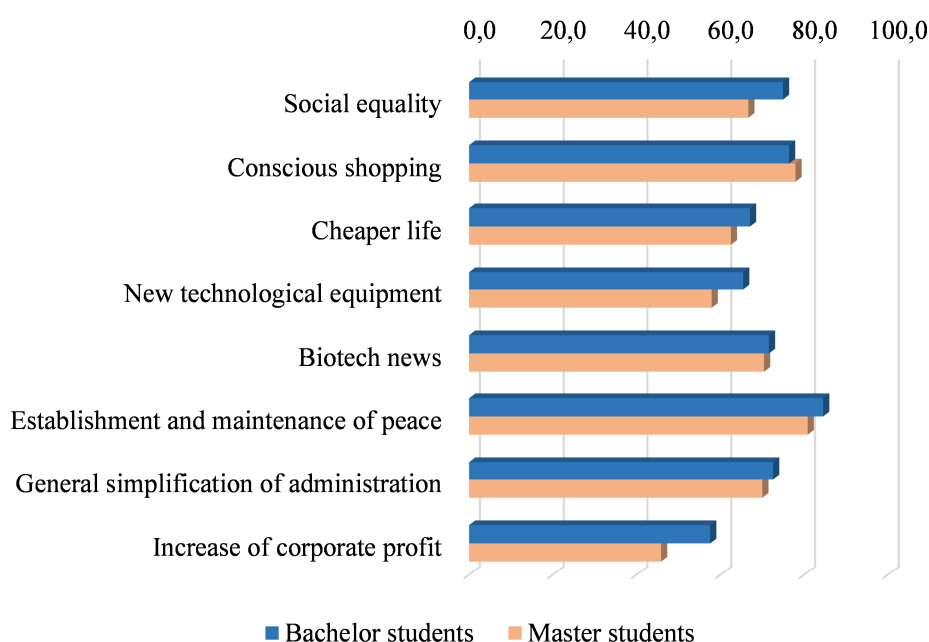


**Figure 1.** Bachelors and master students about sustainability (own edition, data on 0..100 scale)

Figure 1. highlights the differences between the subsamples. Bachelor students give generally higher importance to the studied factors, but significant difference is only detected in case of social equality, new technological equipment and the importance of corporate profit (Table 1.)

Table 1. summarises the results of the analysis between the total sample, bachelor and master level students. Figures are converted to 0.100 scale for an easier overview.

	<b>Total sample</b>	<b>Bachelor students</b>	<b>Master students</b>	<b>Statistical results of comparison*</b>
Social equality	73.5	74.9	66.7	t(267)=2.391 p=.017 d=.413 95% CI [0.073, 0.754]
Conscious shopping	76.7	76.4	77.9	t(267)=-0.479 p=.633 d=-0.077 95% CI [-0.393, 0.239]
Cheaper life	66.2	67.1	62.5	t(267)=1.288 p=.199 d=0.228 95% CI [-0.120, 0.576]
New technological equipment	64.1	65.4	57.9	t(267)=2.048 p=.042 d=0.376 95% CI [0.015, 0.737]
Biotech news	71.4	71.6	70.4	t(267)=.0337 p=.736 d=0.058 95% CI [-0.283, 0.399]
Establishment and maintenance of peace	83.9	84.5	80.8	t(267)=1.131 p=.259 d=0.185 95% CI [-0.137, 0.506]
General simplification of administration	72.1	72.6	70.0	t(61.436)=.0590 p=.557 d=0.139 95% CI [-0.308, 0.566]
Increase of corporate profit	55.5	57.6	45.8	t(62.143)=2.648 p=.010 d=0.586 95% CI [0.144, 1.029]

\*t(df): degree of freedom, p: 2-tailed significance level d: mean difference CI: confidence interval

**Table1.** Opinions about the components of sustainability (own edition, data on 0.100 scale)

### Judgment on CSR

Another interesting question is what the next generation of decision makers think about CSR. CSR may cover the corporate efforts in harmony with the business strategy. However, the tools and methods may give possibilities for increasing profit by mystification of consumers. The survey formed some statements based on expert interviews. Table 2. summarises the results of the total sample and subsamples, including the statistical analysis of comparison. Data collection and presentation uses the same method as in previous chapter.

There are significant differences between bachelor and master students are detected in opinions about the problem-masking role (responses of bachelor students show the lower average) of CSR and the level of required expenses (master students rather believe in the lower expenses than bachelors).

There are non-significant, but other remarkable differences in thinking to highlight. CSR as tool of masking problems and dependence of successfulness on corporation size are to mention because of the inverse evaluation of the subsamples, but the responses show the lower trust in usefulness of CSR among master students.

	Total sample	Bachelor students	Master students	Statistical results of comparison*
Helps to achieve sustainability	67.6	68.4	64.1	t(216)=1.194 p=.234 d=0.214 95% CI [-0.0139, 0.567]
Just a tool of making profit	57.7	58.2	55.5	t(220)=0.658 p=.512 d=0.137 95% CI [-0.0274, 0.548]
Only masks the real problems	51.1	49.3	59.0	t(65.912)=-2.193 p=.032 d=-0.484 95% CI [-0.925, -0.043]
Excellent marketing communication tool	74.6	74.9	73.3	t(220)=0.417 p=.677 d=0.077 95% CI [-0.285, 0.438]
Joins the goals and efforts of the business	64.8	65.4	62.0	t(220)=0.953 p=.342 d=0.169 95% CI [-0.181, 0.519]
Can be successful only for large corporation	49.7	50.1	48.5	t(197)=0.299 p=.765 d=.078 95% CI [-0.437, 0.593]
Expensive to accomplish the actions	65.2	66.9	57.1	t(188)=2.037 p=.043 d=0.493 95% CI [0.016, 0.971]

\*t(df): degree of freedom, p: 2-tailed significance level d: mean difference CI: confidence interval of mean difference

**Table 2.** Opinions about the goals of CSR (own edition, data on 0..100 scale)

## Conclusions

- Most of the respondents have not learned about CSR in details yet (based on the answers 12% has superficial knowledge and know it in details), but it does not hinders the building up a strong and definite opinion.
- Opinions about sustainable development reflects social expectations with a less weight of economic aspects. However, asking about CSR the comprehensive picture shows an opposite opinion.
- There are significant differences between the responses of the bachelor and master only in a few studied factors. The results and other experiences of the research indicates the necessity of rethinking the education and training contents.

## Acknowledgements

The research was carried out as a part of the „TOWARDS science – talent management from classroom to researcher profession” TÁMOP-4.2.2.B-15/1/KONV-2015-0003 project.

## References

- [1] Meadows, D. H., Meadows, D. L., Randers, J., Behrens, W. W., The Limits to Growth, Universe Books, New York, 1972
- [2] Meadows, D. H., Meadows, D. L., Randers, J., Limits to Growth: The 30-Year Update, Chelsea Green Publishing, White River Junction, 2004
- [3] Our Common Future, Oxford University Press, Oxford, 1987
- [4] Carroll, A.B., The Pyramid of Corporate Social Responsibility: Toward the Moral Management of Organizational Stakeholders, Business Horizons. 34(07-08) (1981) 39-48.
- [5] Tóth, G., The Truly Responsible Enterprise, Követ Association, Budapest, 2007
- [6] Ackerman, R. W., Bauer, R.A., Corporate Social Responsiveness, Reston Publishing, Reston, 1976

## Új Pd-Komplexek Azometin-Származékokkal, és Fizikai-Kémiai Vizsgálatuk

ifj. Várhelyi Csaba<sup>1</sup>, Nagy Renáta-Ildikó<sup>1</sup>, Pokol György<sup>2</sup>, Szalay Roland<sup>3</sup>,  
Mihály Judit<sup>4</sup>, Goga Firuța<sup>1</sup>, Golban Ligia-Mirabela<sup>1</sup>

<sup>1</sup>„Babeş-Bolyai” Tudományegyetem, Kémia és Vegyészmérnöki Kar, Kolozsvár

<sup>2</sup>Budapesti Műszaki és Gazdaságtudományi Egyetem, Vegyészmérnöki és Biomérnöki Kar

<sup>3</sup>„Eötvös Loránd” Tudományegyetem, Kémiai Intézet, Budapest

<sup>4</sup>MTA-Természettudományi Kutatóközpont, Anyag- és Környezetkémiai Intézet, Budapest

### KIVONAT

Kutatásunk során új [Pd(monofenil-dioxim)<sub>2</sub>L<sub>2</sub>] (L = 2-amino-pirimidin, 3-hidroxi-anilin, lepidin) típusú komplexeket, valamint Schiff-bázisokkal képzett komplexeket: [Pd(acetonil-aceton)<sub>2</sub>(diamin)], [Pd(dibenzoil-metán)<sub>2</sub>(diamin)] (diamin = o-fenilén-diamin, etilén-diamin, 1,2-, 1,3-propilén-diamin) állítottunk elő PdCl<sub>2</sub>, monofenil-dioxim, ill. a megfelelő Schiff-bázis és amin, ill. diamin reakciója során a megfelelő oldószerben. Szerkezetüket és fizikai-kémiai sajátságait tömegspektrometriával, infravörös- és mágneses magrezonancia spektroszkópiával, por-röntgen diffrakcióval és termoanalitikai módszerekkel (TG, TDG és DTA) vizsgáltuk.

A Pd-komplexek fontos szerepet töltenek be katalizátorként való alkalmazásukban a legkülönbözőbb szerves kémiai reakciókban [1]. Több Pd-katalizálta reakciót ipari körülmények között is megvalósítanak. A Pd drága nemesfém, de ára elenyésző a Rh, Pt, Ir, vagy Os mellett. Biológiai aktivitásukat illetően, bizonyos enzimek inhibitorai, melyek a cukorbetegség kezelésében használatosak, mások glaukoma elleni potenciális gyógyszerek [2]. A Pd-komplexek, a palládium platinához való hasonlósága következtében, potenciális rákellenes szerek [3].

### ABSTRACT

In our research we synthesized novel [Pd(monophenyl-dioxime)<sub>2</sub>L<sub>2</sub>] (L = 2-amino-pyrimidine, 3-hydroxi-aniline, lepidine) type complexes and with different Schiff-bases: [Pd(acetonil-acetone)<sub>2</sub>(diamine)], [Pd(dibenzoyl-methane)<sub>2</sub>(diamine)] (diamine = o-phenylene-diamine, ethylene-diamine, 1,2-, 1,3-propylene-diamine) by reacting PdCl<sub>2</sub>, monophenyl-dioxime, respectively Schiff-bases with amine, respectively diamine in the corresponding solvent. We analyzed their physicochemical properties using mass spectrometry, infrared-, NMR-spectroscopy and thermal analysis (TG, DTG and DTA).

The Pd-complexes have an important role in many organic chemistry reactions as catalysts [1]. Some of them are used in industry. The Pd precious metal price is high, but compared with Rh, Pt, Ir, or Os is infinitesimal. Regarding the biological activity, they inhibit some enzymes which are important in anti-diabetic therapy. Some of the Pd(II) complexes are anti-glaucoma drug candidates [2]. Due to the similarity between Pd and Pt, the complexes of palladium(II) can be considered as potential anticancer agents [3].

## BEVEZETŐ

A palládium kémiajának egyik legfőbb jellemzője, hogy a 4 d elektronhéj teljesen fel van töltve, és egyben könnyen feltörhető, hasonlóan, mint a Pt 5 d elektronhéja. A platinától abban különbözik, hogy sokkal reaktívabb. Ez a jelenség a Pd kémiajában is tükröződik, mint pl. a változó oxidációs állapot (0, I, II, IV).

A  $\text{Pd}^{2+}$  a domináns oxidációs állapot, és általában ezek a származékok diamágnesesek, kis spinű  $d^8$  állapotúak. A  $\text{Pd}^{2+}$  komplexeket képez O-donor (alkoxidok, karboxilátok,  $\beta$ -diketonok és más kelátképző ligandumok), N-donor (aminok, azometinek) és vegyes N, O-kelátképző szerekkel.

Rengeteg ligandum állítható elő kondenzációs reakciók útján karbonil-származékokból különféle amino-származékokkal. Az  $\alpha$ -dioximok  $[\text{Pd}(\text{DioxH})_2]$  típusú komplexeket képeznek ( $\text{DioxH}_2 = \alpha$ -dioxim), ahol a ligandum általában a N-en keresztül kötődik. E származékok enyhén savas közegben képződnek ( $\text{pH} = 1 - 5$ ), ellentétben a Ni-származékokkal, enyhén bázikus közegben oldódnak, pentadentát  $[\text{Pd}(\text{DioxH})_2\text{OH}]$  hidroxokomplexeket képezve. A  $[\text{Pd}(\text{DioxH})_2]$  típusú komplexeket legfőképpen a gravimetriás analitikai meghatározásoknál használják.

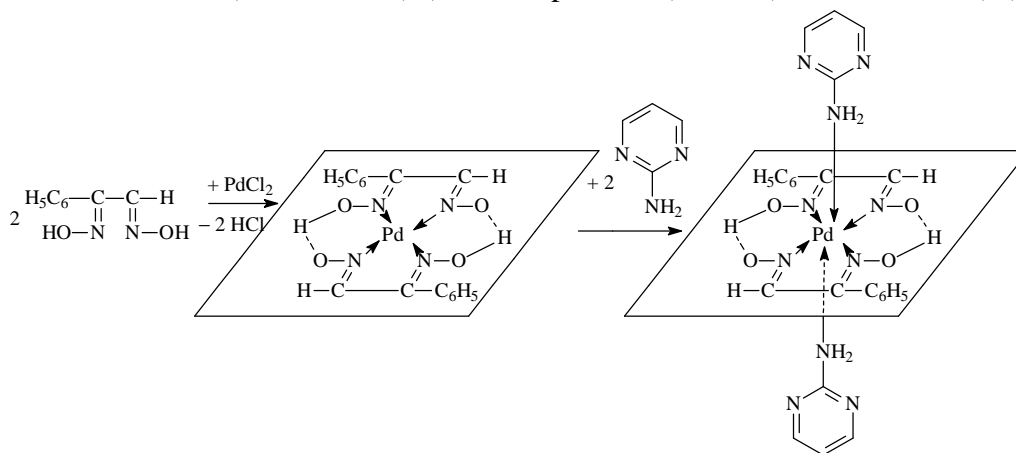
## FELHASZNÁLT ANYAGOK ÉS ELJÁRÁS

**Felhasznált anyagok:**  $\text{PdCl}_2$ , monofenil-dioxim, acetonil-aceton, dibenzoil-metán, 2-amino-pirimidin, 3-hidroxi-anilin, lepidin, o-fenilén-diamin, etilén-diamin, 1,2-propilén-diamin, 1,3-propilén-diamin, Et-OH

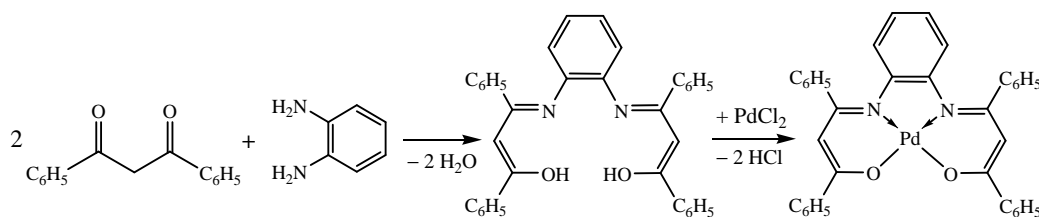
**Eljárás:** a) a  $\text{PdCl}_2$  vizes oldatát monofenil-dioxim etil-alkoholos oldatával elegyítjük, és 1 – 2 órán keresztül forraljuk (mólarány 1:2). Ezután az oldathoz hozzáadjuk a megfelelő amin etil-alkoholos oldatát (Pd/amin mólarány 1:2), és tovább folytatjuk a forralást még 1 – 2 órán át. A keletkezett terméket vákuum alatt szűrjük hidegen, víz-alkohol (1:1) eleggyel mossuk, és levegőn szárítjuk.

b) először előállítjuk a megfelelő Schiff-bázist acetonil-aceton, ill. dibenzoil-metán etil-alkoholos oldatának és a diamin (o-fen, en, 1,2-pn, 1,3-pn) etil-alkoholos oldatának elegyítésével és keverésével hidegen vagy enyhe melegítéssel (mólarány 2:1). A keletkezett Schiff-bázist leszűrjük, majd etil-alkoholban oldjuk, vagy ha nem válik ki, akkor az oldatot használjuk, és a  $\text{PdCl}_2$  vizes oldatával elegyítjük, majd 1 – 2 órán keresztül forraljuk (mólarány 1:1). A keletkezett terméket lehűtjük, vákuum alatt szűrjük, víz-alkohol (1:1) eleggyel mossuk, és levegőn szárítjuk.

Lejátszódo reakciók  $[\text{Pd}(\text{Fenil-DioxH})_2(2\text{-amino-pirimidin})_2]$ ,  $[\text{Pd}(\text{dibenzoil-metán})_2(\text{o-fen})]$ :







## EREDMÉNYEK

Az előállított komplexek mikroszkópos jellemzése és előállítási hozama az 1. táblázatban látható.

1. táblázat. Az előállított komplexek mikroszkópos jellemzése, hozama és móltömege.

Sz.	Vegyület	Számít. móltöm.	Hozam (%)	Mikroszkópos jellemzés
1.	[Pd(Fenil-DioxH) <sub>2</sub> (2-amino-pirimidin) <sub>2</sub> ]	622,92	65	Világos barna színű, háromszög alapú hasábok
2.	[Pd(Fenil-DioxH) <sub>2</sub> (3-HO-anilin) <sub>2</sub> ]	650,97	60	Fekete színű, háromszög alapú hasábok
3.	[Pd(Fenil-DioxH) <sub>2</sub> (lepidin) <sub>2</sub> ]	719,09	50	Barna színű, hosszú háromszög alapú hasábok
4.	[Pd(acetonil-aceton) <sub>2</sub> (o-fen)]	404,79	70	Sötét barna színű, háromszög alapú hasábok
5.	[Pd(acetonil-aceton) <sub>2</sub> (en)]	356,74	55	Világos barna színű, háromszög alapú hasábok
6.	[Pd(acetonil-aceton) <sub>2</sub> (1,2-pn)]	370,77	55	Sötét barna színű, háromszög alapú hasábok
7.	[Pd(acetonil-aceton) <sub>2</sub> (1,3-pn)]	370,77	60	Vöröses barna színű, háromszög alapú hasábok
8.	[Pd(dibenzoil-metán) <sub>2</sub> (o-fen)]	625,02	85	Sárgás barna színű, háromszög alapú hasábok
9.	[Pd(dibenzoil-metán) <sub>2</sub> (en)]	576,97	50	Világos barna színű, háromszög alapú hasábok
10.	[Pd(dibenzoil-metán) <sub>2</sub> (1,2-pn)]	591,00	85	Világos barna, hosszú háromszög alapú hasábok
11.	[Pd(dibenzoil-metán) <sub>2</sub> (1,3-pn)]	591,00	65	Világos lilás-barna színű, háromszög alapú hasábok

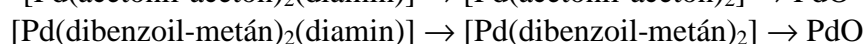
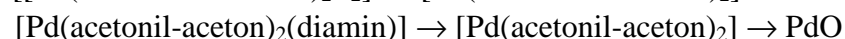
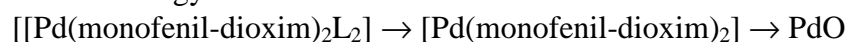
## Tömegspektrometria

A tömegspektrumokat Agilent/Technologies 6320 Mass Spectrometer készülékkel rögzítették. A spektrumokban benne van a várt anyagok molekulatömege és bizonyos bomlási fragmenseket is sikerült azonosítani.

## Hőbontás (TG, DTG, DTA)

A hőbontást egy 951 TG és 910 DSC kaloriméter (DuPont Instruments) készülékkel végeztük Ar vagy N<sub>2</sub> atmoszférában, 10 K/min fűtési sebességgel (mintatömeg: 4 – 10 mg).

A nyert adatokból egy általános bomlási mechanizmust állíthatunk fel:



## Por-Röntgen diffrakciós mérések

A por-röntgen diffrakciós méréseket egy PANalytical X'pert Pro MPD X-ray diffraktométerrel végeztük. A röntgen diffrakciós mérésekkel a komplexeink kristályosságát

vizsgáltuk. Mivel új anyagok, nem találhatók meg a diffraktogramjai a Cambridge-i adatbázisban.

### Infravörös spektroszkópiai vizsgálatok

Az infravörös spektrumokat KBr és polietilén pasztillában vettük fel közepes-IR (4000 – 450  $\text{cm}^{-1}$ ) tartományban, Perkin-Elmer System 2000 FTIR spektrofotométerrel, valamint távoli-IR (500 – 50  $\text{cm}^{-1}$ ) tartományban BioRad FTS-60A FTIR spektrométerrel. A főbb IR adatokat a 2. táblázat tartalmazza.

2. táblázat. Az előállított Pd-komplexek IR adatai.

Vegyület $\text{cm}^{-1}$	$\nu_{\text{N-H}}$	$\nu_{\text{C-H}}$	$\nu_{\text{C=N}}$	$\nu_{\text{C-C}}$	$\nu_{\text{N-O}}$	$\nu_{\text{Pd-N}}$	$\nu_{\text{Pd-O}}$	$\delta_{\text{N-Pd-N}}$
[Pd(Fenil-DioxH) <sub>2</sub> (2-amino-pirimidin) <sub>2</sub> ]	3120	-	1569	1496	1246	484	-	383
[Pd(Fenil-DioxH) <sub>2</sub> (3-HO-anilin) <sub>2</sub> ]	3293	2931	1590	1465	1256	454	-	386
[Pd(Fenil-DioxH) <sub>2</sub> (lepidin) <sub>2</sub> ]	3127	-	1602	1495	1262	499	-	386
[Pd(acetonil-aceton) <sub>2</sub> (o-fen)]	-	2931	1595	1490	-	494	432	398
[Pd(acetonil-aceton) <sub>2</sub> (en)]	-	2905	1637	1404	-	480	444	412
[Pd(acetonil-aceton) <sub>2</sub> (1,2-pn)]	-	2928	1648	1408	-	502	494	399
[Pd(acetonil-aceton) <sub>2</sub> (1,3-pn)]	-	2933	1653	1405	-	518	438	400
[Pd(dibenzoil-metán) <sub>2</sub> (o-fen)]	-	-	1590	1459	-	492	447	399
[Pd(dibenzoil-metán) <sub>2</sub> (en)]	-	-	1587	1451	-	550	468	398
[Pd(dibenzoil-metán) <sub>2</sub> (1,2-pn)]	-	-	1591	1459	-	492	448	399
[Pd(dibenzoil-metán) <sub>2</sub> (1,3-pn)]	-	-	1591	1459	-	493	447	399

### NMR spektroszkópia

A spektrumokat ( $^1\text{H}$  és  $^{13}\text{C}$  NMR) egy Bruker AVANCE spectrométerrel vettük fel 250 MHz ( $^{13}\text{C}$ : 63 MHz) frekvenciával. A [Pd(Fenil-DioxH)<sub>2</sub>L<sub>2</sub>] típusú komplexek esetében az aromás gyűrűk protonjainak a jele 7 – 9 ppm tartományban jelennek meg, az amino-csoport protonjai pedig 2 – 3 ppm között. Az aromás  $^{13}\text{C}$  jelek 126 – 128 ppm tartományban, a többi pedig 76 – 77 ppm értékeknél. A Schiff-bázisokkal képzett komplexek esetében az aromás gyűrűk protonjai ugyancsak 7 – 9 ppm tartományban jelennek meg, az alifás diamintól származó protonok pedig 4,5 – 5 ppm tartományban. Az aromás  $^{13}\text{C}$  jelek 127 – 135 ppm tartományban, a többi pedig 76,5 – 77,5 ppm értékeknél.

### KÖVETKEZTETÉSEK

Munkánk során két típusú Pd-komplexekeket állítottunk elő (dioximokkal és Schiff-bázisokkal), melyek várhatóan biológiai szempontból lesznek jelentősek, mint pl. antibakteriális és antitumor hatás.

### KÖSZÖNETNYILVÁNÍTÁS

A szerzők közül ifj. Várhelyi Csaba köszöni a „Domus Hungarica” alapítványnak, hogy a számára megítélt évi egy hónapos ösztöndíjakkal lehetővé tette a jelen dolgozat létrejöttét.

### IRODALOM

- [1] R. Dileep, B.R. Bhat, *Appl. Organometal.Chem.* (2010) 24, 663
- [2] Qurrat-ul-Ain, et al., *Arabian Journal of Chemistry*, (2015) article in press
- [3] A. Krogul, et al., *Bioorganic & Medicinal Chemistry Letters*, (2013) 23, 2765



## Rare Earth Elements and Plants

Rudolf Kastori, Ivana Maksimović, Marina Putnik-Delić

*Faculty of Agriculture, University of Novi Sad, 2100 Novi Sad, Trg Dositeja Obradovića 8.  
Serbia  
e-mail: kastori@polj.uns.ac.rs*

### Abstract

There has been a growing interest in the study of the rare earth elements (REEs) in recent decades of the last century, with the exploitation of REEs resources and applications in modern industry, medicine, agriculture and biotechnology. The main application of REEs is as new materials for recent technologies in the modern industry and agriculture, where low concentrations of REEs-based fertilizers are used to increase yield and quality of crops. Positive, negative or nil effects of REEs on plant growth, chemical composition and yield were observed in experiments done in many countries, but the physiological and biochemical mechanisms are still not well understood. Essentiality of REEs for living organisms or their threat to the environment has not been identified so far.

### Introduction

The REEs or rare earth metals include 15 lanthanides. The metals scandium and yttrium are often included in the list of REEs. The REEs possess nearly identical chemical and physical properties and comprise a homogenous group of elements in the periodic system. The REEs are widely distributed and present in all parts of the biosphere, often at the level of the other microelements (Kabata-Pendias, 2001). Numerous investigations showed effects of REEs on physiological and biochemical processes, growth, development and yield of plants (Hu et al., 2004). Essentiality of REEs for living organisms has not been identified so far, but REEs can specifically influence their life processes. Detailed review of REEs in biological systems, their implementation, responses of selected crops, and ecological significance is given in publications Horovitz (2000), Tyler (2004), Kastori et al. (2010) and Maksimović et al. (2014a,b).

### Uptake, accumulation and translocation of REEs in plants

Plants can uptake the REEs through the root as well as the aboveground organs. Intensity of uptake of REEs depends of numerous factors (Kastori et al., 2010). There have been determined synergism and antagonism between certain elements of this group during uptake process. The pH value of the environment also affects the REEs uptake. Within the range of pH the uptake efficiency was proportional to the hydrogen ion concentration. Use of EDTA enhances uptake of REEs, since this organic ligand increases desorption of REEs in the soil. It is considered that Casparian strip of the root limits the transport of REEs in the root. Hu et al. (2004) state that the natural translocation rates for REEs from soil to plant are approximately 20%, and for REEs fertilizers this rate was found to be 55-60%. They are mostly accumulated in the root, and less in the stem and reproductive organs (Fig. 1a). The transfer factor of yttrium, in relation to the medium, was much higher in root than in stems and leaves (Maksimović, et al., 2012, 2014b). In general, transfer factor declined with an increase of yttrium concentration in the nutrient medium (Fig. 1b). This is in line with the finding that the uptake rate of REEs from soil to root is much higher than the translocation rate from root to shoot. They are found both inside the cells and in extracellular spaces of plant tissues, where

they form chelate compounds with numerous components of metabolism – amino acids, nucleic acids, proteins etc. Uptake of REEs through the leaf is much faster than through the root. This is not characteristic only for REEs, since the ions of other elements are often much faster taken up through the leaf than through the root and their involvement in the plant metabolism is faster than when taken up through the roots.

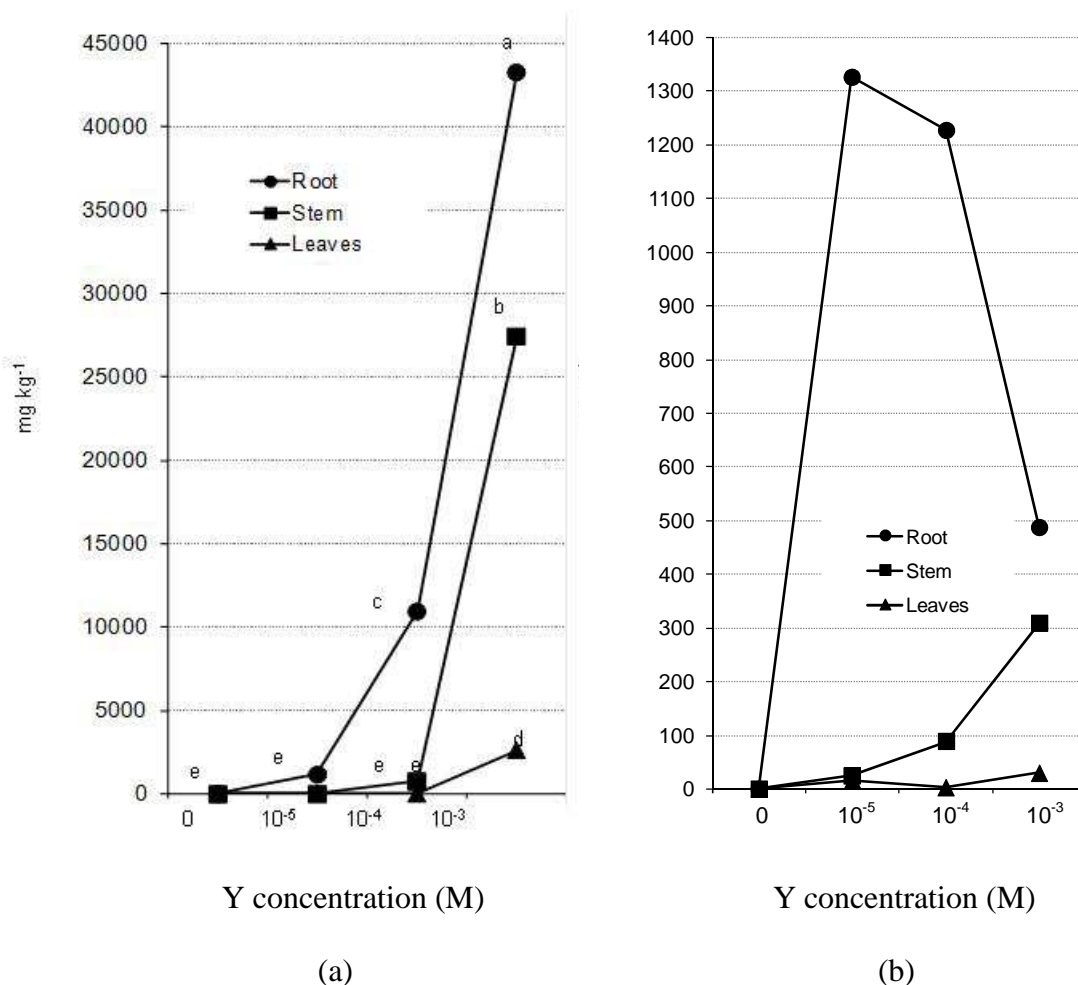


Fig. 1. Concentration (a) and transfer factor of yttrium (b) to sunflower organs in the presence of different yttrium concentrations in nutrient medium (Maksimović et al. 2012)

### Physiological effects of REEs on plants

REEs are not essential for higher plants or for other live organisms, but can specifically influence life processes, such as: promotion and inhibition of growth of organisms, cell proliferation and apoptosis; antioxidant activity and pro-oxidant activity; stabilization and destabilization of cytoskeleton; enhance or jeopardize of membrane permeability; affect regulation of cell signaling system; promote or inhibit bone growth; increase or decrease oxygen affinity for hemoglobin; inhibit muscle contraction; block transmission of neural signals; enhance mineralization or demineralization.

Impact of REEs on plant physiological and biochemical processes was mainly studied by Chinese researchers and the results were mostly published in Chinese language. Detailed review of these and other papers in the field were given by Hu et al. (2004), who cites results of numerous authors who have described effect of certain REEs on activity of some enzymes, the content of phytohormones, productivity and intensity of photosynthesis, chlorophyll

synthesis, translocation of photosynthesis products, water regime of plants and their resistance to water deficiency, symbiotic fixation of atmospheric nitrogen etc. But also, a favorable effect of REEs on seed germination has been described (Bai Bao-Zhang et al., 1988), and effect on morphological characters of plants (Bai Bao-Zhang et al., 1990 a, b). REEs affect the uptake and metabolism of mineral matter in plants. They often stimulate the uptake of certain elements, and decrease the uptake of others.

Research results on the effect of REEs on plant growth are somewhat contradictory. The early findings mostly point to inhibitory effect of these elements on plant growth, first of all lanthanum. The majority of papers published lately point to a stimulating effect of low concentrations of REEs on growth and organic productivity of plants. They were found to affect favorably the yield of many crops such as: rice, sugar cane, sugar beet, soybean, sunflower etc. (Hu et al., 2004). There is far less data in the literature about the single affect of certain REEs elements on life processes in higher plants.

REEs, like all other ions, are toxic when present in excessive concentrations. Mechanisms of their toxicity may include enzyme inhibition, binding to organic ligands, competition for binding sites of some other elements, interactions with proteins, organic acids, carbohydrates and other active molecules, binding cofactors, vitamins, substituting essential metals therefore provoking metal imbalance. They may also be involved in such issues as cation and anion antagonism. In spite of numerous results (Horovitz, 2000), it is not yet clear enough how they affect plant metabolism and human and animal health, which makes is necessary to investigate further on mechanisms of their action.

## Conclusions

It has been found that REEs are widely distributed in plants, as well as that certain plants take up REEs to a different extent. RREs accumulate predominantly in roots. Beneficial, toxic or nil effects of REEs on plant metabolism, growth and crop yield were observed in both controlled and field conditions. Identifying appearance of the uptake, accumulation, distribution of REEs in plants and their particular parts and therefore their entrance into the food chain, as well as their non-specific stimulating or toxic effect on plants, can by very significant ecologically too. Systematic research of the environmental biogeochemical behavior of REEs in soil-plant systems is not sufficient at present and information on their involvement in plant metabolism, and impact on human and animal health is still lacking.

## References

- [1] Z. H. Hu, H. Richter, G. Sparovek, E.Schnug, Physiological and biochemical effects of rare earth elements on plants and their agricultural significance: a review. *J. Plant Nutr.*, 27 (2004) 183-220.
- [2] A. Kabata-Pendias, *Trace Elements and Plants*. Boca Raton, Florida, CRC Press, London, 2001.
- [3] R. Kastori, I. Maksimović, T. Zeremski-Škorić, M. Putnik-Delić, Rare earth elements - Yttrium and higher plants. *Proc. Nat. Sci. Matica srpska* (2010) 118: 87-98.
- [4] B. Bai Bao-Zhang, R. Kastori, N. Petrović, Effect of elements from scandium and lanthanid groups on growth and morphological characters of young sunflower plants. *Helia*, (1990a), 13: 1-9.
- [5] B. Bai Bao-Zhang, R. Kastori, N. Petrović, Effect of elements from scandium and lanthanid groups on some morphological and physiological characters of young soybean plants *Glycine max.* (L.) Merrill. *Agrochimica*, 34 (1990b), 467-474.

- [6] I. Maksimović, R. Kastori, M. Putnik-Delić, M. Borišev, Effect of yttrium on photosynthesis and water relations in young maize plants. *J. Rare Earths.*, 32 (2014a), 371-378.
- [7] I. Maksimović, R. Kastori, M. Putnik-Delić, T. Zeremski, Yttrium – accumulation, translocation and distribution in young sunflower plants (*Helianthus annuus* L). *Fresenius Environmental Bulletin*, 21 (2012), 11-18.
- [8] I. Maksimović, R. Kastori, M. Putnik-Delić, S. Zeljković, Rare earth elements in the environment. *Proceedings of XVI International ECO-Conference, Safe Food*, Novi Sad, (2014b), 81-89.
- [9] C. T. Horovitz, *Biochemistry of Scandium and Yttrium. Part. 2. Biochemistry and Application*. Kulwer Academic/Plenum Publishers, New York, 2000.
- [10] G. Tyler, Rare earth elements in soil and plant systems – A review. *Plant Ecology and Systematics*, 265 (2004), 191-206.

## Copper Recovery from Spent Catalyst used in COSORB Processes

Livia Deveseleanu-Corîci<sup>1\*</sup>, Liliana Cseh<sup>1</sup>, Marcel Lazarovici<sup>2</sup>, Laurențiu Demetrovici<sup>2</sup>,  
Ladislau Andres<sup>3</sup>, Georgeta Simu<sup>4</sup>, Cristina Dehelean<sup>4</sup>, Otilia Costișor<sup>1</sup>

<sup>1</sup> *Institute of Chemistry Timisoara of Romanian Academy, Mihai Viteazul 24, Timisoara 300223, Romania*

<sup>2</sup> *S.C. Pro Air Clean Ecologic S.A., Sulina 6B, Timisoara 300516, Romania*

<sup>3</sup> *National Research and Development Institute for Industrial Ecology – ECOIND, Dambovit Bridge 71-73, Bucharest 060652, Romania*

<sup>4</sup> *“Victor Babes” University of Medicine and Pharmacy, Eftimie Murgu Square 2, Timișoara 300041, Romania*

### Abstract

Environmentally responsible and sustainable waste management derived from technological processes represents an important priority marked by both national and EU legislation. Therefore, exploitation of chemical waste is considered as an obligation for each member state and, by default, for all the factors involved in the products life cycle and also an important economic opportunity.

The main objective of our research project is to reduce the environment pollution with heavy metals and aromatic organic materials by recycling spent catalyst complexes resulted from industrial COSORB processes. In addition, it is economically desirable to recover the metals, which are usually copper and aluminum, from waste materials. Therefore, the present study aimed to develop a process for recovering copper from spent solutions of complexing agents containing cuprous aluminum tetrachloride. The liquid sorbent consisting of bimetallic  $\text{CuAlCl}_4$  in toluene and impurities has been subjected to several separation and analysis procedures for recovering and purification of metals and toluene. The process comprised of (i) treatment of spent solution with different solutions of sodium hydroxide, calcium hydroxide or water; (ii) separating the organic phase and the aqueous phase; (iii) contacting the aqueous phase containing the dissolved cuprous halide with iron, for precipitating copper metal and (iv) recovering the precipitated copper metal.

The separation method employing water showed the best performances in terms of operational simplicity and cost-efficiency. The organic phase after separation contained 84.5 % toluene as major component, 10.0 % toluene oxidation products, 5.4 % xylene, and 0.1 % benzene traces. The inorganic phase contained about 98.5 g/L copper, 40.1 g/L aluminum, 20.0 mg/L zinc, 26.0 mg/L chromium and 18.0 mg/L iron. The yield of copper metal recovered from the spent solution was 91.9 % with 99.35 % purity.

### Acknowledgements

This work was supported by a grant of the Romanian National Authority for Scientific Research, UEFISCDI, project number PN-II-PT-PCCA-2013-4-0612.

## Homoleptic and Heteroleptic Pt(II) Complexes with Potential Biological Activity

Ioana Costinas<sup>1\*</sup>, Carmen Cretu<sup>1</sup>, Ramona Tudose<sup>1</sup>, Liliana Cseh<sup>1</sup>, Viorel Sasca<sup>1</sup>,  
Valentin Badea<sup>2</sup>, Otilia Costisor<sup>1</sup>, Elisabeta I. Szerb<sup>1</sup>

<sup>1</sup> *Institute of Chemistry Timisoara of Romanian Academy, 24, Mihai Viteazul Bvd., 300223-Timisoara, Romania*

<sup>2</sup> *"Politehnica" University of Timisoara, Vasile Parvan Str., Timisoara, Romania*

### Abstract

Metal complexes used as pharmaceuticals have received great attention because of their potential biological activity. The chemistry of platinum(II) complexes has been widely developed since the cytostatic activity of cis-diaminodichloroplatinum(II) (cisplatin) has been discovered [1]. Moreover, transition metal complexes containing planar polycyclic aromatic systems intercalate between the stacked base pairs of DNA. The biological activity of both *cis*- and *trans*-diamine Pt(II) complexes is dramatically enhanced by the presence of aromatic intercalator ligands, due to the influence on both kinetics and thermodynamics of DNA binding [2,3].

The chemistry of Pt(II) complexes is highly versatile, permitting the design and synthesis of a large variety of different structures. By 'smart' molecular engineering, new structures are programmed and obtained continuously, in an attempt to overcome the drawbacks of the cisplatin like tumor resistance, or to lessening unpredictable and severe nephrotoxicity and/or providing oral bioavailability.

Herein, new Pt(II) complexes as DNA intercalators were synthesized and characterized aiming to follow their structure – activity relationships. The synthesis and characterization of the complexes will be presented.

### Acknowledgment

We are thankful to the Romanian Academy (Project 4.1.) for the financial support.

### REFERENCES

- [1] L. Kelland, *Nature Reviews/Cancer*, 7 (2007) 573-584.
- [2] J. C. Garcia-Ramos, R. Galindo-Murillo, F. Cortez-Gusman, L Ruiz-Asuara, *J. Mex. Chem. Soc.*, 57(3) (2013) 245-259.
- [3] H.-K. Liu, P. J. Sadler, *Accounts of Chemical Research*, 44(5) (2011) 349-359.



## **Olajszennyezett Vizek Tisztítása Ózonos Előkezeléssel Kombinált Membránszűréssel - Analitikai Problémák**

### **Purification of Oil Contaminated Waters by Ozonation/Membrane Filtration Method - Analytical Aspects**

**Veréb Gábor, Sulumán Ádám, Kovács Ildikó, Kertész Szabolcs, Beszédes Sándor, Hodúr Cecília, László Zsuzsanna**

*Szegedi Tudományegyetem, Mérnöki Kar, Folyamatmérnöki Intézet,  
6725 Szeged, Moszkvai krt. 9.; \*e-mail: verebg@mk.u-szeged.hu*

#### **1. Abstract**

In the present study different type of analytic methods were applied for the description of the performance of ozonation/membrane filtration combined water purification method in case of oil contaminated water. The investigated micro- and ultra- (PVDF) membranes were not enough effective to the purification of oil contaminated waters. However a short ozonation pre-treatment increased effectively the elimination efficiency in the aspect of extractable oil content. Results highlighted that the decreased values of extractable oil content and chemical oxygen demand do not necessarily mean the reduced quantity of organic contaminants. Moreover, ozonation pre-treatment increased the total organic carbon content of the permeate. The present study highlighted that differences of applied analytic methods can results different conclusions in case of purification of oil contaminated waters.

#### **2. Bevezetés**

Magyarország vízfelhasználásának jelentős részét mélységi vizek kitermeléséből fedezi, melyek szennyeződései közül potenciális veszélyforrást jelentenek a kis koncentrációban jelen lévő ásványi olaj eredetű szennyezések. Az olajos szennyezések az ipari tevékenységek következtében is egyre fokozódó problémát jelentenek. Ezen szennyezések nem távolíthatók el hatékonyan a hagyományos vízkezelési eljárásokkal, sőt esetenként a kezelés során akár az eredetnél károsabb vegyületek is keletkezhetnek, mint például a klóros fertőtlenítés során keletkező klórozott szerves vegyületek [1].

Az alternatív vízkezelési eljárások közül mind a membránszeparáció, mind a nagyhatékonyságú oxidációs eljárások („AOPs”) igen ígéretesek. A membránszűrés előnye, hogy nincs vegyszerigénye, nem történik kémiai átalakulás, így nem képződnek káros melléktermékek. Ugyanakkor az oldott szennyeződések eltávolítására csak az igen kicsiny pórusátmérővel rendelkező „ultra- és nanoszűrők” alkalmazhatóak, melyek azonban extrém magas nyomást igényelnek, ami korlátot szab a gazdaságos alkalmazhatóságnak. Az AOPs előnye hogy a szerves szennyezők széles körét képesek oxidálni, egyes esetekben akár a klasszikus értelemben vett kémiai adalékok hozzáadása nélkül (pl.: fotolízis, fotokatalízis, ózonozás), és elegendő időt biztosítva akár a teljes mineralizáció is elérhető. Hátrányként megemlítendő, hogy nagy szervesanyag tartalom esetén meglehetősen költséges az eljárás. Megoldást jelenthet a mikroszűrés és nagyhatékonyságú oxidációs eljárások kombinációja. A nagyhatékonyságú oxidációs eljárások a membráneltömődés mértékét is befolyásolhatják pl. az oldott anyag hidrofób jellegének csökkenésével [2], illetve a szűrendő komponensek méretének változtatásával [3]. Jelen munkánkban kis mennyiségű kőolajjal ( $c_{\text{kőolaj}}=100$  ppm) szennyezett víz tisztíthatóságát vizsgáltuk ózonos előkezelés, és mikroszűrés kombinálásával.

#### **3. Alkalmazott anyagok és módszerek**

A modellszennyvíz előállításához desztillált vizet és kőolajat (MOL – algyői olajmező nyers kezeletlen ásványi olaja) használtunk fel ( $c_{\text{kőolaj}}=100$  ppm). A modell szennyvizeket ( $V=500$  mL) ultrahangos kezeléssel homogenizáltuk (HIELSCHER UP200S - maximális

amplitúdó, teljes ciklusidő,  $t=6$  perc). Megjegyzendő, hogy a „csak” ultrahangos kezeléssel homogenizált emulzió olajtartalmának egy része gyorsan szétvált, így vizsgálatainkhoz csak az alsó, stabil fázist használtuk fel.

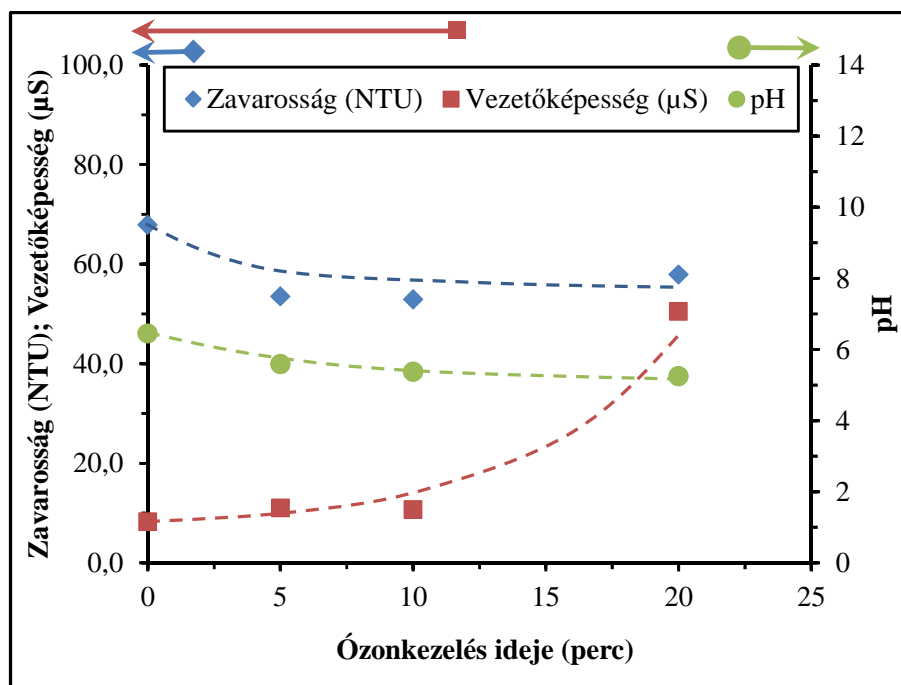
A kezelendő, és a kezelt vizek zavarosságát (*HACH 2100N*), vezetőképességét (*CONSORT C535*), pH-ját (*CONSORT C535*), kémiai oxigénigényét (*LOVIBOND ET 108* roncsoló és fotométer – kálium dikromátos meghatározás), extrahálható olajtartalmát (*WILKS* - *InfraCal TOG/TPH* analizátor; 20 perc extrahálás hexánnal) és teljes szerves széntartalmát (*TELEDYNE TEKMAR*) vizsgáltuk.

Az ózont tiszta oxigénből (*LINDE*, tisztaság: 3.0) állítottuk elő csendes elektromos kisüléssel elven működő ózon generátorral (*WEDECO* - *Ozomatic Modular 4*). Az emulziót tartalmazó elnyeletőedénybe - folyamatos mágneses kevertetés mellett - állandó (1 L/perc) térfogatárammal vezettük be az ózont tartalmazó oxigént. Az elnyeletőedénybe történő belépés előtt, illetve kilépés után átáramlásos küvettában spektrofotométerrel (*WPA LIGHTWAVE S2000*) mértük az ózon koncentrációját, amiből (a térfogatáram ismeretében) kiszámítottuk a különböző idejű ózonkezelések során a kezelt vízben elnyelődő ózon mennyiségét.

A membránszűréshez egy kevertetett cellás membránszűrő berendezést (*MERCK MILLIPORE* – *XFUF04701*) használtunk ( $P=0,1$  MPa – nitrogén palackból, keverési sebesség: 50 rpm, szűrőfelület:  $40\text{ cm}^2$ ). A betáplált szennyvíz minden esetben 50 mL volt, és a mérést 40 mL permeátum átáramlásáig folytattuk (sűrítési arány:  $VRR=5$ ). Az alkalmazott hidrofób membránokat (PVDF -  $0,5\text{ }\mu\text{m}$  illetve PVDF -  $30\text{ kDa}$ ) felhasználás előtt min. 24 óráig áztattuk desztillált vízben.

#### 4. Kísérleti eredmények és kiértékelésük

Először az ózonkezelés modellszennyvízre gyakorolt hatását vizsgáltuk. A nem kezelt, illetve az 5, 10, 20 perces ózonkezelte vizek zavarosságát, vezetőképességét és pH értékeit mutatja be az 1. ábra.



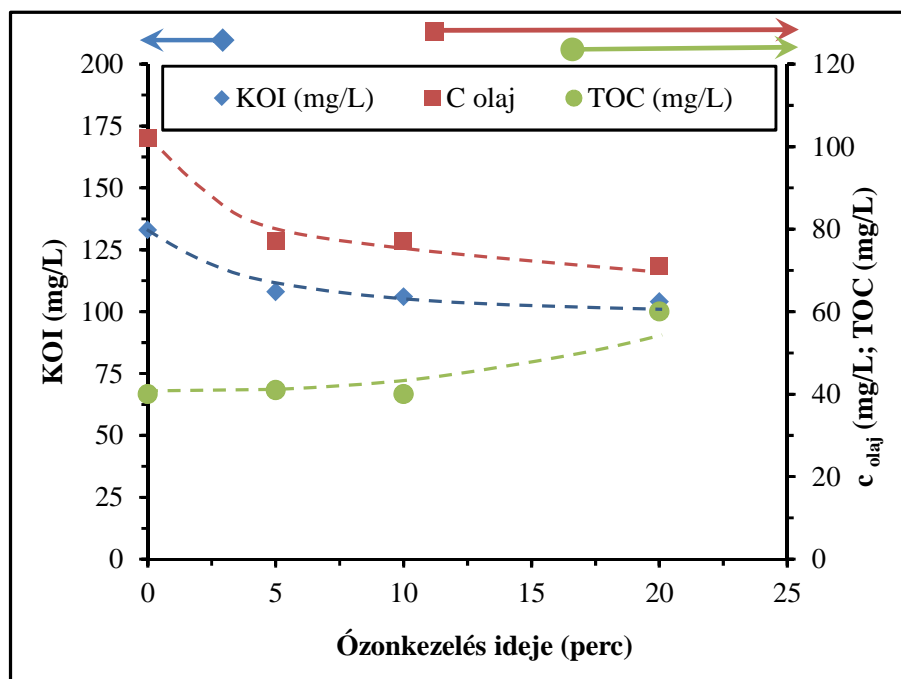
**1. ábra.** Az olajszennyezett víz zavarosságának, vezetőképességének és kémhatásának alakulása az ózonkezelés során

Az ózonkezelés hatására a kezelt víz zavarossága már az első 5 percben kb. 20%-kal csökkent, de a 10 illetve 20 perces kezelt vizek esetén már nem tapasztaltunk további



csökkenést. A csökkenés azzal magyarázható, hogy az oxidáció hatására poláris vegyületek keletkeznek, amelyek megváltoztathatják a cseppek felületi töltését. A cseppek megváltozott anyagi minősége, alakja és mérete megváltoztatja a fényszórást, feltehetően stabilizálja a cseppeket, így befolyásolva a zavarosságot [4]. A vezetőképesség az ózonkezelés hatására nőtt, míg a pH csökkent, mivel az oxidáció hatására a szénhidrogénekből szerves savak és ionok keletkezhetnek [5, 6].

A szennyezés-csökkentés mértékének jellemzésére mértük az extrahálható olajtartalmat, a kémiai oxigénigényt, és teljes szerves széntartalmat is (2. ábra).



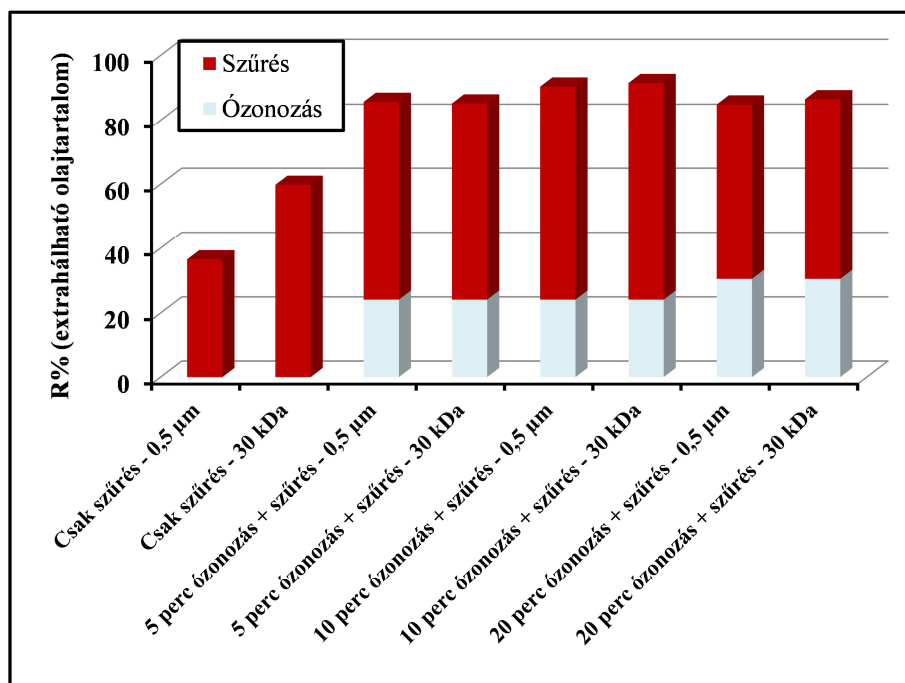
**2. ábra.** Az olajszennyezett víz kémiai oxigénigényének (KOI), extrahálható olajtartalmának (c olaj), és összes szerves széntartalmának (TOC) alakulása az ózonkezelés során

A hexánnal extrahálható olajtartalom csökkent az ózonkezelés hatására, ami részben a tényleges szervesanyag-bontással magyarázható, ugyanakkor az apoláros molekulák oxidációja poláris szerves vegyületek (pl. szerves savak) keletkezéséhez vezet, melyeknek jobb a vízzoldhatósága, ezáltal kisebb arányban jutnak át az extrakció során a szerves fázisba. A kémiai oxigénigény (KOI) az extrahálható olajtartalommal együtt természetesen ugyancsak csökkent az elnyelt ózon mennyiségének növelésével (az oxidáció előrehaladtával). Megjegyzendő azonban, hogy az összes olajtartalom alapján jóval magasabb (~ 350 mg/L) kezdeti kémiai oxigénigényt várnánk, a stabil emulziót képző vizes fázis kémiai oxigénigénye azonban jelentősen kisebb volt, ami a vízben rosszul oldódó szénhidrogének vízfelszínen való kiválásával magyarázható. Az ózonkezelés hatására azonban stabilizálódhat az emulzió a jelen levő szerves sav- és iontartalom növekedése miatt, ami magyarázatot adhat az ózonkezelés során tapasztalt teljes szerves széntartalom (TOC) növekedésére.

Következőekben az ózonnal nem kezelt olajos emulziót mikroszűréssel és ultraszűréssel kezeltük. A 0,5  $\mu\text{m}$  pórusátmérőjű membrán esetén az áteresztőképesség ~50%-kal csökkent a VRR=5 sűrítési arány eléréséig, míg a 30 kDa pórusátmérőjű membrán esetén ~80 %-kal. A szűrési időkben is jelentős különbségek voltak: a „PVDF - 0,5  $\mu\text{m}$ ” membrán esetén, a szűrés 9 percet, a kisebb pórusátmérőjű membránnál 56 percet vett igénybe. Ennek oka (túl azon, hogy az ultraszűrő membrán kezdeti fluxus értéke mindössze ~25%-a a mikroszűrő membránon mért fluxus értéknek), hogy a kisebb pórusátmérőjű membrán esetén az olajcseppek nagyobb eltömődést okoztak. Ezt alátámasztják a fluxusértékek időbeni

alakulására illesztett eltömődési modellek is melyek közül a mikroszűrő membrán esetében az iszaplepeny szűrés modellje, az ultraszűrő membrán esetében a pórusos eltömődés modellje adta a legjobb illeszkedést. A mikroszűrő membrán esetében az ózonos előkezelések (5,10, 20 perc) nem befolyásolták számottevően a fluxus értékeket. A kezdeti fluxus értékekre az ultraszűrés esetén sem volt befolyással az ózonos előkezelés, azonban jelentősen csökkent az eltömődés mértéke. A korábbi ~80%-os fluxus csökkenés helyett mindösszesen 24-35%-os csökkenést mértünk az ózonnal előkezelt olajszennyezett vizek ultraszűrése során ( a már említett VRR=5 sűrítési arány eléréséig). Egy lehetséges magyarázat lehet, hogy az ózonkezelés során olyan átmeneti termékek (pl. ózonidok) keletkezhetnek, amelyek az olajcseppeket merevebbé, kevésbé rugalmassá teszik, ezáltal kevésbé lesznek képesek „bepréselődni” a pórusokba.

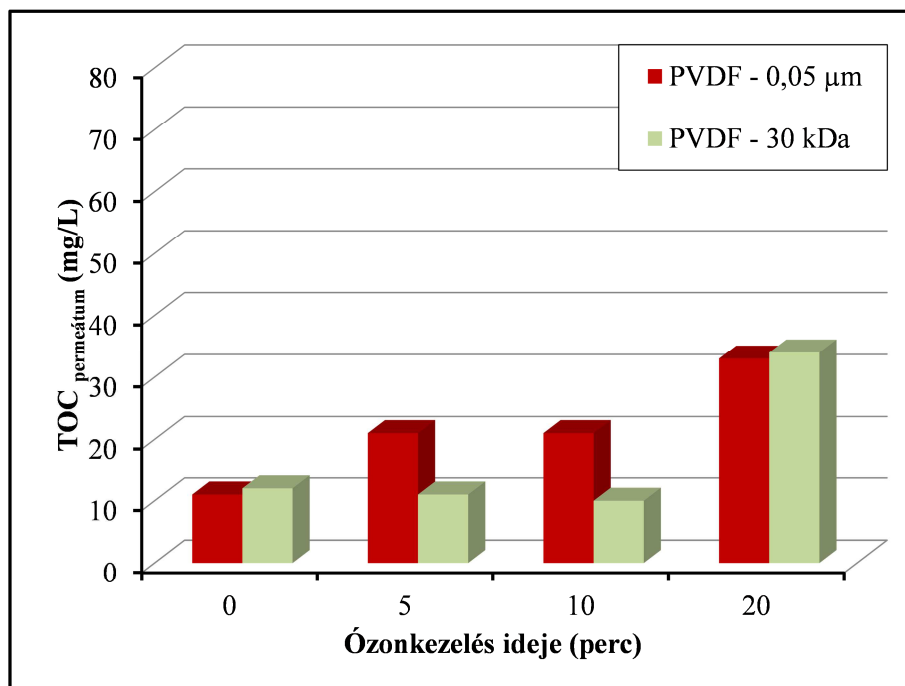
A következőkben azt vizsgáltuk, hogyan változik a szűréssel eltávolítható szennyezőanyag mennyisége az ózonos előkezelés hatására (3. és 4. ábra).



3. ábra. Az ózonos kezelés és membránszűrés hatása az extrahálható olajtartalomra

Az ózonos kezelés a mikroszűrés esetén jelentősen megnövelte a szűréssel eltávolítható olajtartalmat (~36%-ról ~62%-ra emelkedett az eltávolítás hatásfoka), ugyanakkor az ultraszűrő membrán esetében nem volt jelentős hatása. A 3. ábrán látható, hogy az előoxidáció és a membránszűrés kombinálásával mindkét membrán esetében 80-90% körüli eltávolítási hatékonyságot mértünk az extrahálható olajtartalom értékére (az előkezelés ideje nem befolyásolta jelentősen az eltávolítás hatékonyságát). Érdekes továbbá az is, hogy az előkezelt minták esetében a mikroszűrő és az ultraszűrő membrán visszatartása között nincs jelentős eltérés.

Megmértük továbbá a permeátumok összes szerves széntartalmát is, és azt tapasztaltuk, hogy az extrahálható olajtartalom csökkenése ellenére a permeátumban jelen lévő összes szerves szennyezőanyag mennyisége megnőtt az ózonkezelés hatására (4. ábra). Ezen eredmények is alátámasztják, hogy az ózonnal kezelt oldatokban a kis szénatomszámú, vízben jól oldódó szerves vegyületek mennyisége megnőtt.



**4. ábra.** Az ózonos kezelés és membránszűrés hatása a szűrlet összes szerves széntartalmára

## 6. Következtetések

Összességében megállapítható, hogy az alkalmazott mikro- illetve ultraszűrő membránok (PVDF – 0,5 µm és 30 kDa) önmagukban nem mutattak nagy olajvisszatartást (az alkalmazott kísérleti körülmények között), azonban már rövid idejű ózonos előkezelés alkalmazásával is jelentősen növelhető az extrahálható olajtartalom eltávolításának hatékonysága. Az eredmények ugyanakkor egyértelműen rávilágítanak arra a tényre, hogy az extrahálható olajtartalom, és a kémiai oxigénigény csökkenése nem feltétlenül jelenti a szervesanyag tartalom csökkenését. Ellenkezőleg, az ózonos előkezelés hatására a teljes szerves széntartalom megnőtt a szűrletekben. Fontos eredménye a munkának, hogy rávilágít arra a tényre, hogy az olaj/víz emulziók kezelésének vizsgálatánál, eltérő analitikai módszerek alkalmazása akár eltérő következtetések levonását eredményezheti hasonló (vagy akár megegyező) kísérleti körülmények ellenére. Továbbá felhívja a figyelmet az olaj/víz emulziók instabilitásának problémájára, ami tovább nehezíti a helyes következtetések levonását.

## Köszönetnyilvánítás

A munka a Bolyai János Kutatási Ösztöndíj támogatásával készült. A szerzők hálásak továbbá a Nemzeti Kutatási, Fejlesztési és Innovációs Hivatal által biztosított anyagi támogatásért (NKFI témaszám K112096 és K105021) is.

## Irodalomjegyzék

- [1] S.D. Richardson, M. Plewa, E.D. Wagner, R. Schoeny, D.M. DeMarini, Mutat. Res.-Rev. Mutat. Res. 636. (2007) 178.
- [2] S. Geluwe, L. Braeken, B. Van der Bruggen, Water Research, 45. (2011) 3551.
- [3] Zs. László, Sz. Kertész, E. Mlinkovics, C. Hodúr, Sep. Sci. and Techn. 42 (2007) 1627.
- [4] P. Kundu, A. Agrawal, H. Mateen, I.M. Mishra, Chem. Eng. Science 102. (2013) 176.
- [5] L.R. Morrow, W.K. Martir, H. Aghazeynali, Wright D.E. US Patent No. 5.868.945 (1999)
- [6] C. Chen, L. Wei, X. Guo, S. Guo, G. Yan, Fuel Proc. Techn. 124. (2014) 165.

## Kézműves és Kisüzemi Sörök Antioxidáns Kapacitásának Vizsgálata és Annak Függése a Sör Minőségi Jellemzőitől

Czura Bence<sup>1</sup>, Papp Nóra<sup>2</sup>, Stefanovits-Bányai Éva<sup>2</sup>,  
Hegyesné Vecseri Beáta<sup>1</sup>

<sup>1</sup> BCE, Élelmiszertudományi Kar, Sör- és Szeszzipari Tanszék, Budapest,

<sup>2</sup> BCE, Élelmiszertudományi Kar, Alkalmazott Kémia Tanszék, Budapest

email: bence.czura@uni-corvinus.hu

### ABSTRACT

The market of craft beers is growing nowadays and there are many types and technologies, which can make positive or negative effects on the antioxidant capacity of beers. We used 10 different beers in our experiment, included Hungarian and foreign products. We made the measurements with two methods, contained TPC (Total Polyphenol Content) and FRAP (Ferric Reducing Ability of Plasma) methods. The ale samples ranged between 3.5-5.5 mmol GA/L and the lagers between 1.8-4.0 mmol GAE/L. The FRAP values were among 1.6-3.1 mmol AAE/L by ale beers and 0.8-2.5 by lager products. We measured different analytical parameters which can influence the antioxidant capacity of beers. First of all, the beers with higher original extract were mainly ale beers and lower Balling degree were shown by the lagers, and it has been proved by previous researches that the high original extract can increase the antioxidant capacity. The lighter colour, namely the light beers showed lower results compared to the brown/black samples. At last the unpasteurized beers declared nearly higher antioxidant capacity than the unpasteurized products.

### BEVEZETÉS

Az egészséges táplálkozás manapság egyre nagyobb szerepet tölt be a mindennapi emberek életében. Ebben elengedhetetlen szerepe van az antioxidánsoknak, melyek többek között a szabad gyökök elleni küzdelemben töltnek be fontos szerepet. Az utóbbi 1-2 évtizedben egyre nagyobb figyelmet kap, hogy a sör egy olyan élelmiszer, amely nagy mértékben tartalmaz antioxidánsokat [1][2], amely így pozitív hatásokkal rendelkezik élettani szempontból [3].

A sörök antioxidáns-tartalma főképpen az alapanyagokból származik, a malátából és a komlóból, valamint kis részben az élesztőből [4]. Ezek az antioxidánsok lehetnek polifenolok (fenolos savak, flavonoidok) illetve prenilált kalkonok. Számos tanulmányban vizsgálták már a sörök teljes antioxidáns kapacitását in vitro [1] [6]. További kutatások és becslések alapján, az erjesztés típusa, a magasabb extrakttartalom, az élesztő jelenléte a kész sörben, a sör színe illetve a hőkezelés alkalmazása befolyásolhatja a sörök antioxidáns kapacitását.

Megállapították, hogy a sörben lévő polifenolok, már a sör elfogyasztását követő 30. percben detektálhatók voltak a vérplazmában, ami egy felszívó mechanizmus léteire utal az emésztőrendszer felső traktusában [2]. Azonban további tisztázásra van szükség ezen antioxidáns vegyületek kinetikus kezelésével kapcsolatban, beleértve az abszorpció idejét és helyét illetve figyelembe véve az etanol hatását az anyagcsere újtjukra [5] [6].

Kísérletünk célja az volt, hogy a fent említett minőségi jellemzők és egyéb paraméterek (erjesztés típusa, szín, extrakttartalom, hőkezelés, élesztőtartalom) analízise után meg tudjuk határozni melyek azok, amelyek pozitívan és negatívan befolyásolják az antioxidáns kapacitást a sörben.

## ANYAG ÉS MÓDSZER

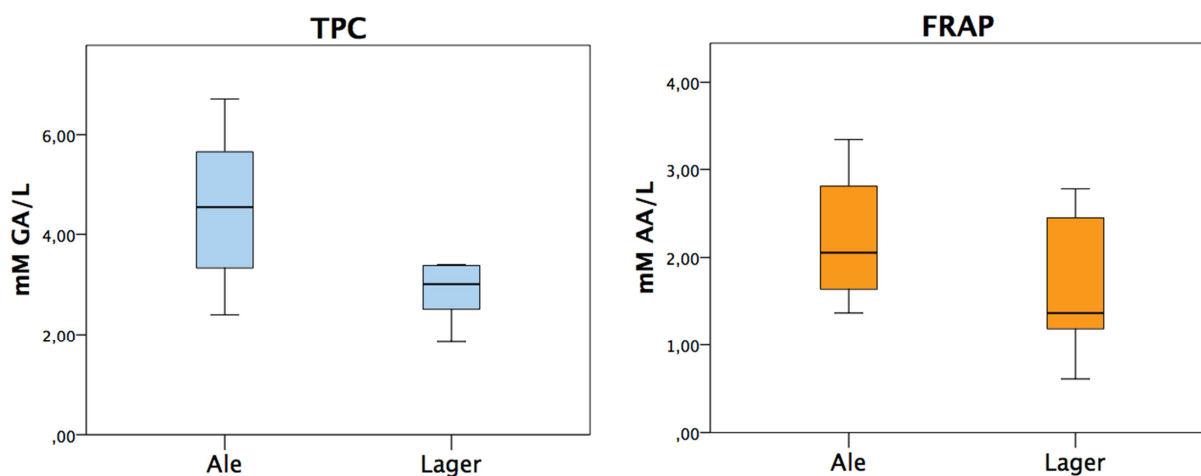
Kísérletünkben 10 különböző magyar illetve külföldi, kisüzemi sörfőzdék termékeit hasonlítottuk össze, amelynek során két különböző módszerrel vizsgáltuk meg az antioxidáns kapacitásukat, és analízist végeztünk a sörök általánosan mérendő analitikai paramétereire. Az összes polifenol-tartalmat (TPC - Total Phenolic Content) [7] szerint határoztuk meg, ahol Folin-Ciocalteu reagenst használtunk, míg a (FRAP – Ferric Reducing Antioxidant Power) minta vasredukáló képességén alapuló antioxidáns kapacitás meghatározó módszernél [8] szerint mértünk. Az eredményeket mmol GSE/L dimenzióban adtuk meg mind a TPC módszernél, és ASE/L dimenzióban a FRAP módszernél. A söranalitikai mérések során meghatároztuk a minták eredeti extrakttartalmát és a színét is. A színmeghatározás spektrofotometriás módszerrel történt, 450 nm-en, amiből kiszámítottuk a sör EBC színértékét. Az eredeti extrakttartalmat Anton Paar DMA 4500-as sűrűségmérővel és azzal összekapcsolt söranalizátorral mértük meg.

## EREDMÉNYEK ÉS ÉRTÉKEKELÉSÜK

Az antioxidáns kapacitás vizsgálatok során kapott eredményeink összhangban állnak a különböző szakirodalmi példákkal [9] [10]. Ennek megfelelően a felsőerjesztésű (ale) sörök mind a két módszernél (TPC, FRAP) nagyobb antioxidáns kapacitással rendelkeztek mint az alsóerjesztésű (lager) minták.

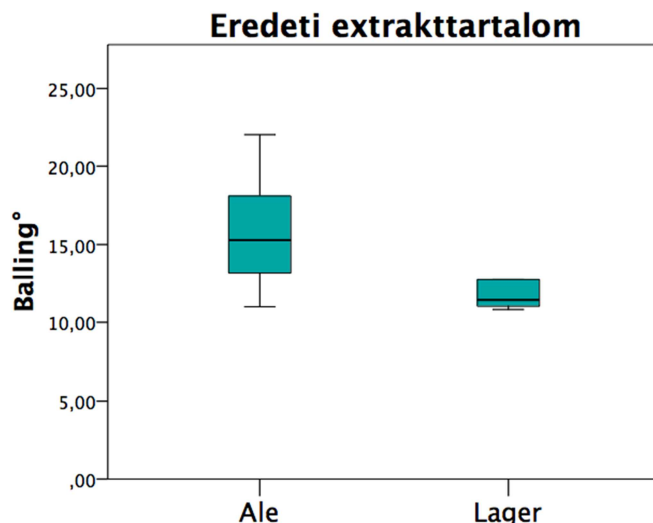
Az eredmények a TPC vizsgálat során az ale típusúaknál 3,5 és 5,5 mmol GSE/L érték között mozogtak, a lagereknél ez a határ 1,8 és 4,0 mmol GSE/L értékeknél húzható meg.

A FRAP módszernél az ale sörök 1,6 és 3,1 mmol ASE/L közé estek, míg a lagerek némileg kisebb eredményt értek el, amely 0,8 és 2,5 mmol ASE/L közé tehető. Ezek az adatok az 1. ábrán kerültek megjelenítésre.



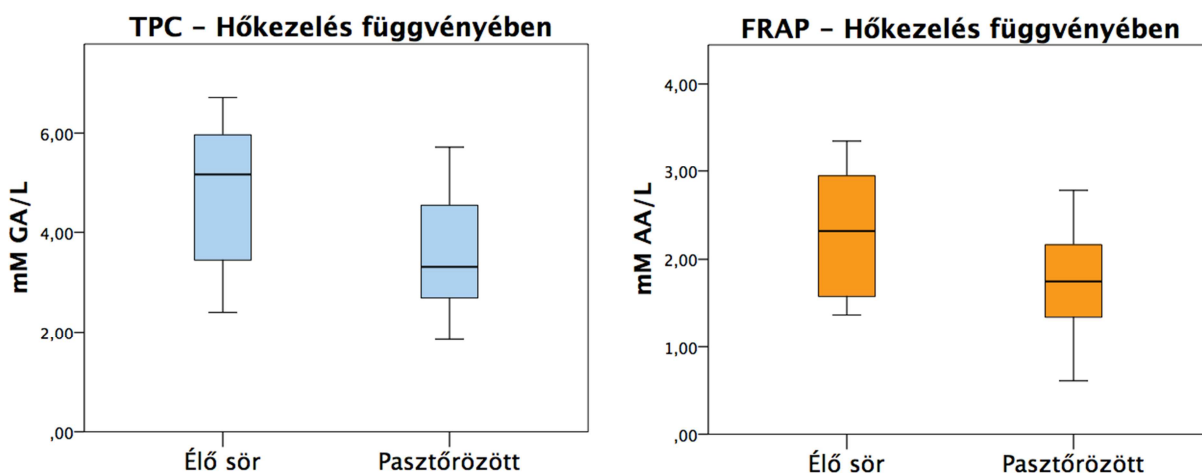
1. ábra. A TPC és a FRAP módszer eredményei a felső- és alsóerjesztésű söröknél.

A söranalitikai mérések során kapott eredmények azt mutatták, hogy a felsőerjesztésű sörök eredeti extrakttartalmi nagyobbak voltak a lager sörökénél. Ezt a 2. ábra mutatja, miszerint az ale sörök 14,2 és 17,5 Balling fok közötti értékekkel rendelkeznek, addig a lager minták 10,8 és 12,8 között helyezkednek el. A szakirodalmi adatok szerint az eredeti extrakttartalom pozitívan befolyásolhatja az antioxidáns kapacitást [11], amelynek megfelelnek az általunk kapott eredmények.



**2. ábra.** Az eredeti extrakttartalom mérés eredményei a felső- és alsóerjesztésű sörökben.

Vizsgáltuk továbbá a eltérést a hőkezelésen átesett és a hőkezelés nélkül forgalomba hozott sörök között. A sörben található enzimekre, antioxidánsokra aktivitására a szakirodalmi példák alapján befolyással lehet a hőkezelés. Ezt alátámasztja a kísérletünk során kapott eredmény, mint hogy az élő sörök magasabb antioxidáns kapacitással rendelkeztek, mint a két mérési módszernél. Az élő sörök a TPC esetében átlagban 4,1 és 5,8 mmol GSE/L között helyezkedtek el, míg a pasztörözött minták 3,1 és 4,2 mmol GSE/L között. Ez az arány a FRAP módszer esetében is nagyjából azonos, ugyanis az élő sörök 1,8 és 2,8 mmol ASE/L közé estek, a pasztörözöttek pedig 1,5 és 2,2 mmol ASE/L közé. Ezek az eredmények a 3. ábrán láthatók.

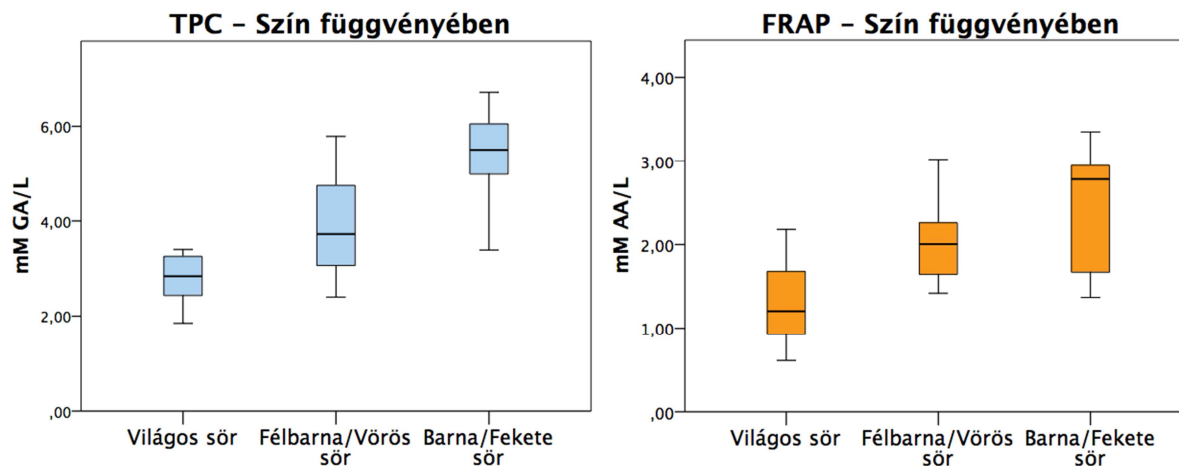


**3. ábra.** A TPC és FRAP módszer eredményei a hőkezelés függvényében.

A nagyüzemi sörökhöz hasonlóan a kézműves söröknél is azt tapasztaltuk, hogy a nagyobb EBC színértékkel rendelkező söröknél nagyobb antioxidáns kapacitás várható [1] [10] [12]. Ennél a vizsgálatnál 3 különböző csoportra (világos, félbarna/vörös, barna/fekete) osztottuk a söröket a Magyar Élelmiszerkönyv szerint, és a 4. ábrán közöljük az eredményeket. Mind a TPC mind a FRAP módszernél esetében a világostól az egyre sötétedő sörmintákig az



antioxidáns kapacitás egy növekvő trendet mutat, mely szerint így világosabb sörök rendelkeznek a legalacsonyabbal (TPC: 2,2-3,3 mmol GSE/L; FRAP: 0,8-1,5 mmol ASE/L), középen a félbarna és vörös sörök helyezkednek el, (TPC: 3,0-4,5 mmol GSE/L, FRAP: 1,8-2,1 mmol ASE/L), míg a legnagyobb antioxidáns kapacitással a barna és a fekete sörök rendelkeznek (TPC: 4,5-5,8 mmol GSE/L, FRAP 1,8-2,8 mmol ASE/L).



4. ábra. A TPC és FRAP módszer eredményei a sörök színének függvényében.

## KÖVETKEZETÉSEK

A hazai és külföldi előállítású kézműves és kisüzemi sörök vizsgálata során megállapítottuk, hogy hasonló trend figyelhető meg az antioxidáns kapacitásban, erjesztés típusa és a színek függvényében. Ahogy a szakirodalmi áttekintés során kiderült, úgy a kísérletünk során is alátámasztottuk, hogy a sötétebb szín, a magasabb extrakttartalom pozitívan befolyásolja az antioxidáns kapacitást, és mivel ezek a sörök gyakran ale típusúak, ezért ez okozhatja a különbséget a felső- és alsóerjesztésű minták között.

## FELHASZNÁLT IRODALOM

- [1].Montanari L., Perretti G., Natella F., Guidi A., Fantozzi P. (1999). Organic and Phenolic Acids in Beer. *LWT – Food Science and Technology*, 32:535
- [2].Nardini M., Natella F., Scaccini C., Ghiselli A. (2006). Phenolic acids from beer are absorbed and extensively metabolized in humans. *The Journal of Nutritional Biochemistry*, 17:14-22
- [3].Halliwell B., Gutteridge JM. (1995). The definition and measurement of antioxidants in biological systems. *Free Radic Biol Med.*, 18(1): 125-126
- [4].Gerhäuser C. (2005). Beer constituents as potential cancer chemopreventive agents. *European Journal of Cancer*, 41: 1941-1954
- [5].Preedy V.R., Iacomino G., Tedesco I., Russo G.L. (2009). Beer in Health and Disease Prevention. 47: 483-490
- [6].Vinson J.A., Mandarano M., Hirst M., Trevithick J.R., Bose P. (2003). *Journal of Agricultural and Food Chemistry*, 51: 5528-5533
- [7].Singleton V.L., Rossi J.A., (1965). Colorimetry of total phenolics with phosphomolybdic-phosphotungstic acid reagents. *Am. J. Enol. Viticult.*, 16: 144–158.
- [8].Benzie I.F.F., Strain J.J. (1996). The ferric reducing ability of plasma (FRAP) as a measure of "antioxidant power": The FRAP assay. *Anal. Biochem.*, 239: 70–76.
- [9].Tafulo P.A.R., Queirós R.B., Delerue-Matos C.M., Ferreira Sales M.G. (2010). Control and comparison of the antioxidant capacity of beers. *Food Research International*, 43: 1702-1709

- [10]. Zhao H., Chen W., Lu J., Zhao M. (2010). Phenolic profiles and antioxidant activities of commercial beers. *Food Chemistry*, 119:1150-1158
- [11]. Zhao H. (2014). Endogenous Antioxidants and Antioxidant Activities of Beers. *Processing and Impact on Antioxidants in Beverages*, 15-24
- [12]. Lugasi A. (2003). Polyphenol content and antioxidant properties of beer. *Acta Alimentaria*, 32 (2): 181-192



## Structural Characterization of 3d Metal Complexes Containing an Unconventional Schiff Base Ligand

Carmen Cretu<sup>1\*</sup>, Diana Aparaschivei<sup>1</sup>, Liliana Cseh<sup>1</sup>, Ramona Tudose<sup>1</sup>, Catalin Maxim<sup>2</sup>, Marius Andruh<sup>2</sup>, Athanasios Salifoglou<sup>3</sup> and Otilia Costisor<sup>1</sup>

<sup>1</sup>*Institute of Chemistry of the Romanian Academy, 300223-Timisoara, Romania*

<sup>2</sup>*Inorganic Chemistry Laboratory, Faculty of Chemistry, University of Bucharest, 020464-Bucharest, Romania*

<sup>3</sup>*Laboratory of Inorganic Chemistry, Department of Chemical Engineering, Aristotle University of Thessaloniki, 54124-Thessaloniki, Greece*

### Abstract

The design of appropriated organic ligands capable of binding metal ions provides a targeted entry to new materials with distinct structural and physicochemical properties. A representative family of such ligands includes Schiff bases. Here, we report new mono, di- and polynuclear materials  $[\text{Co}(\text{L})]_3(\text{ClO}_4)_3 \cdot 4\text{H}_2\text{O}$  (**1**),  $[\text{Zn}_2(\text{L})(\text{CH}_3\text{COO})_2]$  (**2**) and  $[\text{Cu}_3(\text{L})_2(\mu^3\text{-ClO}_4)_{0.66}](\text{ClO}_4)_{1.33} \cdot 1.33\text{CHCl}_3$  (**3**) containing N,N'-bis[(2-hydroxybenzylideneamino)-propyl]-piperazine (**H<sub>2</sub>L**) Schiff base as hexadentate ligand (Figure 1). The X-ray crystallography of the complexes reveal a retaining of the original chair piperazine conformation from the free ligand in the complex **2** and a changing into a boat conformation in the complexes **1** and **3**. Moreover, in the respective complexes a different coordination number as 6 (**1**), 5 (**2**) and 4 and 5 (**3**) was observed upon coordination of the free ligand to Co(III), Zn(II) and Cu(II) ions. The modulatory property of **H<sub>2</sub>L** is reflected upon the molecular assembly and coordination mode of the isolable species.

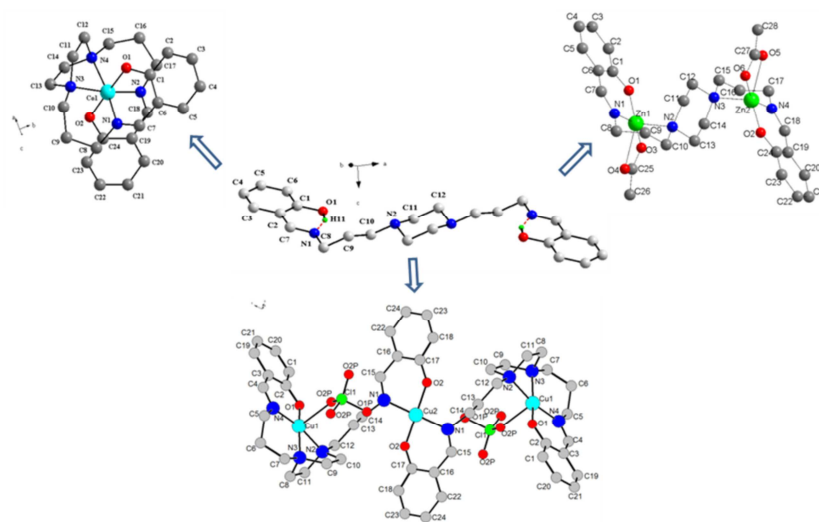


Figure 1. Molecular structure of Schiff base ligand and its metal-complexes

### Acknowledgment

We are thankful to the Romanian Academy (Project 4.1.) for the financial support.

## Lithium Doped Polyphosphoester Composite

Nicoleta Plesu<sup>1\*</sup>, Milica Tara-Lunga-Mihali<sup>1,2</sup>, Smaranda Iliescu<sup>1</sup>, Lavinia Macarie<sup>1</sup>,  
Gheorghe Ilia<sup>1,2</sup>,

<sup>1</sup>*Institute of Chemistry, Romanian Academy, 24 Mihai Viteazu Bvd. 300223 Timisoara, Romania,*

<sup>2</sup>*Vest University Timisoara, Faculty of Chemistry-Biology-Geography, 16 Pestalozzi str., 300115, Timisoara, Romania*

\*email: plesu\_nicole@yahoo.com, nplesu@acad-icht.tm.edu.ro

### Abstract

The effect of lithium triflate on the ionic conductivity of polyphosphoester composite was investigated by electrochemical impedance spectroscopy (EIS). The highest conductivity was obtained for membrane with 15% lithium salt. The ion transport is slow due to the aggregation tendency of ions for composite membrane with higher than 20% lithium salt. The conductivity of all membranes increases linear with the increase of the temperature and shows a thermally activated process.

### Introduction

Composite materials find nowadays easily applications in electronic industry. For instance, in solid polymer electrolytes the increase in conductivity is essential and it can be achieved by adding salts, ionic liquids or inorganic nanoparticles in polymer matrix and their amount is an answer to the required improvement.

Various polymer composites with enhanced mechanical, electrical and thermal stability are reported [1, 2]. High value of ionic conductivity at a temperature close to the melting point was reported for solid polymer electrolytes based on poly(ethyleneglycol) (PEG 2000) and lithium perchlorate [3]. Poly(siloxanes), poly(vinylpyrrolidone), poly(acrylates), poly(ethylenesuccinate), poly(vinylalcohol), poly(ethyleneimine), poly(alkylenesulphides) are also a good candidates for solid polymer electrolytes [4].

The aim of this study is to investigate the electrochemical behavior of polyphosphoester composite doped with lithium salt. The effect of lithium triflate on the ionic conductivity was investigated by electrochemical impedance spectroscopy (EIS).

### Experimental

Composite membranes M, M1, M2 and M3 contain tris(4-hydroxybutylacrylate)-phosphate: polyphosphoester in a 1.5 :1 %wt ratio and different amounts of lithium salts (Aldrich, LiTf) (5-20 %wt.). LiTf was dissolved in methanol (in minimum quantity) and added to polymer mixture together with 0.15% dispersing agent (polyaniline, PANI) and complexation was completed in an oven at 60°C for 6 h. Photoinitiator Darocure 4265 (3%wt, Cognis) was used to cure the composite mixture. To obtain membranes the composite mixture was cast on a Teflon plate and cured by exposure to UV Lamp type Sunray 400SM. In **Table 1** are presented the notations and composition of the prepared lithium polyphosphoester composite membranes.

**Table 1.** The notation and composition of prepared membranes.

Membrane notation	LiTf, % wt	Thickness, $\mu\text{m}$
<b>M1</b>	5	90
<b>M2</b>	10	90
<b>M3</b>	15	110
<b>M4</b>	20	100

### Analysis

Jasco FTIR 4200, Miracle ATR spectrometer with ZnSe crystal plate was used to collect the IR spectra. Ionic conductivity of the membranes was determined by the AC impedance spectroscopy. Autolab 302N potentiostat/galvanostat equipped with the FRA2 impedance module was used for EIS determination. At the point where the phase angle is zero (or close to zero) in Bode diagrams, the impedance is pure ohmic and the ionic conductivity can be determined by the following equation (1):

$$\sigma = h / R_b \cdot A \quad (1)$$

where:  $\sigma$  - ionic conductivity,  $R_b$  – the resistance corresponding to the angle closest to zero in the Bode diagram,  $h$  – the height of the sample between the electrodes,  $A$  – the cross-sectional contact area of the measured sample.

Measurements of composite conductivity function of temperature were performed in the range of 25°C to 90°C and the activation energy was calculated using the Arrhenius equation (2):

$$\sigma(T) = \sigma_0 \exp(-E_a / kT) \quad (2)$$

where:  $\sigma_0$  represents the pre-exponential factor in  $S \cdot cm^{-1}$ ,  $E_a$  is the activation energy in eV, and  $k$  is the Boltzmann constant.

### Results and discussion

The spectra of complexed lithium composite matrix are presented in **Figure 1**. The intensity of the bands associated to P=O ( $1251 \text{ cm}^{-1}$ ) and P-O-C ( $1080 \text{ cm}^{-1}$ ) bonds presented in composite matrix is reduced and slightly shifted to the lower frequency due to the coordinative bond formed between oxygen atoms from phosphate and ether group and lithium ion. This leads to the formation of complexes between polymer and salt.

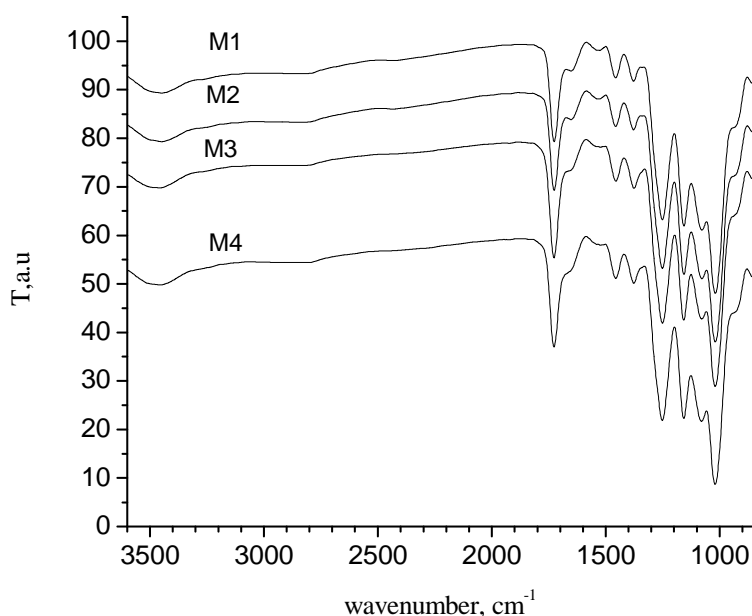


**Figure1.** ATR. Spectra of membranes M1, M2, M3 and M4.

The highest intensity signal is obtained for M3 membrane and pointed out that the amount of lithium salt added in this membrane is the optimum value.

The ionic conductivity ( $\sigma$ ) of membranes was calculated according to Eq. (1), from EIS spectra recorded at Open Circuit Potential (OCP) (**Figure 2a**).

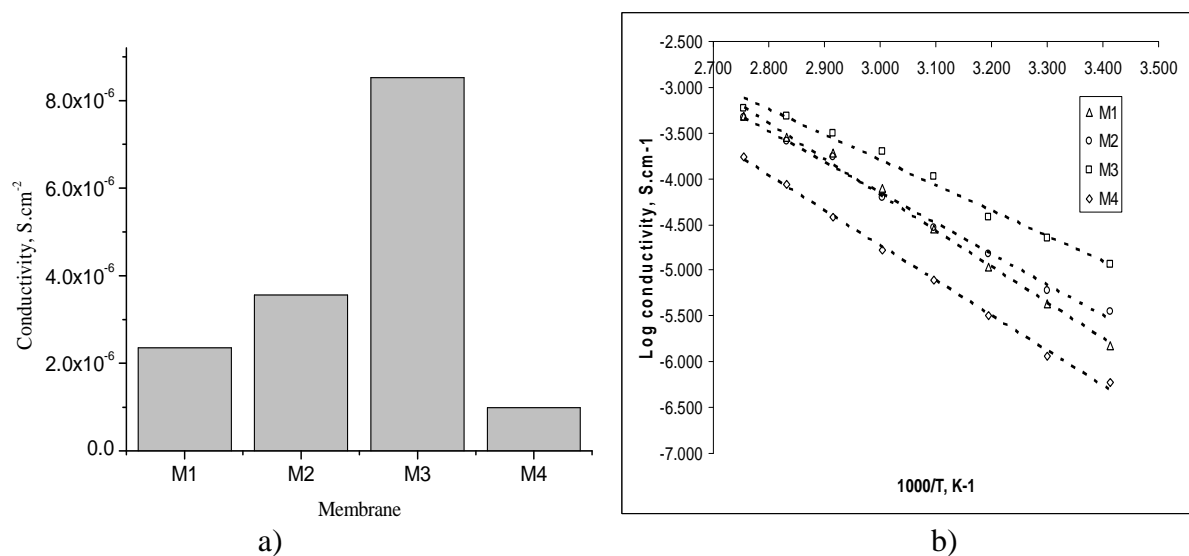


**Figure 2.** Membrane conductivity a) function of membranes composition at 25°C and b) variation with temperature, plotted in Arrhenius coordinates

The conductivities of membranes increase with LiTf content and above a certain amount decrease. The highest conductivity was obtained for membrane based on M3. The conductivity increases with the lithium salt content from 5 to 15% at room temperature and decreases with the increase of lithium salt content from 15 to 20%. The decrease of conductivity was attributed to the decrease of the available number of charge carriers due to ion aggregation. The M3 membrane presents the highest conductivity of  $8.52 \times 10^{-6} \text{ S.cm}^{-1}$ .

The conductivity of all membranes increases with the increase of the temperature. The enhanced conductivity arises from the increase of ions and polymer chains mobility. At high temperatures the polymer chains show a high degree of motion and this leads to compensate the unfavorable retarding effect of the ion clouds. The logarithmic plots show a linear variation of the conductivity vs temperature, which is characteristic for a thermally activated process (**Figure 2b**).

The values for activation energy  $E_a$  and pre-exponential factor calculated from the linear segment of all membranes are presented in **Table 2**.

**Table 2.** The pre-exponential factor and activation energy  $E_a$

PANI, ppm	M1	M2	M3	M4
$\sigma_0$ , S. cm <sup>-1</sup>	7.587	5.910	4.489	6.769
$E_a$ , eV	0.338	0.289	0.238	0.330
R	0.994	0.993	0.989	0.997

The activation energy depends on salt content which is the source of charge carriers in the polymer electrolyte (the decrease of the activation energy is due to the increase number of charge carriers in the polymer electrolyte). It was observed a decrease of activation energy with the increase of salt content till 15% and at 20% salt concentration an increase of

activation energy. With the increase of salt content the number of carriers increase and the conductivity increase. At high ion concentration the number of carriers are diminished and is due to the tendency of ions to aggregate and slow down ion transport.

The  $\sigma_0$  values explain the composite conductivity as a result of the movement of mobile charge carriers in the membranes. Analyzing the data for the pre-exponential factors it was observed that the increase in  $E_a$  (M1 and M2 membranes) tends to be compensating by  $\sigma_0$ . The compensating effect is mentioned in the literature for a lot of semiconductive materials. The data was fitted by the straight line:  $\ln\sigma_0 = 0.119E_a - 1.95$  ( $R^2=0.961$ ) and pointed out the possibility of the carriers to be transported by inter-chain interaction or hopping between localized sites. The slowest macroscopic process will provide the conductivity level.

### Conclusion

Membranes based on PANI-polyphosphoester show conductivity by adding lithium salts. The highest conductivity was obtained for membrane with 15% lithium salt. For the composite membrane with 20% salt content the ion transport is slow due to the aggregation tendency of ions. The linear increase of conductivity with the temperature shows a thermally activated process. The correlation between Arrhenius parameters show transport possibility by inter-chain interaction or hopping between localized sites. The macroscopic conductivity will be determined by the slowest process.

### Acknowledgements

The authors acknowledge for the financial support from Program 2, Project 2.2. of Romanian Academy.

### References

- [1].F.M. Gray, in: V.C.H. Publischers (Eds), Solid Polymer Electrolytes Fundamentals and Technological Applications, New York, 1991.
- [2]. Di Noto V., Lavina S., Giffin G.A., Negro E., Scrosati B., *Electrochim. Acta.* 57 (2011) p. 4.
- [3]. T.H.J. Singh, S.V Bhat., *Bull Mater Sci.* 26 (2003) p.707-714.
- [4].Chandrasekhar, V., *Adv. Polym. Sci.* 135 ( 1998) p.139-205.

## Fertőtlenítés Szerepe Diclofenac-kal Szennyezett Víz Kezelése során

Földényi Rita<sup>\*</sup>, Joó Szilvia

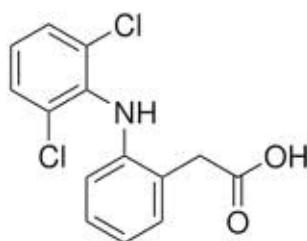
Föld- és Környezettudományi Intézeti Tanszék, Pannon Egyetem, H-8200 Veszprém,  
Egyetem u. 10., Magyarország  
e-mail: foldenyi@almos.uni-pannon.hu

### Abstract

The drug active ingredient “diclofenac” is one of the most frequently identified micropollutants in water resources. Since the addition of chlorine as disinfectant has to be used in the last step of water treatment, its chemical reaction with diclofenac was investigated in the presence of natural organic matter at pH=7. Chlorination and oxidation are parallel reactions but the latter is very slow. The decay of the drug is slower in the presence of humic substances than in their absence but the clay mineral content of the extract prepared from sandy soil can accelerate the chlorination reaction.

### Bevezetés

A gyógyszerhatóanyagok környezeti hatásokra gyakran nem vagy nehezen lebonthatóak és a szervezetben belőlük keletkező metabolitok a szennyvízbe kerülhetnek. Ez az oka annak, hogy az utóbbi években a vízkészletek szennyezőanyagaiként egyre nagyobb figyelmet kapnak. Az ún. nem-szteroid típusú gyulladáscsökkentők közül a diclofenacot (1. ábra) külsőleg és belsőleg is alkalmazzák különböző készítményekben, ezért a környezetben az egyik leggyakrabban kimutatott gyógyszerhatóanyag. Elsősorban nátrium-só formájában kerül forgalomba, amelynek vízoldhatósága különösen jó (szobahőmérsékleten 50 g/l). Jellegzetesen a felszíni vizekben fordul elő, aminek következménye, hogy az üledékben, iszapban is feldúsulhat, de szennyezőként kimutatták felszín alatti vízben és talajban is [1]. Magyarországi gyártása miatt régebben a hatástalan szennyvíztisztítás eredményezte, hogy a Dunában meglehetősen nagy koncentrációban (931 ng/l) fordult elő [2-3].



1. ábra: A diclofenac szerkezeti képlete

Ugyan hazánkban a kitermelt nyersvíznek csak kb. 5 %-a származik közvetlenül felszíni vízből, de az ún. parti szűrészű vízből (felszíni vizek partjai mellett, a felszín alatti áramlásból származó víz, amelynek legalább 50%-a felszíni forrásból származik) 44 %, amelyben a Duna vize is jelentős hányadot képvisel [4]. Emiatt a gyógyszerhatóanyagok közül a diclofenac környezeti analitikai vizsgálatával és a hagyományos módszereknél hatékonyabb bontásával itthoni kutatócsoportok is foglalkoztak [2-3], [5].

Az ivóvíz kezelése során a fertőtlenítést nem kerülhetjük el. Gyakran már a folyamat elején van egy ilyen lépés, de a folyamat legvégén mindig adagolnak fertőtlenítőszert, máskülönb a hálózatban elszaporodnak a mikroorganizmusok. Fertőtlenítésre klór (illetve hypo) mellett klór-dioxid is használható, de ez utóbbi kevésbé terjedt el.

Ismert, hogy a klórozás hatására gyakran toxikus és rákkeltő anyagok keletkeznek [6-8], amelyet a nyers víz bonyolult összetétele miatt szinte lehetetlen megakadályozni.



Mind a felszíni, mind a parti szűrésű víz jellegzetes komponensei a természetes szerves anyagok (NOM), amelyek kolloidális méretük révén a zavarosságot növelik, színük pedig esztétikai szempontból jelent gondot. Bár kifejezetten jó hatással vannak az egészségre, a víz fertőtlenítéskor – különösen az aromás gyűrűkön – klórozódhatnak. Ez volt az oka annak, hogy az ugyancsak aromás gyűrűket tartalmazó diclofenac klór hatására bekövetkező átalakulását humuszanyagok (HS) jelenlétében és homoktalajból készített kivonatban is kövessük, majd a szerves klórtartalom (TOX) meghatározásával következtessünk a klórozott termékek keletkezésének mértékére.

### **Kísérleti rész**

#### **Anyagok**

Modell gyógyszerhatóanyagként a SIGMA ALDRICH Co. által forgalmazott diclofenac nátrium só szolgált.

A vízben oldott természetes szerves anyag nátrium-humát (Roth+Co, Karlsruhe), fulvosav (Organit Kft.) illetve légszáraz dabronyi (Magyarország) homoktalaj volt. Ez utóbbit a talaj legfelső 30 cm-es rétegéből vettük, majd egy órán át golyósmalomban történő őrlést követően 0,5 mm-es részecskeméret alá szitáltuk. A homoktalaj jellegzetes tulajdonságai: fajlagos felülete  $3,85 \text{ m}^2 \text{ g}^{-1}$ ; pH: 5,88, TOC: 16 mg C/ g talaj; fő ásványi alkotók: 55,3 % kvarc, 18,2 % szmektit, 9,9 % albit, 4,8 % csillám, 3,8% mikrolin, 3,6% klorit.

Az oldatok készítéséhez az analitikai tisztaságú  $\text{NaH}_2\text{PO}_4$ ,  $\text{Na}_2\text{HPO}_4$ ,  $\text{Na}_2\text{S}_2\text{O}_3$ ,  $\text{Ca}(\text{NO}_3)_2$  sók szolgáltak, amelyeket a Reanal Hungary Kft.-től vásároltuk.

A klórozási kísérletekhez háztartási boltból származó márkajelzés nélküli tömény hypot használtunk. Ennek aktív klórtartalmát jodometriás titrálással határoztuk meg:  $34,1 \text{ g Cl}_2/\text{l}$ .

A folyadékkromatográfiás mérések során az eluenshez használt HPLC minőségű acetonitril a Spectrum-3D terméke volt.

#### **Diclofenac klórozása**

A vizsgált oldatokat illetve kolloid oldatokat (továbbiakban: oldat)  $0,01 \text{ mol/l}$  pH=7 foszfát-pufferrel készítettük az alábbiak szerint:

- 25 ( $0,0786 \text{ mmol/l}$ ) illetve  $250 \text{ mg/l}$  ( $0,786 \text{ mmol/l}$ ) diclofenac pufferben
- 25 illetve  $250 \text{ mg/l}$  diclofenac  $0,1 \text{ g/L}$  fulvosav pufferelt oldatában
- 25 illetve  $250 \text{ mg/l}$  diclofenac  $0,1 \text{ g/L}$  nátrium-humát pufferelt oldatában
- 25 illetve  $250 \text{ mg/l}$  diclofenac homoktalaj kivonatban ( $5 \text{ g}$  homoktalajt  $50 \text{ ml}$  pufferoldattal rázattunk 30 percen keresztül, majd szobahőmérsékleten egy napig állni hagytuk. Ezután a mintákat redős szűrőpapíron szűrtük.)

A fenti minták  $30 \text{ ml}$ -éhez  $0,065 \text{ ml}$  hypot adtunk ( $73,7 \text{ mg/l Cl}_2 = 1,04 \text{ mmol/l}$  aktív klórtartalom), majd 2 órán keresztül rázattuk, végül a folyamatot egy csepp  $0,1 \text{ mol/l Na}_2\text{S}_2\text{O}_3$  hozzáadásával leállítottuk. Az összehasonlíthatóság érdekében elvégeztük a diclofenac-mentes, csak NOM-tartalmú oldatok klórozását is. A vakmintákhoz nem adtunk hypot. Mindig három párhuzamos mintával dolgoztunk.

#### **Diclofenac fogyasztásának követése**

Elemzésre UV detektorral felszerelt MERCK LaChrom HPLC készüléket használtunk. Az eluens acetonitril és pH=6,5-re beállított  $0,01 \text{ mol/l}$  foszfát-puffer elegye volt 35:65 arányban, a kolonna hőmérséklete  $23^\circ\text{C}$  volt. Az elválasztást  $5 \mu\text{m}$ -es kolonnatöltetű  $250 \times 4,6 \text{ mm}$ -es LiChrospher 100 RP-18 oszlopon (Merck) végeztük, a detektálás  $278 \text{ nm}$ -es hullámhosszon történt. Az injektált térfogat  $10 \mu\text{l}$ /minta volt. A kalibrációt  $0$ - $50$ , illetve  $0$ - $250 \text{ mg/l}$  diclofenac oldat segítségével készítettük.

#### **Összes szerves klórtartalom meghatározása**

Ezt a vizsgálatot a  $250 \text{ mg/l}$  kiindulási koncentrációjú diclofenac mintákkal végzett reakció leállítást követően hajtottuk végre. A szilárd TOX mérés előtt a keletkezett szervesetlen kloridot el kellett távolítani. Az oldatokhoz  $3 \text{ ml}$   $10 \text{ g/l}$  koncentrációjú  $\text{Ca}(\text{NO}_3)_2$  oldatot

adtunk, majd 30 perc rázatás következett, így a szerves anyagokat kicsaptuk, majd bepároltuk. A szilárd maradékot desztillált vízzel mosva azt kloridmentessé tettük (ellenőrzés  $\text{AgNO}_3$ -al), majd újabb bepárlás következett, amikor a maradékot tömegállandóságig szárítottuk.

Az összes szerves halogéntartalmat (TOX) égetéses elven működő Mitsubishi Chemical Model TOX-100 készülékkel határoztuk meg. A kalibrációs görbét pontosan ismert klórtartalmú diclofenac oldatokkal készítettük (0-111,43 mg Cl/l).

### Eredmények, értékelés

A 25 mg/L-es kiindulási koncentrációjú diclofenac-tartalmú oldatok esetében a hypo hatására lejátszódó reakció első rendű kinetikát követ (1. egyenlet, 2.a. ábra).

$$c(t) = c \cdot e^{-k \cdot t}, \quad (1)$$

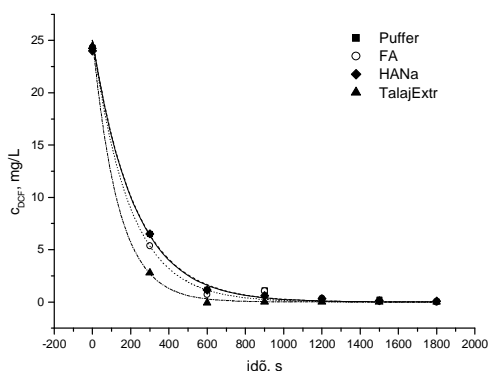
ahol  $c$  az aktuális koncentráció  $t$  időpontban és  $k$  a reakciósebességi állandó.

Jól látható, hogy maximum 30 perc alatt mindegyik modell rendszerben elfogyott a gyógyszerhatóanyag. Az átalakulás a homoktalaj kivonatában volt a leggyorsabb, amiből arra következtethetünk, hogy az extraktumban jelenlévő koloidális méretű agyagásványok katalizálják a folyamatot.

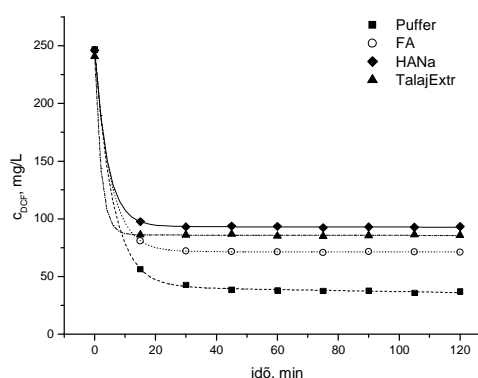
A tízszeres töménységben alkalmazott diclofenac (250 m/L) esetében a folyamat egy idő után jól láthatóan lelassul (2.b. ábra). Ekkor a mérési eredményekre olyan függvényt tudunk illeszteni, ami két – párhuzamosan zajló – elsőrendű reakció összegeként írható le (2. egyenlet).

$$c(t) = c_1 \cdot e^{-k_1 \cdot t} + c_2 \cdot e^{-k_2 \cdot t}, \quad (2)$$

ahol  $c$  az aktuális koncentráció  $t$  időpontban,  $c_1$  és  $c_2$  a két párhuzamos reakció kiindulási koncentrációja (amikor  $t = 0$ ,  $c = c_1 + c_2$ ),  $k_1$  és  $k_2$  a reakciósebességi állandók. Itt is a talajkivonatban indul be leggyorsabban a folyamat, amely egy idő után lelassul.



2.a.



2.b.

**2. ábra:** Diclofenac (DCF) fogyása klórozás hatására puffer oldatban és szerves anyag jelenlétében, pH=7 értéken. 2.a. Kiindulási DCF koncentráció  $c=25$  mg/l.

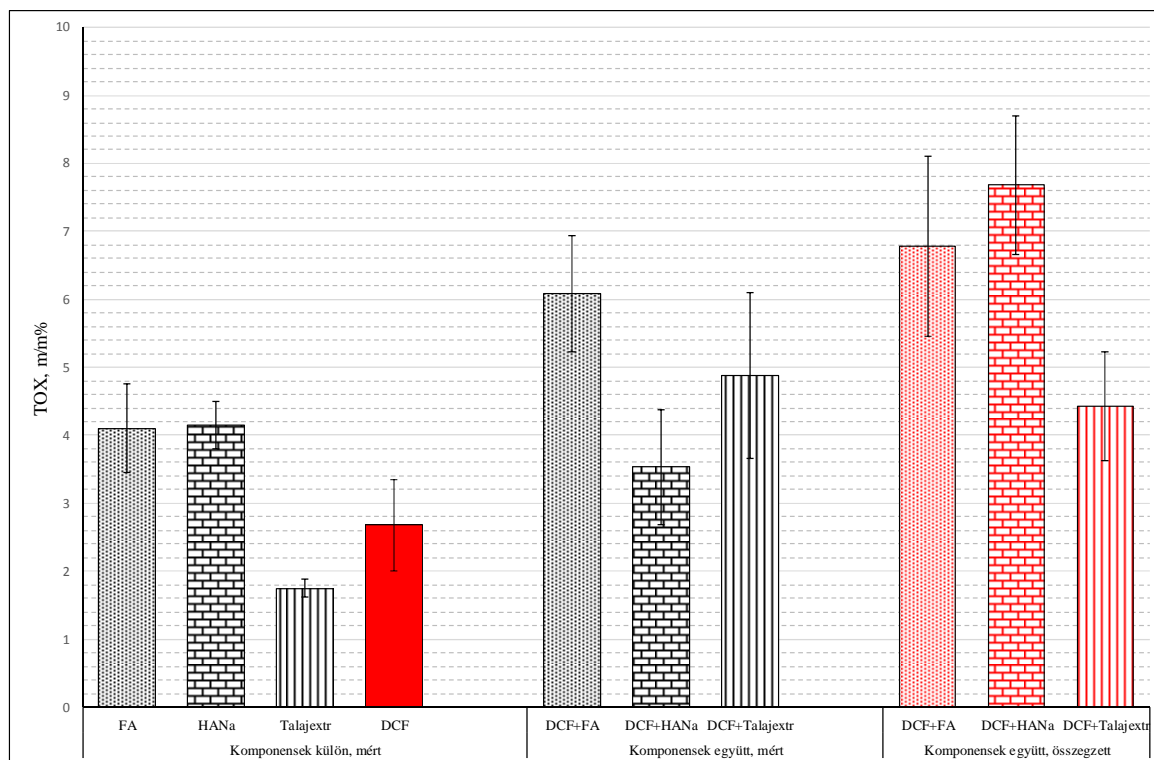
2.b. Kiindulási DCF koncentráció  $c=250$  mg/l

Két óra elteltével a maradék DCF mennyisége a következő sorrendben csökken: HANa > Talajextr > FA > Puffer. Ebből arra következtethetünk, hogy a NOM jelenlétében a



bruttó folyamat lelassul, aminek oka, hogy nemcsak a diclofenac, hanem a szerves anyagok is klórozódnak, ezáltal fogyasztják a hypo aktív klórtartalmát. A másik reakció az oxidáció, amely sokkal lassabban zajlik, ezért oxidált bomlástermékek keletkezésével kevésbé számolhatunk.

Az összes szerves klór meghatározásának alapján mind a humuszanyagok, mind pedig a diclofenac klórozódik hypo hatására önmagában is (3. ábra).



**3. ábra:** Természetes szerves anyagok és diclofenac klórozódása külön-külön és együtt

Amikor a DCF klórozása humuszanyagok jelenlétében zajlik, akkor megfigyelhető, hogy a nátrium-humát esetében a klórtartalom csökken a diclofenac-mentes mintához képest, míg a fulvosav és a homoktalaj-kivonat esetében nő. Hogyha a NOM-tartalmú minták és a DCF klórozásából származó átlag TOX értékeket összeadjuk és összehasonlítjuk ezekkel az eredményekkel, látható, hogy egyedül a homoktalaj kivonattal készített DCF oldat esetében kapunk az elméletinél nagyobb értéket. Ez ismételten arra utal, hogy a kivonatban jelenlévő kolloidális méretű agyagásványok katalizálják a diclofenac klórozását, de közben maguk a humuszanyagok is klórozódnak, ezért az aktív klór elfogy. A nátrium-humát és diclofenac együttes jelenlétben keletkező viszonylag kevés klórozott termék megjelenése és a leglassabb bomlási reakció alapján arra következtethetünk, hogy az oxidáció folyamata valamelyest kedvezményezettebb a többi közeghez képest. Mivel a huminsavról ismert, hogy fotoszenzibilizáló hatással rendelkezik [9-10], feltehető, hogy ezesetben is érvényesül ez a tulajdonsága.

### Következtetések

A diclofenac tartalmú víz fertőtlenítése során klórozás és oxidáció is lejátszódik, de a klórozott termékek keletkezése nagyobb mennyiségben várható, mint az oxidált bomlástermékeké.

Aktív klórtartalmú szennyvíz kibocsátásakor a lebomlatlan gyógyszerhatóanyag klórtartalma növekszik.

A fertőtlenítőszer kis feleslege esetében a humuszanyagok érzékelhetően lassítják a diclofenac fogyását (a bruttó folyamatot), mivel maguk is klórozódnak.

A legkevesebb klórozott termék a nátrium-humát tartalmú modell rendszerben keletkezett, ahol az oxidáció folyamata valamelyest kedvezményezettebb a többi közeghez képest. Mindez feltételezi a humuszanyag fotoszenzibilizáló hatását.

A homoktalaj kivonatban jelenlévő agyagásványok katalitikus hatással rendelkeznek a diclofenac klórozási reakciójában, amelyet mind a fogyási görbe, mind pedig a TOX értékek igazolnak. A keletkezett klórozott termékek nagyobb mennyisége miatt ez nem tekinthető pozitív hatásnak.

Nemcsak esztétikai, hanem humánegészségügyi szempontból is fontos minden kolloidális méretű alkotó eltávolítása az ivóvízből.

### **Köszönetnyilvánítás**

Az anyag „A Pannon Egyetem tudományos műhelyeinek támogatása” című, TÁMOP-4.2.2/B-15/1-2015-0004 azonosító számú projekt keretei között készült el.

### **Irodalomjegyzék**

- [1] T. Heberer, Toxicol. Lett. 131 (2002) 5.
- [2] A. Helenkár, Á. Sebők, Gy. Záray, I. Molnár-Perl, A. Vasanits-Zsigrai, Talanta. 82 (2010) 600.
- [3] M. Varga, J. Dobor, A. Helenkár, L. Jurecska, J. Yao, Gy. Záray, Microchem. J. 95 (2010) 353.
- [4] G. Öllös, Vízisztítás - üzemeltetés, Egri Nyomda Kft., Eger, 1998.
- [5] E. Arany, J. Láng, D. Somogyvári, O. Láng, T. Alapi, I. Ilisz, K. Gajda-Schranz, A. Dombi, L. Kőhidai, K. Hernádi, Sci. Total Environ. 468-469 (2014) 996.
- [6] H. Kim, M. Yu, J. Hazard. Mater. 143 (2007) 486.
- [7] M. Cleuvers, Ecotoxicology and Environmental Safety. 59 (2004) 309.
- [8] E.S. Rigobello, A.D.B. Dantas, L.D. Bernardo, E.M. Vieira, Chemosphere. 92 (2013) 184.
- [9] A.C. Gerecke, S. Canonica, S.R., Müller, M. Schärer, R.P. Schwarzenbach, Environ. Sci. Technol. 35 (2001) 3915.
- [10] R. Földényi, B. Ravasz, Cs. Érsek, T. Ertli, Proc. of the 13<sup>th</sup> Meeting of the International Humic Substances Society, Band 45-II, Universität Karlsruhe (TH), Germany, July 30 to August 4, 2006, 849.

## Látható Fénnyel történő Vízkezelés Rutil Fázisú Titán-dioxid Fotokatalizátorokkal

Tamás Gyulavári<sup>1,3\*</sup>, Gábor Veréb<sup>2,3</sup>, Zsolt Pap<sup>3</sup>, Klára Hernádi<sup>1,3</sup>, András Dombi<sup>3</sup>

<sup>1</sup>Szegedi Tudományegyetem, Természettudományi és Informatikai Kar, Alkalmazott és Környezeti Kémiai Tanszék, 6720 Szeged, Rerrich tér 1.

<sup>2</sup>Szegedi Tudományegyetem, Mérnöki Kar, Folyamatmérnöki Intézet, 6725 Szeged, Moszkvai krt. 9.

<sup>3</sup>Szegedi Tudományegyetem, Természettudományi és Informatikai Kar, Környezetkémiai Kutatócsoport, Tisza Lajos krt. 103.

\*e-mail: gyulavarit@chem.u-szeged.hu

### 1. Abstract

Based on our previous results (discussed below) [1,2] in the present study self-prepared rutile-phased titanium dioxides were synthesized by sol-gel method with the addition of hydrogen peroxide. The characteristic properties (XRD, DRS, IR, specific surface area) and the resulted photocatalytic efficiencies were also investigated. Commercial Aldrich rutile, and Aeroxide P25 were used as reference titanium dioxides. The photocatalytic efficiencies were determined via the decomposition of phenol, and the inactivation of *E. coli* bacteria under visible light irradiation. The IR spectra indicated, that highly efficient Aldrich rutile has Ti-O-O-Ti groups on its surface (at 667 cm<sup>-1</sup> on the IR spectra). Unfortunately the addition of hydrogen-peroxide during the synthesis did not result the appearance of Ti-O-O-Ti groups in measurable amount. However hydrogen peroxide addition resulted increased photocatalytic efficiency in case of a special ratio of the reactants (Ti(OC<sub>4</sub>H<sub>9</sub>)<sub>4</sub>:H<sub>2</sub>O<sub>2</sub>:HCl:H<sub>2</sub>O=1:2:3:50). The DR spectra showed that the resulted photocatalytic efficiencies were mostly related to the band-gap values.

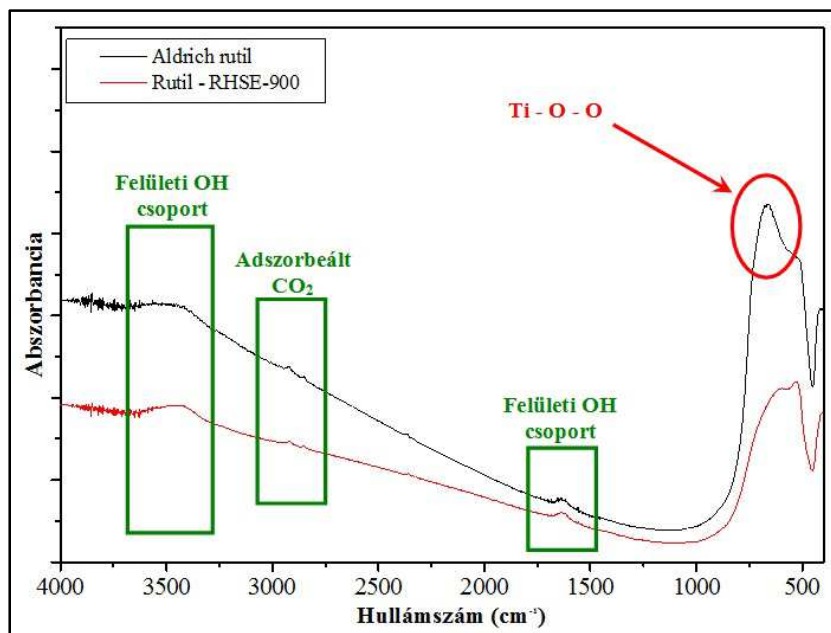
### 2. Bevezetés

Napjaink ígéretes alternatív vízkezelési módszerei a nagyhatékonyságú oxidációs eljárások, melynek egyik típusa a heterogén fotokatalízis. A kezelés során fénnel gerjesztett félvezető fotokatalizátorokat alkalmaznak, melyek felületén összetett gyökös folyamatok során a szennyező anyagok széles köre oxidálható. Fotokatalizátorként szinte kizárólag titán-dioxidot alkalmaznak számos kedvező tulajdonsága miatt. A titán-dioxidnak két gyakorlati jelentőségű kristályfázisa van: az anatáz és a rutil - ez utóbbi látható fénnel is gerjeszthető tiltott sávjának szélessége (3,02 eV –  $\lambda < 410$  nm) miatt.

### 3. Előzmények

Egy korábbi publikációban [1] számos saját készítésű (esetenként adalékolt) és kereskedelmi forgalomban kapható TiO<sub>2</sub> közül a nem adalékolt Aldrich rutil kiemelkedő fotokatalitikus aktivitással bírt rendkívül kicsi fajlagos felülete (3 m<sup>2</sup>/g) ellenére. Egy másik már megjelent közleményben [2] a Tang és társai által leírt előállítási módszert [3] módosítva előállítottunk kis részecskeméretű tisztán rutil fázisú titán-dioxidot (5 nm), majd a részecskeméretet különböző hőmérsékleten történő kalcinálással jelentősen növeltük (~5-300 nm). Az anyagszerkezeti vizsgálatok (XRD, DRS, TEM, BET) alapján megállapítottuk, hogy az Aldrich rutil és a saját készítésű 900 °C-on hőkezelt TiO<sub>2</sub>-RHSE-900 nagyon hasonló anyagszerkezeti tulajdonságokkal bír: hasonló részecskeméret, alak, és részecskeméret eloszlás, azonos fényelnyelés és megegyező fajlagos felület. A fotokatalitikus aktivitásukban azonban drasztikus különbség van. Infravörös spektroszkópiával (1. ábra) megállapítottuk, hogy az Aldrich rutil felülete a 667 cm<sup>-1</sup>-nél megjelenő elnyelési sáv alapján [4] Ti-O-O-Ti

csoportokat tartalmaz, ami egy elektrofil, oxigén-gazdag felületet jelent. Gerjesztés hatására a fotokatalizátornak ez a „peroxidált” felülete azt eredményezheti, hogy az adszorbeálódott oxigén könnyebben befoghat egy elektront elindítva ezzel a gyökös folyamatokat.



1. ábra

Ezen eredményekre alapozva jelen tanulmányban célul tűztük ki, hogy a preparálási módszer módosításával (hidrogén-peroxid hozzáadásával) előállítunk olyan titán-dioxidokat, melyek rendelkeznek az előbbieken említett Ti-O-O-Ti csoportokkal.

#### 4. Alkalmazott anyagok és módszerek

A szintézis során vízhez számított mennyiségű sósavat, hidrogén-peroxidot és titán-tetrabutoxidot adagoltunk a következő anyagmennyiség-arányban:  $\text{Ti}(\text{OC}_4\text{H}_9)_4:\text{H}_2\text{O}_2:\text{HCl}:\text{H}_2\text{O} = 1:1-4:3:50$  (a minták elnevezése a továbbiakban: „Rutil-H1-4” – A „H” a szintézis során alkalmazott hidrogén-peroxidra utal, míg a számok a  $\text{H}_2\text{O}_2:\text{Ti}$  mólarányt jelölik). Az előállított szuszpenziók 168 óra 40 °C-on és 48 óra 55 °C-on történő kristályosítása után azokat Milli-Q vízzel mostuk, szárítottuk, majd achát mozsárban porítottuk.

A fotokatalitikus aktivitást fenol ( $c=10^{-4}$  M) bontásával, illetve *E. coli* K12 baktérium inaktiválásával jellemeztük. A látható fényt sugárzó lámpákkal felszerelt fotoreaktorból vett minták fenol koncentrációját egy Agilent 1100 series típusú HPLC berendezéssel határoztuk meg. A fotokatalitikus fertőtlenítés hatékonyságának jellemzéséhez az említett publikációkban [1,2] részletezett módon előkészített *E. coli* baktérium szuszpenziót öntöttük a fotoreaktorba, majd a megfelelő időközönként vett mintákban lévő élő sejtek számát az agar-agar táptalajon növekvő baktériumtelepek számolásával jellemeztük.

A részecskeméretet és kristályos összetételt egy Rigaku Miniflex II típusú röntgen diffraktométerrel határoztuk meg. A diffúz reflexiós spektrumokat egy ILV-724 jelű diffúz reflexiós modullal ellátott Jasco-V650 diódasoros spektrofotométerrel vettük fel. A fajlagos felületet egy Micromeritics gázadszorpciós műszerrel (Gemini Type 2375) mértük, míg az infravörös spektrumokat egy „FRA 106 Raman” modullal kiegészített „Bruker Equinox 55” típusú spektrométerrel vettük fel.

## 5. Kísérleti eredmények és kiértékelésük

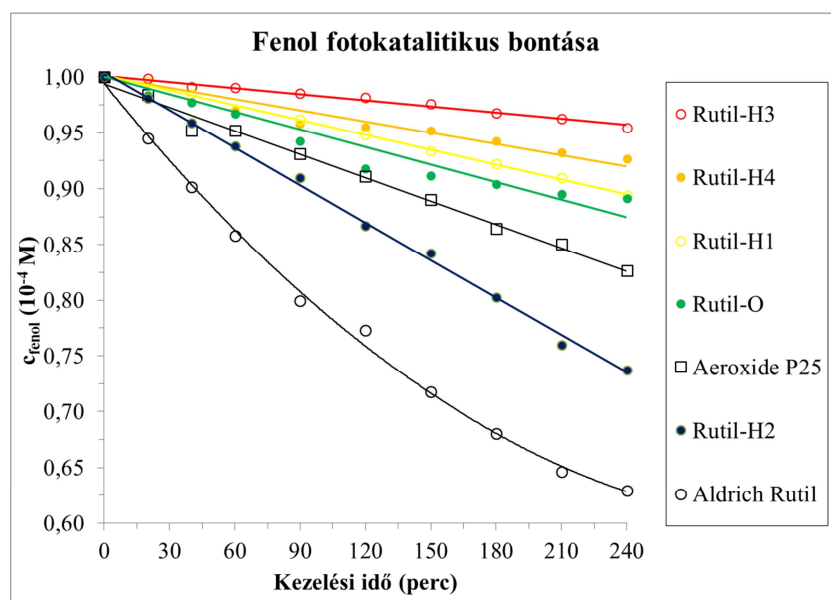
A röntgen diffraktométerrel (XRD) végzett vizsgálatok eredményei, illetve a fajlagos felület értékek az **1. táblázatban** láthatóak.

	Fázisösszetétel - XRD eredmények				Fajlagos felület m <sup>2</sup> /g
	Anatáz		Rutil		
	Tartalom (m/m%)	Részecske méret (nm)	Tartalom (m/m%)	Részecske méret (nm)	
Rutil-0	-	-	100	5,2	197
Rutil-H1	<1	-	>99	7,3	108
Rutil-H2	8	10,7	92	7	117
Rutil-H3	<1	-	>99	6,8	132
Rutil-H4	<1	-	>99	6,9	129
Aldrich rutil	4	315 <sup>TEM</sup>	96	315 <sup>TEM</sup>	3

1. táblázat

Az előállított fotokatalizátorok ~40%-ban tartalmazznak kristályos fázist, melynek a nagy része rutil, egyedül a „Rutil-H2”-es titán-dioxid tartalmaz mérhető mennyiségű anatáz fázist (8%) is. Kijelenthető továbbá, hogy a részecskeméretre és a fajlagos felületre nincs jelentős hatással az alkalmazott  $\text{Ti}:\text{H}_2\text{O}_2$  arány.

A fenol fotokatalitikus oxidációját bemutató **2. ábrán** jól látható, hogy a Rutil-H2-es titán-dioxid fotokatalitikus aktivitása jelentősen meghaladja nem csak a sorozat többi tagjának aktivitását, de az általános referenciaként elfogadott Aeroxide P25 aktivitását is.

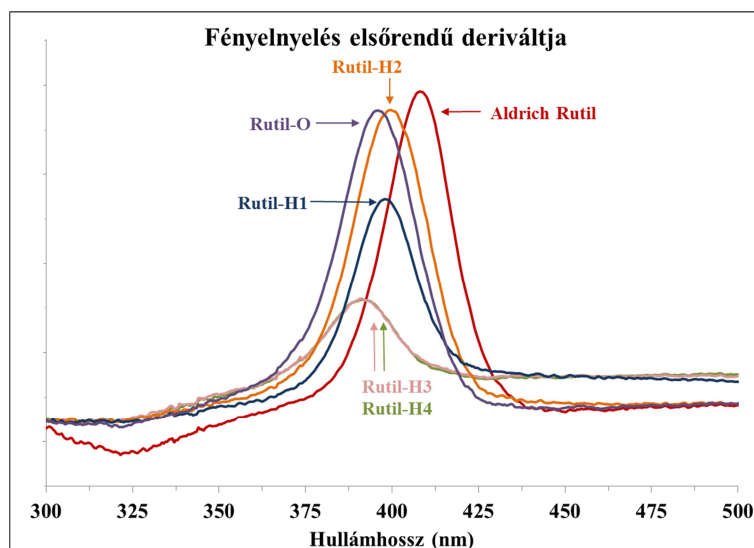


2. ábra

A saját készítésű titán-dioxidok közül egyedül a „Rutil-H2” estén tapasztaltunk fertőtlenítő hatást: 120 perc megvilágítás után az élő baktériumsejtek száma ~75%-al

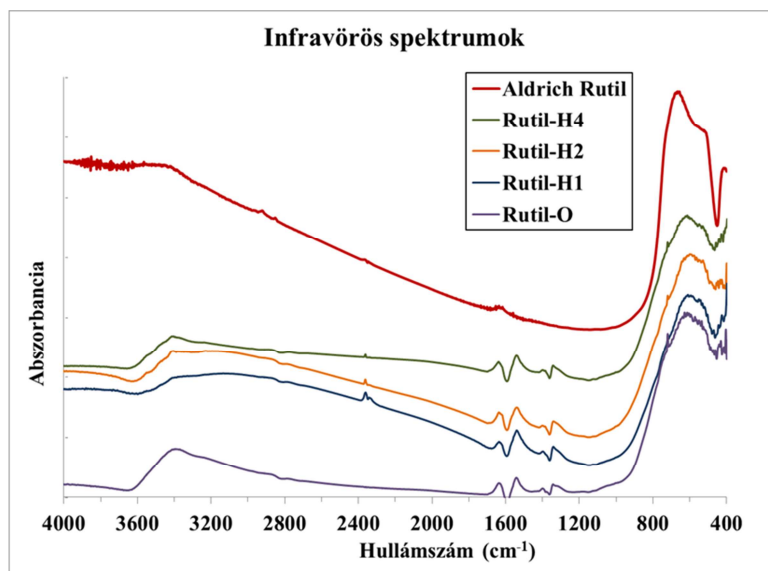
csökkent. Megjegyzendő hogy ez a fertőtlenítő hatás jelentősen elmarad a referencia fotokatalizátorok hatékonyságától [1].

Flak és társai [5] munkája alapján a fotokatalizátorok hullámhossz szerinti reflexiójának elsőrendű deriváltját ábrázolva (**3. ábra**) vizsgálható az egyes fotokatalizátorok gerjeszthetőségének hullámhossz-szerinti függése. Az ábrán levő csúcsok leszálló ágát megfigyelve kijelenthető, hogy valóban a fotokatalitikus aktivitás növekvő sorrendjében következnek (balról jobbra) az egyes fotokatalizátorok. Az eredmények alapján a mért fotokatalitikus aktivitások sorrendje a gerjeszthetőség hullámhossz szerinti függését követi.



3. ábra

Az infravörös spektrumok (**4. ábra**) alapján nem jelenthető ki (ugyanakkor nem is cáfolható) a saját készítésű titán-dioxidokban a Ti-O-O-Ti csoportok jelenléte. Megállapítható azonban hogy nincs jelentős különbség az előállított minták  $667\text{ cm}^{-1}$  hullámszámnál mérhető fényelnyelése között. Vagyis ha sikerült is Ti-O-O-Ti csoportok kialakulását elősegíteni a szintézis során alkalmazott hidrogén-peroxiddal, mennyisége nem emelkedett számottevően a hidrogén-peroxid mennyiségének növelésével.



4. ábra



## 6. Összefoglalás

A leírt módszerrel egyik saját készítésű fotokatalizátor esetén sem sikerült kimutatható mennyiségű Ti-O-O-Ti csoportot beépíteni a felületbe, ugyanakkor megállapítható, hogy az előállítás során adagolt hidrogén-peroxid mennyisége jelentős hatással van a fotokatalizátor hatékonyságára. Csak az alkalmazott anyagok egy speciális arányánál ( $\text{Ti}(\text{OC}_4\text{H}_9)_4:\text{H}_2\text{O}_2:\text{HCl}:\text{H}_2\text{O}=1:2:3:50$ ) figyelhető meg jelentős fotokatalitikus aktivitásnövekedés. A titán-dioxidok hullámhossz szerinti reflexiójának elsőrendű deriváltja szoros összefüggést mutat a fotokatalitikus aktivitással, de a gerjesztési küszöb nem trendszerűen változik az alkalmazott hidrogén-peroxid mennyiségének növelésével. Megemlítendő továbbá, hogy kizárólag az említett arány eredményezte anatóz fázis megjelenését is, aminek érdekessége, hogy a vizsgált titán-dioxidok közül a 3 legaktívabb mindegyike tartalmaz anatóz, és rutil kristályfázist is. Az eredmény összefüggésbe hozható a két kristályfázis néhány publikációban már említett szinergikus hatásával [6-8].

## Köszönetnyilvánítás

A kutatást a Svájci Alap SH7/2/20 projekt támogatta. Gyulavári Tamás köszönetet mond a TÁMOP 4.2.4.A/2-11-1-2012-0001 azonosító számú projektnek. Hálásan köszönjük Dr. Manczinger László, és Lele Mária (SZTE - TTIK - Mikrobiológiai Tanszék) fertőtlenítési vizsgálatokhoz nyújtott segítségét.

## Irodalomjegyzék

- [1] G. Veréb, L. Manczinger, G. Bozsó, A. Sienkiewicz, L. Forró, K. Mogyorósi, K. Hernádi, A. Dombi, Appl. Catal. B-Environ., 129 (2013) 566-574
- [2] G. Veréb, T. Gyulavári, Zs. Pap, L. Baia, K. Mogyorósi, A. Dombi, K. Hernádi, RSC Adv. 5 (2015) 66636-66643
- [3] Z. Tang, J. Zhang, Z. Cheng, Z. Zhang, Mater. Chem. Phys. 77 (2002) 314-317
- [4] V. Etacheri, M. K. Seery, S. J. Hinder, S. C. Pillai, Adv. Funct. Mater. 21(2011) 3744-3752
- [5] D. Flak, A. Braun, B. S. Mun, J. B. Park, M. P. Wojtan, T. Graule, M. Rekas, Phys. Chem. Chem. Phys. 15 (2013) 1417-1430
- [6] N. Balázs, K. Mogyorósi, D. F. Srankó, A. Pallagi, T. Alapi, A. Oszkó, A. Dombi, P. Sipos, Appl. Catal. B-Environ., 84 (2008) 256-362
- [7] K. E. Rajashekhar, L. G. Devi, J. Mol. Catal. A-Chem., 374-375 (2013) 12-21
- [8] D. O. Scanlon, C. W. Dunnill, J. Buckeridge, S. A. Shevlin, A. J. Logsdail, S. M. Woodley, C. R. A. Catlow, M. J. Powell, R. G. Palgrave, I. P. Parkin, G. W. Watson, T. W. Keal, P. Sherwood, A. Walsh, A. A. Sokol, Nat. Mater., 12 (2013) 798-801



## **TiO<sub>2</sub> Nanorészecskékkel Bevonat Membránok Jellemzőinek és Fotokatalitikus Aktivitásának Vizsgálata**

**Kovács Ildikó , Kertész Szabolcs, Beszédes Sándor, Veréb Gábor, Hodúr Cecilia, László Zsuzsanna**

*Szegedi Tudományegyetem, Mérnöki Kar, Folyamatmérnöki Moszkvai krt.9, H-6725 Szeged, Hungary*

*e-mail: zsizsu@mk.u-szeged.hu*

### **Abstract**

Polyethersulfone (PES) membranes are used in a wide range for water and wastewater treatment due to their physical and chemical properties, but despite their improved properties membrane fouling remains a problem. In order to overcome this problem a great deal of interest has been focused on modifying membranes with TiO<sub>2</sub> as a photocatalyst to reduce fouling and to make the organic component removal more efficient.

In this study polyethersulfone membranes with different pore sizes (0.05 and 0.2 µm) were coated with commercial TiO<sub>2</sub> (Aeroxide P25) and synthesized TiO<sub>2</sub> nanoparticles (NP) by filtering the TiO<sub>2</sub> suspension through the membrane. In order to test the photocatalytic activity Acid Red 1 dye solutions were filtered with commercial PES membranes with and without TiO<sub>2</sub> coating. Coated membranes had significantly lower fluxes compared to the neat membranes. Contact angle measurements showed that TiO<sub>2</sub> P25 formed a very hydrophilic coat on the membranes on the contrary TiO<sub>2</sub> NP increased the hydrophobicity of the surface. UV irradiation had an effect on both the neat and coated membranes flux values. Relative dye fluxes were calculated against the equivalent water fluxes and were compared. UV irradiation increased the dye elimination efficiency of the coated membranes, which proves the TiO<sub>2</sub> coatings photocatalytic activity.

### **Bevezetés**

A poliéter-szulfon membránokat széles körben alkalmazzák a vízkezelésben és szennyvíztisztításban jó fizikai és kémiai tulajdonságaiknak köszönhetően. Számos előnyük, mint például a nagy hő tűrő-, kémiai ellenálló képességük, pH tűrésük, valamint különböző pórusméretük ellenére a membráneltömődés nagy gondot jelent a felhasználásukban [1], ezért többek között a membrán anyagába adalékanyagok keverésével történtek próbálkozások a membránok élettartamának növelésére [2]. A membránkészítés során többek között nanorészecskéket is felhasználnak annak érdekében, hogy csökkentsék a membráneltömődést és jobb tulajdonságú membránokat hozzanak létre [3]. Az elmúlt időszakban nagy figyelem irányult a membránok TiO<sub>2</sub>-dal, mint fotokatalizátorral való módosítására, többek között a membrán eltömődés csökkentésére és a szerves anyag eltávolítási hatékonyság növelésére. A TiO<sub>2</sub>-ot előnyben részesítik más félvezetőkkel szemben, jó fizikai és kémiai tulajdonságai, fotokatalitikus aktivitása, hidrofil tulajdonsága és potenciális eltömődés csökkentő hatása miatt [3,4].

A nagyhatékonyságú oxidációs eljárások (AOPs) széles körben kutatottak és alkalmazzák őket a víz, levegő és szennyvízkezelésben egyaránt. Segítségükkel lebonthatók a hagyományos eljárásoknak ellenálló szerves anyagok is [5].

Nanokompozit TiO<sub>2</sub> PES membránok előállítása során a membrán felületét nanorészecskékkel vonják be vagy a nanorészecskéket a membrán anyagába keverik [3, 4]. A javasolt membrán-előállítási módszerek többségében fázis inverziót alkalmaznak megfelelő

menyiségű  $\text{TiO}_2$  hozzáadásával. Alternatív módszer a membránok  $\text{TiO}_2$  szuszpenzióba „mártása” [3]. Rahimpour és társai szerint előnyösebb a membrán felületére felvinni a részecskéket, mint a membrán anyagába keverni azokat. Az első módszer nagyobb permeátum fluxust és kisebb membránellenállást tesz lehetővé [2].

Az Acid Red 1 (AR1, Azophloxine) festéket használtuk modell szennyezőként, hogy meghatározzuk a  $\text{TiO}_2$ -al borított membrán fotokatalitikus aktivitását. Az AR1 festék a textil iparban gyakran alkalmazott festék [6].

A munka során a  $\text{TiO}_2$  P25-el és szintetizált  $\text{TiO}_2$ -al bevont membránok tulajdonságait és a festék eltávolítási hatékonyságot vizsgáltuk a heterogén fotokatalízissel kombinált membránszűrés során, illetve elvégeztük a kísérleteket UV fény alkalmazása nélkül is. A membránfelület nedvesíthetőségét, illetve annak változását peremszög mérések segítségével követtük.

## Kísérleti rész

### Anyagok

Aeroxide P25 titanium dioxide (80% anatáz, 20% rutil) (EVONIK Industries, Németország). A membránszűrés során felhasznált Acid Red 1 (Synthesia, Spanyolország) desztillált vizes oldatának koncentrációja 15 mg/l volt.

### Membrán módosítás

A 0,2  $\mu\text{m}$  és 0,05  $\mu\text{m}$  pórus méretű poliéter-szulfon membránokat (PES-MF és MP005 (NEW LOGIC Research INC, USA)  $\text{TiO}_2$  P25 és szintetizált  $\text{TiO}_2$  nanorészecskékkel (NP) vontunk be. A membránokon 50 ml, 0,4 g/l  $\text{TiO}_2$  szuszpenziót szűrtünk át egy statikus cellában. A 0,1 MPa transzmembrán nyomást inert nitrogén gáz segítségével biztosítottuk. A membránokat használat előtt egy napig desztillált vízben előnedvesítettük.

### Membránszűrés

A membránszűrés kísérleteket egy statikus kevertető cellában (Millipore, N°96) végeztük, amelyet egy kisnyomású higanygőz UV lámpával (Ligtech, Hungary) építettünk egybe, biztosítva, hogy az UV fény megvilágítsa a fotokatalizátorral bevont membrán felületét. A membrán felülete 0.00342  $\text{m}^2$ , a szűrést szobahőmérsékleten. Előkezelésként a statikus cellában 60 percig UV fénnel világítottuk meg a membránokat.

### Analitikai módszerek

A festék koncentrációját spektrofotometriás módszerrel határoztuk meg (Nanocolor® UV/Vis, Macherey-Nagel GmbH, Germany) a festék direkt fényelnyelése alapján  $\lambda=532$  nm-en.

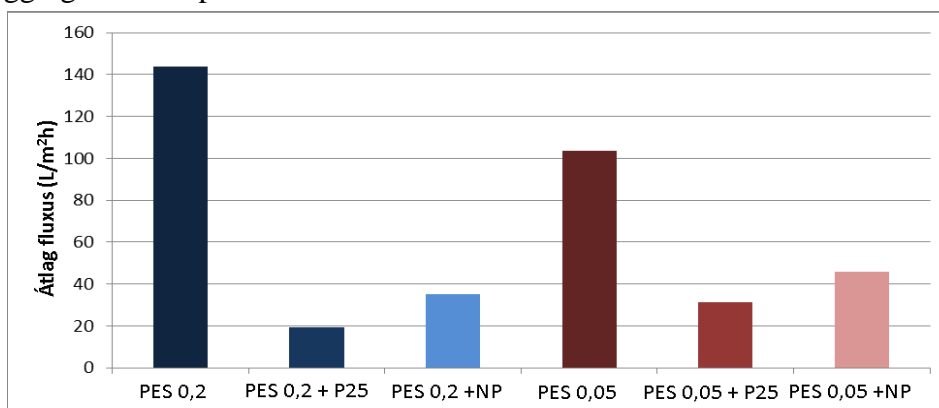
A tiszta és a bevont membránok felületének nedvesíthetőségét desztillált víz peremszög mérésével határoztuk meg (Dataphysics Contact Angle System OCA15Pro, Germany), 10  $\mu\text{l}$  víz óvatos cseppentésével a membrán felületre.

## Eredmények és értékelés

### A membrán tulajdonságainak változása $\text{TiO}_2$ P25 és $\text{TiO}_2$ NP bevonat hatására

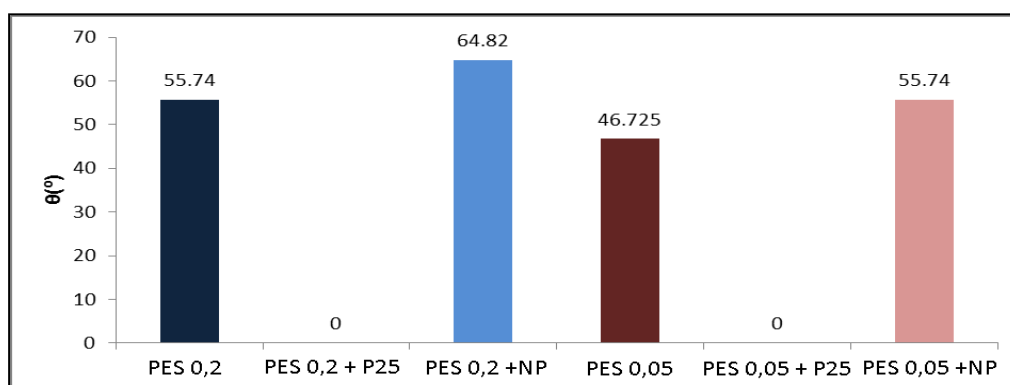
A kísérletek első sorozatában a tiszta 0,2  $\mu\text{m}$  és 0,05  $\mu\text{m}$  pórus méretű poliéter-szulfon membránok valamint a  $\text{TiO}_2$  P25 és  $\text{TiO}_2$  NP-vel borított membránok fluxus értékeit határoztuk meg. A bevont membránok fluxus értékei jelentősen alacsonyabbak voltak a tiszta membránok fluxus értékeihez képest (1. ábra), mivel a membrán felületén a fotokatalizátor réteget képez. A kereskedelemben kapható  $\text{TiO}_2$  P25 elsődleges részecskemérete ~25 nm,

szuszpenzió formában azonban közel egy mikrométeres agglomerátumok alakulnak ki [7]. Hasonló aggregálódást tapasztaltunk a szintetizált  $\text{TiO}_2$  NP esetén is.



1. ábra. A különböző bevonatok hatása az átlagolt vízfluxus értékekre

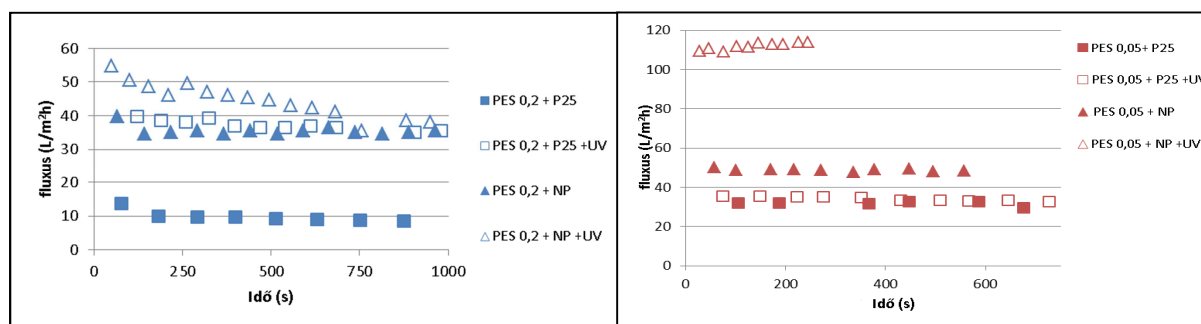
A peremszög mérések alapján elmondható, hogy a  $\text{TiO}_2$  P25 egy rendkívül hidrophil réteget képezett a membrán felületén (a peremszög értéke 0), míg a  $\text{TiO}_2$  NP-vel bevont membránok peremszögértékei magasabbak voltak a tiszta membránokhoz képest, azaz a felület így kevésbé hidrophil. (2. ábra). Érdekes, hogy a felület nedvesíthetősége nem mutatott összefüggést a mért fluxus értékekkel.



2. ábra. Tiszta,  $\text{TiO}_2$  P25 és NP-vel bevont PES membrán felületek nedvesíthetőségei

### AR 1 oldat mikroszűrése

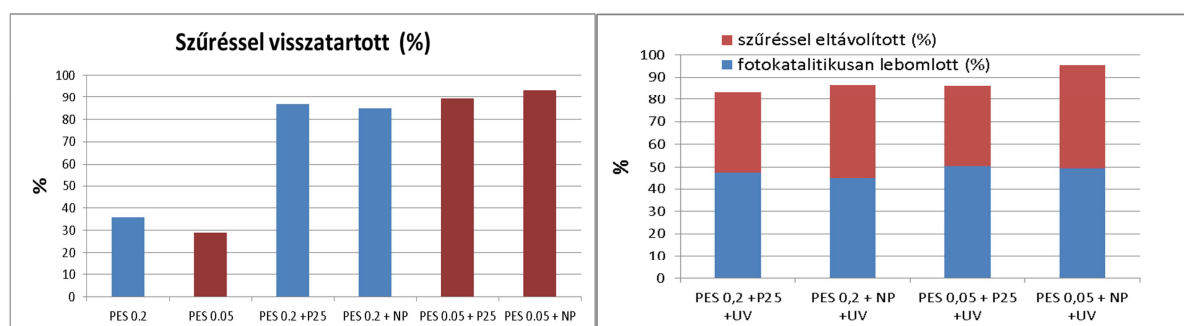
Az AR 1 festék oldatot szűrtük a két különböző fotokatalizátorral bevont két különböző membránnal, UV fény hiányában és jelenlétében is. A megvilágítás hatására a fluxus értékek minden esetben megnövekedtek. (3. ábra).



3. ábra.  $\text{TiO}_2$  P25 és NP-vel bevont PES membránok festék oldat fluxusai

### AR 1 mikroszűrése során a TiO<sub>2</sub> P25 és TiO<sub>2</sub> NP-el bevont membránok fotokatalitikus és eltávolítási hatékonyságai

A következő kísérletsorozatban a TiO<sub>2</sub> P25 és TiO<sub>2</sub> NP-vel borított membránokon AR1 festékkoldatot szűrtünk, és a membrán festék-eltávolítási és fotokatalitikus hatékonyságát vizsgáltuk (4. ábra). Annak érdekében, hogy megállapítsuk, hogy a festék mekkora hányada távolítható el szűréssel és mekkora a heterogén fotokatalízissal, a szűrést elvégeztük UV fénnel megvilágított, illetve meg nem világított membránon is. Azt tapasztaltuk, hogy a pórusmérettől és a fotokatalizátortól függetlenül a bevont membránok nagyobb eltávolítási hatékonyságot mutattak a tiszta membránokhoz képest. A bevont membránok fotokatalitikus aktivitása hasonló volt: a festék koncentrációja kb. a felére csökkent; a membrán a szűrés során további 30-45%-ot tartott vissza. Minden esetben 80%-osnál nagyobb eltávolítás volt mérhető, a legjobb, >95% eltávolítási hatékonyságot a 0,05 µm-es, NP nanorészecskékel bevont membránnal érték el.



4. ábra. Eltávolítási- és fotokatalitikus hatékonyság

### Összefoglalás

Az AR1 festék mikroszűrését végeztük TiO<sub>2</sub> P25-el és TiO<sub>2</sub> NP-el bevont 0,05 µm és 0,2 µm pórus méretű PES membránok segítségével, annak érdekében, hogy meghatározzuk, hogy a bevonattal javítottuk-e a membrán tulajdonságait. A bevont membránok fluxus értékei jelentősen kisebbek voltak a tiszta membránokéhoz képest, ugyanis a fotokatalizátor részecskék egy réteget képeztek a membrán felületén. Peremszög mérések alapján a TiO<sub>2</sub> P25 rendkívül hidrofil réteget képezett a membrán felületén, míg a TiO<sub>2</sub> NP-vel bevont membrán felülete kevésbé volt hidrofil, mint a sima membrán felülete. Eredményeink bizonyítják, hogy a fotokatalizátorral bevont membránok számottevő fotokatalitikus aktivitással rendelkeznek, ami lehetővé teszi a további hasznosíthatóságuk vizsgálatát.

### Köszönetnyilvánítás

A munka a Bolyai János Kutatási Ösztöndíj támogatásával készült. A szerzők szintén hálásak a Nemzeti Kutatási, Fejlesztési és Innovációs Hivatal által biztosított anyagi támogatásért (NKFI témaszám K112096 és K105021). A TiO<sub>2</sub> NP fotokatalizátor előállításáért köszönetet mondunk Kukovecz Ákosnak és Pap Ibolya Zitának.

### Irodalomjegyzék

- [1] J. F. Li, Z. L. Xu, H. Yang, L. Y. Yu, M. Liu, Effect of TiO<sub>2</sub> nanoparticles on the surface morphology and performance of microporous PES membrane, *Applied Surface Science*, 255 (9), 4725-4732 (2009).
- [2] R. Bergamasco, F. V. Silva, F. S. Arakawa, N. U. Yamaguchi, M. H. M. Reis, C. J. Tavares, M. T. P. S. Amorim, C. R. G. Tavares, Drinking water treatment in a gravimetric flow system with TiO<sub>2</sub>coated membranes, 174 (1), 102-109 (2011).

- [3] V. Vatanpour, S. S. Maadaeni, R. A. Khataee, E. Salehi, S. Zinadini, A. H. Monfared, TiO<sub>2</sub> embedded mixed matrix PES nanocomposite membranes: Influence of different sizes and types of nanoparticles on antifouling and performance, *Desalination*, 292, 19-29 (2012).
- [4] A. Razmjoua, J. Mansouri, V. Chen, The effects of mechanical and chemical modification of TiO<sub>2</sub> nanoparticles on the surface chemistry, structure and fouling performance of PES ultrafiltration membranes, *Journal of Membrane Science*, 378 (1-2), 73-84 (2011).
- [5] Cs. Földvary, L. Wojnarovits, The effect of high-energy radiation on aqueous solution of Acid Red 1 textile dye, *Radiation Physics and Chemistry*, 76, 1485–1488 (2007).
- [6] M. Hoffmann, S. Martin, W. Choi, D. Bahnemann, Environmental Applications of Semiconductor Photocatalysis, *Chemical Reviews*, 95, 69-96 (1995).
- [7] K. Mogyorosi, N. Balazs, D.F. Sranko, E. Tombacz, I. Dekany, A. Oszko, P. Sipos, A. Dombi, The effect of particle shape on the activity of nanocrystalline TiO<sub>2</sub> photocatalysts in phenol decomposition. Part 3: The importance of surface quality, *Applied Catalysis B: Environmental* 96 577–585 (2010).

## Confirmation and Differential Diagnosis of Congenital Adrenal Hyperplasia from Dried Blood Spots by UHPLC-MS/MS

Péter Monostori<sup>1\*</sup>, Pál Szabó<sup>2</sup>, Otilia Marginean<sup>3</sup>, Csaba Bereczki<sup>1</sup>, Eszter Karg<sup>1</sup>

<sup>1</sup>*Department of Pediatrics, University of Szeged, Szeged, Korányi fasor 14-15, H-6720, Hungary*

<sup>2</sup>*Institute of Organic Chemistry, Research Centre for Natural Sciences, Hungarian Academy of Sciences, Budapest, Magyar tudósok körútja 2, H-1117, Hungary*

<sup>3</sup>*Pediatric Endocrinology Department of "Louis Turcanu" Children Clinical Hospital, I<sup>st</sup> Pediatric Clinic of "Victor Babes" University of Medicine and Pharmacy, Timisoara, Iosif Nemoianu, nr 2-3, 300011, Romania*

\**e-mail: monostoripeter@gmail.com*

### Abstract

Newborn screening for congenital adrenal hyperplasia (CAH) has high false-positive rates, necessitating confirmation of primary results. We developed a single LC-MS/MS assay for dried blood spots (DBS) that allows concurrent confirmation and differential diagnosis of CAH. All five steroids (cortisol, 21-deoxycortisol, 11-deoxycortisol, 4-androstenedione and 17-hydroxyprogesterone) were baseline resolved and reliably determined (UHPLC: PerkinElmer Flexar FX-10; MS/MS: ABSCIEX QTRAP 5500; column: Phenomenex Kinetex XB-C18). In Hungary-Romania Cross-Border Cooperation Project (HU-RO 0802/008 SCREENGEN), the 21-hydroxylase deficient form of CAH was confirmed in one of a total of 163 samples tested positive in primary screening. Our validated assay can use the same DBS as in primary screening (2<sup>nd</sup>-tier test), eliminating the need for repeated blood sampling and accelerating diagnosis.

### Introduction

Congenital adrenal hyperplasia (CAH), a severe inherited disorder of cortisol biosynthesis, can cause death in early infancy (due to disturbed sodium homeostasis) and prenatal virilisation in affected girls and signs of a postnatal androgen excess in both sexes (caused by an accumulation of steroid precursors, metabolized to androgens) [1].

Newborn screening for CAH is generally performed through measurement of the 17-hydroxyprogesterone (17-OHP) level in dried blood spots (DBSs) by means of a fluorescence immunoassay (DELFI<sup>®</sup>) [1]. However, the number of false-positives in primary CAH screening is high: CAH is confirmed in only around 1-2 of every 100 positive results [1]. Therefore, primary screening results for CAH based on a 17-OHP assay must be confirmed with a second method, preferably using the same DBS specimen as in the primary screening [1].

Liquid chromatography–tandem mass spectrometry (LC-MS/MS) can effectively decrease the number of false-positives in CAH screening [1, 2, 3]. However, earlier assays could not differentiate between the two main forms of CAH, a 21-hydroxylase deficiency and an 11 $\beta$ -hydroxylase deficiency, which together account for >99% of all cases [1]. This requires separation of 21-deoxycortisol (21-Deox) and 11-deoxycortisol (11-Deox), specific for these two forms of CAH [1]. Most previous assays for 21-Deox and 11-Deox did not allow analysis of DBSs [4, 5]; and those which did, achieved acceptable but not baseline resolution of these isobaric analytes [6].

Accordingly, we aimed to develop a single LC-MS/MS assay for the concurrent confirmation and differential diagnosis of CAH through the analysis of 21-Deox, 11-Deox, cortisol (Cort), 4-androstenedione (4-AD) and 17-OHP in DBS. We also set out to apply this method for



newborn screening in the frame of the Hungary-Romania Cross-Border Cooperation Project (HU-RO) 0802/008 SCREENGEN. Cross-border cooperation may be expected to improve the effectiveness of newborn CAH screening and eliminate possible issues (high initial costs and the need for trained analysts) concerning the implementation of the LC-MS/MS technique [7, 8, 9].

## Experimental

For sample preparation, two spots 4.7 mm in diameter (corresponding to 13.6 µl blood) were punched out from filter cards and placed into 96-well round-bottom microtiter plates. For steroid extraction, 200 µl of the deuterated internal standard working solution was added to each vial. The plate was sealed and shaken for 50 min at ambient temperature. After centrifugation, the supernatant (150 µl) was transferred to a second plate and dried for 45 min. The underivatized residues were reconstituted in 45 µl methanol/water 20/80 (v/v), sealed and shaken for 20 min at room temperature.

The analysis was performed on a PerkinElmer Flexar UHPLC system (two FX-10 binary pumps, solvent manager with a degasser, autosampler and thermostatic oven; all *PerkinElmer Inc.*, Waltham, MA, USA), and an AB SCIEX QTRAP 5500 MS/MS triple quadrupole mass spectrometer, controlled by Analyst 1.6.1 software (both *AB SCIEX*, Framingham, MA, USA). Following optimization of the MS/MS settings, 15 µl of sample was analyzed using multi-step gradient elution (total assay time: 13 min) using a Phenomenex Kinetex XB-C18 100x3.0 mm, 2.6 µm core-shell analytical column and a SecurityGuard Ultra Cartridge guard column (both *Phenomenex*, Torrance, CA, USA). Eluents A and B consisted of ultrapure water plus 0.1% formic acid, and methanol plus 0.1% formic acid, respectively.

In the frame of the Hungary-Romania Cross-Border Cooperation Project, DBS samples from newborns screened in county Timis, Romania, and suspected of having CAH on the basis of the primary screening (17-OHP DELFIA<sup>®</sup> assay, *Wallac Oy*, *PerkinElmer Inc.*, *Turku*, *Finland*), were sent to our laboratory. The reported LC-MS/MS assay was applied as a second-tier test, using the same specimen as in the primary screening. After prompt determination of the steroid levels in Szeged, the results were immediately reported to the primary screening centre to facilitate early intervention. The Cross-Border Cooperation Project was approved by the Ethical Committees of all participating institutions (the University of Szeged, the Louis Turcan Emergency Hospital for Children and the Vasile Goldis Western University of Arad).

## Results and discussion

Traditionally, the confirmation of primary CAH screening results was based on LC-MS/MS findings of elevated levels of 4-AD and 17-OHP, a decreased level of Cort and an elevation in the ratio (4-AD+17-OHP)/Cort [3]. In contrast with 4-AD and 17-OHP, 21-Deox and 11-Deox are specific markers for 21-OH and 11β-OH deficiencies, respectively [1]. Thus, their concurrent determination can improve the specificity of the assay and allow the differential diagnosis of the two most frequent forms of CAH [1].

Previous assays for 21-Deox and 11-Deox have almost exclusively used serum samples [4] or urine [5]. However, serum and urine can be obtained only with a delay which can hamper early recognition and treatment. Instead, the analysis of the same DBS specimen as in the primary screening eliminates the need for repeated blood sampling, can shorten time to diagnosis and improve the cost- and time-effectiveness of screening [2]. The avoidance of repeated blood sampling in the large number of false-positive cases can eliminate unnecessary family anxiety and the accompanying increase in the frequency of hospitalization [9].

We have successfully developed a single LC-MS/MS assay for the concurrent confirmation and differential diagnosis of CAH through the analysis of 21-Deox and 11-Deox in DBS



(together with Cort, 4-AD and 17-OHP). This method was validated in terms of linearity, lower limit of detection (LLOD; 1.0-5.0 nM), lower limit of quantitation (LLOQ; 2.5-12.5 nM), intra-assay precision (coefficient of variation, CV: <7%), inter-assay precision (CV: <10%), variation between injections (CV: <5%), retention time stability (CV: <1%) and extraction efficiency (CV: 69.7-85.2% for DBS calibrator vs methanolic standard; and 75.3-90.4% for DBS calibrator vs. spiked whole blood). Excellent baseline resolution ( $R_s > 1.5$ ) was achieved for all five metabolites in DBSs: the  $R_s$  was 4.28 for the pair Cort and 21-Deox; 3.46 for the pair 21-Deox and 11-Deox; 5.68 for the pair 11-Deox and 4-AD; and 6.51 for the pair 4-AD and 17-OHP. A representative LC-MS/MS chromatogram of a DBS calibrator is presented in Figure 1.

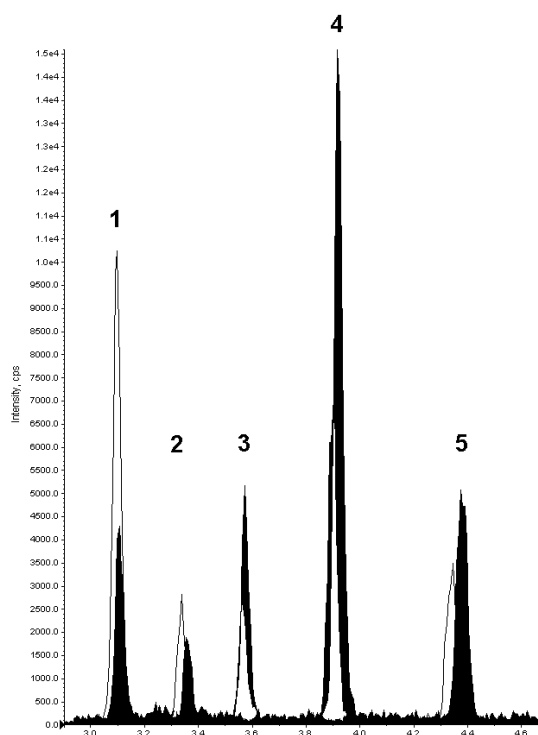


**Figure 1.** Representative LC-MS/MS chromatogram of a DBS calibrator. Peak numbers: 1: Cort; 2: 21-Deox; 3: 11-Deox; 4: 4-AD; 5: 17-OHP (black peaks: unlabelled analytes; unfilled peaks: deuterated internal standards).

In addition, our LC-MS/MS assay proved applicable for the confirmation and differential diagnosis of CAH in cross-border cooperation for newborn screening. A total of 163 newborn DBS samples (including 16 prematures) submitted for second-tier testing were tested with the present assay. The results were compared with reference values of healthy mature newborns and prematures (related to gestational age). The classic 21-hydroxylase deficient form of CAH could be confirmed in one sample on the basis of the markedly elevated levels of 21-Deox, 4-AD and 17-OHP, the increased ratio (21-Deox+17-OHP)/Cort and the decreased Cort level (11-Deox concentration and ratio 11-Deox/Cort were normal). All other samples proved to be false-positives; an 11 $\beta$ -hydroxylase deficiency was not detected.

## Conclusion

An LC-MS/MS method with excellent resolution of 21-Deox and 11-Deox in DBS has been developed, allowing the simultaneous confirmation of CAH and reliable differentiation between its two main forms, the 21-hydroxylase and 11 $\beta$ -hydroxylase deficiencies. The assay can use the same DBS as in the primary screening (second-tier approach), which can facilitate

early therapeutic intervention, improve the cost- and time-effectiveness of screening, and eliminate unnecessary family anxiety by decreasing the high recall rates caused by false-positives. Our method was successfully applied to clinical DBS samples in cross-border cooperation for newborn screening for CAH. The specificity and sensitivity of LC-MS/MS and the use of analyte ratios are expected to facilitate the diagnosis of mild, non-classic CAH.

### **Acknowledgements**

This work was supported by the Hungary-Romania Cross-Border Cooperation Project (HU-RO) 0802/008 SCREENGEN.

### **References**

- [1] P.C. White: *Nat. Rev. Endocrinol.* 5 (2009) 490.
- [2] D. Matern, S. Tortorelli, D. Oglesbee, D. Gavrilov, P. Rinaldo: *J. Inherit. Metab. Dis.* 30 (2007) 585.
- [3] J.M. Lacey, C.Z. Minutti, M.J. Magera, A.L. Tauscher, B. Casetta, M. McCann, J. Lymp, S.H. Hahn, P. Rinaldo, D. Matern: *Clin. Chem.* 50 (2004) 621.
- [4] A.E. Kulle, M. Welzel, P.M. Holterhus, F.G. Riepe: *Horm Res Paediatr* 2013;79:22-31.
- [5] S. Christakoudi, D.A. Cowan, N.F. Taylor: *Steroids*. 78 (2013) 468.
- [6] N. Janzen, S. Sander, M. Terhardt, U. Steuerwald, M. Peter, A.M. Das, J. Sander: *Steroids*. 76 (2011) 1437.
- [7] J.G. Loeber, P. Burgard, M.C. Cornel, T. Rigter, S.S. Weinreich, K. Rupp, G.F. Hoffmann, L. Vittozzi: *J. Inherit. Metab. Dis.* 35 (2012) 603.
- [8] U. Groselj, M.Z. Tansek, A. Smon, N. Angelkova, D. Anton, I. Baric, M. Djordjevic, L. Grimci, M. Ivanova, A. Kadam, V.M. Kotori, H. Maksic, O. Marginean, O. Margineanu, O. Milijanovic, F. Moldovanu, M. Muresan, S. Murko, M. Nanu, B.R. Lampret, M. Samardzic, V. Sarnavka, A. Savov, M. Stojiljkovic, B. Suzic, R. Tincheva, H. Tahirovic, A. Toromanovic, N. Usurelu, T. Battelino: *Mol. Genet. Metab.* 113 (2014) 42.
- [9] J.L. Dhondt: *J. Inherit. Metab. Dis.* 33 (Suppl 2) (2010) S211.

## Neonicotinoid Insecticide Uptake by Maize and Appearance in Guttation Liquid

Mária Mörtl<sup>1\*</sup>, Ágnes Vehovszky<sup>2</sup>, János Győri<sup>2</sup>, Béla Darvas<sup>1</sup>, András Székács<sup>1</sup>

<sup>1</sup>Agro-Environmental Research Institute, National Agricultural Research and Innovation Centre, H-1022 Budapest, Herman O. u. 15, Hungary; <sup>2</sup>Balaton Limnological Institute, Centre for Ecological Research, Hungarian Academy of Sciences, H-8237 Tihany, POB 35, Hungary  
\*e-mail: m.mortl@cfri.hu

### Abstract

Movement of *clothianidin* (CLO) and *thiamethoxam* (TMX) applied as maize seed dressing or spray application has been investigated in different soil types (sandy, clay or loam), and subsequent appearance of these compounds in the guttation liquid of maize are presented. Elution profiles for different soil types were determined in order to explore differences in binding capacity. Soil characterized by high organic matter content retained the ingredients, whereas high clay content resulted in delayed release of the compounds.

Neonicotinoid uptake by non-coated maize plants was also determined *via* guttation liquid measurements after the neonicotinoid ingredients had been applied in spray format. The highest peak concentrations of TMX and CLO (0.546 and 1.83 µg/ml, respectively) were measured from plants planted in sandy soil, but these levels were still substantially lower than levels in samples taken from plants emerged from neonicotinoid-coated seeds (above 100 µg/ml). Moreover, the time of ingredient appearance in guttation liquid was also strongly influenced by soil type.

Cross-contamination was established by measuring neonicotinoid concentrations in guttation liquid in plants emerged from differently coated (CLO and TMX) seeds potted near to each other and the effect of soil type has also been explored. Results for coated (CLO or TMX) and non-coated plants also confirmed that cross-contamination may occur by uptake through soil from neighboring seeds. Differences between non-coated and coated seeds gradually disappeared. This is the first record of neonicotinoid levels in guttation liquid of plants emerged from non-coated maize seeds.

### Introduction

After the introduction of the first commercially available insecticide with a neonicotinoid active ingredient (*imidacloprid*) into the pesticide market in 1991, neonicotinoids rapidly became the most important class of insecticides. Their share in the total global market of insecticides was 28.5% in 2011 [1]. Except for organic farming all of maize seeds planted in North America are coated with neonicotinoids, mainly with *clothianidin* (CLO) or *thiamethoxam* (TMX). They are also routinely applied in developing countries and non-coated seeds are often unavailable for purchase. The current use of systemic pesticides is not sustainable globally [2]. Over 80% of ingredients in seed dressings are not uptaken by target crops [3], and off-target drifting similarly reduces the efficacy of spray applications and causes environmental contamination. Neonicotinoids are persistent in soils under appropriate conditions. Their reported half-lives vary by compound and environmental conditions, but range 150-6900 days for CLO and 35-3000 days for TMX [3]. Due to their good water solubility (e.g. 0.34 g/l and 4.1 g/l for CLO and TMX, respectively) they leach into ground and surface water, and consequently are widely detected in water resources.

Neonicotinoids act as neurotoxic agents to insects and may affect the orientation of bees. Concerns have been raised that their extensive use may contribute to pollinator decline, affecting ecosystem services. Although these compounds were initially regarded less toxic to non-target species compared to other insecticides, they still may pose long-term negative

effects on a wide range of different organisms. Neonicotinoid-related toxic effects on the neuronal connections in the molluscan nervous system have been reported recently [4], but many other examples exist in the literature reviewed in 2015 [5].

Cases of severe bee poisoning and updated risk assessment by EFSA in January 2013 led EU Commission to the conclusion [6] that a high risk for bees cannot be excluded except by imposing further restrictions involving withdrawal of authorization of neonicotinoids and ban of coated seeds for different crops. The restriction applies to the use of CLO, *imidacloprid* and TMX for seed treatment, soil application (granules) and foliar treatment on crops attractive to bees, including certain cereals. Reassessment of these neonicotinoids was scheduled by the EU Commission to be executed by the end on 2015.

Due to their systemic action neonicotinoids are translocated in the entire plant, conferring a long-lasting control of insects. Novel ways of intoxication for bees have been explored *via* the guttation liquid [7], which is excreted in the form of water droplets on the tips of leaves of certain vascular plants. Maize showed high guttation capacity [8], therefore, we selected it as a model species in the present work.

The aim of this work was to study the spread of ingredients in different soil types and to explore the effect of soil quality to CLO and TMX content in guttation liquid. We have also studied the uptake of these active ingredients applied as sprayed format, and their appearance in the guttation liquid of maize plants that emerged from non-coated seeds. Cross-contamination occurring between seeds coated by CLO and TMX has also been studied in different soils. In addition, cross-contamination between coated (CLO or TMX) and non-coated seeds has also been investigated.

## Experimental

Analyses of samples were done on Younglin YL9100 HPLC system equipped with a YL9150 autosampler. A C18 column (150 mm × 4.6 mm i.d., 5µm) was used for the separation at 40°C. Eluent flow rate was 1.0 ml/min with isocratic elution for 5 minutes (70:30 = A:B eluents, A = 90% water : 10% MeOH, B= MeOH). UV detector signals were recorded at  $\lambda=269$  nm for CLO and  $\lambda=252$  nm for TMX. Limits of detections (LODs), determined with standard solutions lied at 10 ng/ml for TMX and below 10 ng/ml for CLO.

Maize seedlings were grown in laboratory in pots and they were obtained from commercially available seeds (DECALB 449 and OCCITAN 380), coated with CLO or TMX. Ingredient contents of coated seeds have been checked.

For investigation of the absorption of neonicotinoids in soils and for spray applications a stock solution containing 2.06 mM of CLO and TMX was prepared and diluted to 8.24 µM in soil adsorption experiments or to 16.5 µM for pre-emergence spray applications.

Three different soil types (sandy, clay, loam) and pumice have been used as a media for growing the maize plants. For the extraction of target compounds from soils a modified QuEChERS method [9] had been chosen as a sample preparation procedure.

The movement of TMX and CLO through a soil column was studied by determination of the elution profiles for clay, loam or sandy soils. Equal molar quantities ( $8.24 \cdot 10^{-7}$  mol) of CLO and TMX were loaded onto the columns, which were then washed with successive 10 ml volumes of water. The neonicotinoid content of the leachates obtained by elution of the active ingredients was determined, as well as the residues in soil were quantified by HPLC.

Vertical spreading of neonicotinoids followed pre-emergence spray application to soil was investigated in pots filled with different soils (loam, clay, sandy). CLO and TMX uptake by plants emerged from non coated maize seeds were studied by analyzing their guttation liquids collected at leaf edges.

Cross-contamination and neonicotinoid uptake by plants from neighboring coated seeds were investigated either with differently coated maize seeds (CLO and TMX) or with non-coated

and coated (CLO or TMX) seeds. Two maize seeds were placed into the same hole and guttation liquid produced by plants were collected and analyzed separately.

## Results & discussion

Water, acetone and acetonitrile were tested as extraction solvents of soil samples, but finally a QuEChERS based sample preparation procedure proved to be suitable method for extraction of TMX and CLO from soils used in this study. Remarkable differences in recoveries concerning water extractions indicate that rate of the leaching can be variable even for these water soluble ingredients.

The effect of soil types on the movement of CLO and TMX in a soil column experiment was significant and elution profiles varied by soil types studied. Poor binding potential of sandy soil probably accounted for high levels of neonicotinoids detected in the first 5<sup>th</sup>-6<sup>th</sup> eluates. High clay content soil showed a greater capacity to bind both TMX and CLO, reflected in their retarded downward movement, continuous leaching and long dissipation. Loam displayed an even stronger retention of both compounds, possibly due to its high organic matter content compared to the two other soil types. According to water solubility data, concentrations measured for TMX were generally higher than that of for CLO. The overall molar ratios of the eluted TMX related to CLO lied at 1.11, 1.46 and 1.33 and 1.26 for sand, clay and loam, indicating the higher mobility of TMX than CLO in all cases. Results are in accordance with binding capacity of soils and with higher water solubility of TMX.

Vertical movement of CLO and TMX and neonicotinoid uptake by non-coated maize plants followed pre-emergence spray application of insecticides to soil show characteristic differences by soil types. The compounds were leached into soil down to the level of seeds with uneven rates, so their uptake and excretion *via* guttation occurred differently. CLO and TMX could be detected immediately in plants emerged in sandy soil. Loam soil retained the substances for a longer period of time, while in the case of clay both compounds appeared shortly after emergence. Peak concentrations determined in guttation liquids of these plants were significantly lower (below 2.0 µg/ml) than the highest levels (over 100 µg/ml) measured for plants emerged from coated seeds. Results reflect the different retention characteristics of investigated soils. Compounds were more retained by higher clay or organic matter content. Plants grown in clay have taken up only 0.021% of applied CLO and 0.042% of TMX, whereas higher rates (0.076 % of CLO, 0.094% of TMX) were detected for plants emerged in sand. Amounts measured for plants grown in loam are negligible.

Leaching of neonicotinoids from one coated seed to another in close proximity and their uptake by plants was evidenced. In case of differently coated seeds (CLO and TMX), cross-contaminations have been observed. Binding capacity of soils plays an important role in the movement of ingredients, therefore, cross-contamination is more pronounced in sandy soil than in soils of high clay and/or organic matter content. When coated and non-coated seeds are potted in close proximity to each other, the neonicotinoids from coated seeds appeared after emergence also in the guttation liquid of plants that emerged from non-coated seeds. In the first period, guttation liquid of maize plants emerged from CLO-coated seeds contained substantially higher amounts of the active ingredient than that of neighboring plants from non-coated seeds (Figure 1) and the concentration rapidly decreased from very high levels. However, significant levels were detected in the guttation liquid of neighboring plants from non-coated seeds as well, whereas there were practically no differences between the two concentrations later from the 24<sup>th</sup> day on. Ratio between the amounts of CLO measured in guttation liquids and coating material was 0.57%. Amounts of CLO taken up by non-coated plants and detected in guttation liquids was 45.7% compared to that of coated seeds.

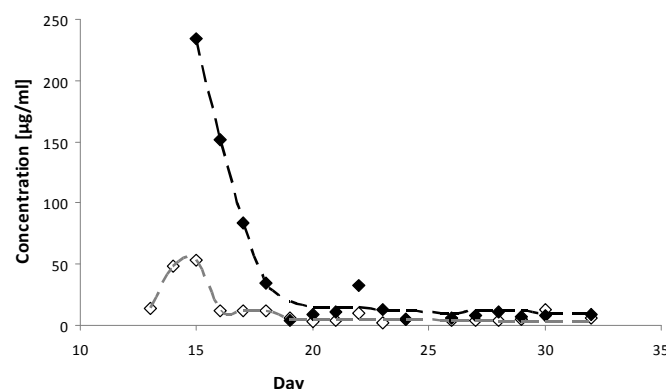


**Figure 1.** CLO levels in the guttation liquid of plants from CLO coated seeds (◆) and neighboring non-coated seeds (◇) grown in sandy soil

### Conclusion

Actual concentrations of neonicotinoids in leachates or in guttation drops are influenced not only by the type of seedling material, but effect of soil type and the application mode (spray or seed coating) also influences the levels of occurrence of these compounds. Our results confirm that high levels of neonicotinoids occur in the guttation liquid of maize. Despite of the fact that neonicotinoids applied as seed coating are targeted to the seed zone, they do not remain associated with the sub-surface soil solution. Our findings provide further evidence of the mobility of these water soluble ingredients, where soil characteristics are of high importance. Insecticides from the field surface move to root zone, and they are also uptaken by non-treated plants. Thus, their systemic effect is not restricted to the plants emerged from coated seeds and could result in exposure of non-target animal species.

### Acknowledgements

This work was supported by the Hungarian Scientific Research Fund (*OTKA 112978*), and received funding from by the Hungarian Ministry of Agriculture (*AD 010* and *AD 006*). Authors thanks Dániel Takács, Csilla Magor and Judit Juracsek for technical support.

### References

- [1] P. Jeschke, R. Nauen, M. Schindler, A. Elbert, J. Agric. Food Chem. 59 (2011) 2897-2908.
- [2] The Task Force on Systemic Pesticides (2015) [http://www.tfsp.info/assets/WIA\\_2015.pdf](http://www.tfsp.info/assets/WIA_2015.pdf)
- [3] D. Goulson, J. Appl. Ecology 50 (4) (2013) 977-987.
- [4] Á. Vehovszky, A. Farkas, A. Ács, O. Stolyar, A. Székács, M. Mörtl, J. Györi, Aquatic Toxicology 167 (2015) 172-179.
- [5] L.W. Pisa, V. Amaral-Rogers, L.P. Belzunces, J.M. Bonmatin, C.A. Downs, D. Goulson, D.P. Kreutzweiser, C. Krupke, M. Liess, M. McField, C.A. Morrissey, D.A. Noome, J. Settele, N. Simon-Delso, J.D. Stark, J.P. van der Sluijs, H. van Dyck, M. Wiemers, Environ. Sci. Pollut. Res. 22(1) (2015) 68-102.
- [6] Commission Implementing Regulation (EU) No 485/2013, <http://eur-lex.europa.eu/LexUriServ/LexUriServ.do?uri=OJ:L:2013:139:0012:0026:EN:PDF>
- [7] V. Girolami, L. Mazzon, A. Squartini, N. Mori, M. Marzaro, A. di Bernardo, M. Greatti, C. Giorio, A. Tapparo, J. Economic Entomology 102 (5) (2009) 1808-1815.
- [8] I. Joachimsmeier, J. Pistorius, U. Heimbach, D. Schenke, W. Kircher, P. Zwerger, 11<sup>th</sup> Int. Symp. of the ICP (2011) Wageningen (The Netherlands). doi: 10.5073/jka.2012.437.020
- [9] M. Anastassiades, S.J. Lehotay, D. Stajnbaher, F.J. Schenck, J. AOAC Int. 86 (2) (2003) 412-431.



## Bio-Nanocomposites - Optoelectronics, Energy Conversion, Biosensors

Richárd Csekő<sup>1,\*</sup>, Emil Nyerki<sup>1</sup>, Balázs Birta<sup>1</sup>, Hüseyin Anil Diblen<sup>1,2</sup>,  
Bilge Hilal Cadirci<sup>2</sup>, Tibor Szabó<sup>1</sup>, Melinda Magyar<sup>1</sup>, Kata Hajdu<sup>1</sup>, Klára Hernádi<sup>1</sup>,  
László Nagy<sup>1</sup>

<sup>1</sup>*Institute of Medical Physics and Informatics, University of Szeged, H-6720, Szeged, Rerrich  
B. tér 1. Hungary*

<sup>2</sup>*Gaziosmanpasa University Tasliciftlik campus, Faculty of Engineering and Natural Sciences,  
Department of Bioengineering*

\**e-mail: Richárd Csekő<csekorichard@gmail.com>*

### Abstract

Biological materials are developed by Nature for extremely efficient, specific and sensitive functions. There are more and more demonstrations recently that it is possible to attach them to nanomaterials combining the advantageous properties of both components. These new types of materials, called *bio-nanocomposites*, open possible directions for new generations of practical applications, e.g. energy conversion and storage, integrated optoelectronics in memory and micro imaging, or sensitive components of analytical (biosensor) devices, etc. In our laboratory recently we have successfully bound representatives of redox proteins (photosynthetic reaction centers and horse radish peroxidase) to inorganic nanostructures and the optoelectronic properties and possible directions of applications are investigated. Examples for applications in environmental field are presented here.

### Introduction

There are many examples that biological materials are used in technical applications (e.g., environmentally friendly biodegradable items and biosensor devices) and vice versa, technical developments (e.g., actuators, artificial tissues, and drug delivery systems) are used in biological systems [1-3]. Because biological materials are developed by Nature for extremely efficient, specific and sensitive functions the use of their exceptional capacity would be beneficial in hybrid systems combining them with inorganic materials. The bio-nanocomposites are of special interest because of their combined advantageous properties and the possibility of the appearance of some new characteristics. Combining different materials (organic or inorganic as well) such substances can be created that pose not only the advantageous properties of the used materials but also new, attractive features can appear. This way there is a good chance to design and tune precisely the characteristics of substrates we need for certain application.

Different biological materials like drugs [4-5], peptides [6], proteins [7], and nucleic acids [8] can be used in combination in nano-hybrid systems as targeted accumulations in vitro and in vivo, e.g. for cancer treatments. Specific biological recognitions are suitable for antibacterial and antiviral targeting by nanomaterials decorated by e.g. antibiotics or antibodies. The unique optical properties of carbon nanotubes can be used for biological imaging [9].

There are many potential applications of bionanocomposite materials in new generations of devices such as biosensors, integrated (opto)electronic devices (switches or converters), photoelectric energy conversion, and (single-molecule) imaging [2,10].

In our laboratory we bound two representatives of redox active proteins (photosynthetic reaction center (RC) and horse radish peroxidase enzyme (HRP)) successfully to various inorganic carrier matrices. Functionalized and non-functionalized single (SWCNT) and multi walled (MWCNT) carbon nanotubes [11], carbon nanotube bundles [12], indium tin oxide



(ITO) [13], porous silicon (PSi) [14] and conducting polymers [15] were used and the functional activities of these samples were demonstrated.

### Aims

The aim of our work is to create functional bio-nanocomposite materials from nano-structured carriers and RC or HRP enzyme proteins. This work requires a continuous design of a measuring system to investigate the basic characteristic (optical characteristics, electric conductivity, redox properties, etc.) of our nanosystems. We would like to design a model or a prototype of a device for possible future application (integrated optical, electric conductance, photocurrent, imaging, biosensors, etc.). There are auxiliary processes providing connecting points for other projects, e.g., using other relevant redox proteins and matrices, or phenomena, which can be investigated.

### Materials and methods

Biological samples RCs were prepared routinely from *Rhodobacter (Rb.) sphaeroides* purple bacterial strains by standard protein purification procedures. HRP was obtained from Sigma. These proteins were bound to different carrier matrices by different methods (physical and chemical binding), which is also routine in our laboratory.

Inorganic carrier matrices Functionalized and non-functionalized single (SWCNT) and multi walled (MWCNT) carbon nanotubes, carbon nanotube bundles were obtained from our collaboration partners (Prof. Klára Hernádi, SZTE AKKT, and Prof. László Forró (EPFL, Switzerland, Lausanne). ITO was purchased from Precision Glass (Germany), porous silicon (PSi) was obtained from Vivechana Agarwal and Gabriela Palestino (Mexico). Conducting polymers were prepared in collaboration with Prof. Csaba Visy (SZTE DPCMC).

Experimental methods Steady state and kinetic absorption spectra were measured by commercial bench top (Unicam) and home built spectrophotometers [16], respectively. Composite electrode samples were prepared and photocurrents were measured by a Metrohm PGSTAT204 potentiostat/galvanostat. Light induced conductivity changes were measured by a programmable Keithley 2400 multimeter.

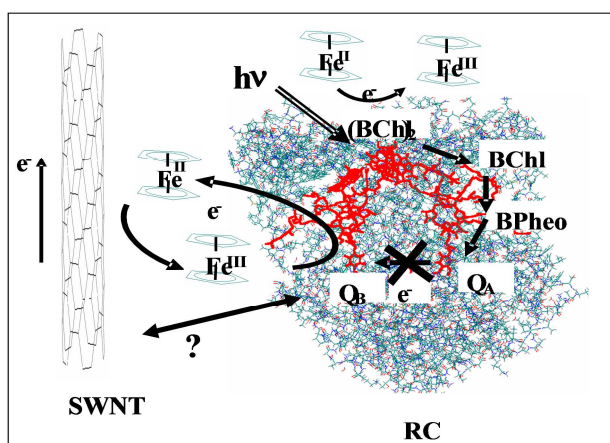
### Results and discussions

#### RC-nanostructures

We already have shown that the integral membrane protein, the photosynthetic reaction center, could be attached to single-walled carbon nanotubes with the apparent binding to specific site(s). Evidence was given that one of the effects of carbon tubes binding included the stabilization of light-induced charge(s) in photosynthetic energy conversion. The attachment of nanotubes increased the lifetime of the  $P^+Q_B^-$  state within the protein, probably due to the slow charge recombination between the oxidized primary electron donor,  $P^+$ , and negative semiquinone forms,  $Q_A^-$  and/or  $Q_B^-$ , the reduced primary and secondary electron acceptor quinones within the protein, respectively. After the excitation, the intraprotein charge movements are followed by slower reorganization of the protein structure (cf. Figure 1).

Specific interactions between the CNTs and RCs can be investigated if specialized chemical (covalent) binding are achieved by several strategies [17]. Common or engineered functional groups (like amine, carboxyl or sulfhydryl) or specialized cross linkers can be used. Several homo- (e.g., glutaraldehyde) and heterobifunctional (e.g., sulfo-SMCC, *N*-(1-Pyrene)iodoacetamide) cross-linkers can be used to bind specific and nonspecific sites of the RCs to different carrier matrices.

**Figure 1.** Schematic presentation of the positions of cofactors, and the path of the electron flow in the RC protein and of the possible interaction between the carbon nanotube and the RC. (BChl)<sub>2</sub>: primary electron donor bacteriochlorophyll dimer; BChl: bacteriochlorophyll monomer; BPheo: bacteriopheophytine; Q<sub>A</sub>: primary quinone; Q<sub>B</sub>: secondary quinone. Black arrows: the electron transport route. X indicates the electron transport step, which is blocked by the inhibitor, terbutryn. Fe<sup>II</sup> and Fe<sup>III</sup> are reduced and oxidized ferrocene, respectively [11].



A promising approach is to bind the RCs to ITO (a transparent conducting electrode) in a photo-electrochemical cell through conducting polymer (Poly(3,4-ethylenedioxythiophene) (PEDOT), Poly[bis(4-phenyl)(2,4,6-trimethylphenyl) amine] (PTAA)). The conducting polymer connects larger amount of RCs and wires electrons to the working electrode. The RC/PTAA/CNT complex showed photochemical activity as indicated by flash photolysis experiments and a photocurrent was measured which was sensitive to the electron transport mediator applied (externally added electron donor/acceptor or specific inhibitor (like terbutryn)).

Photosynthetic RC proteins offer unique applications, for example, their use in the nanostructures or in the optoelectronic systems. In these systems the electron – arising from charge separation – is trapped in the redox components of the RC or its molecular environment and, among other things, can participate in electric circuits. The fabrication of systems for efficient light-energy conversion (e.g., photovoltaics), integrated optoelectronic systems or biosensors (e.g., for specific detection of pesticides) can be visualized for the near future.

Measuring light-induced change in the current (called photocurrent) in an electrochemical cell is an elegant demonstration of the suitability of the photosynthetic systems for photovoltaics, or other practical applications in optoelectronics (e.g. for sensing elements for specific compounds, like pesticides). Two of our RC based composites were successfully tested and found to be active in electrochemical cells. It has been demonstrated that continuous redox turnover of nanocomposite prepared from PTAA/MWCNT and RCs bound to ITO can be driven by light if quinone is added to the solution for mediating the electron transport between the working and the counter electrode.

#### Real time sensing of H<sub>2</sub>O<sub>2</sub> by HRP biosensor

The accurate and sensitive determination of H<sub>2</sub>O<sub>2</sub> is very important in laboratory experiences because it is a product of reactions catalysed by several oxidase enzymes in living cells and it is essential in environmental and pharmaceutical analyses. The fabrication of a device with the sensing component of enzyme protein based (bio-)sensors is a promising way for this purpose because the function of biological molecules is very specific, sensitive and selective. HRP is the most commonly used enzyme in H<sub>2</sub>O<sub>2</sub> detection because it can oxidize xenobiotics in the presence of H<sub>2</sub>O<sub>2</sub>. In order to define the limit of detection (LOD) of H<sub>2</sub>O<sub>2</sub> we made calibrations with guaiacol and amplex red (AR), which chemicals are substrates of HRP. The accumulation of the reaction products, tetraguaiacol and resorufin, then can easily be detected by absorption or emission spectroscopy. In our experiments an enzyme electrode was fabricated from ITO, MWCNT and HRP. LOD was calculated in both cases. The H<sub>2</sub>O<sub>2</sub>

decomposition was about 0.15 nM H<sub>2</sub>O<sub>2</sub>/sec in the case of guaiacol and 0.075 nM H<sub>2</sub>O<sub>2</sub>/sec in the case of AR. Our measurements indicated that the enzyme activity yields 122.8 M [H<sub>2</sub>O<sub>2</sub>]/(M [HRP] · sec) with guaiacol and 49.5 M [H<sub>2</sub>O<sub>2</sub>]/(M [HRP] · sec) with AR [18].

### **Acknowledgements**

Work was supported by grants from Switzerland through the Swiss Contribution (SH/7/2/20), from the National Research, Development and Innovation (NKFI) Fund (OTKA K112688 and PD116739). Thanks are due to the helpful discussions with members of European Cooperation in Science and Technology network, PHOTOTECH COST TD1102 and to Ms. Judit Tóth for the valuable technical assistance.

### **References**

- [1] O. Shoseyov, I. Levy, I. Nanobiotechnology: Bioinspired Devices and Materials of the Future; Humana Press. Inc.: Totowa, NJ, 2008.
- [2] M. Darder, P. Aranda, E. Ruiz- Hitzky, Adv. Mater. 19 (2007) 1309.
- [3] M.T. Giardi, E. Pace, Trends. Biotechnol. 23 (2005) 257.
- [4] R.P. Feazell, N. Nakayama-Ratchford, H. Dai, S.J. Lippard, J. Am. Chem. Soc. 129 (2007) 8438.
- [5] Z. Liu, A.C. Fan, K. Rakhra, S. Sherlock, A. Goodwin, X. Chen, Q. Yang, D.W. Felsher, H. Dai, Angew. Chem. Int. Ed. Engl. 48 (2009) 7668.
- [6] D. Pantarotto, J.P. Briand, M. Prato, A. Bianco, Chem. Commun. 1 (2004) 16.
- [7] N.W.S. Kam, H. Dai, J. Am. Chem. Soc. 127 (2005) 6021.
- [8] Y. Liu, D.C. Wu, W.D. Zhang, X. Jiang, C.B. He, T.S. Chung, S.H. Goh, K.W. Leong, Angew. Chem. Int. Ed. 44 (2005) 4782.
- [9] A. De La Zerda, C. Zavaleta, S. Keren, S. Vaithilingam, S. Bodapati, Z. Liu, J. Levi, T.-J. Ma, O. Oralkan, Z. Cheng, X. Chen, H. Dai, B.P. Khuri-Yakub, S.S. Gambhir, Nat. Nanotechnol. 3 (2008) 557.
- [10] P. Ormos, L. Fábrián, L. Oroszi, E.K. Wolff, J.J. Ramsden, A. Dér, Appl. Phys. Lett. 80 (2002) 4060.
- [11] M. Dorogi, Z. Balint, Cs. Miko, B. Vilenó, M. Milas, K. Hernadi, L. Forro, Gy. Varo, L. Nagy, J. Phys. Chem. B 110 (2006) 21473.
- [12] L. Nagy, K. Hajdu, Sz. Torma, S. Csikós, T. Szabó, M. Magyar, D. Fejes, K. Hernádi, M. Kellermayer, E. Horváth, A. Magrez, L. Forró, Phys. Status Solidi B, 251 (2014) 2366.
- [13] T. Szabó, G. Bencsik, M. Magyar, Cs. Visy, Z. Gingl, K. Nagy, Gy. Váró, K. Hajdu, G. Kozák, L. Nagy, Mater. Sci. Eng. C 33 (2013) 769.
- [14] K. Hajdu, Cs. Gergely, M. Martin, T. Cloitre, L. Zimányi, K. Tenger, P. Khoroshyy, G. Palestino, V. Agarwal, K. Hernádi, Z. Németh, L. Nagy, Langmuir 28 (2012) 11866.
- [15] T. Szabó, M. Magyar, Z. Németh, K. Hernádi, B. Endrődi, G. Bencsik, Cs. Visy, E. Horváth, A. Magrez, L. Forró, L. Nagy, Phys. Status Solidi B, 248 (2012) 2386.
- [16] J. Tandori, L. Nagy, Á. Puskás, M. Droppa, G. Horváth, P. Maróti, Photosynth. Res. 45 (1995) 135.
- [17] L. Nagy, M. Magyar, T. Szabo, K. Hajdu, L. Giotta, M. Dorogi, F. Milano, Curr. Protein. Pept. Sci. 2014;15:363.
- [18] M. Magyar, K. Hajdu, T. Szabó, B. Endrődi, K. Hernádi, E. Horváth, A. Magrez, L. Forró, Cs. Visy, L. Nagy, Phys. Status Solidi B, 250 (2013) 2559.

## Removal of Antibiotics from Aqueous Solution by Bioadsorbant

A. E. Sarrai<sup>\*1, 2, 3</sup>, S. Hanini<sup>1</sup>, N. Kasbadji Merzouk<sup>2</sup>, D. Tassalit<sup>2</sup>, Tibor Szabó<sup>3</sup>, László Nagy<sup>3</sup>

<sup>1</sup>Laboratoire de Biomatiériaux et Phénomènes de Transports LBMPT, Université Yahia Fares, Médéa, Algeria.

<sup>2</sup>Unité de Développement des Equipements Solaires, UDES/Centre de Développement des Energies Renouvelables, CDER, Bou Ismail, 42415, W. Tipaza, Algérie.

<sup>3</sup>Department of Medical Physics and Informatics, University of Szeged, Rerrich Béla tér 1. 3rd floor, H-6701 Szeged, Hungary.

\*Sarrai\_aziz@hotmail.com

### Abstract

In this study, dehydrated wheat bran, which is a natural product grows in the north of Algeria has been used as bioadsorbant for antibiotics removal from aqueous solution. Experimental data showed that the sorption of Tylosin increased with increasing the amount of adsorbent and decreased at high temperature.  $\Delta H^\circ$  and  $\Delta S^\circ$  were calculated from the slope and intercept of plots of  $\ln(k_d)$  versus  $1/T$ , the adsorption process was found to be exothermic and more favourable at low temperature.

### 1. INTRODUCTION

Although antibiotics have been used in large quantities for some decades, until recently the existence of these substances in the environment has received little notice [1]. Antibiotics are gaining recognition as being environmental contaminants, classified as recalcitrant bio-accumulative compounds and are thus regarded as hazardous chemicals [2]. Adsorption method is one of the most efficient methods of removing pollutants from wastewater [3]. It is simple to design and operate; and it is relatively inexpensive and unaffected by the potential toxicity as for biologically based processes [4]. The present work is focused on Tylosin adsorption onto dehydrated wheat bran, the experiments were done in a batch system to evaluate the adsorption capacity of carbon, and adsorption characteristics were evaluated as a function of adsorbent dosage, temperature and thermodynamics parameters.

### 2. MATERIALS AND METHODS

#### 2.1. Preparation of dehydrated wheat bran

The wheat bran provided by SIM Company located in Blida- Algeria; was mixed with sulfuric acid solution in the ratios of 1/1 (starting material/activating agent). The mixture was manually stirred at the beginning to contact wheat bran well with acid and left for 2 h, at the end of the dehydration process, sufficient distilled water was added to the mixture to eliminate dust, impurities and other unwanted chemicals before filtering. This process was repeated until the final pH of the filtrate was about 7.0. The dehydrated material rinsed with distilled water was dried for 24 h in oven at 80 C°. Finally, the powdered sample was kept in a desiccator for future use.

#### 2.2 Adsorption studies

The adsorbed amount of Tylosin (antibiotic selected for study) at equilibrium  $q_e$  (mg.g<sup>-1</sup>) and the percentage removal ( $R\%$ ) were calculated by the following equations:

$$R\% = \frac{(C_0 - C)}{C} * 100 \quad (1)$$

$$q_e = \frac{(C_0 - C_e)}{X} \quad (2)$$

Here  $C_0$  and  $C_e$  are the initial and equilibrium concentrations ( $\text{g.L}^{-1}$ ),  $X$  (g) is the weight of dehydrated wheat bran in one litter and  $C$  is the pollutant concentration at the end of adsorption.

### 3. RESULTS AND DISCUSSION

#### 3.1. Characterization of the adsorbent

Surface structure of dehydrated wheat was analyzed by Scanning Electron Microscope (SEM), the observation from Fig. 1 enabled us to discern the following aspect.

Highly developed porosity all over the entire sample surface with a certain heterogeneity. This porosity can refer to the evaporation of sulfuric acid from the cavities previously occupied by the chemical agent. The presence of pores indicated that there was a good possibility that Tylosin could be trapped and adsorbed onto the surface of dehydrated wheat bran.

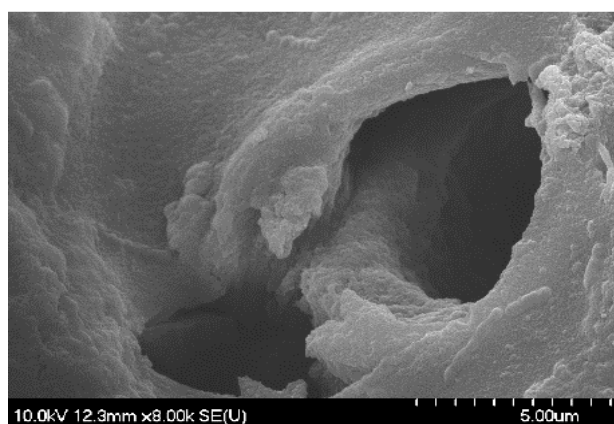


Fig. 1. Scanning electron microscope image of dehydrated wheat bran

#### 3.2. Effect of the operating parameters

##### 3.2.1 Effect of adsorbent dosage

The adsorbent dosage is an important parameter because this determines the capacity of a biosorbent for a given initial concentration. The biosorption efficiency for as a function of biomass dosage was investigated. The results are presented in Fig. 2. It can be seen that percentage of Tylosin adsorption steeply increases with the biomass loading up to 0,8 g/L. This result can be explained by the fact that the biosorption sites remain unsaturated during the biosorption reaction whereas the number of sites available for biosorption site increases by increasing the biosorbent dose [5].

##### 3.2.2. Effect of temperature

Effects of temperature on Tylosin removal are presented in Figure 3. It is concluded from Fig. 3 that Tylosin adsorption decreases with increasing the temperature, which indicated that the lower temperature could be more favourable for Tylosin adsorption onto the dehydrated wheat bran. For further understanding the mechanism of Tylosin adsorption onto the dehydrated wheat bran, thermodynamic analysis was performed. The thermodynamic parameters represented by the change in free energy ( $\Delta G$ ), enthalpy ( $\Delta H$ ), and entropy ( $\Delta S$ ) have an important role to determine spontaneity and heat change for the adsorption process. Equilibrium constant can be used to evaluate the thermodynamic parameters [6].

The van't Hoff equation is used to determine the value of the equilibrium constant with temperature changes. The equation is given as:



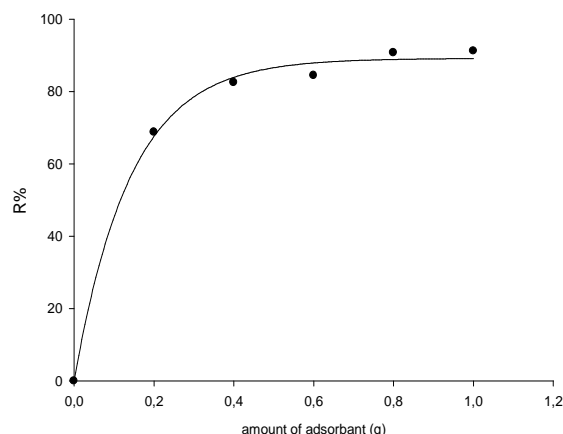


Fig. 2. Adsorbent dosage effect

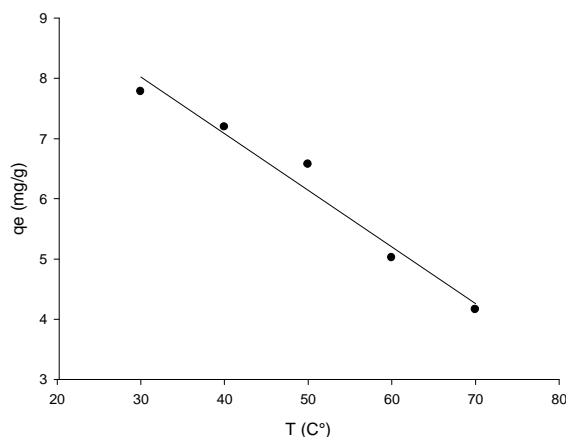


Fig.3. Temperature effect

$$\ln(k_d) = \frac{\Delta S^\circ}{R} - \frac{\Delta H^\circ}{RT} \quad (3)$$

$R$  is the gas constant,  $T$  is temperature and  $\Delta H^\circ$  and  $\Delta S^\circ$  are the standard enthalpy and entropy changes of adsorption, respectively.

The distribution coefficient  $k_d$  [7] can be calculated by using the following equation:

$$k_d = \frac{q_e}{c_e} \quad (4)$$

Fig. 5 shows that  $\ln(k_d)$  vs.  $1/T$  can be fit by the linear equation of van't Hoff (Eq. 3), from which the values  $\Delta H^\circ$  and  $\Delta S^\circ$  were calculated from the slope and from the intercept of the straight line.

The Gibbs free energy of specific adsorption  $\Delta G^\circ$  is calculated using the equation:

$$\Delta G^\circ = \Delta H^\circ - T\Delta S^\circ \quad (5)$$

The calculated thermodynamic parameters of Tylosin adsorption on activated carbon were listed in Table1.

The negative value of enthalpy change  $\Delta H^\circ$  indicates that the adsorption of Tylosin was an exothermic process. The  $\Delta G^\circ$  values were negative at all temperatures and became less negative with increasing temperature, which indicated the spontaneity of the sorption process [8, 9].

Both the negative value of  $\Delta H^\circ$  and the increase in  $\Delta G^\circ$  with an increase in temperature suggested that the reaction was less favourable at higher temperatures.

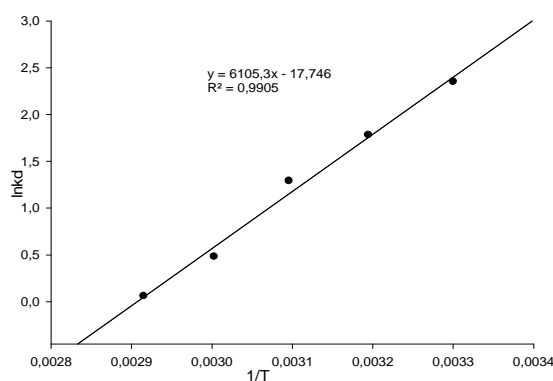

Fig.4.  $\ln(k_d)$  according to the reverse of temperature  $1/T$

Table 1: Thermodynamic parameters for Tylosin adsorption on dehydrated wheat bran.

$T$ (K)	$K_d$ (L.g <sup>-1</sup> )	$\Delta G^\circ$ (kJ.mole <sup>-1</sup> )	$\Delta H$ (kJ.mol <sup>-1</sup> )	$\Delta S$ (kJ.mol <sup>-1</sup> )
303	10.52	-6.057	-50.750	-0.147
313	5.96	-4.582		
323	3.64	-3.107		
333	1.62	-1.632		
343	1.07	-0.157		

#### 4. CONCLUSION

The present investigation shows that the dehydrated wheat bran is an effective bioadsorbant to remove antibiotics compound such as Tylosin from aqueous solutions. The negative value of  $\Delta G$  confirms the spontaneous nature adsorption process. The negative value of  $\Delta H$  indicated the adsorption process was exothermic. The experimental results indicated that Tylosin adsorption is favored for adsorbent dosage higher than 0.8 g.L and at low temperature.

#### 5. REFERENCES

- [1] K.Kümmerer, Antibiotics in the aquatic environment a review-part I, Chemosphere 75(2009) 417-434.
- [2] V. Homem, L. Santos, Degradation and removal methods of antibiotics from aqueous matrices: a review, J. Environ. Manage. 92 (2011) 2304–2347.
- [3] G. Akkaya, I. Uzun, F. Güzel, Adsorption of some highly toxic dyestuffs from aqueous solution by chitin and its synthesized derivative, Desalination. 249(2009) 1115–1123.
- [4] R. Mohd, S. Othman, H. Rokiah, A. Anees, Adsorption of methylene blue on low cost adsorbents: A review, Journal of Hazardous Materials. 177 (2010) 70–80.
- [5] P. Vasudevan, V. Padmavathy, S.C. Dhingra, Biosorption of monovalent and divalent ions on Bakers yeast, Bioresour. Technol. 82 (2002) 285–289.
- [6] D. Xu, X.L. Tan, C.L. Chen, X.K. Wang, Adsorption of Pb (II) from aqueous solution to MX-80 bentonite: effect of pH, ionic strength, foreign ions and temperature, Appl. Clay Sci. 41 (2008) 37–46.
- [7] Q. Zhang, C. Yang, W. Huangc, Z. Dang, X. Shu, Sorption of tylosin on clay minerals. Chemosphere 93 (2013) 2180–2186.
- [8] A. Sarý, M. Tuzen, Kinetic and Equilibrium Studies of Biosorption of Pb(II) and Cd (II) from Aqueous Solution by Macrofungus (Amanita Rubescens) Biomass, Journal of Hazardous Materials, 164 (2009) 1004-1011.
- [9] M. Kara, H. Yuzer, E.Sabah and M.S. Celik, Adsorption of Cobalt from Aqueous Solutions onto Sepiolite, Water Research, 37(2003) 224 – 232.



## Environmental Monitoring of *Glyphosate* and Assessment of its Combined Cytotoxicity with Adjuvants

Marianna Ottucsák, Szandra Klátyik, Gergő Gyurcsó, Mária Mörtl, Béla Darvas,  
András Székács\*

*Agro-Environmental Research Institute, National Agricultural Research and Innovation  
Centre, Herman O. u. 15, H-1022 Budapest, Hungary*

\*e-mail: a.szekacs@cfri.hu

### Abstract

Pesticide toxicology currently focuses mainly on two areas: long-term effects of given compounds and cocktail effects of chemicals, including combined effects of pesticide active ingredients with their adjuvants, as seen in the case of *glyphosate*-based herbicides. In this study surface water pollution in an agricultural region of Hungary by *glyphosate* was determined by ELISA method, and cytotoxic effects on *HEK293* and *NE-4C* cells by *glyphosate*, its formulated herbicide (ROUNDUP®) and adjuvant (polyethoxylated tallowamine, POEA) were compared. ROUNDUP and POEA were found to be equitoxic at short exposures (LC<sub>50</sub>: 10-15 ng/ml in 6 hrs), while *glyphosate* occurred to be of 500-750-fold less toxicity.

### Introduction

The role of pesticides in current industrial agriculture is to suppress damages in crop production by agricultural pests. To achieve such chemical protection, pesticides are used in formulations as mixtures of active ingredient(s) responsible for the main effect of the pesticide preparation with adjuvants added to improve physico-chemical properties, adsorption/penetration capability and other characteristics of the active ingredient(s) [1]. With the worldwide expansion of monoculture-based agriculture, overall pesticide consumption continuously grows not only affecting targeted crop yields, but also causing increasing chemical pressure on the environment. In addition, pesticide residues are often the source of chemical exposure as they enter the food chain upon agricultural practices.

Due to this environmental load and subsequent exposure to numerous non-target organisms, surveys on pesticide residues and their side-effects are expanding [2], and consequently pesticides are subject to strict registration processes specified in corresponding international recommendations [3, 4] and legal regulations [5, 6], and pesticide residues are strictly regulated through their maximal residue levels (MRLs) in food and feed set upon evidence-based scientific risk assessment [7, 8]. General pesticide toxicology research in the 70's was mostly focused on the acute effects. During the late 80's (with the development and extended use of the metabolic bacterial reverse mutation assay developed by Bruce Ames [9] and other microbial mutagenicity tests), attention turned towards mutagenicity, carcinogenicity, teratogenicity and epidemiological examination of pesticides, and toxicity requirements stricened towards candidate pesticide substances. Expanding knowledge justifies why active ingredients in plant protection products have to undergo regular re-assessment. During the past two decades, increasing interest has been expressed in fields, where sufficient knowledge was still lacking: the study of immunomodulant and endocrine disruptive effects [10].

Current toxicology focuses on two main areas: (i) long-term effects of chemicals at doses near the no observed effect level (NOEL) in exposures extending over long periods, even life-times, and (ii) effects of numerous compounds exerting toxicity in parallel, so called cocktail effect. The latter type includes the case of combined effects of active ingredients with their adjuvants. These adjuvants are considered „inert” in terms of the main effects of the pesticide

active ingredient, but they may cause substantial side-effects or increase side-effects of the active ingredients.

#### *Glyphosate*

*Glyphosate* is presently the largest selling herbicide active ingredient in the world, and its market continues to grow in line with restrictions/ban on other herbicides and the increase in the cultivation of *glyphosate*-tolerant (GT) transgenic crops [11]. By blocking the biosynthesis of essential aromatic amino acids through inhibiting the shikimic acid metabolic pathway and also inhibiting photosynthesis, *glyphosate* shows general phytotoxicity, allowing its broad pre-emergent herbicide applications. As a result of the long-term, intensive use, our surveys indicate *glyphosate* as a common contaminant in rivers and other surface waters [12-13]. Formulated preparations of *glyphosate* have been indicated to exert harmful biological effects, for example endocrine disruption [14-15] or teratogenicity [16], even under its no-effect level (NOEL) upon extended chronic exposures. The current evaluation by the UN International Agency for Research on Cancer (IARC) classified *glyphosate* as probably carcinogenic to humans (Group 2A), based on "limited evidence" in human experiments and "sufficient evidence" in animal-experiments [17]. In light of these adverse side effects, the recent re-approval of *glyphosate* has been claimed unacceptable [18]. As *glyphosate* has been reported as common surface water pollutant, and as substantial differences have been evidenced in the toxicity of *glyphosate* and its formulated herbicide products, attributed to side-effects of the adjuvants applied in formulation, our study aimed to evaluate the environmental occurrence of *glyphosate* in surface waters, and to comparatively assess cytotoxicity of *glyphosate*, its formulated herbicide preparation ROUNDUP® and common adjuvant (used also in ROUNDUP) polyethoxylated tallowamine (POEA).

#### **Materials and Methods**

*Glyphosate* and ROUNDUP were obtained commercially, POEA was provided by Lamberti SpA (Albizzate, Italy), chemicals were purchased from Sigma-Aldrich Co. (St. Louis, MO, USA). *Glyphosate* was determined in environmental samples by a commercial enzyme-linked immunosorbent assay (ELISA), cell viability was tested using the thiazolyl blue tetrazolium bromide (MTT) reduction assay detecting mitochondrial respiration intensity [19] on two cell types: a human embryonic kidney cell line expressing adenovirus-specific tumor antigen (HEK293) [20] and a mouse neuroectodermal stem cell line (NE-4C) [21]. HEK293 cells were purchased from Sigma-Aldrich Co., NE-4C cells were kindly provided by the Institute of Experimental Medicine of the Hungarian Academy of Sciences.

#### *Immunochemical analysis of glyphosate*

Immunochemical analysis of *glyphosate* was performed using the ELISA kit by Abraxis LLC (Warminster, PA, USA), validated to determination of *glyphosate* in water (ground/surface/well water). Without sample extraction, water samples were derivatized (acetylated) prior to immunoanalysis, and then were pipetted onto the manufacturer-supplied 96-well microplates. Samples were incubated (30 min) on the microplate with *glyphosate*-specific antibodies, then IgG-specific second antibodies conjugated to a reporter enzyme were added, and upon further incubation (60 min) and washing, substrate (H<sub>2</sub>O<sub>2</sub>) and a chromophore were added, and optical density of the solutions was detected in a MULTISKAN ASCENT microplate reader (Labsystems, Finland). *Glyphosate* concentration was determined using analytical standard and sigmoid (logistic regression) calibration.

#### *Cell culture work*

Cell lines were stored at -196°C in liquid nitrogen, and subsequently thawed in water bath, washed and cultured in buffer medium containing 10% fetal bovine serum. Cells were grown

at 37°C (under an atmosphere of 5% CO<sub>2</sub>, 95% air) to 80% confluence, and prior to cytotoxicity measurement were passed through at least one passage. Upon being washed with serum-free medium buffer, cells were exposed to various chemicals for up to 24 hrs [22]. The MTT cytotoxicity tests were carried out in 96-well microplates. Cells were incubated with *glyphosate*, ROUNDUP and POEA at various concentrations for 2, 6 and 24 hrs in buffer medium with or without serum added [23] and after washing, MTT (0.1 mg/ml in buffer medium) was added, and color development was detected at 570 nm.

## Results and Discussion

### *Determination of glyphosate*

Using the Abraxis ELISA method, *glyphosate* was detected above the practical limit of detection (LOD) (0.12 ng/ml) in half of the surface water samples collected in the autumn period from a maize growing agricultural region of Hungary. *Glyphosate* concentrations showed a somewhat bimodal pattern: concentrations were either below (or in some cases slightly above) the LOD, or were found alarmingly high (0.542±0.003 to 0.984±0.003 ng/ml). In contrast, surface water samples collected in the spring period (before intensive pre-emergent herbicide applications) were found predominantly not to contain *glyphosate* above the LOD, possibly due to a dilution effect in standing water bodies or in rivers.

It has to be noted that the ELISA method is specific only to *glyphosate*, and it doesn't detect its primary metabolite, aminomethylphosphonic acid (AMPA). According to manufacturer's specifications, the cross-reactivity of the detection method for AMPA is slightly above 0.0001%. This means, analysis covers only the presence/absence of the parent compound (*glyphosate*) and not its official residue level, *glyphosate* and its metabolite(s).

### *Cytotoxicity measurements*

ROUNDUP strongly suppressed cell viability, detectable even after 2 hrs of exposure, significantly dropped by 6 hrs, but with no further decay until 24 hrs. POEA caused similarly decreased cell viability above 5 ng/ml concentration, and the effect continuously increased from 2 to 24 hrs of exposure. LC<sub>50</sub> values for ROUNDUP and POEA on NE-4C cells upon 6 hrs of exposition were found to be 15 and 10 ng/ml, respectively, but POEA caused more rapid cytotoxicity. In contrast, cytotoxicity of *glyphosate* (LC<sub>50</sub>: 7.5% µg/ml in 6 hrs) was 500-750-fold lower. ROUNDUP is well known to be cytotoxic by inhibiting mitochondrial respiration (LC<sub>50</sub>: 57.5 µg/ml) [22] and induced cell necrosis by a 15-fold increase in adenylate kinase release. The apoptotic effect of ROUNDUP was seen by an increase in caspase 3/7 activity by 6.29-8.24 times compared to the control level.

## Conclusions

*Glyphosate*-based herbicides present dual hazards in terms of environmental contamination and cytotoxicity. In this study, *glyphosate* was found in half of the surface water samples from a maize growing region of Hungary, with contamination as high as 0.984 ng/ml in a bimodal pattern. POEA, the main adjuvant of *glyphosate*, was found cytotoxic above 1 ng/ml concentration on human cell lines after 2 to 24 hrs of exposure. The results evidenced the hazard of *glyphosate* and even more of its adjuvant POEA on human cell viability, underlying the necessity of toxicological risk assessment of pesticide formulating adjuvants for their combined effects with pesticide residues. Thus, risk assessment has to be extended to toxicological consequences of such parallel exposure.

## Acknowledgments

The authors thank Prof. Emilia Madarász (Institute of Experimental Medicine of the Hungarian Academy of Sciences) for the provision of NE-4C cells and facilities for

cytotoxicity tests on this cell line. The work was supported by project K109865 of the Hungarian Scientific Research Fund (OTKA).

## References

- [1] A.K. Hassall, *The Biochemistry and Uses of Pesticides: Structure, Metabolism, Mode of Action and Uses in Crop Protection*, VCH Publ., London, 1990, pp. 25-56.
- [2] United Nations Environment Programme, *Clearing the Waters: A Focus on Water Quality Solutions*, UNEP Division of Environmental Policy Implementation, Nairobi, Kenya, 2010, pp. 13-16.
- [3] Organisation for Economic Co-operation and Development (OECD), *Water Quality and Agriculture Meeting the Policy Challenge*, OECD Publ., Paris, France, 2012, p. 11.
- [4] Food and Agriculture Organization (FAO), *International Code of Conduct on the Distribution and use of Pesticides*, 2013, FAO, Rome, Italy, 2013, pp. 16-17.
- [5] U.S. Environmental Protection Agency (US EPA), *Pesticide Registration Improvement Extension Act (PRIA 3)*, US EPA, Washington, DC, USA, 2012.
- [6] European Commission (EU), *Regulation 284/2013 (1 March 2013) Setting out the Data Requirements for Plant Protection Products, in Accordance with Regulation 1107/2009 Concerning the Placing of Plant Protection Products on the Market*, 2013.
- [7] World Health Organization (WHO), *International Programme on Chemical Safety, Principles for Modelling Dose-Response for the Risk Assessment of Chemicals, Annex I: Terminology, Environmental Health Criteria 239*, World Health Organization, Geneva, Switzerland, 2009.
- [8] European Food Safety Authority (EFSA), *Scientific Opinion on Risk Assessment Terminology*, EFSA Scientific Committee, Parma, Italy, 2012.
- [9] B.N. Ames, F.D. Lee, W.E. Durston, *Proc. Nat. Acad. Sci. U.S.A.*, 70 (3) (1973) 782-786.
- [10] T. Colborn, D. Dumanoski, J.P. Myers *Our Stolen Future*, Dutton, New York, NY, USA, 1996.
- [11] A. Székács, B. Darvas, *Herbicides – Properties, Synthesis and Control of Weeds*, InTech, Rijeka, Croatia (2012) 247-284.
- [12] M. Mörtl, Gy. Németh, J. Juracek, B. Darvas, L. Kamp, F. Rubio, A. Székács, *Microchem. J.* 2013, 107: 143-151.
- [13] A. Székács, M. Mörtl, B. Darvas, *J. Chem.* (2015) Article ID 717948.
- [14] C. Gasnier, C. Dumont, N. Benachour, E. Clair, M.C. Chagnon, G.-E. Séralini, *Toxicology* 262 (3) (2009) 184-191.
- [15] M. Antoniou, M.E.E.-D.M. Habib, C.V. Howard, R.C. Jennings, C. Leifert, R.O. Nodari, C. Robinson, J. Fagan, *Roundup and Birth Defects*, Earth Open Source, Lancashire, UK, 2011.
- [16] A. Paganelli, V. Gnazzo, H. Acosta, S.L. López, A.E. Carrasco, *Chem. Res. Toxicol.* 23 (2010) 1586-1595.
- [17] International Agency for Research on Cancer, *IARC Monographs* 112 (2015) 1-92.
- [18] N. Swanson, H.W. Ho, in: *Banishing glyphosate*, Institute of Science in Society, London, UK (2015) pp. 64-66.
- [19] T. Mosmann, *J. Immunol. Meth.* 65 (1983) 55-63.
- [20] F.L. Graham, J. Smiley, W.C. Russell, R. Naim, *J. Gen. Virol.* 36 (1) (1977) 59-74.
- [21] K. Schlett, E. Madarász, *J. Neurosci. Res.* 47 (1997) 405-415.
- [22] R. Mesnage, E. Clair, S. Gress, C. Then, A. Székács, G.-E. Séralini, *J. Appl. Toxicol.* 33 (7) (2013) 695-699.
- [23] I. Székács, Á. Fejes, Sz. Klátyik, E. Takács, D. Patkó, J. Pomóthy, M. Mörtl, R. Horváth, E. Madarász, B. Darvas, A. Székács, *Internat. J. Biol., Vet. Food Engineer.* 8 (3) (2014) 213-218.

## Degradation of Monuron in Aqueous Solution by Ionizing Radiation

Krisztina Kovács<sup>1\*</sup>, Viktória Mile<sup>1</sup>, Tamás Csay<sup>1</sup>, Shijun He<sup>2</sup>, Erzsébet Takács<sup>1</sup>, László Wojnárovits<sup>1</sup>

<sup>1</sup>*Institute for Energy Security and Environmental Safety, Centre for Energy Research,  
Hungarian Academy of Sciences, Budapest, Hungary*

<sup>2</sup>*Institute of Nuclear and New Energy Technology (INET), Tsinghua University, Beijing,  
100084 China*

*e-mail: kovacs.krisztina@energia.mta.hu*

### Abstract

In this study ionizing radiation induced degradation of monuron was investigated by  $\gamma$ -radiolysis.  $\gamma$ -radiolysis is one of the Advanced Oxidation processes (AOPs) which is very effective method for the degradation of organic water pollutants. The end-products and transient intermediates were studied in order to describe the degradation mechanism. The main reaction is  $\text{OH}^\bullet$  addition to the aromatic ring forming hydroxyl-cyclohexadienyl type radicals. In addition to this radical, aminyl and phenoxyl radicals have also some contribution to the degradation. Monuron as a halogenated compound is sensitive to the hydrated electron attack. Due to the oxidation, chemical oxygen demand and total organic carbon content decreases during irradiation treatment. The efficiency of oxidation is high compared to other aromatics. Both,  $\text{OH}^\bullet$  and  $e_{\text{aq}}^-$  take part in the dehalogenation reactions.

### Introduction

Phenylurea herbicides are applied for the pre- and post-emergence control of weeds in agricultural and non-agricultural fields. They have a long lifetime [1] and because of their bioaccumulation and persistence they can be detected in the environment [2-4].

Our target of investigation, monuron (3-(4-chlorophenyl)-1,1-dimethylurea) is a phenylurea herbicide. Monuron is known to be carcinogenic on humans [5]. Its decomposition has already been studied by different AOP methods: the most effective method was found to be the photo-Fenton reaction [6].

In our laboratory decomposition of different phenylurea herbicides was investigated by high energy irradiation. This study is a sequence of our studies in which the degradation of a series of harmful organic pollutants was examined by  $\gamma$ -radiolysis [7-8].

### Experimental

Monuron and other chemicals were purchased from Spectrum-3D or Carlo Erba and used without any purification. All solutions were prepared without any buffer addition and pH adjustment. The  $\gamma$ -irradiated samples were first examined by JASCO 550 UV-Vis spectrophotometer with a 1 cm cell applying appropriate dilutions before taking the spectra. The formation and decay of transient intermediates were followed up by pulse radiolysis to investigate the reactions between monuron and  $\text{OH}^\bullet$ , as well as monuron and  $e_{\text{aq}}^-$ .

In irradiated samples other comprehensive characteristics of the solution, such as Chemical Oxygen Demand (COD), Total Organic Carbon (TOC) and Total Nitrogen (TN) contents were also measured using Behrotest TRS 200 COD system and Shimadzu TOC-VCSN equipment, respectively.

The concentration of adsorbable organic halides (AOX) and free chloride ions in solutions were monitored by an AOX equipment and perfectION<sup>TM</sup> Combination Chloride Electrode. Finally, an Agilent Technologies 6410 Triple Quad LC/MS system was used for final products identification.



### Water radiolysis

During water radiolysis reactive primer intermediates (hydrated electron,  $e_{aq}^-$  ( $0.28 \mu\text{mol J}^{-1}$ ); hydroxyl radical,  $\bullet\text{OH}$  ( $0.28 \mu\text{mol J}^{-1}$ ); and hydrogen atom,  $\text{H}^\bullet$  ( $0.062 \mu\text{mol J}^{-1}$ ) and molecular products ( $\text{H}_2$  and  $\text{H}_2\text{O}_2$ ) form. The G-values (yields) of reactive primer intermediates can be seen in the parentheses. These intermediates are responsible for the decomposition of organic substances. The reaction between monuron and individual species were studied under different conditions. In  $\text{N}_2\text{O}$  saturated solution the main reaction partner is  $\bullet\text{OH}$ . In  $e_{aq}^-$  reaction 5 vol% tert-butanol containing solution was saturated by  $\text{N}_2$  to scavenge  $\bullet\text{OH}$  radicals. In the absence of TBA, all 3 primer reactive intermediates have some contribution to the reactions. In aerated saturated solutions,  $e_{aq}^-$  and  $\text{H}^\bullet$  can react with dissolved oxygen. In this case reaction agents are  $\bullet\text{OH}$  and the superoxide radical/perhydroxyl radical pair ( $\text{O}_2^{\bullet-}/\text{HO}_2^\bullet$ ) ( $\text{pK}_a(\text{O}_2^{\bullet-}/\text{HO}_2^\bullet) = 4.8$ ).

### Results and discussion

During spectrometric measurements the reactions of individual species with monuron was studied (Figure 1.). In the UV spectra of monuron there is a well-resolved absorption band at 245 nm. This band is the characteristic excitation band for aromatics. During  $\gamma$ -radiolysis, this band decreases with increasing dose. When  $\bullet\text{OH}$  reacts with monuron, a new band can be observed between 270 and 320 nm. This band may belong to the hydroxylated versions of monuron [7-8]. In both  $\bullet\text{OH}$  and the  $e_{aq}^-$  reactions, a slight shift of absorption band at 245 nm can be seen to shorter wavelength due to the dehalogenation.

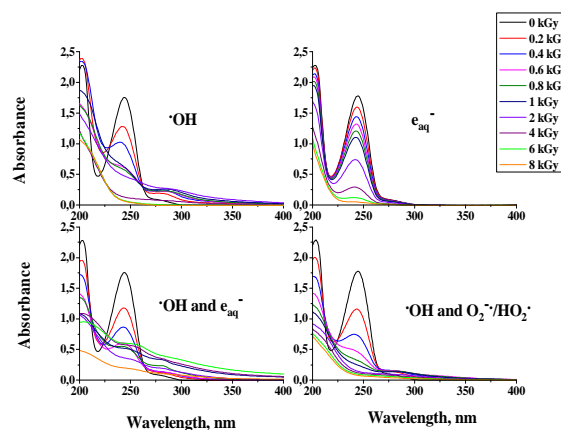


**Figure 1.** Absorption spectra of  $1 \times 10^{-4} \text{ mol dm}^{-3}$  monuron irradiated with 0–8 kGy doses: (a) in  $\text{N}_2\text{O}$  saturated, (b) in  $\text{N}_2$  saturated containing 5 vol. % TBA, (c) in  $\text{N}_2$  saturated and (d) in aerated solutions.

In pulse radiolysis experiments the reaction between monuron and  $\bullet\text{OH}$  was investigated (Figure 2.). In the transient spectra the absorption bands between 300–400 nm and above 400 nm showed time dependence. Based on this spectra, we assumed that there are least 2 intermediates in this reaction. The absorption band between 300 and 400 nm may belong to the hydroxycyclohexadienyl type radical. The measurements were also repeated in the presence of  $1 \times 10^{-4} \text{ mol dm}^{-3} \text{ K}_3\text{Fe}(\text{CN})_6$ ,  $\text{Fe}(\text{CN})_6^{3+}$  reacts OH adduct forming corresponding phenolic compound [9]. The spectra clearly indicated the peak at 350 nm belonging to the OH adduct. The band above 400 nm with a maximum at 450 nm may be due to the phenoxyl or aminyl type radicals. It will be show later phenoxyl radical formation is more probable than aminyl radical formation. The rate coefficients of the reaction between monuron and  $\bullet\text{OH}$ , as well as monuron and  $e_{aq}^-$  were determined to be (Figure 2. Inset):  $2.1 \pm$

$0.9 \times 10^9 \text{ mol}^{-1} \text{ dm}^3 \text{ s}^{-1}$  and  $7.4 \pm 0.2 \times 10^9 \text{ mol}^{-1} \text{ dm}^3 \text{ s}^{-1}$ , respectively. Based on the rate coefficients, the electron withdrawing effect of chlorine atom increases the rate of nucleophile reaction and decreases that of electrophile reaction compared to other phenylureas [10].

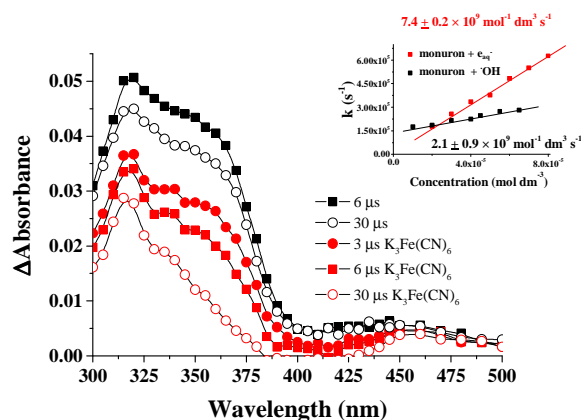


**Figure 2.** Transient absorption spectra of  $1 \times 10^{-4} \text{ mol dm}^{-3}$   $\text{N}_2\text{O}$  saturated monuron solution 6 and 30  $\mu\text{s}$  after the electron pulse, and also with  $1 \times 10^{-4} \text{ mol dm}^{-3}$   $\text{K}_3\text{Fe}(\text{CN})_6$  added to the previous solution 3, 6 and 30  $\mu\text{s}$  after the electron pulse. Inset: Concentration dependence of the pseudo-first-order rate coefficient of absorbance build-up

The rate of oxidation and mineralisation can be described by COD and TOC measurements (not shown). We can get some information on the fate of N-atoms in the molecule based on TN tests. In irradiated samples COD and TOC values decrease due to the oxidation (not shown). The efficiency of oxidation can be characterized by the ratio of rate of oxidation and the number of moles of  $\cdot\text{OH}$  injected into  $1 \text{ dm}^3$  solution [11]. Based on this, one-electron-oxidant  $\cdot\text{OH}$  finally leads to  $\sim 4.4$  electron oxidations. TN value changes just slightly with the absorbed dose which shows that the larger part of N-atoms remain in the solution as organic or inorganic nitrogen compounds during  $\gamma$ -radiolysis.

To follow up dechlorination processes, chloride release and the AOX content were measured (Figure 3.). Based on results, the most intense chloride release was observed in aerated solutions in the first stage of degradation. Above 4 kGy, chloride release was higher in  $\cdot\text{OH}$  reactions. The chloride release in  $\cdot\text{OH}$  reaction is assumed to be due to radical addition to the carbon atom with chlorine, and by HCl elimination from the adduct, in the reaction a phenoxy radical also forms.

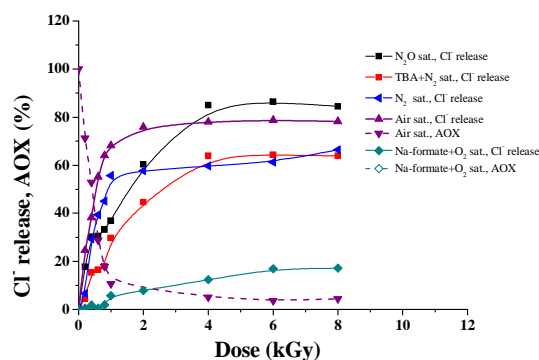


**Figure 3.** Chloride release in different solutions and AOX in air saturated solution ( $1.1 \times 10^{-4} \text{ mol dm}^{-3}$ ) and in oxygen saturated Na-formate containing solution.



The presence of hydrated electron in the reaction mixture promotes dehalogenation processes. In addition to change of adsorbable organic chlorine content was measured in air saturated solutions because the highest in chloride release yield was observed under these conditions. The results showed that complete dehalogenation may take place during the reactions.

The identification of final products was carried out in aerated solution at 0.5 kGy dose. 10 end-products were identified. Particularly, hydroxylated versions of monuron form. During the decomposition of monuron,  $\bullet\text{OH}$  may react with both aromatic ring and methyl group on the terminal N-atom. Based on the distribution of products, the main reaction takes place between  $\bullet\text{OH}$  and aromatic ring. Dechlorination processes may occur through OH/Cl substitution or phenoxyl radical formation. Phenoxyl radical formation have some contribution to the phenol type products formation and ring fragmentation in the presence of dissolved oxygen.

### Conclusion

$\gamma$ -irradiation is a very effective method for the decomposition of monuron. During decomposition, hydroxylated molecules form through hydroxycyclohexadienyl type radical intermediates. In  $\text{N}_2\text{O}$  reactions phenoxyl and aminyl type radicals also take part in the degradation. The presence of chlorine atom in monuron increases the rate of oxidation and the efficiency of decomposition. During decomposition, dechlorination processes occur through phenoxyl radical formation and/or OH/Cl substitution.

### Acknowledgements

The authors thank Hungarian Science Foundation (OTKA, NK 105802), the Swiss-Hungarian project (No SH7/2/14) and International Atomic Energy Agency (Contract No. 16485 and HUN8008) for the support. The International Atomic Energy Agency is thanked for financing scientific training of Dr. He. Finally, the authors thank University of Szeged for the AOX measurements.

### References

- [1] J. W. Eichelberger, J. J. Lichtenberg, Persistence of pesticides in river water. *Environ. Sci. Technol.* 5 (1971) 541–544.
- [2] N. H. Spliid, B. Kjøppen, *Chemosphere* 37, (1998) 1307-1316.
- [3] J. A. Field, R. L. Reed, T. E. Sawyer, M. Martinez, *J. Agric. Food Chem.* 45 (1997) 3897-3902.
- [4] E. M. Thurman, K. C. Bastian, T. Mollhagen, *Sci. Total Environment* 248 (2000) 189-200.
- [5] N. N. Ragsdale, R. E. Menzer, *Carcinogenicity and Pesticides: Principles, Issues, and Relationships*. American Chemical Society, Washington, DC (1989).
- [6] M. Bobu, S. Wilson, T. Greibrokk, E. Lundanes, I. I. Siminiceanu, *Chemosphere* 63 (2006) 1718–1727.
- [7] K. Kovács, V. Mile, T. Csay, E. Takács, L. Wojnárovits, *Environ Sci Pollut Res.* 21: (2014) 12693–700.
- [8] K. Kovács, S. He, V. Mile, T. Csay, E. Takács, L. Wojnárovits, *Chemistry Central Journal.* 9:21 (2015) doi:10.1186/s13065-015-0097-0.
- [9] S. C. Choure, M. M. M. Bamatraf, B. S. M. Rao, Ranjan Das, H. Mohan, J. P. Mittal, *Phys. Chem. A* 101 (1997) 9837-9845.
- [10] L. Wojnárovits, E. Takács, *Radiat Phys Chem.* 96 (2014) 120–34.
- [11] R. Homlok, E. Takács, L. Wojnárovits, *Chemosphere* 91 (2013) 383–389.

## Az Oldható Elemtartalmak Változása Meszes Csernozjom Talajon Beállított Nehézfém Terheléses Szabadföldi Tartamkísérletben

Szabó Anita, Pokovai Klára, Rékási Márk, Csathó Péter, Kádár Imre, Lehoczky Éva

*Talajtani és Agrokémiai Intézet, Agrártudományi Kutatóközpont, Magyar Tudományos Akadémia, 1022 Budapest, Herman Ottó út 15.  
e-mail: szabo.anita@agrar.mta.hu*

### Abstract

The 1<sup>st</sup> to 18<sup>th</sup> year changes in the easily soluble element contents (NH<sub>4</sub>-acetate + EDTA) were investigated in the ploughed layer of a long-term heavy metal load field trial, set up on a Mezőföld calcareous chernozem soil in Hungary, in Spring 1991. The thirteen potentially harmful elements (Al, As, Ba, Cd, Cr, Cu, Hg, Mo, Ni, Pb, Se, Sr, Zn) were applied at the beginning of the experiment in soluble salt forms, in 0/30, 90, 270, 810 kg·ha<sup>-1</sup> element doses. The easily soluble element contents decreased sharply in the first years, which was followed by an equilibrium at a low concentration level. Cadmium was the only exception, which element, even in the 18<sup>th</sup> year after application, showed equilibrium at relatively high, around 100 mg·kg<sup>-1</sup> LE-Cd level.

Soil analyses were accompanied by young plant analyses, as well as main product and by-product harvested crop analyses. In certain years, household animal feeding experiments were also carried out for investigating the behaviour of the heavy metals in the food chain.

### Bevezetés

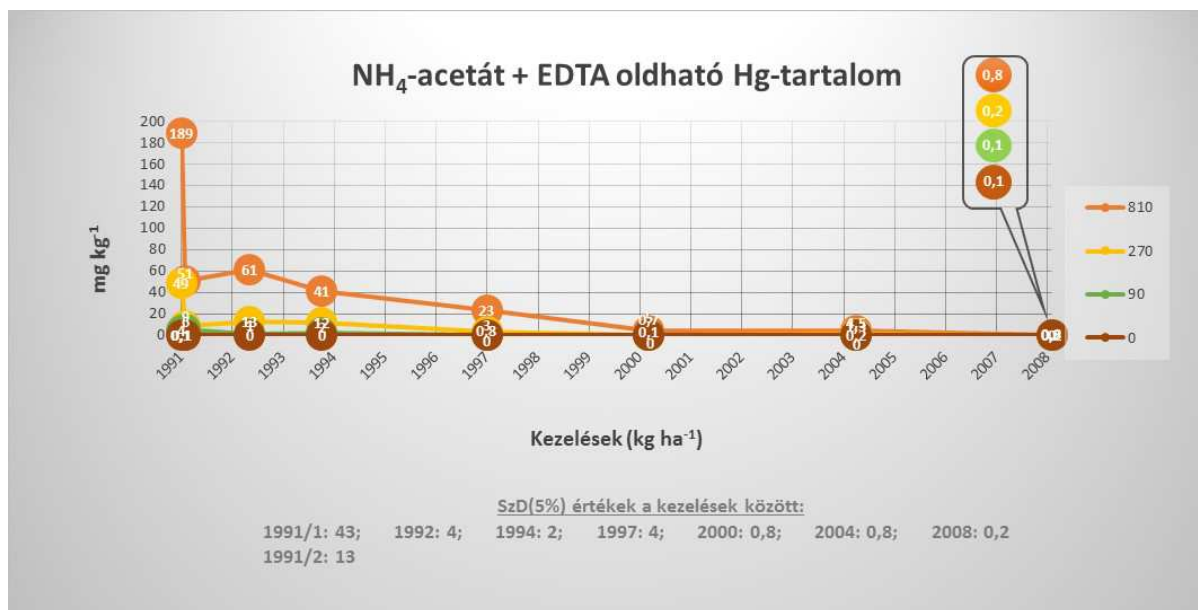
A talajok, a tápláléklánc nehézfém-forgalmának vizsgálatát megkülönböztetett figyelem kíséri az utóbbi években: egyfelől a környezetvédelmi szemlélet térnyerése következtében mind a tudományos kutatás, mind a közvélemény területén, másfelől pedig az analitikai módszerek a műszeres vizsgálatok fejlődése nagyobb pontossága következtében [1, 2, 3, 4, 5].

### Anyag és módszer

Mezőföldi meszes csernozjom talajon, az MTA ATK TAKI Nagyhörcsöki kísérleti telepén, tizenhárom potenciális toxikus elem (Al, As, Ba, Cd, Cr, Cu, Hg, Mo, Ni, Pb, Se, Sr, Zn) oldható sójának 0/30, 90, 270, 810 kg/ha elemtartalom adagjával 1991 tavaszán beállított szabadföldi nehézfém terheléses kísérletben vizsgáltuk a talaj könnyen oldható (NH<sub>4</sub>-acetát + EDTA, [6]) elemtartalmainak 1-18. évi változását a szántott rétegben. Egyes években az „összes” (cc. HNO<sub>3</sub> + cc. H<sub>2</sub>O<sub>2</sub>) elemtartalmakat is meghatároztuk, illetve mélységi talajmintavételekre is sor került az egyes elemek mélységi elmozdulásának tanulmányozására.

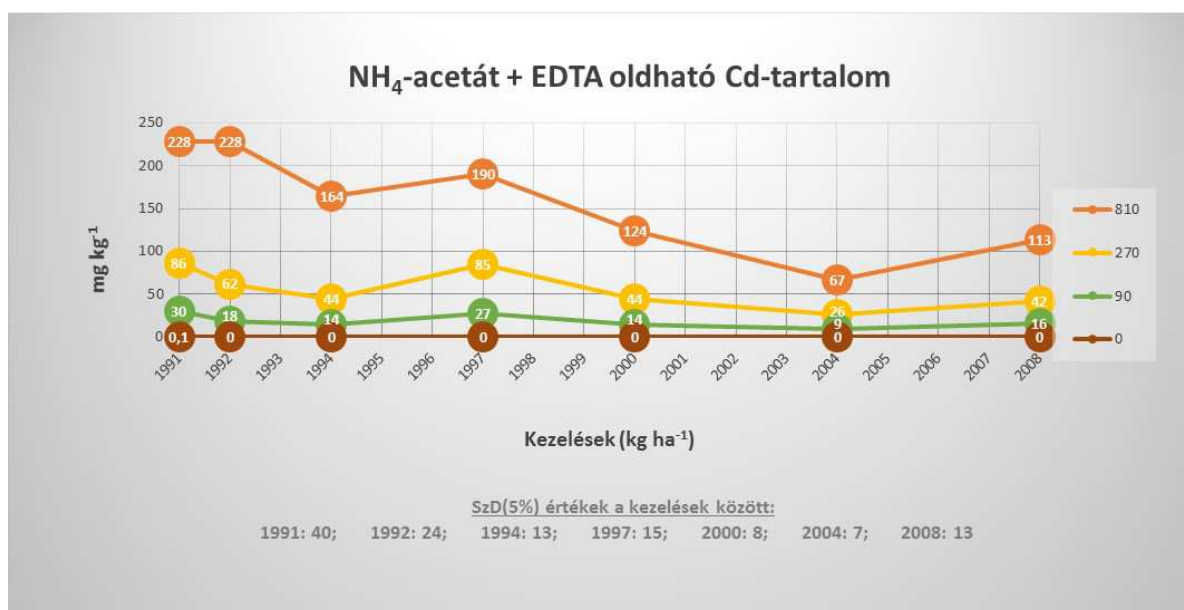
### Eredmények és értékelésük

A talaj szántott rétegében az oldható elemtartalmak a legtöbb elemnél előbb erőteljes csökkenést, majd, alacsony koncentrációnál egyfajta egyensúlyi állapotot mutattak. Ez alól talán a Cd volt kivétel, amely elem még a 18. évben is nagy, 100 mg/kg körüli LE-oldható elemtartalmaknál jelezte az egyensúlyi állapotot. A könnyen oldható elemtartalmak változása alapján tehát az elemek két fő csoportba voltak sorolhatók. Az elemek 1. csoportbeli viselkedését a Hg példáján, a 2. csoportbelit a csoportot egyedülként képviselő Cd példáján szemléltetjük (1. és 2. ábra).



**1. ábra:** A talaj LE-oldható Hg-tartalmának változása a kísérlet 1-18. évében.  
Meszes csernozjom, Nagyhorcsók, 1991-2008.

A 810 kg/ha adagú terhelés 18. évi utóhatásában az alábbi LE-oldható elemtartalmakat mértünk: As: 24 mg/kg (a kontrollon <0,1); Ba: 69 (20) mg/kg; Cd: 113 (<0,1) mg/kg; Cr: 1,5 (<0,1) mg/kg; Cu: 105 (4) mg/kg; Hg: 0,8 (0,1) mg/kg; Mo: 30 (<0,1) mg/kg; Ni: 55 (3) mg/kg; Pb: 99 (5) mg/kg; Se: 1,9 (0,1) mg/kg; Sr: 110 (31) mg/kg, és Zn: 59 (2) mg/kg.



**2. ábra:** A talaj LE-oldható Cd-tartalmának változása a kísérlet 1-18. évében.  
Meszes csernozjom, Nagyhorcsók, 1991-2008.

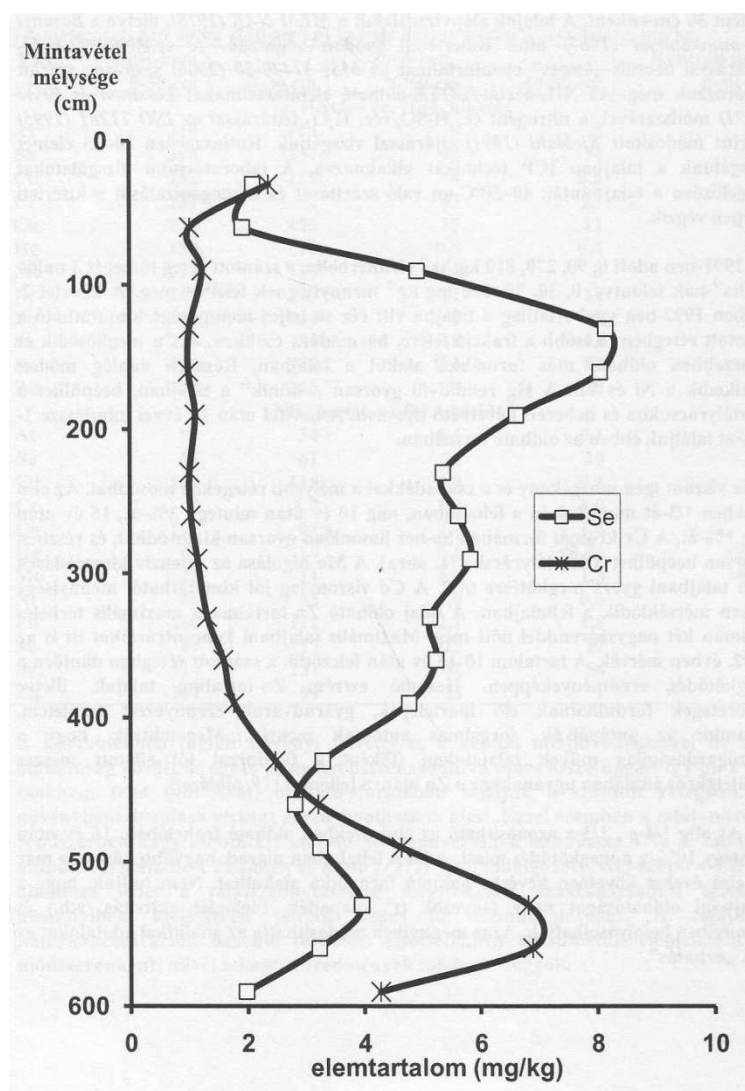
A 18. évben tehát a talaj könnyen oldható elemtartalmakban a kontrollhoz képest a Ba, és a Sr még mindig mintegy három-négyszeres, a Hg mintegy nyolcszoros, a Cr mintegy tizenötszörös, a Pb, az Se és a Ni mintegy húszszoros, a Cu mintegy huszonötszörös, a Zn mintegy harmincszoros, az As mintegy kétszázötvenszörös, a Mo mintegy háromszázszoros, míg a Cd több mint ezerszeres (!) többleteket mutattak. A talaj nagy természetes Al-tartalma következtében már a 3. évben is csupán 20 %-os növekedést lehetett kimutatni a LE-oldható

Al-tartalmakban, mely különbség a későbbi években minimálisra csökkent.

A kísérlet 3. évében a szántott rétegben átfogó vizsgálatokat végeztünk mind az „összes” (cc.  $\text{HNO}_3$  + cc.  $\text{H}_2\text{O}_2$ ), mind a könnyen oldható ( $\text{NH}_4$ -acetát + EDTA, [6]) elemtartalmak vonatkozásában. Mindkét módszernél meghatároztuk az un. visszamérési %-ot, azaz hogy a 3. évben a kísérlet beállításakor kijuttatott elem mennyiségek hány %-a volt az „összes”, illetve a könnyen oldható formában kimutatható.

Ami az „összes” tartalmakat illeti látható, hogy – a szórásokat figyelembe véve – a kísérlet 3. évében az átlagos visszamérhetőségi sorrend az alábbi: Pb, Sr, Ba, Ni, Zn, Cu, Se, As, Hg, Cr, Cd, Mo, Al. Azaz, a talajba jutott szennyező elemek közül 1994-ben (3 év után) a szántott rétegben kimutatható: Pb, Sr, Ba, Ni, Zn 90 % felett; Cu, Se, As, Hg 60–90 % között; Cr, Cd, Mo 30–60 % között; míg az Al 10 % alatt.

A könnyen oldható tartalmakat illetően, szintén a kísérlet 3. évében, az átlagos visszamérési sorrend az alábbiak adódott: Pb, Sr, Cu, Zn, Cd, Ni, Se, Ba, As, Hg, Mo, Cr, Al. Azaz a talajba jutott szennyező elemek közül 1994-ben a szántott rétegben kimutatható: Pb 90 % felett; Sr és Cu 60–90 % között; Zn, Cd, Ni, Se 30–60 % között; Ba, As, Hg 10–30 % között; míg a Mo, Cr és Al 10 % alatt.



**3. ábra:** A talaj szelvény LE-oldható Cr-, illetve Se-tartalmának változása a kísérlet 15. évében a legnagyobb, 810 kg/ha elemterheléses kezelésben.

Meszes csernozjom, Nagyhörcsök, 2005.

A könnyen oldható só formájában kijuttatott 13 elem mélységi elmozdulásáról szintén a 3. évben végeztünk átfogó vizsgálatokat a 0-20, 20-40, és 40-60 cm rétegekben. Ezek alapján az Al lemosódását kizárhatónak, az As-t, Ba-t, Cu-t, Hg-t, Mo-t, Ni-t, Se-t, Sr-t, Zn-t kérdésesnek, a Cd-t és a Pb-t valószínűnek, a Cr-t kifejezettnek nyilvánítottuk.

A kísérlet 15. évében a 0-6 m mélységig elvégzett vizsgálatok ugyanakkor azt jelezték, hogy a Cr mellett a Se lemosódása is kifejezett volt, hiszen még a 6 m-es mélységben is kimutathatók voltak ezek az elemek (Se: 2 mg/kg; Cr: 4 mg/kg). A kontroll kezelésekben ez a két elem <0,1 illetve 0,2 mg/kg értékeket mutatott a teljes szelvényben (**3. ábra**).

### **Következtetések**

Annak ellenére, hogy a jogszabályokban a talajok „összes” elemtartalmára találunk határértékeket [7], fontos lehet a könnyen oldható elemtartalmak ismerete is. Ez utóbbiak vélhetően szorosabb összefüggéseket mutathatnak a fitotoxicitás mértékével, a potenciálisan káros elemek növényi felvételével, táplálékláncon belüli viselkedésével. Mivel kísérletünkben mértük a betakarított termések mennyiségét, illetve fiataalkori, illetve betakarításkori növényvizsgálatokra is sor került, a későbbiekben a talaj könnyen oldható elemtartalmi és a termés mennyiségek, illetve a talaj könnyen oldható elemtartalmi és a növény által felvett elem mennyiségek/koncentrációk közötti összefüggések vizsgálatával ezen könnyen oldható talajvizsgálati eredmények még jobban értelmezhetővé válnak.

### **Köszönetnyilvánítás**

A nehézfém-terheléses szabadföldi tartamkísérlet beállítására a Környezetvédelmi és Területfejlesztési Minisztérium anyagi támogatásával került sor.

### **Irodalom**

- [1] D.C. Adriano, Trace elements in the terrestrial environment. Springer-Verlag, New York – Berlin – Heidelberg – Tokyo, 1986, pp. 533.
- [2] B. J. Alloway, Heavy Metals in Soils. Blackie & Son, Ltd. London, 1990, pp. 339.
- [3] P. Csathó, A környezet nehézfém szennyezettsége és az agrártermelés. MTA TAKI. Budapest, 1994, pp. 176.
- [4] I. Kádár, A talaj-növény-állat-ember tápláléklánc szennyeződése kémiai elemekkel Magyarországon. MTA TAKI. Budapest, 1995, pp. 388.
- [5] I. Kádár, A főbb szennyező mikroelemek környezeti hatása. MTA ATK TAKI. Budapest, 2012, pp. 360.
- [6] E. Lakanen, R. Erviö, A comparison of eight extractants for the determination of plant available microelements in soils. Acta Agr. Fenn. 123 (1971) 223.
- [7] 10/2000. (VI. 2.) KÖM–EüM–FVM–KHVM együttes rendelete a felszín alatti víz és földtani közeg minőségi védelméhez szükséges határértékekről. Magyar Közlöny. 53 (2000) 3156.



## Cisztein Tartalmú Oligopeptid Toxikus Fémionokkal Való Kölcsönhatásának Vizsgálata Analitikai Felhasználás Céljából

Szekeres Levente István, Jancsó Attila, Bálint Sára, Tóth Anikó

Szegedi Tudományegyetem, Szervetlen és Analitikai Kémiai Tanszék,  
6720 Szeged, Dóm tér 7.  
slevente@chem.u-szeged.hu

Napjainkban a szenzorfejlesztéssel kapcsolatos kutatások fő irányvonala a minél kompaktabb, egyszerű, laboratóriumi környezeten kívül is alkalmazható technikák fejlesztése. Egyik fontos feladat ezen belül a különböző toxikus fémionok kimutatása, melyek természetes előfordulásukon túl számos emberi eredetű szennyező forrásból is a környezetbe kerülhetnek, ahonnan a humán szervezetbe jutva különböző akut és krónikus káros hatásokat indukálásért felelősek. Érzékelésük megoldható lehet toxikus fémionok erős és szelektív megkötésére képes biomolekula receptorokat tartalmazó kemoszenzorok segítségével. A számos fémion szállító-, illetve fémion-kötő fehérjében megtalálható CXXC motívum alapján egy rövid, terminálisan védett oligopeptidet terveztünk. A toxikus fémionok tiol csoportokhoz fűződő nagy affinitása miatt, elsősorban a Cys oldalláncok esetében számíthatunk koordinációra, melynek kialakulását a Tyr aminosav fluoreszcens jelének változásán keresztül terveztük követni.

A peptid kölcsönhatását higany(II), kadmium(II) ionokkal, illetve arzénessavval ( $\text{H}_3\text{AsO}_3$ ) kívántuk megvizsgálni. A kölcsönhatásokat pH-potenciometria, fluorimetria, UV-,  $^1\text{H}$ -NMR, szinkrotron radiációs CD spektroszkópia módszerekkel vizsgáltuk.

Cd(II) ionokkal számottevő kölcsönhatás csupán pH = 3,5 értéktől volt megfigyelhető. A fluoreszcens kvencselés nem lineárisan nő a fémion - ligandum aránnyal. A trendben jelentős mértékű törés észlelhető kétszeres ligandumfeleslegnél, ami a monokomplexek mellett biszkomplexek képződését támasztja alá.

A Hg(II) esetében megállapítottuk, hogy már egészen savas pH-tól kiemelkedő stabilitású Hg(II):DY = 1:1 összetételű komplexek képződnek, melyek magasabb pH értékeken négyes koordinációs számú biszkomplexszé alakulnak tetraéderes szimmetriával elrendeződő donatoratomokkal. Fluorimetriás mérésekkel kimutattuk, hogy a fémion kötődése koncentráció arányos fluoreszcencia csökkenést eredményez 1:1 fémion:ligandum arányig pH = 2 - 6 tartományban, mely jelenség alkalmassá teheti a rendszert Hg(II) ionok detektálására.

Az arzénessav és DY között szintén kimutatható volt mérsékelt kölcsönhatás. Savas körülmények között a komplexképződés lassú. A koordináció még pH = 7,0, 1:1 összetétel mellett, 1mM koncentrációban sem teljes, így a rendszert alkalmatlannak találtuk fluorimetriás mérések kivitelezésére.

A potenciális receptorként való alkalmazhatóság tesztelése céljából a DY peptidet szilárd gyanta, üveg, illetve kvarc hordozón rögzítve is előállítani kívántuk, melynek kivitelezése még folyamatban van.



## **Poster Proceedings**

## Pollution from Meat Processing Factories

**Dragan Adamović<sup>1\*</sup>, Mirjana Vojinović- Miloradov<sup>1</sup>, Jelena Radonić<sup>1</sup>, Maja Turk-Sekulić<sup>1</sup>, Savka Adamović<sup>2</sup>**

<sup>1</sup>*Department of Environmental Engineering and Occupational Safety and Health, Faculty of Technical Sciences, University of Novi Sad, 21000 Novi Sad, Trg Dositeja Obradovića 6, Serbia*

<sup>2</sup>*Department of Graphic Engineering and Design, Faculty of Technical Sciences, University of Novi Sad, 21000 Novi Sad, Trg Dositeja Obradovića 6, Serbia*  
*e-mail: draganadamovic@uns.ac.rs*

### Abstract

A basic understanding of the nature of meat plant wastewaters and factors that influence these wastewaters is essential for the control of wastewater volume and waste loads. Analyzing waste characteristics of the meatpacking industry is not a simple matter. It is difficult to characterize a “typical” plant and its associated wastes, owing to the many procedures and facets of meat-processing operations. However, some similarities have emerged during extensive study and research.

**Key words:** Meat industry, wastewater, solid waste, waste gas stream

### Introduction

Key resources used by the meat processing industry include: water, raw materials and energy. The meat processing industry uses large quantities of water. Water is used as a component of final products, an initial and intermediate cleaning source, an efficient transportation conveyor of raw materials, and the principal agent used in cleaning of plant machinery and areas. Although water use will always be a part of the meat processing industry, it has become the principal target for pollution prevention. The quantity of processing wastewater and its general quality, are both economic and environmental factors in the treatability and disposal of wastewater [1].

The waste load from a meat processing plant is a result of blood, flesh particles, soluble proteins and waste materials which are intentionally or inadvertently released to the sewer system. There are three proven ways to reduce waste load as well as water use and wastewater discharge. First is to operate the plant more efficiently. Second is to make process modifications to reduce water use and waste, and third is to consider pretreatment steps to reduce the waste load.

Water, sewer and overload costs are significant to any meat plant. Well-trained employees, modern technology and management support are necessary to achieve cost reduction through reduced use of water and generating fewer amounts of waste.

Water is a basic and necessary tool for the meat industry. In meat processing and quality control, water helps to cleanse the product and remove unwanted materials. But in wastewater handling, water flushes organic and inorganic matter to the sewer. Wastewater treatment is basically a processing system to separate the organic and inorganic matter from the water that collected it. Thus, keeping organic and inorganic matter out of the water eliminates the necessity for treatment. The goal of every wastewater engineer is to remove organic solids without discharging them to the sewer, and to use an absolute minimum of water for the essentials of sanitation.

### **Meat processing wastewaters**

The meat industry is a branch of the food industry, which causes degradation of the environment to a large extent. The wastewater produced in it contains a variety of organic and inorganic pollutants, has a high concentration of etheric extract, suspended and biogenic matter as well as variable concentrations. A basic understanding of the nature of meat plant wastewaters and factors that influence these wastewaters is essential for the control of wastewater volume and waste loads.

Typical slaughterhouse and packing house wastes are generally high in 5-day biochemical oxygen demand (BOD<sub>5</sub>), chemical oxygen demand (COD), total suspended solids (TSS), floatable material and grease (FOG). The amounts of wastewater generated and pollutant load depend on the kind of meat being manufactured.

Chemical oxygen demand (COD) and biochemical oxygen demand (BOD<sub>5</sub>) are common measurements used to determine water quality. They measure the strength of the waste stream by measuring the oxygen required to stabilize the wastes. COD and BOD<sub>5</sub> are important to the meat processing industry because they can be used to indicate lost product and wasteful practices. High BOD<sub>5</sub> and COD levels indicate increased amounts of product lost to the waste stream. Measurements at various process locations can help locate sources of waste. [2]

The waste is usually at an elevated temperature and may contain organic material: blood, bits of flesh, fat, manure, dirt and viscera. It may contain pathogens, including Salmonella and Shigella bacteria, parasite eggs, and amoebic cysts. Pesticide residues may be present from treatment of animals or their feed. Chlorides, phosphorus and nitrogen compounds are also found in the waste load. Chloride levels may be very high (up to 77,000 mg/L) from curing and pickling processes.

Separation of product from wastes at each stage is essential to maximize product recovery and reduce waste loads. The materials being handled are all susceptible to decay. hence, cleanliness is very important.

Water management should achieve the necessary cleanliness without waste. The amounts and strength of wastes can be reduced by good practices such as dry removal of solid waste and providing screens on wastewater collection channels [3].

The principal operations and processes in meatpacking plants where wastewater originates are:

- Animal holding pens
- Slaughtering
- Cutting
- Meat processing
- Secondary manufacturing (by-product operations)
- Cleanup operations

In-plant measures such as the following can be used to reduce the odor nuisance and generation of solid and liquid wastes from the production processes:

Recover and process blood into useful byproducts [4,5]. Allow enough time for blood draining. By reducing the volume of blood lost to the effluent stream by only 100L each day, a meat plant disposing of its effluent by land application could reduce the land area required by 2.5 ha. This blood, if recovered for blood processing, also represents a gain in product revenue. Blood recovery, grease recovery, separate paunch manure handling and efficient rendering operations can reduce waste loads substantially and may also produce salable by-products.

Minimize water consumed in the production processes, for example, by the use of taps with automatic shut-off, the use of high water pressure and improvement of the process lay-out.

Reduce the liquid waste load by preventing all solid wastes and all concentrated liquids from entering the wastewater stream by covering collection channels in the production area with

grids to reduce the amount of solids entering wastewater.

Separate cooling waters from process and waste waters and recirculate cooling water.

Implement dry pre cleaning of equipment and production areas prior to wet cleaning. Dry cleaning methods should be used to collect the solids as close to source as possible this maximizes recovery for rendering. Dry cleaning before hosing down the floor will reduce the amount of water used for cleaning.

Equip the outlets of wastewater channels with screens and fat traps, to recover and reduce the concentration of coarse material and fat in the combined wastewater stream. Optimize the use of detergents and disinfectants in washing water.

Remove manure from the stockyard and from intestine processing in solid form.

For meat plants that do not carry out on-site rendering, blood processing or other major by product processing operations, it is estimated that the feces and gut contents would typically account for more than 75% of the phosphorous and 50% of the nitrogen, sodium and organic loading in primary screened or settled effluent from the plant.

Odor reduction is the most important air pollution issue in rendering plants and can be achieved by: minimizing the stock of raw material and storing it in a cold, closed, well-ventilated place. Pasteurization the raw material before processing it in order to halt biological processes that generate odor. Installing all equipment in closed spaces and operating under partial or total vacuum. Keeping all working and storage areas clean.

### **Treatment Technologies**

Choice of technology for treatment of waste water is not an easy and irresponsible task. Industrial wastewater components show different degrees of environmental nuisance and contamination hazard due to their chemical characteristics as well as excessive concentration. Therefore, the treatment of wastewater, which is particularly hazardous to the environment, requires a number of complementary techniques that sufficiently remove pollutants and enable the wastewater to be discharged into receiving water or be reused for industrial purposes. Abattoirs and the meat processing industry use a huge amount of water. The whole chain from cattle delivery, slaughtering and processing to the final cleaning is subject to strict hygiene regulations. That is why large amounts of wastewater accrue that is highly polluted with organic substances- containing blood and dissolved proteins, fat, straw, sawdust and residues of animal excrements. Since the wastewater contains substantial amounts of proteins, it putrefies easily and gives off nasty smells. Especially if this wastewater cannot be disposed fast and reliably, germs and insect attacks, threatens the plant.

The wastewaters of meat processing industry are suitable for biological treatment and (except for the very odor rendering wastewater) could be discharged to a municipal sewer system after flow equalization if the capacity exists. Especially abattoirs have to deal with unpleasant smells due to the accrual of ammonia and hydrogen sulphide as well as the accumulation of solids from deposition. Oftentimes this leads to complaints from residents and the formation of action groups targeting the companies. Sewage authorities usually require pretreatment of the wastewater before its discharge into the sewer. Mechanical pre-cleaning is very important, particularly for municipal wastewater, in order to ensure the efficient functioning of the wastewater technology in the following treatment steps. The pre-cleaning will prevent blockages and damages and thus unnecessary maintenance schedules and superfluous cost. Screens and fat traps are the minimum level of pretreatment in any system.

If the wastewater contains water-insoluble substances or colloids, for instance, sedimentation, filtration or centrifugal separation becomes necessary to achieve efficient wastewater treatment. Flotation (in some cases aided by chemical addition) may also be provided to remove suspended solids and emulsified fats, which can be returned to the rendering plant. The choice of an appropriate biological treatment system will be influenced by a number of

factors, including wastewater load and the need to minimize odors. Rendering wastewater typically has a very high organic and nitrogen load and extended aeration is an effective form of treatment, but care must be taken to minimize odors.

Disinfection of the final effluent may be required if high levels of bacteria are detected. Ponding is a simple solution but requires considerable space. Chemical methods, usually based on chlorine compounds, are an alternative.

Biofilters, carbon filters, and scrubbers are used to control odors and air emissions from several processes including ham processing and rendering. Recycle of exhaust gases from smoking maybe feasible in cases where operations are not carried out manually and smoke inhalation by workers is not of concern.

## Conclusion

Production of wastes during the processing of meat products is not desirable because it significantly deteriorates the quality of the final product as well as causes some serious health threats if not properly disposed-off. The majority of the waste, in the meat industry is produced during slaughtering. The composition of waste generated by the meat industry depends on species of animals slaughtered. The waste material of the meat processing industry contains plentiful amount of organic compounds due to which its disposal is quite difficult. Efficient utilization of by-products has direct impact on the economy and reduce environmental pollution.

Meat by-products have been used all over the world since decades but due to certain health concerns there is need to develop new technologies for safe processing and efficient utilization. This is also very important to develop meat by-products with maximum cost-benefit ratio in the future for the viability of meat industry. Additionally, more research is needed to develop some innovative methods for the treatment of meat industry wastes. Moreover, modern extraction methods such as solvent extraction, microfiltration, solid phase extraction and super critical fluid extraction should be applied to extract several bioactive compounds from the effluents of the meat processing industries.

Wastewater from the meat industry is very difficult to purify due to its specific characteristics, irregular scatter, and considerable amounts of organic, mineral and biogenic matter. It can also be satisfactorily treated so that it can be reused in the production cycle of a plant. In addition to wastewater management, this study promotes good practice in the management of gas and solid waste stream in meat processing industry. This system has considerable advantages in terms of environmental protection, power savings and cost-effectiveness.

## Acknowledgements

*This research was supported by Ministry of Education, Science and Technological Development, Republic of Serbia (III46009).*

## References

- [1] M. Cosmin, A. Florin, Assessing the power generation solution by thermal chemical conversion of meat processing industry waste. *Energy Procedia*, 50, (2014) 738–743.
- [2] V. Elaine , L.S. Robson, A. Waldir, A.A. Chtistine, S. Maurício, F.P.M. Regina, Organic solid waste originating from the meat processing industry as an alternative energy source. *Energy*, 36, (2011) 3897–3906.
- [3] I.S. Arvanitoyannis, D. Ladas, Meat waste treatment methods and potential uses. *International Journal of Food Science and Technology*, 43, (2008) 543–559.
- [4] A.O. Jack, P.H. Yun-Hwa, Blood-derived products for human consumption. *Revelation and Science*, 1, (2011) 14–21.

[5] W. Russ, R.M. Pittroff, Utilizing waste products from the food production and processing industries. *Critical Reviews in Food Science and Nutrition*, 44, (2004) 57–62.



## The Combined Electrocoagulation/Flotation and Adsorption Processes for Organic Substances Regeneration of Waste Printing Developer

Savka Adamovic<sup>1</sup>, Miljana Prica<sup>1</sup>, Bozo Dalmacija<sup>2</sup>, Jelena Trickovic<sup>2</sup>, Marijana Kragulj<sup>2</sup>, Snezana Maletic<sup>2</sup>, Dragan Adamovic<sup>1</sup>

<sup>1</sup>University of Novi Sad, Faculty of Technical Sciences, Trg Dositeja Obradovica 6, 21000 Novi Sad, Serbia

<sup>2</sup>University of Novi Sad, Faculty of Sciences, Trg Dositeja Obradovica 3, 21000 Novi Sad, Serbia

e-mail: adamovicsavka@uns.ac.rs

### Abstract

This paper investigates the possibility of reducing the content of organic substances in waste printing developer using a combination of electrocoagulation/flotation (ECF) and adsorption (AD) processes. The content of organic substances in waste printing developer was monitored by analysis of total organic carbon (TOC), chemical oxygen demand (COD) and biological oxygen demand (BOD<sub>5</sub>) before and after the ECF and AD processes, respectively. When combining the two processes, a removal of 99.4, 92.9 and 96.0% of the TOC, COD and BOD<sub>5</sub> was achieved, respectively. Obtained results confirm the improvement in the printing industrial effluent quality and height removal of organic substances by the combined ECF and AD treatments.

**Keywords:** electrocoagulation/flotation, adsorption, treatment, organic substances

### Introduction

The ECF process involves the passage of an electric current into the reaction cell using sacrificial aluminum or iron electrodes. The generation of the metal ions takes place at the anode by dissolving electrically metal electrodes. These ions, at an appropriate pH, can form wide ranges of coagulated species such as corresponding aluminum or iron hydroxides and/or polyhydroxides that destabilize and aggregate the suspended particles or precipitate and adsorb dissolved contaminants. Also, electrooxidation, surface complexation, electrostatic attraction, and chemical modification occur in the ECF reactor. The flocks generated of coagulated species and the pollutants then can be removed using liquid-solid separation methods, such as, settling, flotation, or filtration [1, 2, 3]. The typical benefits of the ECF process are: no liquid chemical is added; alkalinity is not consumed, pH adjustment is not needed, requires less dosage and produces less sludge, the space required for apparatus is small because ECF does not require chemical storage, dilution, and rapid mixing, short reaction time (few minutes), oxidation or reduction of much pollutant, coagulation and flocculation of finest colloids and economic advantages [1, 2].

Research has shown that ECF is an effective treatment for removing pollutants from lowland surface water, urban wastewaters, synthetic colloid-polluted wastes, restaurant effluents, metal plating wastes, actual industrial discharges, cardboard paper mill effluents, etc. [3, 4]. Also, ECF was not used for treatment of waste offset printing effluent such as waste printing developer (WPD). As can be seen, ECF has a wide application field and it can also be effective for complicated wastewater which contains: heavy metals, oils, turbidity, color, bacteria, algae and microorganisms, tannin, dyes, organic matter (BOD and COD), suspended solids, and colloids [3, 5].

Also, the AD is a very well known, effective and commercially applicable water and wastewater treatment process, which is gaining prominence as a means of reducing inorganic

and organic concentrations in industrial effluents [2, 3, 6, 7]. Adsorption has been found to be superior to other techniques for water and wastewater re-use in terms of the initial cost, simplicity of design, ease of operation and insensibility to toxic substances [8]. Activated carbon is one of the commercially applicable and most effective adsorbent, which are remove different types of dyes, organic and inorganic pollutants such as metal ions, phenols, pesticides, chlorinated hydrocarbons, humic substances, PCBs, detergents, organic compounds which cause taste and odor, and many other chemicals and organisms [7]. Nevertheless, as an individual process for treating effluents, AD requires overdoses of the adsorbent. In addition, the regeneration of the activated carbon is very complicated and expensive [3].

In the recent years, the potential of ECF technology for the treatment of industrial effluents is tried to be even further increased by the synergistic combination with other treatment technologies, such as ozonation, adsorption, ultrasound irradiation, and pulses [6]. Barrera-Díaz et al. [6] reported that the use of an ECF treatment in combination with AD take place within the two systems. In the first system ECF treatment was combined with AD as a pre-treatment step to enhance AD capability of adsorbents. Also, this coupling technology has been studied in systems in which an adsorbent used for the fast removal of pollution from wastewater is continuously regenerated using electrolysis.

Materials being used in the printing industry are very diverse and complex and they influence the quality of printing products to a great extent. The knowing of the structure and characteristics of the materials and their exploitative properties conditions the choice of the optimal technological procedure in the printing industry [9]. Also, the characteristics of the waste printing materials have a major impact on the environment. The WPD is expected to contain residual ingredients and products present in the offset plate surface such as organic binders and photo-sensitive compounds. Also, in the preservation process, plate is covered with a thin solution of "gum arabic" or similar chemical. These processes resulted in high amount of organic substances witch were originated from plate surfaces and chemicals [10].

The objective of this paper is to investigate the maximum TOC, COD and BOD<sub>5</sub> removal from WPD by combining ECF and AD treatments. The ECF treatment with iron electrodes, as a pre-treatment, was followed by AD of residual organic substances on commercially powder activated carbon (Norit W35).

## Experimental

### The waste printing developer

In the plate development process, initial printing developer was dispensed in quantities of 100 mL per m<sup>2</sup> of plate. After the development process, the obtained WPD cumulatively was collected in containers of 20 L. The WPD was collected from the offset printing facility in Novi Sad, Republic of Serbia.

### The electrocoagulation/flotation treatment of the WPD

The ECF experiments was performed in a batch cell (borsilicate glass of 250 mL) with four plate iron electrodes (dimensions of 10 cm × 5 cm × 0.1 cm) connected in a parallel (bipolar) mode. Only the outer electrodes have been connected to the DC power supply (DF 1730LCD). The current density of 8 mA cm<sup>-2</sup> was applied for the interelectrode distance of 0.5 cm and operating time of 60 minutes. The ECF treatment was carried out at the ambient temperature (25±1°C), with 220 mL aliquots of the WPD which has been mixed with the 0.5 g of sodium chloride as a conductor. Then the ECF treated WPD was filtered through a set of membrane filtration with Millipore vacuum pump and cellulose nitrate filter (pore size of 0.45µm). Supernatant has then been used for the analyses of TOC, COD and BOD<sub>5</sub>. Before

each run, iron electrodes have been mechanically polished with abrasive paper, rinsed with distilled water, dried, dipped for 10 min in a 5 M solution of hydrochloric acid, rinsed with distilled water, and placed vertically in the ECF cell [10].

### Adsorption treatment of the WPD

The adsorption (AD) treatment were run in duplicate at room temperature ( $25\pm1^\circ\text{C}$ ) in 1100 mL plastic bottle. The amount ( $10\text{ g L}^{-1}$ ) of powder activated carbon (Norit W35) was added to 1L of ECF treated WPD. The head space in bottle was kept at a minimum in order to minimize the loss of compounds during the experiment due to evaporation. The amount of adsorbent (10 g) and the equilibration period of 30 minutes were selected based on a preliminary kinetics experiment which was performed with amount of 5, 10, 15  $\text{g L}^{-1}$ , respectively, and operating times over 6h. The ECF treated WPD was filtered through a set of membrane filtration with Millipore vacuum pump and cellulose nitrate filter (pore size of  $0.45\text{ }\mu\text{m}$ ). Supernatant has then been used for the analyses of TOC, COD and  $\text{BOD}_5$ .

### Analytical procedure and calculation

Measurements of TOC were performed after sample acidification with concentrated hydrochloric acid to  $\text{pH} = 2$  and membrane filtration with cellulose nitrate filter (pore size of  $0.45\text{ }\mu\text{m}$ ). The TOC was measured using an Elementar Germany Liqui TocII analyzer, according to SRPS ISO 8245 (2007) method [11]. For COD determination, calculated from the consumption of  $\text{Cr}_2\text{O}_7^{2-}$ , SRPS P-IV-10 method was used [12]. The  $\text{BOD}_5$  was determined by SRPS EN 1899-1:2009 [13].

The removal efficiencies of investigated parameters (TOC, COD and  $\text{BOD}_5$ ) by ECF or AD treatments were evaluated by the following universal equation [5, 10]:

$$E_x (\%) = \frac{X_o - X_t}{X_o} \times 100 \quad (1)$$

where  $X_o$  – the initial values of investigated parameters in the WPD before of certain treatment (ECF or AD), and  $X_t$  – the final values of investigated parameters in the WPD after of certain treatment.

### Results and discussion

The initial values of TOC, COD and  $\text{BOD}_5$  in the WPD and values of investigated parameters after ECF and AD treatments of WPD are presented in Table 1.

Table 1. The values of TOC, COD and  $\text{BOD}_5$  in the WPD and before and after ECF and AD treatments

Parameter	WPD	ECF treated WPD	AD treated WPD	Efficiency (%)		
				ECF treatment	AD treatment	ECF + AD treatment
TOC ( $\text{mg L}^{-1}$ )	60800	1740	391	97.1	77.5	99.4
COD ( $\text{mg L}^{-1}$ )	21100	11300	1499	46.5	86.7	92.9
$\text{BOD}_5$ ( $\text{mg L}^{-1}$ )	9400	5350	372	43.1	93.0	96.0

The results indicate that the ECF treatment reduces TOC, COD and  $\text{BOD}_5$  values by 97, 46.5 and 43.1%, respectively, which still does not comply with environmental discharge standards. In relation to ECF process, AD process removes almost twice more COD and  $\text{BOD}_5$  values. Thus, additional techniques such as AD are needed to improve the quality of the wastewater.

AD process used as a secondary treatment is effective and requires limited amounts of activated carbon. According to Linares-Hernández et al. [4] the use of an ECF treatment as a pre-treatment step to enhance AD capability of adsorbents can be justified if the resulting industrial wastewater quality expressed as color and COD removal is good. Thus, the coupling of electrochemical and adsorption processes might prove a judicious choice for treating industrial wastewater with mixtures of different types of pollutants [4].

The combined ECF and AD processes are able to eliminate TOC, COD and BOD<sub>5</sub> from printing industry effluent, respectively. The overall elimination reaches of TOC, COD and BOD<sub>5</sub> are 99.4, 92.9 and 96.0%, respectively.

### **Conclusion**

The proposed combined ECF (with iron electrodes) and AD (with activated carbon Norit W35) treatments used in this study excellently reduce the concentration of organic substances in waste printing effluent. The removal efficiency of TOC, COD and BOD<sub>5</sub> from WPD by combined ECF and AD processes are 99.4, 92.9 and 96.0%, respectively. In the future, the combined effect of ECF and AD treatments could be applied to other effluents of printing industry.

### **Acknowledgements**

The authors acknowledge the financial support of the Ministry of Education, Science and Technological Development, Republic of Serbia (Project No. III43005).

### **References**

- [1] Y.M. Cho, G.W. Ji, P.J. Yoo, C.W. Kim, K.B. Han, *Korean J. Chem. Eng.* 25 (2008) 1326.
- [2] Y. Ait Ouaisa, M. Chabani, A. Amrane, A. Bensmaili, *Chem. Eng. Technol.* 36 (2013) 147.
- [3] S. Bellebia, S. Kacha, A.Z. Bouyakoub, Z. Derriche, *Environ. Prog. Sustain. Energy.* 31 (2012) 361.
- [4] I. Linares-Hernández, C. Barrera-Díaz, G. Roa-Morales, B. Bilyeu, F. Ureña-Núñez, J. Hazard. Mater. 144 (2007) 240.
- [5] C.A. Martínez-Huitle, E. Brillas, *Appl. Catal. B.* 87 (2009) 105.
- [6] C.E. Barrera-Díaz, G. Roa-Morales, P. Balderas Hernández, C.M. Fernandez-Marchante, M.A. Rodrigo, *Journal of Electrochemical Science and Engineering.* 4 (2014) 285.
- [7] V.K. Gupta, Suhas J. *Environ. Manage.* 90 (2009) 2313.
- [8] N.V. Narayanan, M. Ganesan, *J. Hazard. Mater.* 161 (2009) 575.
- [9] S. Adamović, M. Prica, J. Radonić, M. Turk Sekulić, S. Pap, *J. Graph. Eng. Des.* 5 (2014) 9.
- [10] S. Adamovic, M. Prica, B. Dalmacija, S. Rapajic, D. Novakovic, Z. Pavlovic, S. Maletic, *Arabian Journal of Chemistry.* (2015), [dx.doi.org/10.1016/j.arabjc.2015.03.018](https://doi.org/10.1016/j.arabjc.2015.03.018).
- [11] SRPS ISO 8245, Water quality - Guidelines for the determination of total organic carbon (TOC) and dissolved organic carbon (DOC), Institute for Standardization of Serbia, Belgrade, Serbia, 2007 (In Serbian).
- [12] S. Škunca-Milovanović, R. Feliks, B. Đurović, *Drinking water. Standard methods for testing hygienic safety.* Federal Office of Public Health, NIP "Economic Review", Belgrade, 1990 (In Serbian).
- [13] SRPS EN 1899-1:2009, Water quality - Determination of biochemical oxygen demand after n days (BOD<sub>n</sub>) - Part 1: Dilution and seeding method with allylthiourea addition.

## **Rabbits *in vivo* Experiments and Hematological Evaluation after Iron Toxicity**

**Mirela Ahmadi<sup>1\*</sup>, Dorel Dronca<sup>2</sup>, Cornelia Milovanov<sup>1</sup>, Oana Boldura<sup>1</sup>, Ioan Hutu<sup>1</sup>,  
Calin Mircu<sup>1</sup>, Camelia Tulcan<sup>1</sup>**

<sup>1</sup>*Faculty of Veterinary Medicine, University of Agriculture Sciences and Veterinary Medicine of Banat "King Michael 1st of Romania", 300645 - Timisoara, Calea Aradului, 116, Romania*

<sup>2</sup>*Faculty of Animal Sciences and Biotechnologies, University of Agriculture Sciences and Veterinary Medicine of Banat "King Michael 1st of Romania", 300645 - Timisoara, Calea Aradului, 116, Romania*

*e-mail: ddronca@animalsci-tm.ro*

### **Abstract**

Iron is essential elements for human, animals and plant organism. The depletion of organism in iron leads to modification in the concentration of hemoglobin which is responsible for oxygen transportation. Also, overload of iron represents a possible intoxication that can affect negatively the liver tissue and then all cells. Our experiments was conducted on two groups (control and experimental) of rabbits – German Lop Eared Rabbits breed, and we administrated ferrous gluconate (10mg/kg body weight) to the experimental group, two times. Also, during the experiment the rabbits had a special diet with plants from garden administrated fresh. The plants have very good antioxidant properties, and can prevent the iron intoxication and also participate intense to detoxification of the liver after iron overload. Hematological analysis were preformed for red blood cells, hemoglobin, hematocrit, mean corpuscular volume, mean corpuscular hemoglobin, mean corpuscular hemoglobin concentration, red cell distribution width, platelet and leukocyte evaluation. The results demonstrated a very good protective action of the diet plants, meaning that the hematological parameters were not out of normal range after iron overload.

**Key words:** rabbit, iron, protective diet

### **Introduction**

Iron is an essential element found all over in living organisms and environment; is a transitional metal, and is the fourth most representative metal in the Earth's crust. Biochemical properties of iron are various being involved in many oxido-reduction processes – by changing the oxidation states from  $\text{Fe}^{2+}$  to  $\text{Fe}^{3+}$  or reverse. Iron is present in different essential compounds in organism, but most known is the prophyrinic compound that contain ferric ion – hemoglobin. Also, many enzymes activity are depending on the presence of iron. Main functions of iron in living organism are: growth-promoting capacity, transportation of oxygen, in energetic metabolism: conversion of glucose from blood in energy, DNA synthesis, and more others (Seo et al., 2014). The lost of iron from organism has to take in view the urination, sweating, defecation, old skin cells exfoliating, and bleeding (menstruation).

The quantum of iron from organism is very important, and the equilibrium between the intake and excretion has to be very well managed by living organism because also the excess and deficiency (microcytic or hypochromic or severe anemia; primary and secondary hemochromatosis) can have severe consequences (Ludwiczek et al., 2005; Chua et al., 2007; Naigamwalla et al., 2012). However, in case of insufficient iron, the concentration of hemoglobin is also reduces that lead to a decrease of oxygen transport with consequences



such as fatigue, vertigo, or loss of energy in case of athletes (Mettler and Zimmermann, 2010).

Iron bioavailability is depending by dietary composition, and very important by the chemical form of the iron salt (Hurrel and Egli, 2010).

More of 90% of necessary iron has to come from endogenous sources because of the metabolic pathway of iron in concordance with the red cells. The necessary iron for organism has to count the losses of iron and the needs of iron for growth and has to be provided by a proper diet. Also, the dietary characteristic influences the iron bioavailability as non-heme-iron (present in plants and animals) and heme-iron (from hemoglobin and myoglobin). Between these two iron forms, the heme-iron is better absorbed compared to non-heme-iron. However, there are some other factors that influence the iron absorption, such as the presence of some chemical compounds that bound the iron and made it insoluble, and finally is excreted by feces. These compounds are usually acids like phytate (myo-inositol hexakisphosphate) well presented in some plants with green leaves and some grains (Gupta et al., 2015; Hurrell and Egli, 2010; Sotelo et al., 2010).

## Experimental

For this experimental data we used German Lop Eared Rabbits breed, as two groups of animals: one control group and one experimental group (Dronca, 2007). Each group of rabbits was formed by five animals. The animals where in a well suited placed, without to be stressed, and had well physiological conditions according with specific laws concerning animal protection in scientific researches (Romanian Law nr 205/2004; Directive 86/609/EEC from November 24, 1986 for Protection of Vertebrate Animals Used for Experimental and Other Sciences Purpose and Directive 2010/63/EU for Protection of Animals Used for Experimental and Other Scientific Purposes). The environment was well ventilated and the diet was establish in order to bring a toxicity protection against iron overload (Hazra et al, 2012). Dietary feed including organic plants from garden that provided a protective and a pro-active antioxidant protection (well-ahead of the addition of the toxicity of iron administration). The rabbits had in their diet one time a week oat (*Avena sativa*), dry alfalfa (*Medicago sativa*), carrots (*Daucus carota subsp sativus*), clover (*Trifolium*), garden parsley (*Petroselinum crispum*), leek (*Allium ampeloprasum*), chives (*Allium tuberosum*), coriander (*Coriandrum sativum*), and fenugreek (*Trigonella foenum-graecum*). These plants were organic plants, cultivated in our garden, and were fresh administrated in the rabbit's diet.



We choose to administrate iron as Fe(II)-gluconate hydrated (Fluka) because it was commercially available, is water soluble and the iron from this product has good bioavailability in animal organism. We administrated iron such as ferrous gluconate ( $C_{12}H_{26}FeO_{16}$ ) as a solution that provided  $10\text{mg Fe}^{2+}$  / body weight for every rabbit from the experimental group, twice times during our experiment, with a pause between administrations of 7 days. The animals from control and experimental group where introduced into the experiment right after the weaning period (after five weeks of life), the weight of the rabbits was between 580g and 800g (weight mean was 703g and SD was 89.19) and the experiment was conducted during 43 days during the summer time. Blood samples were collected for hematological determinations. By tube inversions we ensure mixing of anticoagulant K3EDTA with blood to prevent clotting. Sampling the blood from rabbits had in view the good practice guidelines (Waynforth et al., 1998). Complete blood count was



analyzed in the authorized bioclinical laboratory in Timisoara, with Impedance Analysis System, Flow Cytometry method.

### Results and discussion

Our experiment wants to have in consideration the evaluation of some hematological parameters after iron overload in experimental rabbits compared to the control group. In the figure 1 we present the results of red blood cells (RBC or erythrocytes), hemoglobin (HB), hematocrit (HC), mean corpuscular volume (MCV), Mean corpuscular hemoglobin (MCH), Mean corpuscular hemoglobin concentration (MCHC), Red cell distribution width (RDW), platelet (PL) and leukocyte (WBC – white blood cells).

The hemoglobin (HB) is the protein that participate to oxygen carrying in blood. Hematocrite (HC) represents the percent (%) of the red blood cells from the total blood volume. The red blood cells (RBC) indicates more informations about the heath status, and these tests are: mean corpuscular volume (MCV) that represents an avarage size of a single red blood cell; mean corpuscular hemoglobin (MCH) that presents the avarage of hemoglobin inside a red blood cell; mean corpuscular hemoglobin concentration (MCHC) represents a calculation of an avarage hemoglobin concentration inside the red blood cells; red cell distribution width (RDW) represent a calculation of RBCs size variation.

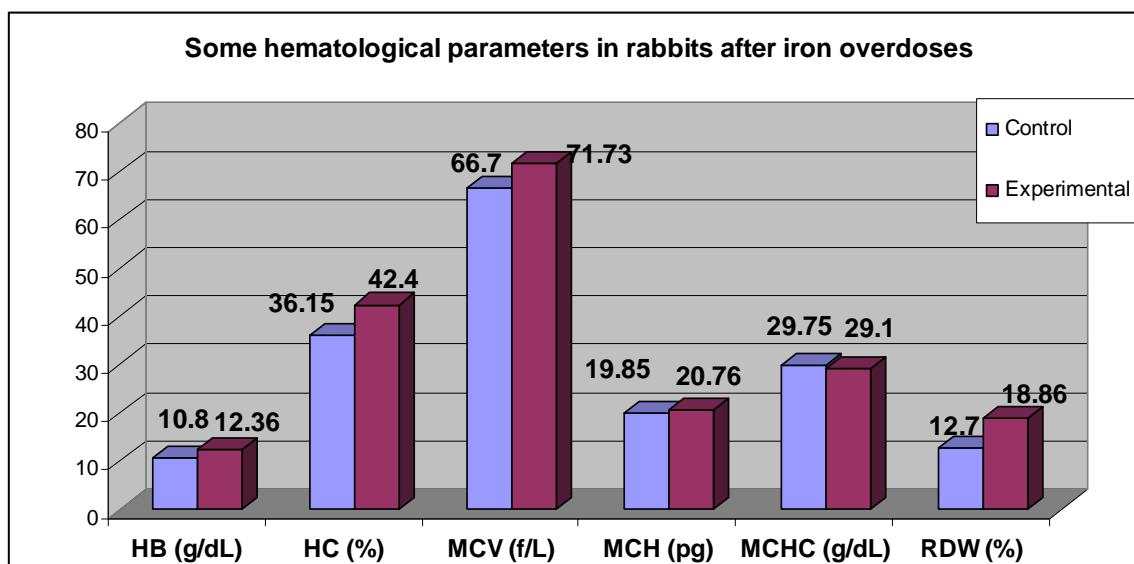


**Figure 1.** Variation of some blood hematological parameters of rabbits

After iron glconate administration for a very short time, the rabbits accumulates more iron compated to the control group, but compared to the normal range of these parameters the values from experiment are in normal range. This can be explained that all animals where feeded wit a special detoxifiant diet, based on different plants with protective action against iron intoxication.

Evaluation of reb blood cells (RBC) represent the total number of red blood cells (also named erythrocytes) presented in total blood. The platelet evaluation presents the cell fragments that play a vital role for normal blood clotting and the platelet count is the plateles number from blood; mean platelet volume (MPV) is more often raported together with reticulocyte count (CBC) and with platelet distribution width (PDW) – that reflects the uniformity of plateles in size.

Figure 2 presents the variation of red blood cells (RBC) and platelets in rabbits for control group and experimental group – after administration of moderate excess or iron.

Concentration of RBC and platelets is easily increased in the experimental rabbits that is normal because of the total iron intake in a short time.

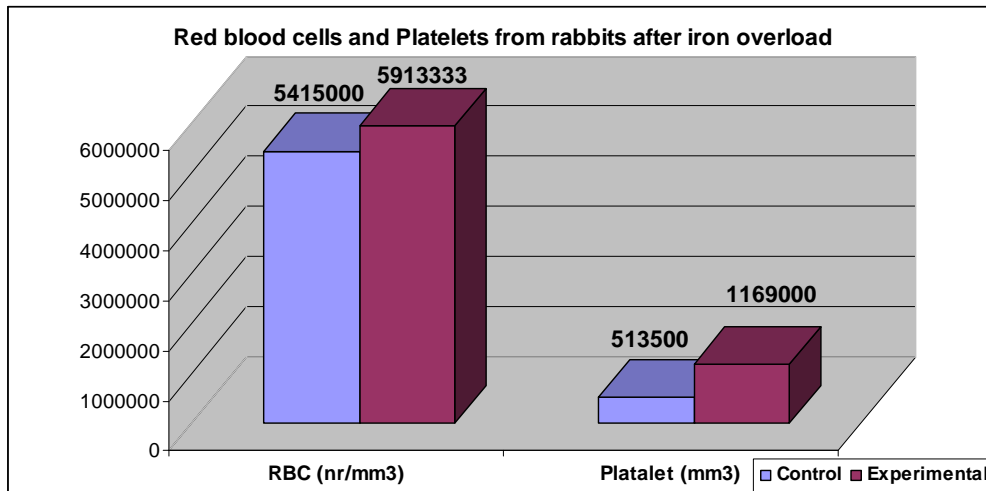


**Figure 2.** RBC and platelets

Evaluated of WBC – total number of white blood cells, present a response of the organism against infection and cancer and also play a very important role in allergic reactions and inflammation. White blood cells differentiate various types of white blood cells, such as: neutrophils, lymphocytes, monocytes, eosinophils, and basophiles.

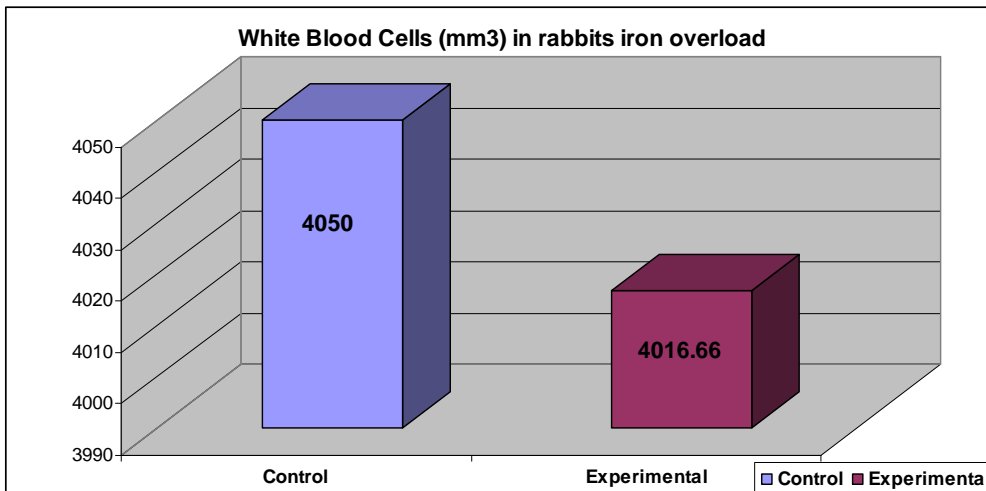


**Figure 3.** WBC after iron overload in rabbits

White blood cells number is higher in the control group compared to the experimental group, but both values are in the normal range for rabbits. This explains that the immunity is not affected by administration of iron overload for a very short time or another explanation could be linked to the diet that could protect the body from an infection of low immunity.

### Conclusion

Iron is an element essential for a good health status, but out of the normal range can affect the immunity, the resistance to effort, can lead to anemia, or in overload case can affect the liver tissue or all the cells integrity.

Diet based on different plants administered fresh, can prevent and can counteract the moderate toxicity of administration of iron in high concentration for a short time to the

rabbits. Iron overload can not affect negatively the health status to the rabbits if the diet is conducted to assure a protective action against iron toxicity.

Hematological determination after iron overload for a short time to the rabbits feed with a protective fresh diet, does not affect the normal values for red blood cells, hemoglobin, hematocrit, mean corpuscular volume, mean corpuscular hemoglobin, mean corpuscular hemoglobin concentration, red cell distribution width, platelet and leukocyte evaluation.

## **References**

- [1] A.C. Chua, R.M. Graham, D. Trinder, J.K. Olynyk, *Crit. Rev. Clin. Lab. Sci.*, 44, (2007), 413-59.
- [2] D. Dronca, *Ameliorarea genetica a populatiilor de animale*, Ed. Mirton, Timișoara, 2007
- [3] R.K. Gupta, S.S. Gangoliya, N.K. Singh, *J. Food Sci. Technol.*, 52 (2015), 676-84
- [4] B. Hazra, R. Sarkar, N. Mandal, *American J. Pharmacol. Toxicol.*, 201, (2012), 109-122
- [5] R. Hurrell, I. Egli, *Am J Clin Nutr*, 91, (2010), 1461S-7S
- [6] S. Ludwiczek, I. Theurl, S. Bahram, K. Schumann, G. Weiss, *J. Cell Physiol.*, 204, (2005), 489-99 I
- [6] S. Mettler, M.B. Zimmermann, *European J. Clin. Nutr.*, 64, (2010), 490-494
- [7] D.N. Naigamwalla, J.A. Webb, U. Giger, *Can. Vet. J.*, 53, (2012), 250-256
- [8] R. Sarkar, B. Hazra, N. Mandal, *Indian J. Exp. Biol.*, 51 (2013), 165-73
- [9] S.W. Seo, D. Kim, H. Latif, E.J. O'Brien, R. Szubin, B.O. Palsson, *Nat. Commun.* 5, (2014), 5910
- [10] A. Sotelo, L. Gonzalez-Osnaya, A. Sanchez-Chinchillas, A. Trejo, *Internat. J. Food Sci. and Nutr.*, 61 (2010), 29
- [11] H.B. Waynforth, P. Brain, T. Sharpe, D.F. Stewart, K.A. Applebee, P.G.G. Darke, *Good Practice guidelines in Collection of Blood Samples (rat, Mouse, Guinea Pig, Rabbit)*, Laboratory Animal Science Association, Series 1 / Issue 1 – October 1998
- [12] \* \* \* Romanian Law nr 205/2004 (Art. 7, 8, 22), publ. in M.O. of Romania, Part I, Nr. 531/14.06.2004
- [13] \* \* \* Directive 86/609/EEC from November 24, 1986 for Protection of Vertebrate Animals Used for Experimental and Other Sciences Purpose
- [14] \* \* \* Directive 2010/63/EU of the European Parliament and of the Council of 22 September 2010 for Protection of Animals Used for Experimental and Other Scientific Purposes

## p-Nitrophenol Adsorption on Polystyrene-Co-Divinylbenzene Functionalized Copolymers

Roxana Babuța<sup>1\*</sup>, Adriana Popa<sup>2</sup>, Cornelia Păcurariu<sup>1</sup>,  
Ecaterina Stela Drăgan<sup>3</sup>, Ioan Lazău<sup>1</sup>

<sup>1</sup>Politehnica University Timișoara, Faculty of Industrial Chemistry and Environmental Engineering, 6 Pîrvan Blv., RO-300223, Timișoara, România

<sup>2</sup>Institute of Chemistry Timișoara of Romanian Academy, Romanian Academy, 24 Mihai Viteazul Blv., RO-300223, Timișoara, România

<sup>3</sup>"Petru Poni" Institute of Macromolecular Chemistry, Aleea Grigore Ghica Voda 41 A, 700487 Iași, România  
e-mail: babuta.roxana@yahoo.com

### Abstract

The removal of phenolic compounds from wastewater is of significant importance due to the damages caused to the environment and human life [1-3]. The polymeric adsorbents were intensely studied in the adsorption processes and are now considered efficient in the removal of different pollutants from wastewater, including phenolic compounds [4-6].

In this study we introduce two new polystyrene-co-divinylbenzene copolymers, functionalized with carboxylic groups. The two copolymers, PC12 (with 12% divinylbenzene) and PC6.7 (with 6.7% divinylbenzene) were characterized and tested as adsorbents for the removal of p-nitrophenol from aqueous solution. The effect of different parameters on the removal efficiency was investigated. The kinetics and adsorption isotherm were also evaluated.

The copolymers were characterized by means of IR spectroscopy. FTIR spectra were carried out using a Shimadzu Prestige-21 spectrometer in the range 400–4000 cm<sup>-1</sup>, using KBr pellets and resolution of 4 cm<sup>-1</sup>. N<sub>2</sub> adsorption-desorption isotherms of copolymers were performed on Micromeritics ASAP 2020 instrument. The specific surface area was calculated using the Brunauer-Emmett-Teller (BET) method and the pore size distribution using the Barrett-Joyner-Halenda (BJH) method from the desorption curves. Thermal analysis (TG/DSC) was carried out using a NETZSCH-STA 449C instrument. The curves were recorded in the range of 25–1200 °C with a heating rate of 10 K min<sup>-1</sup>, using platinum crucibles. The experiments were carried out in artificial air at a flow rate of 20 mL min<sup>-1</sup>. The morphology of the nanopowders was investigated by scanning electron microscopy (SEM), using a FEI Quanta FEG 250 microscope.

The adsorption experiments were performed at 25 °C, using 50 mg adsorbent added at 25 mL p-nitrophenol solution with initial concentrations of 100 mg L<sup>-1</sup>. All experiments were performed at a 200 rpm shaking speed for 8 h to ensure the equilibrium of the adsorption process. The p-nitrophenol concentration was monitored by spectrophotometric analysis using a Shimadzu UV-VIS Spectrophotometer. The absorbance values were measured according to the maximum UV-absorption, at the wavelength of 316 nm.

The copolymers proved a good adsorption capacity. The removal efficiency of p-nitrophenol using PC6.7 adsorbent was 86% while using PC12 was 78%.

The experimental data were fitted with Langmuir, Freundlich, Redlich-Peterson and Sips isotherms. The maximum adsorption capacity of p-nitrophenol, resulted from Langmuir isotherm was 213.4 mg g<sup>-1</sup> using PC6.7 adsorbent and 80.8 mg g<sup>-1</sup> using PC12.

### Acknowledgements

This work was partially supported by the strategic grant POSDRU/159/1.5/S/137070 (2014)

of the Ministry of Labor, Family and Social Protection, Romania, co-financed by the European Social Fund – Investing in People, within the Sectoral Operational Programme Human Resources Development 2007-2013.

### **References**

- [1] E. Bazrafshan, F.K. Mostafapou, H.J. Mansourian, *Health Scope*. 2 (2013) 65-66.
- [2] E.O. Igbinosa, E.E. Odjadjare, V.N. Chigor, I.H. Igbinosa, A.O. Emoghene, F.O. Ekhaize, N.O. Igiehon, O.G. Idemudia, *Scientific World J.* 2013 (2013) 1-11.
- [3] J. Michałowicz, W. Duda, *Pol. J. Environ. Stud.* 16 (2007) 347–362.
- [4] Lin S.-H., Juang R.-S. *J. Environ. Manag.* 90 (2009) 1336–1349.
- [5] C. Păcurariu, G. Mihoc, A. Popa, S.G. Muntean, R. Ianoș, *Chem. Eng. J.* 222 (2013) 218–227.
- [6] M. Sobiesiak, B. Podkościelna, *App. Surf. Sci.* 257 (2010) 1222–1227.

## TiO<sub>2</sub> Thin Films on Si Substrate Obtained by PLD for Sensing Applications

Cornelia Bandas<sup>1</sup>, Ileana Cernica<sup>2</sup>, Corina Orha<sup>1</sup>, Stefania Rus<sup>1</sup>, Carmen Lazau<sup>1\*</sup>

<sup>1</sup>*Department of Condensed Matter, National Institute for Research & Development in Electrochemistry and Condensed Matter, Plautius Andronescu Street, No.1, 300224 Timisoara, Romania*

<sup>2</sup>*National Institute for Research and Development in Microtechnologies, Bucharest, 126A, Erou Iancu Nicolae Street, 077190, Bucharest, Romania*  
*e-mail: carmen.lazau@gmail.com*

### Abstract

Titanium dioxide (TiO<sub>2</sub>) thin films were deposited by pulsed laser deposition on Si substrate. An KrF excimer laser with wavelength of 248 nm was used for the irradiation of TiO<sub>2</sub> targets. The substrates were heated during the film deposition at 400°C under an oxygen pressure of 35 mTorr, 50 mTorr and 65 mTorr. The XRD results reveal the growth of TiO<sub>2</sub> thin film deposited on Si substrate in pure anatase phase. AFM topography of as deposited film indicates the formation of uniform TiO<sub>2</sub> on substrate and particles size depending of the oxygen pressure. The optical properties of films have been recorded using UV-Vis spectrophotometer in the wavelength range 400-800 nm.

### Introduction

TiO<sub>2</sub> thin films have been synthesized by using numerous methods including sol-gel [1], plasma oxidation [2], chemical vapor deposition (CVD) [3], metal organic chemical vapor deposition (MOCVD) [4], reactive magnetron sputtering [1], plasma-enhanced ALD (PEALD) and pulsed laser deposition (PLD) [5]. Among these techniques, PLD is one of the most promising techniques for the formation of complex oxide heterostructures, superlattices, and well controlled interfaces at high melting points of oxide materials. This technique generally enables the deposition of highly dense films and has proven its efficiency in growing oxides of complex stoichiometry [6]. TiO<sub>2</sub> has been proven to be an effective material for applications such as photocatalysis [7, 8], dye sensitized solar cells [9], heterogeneous catalysis [10], self-cleaning surface coatings, sensors and anti-reflection coatings [5]. TiO<sub>2</sub> thin film prepared by PLD has been studied by various research groups [10, 11]. However, different type of targets (*i.e.* Ti and TiO<sub>2</sub>), variation in substrate materials, widerange of operation pressures, and the differences in synthesis temperatures make it difficult to compare and understand the differences in properties of the thin films [12]. TiO<sub>2</sub> is one of the most important semiconductors with high photocatalytic properties, stability, non-toxicity, wide band gap and high dielectric constant. TiO<sub>2</sub> can exist in three crystallographic phases: anatase, rutile and brookite. The dielectric constant of TiO<sub>2</sub> increases from amorphous to anatase and rutile phase [5]. The band gap of TiO<sub>2</sub> changes from 3.2 to 3.5 eV depending of crystalline phase. The anatase and rutile multiphase structures were observed in TiO<sub>2</sub> thin films by several researchers [13]. Variation in PLD deposition parameters such as oxygen pressure and target temperature results in the growing of TiO<sub>2</sub> thin films with different chemical and physical properties. It has been reported that the deposition of TiO<sub>2</sub> films on Si substrates at higher temperature leads to increase in oxygen vacancies as the surface Si atoms easily capture oxygen atom from TiO<sub>2</sub> [5].

In this paper, we report the successful growth of pure anatase phase TiO<sub>2</sub> thin films on Si substrate by PLD method. As TiO<sub>2</sub> target we used pure Ti foil, at fixed heated temperature 400°C and different conditions of oxygen pressures. Besides the composition and structure evolution as a function of oxygen pressure, we investigated the optical properties of the



deposited thin films for further sensing applications.

## Experimental

TiO<sub>2</sub> thin films were deposited on Si substrate by PLD technique using a NANO PLD-1000 system, PVD products. The KrF excimer laser Lambda Physik COMPex PRO 110 F with wavelength of 248 nm was used for deposition. The target used for ablation was commercial titanium foil with high purity (Aldrich, 99.97%). The target to substrate distance and deposition temperature was kept 75 mm and 400°C, respectively. To avoid major changes in the surface morphology of the target, which have negative effects on the deposition process, the substrates were rotated during the multiple laser irradiations with 10 rpm. The laser spot area on the Si surface was about 10 mm<sup>2</sup> and the laser pulse energy about 0.2 J. The laser beam incidence angle onto the target was chosen of 60°. Thus, the laser fluence onto the target surface was about 2 J/cm<sup>2</sup>.

The irradiation chamber was previously evacuated down to a residual pressure of  $8 \times 10^{-6}$  Torr. High purity oxygen (99.99%) was then circulated inside the irradiation chamber through a calibrated gas inlet system. The oxygen pressure measured with an MKS controller was varying at 35 mTorr (TiO<sub>2</sub>/Si-35), 50 mTorr (TiO<sub>2</sub>/Si-50) and 65 mTorr (TiO<sub>2</sub>/Si-65). The substrates were heated during the thin film deposition process at 400°C fixed temperature. Prior to introduction inside the deposition chamber, the Si substrates were carefully cleaned in ultrasonic bath in acetone, ethanol and distilled water for the removal of the impurities present on the surface. The films were annealed for 5 min after deposition.

The surface morphologies of the deposited TiO<sub>2</sub> thin films were investigated by atomic force microscopy (AFM) using a Nanosurf® EasyScan 2 Advanced Research AFM apparatus. The crystalline phase of the deposited thin films was studied by X-ray diffraction (XRD) with a PANalytical X'PertPRO MPD Diffractometer, Cu tube. The transmittance spectra for TiO<sub>2</sub> thin films on Si substrate annealed at 400°C were obtained in the range of 400-800 nm using the Lambda 950 Perkin Elmer UV-Vis spectrophotometer.

## Results and discussion

TiO<sub>2</sub> thin films on Si substrate were characterized using XRD, AFM and UV-Vis spectroscopy. Influence of oxygen pressure on morphological and optical properties of TiO<sub>2</sub> thin films were discussed in detailed below.

### *X-ray diffraction analysis*

X-ray diffraction of different TiO<sub>2</sub> thin films are shown in Fig.1. The spectra were recorded by using X-ray reflectivity module and the sample was aligned both to  $2\theta$  and  $\omega$  angle. XRD pattern was recorded at  $\omega = 4^\circ$  and  $2\theta$  between  $24^\circ - 37^\circ$  with a time per step about 200 s. For a better accuracy for each sample the analysis time was about 420 minutes. In the present study the diffractograms of all thin films deposited at different oxygen pressure (Fig.1 a-c) contain one intense line at  $25.54^\circ$  attributed to (101) lattice plane reflection of the tetragonal anatase TiO<sub>2</sub> phase indexed by Program XPert High Score-Plus (Ref. code 01-073-1764). It can be observed also the line at  $24.56^\circ$  attributed to (400) lattice plane assigned to SiO<sub>2</sub> indexed by Program XPert High Score-Plus (Ref. code 00-025-1332). Appearance of SiO<sub>2</sub> peak in XRD pattern is probably because of highly oxidant medium and a heating temperature inside reaction chamber.

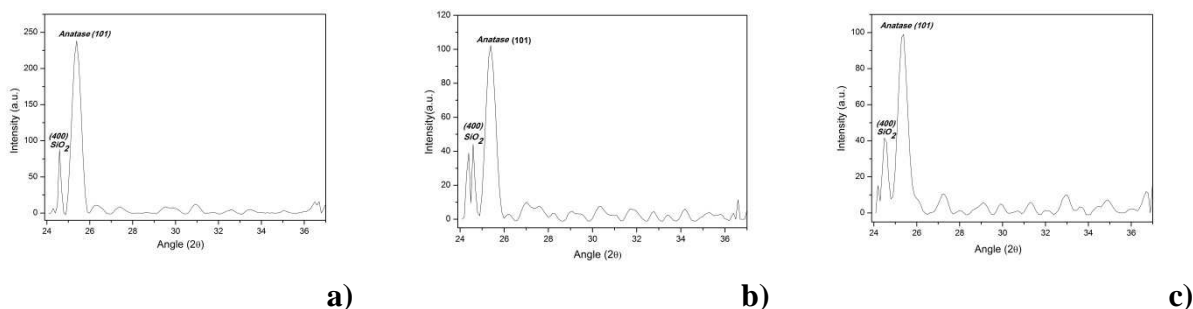


**Figure 1.** XRD pattern of thin films TiO<sub>2</sub>/Si-35(a), TiO<sub>2</sub>/Si-50(b) and TiO<sub>2</sub>/Si-65(c)

### AFM microscopy

AFM images were recorded in the contact mode, at the scale of  $(2 \times 2) \mu\text{m}^2$ . Figure 2 shows the 3D AFM images measured in deflection mode for deposited TiO<sub>2</sub> films on Si substrate. AFM images obtained in different areas of the films showed that the TiO<sub>2</sub>/Si films reveal a homogenous nanostructure and a uniform deposition. Particle size analysis has been carried out on TiO<sub>2</sub> films surface using Nanosurf software by considering the image sizes of about  $220 \text{ nm} \times 220 \text{ nm}$  and the corresponding size distributions are shown in Fig. 2 b, c and f. The average nanostructure size obtained for TiO<sub>2</sub>/Si-35 (Fig. 2b) is about 16 nm, and when the oxygen pressure increased at 50 mTorr (Fig. 2d) and respectively 65 mTorr (Fig. 2f) the particle sizes decreased at 5 nm.

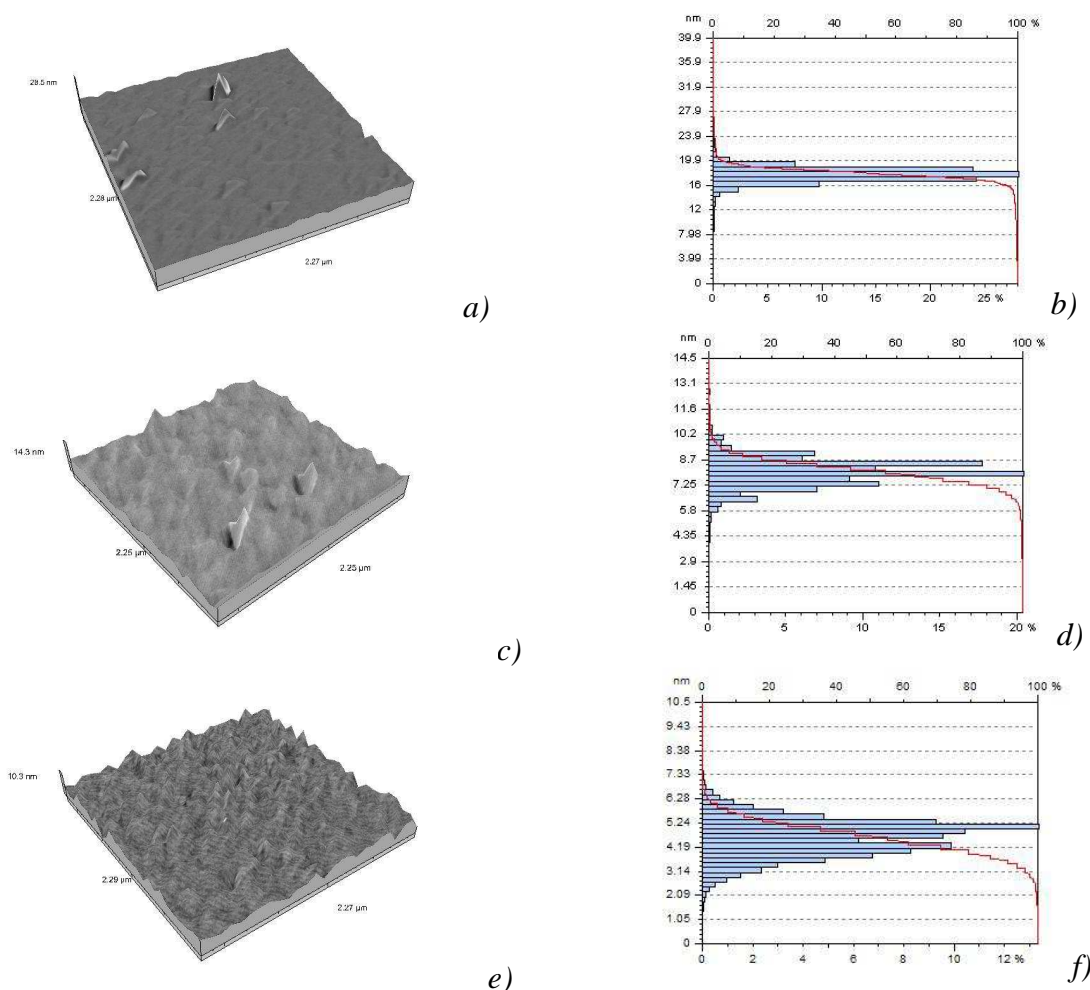


**Figure 2.** 3D AFM topography and particle size distribution of  $2 \mu\text{m} \times 2 \mu\text{m}$  scan area for TiO<sub>2</sub>/Si-35 (a, b), TiO<sub>2</sub>/Si-50 (c, d) and TiO<sub>2</sub>/Si-65 (e, f)

### Optical characteristics

The transmittance spectra in the wavelength range 400-800 nm of the TiO<sub>2</sub> films are shown in Fig. 3. The transparency of the films lies between 25% and 35% in the spectra of the deposited films. The oscillations are absent in the optical spectra probably because the films are so thin (< 100 nm). The optical transmission of TiO<sub>2</sub> films in the visible wavelength region reduces with the increase of oxygen pressure indicating lower defect density near the band edge [15].

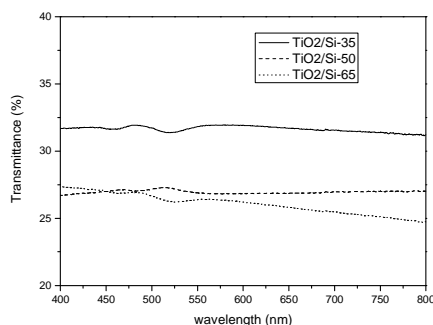


**Figure 3.** Optical transmittance of TiO<sub>2</sub> thin films

### Conclusion

TiO<sub>2</sub> films have been deposited on Si substrate using PLD method in an oxygen atmosphere. The deposited films were characterized by XRD, AFM and UV-Vis techniques. XRD spectra suggested the formation of anatase TiO<sub>2</sub> independently of oxygen pressure. AFM topography of as deposited films indicates the uniformity of TiO<sub>2</sub> layer with an average size of 16 nm for a oxygen pressure of 35 mTorr, respectively 5 nm for 50 and 65 mTorr. The transparency in the visible range was found to be 35 % which fulfill the requirements of the sensing applications.

**Acknowledgements:** This study was supported by research funds of project PN 09 34 01 08, contract no. 34N/2014.

### References

- [1] E. Gyorgy, G. Socol, E. Axente, I.N. Mihailescu, C. Ducu, S. Ciuca, Appl. Surf. Sci. 247 (2005) 429.
- [2] J.C. Tinoco, M. Estrada, G. Romero, Microelectron. Reliab. 43 (2003) 895.
- [3] Y.H. Lee, K.K. Chan, M.J. Brady, J. Vac. Sci. Technol. A 13 (1995) 596.
- [4] T. Asanuma, T. Matsutani, C. Liu, T. Mihare, M. Kiuchi, J. Appl. Phys. 95 (2004) 11.
- [5] R.R. Mohanta, V.R.R. Medicherla, K.L. Mohanta, Nimai C. Nayak, S. Majumder, V. Solanki, S. Varma, K. Bapna, D.M. Phase, V. Sathe, Appl. Surf. Sci. 325 (2015) 185.
- [6] V. N. Cancea, V. Ion, M. Filipescu, M. Dinescu, Physics AUC, 23 (2013) 18.
- [7] H. Fujishima, K., Nature 238 (1972) 37-38.
- [8] H. Lin, C. P. Huang, W. Li, C. Ni, S. I. Shah, Y. H. Tseng, Appl. Catal. B – Environ. 68 (2006) 1.
- [9] A. Hagfeldt, M. Gratzel, Accounts of Chemical Research 33 (2000) 269.
- [10] M. Valden, X. Lai, D. W. Goodman, Science 281 (1998) 1647.
- [11] T. Nakamura, T. Ichitsubo, E. Matsubara, A. Muramatsu, N. Sato, H. Takahashi, Acta Materialia 53 (2005) 323.
- [12] A. Singh, Z. R. Khan, P.M. Vilarinho, V. Gupta, R.S. Katiyar, Mat. Res. Bull. 49 (2014) 531.
- [14] S.I. Kitazawa, Y. Choi, S. Yamamoto, T. Yamaki, Thin Solid Films 515 (2006) 1901.
- [15] S. Khana, I. Ahmed, A. Shah, Appl. Surf. Sci. 317 (2014) 607.

## **Influence of Termic Treatment on *Armoracia Rusticana* Roots and Leaves, Total Polyphenols Content**

**Despina-Maria Bordean \*, Marinel Horablaga, Ioan Gogoasa, George Andrei Draghici, Lidia Sida, Luminita Pirvulescu \*\*, Luminita Cojocariu, Aurica Breica Boroza**

*Banat's University of Agricultural Sciences and Veterinary Medicine, 119, C. Aradului, 300645-Timisoara, Romania*

*\*e-mail: despina.bordean@gmail.com*

*\*\*e-mail: pirvulescu\_l@yahoo.com*

### **Abstract**

The studies were conducted on Romanian horseradish originated from three domestic farms, located in the plains, hills and mountain areas. The localization of the horseradish plant as well as processing and temperature treatment seems to have a big effect on total polyphenols content (TPPC) of roots and leaves. The modifications of TPPC are due to the increasing and decreasing of temperature and they maintain the same profile irrespective of the locations

### **Introduction**

*Armoracia Rusticana* contains a complex mixture of polyphenols and presents a high total antioxidant activity, confirmed also by the experimental studies.

Polyphenols are chemical compounds with more than one aromatic hydroxyl group on the aromatic ring inserted. Due to this structure, the redox properties, can be oxidized by the Folin Ciocalteu which form a blue coloration with maximum absorption at 750 nm [5].

“Phenolic composition of plants is affected by different factors –variety, genotype, climate, harvest time, storage, processing, and treatment” (Marrelli et al., 2012, cited by Tomsone L. and Zanda K., 2014) [4,8].

### **Experimental**

The studies were conducted on Romanian horseradish originating from three domestic farms, located in the plains, hills and mountain areas [2] from where the samples were freshly harvested. The study was carried out in our laboratory (Environmental Research Test Laboratory, All samples were separated and rinsed in distilled water to remove potential impurities. The samples were washed with double distilled water and spread on clean plastic trays to allow the water to drain off.

Drying of leaf samples was performed in a vacuum oven at 60 °C for 36 hours and for the roots samples 48 hours. After drying, the samples were ground in a special mill plant. The freezing of samples were done at a temperature of -20 C°. The alcoholic extracts were obtained from the roots and leaves dried in the oven and the sample frozen in the freezer. and fresh roots and leaves were used as control batch.

The total phenolic content (TPPC) of the plant extracts was determined according to the Folin -Ciocalteu spectrophotometric method. The absorbance was measured at 750 nm and total phenols were expressed as the gallic acid equivalents (GAE) 100 g<sup>-1</sup> fresh weight (FW) of plant material. To determine the total polyphenolic content, the alcoholic extracts were diluted 1:10. 0.5 mL alcoholic extract were mixed with 2.5 ml of Folin and Ciocalteu 1:10 solution and 2 mL 7.5% sodium carbonate solution.

All reagents used in the present study were of analytical grades and double distilled water was used throughout the analyses.

The data were statistically analyzed and graphically represented using PAST software [3].

## Results and discussion

The roots present 5 times less TPPC (57.49 - 73.42 mg GAE 100g<sup>-1</sup>FW) compared to the leaves content (316.12 - 399.28 mg GAE 100g<sup>-1</sup>FW) (figure1 and 2).

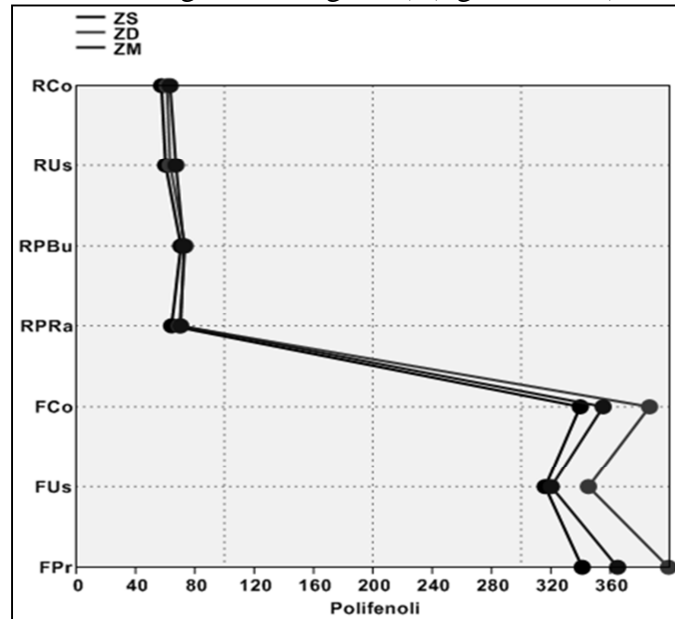


**Figure 1.** Horseradish Polyphenols concentrations based on the area of origin of samples  
*Legend: FPr = Fresh horseradish leaves; FUs = Dry horseradish leaves; FCo = Frozen leaves; RPRa = Grated horseradish; RPBu = Horseradish pieces; ZS = plain area; ZD = hills area; MA = mountain area*

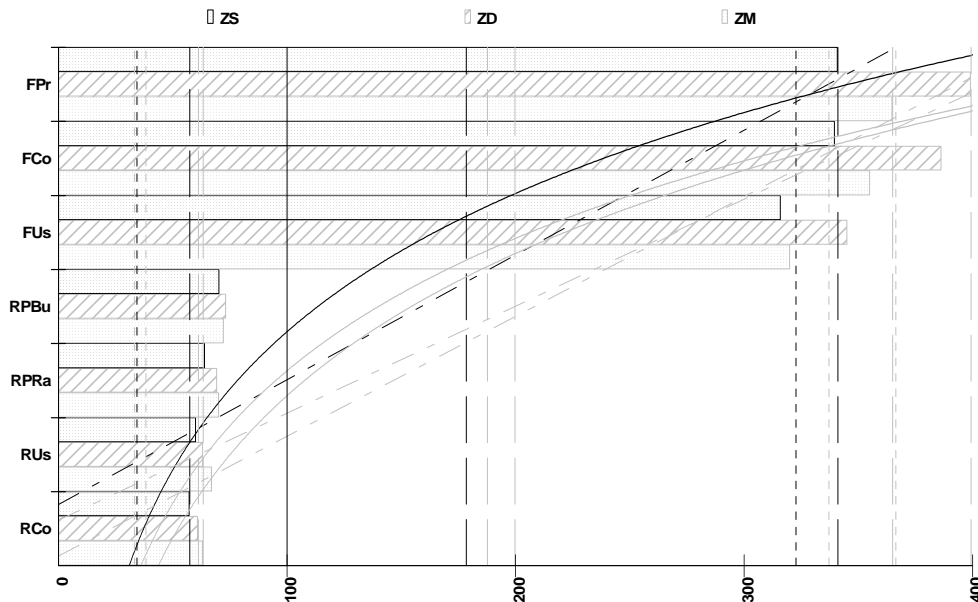


**Figure 2.** Horseradish roots and leaves TPPC profiles evolution  
*Legend: FPr = Fresh horseradish leaves; FUs = Dry horseradish leaves; FCo = Frozen leaves; RPRa = Grated horseradish; RPBu = Horseradish pieces; ZS = plain area; ZD = hills area; MA = mountain area*

Higher content of TPPC in horseradish leaves compared to roots is confirmed by other scientific studies (Calabrone L. et al, 2015, Tomsone L. et al, 2010), [1, 6].

The horseradish leaves show the highest variation in polyphenol content compared to the roots content. The highest TPPC (figure 1), irrespective of the preserving method show the horseradish samples collected from the hills area (fresh: 399.28 mg GAE 100g<sup>-1</sup>FW; dry: 345.27 mg GAE 100g<sup>-1</sup>FW; frozen: 386.50 mg GAE 100g<sup>-1</sup>FW).

In the case of horseradish roots preparation, grated horseradish presents less TPPC compared to horseradish sliced in small pieces (figure 1 and 2), which is confirmed by (Marrelli et al., 2012)[4, 7].

## **Conclusion**

The modifications of TPPC are due to the increasing and decreasing of temperature and they maintain the same profile irrespective of the locations of the plant.

After the analysis it is concluded that the best method for preserving TPPC of horseradish leaves is by freezing and for the roots by drying. At the same time we could observe that different environmental conditions of the plants locations affect TPPC significantly.

The highest content of polyphenolic compounds was in horseradish leaves extracts, and these extracts could be incorporated in foods especially meat products.

## **References**

- [1] L. Calabrone, M. Larocca, S. Marzocco, G. Martelli, and R. Rossano, Food and Nutrition Sciences, 6, (2015), pp.64-74. <http://dx.doi.org/10.4236/fns.2015.61008>
- [2] A.G Draghici., L. Sida, D. Raican, T.A. Szijarto, L. Sirbu, A. B. Borozan, L. Pirvulescu, D-M. Bordean, The 6th International Conference on Food Chemistry, Engineering & Technology, May (2015), Timisoara, [http://www.usab-tm.ro/utilizatori/tpa/file/simpozion%202015/Programme\\_Conference%20on%20Food%20Chemistry,%20Engineering%20&%20%20%20Technology\\_Timisoara\\_Book-of-Abstract.pdf](http://www.usab-tm.ro/utilizatori/tpa/file/simpozion%202015/Programme_Conference%20on%20Food%20Chemistry,%20Engineering%20&%20%20%20Technology_Timisoara_Book-of-Abstract.pdf).
- [3] O. Hammer, D. A. T. Harper, P. D Ryan, 2001, Palaeontologia Electronica, 4: 1-9.
- [4] M. Marrelli, F. Menichini, G.A. Statti, M. Bonesi, P. Duez, F. Menichini, F. Conforti, Food and Chemical. Toxicology, No. 50, (2012), pp. 726–733.
- [5] M-A Poiana, D. Moigradean, D. Raba, L-M. Alda, M. Popa, Journal of Food, Agriculture & Environment Vol.8 (1), January (2010), Helsinki, Finland, ISSN 1459-0255, p.54-58, [www.world-food.net/scientificjournal.php](http://www.world-food.net/scientificjournal.php)
- [6] L. Tomsone, Z. Kruma, T. Talou, T. M. Zhao, Journal of Hygienic Engineering and Design, (2010), p.16–24, UDC 635.162:542.613]:615.272, [http://www.jhed.mk/filemanager/JHED10/02.FQS/04.Full paper Zanda Kruma.pdf](http://www.jhed.mk/filemanager/JHED10/02.FQS/04.Full%20paper%20Zanda%20Kruma.pdf)
- [7] L. Tomsone, Z. Kruma, R. Galoburda, F. Dimins, V. Kreicbergs, 2<sup>nd</sup> International Conference on Nutrition and Food Sciences, IPCBEE vol. 53 (2013), IACSIT Press, Singapore, p: 6-10, DOI: 10.7763/PCBEE. 2013. V53. 2, <http://www.ipcbee.com/vol53/002-ICNFS2013-F0004.pdf>
- [8] L. Tomsone, Z. Kruma, FOODBALT Proceedings, (2014), pp:192-197, [http://llufb.llu.lv/conference/foodbalt/2014/FoodBalt\\_Proceedings\\_2014-192-197.pdf](http://llufb.llu.lv/conference/foodbalt/2014/FoodBalt_Proceedings_2014-192-197.pdf)



## Evaluation of Tomato Yield Using Statistical Tests

Diana Moigradean<sup>1\*</sup>, Mariana-Atena Poiana<sup>1</sup>, Liana-Maria Alda<sup>1</sup>, Simion Alda<sup>2</sup>,  
George-Andrei Draghici<sup>1</sup>

<sup>1</sup> Faculty of Food Processing Technology, Banat's University of Agricultural Sciences and Veterinary Medicine „King Mihai I of Romania” from Timisoara, Calea Aradului 119, Timisoara, RO 300645, Romania

<sup>2</sup> Faculty of Horticulture and Forestry, Banat's University of Agricultural Sciences and Veterinary Medicine „King Mihai I of Romania” from Timisoara, Calea Aradului 119, Timisoara, RO 300645, Romania  
e-mail: dimodean@yahoo.com

### Abstract

The main objective of this study is to calculate the correlation existed between the NPK mineral fertilization doses on tomato yield using statistical tests (multiple regression analysis of variance, the F-test, value of R and  $R^2$ , Durbin–Watson test). A field experiment was using two tomatoes samples in different precocity steady (Export II and Ace Royal) cultivated in Romanian west area. Multiple regression analysis of variance on the influence of fertilization on the yield of Export II cultivar show that 90.28% of the production variability is due to the influence of these three macronutrients (NPK) while the yield of Ace Royal cultivar the percentage is 97.78%. The tomato yield increases with the fertilization doses and nitrogen fertilization has a major influence distinctly significant on achieving production, while the fertilization with potassium is lower but superior to phosphorus fertilization for two tomato cultivar.

### Introduction

Consumption of vegetables and fruits is very important for human nutrition [2]. Tomato (*Lycopersicum esculentum*) is one of the popular and most consumed vegetable in the world. Romania produces about 745 thousands tons tomatoes/year, current average productivity is 16 - 18 tons per hectare (t/ha) [9]. Multiple regression analysis model provides not only a statistical test of the models ability to predict the outcome variable (the F-test), but also the value of R and the adjusted  $R^2$  [1]. The Durbin-Watson statistic (DW) is a commonly used and routinely reported diagnostic test for the presence of first-order auto or serial correlation in the error of a time-series regression model [3]. Its value always lies between 0 and 4. A value of 2 indicates there appears to be no autocorrelation. If the Durbin-Watson statistic is substantially less than 2, there is evidence of positive serial correlation [3, 4].

### Experimental

Fertilization was control (without fertilizers) and mineral fertilizers (NPK) in variable doses:  $N_{30}P_{30}K_{30}$ ,  $N_{45}P_{45}K_{45}$ ,  $N_{60}P_{60}K_{60}$ ,  $N_{120}P_{60}K_{60}$ . Were use dry/granulated fertilizers NPK 15:15:15 and the nitrogen high dose supply with urea application. The fertilization doses and the application methods in tomatoes fertilization were to determine in correlations between agro chemistry factors [8].

Regression analysis is defined as another technique for measuring the linear association between x (independent variable) and y (dependent variable) and shown as ( $Y=a+b_1X_1+b_2X_2+b_3X_3...+b_nX_n$ ) which is used extensively in forecasting. Multiple regression analysis model provides not only a statistical test of the models ability to predict the outcome variable (the F-test), but also the value of R and the adjusted  $R^2$  [1, 7]. Data collected was subjected to analyses using statistical package ANOVA.

## Results and discussions

The experience was done in a cambic cernosium soil, with low acidity reaction and the high natural fertility potential favorable vegetables cultivation. The analysis show that soil its favorable for tomatoes cultivation [6]. Liptay and al. [5] has showed that with increasing nitrogen fertilization doses increased tomatoes production. As can be observed from Figure 1, the tomato yield increases from control to highest fertilization doses for both varieties.

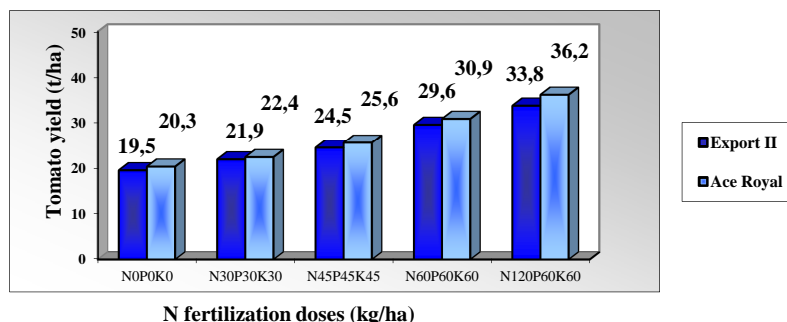


**Figure 1.** Tomato yield

Multiple regression analysis of variance on the influence of the three macronutrients on the yield of Export II tomato cultivar (Table 1) show that 90.28% of the production variability is due to the influence of the macroelements. Of these, it is observed that nitrogen fertilization has a major distinctly significant contribution (82.98%) to achieving the high yield, while potassium (15.15%) and phosphorus (1.87%) fertilization has small and very small influence on the production. Other sources, were not significant, and did not have much contribution to the tomato yield.

**Table 1.** The multiple regression analyses of variance between Export II cultivar production and nitrogen, phosphorus and potassium fertilization doses

Variability source	SP	GL	S <sup>2</sup>	F test
Regression	168.22 (100%)	3	56.07	F = 65.20**
N dose (x <sub>1</sub> )	139.59 (82.98%)	1	139.59	F = 162.31**
P dose (x <sub>2</sub> )	3.12 (1.87%)	1	3.12	F = 3.62ns
K dose (x <sub>3</sub> )	25.51 (15.15%)	1	25.51	F = 29.66**
Other sources	18.10	21	0.86	
Sum	186.32	24		

ns: non significant; \*: significant; \*\*: distinct significantly; \*\*\*: major distinct significantly  
 $y = 23.407 + 0.032x_1 + 2.546x_2 - 2.525x_3$ ;  $R^2 = 0.9028$ ;  $R = 0.9501$ ;  $SDE = 2.206$  t/ha;  $DW = 3.06$

The regression model adopted for the analysis of relationships between production and different macroelements, shows a strong statistical assurance, assessing the production with an error of  $\pm 2.206$  t/ha, while the estimated production without fertilization is about 23 t/ha. Because the DW index is 3.06, the any errors that accompanying experimental results are not autocorrelation and the macroelements order in the regression equation not affect the estimated production.

Eliminating the effect of phosphorus fertilization, on the results of multiple regression analysis of variance with two independent variables (Table 2) shows that 76.38% of Export II tomato yield is influenced by the effect of nitrogen and potassium doses applied.

In Figure 2 was noted that there is a linear relationship, positive and highly significant between the nitrogen doses applied and Export II tomato yield, such as the production increases proportionally with the nitrogen applied to 272.5 kg/ha, where obtaining the highest estimated tomato yield of 31 t/ha.

**Table 2.** The multiple regression analyses of variance between Export II cultivar production and nitrogen and potassium fertilization doses

Variability source	SP	GL	S <sup>2</sup>	F test
Regression	142.30 (100%)	2	71.15	F = 35.52**
N dose (x <sub>1</sub> )	139.58 (98.08%)	1	139.58	F = 69.79**
K dose (x <sub>3</sub> )	2.722 (1.92%)	1	2.72	F = 1.36ns
Other sources	44.02	22	2.00	
Sum	186.32	24		

$$y = 23.428 + 0.033x_1 + 0.019x_2; R^2 = 0.7638; R = 0.8739; SDE = 2.887 \text{ t/ha}; DW = 3.15$$

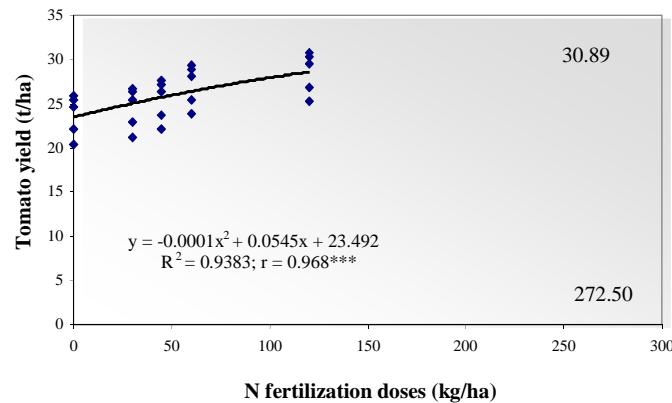


**Figure 2.** Regression between the production and nitrogen dose of Export II tomato variety

In Table 3 it is noted that 98% of the Ace Royal tomato yield can be explained as the result of NPK fertilization. The fertilization with nitrogen has a major influence distinctly significant on achieving production (78.64%), following the contribution with potassium (20.32%) and phosphorus (0.98%) fertilization.

**Table 3.** The multiple regression analyses of variance between Ace Royal cultivar production and nitrogen, phosphorus and potassium fertilization doses

Variability source	SP	GL	S <sup>2</sup>	F test
Regression	203.69 (100%)	3	67.89	F = 188.60**
N dose (x <sub>1</sub> )	160.20 (78.64%)	1	160.20	F = 445**
P dose (x <sub>2</sub> )	1.97 (0.98%)	1	1.97	F = 5.47ns
K dose (x <sub>3</sub> )	41.52 (20.32%)	1	41.52	F = 115.33**
Other sources	7.66	21	0.36	
Sum	211.35	24		

$$y = 24.422 + 0.039x_1 + 2.686x_2 - 2.67x_3; R^2 = 0.9778; R = 0.9888; SDE = 2.268 \text{ t/ha}; DW = 2.99$$

According to the distinct significantly regression model, the control samples obtain a production about 24 t/ha, by an error about  $\pm 2.26$  t/ha. DW coefficient values (2.99) indicate that the order of the three variables does not affect the results of estimated tomato yield [1].

**Table 4.** The multiple regression analyses of variance between Ace Royal cultivar production and nitrogen and potassium fertilization doses

Variability source	SP	GL	S <sup>2</sup>	F test
Regression	177.84 (100%)	2	88.92	F = 58.50**
N dose (x <sub>1</sub> )	176.20 (99.07%)	1	176.20	F = 115.92***
K dose (x <sub>3</sub> )	1.64 (0.93%)	1	1.64	F = 1.08ns
Other sources	33.51	22	1.52	
Sum	211.35	24		

$$y = 24.444 + 0.039x_1 + 0.015x_2; R^2 = 0.8414; R = 0.9173; SDE = 2.359 \text{ t/ha}; DW = 3.13$$

Considering only fertilization with nitrogen and potassium (Table 4), shows that these macrolements influenced by 84% the Ace Royal tomato yield, under a major distinct significant contribution of nitrogen (99.07%).

Figure 3 illustrates the result of the correlation between nitrogen fertilization doses and productions; the highest estimated Ace Royal tomato yield (35 t/ha) is obtained at the optimal dose of about 274 kg/ha.

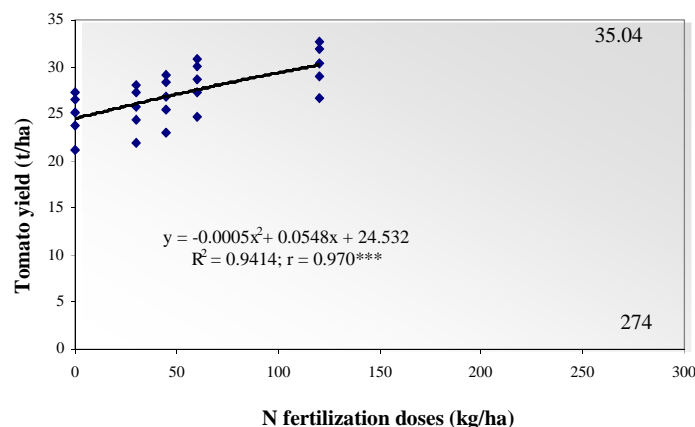


**Figure 3.** Regression between the production and nitrogen dose of Ace Royal tomato variety

Nitrogen was more efficiently exploited by Ace Royal tomato variety compared with the Export II variety, which on the optimal fertilization dose has achieved an increase of 4.0 t tomato/ha.

### Conclusion

The tomato yield increases with the fertilization doses. The fertilization with  $N_{120}P_{60}K_{60}$  determinate maximum tomato yield (34 t/ha for Export II variety and 36 t/ha for Ace Royal variety).

Using statistical methods show that the highest tomato yield (31 t/ha) is obtained at the optimal nitrogen dose of 272 kg/ha for Export II variety and for Ace Royal variety the highest estimated tomato yield (35 t/ha) is obtained at the optimal nitrogen dose of 274 kg/ha.

The nitrogen fertilization has a major influence on tomato yield, followed by fertilization with potassium and phosphorus by two tomato cultivars.

### References

- [1] C. Benkovitz, LN. Oden, Environ. Software. 2 (1987), 85-88.
- [2] D.M. Bordean, I. Gergen, I. Gogoasa, G. Oprea, L. Pirvulescu, L.M. Alda, S. Alda, A.B. Borozan, M. Harmanescu, J. Food Agric. Environ. 9(1), (2011), 680-683.
- [3] J. Durbin, G.S. Watson, Biometrika. 37 (1950), 409-428.
- [4] J. Durbin, G.S. Watson, Biometrika. 38 (1951), 159-179.
- [5] A. Liptay, S. Nicholls, J., Am. Soc. Hortic. Sci. 118 (1993), 339-342.
- [6] B. Manescu, M. Stefan, Comparated horticultural systems, Ceres (Eds.), Bucuresti, 2003.
- [7] D. Moigradean, M.A. Poiana, L.M. Alda, D.V. Dogaru, S. Alda, A. Lazureanu, Proceeding of the Third International Conference „Research people and actual tasks on multidisciplinary sciences”, Lozenec, Bulgaria, (1) 2011, pp. 51-55.
- [8] \*\*\* Agrochemical soil analysis methodology for establish the need amendaments and fertilizers (M.A.I.A.), Romania, 1983.
- [9] \*\*\* Romanian Statistical Yearbook, 2013.

## Bio-Minerals Contribution of Seasonal Fruits to the Recommended Dietary Allowances

Ioan Gogoasă<sup>1\*</sup>, Liana Maria Alda<sup>1</sup>, George Andrei Drăghici<sup>1</sup>, Despina-Maria Bordean<sup>1\*\*</sup>, Adina Negrea, Gheorghița Jigoria<sup>1</sup>, Ariana Velciov<sup>1</sup>, Maria Rada<sup>3</sup>, Antonela Cozma<sup>1</sup>, Iosif Gergen<sup>1</sup>

<sup>1</sup>Banat's University of Agricultural Science and Veterinary Medicine "King Mihai I of Romania", Romania

<sup>2</sup>Politehnica University - Timisoara, Romania

<sup>3</sup>Victor Babes University of Medicine and Pharmacy, Timisoara, Romania

\*ionelgogoasa@yahoo.com

\*\*despina.bordean@gmail.com

### Abstract

The paper presents data regarding the distribution of some mineral bio elements in three assortments of fall fruits – apples, pears and quinces – cultivated in a hill area of Banat, Romania, and an estimate of their mineral supply.

Experimental results obtained through the ICP-MS technique show that the fruits analysed have important contents of K, Ca, Mg, and Na, and appreciable contents of Fe, Mn, Zn, and Cu.

Calculus shows that a consumption of 400 g of fresh fruits (edible parts) supplies the necessary daily amount of macro elements: 14.66% K – in males and females, 9.50% Mg – in females and 7.24% Mg – in males, 2.76% Ca – in males and in females, and 0.18% Na – in males and females. Microelement supply is slightly higher: 16.45% Fe – in males and 7.31% Fe – in females, 12.22% Mn – in females and 9.57% Mn – in males, 9.33% Cu – in males and 5.45% Cu – in females and 3.96% Zn – in males.

### Introduction

Apples, pears and quinces, as fall fruits [11] are a true treasure of antioxidants, vitamins, fibers and minerals [1, 6, 8, 9]. Their nutritive and therapeutic features are determined by the contents in and nature of minerals some of which are essential bio elements for the good functioning of the human body: Ca, Mg, K, P, Fe, Mn, Zn, Cu, Cr, I, Se, etc [4, 3, 5]. This is why we believe it is important to know the share of minerals in different fruits and to estimate their mineral supply.

We determined the concentrations of Na, K, Ca, Mg, Fe, Mn, Zn, Cu, Co, Cr, Ni, Pb and Cd in apples, pears and quinces cultivated in a pollution-free hill area of Banat, Romania. Experimental results allowed us to calculate the mineral supply by these fruits and to estimate the degree of supply of the necessary Na, K, Ca Mg, Fe, Mn, Zn and Cu in the recommended dietary allowances containing fresh fruits.

### Experimental

To carry out the experiment, we used three native assortments of fall fruits – apples, pears and quinces – harvested from a hill area of Banat, Romania, known as a pollution-free area.

The total concentration of macro- and micro-elements such as Na, K, Ca, Mg, and Fe, Mn, Zn, Cu, Co, Ni, Cr, Pb, and Cd, respectively, in fresh fruit samples was assessed using the ICP-MS spectrometry technique after calcinations of the samples at 550<sup>0</sup>C and extracting from the mineral residue with HNO<sub>3</sub>, solution of 0.5N [2, 3].

To measure absorbance, we used the Bruker – Aurora M 90 spectrometer, choosing the working parameters after the recommendations of the producers.

## Results and discussion

Experimental results after determining minerals in the three assortments of fresh fruits analysed are shown in Tables 1 and 2 below.

**Table 1. Concentration of Na, K, Ca and Mg (mean values) in some fall fruits**

Specification	Macroelements, mg/kg fresh fruit			
	Na	K	Ca	Mg
<b>Apples</b>	4.20	1079	51.2	44.5
<b>Pears</b>	12.5	2551	81.9	112
<b>Quinces</b>	3.10	1538	72.8	72.3
<b>Mean values</b>	<b>7</b>	<b>1723</b>	<b>69</b>	<b>76</b>

**Table 2. Concentration of Fe, Mn, Zn, Cu, Cr, Co, Ni, Pb and Cd (mean values) in fall fruits**

Fruit	Micro-elements, mg/kg fresh fruit								
	Fe	Mn	Zn	Cu	Cr	Co	Ni	Pb	Cd
<b>Apples</b>	2.18	0.44	0.22	0.07	0.01	0.01	0.01	< 0.01	SLD
<b>Pears</b>	3.14	0.44	1.39	0.25	0.01	0.02	0.01	< 0.01	SLD
<b>Quinces</b>	4.54	0.78	1.67	0.32	0.02	0.01	0.09	< 0.01	SLD
<b>Mean values</b>	<b>3.29</b>	<b>0.55</b>	<b>1.09</b>	<b>0.21</b>	<b>0.01</b>	<b>0.01</b>	<b>0.04</b>	<b>0.00</b>	<b>0.00</b>

As shown in Tables 1 and 2, the share of minerals in the fruit assortments analysed is uneven. Of the total elements analysed, the best represented are macro-elements, i.e. over 99%. Among them, K is the best represented, followed by Magnesium and Calcium, and by Sodium, respectively.

Potassium was determined within concentration limits of 1079 mg/kg (apples) and 2551 mg/kg (pears), its value reaching 1723 mg/kg.

Magnesium was determined in much smaller concentrations than Potassium, its concentration ranging between 44.5 and 112 mg/kg; pears are the richest fruits in Mg.

Calcium was determined in much smaller concentrations than Potassium (51.2 mg/kg – 81.9 mg/kg), the mean value of its concentration being 69.00 mg/kg, relatively close to the concentration of magnesium.

Sodium was determined in the lowest concentration compared to K, Ca and Mg, the mean value of its concentration being 7 mg/kg. The highest values were in pears (12.5 mg/kg), while the lowest were in quinces (4.2 mg/kg) and apples (3.10 mg/kg).

Microelements were identified in much smaller concentrations compared to macro-elements (Table 2). There was also uneven distribution of microelements: the best represented was Fe, followed by Zn, Mn, and Cu. The rest of microelements, Cr, Co, Ni, Pb and Cd, in working conditions, were identified in extremely small concentrations, at the limit or beneath the limit of detection of the apparatus.

Iron was determined in concentrations between 2.18 mg/kg (apples) and 4.54 mg/kg (quinces); the mean value of the concentration of Fe was 3.29 mg/kg.

Zinc was determined in smaller concentrations than Fe, but in larger concentrations than Mn and Cu, and much larger than Mn and Cu. The concentration of Zn ranged between 0.22 mg/kg (apples) and 1.17 mg/kg (quinces); quinces and pears are richer in Zn.

Manganese was determined within close concentration limits, i.e. between 0.44 mg/kg (apples and pears) and 0.78 mg/kg (quinces); the mean concentration of Mn was 0.55 mg/kg.



Copper was determined in small concentrations ranging between 0.07 mg/kg (apples) and 0.32 mg/kg (quinces), the mean concentration reaching 0.21 mg/kg; quinces are the richest in copper.

Zinc and Copper, essential bio elements, can harm above certain concentration limits. Comparing the values determined with maximum admitted limits [10], we see that the fruits we analysed do not show any contamination risk by Zn and Cu.

Cobalt, Chromium and Nickel were identified in extremely small concentrations, which explains why we did not consider them in estimating mineral supply.

Lead and Cadmium, high toxicity metals, were practically not determined under experimental conditions; therefore, there is no contamination risk by Pb and Cd.

We can say that the fall fruits we analysed have important amounts of K, Ca, Mg, and Na, appreciable amounts of Fe, Mn, Zn, and Cu and no risk of contamination by toxic elements.

The mean values of the concentrations of Na, K, Ca, Mg, Fe, Zn, Mn, and Cu in the assortments of fall fruits we analysed (Tables 1 and 2) and the recommended mineral intake [12] allowed us to estimate their supply in the recommended dietary allowances [7, 12].

The mineral supply, i.e. the degree of coverage of the recommended dietary allowances of minerals calculate for 400 g of fresh fruit (the equivalent of two medium-size apples eaten at two main meals) is shown in Table 3 below.

**Table 3. Mean supply with some bio elements of the recommended dietary allowances for a mean consumption of 400 g of fresh fruit**

Group/Life Stage	Bio element supply of the RDA (%)							
	Na	K	Ca	Mg	Fe	Mn	Zn	Cu
<b>Males, aged 30-70</b>	0.18	14.66	2.76	7.24	16.45	9.57	3.96	9.33
<b>Females, aged 30-70</b>	0.18	14.66	2.76	9.50	7.31	12.22	5.45	9.33

The mean supply of bio elements in the recommended dietary allowances by fall fruits has different values depending on the nature of the element and on the category of consumer (male or female).

In the case of macro-elements, the supply of minerals reached 14.66% K – in males and females, 9.50% Mg – in females and 7.24% Mg – in males, 2.76% Ca – in males and females, and 0.18% Na – in males and females.

The supply in microelements is slightly higher: 16.45% Fe – in males and 7.31% Fe – in females, 12.22% Mn – in females and 9.57% Mn – in males, 9.33 % Cu – in males and females, and 5.45% Zn – in females and 3.96% Cu – in males.

## Conclusions

The analysed Fall fruits are to be noted for their important contents of K, Ca, Mg, and Na and for their appreciable amounts of Fe, Mn, Zn, and Cu, showing no contamination risk by toxic elements.

The mean values of the mineral supply in the recommended dietary allowances, under experimental conditions, show that these fruits could be taken into account as an alternative supplementary source of certain bio elements such as K, Mg, Fe, Mn, and Cu.

## Acknowledgements

We thank Prof.Dr.Eng. Petru Negrea for ICP-MS spectrometry, Politehnica University - Research Institute for Renewable Energy (ICER) – Timisoara.

## References

- [1]. I.J. Cindric, I. Krizman, M. Zeimer, Š. Kampic, G. Medunic, G. Stinger, Food Chem 135 (4), pp. 2675-2680, (2012).
- [2]. A. Dehelean and D.A. Magdaş, The Scientific World Journal, Volume 2013, pp. 285-289, (2013).
- [3]. I.Gogoasă, L.M. Alda, D. Bordean, M. Rada, A. Velciov, S. Popescu, S. Alda, I. Gergen, Journal of Horticulture, Forestry and Biotechnology, Volume 18(4), pp. 108-112, (2014).
- [4]. M. Grembecka, P. Szefer, Grembecka M, Szefer P., Environmental Monitoring and Assessment , Volume 185, Issue 11, pp. 9139-9160, (2013).
- [5]. R. C., Hegheduş-Mîndru, G. Hegheduş, P. Negrea, R. Şumălan, A. Negrea, D. Ştef, Annals of Agricultural and Environmental Medicine, Vol 21, No 1, 98–105, (2014).
- [6]. C. Ji-luan; WU, Ji-hong; J. Ying, HU Xiao-song, Spectroscopy and Spectral Analysis, Volume 9, Number 2, pp. 496-498 (2009).
- [7]. O.A. Levander, Hortscience, Vol. 25(12), (1990).
- [8]. O. Rop, J. Balík , V. Řezníček, T. Juríková, P. Škardová, P. Salaš, J. Sochor , J. Mlček and D. Kramářová, Czech J. Food Sci. Vol. 29, No. 1: 65–73, (2011).
- [9]. D. Todea, O. Cadar, D. Simedru, C. Roman, C. Tanaselia, I. Suatean, A. Naghiu, Not Bot Horti Agrobi, 42(2), pp.523-52, (2014).
- [10]. ORDIN nr. 975/1998 al Ministerului Român de Sanatate Publica JECFA, (2005).
- [11]. <http://incomemagazine.ro/articole/topul-celor-mai-sanatoase-fructe-ale-toamnei>.
- [12]. www.nap.edu. Dietary Reference Intakes (DRIs): Recommended Dietary Allowances and Adequate Intakes, Elements.

## The Influence of Total Chromium Soil Content on the Maize Zinc Levels, in a Polluted Area

Liana Maria Alda\*, Simion Alda, Diana Moigradean\*\*, Teodor Cristea, George Andrei Draghici, Luminita Pirvulescu, Iosif Gergen

<sup>1</sup>Banat's University of Agricultural Science and Veterinary Medicine "King Mihai I of Romania", 300645 Timisoara 119, Calea Aradului, Romania;

\*e-mail: lianaalda@yahoo.com

\*\*e-mail: dimodean@yahoo.com

### Abstract

Chromium compounds are highly toxic to plants and are detrimental to their growth and development. Cr is toxic to most higher plants at 100  $\mu\text{MKg}^{-1}$  dry weight, while Zn is an essential plant nutrient. The essentiality of Zn in plants was first shown in maize. The aim of this paper was to determine the influence of Cr contaminated soils on the accumulation of Zn in maize (*Zea mays L.*) grains, sampled from Tarnaveni area (Mures County, Romania), a well known industrial center. The heavy metals contents in soils and maize were determined by flame atomic absorption spectrometry using a ContrAA 300 spectrophotometer with high resolution continuum source. In soil, Cr contents ranged from 9.7 ppm to 80.73 ppm and Zn from 21.77 to 99.87 ppm. In corn, the values for Cr are between 0.081 to 0.11 ppm and for Zn between 44.74 to 132.66 ppm. Mathematical modeling indicates that chromium in the soil might be the one which is determining the evolution of zinc corn content.

### Introduction

Zinc is an essential plant nutrient. The essentiality of Zn in plants was first shown in maize [12]. Zinc deficiency is one of the most widespread micronutrient deficiencies in plants and causes severe reductions in crop production [5].

Chromium compounds are highly toxic to plants and are detrimental to their growth and development. Although some crops are not affected by low Cr concentration ( $3.8 \times 10^{-4} \mu\text{M}$ ) [9,10], Cr is toxic to most higher plants at 100  $\mu\text{MKg}^{-1}$  dry weight [6].

Soil pH is influencing the accumulation of chromium in plants, observation confirmed by various literature data[2].

Barcelo et al. found high correlation between chlorophyll pigments and Fe and Zn uptake in Cr-stressed plants [1].

The accessibility of metals for plants depends on soil reaction, mineral colloids, soil humidity, microbiological activity and organic matter content [16]. Literature contains numerous data on the distribution of minerals in plants from spontaneous flora or cultivated in different geographical areas, as well as a series of mineral analysis techniques [3,4,7].

The aim of this paper was to determine the influence of Cr contaminated soils on the accumulation of Zn in maize (*Zea mays L.*) grains, sampled from Tarnaveni area (Mures County, Romania), a well known industrial center.

### Experimental

The prelevations points are located in a polluted area (Tărnaveni- Mures County, Romania). Soil and maize samples were collected from four familiarly farms located in the studied area. From each prelevation points (PP) were collected soil (0-40 cm depth) and maize samples. Determination of pH has been accomplished in watery suspension in report with the soil: water of 1:2.5.

The heavy metals contents in soils and maize were determined by flame atomic absorption spectrometry using a ContrAA 300 spectrophotometer with high resolution continuum source (Analytik Jena, Germany).

The FAAS determination of minerals, in the analysed samples needed two working steps: mineralisation through calcination followed by the solubilisation of the inorganic matter in nitric acid 0.5 N up to 50 ml. The solutions obtained were used for total metal content determinations [11].

*Statistical analysis.*

*Cluster analysis* permits to form groups of related variables (similar to what is done in factor analysis), in such a way that objects in the same group (called a cluster) are more similar to each other than to those in other groups (clusters) [14]. Cluster analysis was performed using PAST (version 2.14), [8].

*Principal Components Analysis* (PCA) is a mathematical model that permits to identify patterns in data by expressing the data to highlight their similarities and differences [8].

## Results and discussion

The pH level of soil, in studied area, registered values between 7.67 and 8.73.

The results were expressed in ppm ( $\text{mgKg}^{-1}$  dry weight).

Regarding the heavy metals contents in soil, Cr ranged from 9.7 ppm to 80.73 ppm and Zn from 21.77 to 99.87 ppm.

In corn, the values for Cr are between 0.081 to 0.11 ppm and for Zn between 44.74 to 132.66 ppm. Each value is an average of 3 replicates.

According to Table 1 (the maximum admitted concentrations for soils), in the sensitive areas revealed to be exceeded for Cr (30 ppm) in 3 sites.

The soil levels of Zn do not exceed the reference value (100 ppm) in the sensitive area.

**Table 1:** Romanian guideline on the admitted concentrations of Cr and Zn in soil [19]

Element	RVS(ppm)	ALVS(ppm)	AITV(ppm)
Cr	30	100	600
Zn	100	300	1500

**Legend:** RSV = Reference value in the sensitive area, ALVS = Alert level value in the sensitive area, AITV = Area intervention threshold value

Further, mathematical modeling indicates that chromium in the soil might be the one which is determining the evolution of zinc corn content, in all four locations (Figure 1 and 2).

Spatial interpolation map (Figure 3) highlights that the level of Zn in corn depends on the total chromium soil content for all the analyzed samples.

Our research is in accord with other studies [8] who found high correlation between Zn uptake in Cr-stressed plants.

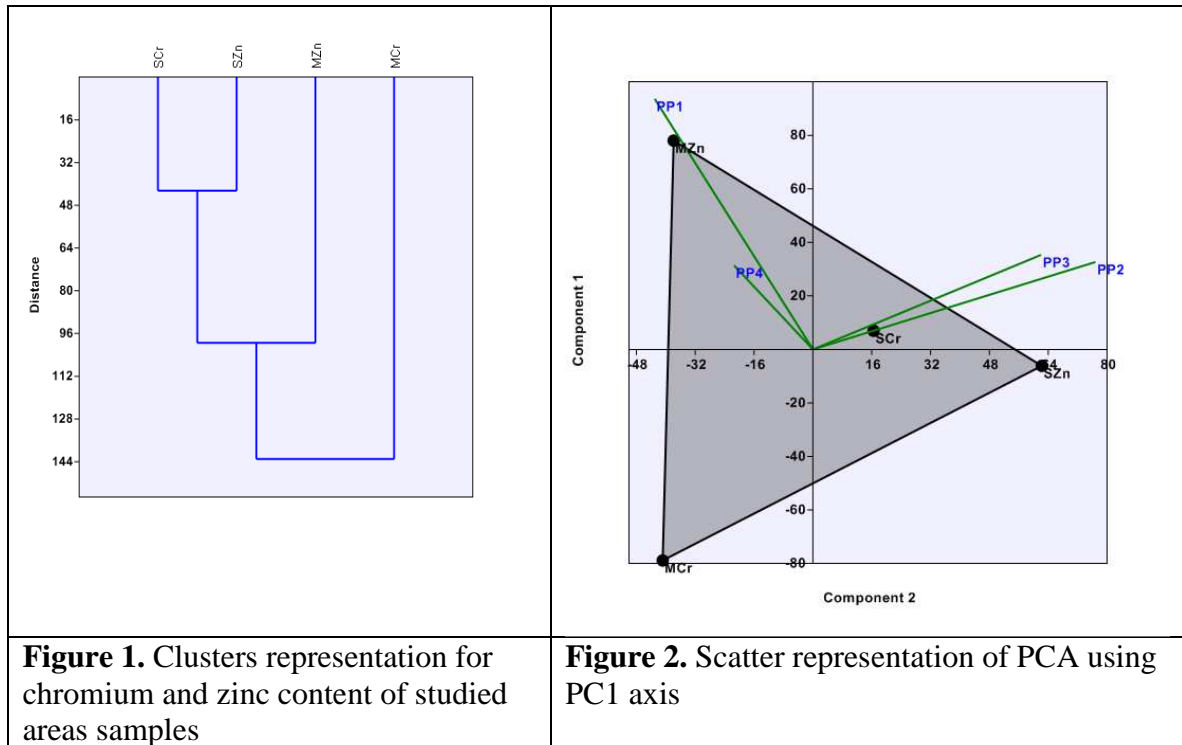


**Figure 1.** Clusters representation for chromium and zinc content of studied areas samples

**Figure 2.** Scatter representation of PCA using PC1 axis

**Legend:** SCr=Cr contents in soil, SZn=Zn contents in soil, MCr=Cr contents in maize, MZn=Zn contents in maize;

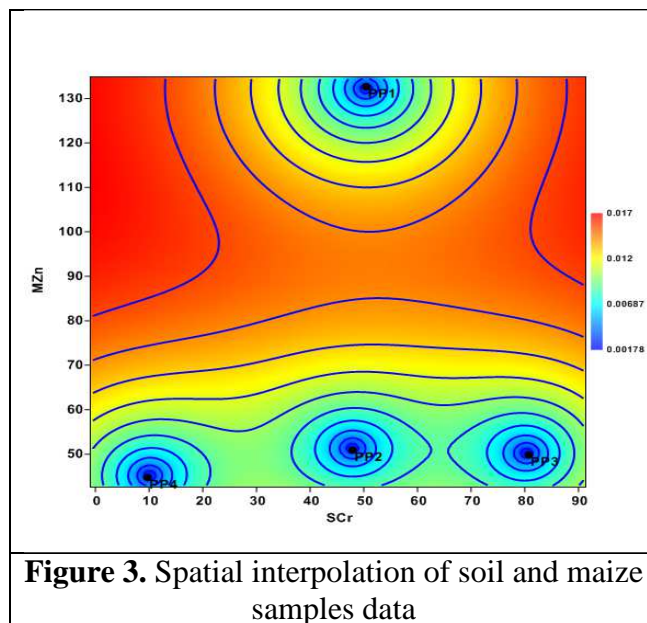


**Figure 3.** Spatial interpolation of soil and maize samples data

## Conclusions

In soil, sampled from Tarnaveni area, Cr ranged from 9.7 ppm to 80.73 ppm and Zn from 21.77 to 99.87 ppm.

In corn, the values for Cr were between 0.081 to 0.11 ppm and for Zn between 44.74 to 132.66 ppm.

Mathematical modeling indicates that chromium in the soil might be the one which is determining the evolution of zinc corn content.

## References

- [1] J. Barcelo, C. Poschenriender, A. Ruano, B. Gunse, *Plant Physiol Suppl*, 1985;77:163 – 4.
- [2] D. M. Bordean, 2012, *Journal of Horticulture, Forestry and Biotechnology*, 16(2), 106-111.
- [3] D. M. Bordean, I. Gergen, M. Harmanescu, L. Pirvulescu, M. Butur, C. I. Rujescu, 2010. *J Food Agric & Environ*, 8(2), 1054-1057.
- [4] D. M. Bordean, I. Gergen, I. Gogoasă, G. Oprea, L. Pirvulescu, L. M. Alda, M. Harmanescu, 2011, *J Food Agric & Environ*, 9(1), 680-683.
- [5] I. Cakmak, 2000, *Tansley Review No. 111, New Phytologist*, 185-205.
- [6] FT Davies, JD Puryear, RJ Newton, JN Egilla, JS Grossi., *J Plant Nutr*, 2002, 25:2389–407.
- [7] I. Gogoasa., V. Jurca, L. M. Alda, A. Velciov, M. Rada, S. Alda, C. Sirbulescu, D.M. Bordean, I. Gergen, 2013, *Journal of Horticulture, Forestry and Biotechnology Volume 17(4)*, 65- 67.
- [8] O. Hammer, D. A. T. Harper, P. D. Ryan, 2001, *Palaeontologia Electronica*, 4: 1-9.
- [9] Jr EWD Huffman, HW. Allaway, *J Agric Food Chem* 1973a, 21, 982 – 6.
- [10] Jr EWD Huffman, HW. Allaway, *Plant Physiol* 1973b, 52, 72 – 5.
- [11] R. Lacatusu, A. R. Lacatusu, 2008, *Carpth. J. of Earth and Environmental Science*, 3, pp. 115–129.
- [12] P. Mazé, 1915, *Comptes Rendus Hebdomadaires des Séances de L'académie des Sciences* 160: 211–214.
- [13] *Monitorul Oficial al Romaniei*, No. 303 bis/ 6 XII 1997/ OM 756/1997, 1997, <http://mmediu.ro/new/wp-content/uploads/2014/10/OM-184-1997-bilant-de-mediul-si-OM-756-1997-evaluarea-poluării-mediului.pdf>.
- [14] M. Norušis, IBM SPSS Statistics Guides, 2011, [http://www.norusis.com/pdf/SPC\\_v13.pdf](http://www.norusis.com/pdf/SPC_v13.pdf);
- [15] F. Skoog, 1940, *American Journal of Botany*, 27, 939–951.
- [16] D. S. Ștef, I. Gergen, T. I. Trașcă, M. Hărmănescu, L. Ștef, M. Drugă, G. Heghedus-Mindru, 2010, *Scientific Papers Animal Science and Biotechnologies*, 43(1), 127-132.



## Improved Electrical Response in GdMnO<sub>3</sub> Doped (K, Na)NbO<sub>3</sub> Piezoelectric Speaker

Bucur Raul Alin, Bucur Alexandra Ioana

National Institute for Development and Research in Electrochemistry and Condensed Matter  
Timisoara, Condensed Matter Department, no. 1 Plautius Andronescu, 300224, Romania,  
Tel./Fax.: +40 0256 204698;  
e-mail: raul\_alin\_bucur@yahoo.com

### Abstract

[(K<sub>0.368</sub>Na<sub>0.432</sub>)Li<sub>0.5</sub>][Nb<sub>0.86</sub>Sb<sub>0.04</sub>Ta<sub>0.1</sub>]O<sub>3</sub> doped with 0.5 mol% GdMnO<sub>3</sub> piezoelectric speakers were obtained, with good frequency sensibility in the range 20 Hz – 20 kHz. The additive used distorts the crystalline structure to a mixture of orthorhombic and tetragonal phases at room temperature. Also the dopants used shift the high temperature phase transitions toward room temperature. Good piezoelectric properties were obtained for doped samples, with an optimum piezoelectric charge constant  $d_{33}$  of 127 for [(K<sub>0.368</sub>Na<sub>0.432</sub>)Li<sub>0.5</sub>][Nb<sub>0.86</sub>Sb<sub>0.04</sub>Ta<sub>0.1</sub>]O<sub>3</sub> - 0.5 mol % GdMnO<sub>3</sub>, a planar coupling coefficient of 0.39 and a quality factor of 102.

### Introduction

The most common piezoelectric ceramics used nowadays for actuators and sensors applications are lead oxide based ferroelectrics, especially Pb(Zr,Ti)O<sub>3</sub> (noted as PZT). Their excellent piezoelectric and dielectric properties [1], make such materials a suitable choice for commercial products. Nevertheless, a major issue of these materials is the toxicity of Pb compounds, relative to the environment and man. As a result of E.U. directives on waste from electrical and electronic equipment (WEEE) and restriction of hazardous substances (RoHS) [2], the latest trends in scientific research are oriented toward “environmental friendly” materials. As a consequence, many lead free piezoelectric materials are nowadays intensively studied: modified BaTiO<sub>3</sub> [3], bismuth layer structure ferroelectrics [4], (Na<sub>0.5</sub>Bi<sub>0.5</sub>)TiO<sub>3</sub> [5] and (K<sub>0.5</sub>Na<sub>0.5</sub>)NbO<sub>3</sub> (denoted as KNN) [6, 7]. Presently, the most promising lead-free piezoelectric ceramics are based on potassium sodium niobate modified with different additives, sintering aids or doped with other perovskite structures.

The purpose of this work is to fabricate piezoelectric speakers based on lead free materials. [(K<sub>0.368</sub>Na<sub>0.432</sub>)Li<sub>0.5</sub>][Nb<sub>0.86</sub>Sb<sub>0.04</sub>Ta<sub>0.1</sub>]O<sub>3</sub> was previously reported with improved piezoelectric properties [8], due to the presence of morphological phase boundaries between orthorhombic and tetragonal crystalline phases at room temperature. GdMnO<sub>3</sub> was considered in this work to improve the piezoelectric properties and frequency response of the lead free piezoelectric speaker. The ceramics obtained were characterized using x-ray diffraction (PANalytical X'Pert Pro MPD) and scanning electron microscope (Inspect S Phillips). Dielectric measurements were performed with a programmable RLC-meter TEGAM-3550, ferroelectric hysteresis loop was obtained using a Sawyer-Thomson circuit and an Atten ADS 1152CML digital storage oscilloscope. A complete set of piezoelectric properties were obtained using a network analyzer Agilent E5100A. The relative sound pressure generated by the piezoelectric speaker was recorded using Audacity 2.0.5 software.

### Experimental

Solid state reaction was used to prepare (K<sub>0.5</sub>Na<sub>0.5</sub>)NbO<sub>3</sub> noted KNN, [(K<sub>0.368</sub>Na<sub>0.432</sub>)Li<sub>0.5</sub>][Nb<sub>0.86</sub>Sb<sub>0.04</sub>Ta<sub>0.1</sub>]O<sub>3</sub> noted KNLNST, and [(K<sub>0.368</sub>Na<sub>0.432</sub>)Li<sub>0.5</sub>][Nb<sub>0.86</sub>Sb<sub>0.04</sub>Ta<sub>0.1</sub>]O<sub>3</sub> – 0.5 mol% GdMnO<sub>3</sub> noted KNLNST-0.5GM. All the samples were calcined at 880° C with a 5 deg·min<sup>-1</sup> slope and a five hours dwell time. The

resulting powders were mixed with a 5 mass% PVA binder, cold pressed at 200 MPa into disk samples of 10 mm in diameter and 0.5 mm thickness, respectively into bar shapes of 6 mm in length and 1.8 mm in width/thick, and sintered at 1090°C for 3 hours. Silver electrodes were formed on each side of the disks. The ceramics were poled in silicone oil at room temperature under a direct current electric field of 4 kV/mm for 30 min. The piezoelectric speakers were then constructed from poled disk glue with silver paint to a thin metal plate, serving as a mechanical amplification of the vibrations produced by the piezoceramic.

## Results and discussion

The X ray diffraction patterns presented in figure 1 of KNN and doped KNN ceramics, shows a perovskite phase structure, with no secondary phases present. The presence of additive change the crystalline structure at room temperature from orthorhombic for KNN, to a mixed orthorhombic-tetragonal for KNLNST and KNLNST-0.5GM, visible from the diffracted angles shift presented in the inset.

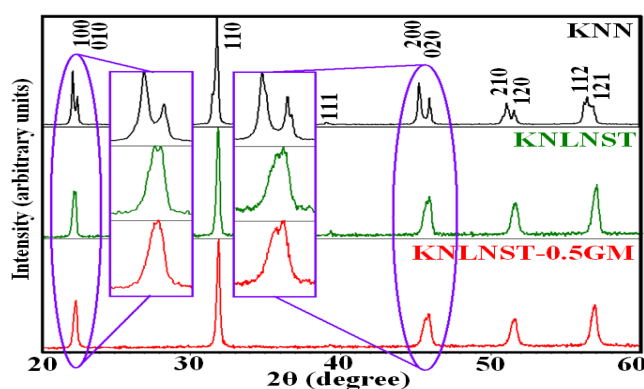


**Figure 1.** X ray diffractions of the sintered ceramics.

The dielectric constant (figure 2) was measured from room temperature up to 430° C, at 1 kHz. For the reference sample KNN, we can noticed two inflexions of the dielectric constant, corresponding to different phase transitions: from room temperature, where the system crystallize in orthorhombic crystal structure, at 210°C the system distorts to tetragonal and then to cubic at 410°C (Curie temperature). Similar behavior was noticed for doped KNN samples, but all the phase transition temperatures are significantly shifted to lower temperatures: 80°C for orthorhombic - tetragonal and 295°C for the Curie temperature for KNLNST, respectively 65°C and 260°C for KNLNST-0.5GM.

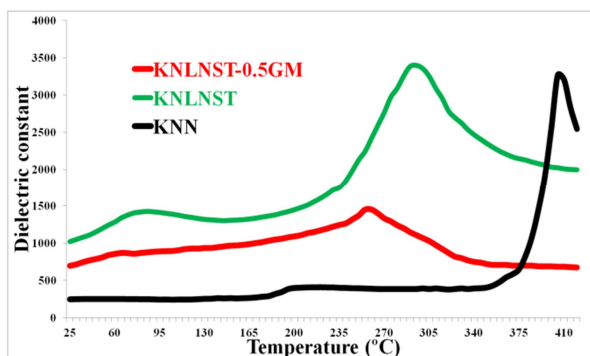


**Figure 2.** The temperature dependence of the dielectric constant for sintered ceramics.

From the hysteresis loops of the unpoled ceramics (figure 3), we can conclude that all the additives used contribute to a softening of ferroelectric properties. From 13.2  $\mu\text{C}/\text{cm}^2$  for

KNN, the remnant polarization increase up to  $13.5 \mu\text{C}/\text{cm}^2$  for KNLNST, respectively  $14.5 \mu\text{C}/\text{cm}^2$  for KNLNST-0.5GM. The coercive field however drops from 20 kV/cm for KNN, down to 15 kV/cm for KNLNST, respectively 14 kV/cm KNLNST-0.5GM. The observed softening of ferroelectric properties is to be related to a higher freedom of domain walls, due to the presence of dopants, since a lower electrical field is necessary to reduce the remnant field to zero.

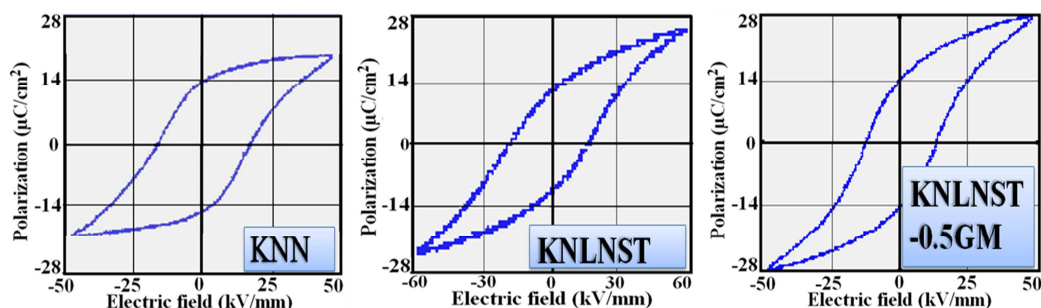


**Figure 3.** Room temperature hysteresis loops of sintered thin ceramic disks.

After poling of the ceramics at room temperature, in silicon oil under an electric field of 4 kV/mm, the samples were aged for 1 day. Resonance and anti-resonance curves (figure 4) were obtained at room temperature. For a complete determination of piezoelectric coefficients, both radial mode (left) and length mode (right) oscillations were obtained. For the reference sample KNN, poor frequency response was obtained, with badly outlined resonant frequencies and phases shift. An improved and sharper response was obtained for KNLNST and KNLNST-0.5GM ceramics in radial mode. An optimum frequency response was observed for KNLNST-0.5GM in length mode, suggesting improvements of piezoelectric properties.

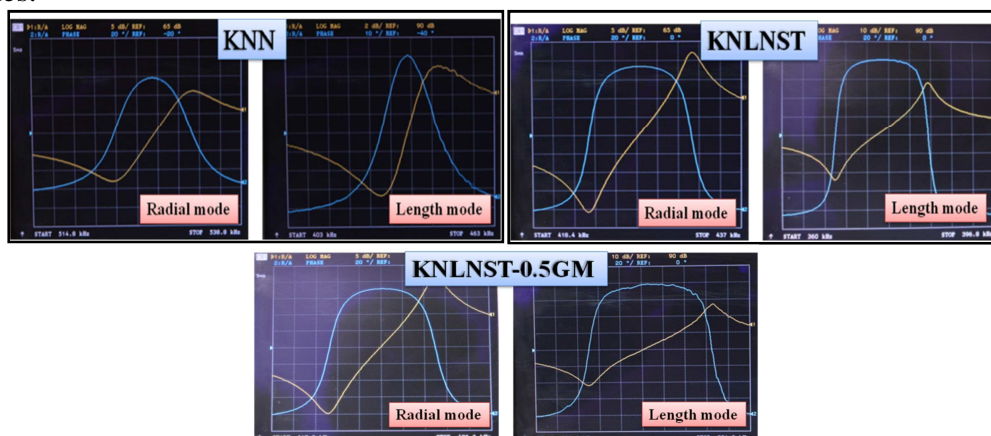


**Figure 4.** Resonance and anti-resonance curves in radial and length mode.

The frequency response of the piezoelectric speakers, in terms of relative sound pressure, was evaluated in the range 50 Hz- 20000 Hz. The speaker based on KNN (insets in figure 5), responds very well to frequencies up to 180 Hz, and has a moderate response for 180 Hz-2000 Hz, with a rapid decrease in sensibility for higher frequencies. In the case of the piezoelectric speaker based on KNLNST (figure 5 in the middle), the relative sound pressure recorded show an improved frequency response compared to pure KNN. The speaker maintains a good sensibility to low frequencies (20 Hz -180 Hz) but an increased sensibility is noticed in the frequency range 200 Hz – 4 kHz. At higher frequencies, we notice a similar rapid decrease in sensibility as KNN. For KNLNST-0.5GM, the maximum frequency sensibility is obtained, particularly in the range 600 Hz – 10 kHz. Good piezoelectric

properties were obtained for doped samples (table 1), with an optimum piezoelectric charge constant  $d_{33}$  of 127 for KNLNST-0.5GM, planar coupling coefficient of 0.39 and a quality factor of 102.

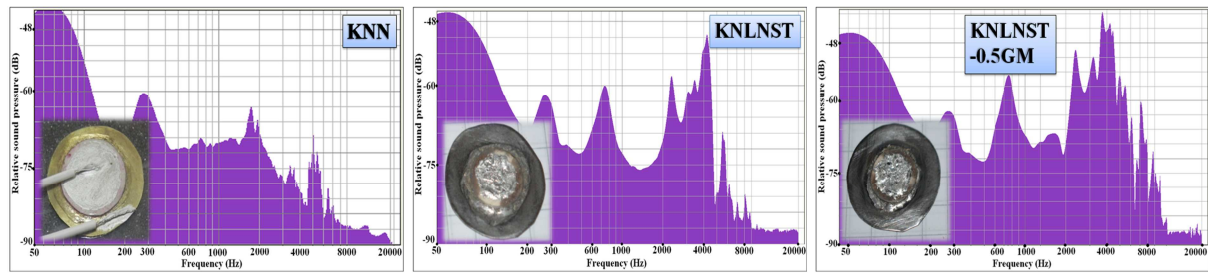


**Figure 4.** Relative sound pressure response of KNN based speakers, and insets illustrating the piezoelectric speaker disks.

**Table 1.** Piezoelectric properties of sintered ceramic.

Properties	KNN	KNLNST	KNLNST-0.5GM
<b>Q</b>	407	158	102
<b><math>k_{31}</math></b>	0.19	0.21	0.17
<b><math>k_p</math></b>	0.35	0.38	0.39
<b><math>S_{11}^E [10^{-12} \text{ m}^2/\text{N}]</math></b>	7.4	5.9	10.1
<b><math>S_{12}^E [10^{-12} \text{ m}^2/\text{N}]</math></b>	2.5	2.4	4.1
<b><math>S_{11}^D [10^{-12} \text{ m}^2/\text{N}]</math></b>	6.76	5.68	9.83
<b><math>d_{31} [10^{-12} \text{ C/N}]</math></b>	28.8	41.7	45.9
<b><math>g_{31} [10^{-3} \text{ Vm/N}]</math></b>	9.4	5.7	7.1
<b><math>k_{33}</math></b>	0.38	0.42	0.42
<b><math>d_{33} [10^{-12} \text{ C/N}]</math></b>	82	93	127
<b><math>g_{33} [10^{-3} \text{ Vm/N}]</math></b>	17.3	14.6	10.1
<b><math>S_{33}^D [10^{-12} \text{ m}^2/\text{N}]</math></b>	9.4	20	11.1
<b><math>S_{33}^E [10^{-12} \text{ m}^2/\text{N}]</math></b>	10.5	21.1	13.1

## Conclusion

We have successfully obtained  $(\text{K}_{0.5}\text{Na}_{0.5})\text{NbO}_3$ ,  $[(\text{K}_{0.368}\text{Na}_{0.432})\text{Li}_{0.5}][\text{Nb}_{0.86}\text{Sb}_{0.04}\text{Ta}_{0.1}]\text{O}_3$ ,  $[(\text{K}_{0.368}\text{Na}_{0.432})\text{Li}_{0.5}][\text{Nb}_{0.86}\text{Sb}_{0.04}\text{Ta}_{0.1}]\text{O}_3 - 0.5 \text{ mol\% GdMnO}_3$  piezoelectric speakers. At room temperature Li, Sb and Ta distorts the crystalline structure from orthorhombic to a mixed orthorhombic-tetragonal, while  $\text{GdMnO}_3$  maintain such distortion. The remnant polarization increase from  $13.2 \mu\text{C}/\text{cm}^2$  for KNN, to  $14.5 \mu\text{C}/\text{cm}^2$  for KNLNST-0.5GM. Compared to the reference sample KNN, the presence of additive decrease the coercive field, suggesting a softening of ferroelectric properties. Also the additives decrease the temperature of all phase transitions. Good piezoelectric properties were obtained for doped samples, with an optimum piezoelectric charge constant  $d_{33}$  of 127 for KNLNST-0.5GM, planar coupling coefficient of 0.39 and a quality factor of 102. The piezoelectric speaker based on  $[(\text{K}_{0.368}\text{Na}_{0.432})\text{Li}_{0.5}][\text{Nb}_{0.86}\text{Sb}_{0.04}\text{Ta}_{0.1}]\text{O}_3 - 0.5 \text{ mol\% GdMnO}_3$  has the best frequency response in the range 20 Hz -20 kHz. The high relative sound pressures recorded suggest that this composition can be successfully used for practical applications.

## References

[1] B. Jaffe, W. Cook, H. Jaffe, Piezoelectric Ceramics, Academic Press, NY, 1971, p. 92.

- [2] E.U. directives on waste from electrical and electronic equipment: 2002/95/EC and 2008/35/EC
- [3] R.A. Bucur, A.I. Bucur, S. Novaconi, I. Nicoara, J. Alloy. Compd. 539 (2012), 148–153.
- [4] T. Takenaka, H. Nagata, *Ferroelectrics* 336 (2006) 119.
- [5] Y.M. Li, W. Chen, Q. Xu, J. Zhou, H.J. Sun, M.S. Liao, *J. Electroceram.* 14 (2005) 53.
- [6] R. Bucur, A. Bucur, I. Nicoara, *Lead-free piezoelectric ceramics*, 11th ISIRR Szeged 2010.
- [7] R. Bucur, I. Badea, A. Bucur, S. Novaconi, *Lead free piezoelectric buzzers based on (K, Na)NbO<sub>3</sub>*, 20th ISIRR Szeged 2014.
- [8] Z.W. Chen, J.G. Hu, *Trans. Nonferrous Met. Soc. China* 18 (2008), 623-626.

## Pesticide Residues in Maize by LC-MS/MS

Gorica Vuković<sup>1\*</sup>, Vojislava Bursić<sup>2</sup>, Maja Meseldžija<sup>2</sup>, Bojana Špirović-Trifunović<sup>3</sup>,  
Snežana Tanasković<sup>4</sup>

<sup>1</sup>*Institute of Public Health, Bul. despota Stefana 54a, Belgrade, Serbia*

<sup>2</sup>*Faculty of Agriculture, University of Novi Sad, Trg Dositeja Obradovića 8, Novi Sad, Serbia*

<sup>3</sup>*Faculty of Agriculture, University of Belgrade, Nemanjina 6, Zemun, Serbia*

<sup>4</sup>*Faculty of Agronomy Čačak, University of Kragujevac, Cara Dušana 34, Čačak, Serbia*  
e-mail: goricavukovic@yahoo.com

### Abstract

The liquid chromatography tandem-mass spectrometry (LC–MS/MS) with ESI was applied for the detection of 60 pesticides residues in maize, extracted with QuEChERS. The average recoveries for all analites were 83.7-121.9% (RSDs 4.82-15.34%). The obtained  $R^2$  values for all investigated pesticides were higher than 0.99. The LOQs of 0.01 mg/kg confirm that the method is appropriate for the determination of pesticide residues in all investigated vegetables according to the regulations of the Serbian and EU MRLs. One sample was with no detected pesticide residues and in three samples only one pesticide residue was detected. The multiple detections were confirmed in three analyzed samples. All the detections were below the MRLs.

### Introduction

Maize (*Zea mays*) is an annual plant – a crop from grass family (*Graminae*) the cultivation of which is widespread due to the fact that it is used as food and feed. Its grains, as basic raw material, are of particular significance as they contain 70-75% of carbohydrates, 10% of proteins, about 5% of oil, 15% of mineral compounds as well as 2.5% of cellulose.

The goal of modern agricultural production is obtaining high and qualitative yields of agricultural products [1-2]. To achieve these results and to obtain qualitative and quantitative justified yields it is necessary to apply plant protection products. The use of pesticides in agriculture continues to increase as much as food is needed to meet the demands of the growing population and also for the export [3]. The human exposure to low doses of pesticides through food consumption has led to chronic toxicity which can lead to birth defects, cancers, endocrine disruption or reproductive dysfunctions [4]. Crop protection problems refer to all the biotic and abiotic factors [5].

Based on the register of plant protection products sold in Serbia, 239 products have been registered for maize protection, which emphasizes the need for pesticide residues control regarding this crop [6].

That is why the aim of this study has been to determine the content of 60 pesticides in maize samples by the validated multiresidue method using liquid chromatography tandem mass spectrometry (LC–MS/MS).

### Experimental

**Plant material.** The seven maize samples were collected directly from the farmers from Rivnica and Novi Slankamen, Vojvodina, Serbia.

The sampling was carried out in accordance with the “Regulations over the methods of food sampling and testing aimed at the determination of plant protection product residues in food” [7] which defines the sampling methods and the minimum size of laboratory samples.



Seven average samples of maize were taken at the stage of technological maturity from the farmers. The samples were put into polyethylene bags and promptly transported to the laboratory. Each sample was homogenized on the arrival in the laboratory and kept in the freezer at the temperature of -18 °C till being analyzed [8].

**Sample analyses.** For LC analysis, an Agilent 1200 HPLC system with a binary pump was used. For chromatography separation, Zorbax XDB C18 analytical column of 50 × 4.6mm and 1.8 µm particle size (Agilent Technologies) was used. For the mass spectrometric analysis, an Agilent 6410B Triple-Quad LC/MS system was used. Agilent by MassHunter Workstation Software version B.04. was applied for the method acquisition and data processing.

**Validation.** The method was validated according to SANCO/12571/2013.

The limit of detection - LOD was determined as the lowest concentration giving a response of three times the average baseline. The ratio signal/noise in the obtained chromatograms for the LOD was calculated by MassHunter Qualitative Software.

The linearity was checked using matrix matched standards (MMS) at the concentrations of 5.0, 10.0, 25.0, 50.0 and 100.0 ng/mL.

The recovery was checked by enriching 5 g of a blank sample with the mixture of pesticide standard of 10 µg/ml in the amount of 50 and 25 µL (final mass concentration 0.10 and 0.05 mg/kg) and with the mixture of pesticide standard of 1 µg/mL in the amount of 100 µl (final mass concentration 0.01 mg/kg) with the addition of the internal standard carbofuran-D3.

**Pesticide extraction.** A 5 g of homogenate samples was weighed into 50 mL PP centrifuge tube. Five milliliters of water was added and mixed by vortex. For the extraction of the pesticides, 10 mL of acetonitrile was added and the tube was shaken for 30 sec. A mixture of 21 g of NaCl, 4g of MgSO<sub>4</sub>, 1 g of trisodium citrate dehydrate, and 0.5 g of disodium hydrogencitrate sesquihydrate was added, and the tube was vigorously shaken for 1 min, followed by centrifugation for 5 min at 3500 rpm. An aliquot of 6 mL of the supernatant acetonitrile phase was transferred into 15 mL PP centrifuge tube containing 150 mg PSA and 900 mg MgSO<sub>4</sub>, and the tube was vigorously shaken for 30 sec. One milliliter of aliquot evaporated nearly to dryness and reconstituted in 1 mL of mixture methanol/water (50:50, V/V) contained 0.1% of formic acid.

## **Results and discussion**

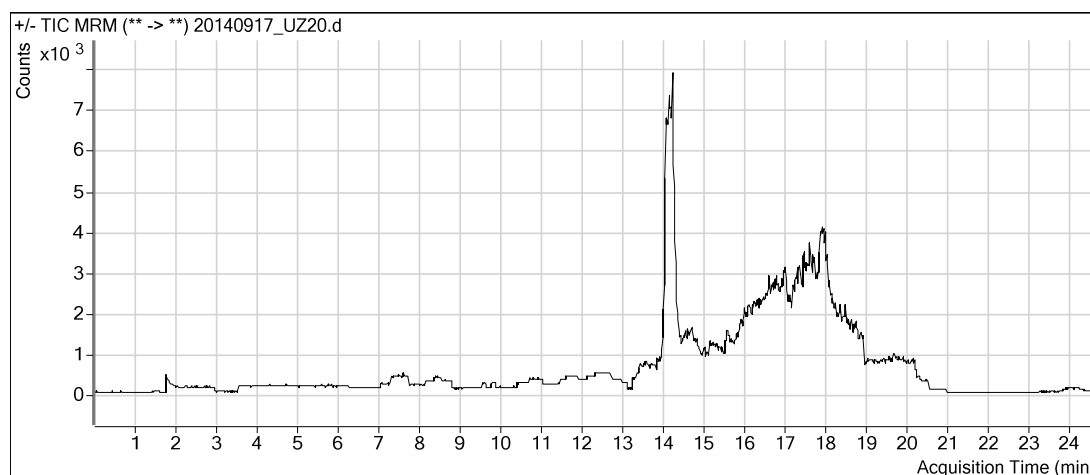
The LC-MS/MS was used for the simultaneous residue determination of 60 pesticides in the maize samples. The validated method which uses the LC-MS/MS provides a very high sensitivity, good reproducibility, appropriate linearity and can be applied with the high reliability to the analysis of investigated pesticide residues in maize samples.

The LOQs was 10 mg/kg with the average recoveries for all analites from 83.7 to 121.9% (RSDs 4.82-15.34%). The obtained coefficients of correlations ( $R^2$ ) values for all investigated pesticides were higher than 0.99.

The analyses of the obtained data from the LC-MS/MS analyses show that the most frequently detected pesticides were pirimifos-methyl, metalaxyl-M and acetamiprid.

One maize sample was with no pesticide residues detection, or detections were below the LOQ. In three samples one pesticide was detected: acetamiprid, pirimifos-methyl and metalaxyl-M, respectively. Three samples were with multiple detections, two with four and one with three detected pesticides (sample number 1. acetamiprid, difenoconazol and metalaxyl-M; sample number 6. carbendazim, metalaxyl-M and pirimifos-methyl and sample number 7. clothianidin, metalaxyl-M, pirimifos-methyl and thiametoxam).

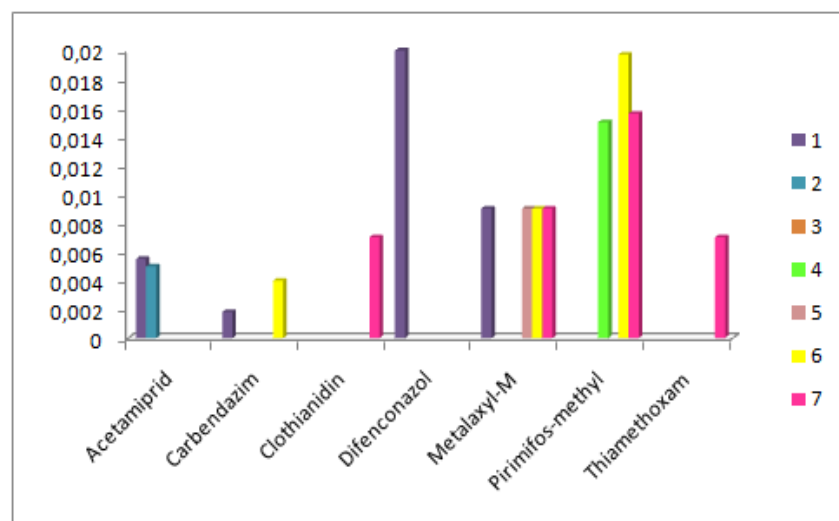
**Figure 1.** LC-MS/MS chromatogram of a maize sample



Off. Gazzete RS No 29/2014 regulates the maximum limits the amount of pesticide residues in agricultural products whereby the Regulations are in compliance with the MRLs as regulated in the European Union, i.e. by Regulation 396/2005.

When comparing the detected values of pesticides in the analyzed maize samples with the MRL values all the detections were found to be in accordance with their limits.

**Figure 2.** Detected pesticides in maize samples (mg/kg)



## Conclusion

The high percentage of samples (85.71%) positive to the pesticide residues which are below the MRL values, emphasizes the need for the continuous food safety control in the production, in order to successfully prevent harmful effects of pesticides on the healths of humans and animals, as well as to secure the obligatory adherence to the rules of GAP-a (Good Agricultural Practice).

However, the alarming fact is that farmers, in their production, tend to use the compounds, i.e. active substances which have not been registered and are not allowed for use in maize protection. Among the detected insecticides there are acetamiprid, thiamethoxam, clothianidin and pirimifos-methyl which are not registered for the application on maize as well as the

detected fungicides carbendazim and difenoconazol. The only detected pesticide permitted to be used on this crop is the fungicide metalaxyl-M.

It is interesting to note that, although a large number of herbicides are used for maize protection from weeds, none were registered in the investigated samples.

## **References**

- [1] R. Baličević, V. Rozman, E. Raspudić, M. Brmež, Z. Lončarić, V. Bursić, M. Ravlić, A. Sarajlić, P. Lucić, P., 50<sup>th</sup> Croatian and 10<sup>th</sup> International Symposium on Agriculture, Opatija, Croatia, Proceedings, (2015) 49
- [2] V. Bursić, G. Vuković, R. Čabilovski, M. Meseldžija, A. Popović, R. Baličević, N. Budić, Plant doctor, 43 (3) (2015) 272.
- [3] O. Akoto, H. Andoh, G. Darko, K. Eshun, P. Osei-Fosu, Chemosphere. 92 (2013) 67.
- [4] S. A. Mansour, M. H. Belal, A. A. K. Arab, M. F. Gad, Chemosphere. 75 (2004) 601.
- [5] M.O. Ofor, I. I Ibeawuchi, A. M. Oparaeke, Nat. Sci. 7(12) (2009) 8.
- [6] S.Lj. Savcic-Petric, Plant protection products on the Serbian market 2015, Plant Doctor, (2015), pp.42-56
- [7] Off. Gazzete RS No. 110/2012.
- [8] SANCO/12571/2013, Method validation and quality control procedures for pesticide residues analysis in food and feed.
- [9] Off. Gazzete RS No. 29/2014
- [10] Regulation EC No 396/2005, Official Journal of the European Union (2005).

## Determination of Pesticide Residues in Honeybees by GC-MS and LC-MS/MS

Vojislava Bursić<sup>1\*</sup>, Gorica Vuković<sup>2</sup>, Sonja Gvozdenac<sup>1</sup>, Mira Pucarević<sup>3</sup>, Tijana Zeremski<sup>4</sup>, Zoran Stojanović<sup>5</sup>, Rada Đurović-Pejčev<sup>6</sup>

<sup>1</sup>*Faculty of Agriculture, University of Novi Sad, Trg Dositeja Obradovića 8, Novi Sad, Serbia*

<sup>2</sup>*Institute of Public Health, Bul. despota Stefana 54a, Belgrade, Serbia*

<sup>3</sup>*EDUCONS University, Faculty for Environmental Protection, Sremska Kamenica*

<sup>4</sup>*Institute of Field and Vegetable Crops, Maksima Gorkog 30, Novi Sad, Serbia*

<sup>5</sup>*Republic Hydrometeorological Service of Serbia, Kneza Višeslava 66, Belgrade, Serbia*

<sup>6</sup>*Institute of Pesticides and Environmental Protection, Banatska 31b, Belgrade, Serbia*  
e-mail: bursicv@polj.uns.ac.rs

### Abstract

In recent years, a significant decline in populations of honeybees (*Apis mellifera*) has been recorded. GC/MSD and LC-MS/MS were used to determine pesticide residues in honeybee samples. By GC/MSD analysing six samples of dead honeybees the acetochlor, metolachlor, propiconazole and difenoconazol were detected. By LC-MS/MS analysing thiamethoxam and acetamiprid were detected.

### Introduction

In recent years, a significant decline in populations of honeybees (*Apis mellifera*) has been recorded. Through his abuse of the natural environment a man has continually caused damage to the ecosystem and, among other things, has brought about the decrease in the number of bee colonies. Honeybees can be used as the indicators of environmental pollution because of their morphological characteristics and the intense foraging activity, and their ability to retain and bioaccumulate in their bodies substances which they are in close contact with during pollination [1]. In the countries that have a long history of using pesticides in agriculture, such as Serbia [2], one can point to these agrochemicals as one of the important factors underlying wild bee and honey bee colony losses [3]. Growing concern about the impact of pesticides on pollinators is reflected in the enormous literature on the topic in the past few years [4]. The literature of the subject concludes that the presence of pesticides in pollen, honey, wax and other matrices in beehives presents a risk totally different from the effect caused by spraying with plant protection products [3].

According to the data by the Association of bee-keepers of Vojvodina 3200 hives were destroyed in Vojvodina from 2007 to 2012 due to the application of pesticides. The losses of bee colonies are of alarming proportion not only for bee-keepers, honey quality and honey consumers but for agricultural production and the market itself as well [5-7].

The analytical determination of pesticides, although by research groups considered a routine procedure, still constitutes a major challenge especially due to the increasing demand for low limits of detection (LODs) and the complexity of the matrices. The requirement for low LODs is linked to bee toxicity since the honeybee oral LD<sub>50</sub> and contact LD<sub>50</sub> are in the ng/g scale for many pesticides. Thus liquid chromatography tandem mass spectrometry (LC-MS/MS) has been used by various researchers [8].

In this article, we describe the evaluation and adaptation of the QuEChERS approach in combination with GC/MSD and LC-MS/MS used to determine pesticide residues in honeybee samples.

## Experimental

**Chemicals and apparatus.** All solvents were of HPLC grade and were obtained from Merck (Darmstadt, Germany). The certified pesticide analytical standards were purchased from Sigma-Aldrich and Dr. Ehrenstorfer (Augsburg, Germany).

For LC analysis, an Agilent 1200 (Agilent Technologies, USA) HPLC system with a binary pump was used. Chromatography separation was achieved using Zorbax C18, 50x4.6 mm, 1.8  $\mu$ m analytical column from Agilent at a flow rate of 0.4 ml/min with mobile phase consisting of water/methanol with 0.1% formic acid in gradient mode. For the mass spectrometric analysis, an Agilent 6460 Triple-Quad LC/MS system was applied. Agilent MassHunter version B.04.00 software was used for the data acquisition and processing. The analysis was performed in the positive ion mode. The multi source values were as follows: drying gas (nitrogen) temperature 300 °C, drying gas flow rate 5 L/min, nebulizer pressure 40 psi and capillary voltage 3000 V. The detection was performed using the multiple reactions monitoring mode (MRM).

For GC analysis, the Hewlet Packard GC System model 6890, auto sampler Agilent 6890 series injector. The Mass spectrometer Hewlet Packard 5973. GC capillary column: HP5MS (30 m x 0.25 mm x 0.25  $\mu$ m (5%-Phenyl)-methylpolysiloxane)). Carrier gas: helium, constant pressure 21.82 psi (RTL Pestf-PTV method). GC temperature program: 2 min -70 °C, 25 °C/min to 150 °C (0 min), 3 °C/min to 200 °C (0 min), 8 °C/min to 280 °C (10 min). Stop time was 41.87 min. The injection volume was 5  $\mu$ L (PTV, solvent vent mode). PTV temperature program: 0.04 min on 70 °C, 10 °C/sec to 280 °C (10 min), 250 °C (10 min). Vent flow: 50 mL/min. Vent press: 0.00 psi hold 0.04 min. Purge flow: 60 mL/min start on 2 min. Gas saver: Off. Acquisition mode: SCAN, type of ionisation: EI. Temperature of transfer line was 280 °C. Temperature MS quadropole of 150 °C, with the ion source temperature of 230 °C.

**Validation parameters.** The validated QuEChERS method according to SANCO/12571/2013 was used for the pesticide residues detections in honeybees. The LOD was calculated by MassHunter Qualitative Software. The linearity was checked using matrix matched standards (MMS) at the concentrations of 10.0-200.0 ng/mL for GC/MSD and 1.0-20.0 ng/mL for LC-MS/MS with the  $R^2 > 0.99$  for all investigated pesticides. The recovery for the final mass concentration of 0.01 and 0.002 mg/kg was in the range from 89.7-127.4 $\pm$ 5-14.8% (for LC-MS/MS) with the addition of the internal standard acetamiprid-D5.

### Pesticide extraction

2 g sample +10 mL d. H <sub>2</sub> O + 10mLMcCN + 100 $\mu$ L ISTD (10 $\mu$ g/mL Acetamiprid-D5)
--

↓ Shake vigorously for 1 min

Add 4g MgSO <sub>4</sub> , 1g NaCl, 1g Na <sub>3</sub> Citrate dihydrate, 0.5g Na <sub>2</sub> HCitrat sesquihydrate Shake tube immediately for 1 min
--

↓ Centrifuge for 5 min at 3500 rpm

Transfer 8 ml of the extract into a PP tube and stor 1 h in the freezer
---

Transfer 5 ml of the extract into a PP tube containing MgSO <sub>4</sub> , PSA, C18; Shake for 30 s
---

↓ Centrifuge for 5 min at 3500 rpm

Transfer 200 $\mu$ L into a vial, evaporate to dryness
--



Reconstitute in 200  $\mu$ L of mobile phase  
then LC-MS/MS

Transfer 2 mL into a vial, evaporate to dryness
---



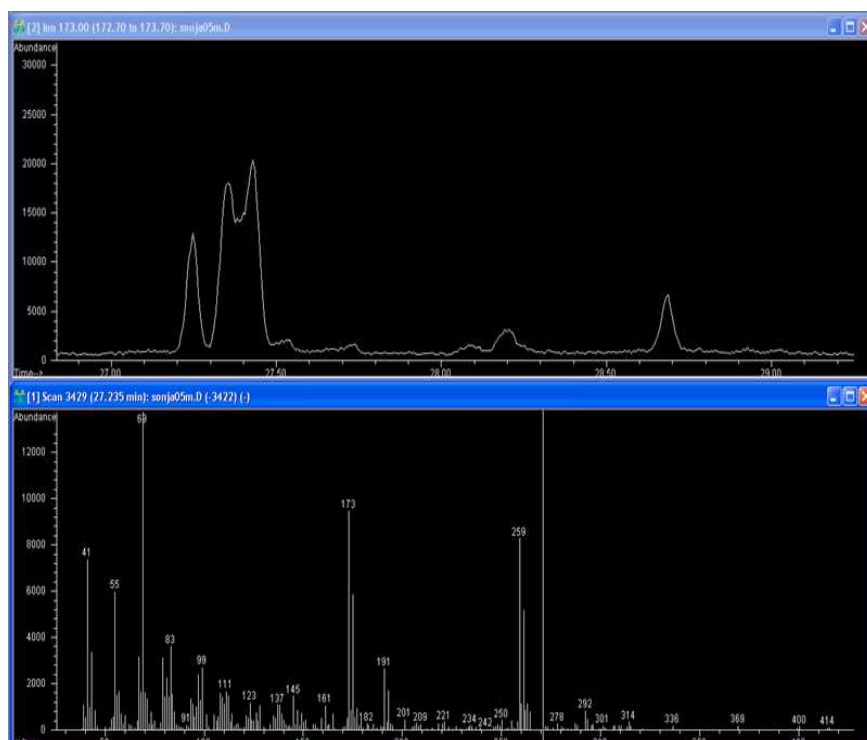
Reconstitute in 1 mL of hexan/acetone  
then GC-MS

## Results and discussion

The analysis comprised the detection of pesticide residues in six honeybees samples collected from the localities of Čerević and Radojevo. The validated QuEChERS method according to

SANCO/12571/2013 was used for the pesticide residues detections in honeybees by LC-MS/MS and GC-MS.

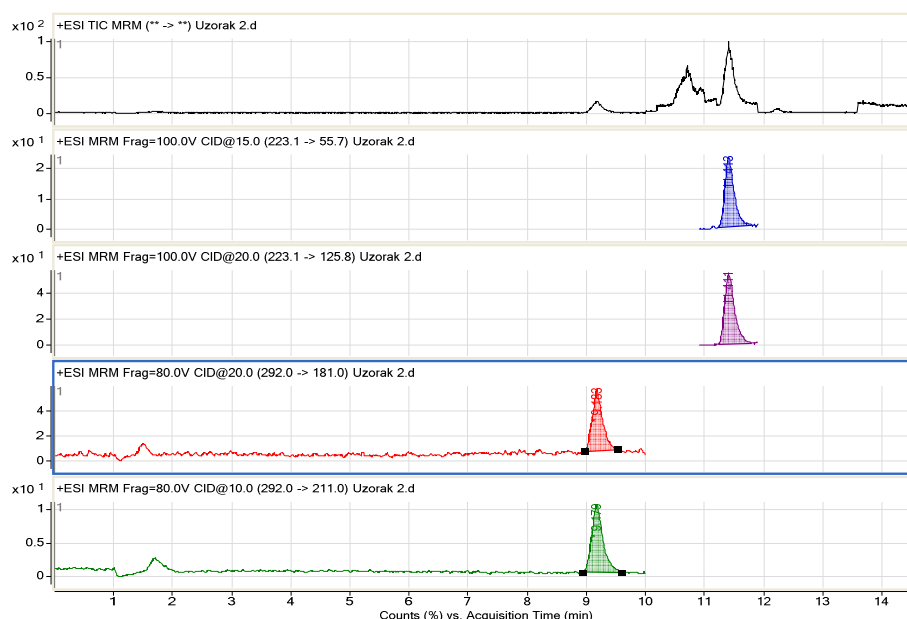
**Figure 1.** Detected pesticides in a honeybees sample obtained by GC-MS



By GC/MSD analysing six samples of dead honeybees the acetochlor, metolachlor, propiconazole and difenoconazol were detected. The detections of acetochlor were in the range from 12.8 to 18.5 ng/g, for metolachlor 49-72 ng/g, for propiconazole 19 to 29 ng/g, and for difenoconazol from 390 to 420 ng/g. Acute oral toxicity expressed as LD<sub>50</sub> for acetochlor and propiconazol is >100 µg/bee, while the acute contact LD<sub>50</sub> is >200 µg/bee while for difenoconazol acute oral is >100, and the acute contact is >187 µg/bee. According to EPA, metolachlor is not bee toxic [3].

By LC-MS/MS analysing thiamethoxam and acetamiprid were detected. In one sample thiamethoxam was found at the concentration level of 18 µg/kg, and acetamiprid was found in three samples between 0.012 and 0.033 mg/kg. Acute oral toxicity expressed as LD<sub>50</sub> for acetamirid is 14.53 µg/bee, while the acute contact LD<sub>50</sub> is 8.09 µg/bee; for thiamethoxam acute oral is 0.005, while the acute contact is 0.024 µg/bee.



**Figure 2.** Detected pesticides in a honeybees sample obtained by LC-MS/MS

A typical risk assessment considers only the acute toxicity of pesticides by contact or oral exposure in 24/48 hours, thus ignoring the negative effects derived from the constant exposure to pesticide residues over longer periods [3].

## Conclusion

Taking into consideration the results GC-MS and LC-MS/MS analyses of honeybees samples, there is a significant and justified doubt that the detected pesticides brought about the death of honeybees.

## References

- [1] Ž. Bargańska, M. Ślebioda, J. Namieśnik, *Molecules*. 19 (2014) 2911.
- [2] V. Bursić, G. Vuković, N. Vuković, N. Čuk, S. Gvozdenac, M. Meseldžija, A. Popović, „XX Savetovanje o biotehnologiji sa međunarodnim učešćem“ Univerzitet u Kragujevcu, Agronomski fakultet u Čačku, 13-14.03., *Proceedings*, 20 (2015) 491.
- [3] F. Sanchez-Bayo, K. Goka, *Plos One*, 9(4) (2014) 1.
- [4] J. L. Osborne, *Nature*. 491 (2012) 43.
- [5] V. Bursić, G. Vuković, N. Vuković, M. Pucarević, S. Gvozdenac, T. Zeremski, M. Cara, 5<sup>th</sup> CASEE conference, 25-27 May, University of Novi Sad, Faculty of Agriculture, Serbia, *Book of abstracts*, (2014) 46-47.
- [6] Peći A., Pesticidet po “vdesin” bletët, *Grupimi Ekolevizja korrik* (2014).
- [7] V. Bursić, G. Vuković, M. Pucarević, S. Gvozdenac, T. Zeremski, A. Popović, B. Špirović-Trifunović, 7<sup>th</sup> Symposium: Chemistry and Environmental Protection, Palić, Serbia, June 9-12, *Book of abstracts*, 352.
- [8] K. Kosiotis, C. Anagnostopoulos, P. Anastasiadou, K. Machera, *Sci. Total. Environ.* 485-486 (2014) 633.
- [9] SANCO 12571/2013, Guidance document on analytical quality control and validation procedures for pesticide residues analysis in food and feed (2013).

## Reduced Use of Pesticides in Tick Control in the Urban Environment

Aleksandra Petrović<sup>1\*</sup>, Aleksandar Jurišić<sup>1</sup>, Ivana Ivanović<sup>1</sup>, Dragana Rajković<sup>1</sup>,  
Branka Ljevnaić-Mašić<sup>2</sup>, Aleksandra Popović<sup>1</sup>, Miloš Petrović<sup>1</sup>

<sup>1</sup>Department of Environmental and Plant Protection, Faculty of Agriculture, University of Novi Sad, 21000 Novi Sad, Trg Dositeja Obradovića 8, Serbia

<sup>2</sup>Department of Field and Vegetable Crops, Faculty of Agriculture, University of Novi Sad, 21000 Novi Sad, Trg Dositeja Obradovića 8, Serbia  
e-mail: petra@polj.uns.ac.rs

### Abstract

Urban environment usually consists of wide range of heterogeneous ecosystems with diverse and complex interactions. All green areas, especially parks and lawns, represent suitable habitats for ticks, as they provide all necessary features to complete a ticks' life cycle. Vegetation cover and the presence of suitable hosts are crucial for tick population persistence. Therefore, vegetation management as a preventive method should have the fundamental role in tick control. The aim of this research was to determine whether regular and frequent mowing and vegetation management have influence on the efficacy of tick control program. The tick presence and abundance were observed at seven localities, from February till October during 2014. The total number of collected ticks was 1.241 and two tick species were identified: *Ixodes ricinus* and *Dermacentor marginatus*. Ticks were present at all prospected localities except Dunavski Park. The highest number of collected ticks was obtained at Park of Poplar Research Institute and the lowest at Kamenica Park. In order to obtain one integrated, but adequate, environmental safe and less expensive method for tick control, it is necessary to integrate constant monitoring of tick populations, mowing as a preventive method and control of potential tick hosts.

### Introduction

Urban environment usually consists of wide range of heterogeneous ecosystems with diverse and complex interactions. Almost all areas in the cities are managed and manipulated by man [1]. All green areas, especially parks and lawns, represent suitable habitats for ticks, as they provide all necessary features to complete a tick life cycle. Vegetation cover and the presence of suitable hosts for adult ticks are crucial for tick population persistence [2]. The successful survival of ticks in certain habitats depends on optimal temperature and humidity. Exophilic ticks which live in the lower parts of vegetation, litter and upper layer of the soil are especially dependent on these microclimate features [3]. Furthermore, even one species of medium-sized hosts (hare, hedgehog) could support the tick population, but the size of the locality, the type of adjacent territories, the scale of anthropogenic influence and the degree of its isolation from other potential tick localities are also important [3]. Different human activities could change microclimatic conditions that influence ticks' development and their hosts [4].

Ticks have always been a part of urban fauna. The urbanization and human activities connected with it may often positively influence the occurrence and abundance of ticks, both in short- and in long-term perspectives [5].

Urban forest parks are different in their size and position in the city. Some of them are in the central areas so they have rather weak or no connection at all with natural forests. They are exposed to the strong anthropogenic influence and the abundance of all tick stages in such localities is usually very low. Oppositely, parks placed at the edges of the cities, in the semi-urban areas, have good connection with surrounding forests or agroecosystems. Although the

anthropogenic influence could be high at these localities, the number of potential hosts is higher.

Worldwide, researchers are making a great effort to develop the most efficient method for tick control, especially in urban areas. The application of insectoacaricides based on synthetic pyrethroids today is the most frequent. However, the excessive use of these pesticides in tick control could be dangerous for human and animal health and cause environmental pollution. Certain tick species are sensitive to desiccation and usually search for sufficient humidity in microhabitats at ground levels or sheltered by vegetation cover. During unfavorable microclimatic conditions a great number of different tick stages dies, considerable number finds shelters at surface ground layer, and certain number even permanently leaves the habitat [4]. Therefore, vegetation management as a preventive method should have the crucial role in tick control.

The aim of this research was to determine whether regular and frequent mowing and vegetation management have influence on the efficacy of tick control program.

## Experimental

### *Tick sampling and identification*

The tick presence and abundance were observed at seven localities, from February till October during 2014. Ticks were sampled according to “Flag-hour” method [6]. White flannel cloth (1x1.6 m) was dragged through the low vegetation and soil surface for an hour, through the chosen transect in total length of 100 m. Five transects were chosen for each locality. Both sides of the cloth were carefully examined every 20 m, and all ticks were collected. Ticks were placed in the plastic tubes with a small cotton ball soaked into water to prevent desiccation and closed with perforated plastic stopper for sufficient ventilation. Ticks were sampled monthly, from 10 am till 6 pm, if the weather conditions were suitable.

Ticks were identified according to identification keys [7]. All tick stages (larvae, nymphs and adults) were identified and counted.

### *Localities*

The study was performed at seven localities in Novi Sad (Province of Vojvodina, Serbia), based on tick abundance, floristic composition and everyday human activities. Five of them were in urban areas of the city with high anthropogenic influence: Railway Station Park (9 ha, N45°15'841, E19°49'403), Omladinski Park (3 ha, N45°15'443, E19°51'219), Dunavski Park (4 ha, N45°15'198, E19°51'053), Limanski Park (10 ha, N45°14'201, E19°50'347), Futoški Park (5 ha, N45°15'020, E19°49'376). The sixth locality, Kamenica Park (18 ha, N45°13'663, E19°50'776) was in semi-rural area, near the city, known for picnic places, trim, jogging and cycling pathways. The seventh locality, The Park of Poplar Research Institute (50 ha, N45°17'586, E19°53'754), has never been under any chemical control program, and therefore was set as a control locality.

All prospected localities are park-forest type habitats, a combination of meadow vegetation and deciduous trees. The plant species were identified according to standard identification keys [8, 9 and 10]. The dominant tree species were: poplars (*Populus sp.*), sweet chestnut (*Castanea sativa*), silver birch (*Betula pendula*), oaks (*Quercus sp.*), white willows (*Salix alba*), plane trees (*Platanus sp.*), silver lime (*Tilia tomentosa*), maples (*Acer sp.*), field maple (*Acer campestre*), hornbeam (*Carpinus betulus*). The shrub vegetation was consisted of: forsythia (*Forsythia sp.*), dog-rose (*Rosa canina*), wild privet (*Ligustrum vulgare*) and hazel (*Corylus avellana*). The species of Poaceae family were dominant at all prospected localities: wall barley (*Hordeum murinum*), yellow foxtail (*Setaria glauca*) and meadow grasses (*Poa sp.*), but also: dandelion (*Taraxacum officinale*), Shepherd's-purse (*Capsella bursa pastoris*), greater plantain (*Plantago major*), fat-hen (*Chenopodium album*), amaranth (*Amaranthus*

*retroflexus*), cleavers (*Galium aparine*) and red clover (*Trifolium pratense*).

### Results and discussion

The total number of collected ticks was 1.241 and two tick species were identified: *Ixodes ricinus* Linnaeus 1758 and *Dermacentor marginatus* Sulzer 1776. Ticks were present at all prospected localities except Dunavski Park. The highest number of collected ticks was obtained at Park of Poplar Research Institute and the lowest at Kamenica Park (Tab. 1.). Larval stages were collected only at Park of Poplar Research Institute. This locality has never been treated with any insectoacaricides. The tick populations here are persistent and independent, so they could be marked as self-sufficient populations which can persist and flourish without replenishment [3].

**Table 1.** The number of collected ticks in parks in Novi Sad

	February	March	April	May	June	July	August	September	October	Total number
Park of Poplar Research Institute	6	11	21	57	493	321	62	65	52	1080
Kamenica Park	0	2	1	0	0	0	0	1	1	5
Railway Station Park	0	1	2	9	5	3	1	3	2	26
Omladinski Park	3	5	9	24	18	9	5	9	7	89
Dunavski Park	0	0	0	0	0	0	0	0	0	0
Limanski Park	0	0	1	3	2	0	0	1	0	7
Futoški Park	0	3	4	8	8	5	2	2	2	34

Kamenica Park, Dunavski Park and Limanski Park were properly maintained throughout the year: regularly and frequently mowed, the litter was regularly collected and the chemical treatments were applied two to three times during the season (April, May/June, September). Because of high anthropogenic presence at these localities, the number of potential host species was low (lizards, birds, cats and dogs). On the contrary, Railway Station Park, Omladinski Park and Futoški Park were mowed only once or twice during the year and the litter were not regularly collected. Although the chemical treatments were applied too, these localities had relatively high densities of tick populations. The highest abundance of ticks was noticed in shrub belt on the edge of these parks. Additionally, at these localities more potential host species were present: lizards, birds, rats, mice, hedgehogs, squirrels, cats, dogs and sometimes hares.

Tick populations noticed in Kamenica Park, Dunavski Park and Limanski Park could be described as dependent or temporary, as these populations cannot persist without constant replenishment or they are short-lived populations in unfavorable habitats which are periodically appearing after tick specimens importation by their hosts from the outside. Railway Station Park, Omladinski Park and Futoški Park have semi-independent population of ticks that could not be maintained without replenishment [3].

The constant presence of *I. ricinus* and *D. marginatus* in Railway Station Park, Omladinski Park and Futoški Park could be explained by ticks' specific microclimatic requirements such as temperature and constant humidity which was obtained by unmowed vegetation cover. The ideal habitat for *I. ricinus* in continental Europe is a deciduous forest with damp soil covered with rich undergrowth [11]. Although treatments were applied at these localities too, the

persistent ticks' populations could be explained by unregularly mowing which provided certain degree of humidity and higher number of different host species.

### **Conclusion**

The modern urban areas represent perfect habitat for ticks, as they could complete their developmental cycles feeding on different but always present hosts. Proper vegetation covering and constant presence of adult tick hosts support persistence of the tick population. In order to obtain one integrated, but adequate, environmental safe and less expensive method for tick control, it is necessary to integrate constant monitoring of tick populations, mowing as a preventive method and the control of potential tick hosts. In that way the use of pesticides will be reduced in the urban areas and the program would be economically justified and environmental safe.

### **Acknowledgements**

The authors acknowledge the financial support of the Ministry of Education and Science, Republic of Serbia, Project Ref. TR31084.

### **References**

- [1] P. Bolund, S. Hunhammar. *Ecological Economics*. 29 (1999) 293.
- [2] I. Uspensky. *Proceedings of the Conference GERI 2015 (Genes, Ecosystems and Risk of Infection)*, Crete, Greece, 21-23 April, 2015.
- [3] I. Uspensky. *Proceedings of the 8th International Conference on Urban Pests*, Zurich, Switzerland, 20 – 23 July, 2014, 203.
- [4] A. Jurisic, A. Petrovic, D. Rajkovic, S. Nicin. *Exp. Appl. Acarol.* 52 (2010) 101
- [5] I. Uspensky. *Ticks and Tick-borne Diseases* 5 (2014) 41.
- [6] G.O. Maupin, D. Fish, J. Zultowsky, E.G. Campos, J. Piesman. *Am. J. Epidemiol.* 133(11) (1991) 1105.
- [7] A.Estrada-Peña, A. Bouattour, J.Camicas, A. Walker. *Ticks of domestic animals in the Mediterranean Region. A guide to identification of species*. University of Zaragoza, Spain. 2004.
- [8] M. Josifović, (ed.). *Flora SR Srbije, I-IX*, SANU, Beograd, Srbija, 1970-1977.
- [9] M. Sarić, (ed.): *Flora Srbije X*, SANU, Beograd, Srbija, 1986.
- [10] F. Rose: *The Wild Flower Key*. Penguin Books Ltd, England, 1981
- [11] L. Gern, E. Rouvinez, L.N. Toutoungi, E. Godfroid. *Folia Parasitologica*. 44 (1997) 309.

## Assessment of Serum Metallograms in Patients with Purine Urolithiasis Before and After Treatment

Zeno Gârban<sup>1,2</sup>, Alin Cumpănaș<sup>3</sup>, Adina-Elena Avacovici<sup>2</sup>, Cornel Baltă<sup>4</sup>, Ludovic Sayti<sup>5</sup>, Sorin Marinescu<sup>5</sup>, Mirela-Minerva Nedelcu<sup>6</sup>

*1) Department of Biochemistry and Molecular Biology (former), Faculty of Food Products Technology, University of Agricultural Sciences and Veterinary Medicine of Banat "King Michael I of Romania" from Timișoara, Calea Aradului No. 119, RO-300 645 Timișoara, Romania; 2) Working Group for Xenobiochemistry, Romanian Academy-Branch Timișoara, Bd. M. Viteazu Nr.24, RO-300 223 Timișoara, Romania; 3) Clinic of Urology, Faculty of Medicine, University of Medicine and Pharmacy „Victor Babeș”, Timișoara, Bd. Iosif Bulbuca Nr.10, Timișoara, Romania; 4) West University „Vasile Goldiș” Arad, Faculty of Medicine, Arad, Romania; 5) Institute of Chemistry of the Romanian Academy, Bd. M. Viteazu Nr.24, Timișoara, Romania; 6. Clinical Laboratory, Municipal Hospital, Str. G.Dima, Nr.5, Timișoara, Romania  
E-mail: zeno.garban@yahoo.com*

### ABSTRACT

Investigations on the homeostasis of the hydroelectrolytic metabolism is important in the assessment of the uroconcrements' biogenesis and of the therapeutic effects (based on diverse procedures).

Our investigations have been performed on patients with purine urolithiasis included in two groups, according to the applied treatment for the removal of the uroconcrements. A group included 23 patients who underwent surgical treatment and the other group included 18 patients treated with Extracorporeal Shock-Wave Lithotripsy (ESWL). Before and after the therapeutic procedure the serum metallograms of the main alkaline (Na, K) and alkaline-earth (Ca, Mg) metals were determined by using spectrophotometry. The obtained results revealed post-treatment changes in the serum metallogram as follows: increase of natriemia and calcemia; decrease of kaliemia and magnesemia in both groups. The find data show the dyshomeostasis of the main alkaline and alkaline-earth metals after the treatment underlying their implication in urolithogenesis.

**Keywords:** serum metallogram, purine urolithiasis; ESWL and surgery treatment

### INTRODUCTION

Metals are important components of the human organism which are neither produced nor destroyed by the organism and are present in our environment, i.e. food, water, air, soil.

In the investigation of urolithiasis not only the biogenesis mechanisms of concrements formation and problems related to their prevention, metaphylaxy and therapy, but also the quantum of metals in blood serum and biologic fluids are of great importance.

The homeostasis of the hydroelectrolytic metabolism presents a major interest because metals are compounds playing the role of starters in the urolithogenetic processes (Coe and Parks, 1988; Drăgan et al., 1994; Gârban et al., 1998; Kok, 2002). As known, in the first stage of the process –the heterogenous nucleation - the metals intervene and become fixed to inorganic, organic anions or organic compounds with negative polarity. In this way are formed the so called starters or primers which facilitate the precipitation of electrolytes (Matouschek and Huber, 1981).

Mineral compounds, generally, and metals particularly, in the human organism can be evaluated under various aspects presenting interest for physiology, biochemistry, morphology and, evidently, pathology.



From pathological point of view the approach of this problem can be made in relation with patobiochemistry, physiopathology, respectively morphopathology.

In the organism the development of the normal physiological processes is conditioned by the maintenance of the biochemical homeostasis of the carbohydrate, lipid, protein and hydroelectrolytic metabolisms.

Lithogenesis, in general, is considered as a disturbance of the hydroelectrolytic metabolism, thus a dyshomeostatic phenomenon. To this one can add the dyshomeostasis of specific metabolites, e.g. oxalates, phosphates, urates, cystine, cholesterol a.o. (Coe and Park, 1988; Kok, 2002; Villegas et al., 2012).

The aim of this paper was to find out if the serum metallograms are or not disturbed by the applied treatment.

## MATERIALS AND METHODS

*Clinical cases.* The initiated study have been made on two groups of patients with urolithiasis admitted to the Urological Clinic Timișoara. A group was formed by 23 kidney stone patients - surgically (SU) treated for the removal of calculi and the other group was constituted by 18 kidney stone patients treated with Extracorporeal Shock -Wave Lithotripsy (ESWL).

*Clinical chemistry investigations.* In the studied group of patients there were determined the concentrations of the main alkaline (Na, K) and alkaline-earth (Ca, Mg) metals in the serum, before and after the intervention. The concentration of the alkaline and alkaline-earth metals in serum and urine of kidney stone patients was studied before (48 hours) and after (72 hours) the treatment in order to find out the role and participation at the formation of concrements. Concentrations of Na and K were determined by flame photometry, of Ca by volumetric and of Mg by spectrophotometric method (Kaplan and Pesce, 2010). Details concerning this methods were presented in a previous paper (Drăgan et al., 1994; Villegas et al., 2012; Gârban, 2015).

*Statistical evaluation.* Was done by a one-way analysis of variance (ANOVA), followed by the Tukey HSD post-hoc test. The obtained data are expressed as mean (X) and standard deviation (SD).

## RESULTS AND DISCUSSIONS

Investigations concerning the metals present in biologic fluids and in tissues are of importance for defining the homeostatic status and eventually, the perturbations of biochemical homeostasis (Gârban et al., 1981; Matouschek and Huber, 1981; Hesse et al., 1993). Metals play an important role in the organism. In the case of lithiasis biogenesis caused by morphophysiologic and/or biochemical factors, metals can be found – in certain cases – in increased amounts contributing at the constitution of crystallization nuclei as precursors of lithiasic concrements (Coe and Parks, 1988; Gârban et al., 1998). These can be formed at the level of urinary tract, gall bladder, salivary gland etc.

The concentration of metals is maintained in the body through homeostatic mechanisms being influenced by environmental factors, age, bioaccumulation processes. Metals in excess can lead to competitive interactions in biological systems modifying the normal metabolic status and inducing certain diseases.

Metal ions presence in blood and urine depends on dynamic characteristics of biologic processes: hydroelectrolytic metabolism, chronobiochemistry, homeostasis. Any hydroelectrolytic imbalance that involves the modification of ions concentration depends on diverse factors, among which a major role plays the nutritional status and the morphofunctional characteristics of the body.

Renal calculi can be removed surgically or disintegrated using Extracorporeal Shock - Wave Lithotripsy (ESWL). Diverse surgical interventions as well as the procedures of ESWL are followed by homeostatic modifications decelated through the investigation of serum and urine metabolites (Drăgan et al., 1994; Saxby et al., 1997).

Calculi removal through surgical treatment or ESWL is followed by modifications of the biochemical homeostasis. These can be observed in laboratory investigations specific for clinic chemistry. Of main importance are the electrolytes because the lithogenetic process is a disorder of the hydroelectrolytic metabolism.

Use of ESWL is beneficial being a non invasive technique; the residues obtained pass spontaneously through the urinary tract (Segura, 1990; Drăgan et al., 1994; Avacovici, 2012). The method is successfully applied for renal and vesical calculi with a diameter between 4-20 cm. Recovery time following ESWL is expected to be minimal. Patients resume activity within a few days after treatment

Obtained data - concerning the aspects of  $\text{Na}^+$ ,  $\text{K}^+$ ,  $\text{Ca}^{2+}$  and  $\text{Mg}^{2+}$  ions homeostasis - are presented and discussed separately on both patients groups, i.e. SU-treated and ESWL-treated.

Table 1 presents the values of the metals concentration from the blood serum of patients from the SU-treated group. Determinations on metals were performed before and after surgical treatment. The analytical data are expressed in mmol/L (mM/L).

**Table 1:** Serum metallogram of patients with urolithiasis surgically treated

Specification		UM	Number of patients (n)	Pre-treatment		Post-treatment		$\square X$ ( $X_1 - X_2$ )
				$n_1$	$X_1 \pm DS$	$N_2$	$X_2 \pm DS$	
Alkaline metals	Na	mM/L	23	23	136.12 $\pm$ 23.81	21	143.91 $\pm$ 30.16	+ 7.79
	K		23	23	4.46 $\pm$ 0.34	21	4.26 $\pm$ 0.48	- 0.20
Alkaline -earth metals	Ca		23	23	2.59 $\pm$ 0.29	21	2.73 $\pm$ 0.61	+ 0.14
	Mg		23	23	1.15 $\pm$ 0.23	21	1.07 $\pm$ 0.26	- 0.08

$n$ - number of patients with purine urolithiasis;  $n_1$  - number of patients investigated before (pre-) treatment;

$n_2$  - number of patients investigated after (post) treatment.

Data concerning metal concentrations in the serum of the ESWL treated group of patients, presented in Table 2, revealed also a post-treatment dyshomeostasis.

**Table 2:** Serum metallogram of patients with urolithiasis treated by Extracorporeal Shock-Wave Lithotripsy

Specification		UM	Number of patients (n)	Pre-treatment		Post-treatment		$\square X$ ( $X_1 - X_2$ )
				$n_1$	$X_1 \pm DS$	$N_2$	$X_2 \pm DS$	
Metale alcaline	Na	mM/L	18	18	138.93 $\pm$ 29.16	17	143.69 $\pm$ 45.13	+ 4.76
	K		18	18	4.49 $\pm$ 0.37	17	4.21 $\pm$ 0.52	- 0.28
Metale alcalino-terose	Ca		18	18	2.51 $\pm$ 0.26	17	2.72 $\pm$ 0.37	+ 0.21
	Mg		18	18	1.08 $\pm$ 0.17	17	1.04 $\pm$ 0.29	- 0.04

One can remark that post-treatment the concentration of sodium and calcium increases and the concentration of potassium and magnesium moderately decreases. Results concerning the concentration of alkaline and alkaline-earth metals in blood serum show a post-treatment dyshomeostasis.

Our analytical investigations revealed data that are in the range of analytical values from literature. For serum, Na 100-142 mM/L, K 3.5 - 4.5 mM/L; Ca 2.25 – 2.60 mM/L; Mg 0.7 – 1.11 mM/L. In the case of urinary metallograms in literature are mentioned the following values: Na 100 – 300 mM/24h; K 40 – 100 mM/24h; Ca 1.25 – 7.50 mM/24h; Mg 2.5 – 8.2 mM/24h (Kaplan and Pesce, 2010; Gârban, 2015).

Preliminary papers (Drăgan et al., 1994; Drăgan and Gârban, 2002) showed slightly different values that could be explained by the distribution of metal ions in the intracellular environment.

### CONCLUSIONS

1. Serum metallograms of the main alkaline (Na, K) metals in surgically and ESWL treated kidney stone patients revealed the increase of natriemia and decrease of kaliemia after the treatment.
2. Serum metallograms of alkaline-earth (Ca, Mg) metals in both groups of subjects revealed the post-therapeutic decrease of magnesemia and the increase of calcemia.

**Acknowledgements.** The present paper complies with the topics of the «Working Group for Metal Research in Biological Systems» created in 1979 at the Institute of Public Health Timișoara. It is to mention that this Working group was implicated also in the organization of the series of the International Symposium “Metal Elements in Environment, Medicine and Biology” (Timișoara-Romania) and printing of the in extenso papers of the meetings in Tomes I-X (1994-2010)

### REFERENCES

1. Avacovici Adina-Elena – *Investigations on purine metabolites and specific metal ions in the biogenesis of lithiasic uroconcrements* (in Romanian) – Ph. D. Thesis, Universitatea “Politehnica” Timișoara, 2012
2. Coe F.L., Parks J.H. - *Nephrolithiasis.*, 2nd ed., Year Book Medical Publishers Inc., Chicago-London-Boca Raton, 1988.

3. Drăgan P., Daranyi Gabriela, Bucuraș V., Agapie D., Botoca M., Patroi Delia, Gârban Z. - Investigations on the composition and etiopathogeny of lithiasis. XVIII. Dishomeostasy of some alkaline and alkaline-earth metals in pre-, postsurgical and ESWL treatment of urolithiasis, pp.91-94, in *Metal Elements in Environment, Medicine and Biology*, Tome I (Eds. Drăgan P., Gârban Z.), Publishing House Mirton Timișoara, 1994.
4. Drăgan P., Gârban Z. - New data regarding the metallogram of the patients with urolithiasis before and after surgical and ESWL treatment, pp.77-82, in *Metal Elements in Environment, Medicine and Biology*, Tome V (Eds. Gârban Z., Drăgan P.), Publishing House Eurobit, Timișoara, 2002.
5. Gârban Z., Cristescu Lucia, Mihalca Victoria, Drăgan P. – Consideration on the bioinorganic mechanism in purine urolithiasis pathogenesis (in Roumanian), *Timișoara Medicală*, 1981, XXVI, 4, 54-61.
6. Gârban Z., Daranyi Gabriela, Drăgan P., Avacovici Adina – Metallograms in simple and mixed urolithiasis. *J. Trace Elements Experimental Medicine*, 1998, 11, 376
7. Gârban Z. – *Biochemistry: comprehensiv treatise, Vol. I* (in Roumanian), Ed. 5-a, Editura Academiei Române București, 2015
8. Hesse A., Siener R., Heynck, Jahnen A. – The influence of dietary factors on the risk of urinary stone formation, *Scanning Microsc.*, 1993, 7, 1119-1137
9. Kaplan L.A., Pesce A.J. - *Clinical chemistry: theory, analysis, correlation*, 5th edition, Elsevier Mosby, St. Louis, 2010.
10. Kok D.J. – Clinical implications of physico-chemistry of stone formation, *Endocrinol. Metab. Clin. North Am.*, 2002, 31, 855-867
11. Matouschek E., Huber R.D. – *Urolithiasis: Pathogenese, Diagnostik, Therapie*. Schattauer Verlag Stuttgart-New York, 1981
12. Saxby M.F., Sorahan T., Slaney P., Coppinger S.W. – A case-control study of percutaneous nephrolithotomy versus extracorporeal shock wave lithotripsy, *Brit. J. Urol.*, 1997, 79:317,
13. Segura J.W. – Role of percutaneous procedures in the management of renal calculi, *Urol. Clin. North Am.*, 1990, 17, 207
14. Villegas R., Xiang Y.B., Elasy T., Xu W.H., Cai H., Cai Q., Linton M.F., Fazio S., Zheng W., Shu X.O. – Purine rich foods, protein intake and the prevalence of hyperuricemia: The Shanghai Men`s Health Sudy, *Nutr. Metab. Cardiovasc. Dis.*, 2012, 22(5), 409-416 doi: 10.1016/j.numecd.2010.07.012, epub 2011 Jan 28

## Fortified Foods with Mineral Elements - Conceptual and Applicative Data

Gârban Gabriela<sup>1</sup>, Muselin Florin<sup>2</sup>, Negrea Adina<sup>3</sup>, Ujhelyi Robert<sup>4</sup>,  
Romînescu Ramona<sup>7</sup>, Gârban Zeno<sup>6,7</sup>

1) Laboratory of Environment and Nutrition, National Institute of Public Health - Branch Timișoara, Bd. Dr. V.Babeș Nr.16, RO-300 226 Timișoara, Romania; 2) Faculty of Veterinary Medicine, University of Agricultural Sciences and Veterinary Medicine of Banat "King Michael I of Romania" from Timișoara, Calea Aradului No. 119, Timișoara, Romania; 3) Faculty of Industrial Chemistry and Environmental Engineering, University Politehnica Timișoara, P-ta Victoriei Nr.2, Timișoara, Romania; 4) Medical Department, S.C. CaliVita International, Timișoara, Romania; 5) School Group for Food Industry, Calea Bogdăneștilor Nr.32/A, Timișoara, Romania; 6) Department of Biochemistry and Molecular Biology (former), Faculty of Food Products Technology, University of Agricultural Sciences and Veterinary Medicine of Banat "King Michael I of Romania" from Timișoara, Calea Aradului No. 119, Timișoara, Romania; 7) Working Group for Xenobiochemistry, Romanian Academy-Branch Timișoara, Bd. M.Viteazu Nr.24, Timișoara, Romania  
E-mail: gabriela.garban@gmail.com

### ABSTRACT

In the last decade food business operators are selling more and more foods to which vitamins and minerals were added. The reason is to restore their content where this has been reduced during processing, storage or handling procedures. Beside the mentioned micronutrients, other ingredients might be used in food manufacturing, too. Among such substances one can mention : amino acids, essential fatty acids, fibre, various plants and herbal extracts. At the Community level the Regulation (EC) 1925/2006 harmonises the effective functioning of the internal market as regards the addition of vitamins and minerals and certain other substances to foods. For an efficient monitoring of foods to which vitamins and minerals and other substances have been added the manufacturer or the person placing such foods on the market must notify the competent authority of that placing on the market or on the withdrawal of the product from the market.

**Key words:** fortified foods - mineral elements

### INTRODUCTION

During processing, storage and handling processes the final food product may loose micronutrients, mainly vitamins and minerals. Also, there are regions where the soil is spoiled in some minerals and the resulted crops and vegetables will be also poor in essentials minerals, necessary for the optimal functioning of the organisms. Therefore food business operators started to add some vitamins, minerals and other substances to some foods.

Food or foodstuffs, according to the definition given in the Regulation 178/2002, means „any substance or product, whether processed, partially processed or unprocessed, intended to be, or reasonably expected to be ingested by humans”. ”Food includes drink, chewing gum and any substance, including water, intentionally incorporated into the food during its manufacture, preparation or treatment”.

The European Community Regulation 1925/2006 establishes the same rules for all Member States regarding fortified foods.

## **1. MINERAL ELEMENTS IN FOODS - OVERVIEW**

From nutritional point of view the minerals (beside vitamins) are included in the group of micronutrients. Minerals are essential nutrients to life, are needed in small amounts and participate in numerous catabolic and anabolic reactions in various biochemical pathways. Beside other nutrients the mineral compounds participate in physiological processes which assure the health maintenance. For the human organism there are essential about twenty eight elements, e.g. Ca, Mg, Na, K, Zn, Fe, Cu, Se, I etc. (Berdanier, 1998; Richardson, 2007)

Mineral micronutrients are generally divided in two sub-categories accordingly to their chemical characteristics: the micronutrients with cationic nature (metals) and micronutrients with anionic nature (non-metals). Also, taking in account the amount of this elements that is found in the organism, the mineral nutrients can be classified in macroelements, e.g.: Na, K, Ca, Mg, P, Cl etc. and trace elements, e.g.: Zn, Fe, Cu, I, Se.

They are often found as cofactors in enzymes, e.g.:  $Zn^{2+}$  in alcohol dehydrogenase;  $Mn^{2+}$  in phosphotransferase;  $Fe^{2+}$  in the lysosomal myeloperoxidase; selenium in the metalloenzyme glutathione peroxidase etc. (Champe and Harvey, 1987; Chaney, 1992). Minerals can be present also in the composition of some hormones, e.g.: iodine in thyroid hormones ; in certain amino acids, e.g.: selenomethionine; in hemoglobin or myoglobin.

Deficiency of minerals and especially of trace elements in food are actually more likely to occur than is vitamin deficiency. Because of differing geologic conditions minerals and trace elements may scarce in the soil of certain region and rich in those of other regions (O'Dell and Sunde, 1997; Gârban and Gârban, 2003). The insufficiency or lack of one or more minerals leads to dysmineraloses.

## **2. FORTIFIED FOODS : FOOD CATEGORIES, LEGISLATION**

According to the European Food Safety Authority (EFSA) and Codex Alimentarius Commission various food categories can be fortified. Regulation (EC) No 1925/2006 of the European Parliament and of the Council establishes the rules for the addition of vitamins and minerals to foods and the use of certain other substances or ingredients in foods. In Annexes I and II of that Regulation are the lists of vitamins and minerals, and for each of them the forms, that may be added to food.

In the meantime EFSA evaluated new vitamin and mineral forms. The substances which have received favourable scientific opinion were added to the lists with the Commission Regulation (EC) No 1170/2009. In Annex III of this Regulation the new list of „Vitamin formulations and mineral substances which may be added to foods” can be find.

In case of fortified foods it is also necessary to have in view the Commission Directive 2008/100/EC amending Council Directive 90/496/EEC on nutrition labeling for foodstuffs as regards recommended daily allowances, energy conversion factors and definitions, because the addition of a vitamin or a mineral to a food shall result in the presence of that vitamin or mineral in the food in at least a significant amount where this is defined according to the Annex to Directive 90/496/EEC.

Various diseases can reduce the mineral nutrients intake and especially those that interfere with the ingestion, digestion, absorption and requirement of nutrients: celiac disease, Crohn disease, irritable bowel syndrome, lactose intolerance, bacterial, viral and parasitic infections (Chaney, 1982; Shrimpton, 1997).

Evidence from recent studies revealed that mineral trace elements supplementation may help to prevent various forms of cancer, heart disease and some other degenerative processes.

A way to increase the mineral micronutrient levels from diet is food fortification by adding such nutrients during the food processing or the consumption of food supplements with specific minerals.



### 3. MINERAL ELEMENTS IN FORTIFIED FOODS

Mineral micronutrients can be found in various chemical forms with different levels of absorption at the level of gastrointestinal tract and with various degrees of bioavailability. Therefore the regulatory institutions must establish which forms are safer and have a higher bioavailability. Recently the European Commission had issued Regulation 1170/2009 amending Directive 2002/46/EC and Regulation 1925/2006/EC regarding the lists of vitamins and minerals and their forms that can be added to foods, including food supplements. The *nutritional reference value* (NRV) for minerals and vitamins are specified in Regulation 1169/2011.

#### 3.1. Macro- and micronutrients with cationic character

Regulation EC 1170/2009 of the European Parliament and the Council establishes the nutrients and their chemical forms which may be added to foods. Detailed data referring to the chemical forms of micronutrients with cationic character are presented in table 1.

**Table 1.** Chemical formulations of the cationic mineral substances which may be added to foods

Micronutrient	Measure unit	NRV	Chemical formulations
Potassium	mg	2000	bicarbonate ; carbonate ; chloride ; citrate ; gluconate ; glycerophosphate ; lactate ; hydroxide ; salts of orthophosphoric acid
Calcium	mg	800	carbonate; chloride; citrate malate; salts of citric acid; gluconate; glycerophosphate; lactate; salts of orthophosphoric acid ; hydroxide ; malate ; oxide ; sulphate
Magnesium	mg	375	acetate; carbonate ; chloride ; salts of citric acid ; gluconate ; glycerophosphate ; salts of orthophosphoric acid; lactate; hydroxide; oxide ; magnesium potassium citrate; sulphate
Iron	mg	14	ferrous bisglycinate; ferrous carbonate; ferrous citrate; ferric ammonium citrate; ferrous gluconate; ferrous fumarate ; ferric sodium diphosphate ; ferrous lactate; ferrous sulphate; ferric diphosphate (ferric pyrophosphate) ; ferric saccharate ; elemental iron (carbonyl + electrolytic + hydrogen reduced)
Zinc	mg	10	acetate ; bisglycinate ; chloride ; citrate ; gluconate ; lactate ; oxide ; carbonate ; sulphate
Manganese	mg	2	carbonate ; chloride ; citrate ; gluconate ; glycerophosphate ; sulphate
Copper	mg	1	cupric (Cu II) salts: cupric carbonate ; cupric citrate ; cupric gluconate ; cupric sulphate ; copper lysine complex
Chromium	mg	40	chromium (III) chloride and its hexahydrate ; chromium (III) sulphate and its hexahydrate
Molybdenum	µg	50	ammonium molybdate (molybdenum (VI); sodium molybdate (molybdenum (VI)

Various organisms such as the Scientific Committee on Food (SCF), the European Food Safety Authority (EFSA a.o. are involved in the establishment of the tolerable upper intake of minerals. According to SCF and EFSA the tolerable upper intake levels for some of the cationic minerals are : Ca – 2500 mg, Mg – 250 mg, Cu – 5 mg, Zn – 25 mg

### 3.2 Micronutrients with anionic character

The micronutrients with anion specificity (i.e. non-metals) which may be added to foods are, according to the Regulation EC 1170/2009 of the European Parliament and the Council : iodine, selenium, fluoride and boron.

The chemical formulations of micronutrients with anionic character as well as their NRV are given in table 2.

**Table 2.** Chemical formulations of the anionic mineral substances which may be added to foods

Micronutrient	Measure unit	NRV	Chemical formulations
Fluoride	mg	3.5	sodium fluoride ; potassium fluoride
Iodine	µg	150	sodium iodide ; sodium iodate ; potassium iodide ; potassium iodate
Selenium	µg	55	selenium enriched yeast ; sodium selenate ; sodium hydrogen selenite ; sodium selenite
Boron	mg	NE*	boric acid ; sodium borate

\*NE – not established

From the anionic minerals used in fortified foods selenium and iodine are more often found. Less often is used boron. In the case of anionic nutrients the tolerable upper intake levels, according to Scientific Committee on Food (SCF) and the European Food Safety Authority (EFSA) are: F – 7 mg, I – 600 µg, Se – 300 µg, B – 10 mg/day.

The presence of too small and insignificant amounts of micronutrients in foods would not offer any benefit to consumers and would be misleading. Thus, in order to be allowed to be declared in nutrition labelling, vitamins and minerals added to foods should be at least a significant amount, i.e. 15% of the RDA per 100g or 100ml (Annex of Directive 90/496/EEC).

### CONCLUSIVE DATA

1. In case of fortified foods an important aspect is related to the source compounds of minerals, namely the chemical formulations which can be used in their manufacture.
3. Mostly the following food categories are fortified : beverages excluding dairy products; dairy products and analogues; cereals and cereal products; confectionary; fats and oils, and fat emulsions.

### REFERENCES

1. Berdanier C.D. - *Advanced Nutrition: Micronutrients*. CRC Press, Boca Raton, 1998.
2. Brody T. – *Nutritional biochemistry*, Academic Press, San Diego, 1994.
3. Champe P.C., Harvey R.A. – Nutrition, pp. 297-309, in *Illustrated Review Biochemistry* (Champe P.C., Harvey R.A., Eds.), J.B. Lippincott Comp, Philadelphia, 1987.
4. Chaney S.G. – Principles of nutrition II. Micronutrients, pp.1115-1147, in „*Textbook of Biochemistry*” (Devlin T.M., Ed.), Wiley-Liss Inc., New York-Chichester-Brisbane-Toronto-Singapore, 1992.

5. Gârban Z., Gârban Gabriela – *Human nutrition* (in Romanian), Vol.I , ed. 3, Ed. Orizonturi Universitare, Timișoara, 2003.
6. O'Dell B.L., Sunde R.A. (Eds.) - *Handbook of nutritionally essential mineral elements*. New York, Marcel Dekker Inc., 1997.
7. Richardson D.P. - Risk management of vitamins and minerals: a risk categorisation model for the setting of maximum levels in food supplements and fortified foods, *Food Science and Technology Bulletin: Functional Foods*, 2007, 4 (6), 51–66.
8. Shrimpton D. H. - *Vitamins and minerals: a scientific evaluation of the range of safe intakes*, Council for Responsible Nutrition, UK, 1997.
9. \*\*\* - Regulation (EC) No 1925/2006 of the European Parliament and of the Council of 20 December 2006 on the addition of vitamins and minerals and of certain other substances to foods
10. \*\*\* - Commission Regulation (EC) No. 1170/2009 of November 2009 amending Directive 2002/46/EC and Regulation (EC) No 1925/2006 as regards the lists of vitamins and minerals and their forms that can be added to foods, including food supplements. *Official Journal of the European Union*, 1,12,2009
11. \*\*\* - Regulation (EU) No 1169/2011 of the European Parliament and of the Council of 25 October 2011 on the provision of food information to consumers, amending Regulations (EC) No 1924/2006 and (EC) No 1925/2006 of the European Parliament and of the Council, and repealing Commission Directive 87/250/EEC, Council Directive 90/496/EEC, Commission Directive 1999/10/EC, Directive 2000/13/EC of the European Parliament and of the Council, Commission Directives 2002/67/EC and 2008/5/EC and Commission Regulation (EC) No 608/2004

## Single Crystalline Micrometric Magnetite for Magnetic Resonance Imaging

Corina Beljung<sup>1</sup>, Mihaela Luminita Kiss<sup>1</sup>, Adrian Ieta<sup>2</sup>, Marius Chirita<sup>3,\*</sup>

<sup>1</sup>Politehnica University, Timisoara; <sup>2</sup> Department of Physics, SUNY Oswego, NY, USA;

<sup>3</sup>National Institute for Research and Development in Electrochemistry and Condensed Matter, Timisoara;

\*email: chirifiz@gmail.com

A major drawback of using metal oxide nanoparticles as contrast agent in MRI is related to their low saturation magnetization mainly due to their particle size. The current works seeks to solve this problem by increasing the number of nanoparticles, of micrometer sized clustered particles. The studies shows that to be effective in improving MRI signal, millions of ultrasmall superparamagnetic iron oxide nanoparticles are needed to mark a single cell which is a difficulty. A better solution to this problem is to use singlecrystalline particles, in micrometer domain. Micrometric magnetite singlecrystals with average size of 10 $\mu$ m (along the <001> axis) with unusual superparamagnetic behavior at room temperature was synthesized by us through hydrothermal decomposition of Fe<sup>3+</sup>-Na<sub>4</sub>EDTA complex. Based on this lately original results regarding the obtaining of single crystalline micrometric domain (10-50 $\mu$ m) iron oxide (magnetite) with superparamagnetic behaviour generic named by as **SCMSPIO**, we believe that it could be involved in many interesting applications including their formulation as T<sub>2</sub> contrast agents for successfully exploring by MRI.

Single crystals of Fe<sub>3</sub>O<sub>4</sub> with micrometric dimensions of 10 $\mu$ m and superparamagnetic behaviour were synthesized. We tasted these particles as contrast agent in MRI experiments and at this stage of experiments the nuances of grey which we obtained show promising effects and they correspond to our objective (see figures 1 an 2 presented below).

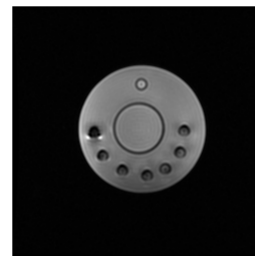
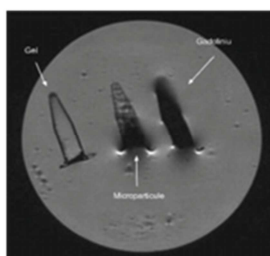
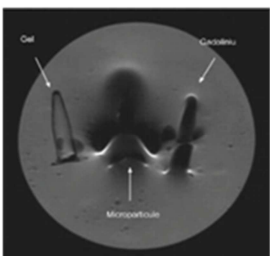
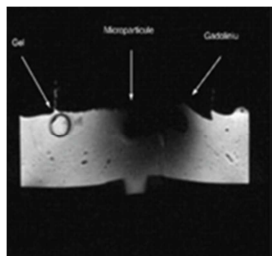


Fig. 1, Three representative phantoms

Fig.2, The grey nuances

The results indicate that the choice of appropriate concentration might give a good contrast in MRI applications. Further in vivo experiments on animals are in progress. Taking into account the dimensions of the cells (10 $\mu$ m -100 $\mu$ m), this particle could be appropriate for other medical applications such as intracellular hyperthermia, controlled drug delivery system (site specific drug delivery), cellular Magnetic Resonance Imaging (MRI), monitoring cell migration for cell therapy, multimodal cancer therapy, immunomagnetic separation of cells, detection, immobilization and modification of biologically active compounds, cell labelling; magnetic separation of cells, magnetic resonance contrast agents, gene delivery, multi-modal cancer therapy.

**Keywords:** MRI, superparamagnetic, magnetite, micrometric, biomedical.

## Influence of CO<sub>2</sub> upon UV-Vis spectroscopy of silica-tetra-3,4-dimethoxy-phenyl-porphyrin hybrid nanomaterial

Ionela Creanga<sup>1</sup>, Anca Palade<sup>1</sup>, Anca Lascu<sup>1</sup>, Ileana Cernica<sup>2</sup>, Mihaela Birdeanu<sup>1,3</sup>,  
Eugenia Fagadar-Cosma<sup>1</sup>

<sup>1</sup>*Institute of Chemistry Timisoara of Romanian Academy, 24 M. Viteazul Ave, 300223-Timisoara, Romania*

<sup>2</sup>*National R&D Institute for Microtechnology, 126 A Erou Iancu Nicolae Str., Voluntari, 077190 Bucharest, Romania*

<sup>3</sup>*National Institute for Research and Development in Electrochemistry and Condensed Matter, 1 PlautiusAndronescu Street, 300224 Timisoara, Romania*

### Abstract

A symmetrical substituted aryl porphyrin was incorporated by sol-gel method to generate a silica hybrid nanomaterial that preserves the UV-vis absorption properties of bare porphyrin. The novel hybrid demonstrated to be a sensitive material for CO<sub>2</sub> detection. The sol-gel synthesis was monitored by UV-vis spectroscopy. Atomic force microscopy was performed for the hybrid before and after CO<sub>2</sub> detection and important changes in the aggregation behavior of the nanomaterial were observed.

**Keywords:** porphyrin-silica hybrid, sol-gel, UV-vis, CO<sub>2</sub> detection, AFM

### Introduction

In 1997, for the first time a phosphorescence signal from a porphyrin encapsulated in a sol-gel matrix was used for gaseous oxygen sensing [1]. This result accelerated work into other optical sensors using water-insoluble luminescent dye/sol-gel matrices.

Sol-gel process affords easy immobilization of any porphyrin retaining the optical and sensing properties of the dye, due to the high homogeneity of the porphyrin molecules into the sol-gel matrices. The critical issues remain the tailoring of sol-gel materials to inhibit leaching of porphyrin, and to achieve enhanced sensor performance in terms of stability, response time, sensitivity, repeatability and selectivity.

Based on our previous studies regarding CO<sub>2</sub> detection [2] in this paper the porphyrin was incorporated into a silica matrix by sol-gel method in two steps acid-base catalysis and used as optical sensor for the detection of CO<sub>2</sub> in wet environment.

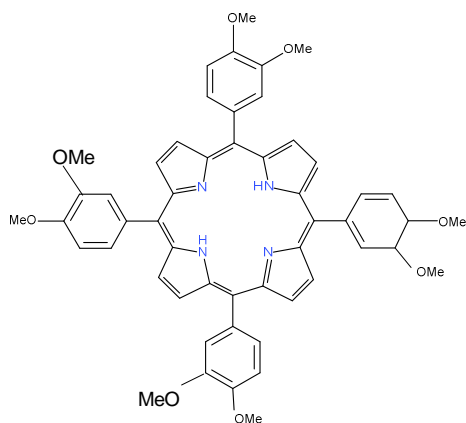


**Figure1.** Structure of tetra (3,4-dimethoxy-phenyl)-porphyrin.

## Experimental

### 2.1. Reagents

All reagents used in this work were *p a* grade provided by Merck, Fluka and Sigma-Aldrich.

2.2. *Sol-gel synthesis* was done by adapting previously reported paper [3]. A mixture of H<sub>2</sub>O (2,730g; 0,152mmol) and HCl 37% (0,037g; 1,01 mmol) were added by dripping under continuous stirring to a solution of TEOS (7,9g; 0,038moli) dissolved into EtOH (6,98g; 0,152 mmol) containing a mixture of 8 mg porphyrin ( $0.88 \times 10^{-5}$  mmol) dissolved in 14 ml THF. The molar ratios were: TEOS:EtOH:H<sub>2</sub>O:HCl= 1:4:4:0,01. After 40 minutes, the second basic step was started by slowly adding of NH<sub>3</sub> 1.6g (solution of NH<sub>3</sub> 25%+9g H<sub>2</sub>O). Transparent gel colored in violet was obtained instantly.

### 2.3. Apparatus

UV-visible spectra were registered on JASCO UV- V-650 visible spectrometer using 1 cm pass cells. Atomic force microscopy (AFM) investigations were performed on Nanosurf®EasyScan 2 Advanced Research AFM. AFM images were obtained in contact mode.

## Results and discussion

The hybrid material was characterized after first step of acid catalysis and in the final step of base catalysis. As revealed by Figure 2, the properties of porphyrin are preserved in both steps of catalysis. Our interest was to incorporate into the hybrid a porphyrin that is neutral, not a protonated one, so that we choose for the tests to CO<sub>2</sub> detection the hybrid preserving the properties of the initial porphyrin base that is the hybrid after gelation in the basic step.

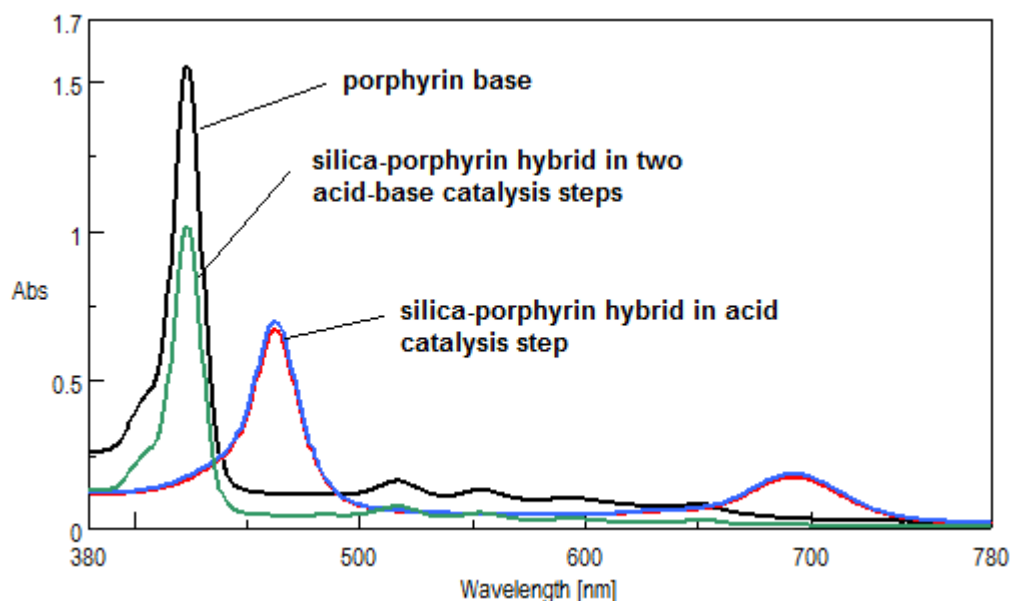


**Figure 2.** The UV-vis of the bare porphyrin and of the hybrids, at the same concentration in THF

The selected hybrid was further subjected to test to CO<sub>2</sub> and by increasing the quantity of gas introduced in the vial containing the gel (rate of 1 $\mu$ L/min), the intensity of the Soret band of the nanomaterial increased also, as presented in Figure 3. The dependence between the intensity of the Soret band of the silica-porphyrin hybrid and the CO<sub>2</sub> concentration is linear. A very good correlation coefficient is obtained.



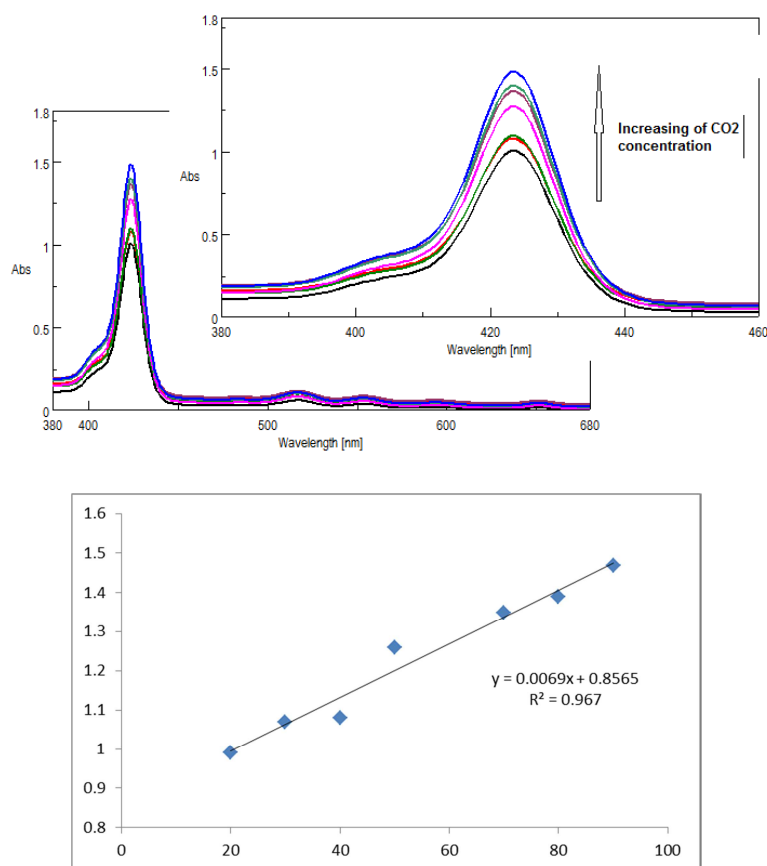


**Figure 3.** UV-vis spectra showing the linear dependence between CO<sub>2</sub> increasing of concentration and the increase of Soret band intensity for porphyrin-silica hybrid.

Due to the fact that the shape of the spectrum does not change during experiments we cannot presume that the mechanism of detection is based on the increase of acidity of the medium by CO<sub>2</sub> introduction. So other hypothesis can be some adsorption phenomena of CO<sub>2</sub> that might be accompanied by morphology and topography changes of the hybrid material. The aggregates of hybrid before CO<sub>2</sub> addition, investigated by AFM, look uniform, with small pores and with mean surface of islands of 0.0025  $\mu\text{m}^2$  as presented in Figure 4.

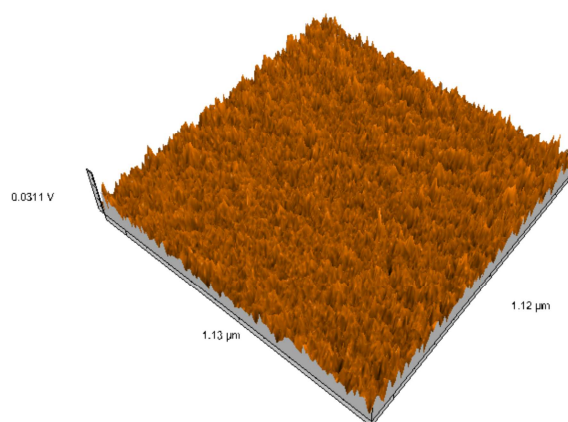


**Figure 4.** The surface image of hybrid nanomaterial before CO<sub>2</sub> addition.

The aggregates of hybrid after CO<sub>2</sub> interference are significantly bigger, look like irregular straw –type assemblies having the height of 68 nm, the mean surface of 0.0181  $\mu\text{m}^2$  and the

mean volume of  $0.00013 \mu\text{m}^3$ . The diameter is varying in the range of 366 nm up to 791 nm (Figure 5).

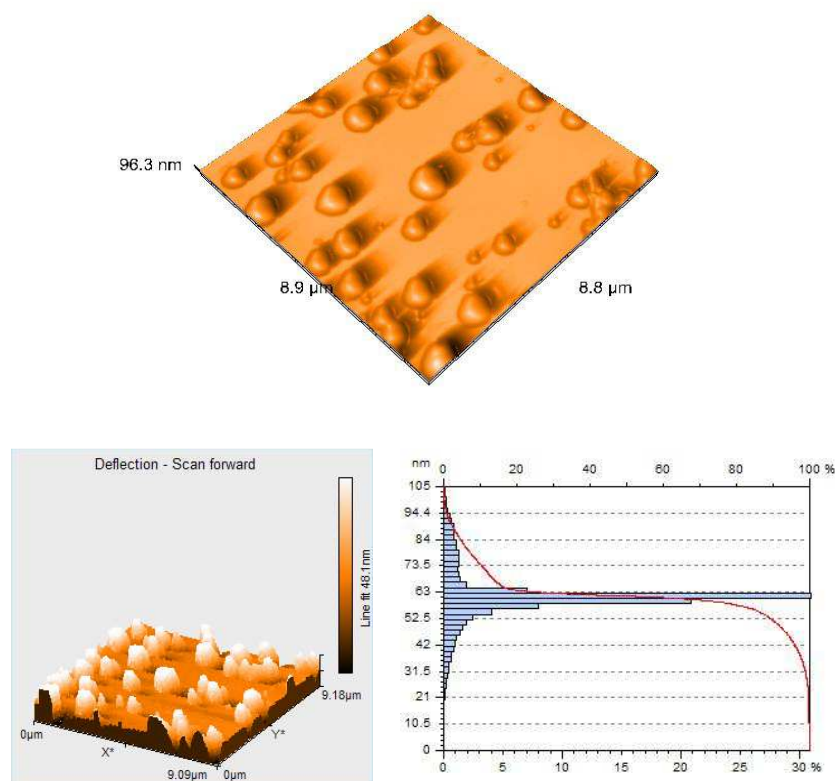


**Figure 5.** The surface image of hybrid nanomaterial after CO<sub>2</sub> addition.

## Conclusion

A symmetrical A<sub>4</sub>B substituted porphyrin was incorporated into a silica matrix by sol-gel method in two steps acid-base catalysis and used as optical sensor for the detection of CO<sub>2</sub> in wet environment.

By increasing the quantity of CO<sub>2</sub> gas introduced in the vial containing the gel the intensity of the Soret band of the nanomaterial increased also, the dependence between being linear.

AFM studies show important changes regarding the surface morphology before and after CO<sub>2</sub> addition to the hybrid nanomaterial, these indicating a probable absorption mechanism, not one based on acidity changes, as expected.

## Acknowledgements

The authors from Institute of Chemistry Timisoara of Romanian Academy are kindly acknowledging the support from Program 3-Porphyrins/2015 and STAR Programme-SAFEAIR Project 76/2013.

## References

- [1] L. Sang-Kyung, O. Ichiro, Anal. Chim. Acta 342 (1997) 181-188.
- [2] E. Fagadar-Cosma, D. Vlascici, G. Fagadar-Cosma, A. Palade, A. Lascu, I. Creanga, M. Birdeanu, R. Cristescu, I. Cernica, Molecules 19(12) (2014) 21239-21252.
- [3] E. Fagadar-Cosma, C. Enache, G. Fagadar-Cosma, C. Savii, J. Optoelectron. Adv. Mat. 9 (2007) 1878.

## Detection of Phosphine Derivates Using Metalloporphyrins

Anca Palade<sup>1</sup>, Ionela Creanga<sup>1</sup>, Anca Lascu<sup>1</sup>, Eugenia Fagadar-Cosma<sup>1</sup>Institute of Chemistry Timisoara of Romanian Academy, M.Viteazul Ave, No. 24,  
300223-Timisoara, Romania**Abstract**

Starting from the knowledge that phosphine derivatives exhibit medium/high toxicity, in this study we focused on the behavior of Co(II)- 5,10,15,20-tetratolyl-porphyrin (CoTTP) and Mn(III)-5,10,15,20-tetraphenyl-porphyrin chloride (MnTPPCL) as active UV-vis chromophores for the detection of triphenylphosphine oxide (LC50=12.2µg/mL, LC90=29.5µg/mL). The increase of triphenylphosphine oxide concentration generates the hypochromic effect on the Soret bands of the two metalloporphyrins. A comparison regarding the efficiency of the two metalloporphyrins in detecting phosphine derivatives was done.

Keywords: Co(II)-tetratolylporphyrin, Mn(III)-tetraphenylporphyrin, UV-vis, phosphine derivatives-detection, AFM.

**Introduction**

Due to  $d\pi$ - $p\pi$  bonding that diminishes the electron density on oxygen, tertiary phosphine oxides are weak bases. Triphenylphosphine oxide ( $\text{Ph}_3\text{PO}$ ) is a widely used reagent material for synthesis of organophosphorus compounds and as catalyst, cocatalyst, Lewis base and monodentate neutral oxygen donor ligand. It is already known that Mn and Mg have a strong affinity to PO group in  $\text{Ph}_3\text{PO}$  [1] and the coordination chemistry of P=O ligands and their coordination capabilities were largely studied [2].

Complexes of lanthanide nitrates with phosphine oxides have been investigated since the 1960s [3]. Due to its versatile ligand properties triphenylphosphine oxide was used in synthesis of  $\text{TiO}_2$ -hybrids incorporating  $\text{Eu}^{3+}$  in order to improve  $\text{Eu}^{3+}$  luminescence [4] or in the polymeric composites for the detection of dopamine [5]. The detection of  $\text{Ph}_3\text{PO}$  was reported by  $^{31}\text{P}$ -NMR in complexes to silanes, siloxanes and stannanes [6] but in this study, related to our previous research [7] we proposed a facile and non-toxic detection, using a Mn-porphyrin, namely: Mn(III)-5,10,15,20- tetraphenyl-21H,23H porphyrin chloride (structure in Figure 1).

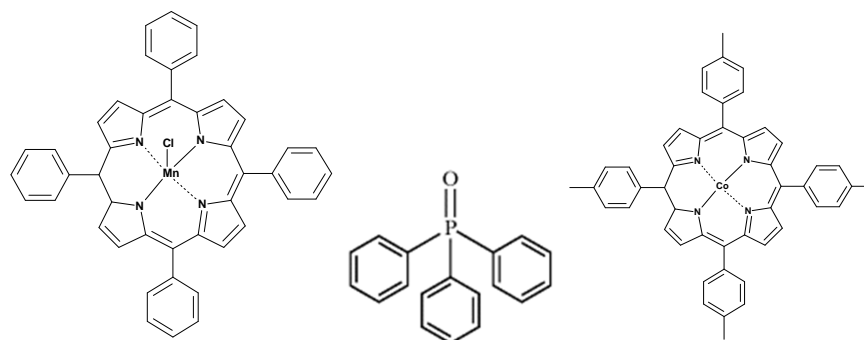


**Figure 1.** Structures of Mn(III)-5,10,15,20-tetraphenyl-porphyrin chloride (MnTPPCL), triphenylphosphine oxide and Co(II)- 5,10,15,20-tetratolyl-porphyrin (CoTTP).

**2. Experimental****2.1. Reagents**

All reagents used in this work were *purum analiticum*, provided by Merck, Fluka and Sigma-Aldrich. The porphyrin bases, were synthesized according to our previous report [8]. The

manganese and cobalt complexes were prepared [9] using large excess of salts (mole ratio 1/20 porphyrin/salts). Stock solutions of metalloporphyrins  $0.5 \times 10^{-5}$  M and  $2 \times 10^{-4}$  M solution of triphenylphosphine oxide, all dissolved in toluene have been prepared for UV-vis experiments.

## 2.2. Apparatus

UV-visible spectra were registered on JASCO UV- V-650 visible spectrometer using 1 cm pass cells. Atomic force microscopy (AFM) investigations were performed on Nanosurf®EasyScan 2 Advanced Research AFM. AFM images were obtained in contact mode.

## Results and discussion

Complete considerations regarding the UV-vis hyper spectra of Mn-metalloporphyrin were presented in the reported paper [8].

The UV-vis spectrum of triphenylphosphine oxide in toluene has the absorption maximum at 283 nm and do not influence these determinations.

For the UV-vis detection of triphenylphosphine oxide a spectrophotometric titration was performed by adding 100  $\mu$ L triphenylphosphine oxide in toluene to each metalloporphyrin solution dissolved in toluene.

By increasing concentration of triphenylphosphine oxide we noticed a continuous decrease in intensity of the Soret bands of both metalloporphyrins, as shown in Figures 2, 3 and 4. The dependence between the intensity of absorption measured at Soret band and the concentration of triphenylphosphine oxide is linear, characterized by a very good correlation coefficient of 0.978.

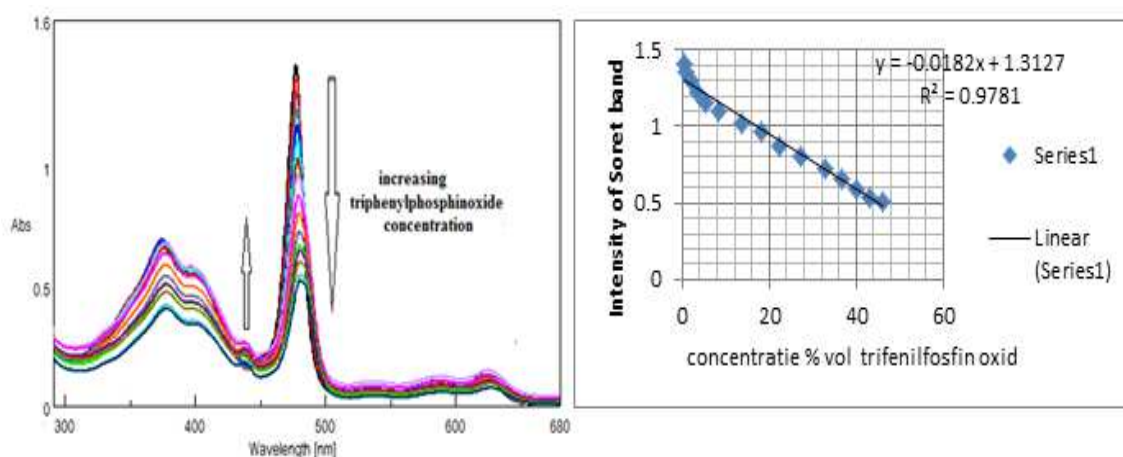


**Figure 2.** UV-vis spectra showing the linear dependence of triphenylphosphine oxide increasing concentration and MnTPPCl, in toluene.

Besides, a novel peak is formed at 437 nm, as a proof of the new complex formation, its intensity increasing as the phosphine derivative content is increasing. Figure 4 displays the effect of increasing the concentration of triphenylphosphine oxide on UV-vis spectrum of CoTTP. The same phenomenon is produced, the Soret band intensity is decreasing by increasing the concentration of the triphenylphosphine oxide, but the dependence is not a regular one.

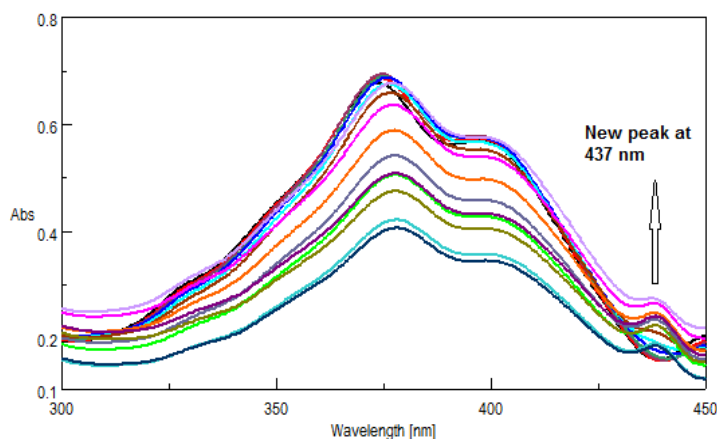


**Figure 3.** UV-vis spectra revealing a novel peak generated by the complex formation between triphenylphosphine oxide and MnTPPCL, in toluene.

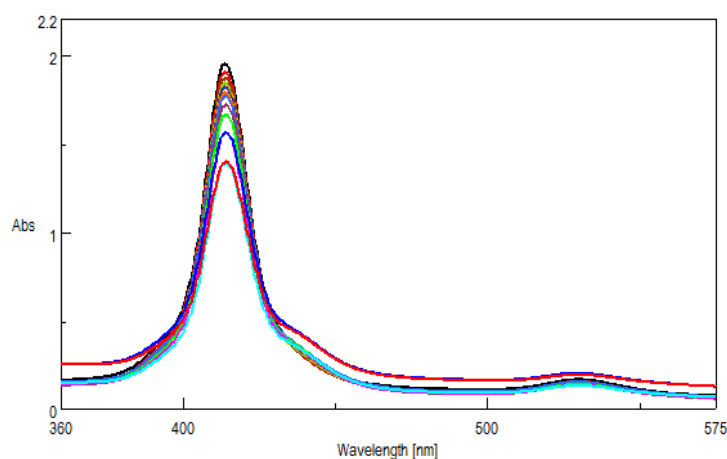


**Figure 4.** The influence of increasing triphenylphosphine oxide concentration on UV-vis spectra of CoTTP.

The explanation of the lower quality detection provided by Co-porphyrin can be that triphenylphosphine oxide is relatively basic and is a better ligand for hard or intermediate metal centers, as manganese case is.

### Conclusions

The metalloporphyrins are a class molecules with excellent sensing properties. With the increase of amount of the phosphine oxide, a continuous decrease regarding the intensity of the Soret bands of the two metalloporphyrins tested for detection qualities was put into evidence. A novel peak in the UV-vis spectrum at 437 nm proved the complex formation between the Mn-porphyrin and the phosphorus derivative. This Mn-metalloporphyrin offers a good base to develop a novel sensor for small amounts of toxic  $\text{Ph}_3\text{PO}$ .

### Acknowledgements:

The authors from Institute of Chemistry Timisoara of Romanian Academy are kindly acknowledging the support from Program 3-Porphyrins/2015 and STAR Programme-SAFEAIR Project 76/2013.

## References

- [1] G. Ciani, M. Manassero, M. Sansoni, J. Inorg. Nucl. Chem. 34(5) (1972) 1760–1762.
- [2] T.S. Lobana, N. Bala, Transit. Metal Chem. 19 (1) (1994) 115–116.
- [3] S. Xu, M. Liu, H.-L. Han, (...), Y.-Y. Chen, J.-Y. Yao, Polyhedron 85 (2015) 69–75.
- [4] Y. Lv, J. Zhang, W. Cao, Y. Fu, X. Wu, J. Alloy Compd. 462 (1–2) (2008) 153–156.
- [5] S. Köytepe, A. Paşahan, E. Ekinçi, B. Alici, T. Seçkin, J. Polym. Res. 15 (3) (2008) 249–257.
- [6] M. Zeldin, P. Mehta, W. Vernon, Inorg. Chem. 18 (2) (1979) 463–466.
- [7] A. Palade, A. Lascu, I. Creanga, G. Fagadar-Cosma, M. Birdeanu, E. Fagadar-Cosma, DJNB 10 (3) (2015) 729 – 735.
- [8] E. Fagadar-Cosma, C. Enache, I. Armeanu, D. Dascalu, G. Fagadar-Cosma, M. Vasile, I. Grozescu, Mat. Res. Bull. 44 (2009) 426–431.
- [9] E. Fagadar-Cosma, M. Mirica, I. Balcu, C. Bucovicescu, C. Cretu, I. Armeanu, G. Fagadar-Cosma, Molecules 14(4) (2009) 1370–1388.



## Preliminary Study of the Blood Brain Barrier Penetration of Some Organic Compounds and Drugs

*Luminita Crisan, Liliana Pacureanu*

*Department of Computational Chemistry, Institute of Chemistry of Romanian Academy,  
Timisoara, 24 Mihai Viteazul Avenue, 300223 Timisoara, Romania  
e-mail: lumi\_crisan@acad-icht.tm.edu.ro*

### Abstract

Partial Least Squares (PLS) regression of blood–brain permeation data (logBB) including 348 diverse organic compounds and drugs was built using 903 Dragon descriptors. The prediction performance of the obtained PLS model is acceptable: the squared correlation coefficient (cumulative sum of squares of all the Y's explained by all extracted components)  $R^2_{Y(CUM)} = 0.822$ , the crossvalidated correlation coefficient (cumulative fraction of the total variation of the Y's that can be predicted by all the extracted components)  $Q^2_{Y(CUM)} = 0.640$ , the number of independent variables,  $X=487$ , for a dataset of 342 compounds (six compounds was outliers). The Y-randomization test demonstrated the absence of chance correlation which is confirmed by the lower values of regression line intercepts for  $R^2_{X(CUM)}$  (0.307) and  $Q^2_{(CUM)}$  (-0.320). The descriptors such as polar surface area (N,O and N,O,S,P polar contributions), octanol-water partition coefficient (Ghose-Crippen and Moriguchi), hydrophilic factor, complementary information content index and the number of H-bond donor atoms showed the largest Variables Importance in the Projection (VIP) values and can influence the logBB. The values of logBB predicted by our model display lower differences against experimental values of 342 compounds than logBB values predicted by QikProp.

### Introduction

The blood–brain barrier (BBB) is a complex system implicated in the normal function of the central nervous system (CNS) through: (i) strictly limiting the passive diffusion of polar substances from the blood to the brain; (ii) mediating the transport of nutrients to the brain and of toxic metabolites and xenobiotics from the brain; (iii) overseeing the migration of circulating immune cells. [1-3] Penetration of blood-brain barrier, represents one of the most important and challenging areas in drug discovery. The presence of the BBB makes difficult the development of new therapies for brain diseases including meningitis, brain abscess, epilepsy, multiple sclerosis, neuromyelitis optica, late-stage neurological trypanosomiasis, Alzheimer's disease, cerebral edema, HIV encephalitis, etc [4]. To measure the drug transport across the blood brain barrier the blood–brain partition coefficient, logBB has been defined, [5]  $\log BB = \log(C_{\text{brain}}/C_{\text{blood}})$ , where  $C_{\text{brain}}$  and  $C_{\text{blood}}$  are the equilibrium concentrations of the drug in the brain and the blood, respectively.

*In vitro* experimental determination of BBB permeation is expensive, time consuming and requires compound's stability, purity and assay special conditions, while *in vivo* determinations based on radiolabeled compounds are required in some cases. [6] In 1988 the first theoretical model for a large number of H<sub>2</sub> histamine receptor agonists predicting logBB values has been reported. [7] Ever since many attempts to correlate the experimental blood-brain concentration ratio values with physico- chemical parameters have been reported. [8-24]

In this study the prediction of logBB values based on a larger dataset of compounds belonging to different structural classes collected from literature [12, 22, 23, 25-33] is reported. The aim is to build a comprehensive and general model for the blood brain barrier penetration of different organic compounds and drugs.

## Methodology

**Dataset.** In our study we combined various literature data sets to collect a large-scale logBB dataset comprising 348 experimental logBB values. These dataset are available upon request from the authors and contains compounds that belong to different structural classes: 197 compounds classified as permeable showing positive logBB values, ranging from 0 to 1.64, and 151 compounds classified as non-permeable displaying negative logBB value, ranging from -0.01 to -2.15.

**Descriptors.** The following classes of descriptors were calculated with the help of Dragon software [34]: of 1D-functional groups, 1D-atom centered fragments, 2D-topological descriptors, 2D walk and path counts, 2D-autocorrelations, 2D-connectivity indices, 2D-information indices, 2D-topological charge indices, 2D-Eigenvalue-based indices, 2D-topological descriptors, 2D-edge adjacency indices, 2D-Burden eigenvalues, molecular properties, 2D-binary fingerprints and 2D-frequency fingerprints starting from the SMILES codes. Molecular descriptors were checked and constant or near-constant variables were excluded. If two descriptors register a correlation coefficient of 0.99 one of them was eliminated. The final set of descriptors used in PLS investigation included 903 molecular descriptors. The complete list of molecular descriptors and their meaning are provided on the Dragon website.[34]

**PLS method.** PLS analysis is a linear modeling technique [35] aimed at finding the relationship between the independent variable X-matrix (Dragon descriptors) and response Y-matrix (logBB). The information contained in the descriptor X-matrix is projected on a smaller number of latent variables called PLS components, denoted by A. The prediction of Y-values is carried out by extracting a set of 125 orthogonal components from the initial X-matrix, which display the highest predictive power. The number of A factors was determined using the cross-validation method leave seven out, with maximum number of iterations when fitting the model of 200, whereas the confidence level was set at 95%. The VIP reflects the influence of the variables in the PLS model concerning the property Y (i.e., its correlation to all responses), and independent variables X [36]. To evaluate the robustness of the PLS model obtained we used the response permutation method implemented in SIMCA package [36].

**Robustness of the QSAR models.** Golbraigh demonstrated that the  $Q^2$  is not adequate to assess the predictive ability of the QSAR model. [37] Therefore, Y-randomization test is a widely used technique to evaluate the robustness of a QSAR model. [38] It consists in building a number of QSAR models using the initial descriptor matrix and the randomized Y variable. The plot showing  $R^2Y_{(CUM)}$  (cumulative sum of squares of all the Y's explained by all extracted components) and  $Q^2_{(CUM)}$  (cumulative fraction of the total variation of the Y's that can be predicted by all the extracted components) for all PLS-DA models (all the Y permuted models, and also the initial model) on the Y-axis and the correlation coefficients between randomized and original response variables on the X-axis was analyzed [37]. If the Y-axis intercept of the regression line does not exceed 0.3–0.4 for  $R^2Y_{(CUM)}$ , and 0.05 for  $Q^2_{(CUM)}$ , the model is considered free of chance correlation. [38] The selected PLS model was subjected to 999 Y-randomizations.

**LogBB prediction by QikProp.** The QikProp software [39] developed by Professor William L. Jorgensen [40] fitted to 710 compounds including 500 drugs, one of the state of the art tools in predicting log(BB) was used as reference for our model. In addition to predicting the absorption, distribution, metabolism, and excretion (ADME) physically and pharmaceutically relevant properties of organic molecules or drugs, QikProp provides ranges for comparing a particular molecule properties.

## Results and discussions

In order to correlate the experimental logBB values with structural descriptors, the PLS calculations were initiated for 903 descriptors and 348 log BB values [36]. From the 125 principal components resulted, the first 10% of the components already explain 54% of the information content of the X-matrix. The first PLS model was constructed using the initial X matrix, was not satisfactory, therefore we proceed to the improvement of the statistics as follows: (i) the normal probability plot of Y standardized residuals - standard deviation higher than  $\pm 3$  - was the criterion for gradually eliminating the outliers; (ii) the overfit was reduced by excluding the noise variables (variable coefficient values close to 0). Therefore, six compounds were identified as outliers as their standard deviations exceeded  $\pm 3SD$  ( $\pm 3.04$  to  $\pm 4.31$ ) and 416 noise variables were progressively eliminated. The statistical parameters of the final model are suitable for a large dataset of compounds. The cumulative sum of squares (SS) of all the X values explained by all extracted components  $R^2_{X(CUM)} = 0.559$ , the cumulative SS of all the Y's explained by all extracted components  $R^2_{Y(CUM)} = 0.822$ , and the fraction of the total variation of Y values that can be predicted for all extracted principal components  $Q^2_{Y(CUM)} = 0.640$ . The variables which influence markedly our PLS model ( $VIP > 1.6$ ) include several straightforward descriptors such as polar surface area (PSA - N,O and N,O,S,P polar contributions), octanol-water partition coefficient (Ghose-Crippen and Moriguchi), hydrophilic factor, complementary information content index and the number of H-bond donor atoms. This is in accord with well accepted parameters such as lipophilicity, hydrogen bonding capacity, molecular charge, molecular size, molecular shape, and molecular flexibility which was correlated with log BB. [5] Complementary information content index is an topological index which is calculated based on Shanon information theory [41] Generally speaking, the molecular topology is correlated with a large number of molecular and biological properties. In particular, the topological indices of zero order are of special importance for the suitable description of molar volume of organic compounds which in turn is correlated with logBB [42]. Higher polarity and hydrogen bonding are detrimental for blood-brain penetration, whereas higher molecular volume was positively correlated. [5] PSA is highly correlated with the hydrogen bonding capacity of a compound. [5] Norinder and Haeberlein [43] observed a linear correlation between PSA and the sum of N + O atoms, and concluded that  $(N + O) \leq 5$  is favorable for blood brain penetration. Clark, [44] stated that logP is favorable to get positive values of log BB.

The predictive capacity or validity of a QSAR model is a measure of how accurately the model can predict the biological activity of the set of compounds. The final model was internally validated using, the Y-permutation procedure using 999 randomizations to cover the complete dataset, each time forming a distinct set. The scrambled models were constructed with the same number of latent variables as the final model. The plot displayed in Figure 1 demonstrates that the Y-intercept (logBB-intercept) of the  $R^2_{X(CUM)}$  and  $Q^2_{Y(CUM)}$  lines has lower values and indicates no chance correlation for the selected model.

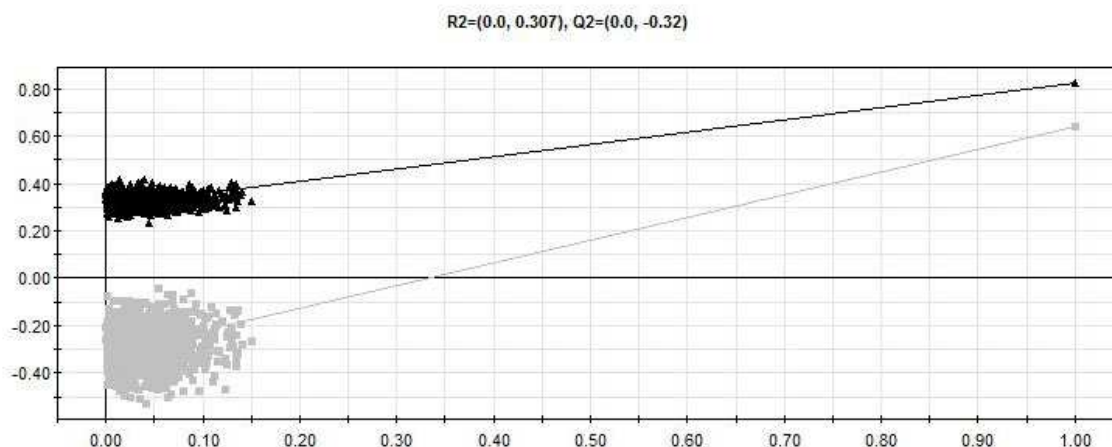


**Figure1.** Y - Randomization results for the final PLS model. The x-axis reports the correlation coefficient between original and permuted response data, while on the y-axis are represented  $R^2$  (black triangles) and  $Q^2$  (grey squares) values for the 999 randomized models

Several descriptors displaying higher VIP (Variables Importance in the Projection) values might play a critical role in defining BBB permeability of organic compounds. The top ten descriptors according to VIP magnitudes included in the PLS model are shown in Table 1.

**Table 1.** The most relevant descriptors of the PLS model

Var ID	VIP	VIPcvSE	CoeffCS	CoeffCScvSE	Descriptor significance
ALOGP	2.014	0.028	0.035	0.009	Ghose-Crippen octanol-water partition coeff. (logP)
MLOGP	1.926	0.035	0.032	0.010	Moriguchi octanol-water partition coeff. (logP)
BLTD48	1.926	0.035	-0.032	0.009	Verhaar Daphnia base-line toxicity from MLOGP (mmol/l)
TPSA(NO)	1.823	0.021	-0.031	0.007	Topological polar surface area using N,O polar contributions
MLOGP2	1.813	0.029	0.029	0.016	Squared Moriguchi octanol-water partition coeff.
TPSA(Tot)	1.759	0.015	-0.031	0.008	Topological polar surface area using N,O,S,P polar contributions
Hy	1.729	0.049	-0.030	0.022	Hydrophilic factor
ALOGP2	1.722	0.025	0.024	0.009	Squared Ghose-Crippen octanol-water partition coeff.
CIC1	1.636	0.027	0.017	0.011	Complementary Information Content index (neighborhood symmetry of first order)
nHDon	1.629	0.040	-0.033	0.022	Number of donor atoms for H-bonds (N and O)

\*VIP = The influence of every term in the matrix X on all the Y's; VIPcvSE = The jack knife standard error of the VIP computed by seven rounds of cross validation; CoeffCS = PLS regression coefficients corresponding to centered and scaled X, and scaled (but uncentered) Y; CoeffCScvSE = The jack knife standard error of the coefficients CoeffCS computed by seven rounds of cross validation.

For the same dataset of compounds QplogBB (Predicted brain/blood partition coefficient) was calculated with QikProp module from Schrödinger suite. The logBB predicted by our model register lower differences with respect to experimental values than QikProp calculations (see

Figure 2). The highest number of compounds displaying low differences to experimental values (0.05-0.3) is predicted by our PLS model, whereas QikProp predictions exhibit higher differences against experiment.

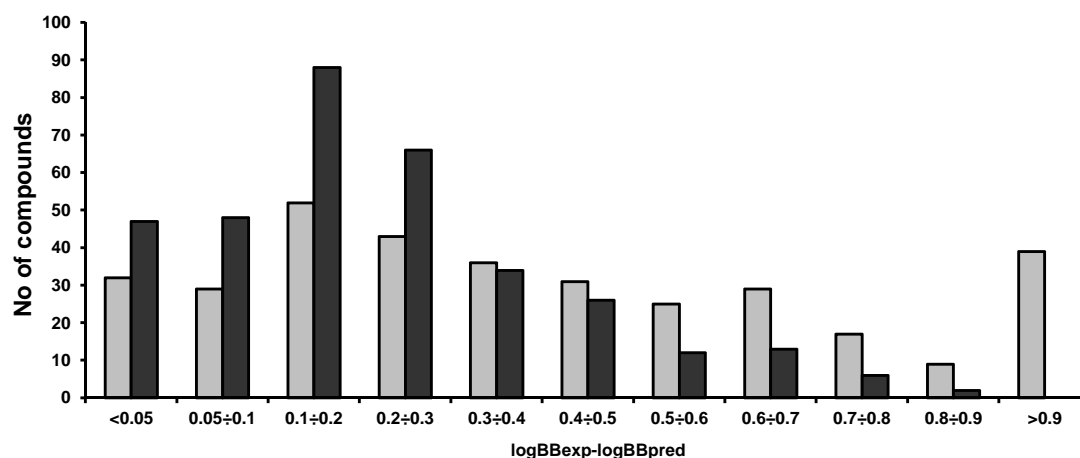


**Figure 2.** The number of compounds versus logBBexp-logBBpred; black bars render the PLS model and grey bars depict the QikProp prediction.

These results can be explained by the fact that the domain of applicability of the regression equation used by QikProp, is based on N=104 compounds of the molecular weight between 20-525 Da, while the molecular weight for our dataset of N=348 compounds ranges 16-1202 Da.

### Conclusions

We have applied a PLS approach to a dataset of 348 compounds with known experimental logBB values, which belong to different structural classes. Some straightforward descriptors such as topological polar surface area, octanol-water partition coefficient and the number of H-bond donor atoms influence the developed PLS model, showing VIP values higher than 1.6. The final PLS model built on a large dataset excluded the risk of arbitrary correlation. Further QSAR experiments using diverse modeling methodologies including 3D descriptors and additional compounds will be pursued.

### Acknowledgements

We thank Dr. Erik Johansson (Umetrics, Sweden) for kindly providing the SIMCA P 9.0 program package (L. Kurunczi laboratory) and to Dr. Simona Funar-Timofei for the access to DRAGON software. This project was financially supported by the Project No. 1.2 of the Institute of Chemistry of Romanian Academy, Timisoara.

### References

- [1] N.J. Abbott, A.A. Patabendige, D.E. Dolman, S.R. Yusof, D.J. Begley, *Neurobiol. Dis.* 37 (2010) 13.
- [2] D.J. Begley, M.W. Brightman, *Prog. Drug. Res.* 61 (2003) 39.
- [3] H. Wolburg, S. Noell, A. Mack, K. Wolburg-Buchholz, P. Fallier-Becker, *Cell. Tissue Res.* 335 (2009) 75.
- [4] S. Paris-Robidas, V. Emond, C. Tremblay, D. Soulet, F. Calon *Mol Pharmacol.* (2011) 80, 32.
- [5] U. Bickel, *NeuroRx.* 2 (2005) 15.
- [6] A. Reichel, D.J. Begley, *Pharm. Res.* 15 (1998) 1270.



- [7] R.C. Young, R.C. Mitchell, T.H. Brown, C.R. Ganellin, R. Griffiths, M. Jones, K.K. Rana, D. Saunders, I.R. Smith, N.E. Sore, T.J. Wilks, *J. Med. Chem.* 31 (1988) 656.
- [8] F. Lombardo, J.F. Blake, W.J. Curatolo, *J. Med. Chem.* 39 (1996) 4750.
- [9] M.H. Abraham, K. Takacs-Novak, R.C. Mitchell, *J. Pharma. Sci.* 86 (1997) 310.
- [10] U. Norinder, P. Sjöberg, T. Osterberg, *J. Pharma. Sci.* 87 (1998) 952.
- [11] D.E. Clark, *J. Pharma. Sci.* 88 (1999) 815.
- [12] J. Kelder, P.D.J. Grootenhuis, D.M. Bayada, L.P.C. Delbressine, J.P. Ploemen, *Pharma. Res.* 16 (1999) 1514.
- [13] P. Crivori, G. Cruciani, P.A. Carrupt, B. Testa, *J. Med. Chem.* 43 (2000) 2204.
- [14] P. Ertl, B. Rohde, P. Selzer, *J. Med. Chem.* 43 (2000) 3714.
- [15] G.M. Keseru, L. Molnar, *J. Chem. Inf. Comput. Sci.* 41 (2001) 120.
- [16] R. Liu, H. Sun, S.S. So, *J. Chem. Inf. Comput. Sci.* 41 (2001) 1623.
- [17] K. Rose, L.H. Hall, L.B. Kier, *J. Chem. Inf. Comput. Sci.* 42 (2002) 651.
- [18] T. Hou, X. Xu, *J. Mol. Model.* 8 (2002) 337.
- [19] M.C. Hutter, *J. Comput. Aided Mol. Des.* 17 (2003) 415.
- [20] M.H. Abraham, *Eur. J. Med. Chem.* 39 (2004) 235.
- [21] A. Yan, H. Liang, Y. Chong, X. Nie, C. Yu, *SAR QSAR Environ. Res.* 24 (2013) 61.
- [22] R. Narayanan, S.B. Gunturi, *Bioorg. Med. Chem.* 13 (2005) 3017.
- [23] L. Zhang, H. Zhu, T.I. Oprea, A. Golbraikh, A. Tropsha, *Pharm. Res.* 25 (2008) 1902.
- [24] M. Muehlbacher, G.M. Spitzer, K.R. Liedl, J. Kornhuber, *J. Comput. Aided Mol. Des.* 25 (2011) 1095.
- [25] S.R. Mente, F. Lombardo, *J. Comput. Aided Mol. Des.* 19 (2005) 465.
- [26] S. Vilar, M. Chakrabarti, S. Costanzi, *J. Mol. Graph. Model.* 28 (2010) 899.
- [27] J.A. Platts, M.H. Abraham, Y.H. Zhao, A. Hersey, L. Ijaz, D. Butina, *Eur. J. Med. Chem.* 36 (2001) 719.
- [28] M.H. Abraham, A. Ibrahim, Y. Zhao, W.E. Acree, *J. Pharm. Sci.* 95(2006) 2091.
- [29] P. Garg, J. Verma, *J. Chem. Inf. Model.* 46 (2006) 289.
- [30] A. Guerra, J.A. Pa'ez, N.E. Campillo, *QSAR Comb. Sci.* 27 (2008) 586.
- [31] K. Rose, L.H. Hall, L.B. Kier, *J. Chem. Inf. Comput. Sci.* 42 (2002) 651.
- [32] D.A. Konovalov, D. Coomans, E. Deconinck, Y. Vander Heyden, *J. Chem. Inf. Model.* 47 (2007) 1648.
- [33] M. Zerara, J. Brickmann, R. Kretschmer, T.E. Exner, *J. Comput. Aided Mol. Des.* 23 (2009) 105.
- [34] Dragon Professional 5.5/2007 is software of Talete S.R.L., Milano, Italy.
- [35] S. Wold, M. Sjöström, L. Eriksson, *Chemometr. Intell. Lab.* 58 (2001) 109.
- [36] SIMCA-P+ version 9.0, Umetrics AB, Sweden. <http://www.umetrics.com>.
- [37] A. Golbraikh, M. Shen, Z. Xiao, YD Xiao, K.H. Lee, A. Tropsha, *J. Comput. Aided Mol. Des.* 17 (2003) 241.
- [38] L. Eriksson, E. Johansson, N. Kettaneh-Wold, S. Wold, in: *Multi- and megavariate data analysis: principles and applications*, Umetrics AB, Umea, 2001, pp 92–97, pp 489–491.
- [39] QikProp, version 3.9, Schrödinger, LLC, New York, NY, 2014.
- [40] W.L. Jorgensen, E.M. Duffy, *Bioorg. Med. Chem. Lett.* 10 (2000) 1155.
- [41] C.E. Shannon, *Tech. J.* 27 (1948), 379.
- [42] A.R. Katritzky, E. Gordeeva, *J. Chem. Inf. Comput. Sci.* 33 (1993) 835.
- [43] U. Norinder, M. Haeberlein, *Adv. Drug Deliv. Rev.* 54 (2002) 291.
- [44] D.E. Clark, *J Pharm Sci* 88 (1999) 815.



## Modeling of Mannich Bases Fungicidal Activity by the MLR Approach

Simona Funar-Timofei, Ana Borota, Alina Bora, Ramona Curpan, Sorin Avram

Computational Chemistry Department, Institute of Chemistry Timisoara of the Romanian Academy, 24Mihai Viteazul Bvd., 300223, Timisoara, Romania

### ABSTRACT

In the present paper, we have carried out quantitative structure-fungicidal activity relationships analysis on a novel series of Mannich bases with trifluoromethyl-1,2,4-triazole and substituted benzylpiperazine moieties reported to have improved fungicidal activity against *Fusarium oxysporum f.sp. cucumerinum*. The chemical structures were energy minimized based on semiempirical quantum chemical method RM1. The molecular descriptors were calculated using the DRAGON, InstantJchem and ChemProp software. Several models for the prediction of fungicidal activity have been drawn up by using the multiple regression technique (MLR). The genetic algorithm approach was employed for variable selection method to search for the best ranking models. The predictive ability of the MLR models was validated using an external test set of 5 out of 18 molecules. The best MLR model was chosen by observing acceptable  $r^2$ ,  $r_{adj}^2$  and  $q_{LOO}^2$  values, low residual errors and high Multi-Criteria Decision Making (MCDM) scores. The MLR equation suggests the positive impact of GETAWAY and edge adjacency matrix descriptors on the fungicidal activity. The high acidic character of the molecule increase the fungicidal activity.

### INTRODUCTION

Triazoles are often used in pharmacology, medicine and agriculture, having a broad spectrum of biological activities such as antimicrobial, cytotoxic, antihistaminic, anticonvulsant, analgesic, anti-inflammatory, insecticidal, antimycotic, antimycobacterial, anticancer, antiprotozoal, antimalarial and anti-ulcer activity [1].

Molecules containing thiazole ring systems are important because of their low toxicity and excellent biological activity [2].

Triazoles undergo different types of reactions to yield other heterocyclic compounds, e.g., mannich bases, thioureas, thioethers, schiff bases, triazolothiadiazoles, triazolothiazines, triazolothiazepines and triazolothiadiazines. They are not only transition compounds but they are also very effective organic compounds [3].

Triazole compounds have shown a great efficacy against antifungal infections. The mechanism of inhibition of fungal growth is well established. Thus, the azoles antifungal action is performed in two steps: (i) inhibition of ergosterol synthesis, a major component of fungal membrane and (ii) the blocking of P450-dependent enzyme *i.e.*, lanodterol 14- $\alpha$ -demethylase (CYP 51) [4]. Triazole fungicides are widely used broad-spectrum fungicides that inhibit the sterol 14- $\alpha$ -demethylase, an enzyme involved in the biosynthesis of ergosterol [5].

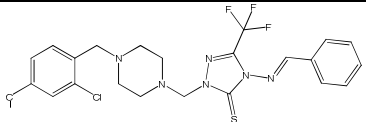
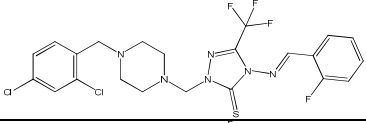
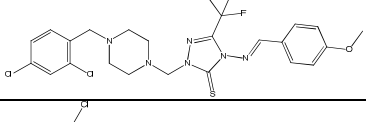
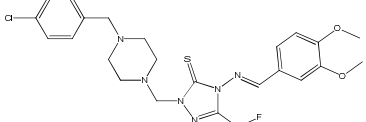
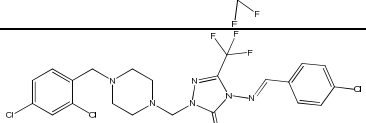
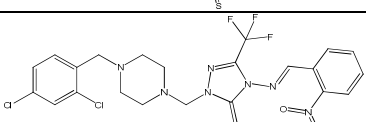
A series of novel 18 trifluoromethyl-substituted 1,2,4-triazole Mannich bases containing substituted benzylpiperazine ring have been synthesized and investigated for their herbicidal, fungicidal and plant growth regulators activity [6] (Table 1).

The current paper presents a quantitative structure-activity relationships study for this series of 1-[(4-substituted-benzylpiperazin-1-yl)methyl]-4-(substituted)benzylideneamino-3-trifluoromethyl-1H-1,2,4-triazole-5(4H)-thiones using multiple linear regression (MLR). These compounds were optimized using the RM1 semiempirical molecular orbital method

[7]. Descriptors calculated for the RM1 geometries were related to the mycelial growth inhibition activity against the *Fusarium oxysporum f. sp. cucumerinum* fungi test [6].

**Table 1.** The chemical structure of trifluoromethyl-substituted 1,2,4-triazole Mannich bases and their *Fusarium oxysporum f. sp. Cucumerinum* experimental relative inhibition rates (RIR)\*

No	Structure	RIR	HATS8u	R2u	EEig11r	Strongest basic pKa	$\Delta H_f$ kcal/mol
1		0.101	0.402	2.004	2	7.74	-3.69
2		0.804	0.271	2.103	2.167	7.74	-47.91
3		0.187	0.426	1.972	2	7.74	-81.18
4		0	0.428	1.966	2.167	7.74	-86.31
5		0	0.398	2.032	2.167	7.74	-73.76
6		0.402	0.383	2.015	2.332	7.74	-40.62
7		0.509	0.341	2.082	2.167	6.76	-36.52
8		0.719	0.271	2.129	2.333	6.76	-16.05
9		0.604	0.405	1.995	2.167	6.76	-49.72
10		0.401	0.357	2.061	2	6.76	-83.93
11		0.303	0.398	2.03	2.167	6.76	-17.43
12		0.502	0.401	2.009	2.332	6.76	-11.65

13		0.708	0.355	2.109	2	6.01	-19.18
14		0.826	0.286	2.116	2.167	6.01	-64.77
15		0.504	0.388	2.014	2	6.01	-58.49
16		0.705	0.416	2.041	2.167	6.01	-93.71
17		0.607	0.389	2.043	2	6.01	-45.43
18		0.608	0.386	2.034	2.167	6.01	-48.14

\* HATS8u represents average-weighted autocorrelation of lag 8 / unweighted (GETAWAY descriptor); R2u - R autocorrelation of lag 2 / unweighted (GETAWAY descriptor); EEig11r - eigenvalue 11 from edge adj. matrix weighted by resonance integrals (Edge adjacency index); heat of formation ( $\Delta H_f$ ) of the energy optimized structure.

## MATERIALS and METHODS

### Definition of target property and molecular structures

A series of 18 trifluoromethyl-substituted 1,2,4-triazole Mannich bases containing substituted benzylpiperazine ring (Table 1) was used, having the fungicidal *Fusarium oxysporum f. sp. Cucumerinum* relative inhibition rate (RIR, expressed in %) as dependent variable.

All geometries of the title fungicides were minimized with the semiempirical RM1 quantum chemical approach [7] using the semiempirical NDDO module of Schrödinger software (Schrödinger, LLC, New York, NY, 2015). The following quantum chemical descriptors were derived for the RM1 geometries: electronegativity, hardness, chemical potential, electrophilicity, HOMO and LUMO molecular orbital energies, heat of formation, dipole moment, molecular surface area, softness, maximum average local ionization energy on the molecular surface, minimum average local ionization energy on the molecular surface, mean average local ionization energy on the molecular surface, maximum electrostatic potential on the molecular surface, minimum electrostatic potential on the molecular, mean electrostatic potential on the molecular surface, electrophilic superdelocalizability, nucleophilic superdelocalizability, radical superdelocalizability, atom self polarizability. The outlines of the calculated quantum chemical parameters provide additional information about the activity of the studied compounds.

Structural 0D, 1D, 2D and 3D descriptors were calculated for the lowest energy compounds using the DRAGON (Dragon Professional 5.5 (2007), Talete S.R.L., Milano, Italy), InstantJchem (which was used for structure database management, search and prediction) (InstantJchem 15.7.27, 2015, ChemAxon (<http://www.chemaxon.com>) and ChemProp (UFZ

Department of Ecological Chemistry 2014. ChemProp 6.2, <http://www.ufz.de/index.php?en=6738>) software.

The variables were normalized using the following equation (1):

$$XT_{mj} = \frac{X_{mj} - \bar{X}_m}{S_m} \quad (1)$$

where for each variable  $m$ ,  $XT_{mj}$  and  $X_{mj}$  are the values  $j$  for the variable  $m$  after and before scaling respectively,  $\bar{X}_m$  is the mean and  $S_m$  the standard deviation of the variable.

Structural descriptors were correlated with the fungicide relative inhibition rate by multiple linear regression (MLR). MLR calculations were combined with a genetic algorithm for variable selection included in the QSARINS v.2.2 program [8]. The RQK fitness function, with leave-one-out cross-validation correlation coefficient was used as constrained function to be optimized. The dataset was divided into training set and a randomly selected (30% of the total number of compounds) test set. Compounds 7, 9, 10, 13, 18 (Table 1) were included in the test set. Validation is a crucial aspect of any quantitative structure–activity relationship (QSAR) analysis [9, 10]. In this light, the developed MLR models were validated using internal and external validation.

### Model validation

All the statistical tests were performed at a significance level of 5 %. In MLR models, outliers were detected by a value of residual greater than 2.5 times, the value of standard error in calculation.

For internal validation results several measures of robustness were employed: leave-one-out cross-validation ( $Q^2_{LOO}$ ), Y-scrambling and  $Q^2_{LMO}$  leave-more-out (LMO) cross-validation (carried out for 30% of data out of training, each run).

Y-scrambling testing was repeated 2000 times. It is used for checking the robustness of a QSAR model and the statistical significance of the estimated predicted power. Satisfactory leave-one-out cross-validation values are stable and predictive if validated by the leave-more-out (LMO) procedure.

The data over fitting and model applicability was controlled by comparing the root-mean-square errors of training ( $RMSE_{tr}$ ) and validation ( $RMSE_{ext}$ ) sets. To test the predictive power of the model, several parameters were calculated:  $Q^2_{F1}$  [11],  $Q^2_{F2}$  [12],  $Q^2_{F3}$  [13],  $RMSE_{ext}$ ,  $MAE_{ext}$  (mean absolute error for test set) and the predictive  $r^2$  ( $r^2_{pred}$ ) test [14]. It is considered that for a predictive QSAR model, the value of  $r^2_{pred}$  should be higher than 0.5.

The Multi-Criteria Decision Making (MCDM) [15] is a technique that summarizes the performances of a certain number of criteria simultaneously, as a single number (score) between 0 and 1. A desirability function, takes values ranging from 0 to 1 (where 0 represents the worst validation criteria value and 1 the best) and is associated to every validation criteria. The geometric average of all the values obtained from the desirability functions gives the MCDM value. The 'MCDM all' scores were calculated using all the criteria: fitting, cross-validated and external and were used to choose the best MLR models.

## RESULTS AND DISCUSSION

A training set of 12 compounds and five test compounds (no.: 7, 9, 10, 13, 18) were used to build the models and to measure their performances. Compound 2 was found as outlier and was excluded from the final MLR models. Starting from all calculated descriptors several one and two descriptor models were generated (Table 2). Structural parameters derived from the

InstantJChem, Dragon and ChemProp programs and quantum chemical descriptors obtained from the RM1 geometries were employed in the MLR calculations. Variable selection was carried out by the genetic algorithm, using the leave-one-out fit criterion as constrained function to be optimized. Several fitting and predictability criteria were employed for model validation (see Tables 2 and 3). Satisfactory MLR models were obtained. Good fitting results were obtained for all MLR models. The predictive ability of models 3 and 4 is acceptable (except the  $Q_{F2}^2$  value), the “MCDM all” scores indicating as satisfactory models 3 and 4, too.

**Table 2.** Internal validation parameters of the MLR models (training set)

Model	Variables	$r_{\text{training}}^2$	$r_{\text{adj}}^2$	$q_{\text{LOO}}^2$	RMSE <sub>tr</sub>	MAE <sub>tr</sub>	$r_{\text{scr}}^2$	$q_{\text{scr}}^2$	$q_{\text{LMO}}^2$	MCDM all	F
1	Strongest basic pKa HATS8u	0.839	0.803	0.735	0.110	0.095	0.188	-0.494	0.699	0	23.38
2	Strongest basic pKa R2u	0.823	0.783	0.715	0.116	0.095	0.180	-0.499	0.667	0	20.86
3	Strongest basic pKa EEig11r	0.818	0.777	0.683	0.117	0.105	0.183	-0.468	0.636	0.610	20.16
4	Strongest basic pKa	0.705	0.675	0.583	0.149	0.127	0.092	-0.312	0.572	0.663	23.87

\*  $r_{\text{training}}^2$  -correlation coefficient;  $r_{\text{adj}}^2$  -adjusted correlation coefficient;  $q_{\text{LOO}}^2$  - leave-one-out cross-validation correlation coefficient; RMSE<sub>tr</sub>-root-mean-square errors; MAE<sub>tr</sub>-mean absolute error;  $r_{\text{scr}}^2$  - correlation coefficient of the randomized responses;  $q_{\text{scr}}^2$  - cross-validation correlation coefficient of the randomized responses;  $q_{\text{LMO}}^2$  -leave-more-out cross-validation correlation coefficient; MCDM all-Multi-Criteria Decision Making scores using all the fitting, cross-validated and external criteria; F-Fischer test.

**Table 3.** External validation parameters of the MLR models (test set)

Model	$Q_{F1}^2$	$Q_{F2}^2$	$Q_{F3}^2$	RMSE <sub>ext</sub>	MAE <sub>ext</sub>	$r_{\text{pred}}^2$
1	0.699	-0.030	0.853	0.105	0.074	0.699
2	0.537	-0.583	0.774	0.131	0.102	0.537
3	0.731	0.081	0.869	0.100	0.092	0.731
4	0.811	0.352	0.908	0.084	0.072	0.810

\*  $Q_{F1}^2$ ,  $Q_{F2}^2$ ,  $Q_{F3}^2$  -external validation parameters; RMSE<sub>ext</sub>-root-mean-square errors; MAE<sub>ext</sub>-mean absolute error;  $r_{\text{pred}}^2$  -predictive  $r^2$

The best MLR model was chosen by observing the acceptable  $r_{\text{training}}^2$ ,  $r_{\text{adj}}^2$ ,  $q_{\text{LOO}}^2$  and  $r_{\text{pred}}^2$ , values, high ‘MCDM all’ scores and low residual errors. Based on these criteria, the best MLR model could be considered equation 3 (Table 2):

$$\text{RIR} = 0.583(\pm 0.07) - 0.553(\pm 0.09)\text{Strongest basic pKa} + 0.2445(\pm 0.10)\text{EEig11r}$$

$$N_{\text{training}} = 12 \quad N_{\text{test}} = 5 \quad r_{\text{training}}^2 = 0.818 \quad \text{SEE} = 0.135 \quad r_{\text{adj}}^2 = 0.777 \quad q_{\text{LOO}}^2 = 0.683 \quad q_{\text{LMO}}^2 = 0.636$$

where: SEE represents the standard error of estimates, F – the Fischer test

The differences between  $r_{\text{training}}^2$  and  $r_{\text{adj}}^2$  of 0.0406, between  $r_{\text{training}}^2$  and  $q_{\text{LOO}}^2$  of 0.1345, and between  $q_{\text{LOO}}^2$  and  $q_{\text{LMO}}^2$  of 0.0474, indicate that model 3 is robust and has low over fitting effects. The low differences between the root-mean-square errors and between the mean absolute errors of the training and validation sets point to good fitting results and a robust model ( $\text{RMSE}_{\text{tr}} - \text{RMSE}_{\text{ext}} = 0.017$ ;  $\text{MAE}_{\text{tr}} - \text{MAE}_{\text{ext}} = 0.013$ ).

In order to check the reliability of the proposed equation, the observed versus predicted activities RIR values according to the QSAR equation using molecular descriptors, the Williams and the Y-scramble plots predicted by the MLR 3 model are outlined in Figures 1, 2 and 3, respectively.

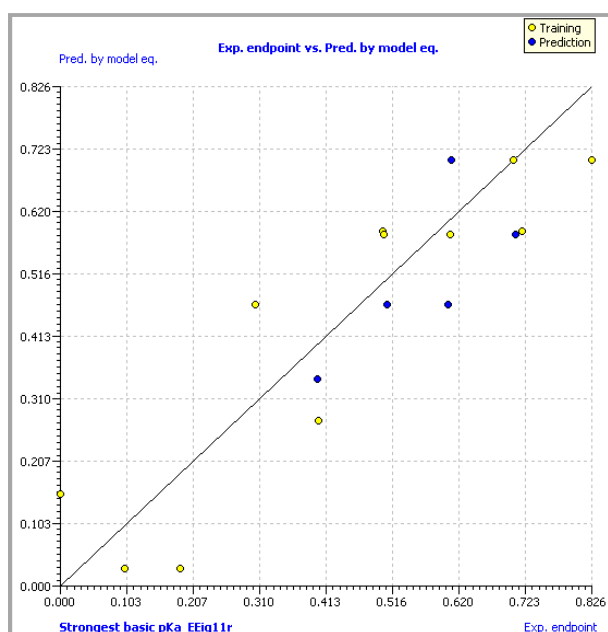


**Fig. 1.** Experimental *versus* predicted RIR values for the MLR3 model (Table 2).

Generally, the Williams plot is used to identify compounds with the greatest structural influence ( $h_i > h^*$ ;  $h_i$  = leverage of a given chemical;  $h^*$  = the warning leverage) in developing the model. The Williams plot for the training set presented in Figure 2, establishes applicability domain of the model within  $\pm 2.5\sigma$  and a leverage threshold  $h^* = 0.750$ . It is obvious from Figure 2 that all the compounds in the dataset are within the applicability domain of the model.



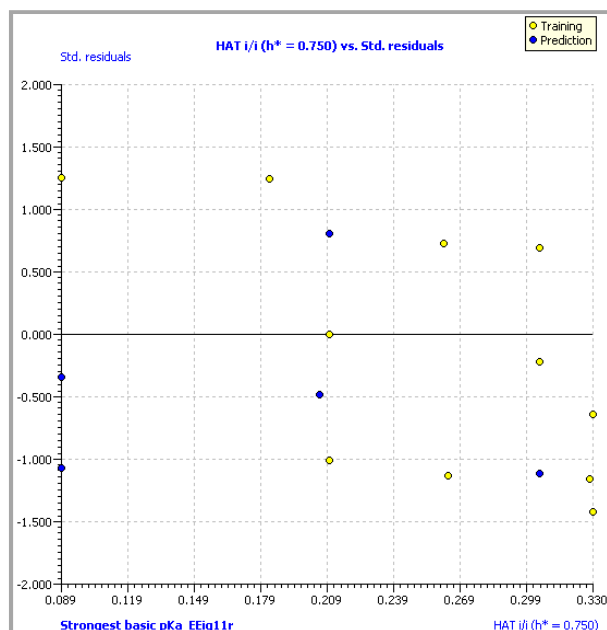


**Fig. 2.** Williams plot predicted by the MLR3 model (Table 2).

Y-scramble test was verified if the developed QSAR model is robust and not derived due to chance. The models are expected to have significant low scrambled  $r^2$  ( $r_{scr}^2$ ) and cross-validated  $q^2$  ( $q_{scr}^2$ ) values for several trials, which confirm the robustness of the developed models. From Figure 3 one can observe that in case of all the randomized models, the values of  $r_{scr}^2$  and  $q_{scr}^2$  were  $< 0.5$ . The low calculated  $r_{scr}^2$  and  $q_{scr}^2$  values (Table 2, Figure 3) indicate no chance correlation for the chosen model.

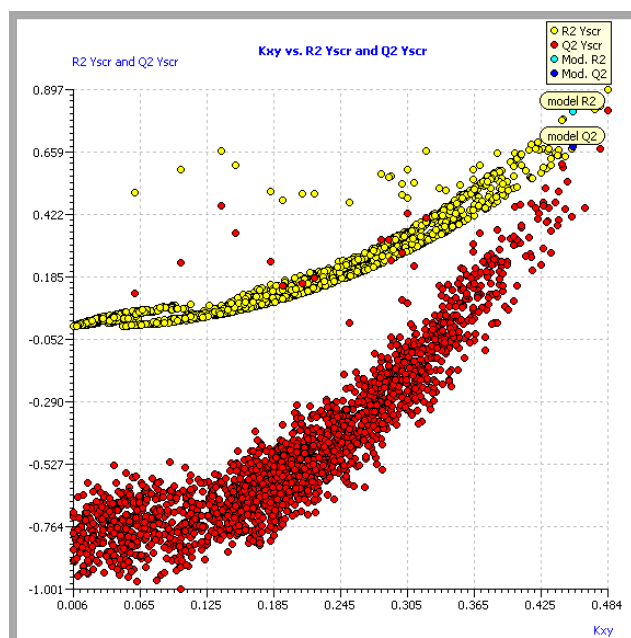


**Fig. 3.** Y-scramble plots for the MLR 3 model.

The predictive ability of the MLR models 3 and 4 is acceptable, according to the  $Q_{F1}^2$ ,  $Q_{F3}^2$  and  $r_{pred}^2$  values, model 4 having lower fitting results compared to model 3.

## CONCLUSIONS

In this study we developed MLR models for a series of trifluoromethyl-1,2,4-triazole derivatives with fungicide activity against *Fusarium oxysporum f.sp. cucumerinum*. Cross-validation (LOO and LMO), 'MCDM all' scores, y-scrambling test and applicability domain analysis validate the internal and external predictabilities of the models developed using the training and test sets. The y-randomization test outcomes ensure that the developed MLR model is robust and not derived merely due to chance. Moreover, the applicability domain evaluation confirms that the developed model is reliable to make predictions, which were checked by several external validation criteria.

The chosen regression equation 3 indicates that low values of the 'strongest basic pKa' descriptor (more acidic fungicides) and high values of the EEIG11r descriptor increase the RIR values, respectively the fungicide activity.

We conclude that GETAWAY and edge adjacency matrix descriptors provide the highest contribution to the fungicidal activity for the data set studied herein, the acidic ability influencing the fungicide inhibition rate.

## ACKNOWLEDGEMENT

This project was financially supported by the Project No. 1.1 of the Institute of Chemistry of Romanian Academy, Timisoara. The authors are indebted to the Chemaxon Ltd., Prof. Paola Gramatica from The University of Insubria (Varese, Italy) and Prof. Gerrit Schüürmann from Helmholtz Centre for Environmental Research (UFZ, Leipzig, Germany) for giving access to their software.

## REFERENCES

- [1]. Kumar S.S.; Kavitha H.P. (2013). Synthesis and Biological Applications of Triazole Derivatives - A Review, *Mini-Reviews in Organic Chemistry*, 10(1), p. 40-65.
- [2]. Qin X., Yu H. B., Dai H., Qin Z. F., Zhang X., Bing G. F., Wang T. T., Fang J. X. (2010). Synthesis and plant-growth regulatory activities of novel imine derivatives containing 1H-1,2,4-triazole and thiazole rings. *Chinese Chem. Lett.*, 21, p. 283-286.
- [3]. Güniz Küçükgül S., Çıkla-Süzgün P. (2015). Recent advances bioactive 1,2,4-triazole-3-thiones. *Eur. J. Med. Chem.* 97, p. 830-870.
- [4]. Khana I. A., Ahmada M., Aslamb S., Saife M. J., Zahoor A. F., Raza Naqvia S. A., Mansha A. (2015). Recent advances in the synthesis of triazole derivatives, *AFINIDAD LXXII, Enero - Marzo*, 569, p.64-77.
- [5]. Buerge J.I., Poiger T., Buser H.R. (2006). Influence of pH on the stereoselective degradation of the fungicides epoxiconazole and cyproconazole in soils. *Environ. Sci.Technol.*, 40, p. 5443-5450.
- [6]. Wang B.-L., Liu X.-H., Zhang X.-L., Zhang J.-F., Song H.-B., Li Z.-M. (2011). Synthesis, structure and biological activity of novel 1,2,4-triazole Mannich bases containing a substituted benzylpiperazine moiety. *Chem. Biol. Drug. Des.*, 78, p. 42-49.
- [7]. Rocha G.B., Freire R.O., Simas A.M., Stewart J.J.P. (2006). RM1: a Reparameterization of AM1 for H, C, N, O, P, S, F, Cl, Br, and I. *J. Comput. Chem.*, 27(10), p. 1101-1111.
- [8]. Gramatica P., Chirico N., Papa E., Cassani S., Kovarich S. (2013). QSARINS: A new software for the development, analysis, and validation of QSAR MLR models. *J. Comput. Chem.*, 34, p. 2121-2132.
- [9]. Guidance Document on the Validation of (Quantitative) Structure-Activity Relationship [(Q)SAR] Models. (2007), OECD Environment Health and Safety Publications Series on Testing and Assessment No. 69. OECD: Paris, (<http://www.oecd.org/officialdocuments/publicdisplaydocumentpdf/?doclanguage=en&cote=env/jm/mono%282007%292>)

- [10]. Topliss J. G., Edwards R. P. (1979). Chance factors in studies of quantitative structure-activity relationships. *J. Med. Chem.*, 22, p.1238–1244.
- [11]. Shi L.M., Fang H., Tong W., Wu J., Perkins R., Blair R.M., Branham W.S., Dial S.L., Moland C.L., Sheehan D.M. (2001). QSAR models using a large diverse set of estrogens. *J. Chem. Inf. Model.* 41, p.186–195.
- [12]. Schüürmann G., Ebert R.U., Chen J., Wang B., Kuhne R. (2008) External validation and prediction employing the predictive squared correlation coefficient test set activity mean vs training set activity mean. *J. Chem. Inf. Model*, 48, p. 2140–2145.
- [13]. Consonni V., Ballabio D., Todeschini R. (2009). Comments on the definition of the Q2 parameter for QSAR validation. *J. Chem. Inf. Model*, 49, p. 1669–1678.
- [14]. Roy P.P., Paul S., Mitra I., Roy K. (2009). On two novel parameters for validation of predictive QSAR models. *Molecules*, 14, p. 1660-1701.
- [15]. Keller H.R., Massart D.L., Brans J.P. (1991). Multicriteria decision making: a case study. *Chemom. Int.Lab. Syst.*, 11, p.175-189.

## Magnesium Silicate Functionalized with Sodium- $\beta$ -Glycerophosphate used for Sr(II), Cs(I), Tl(I) Adsorption

Andreea Gabor<sup>1\*</sup>, Corneliu-Mircea Davidescu<sup>1</sup>, Adina Negrea<sup>1</sup>, Mihaela Ciopec<sup>1</sup>, Petru Negrea<sup>1</sup>

<sup>1</sup>University Politehnica Timisoara, Faculty of Industrial Chemistry and Environmental Engineering, Blv. Vasile Parvan 6, 300223, Timisoara, Romania  
e-mail: emeline\_gabor@yahoo.com

### Abstract

In this research Sr(II), Cs(I), Tl(I) were removed through adsorption using a functionalized solid support, magnesium silicate with sodium- $\beta$ -glycerophosphate. The influence of the initial concentration of metal in the solution and of the contact time were investigated. The adsorption process runs quickly obtaining the highest adsorption capacity for Sr(I) 7 mg/g.

### Introduction

One important problem in using nuclear energy are the nuclear waste, because they contain radioactive elements that are very harmful for the environment and for humans. Two of those elements are the metals Sr(II) and Cs(I). Sr-90 and Cs-137 have long half-lives, 28 years, 30 years, respectively, and are contained in acidic high level liquid waste [1]. Being heat emitting nuclides [2] and a source of  $\beta$ -radiation [3] it is necessary to remove them from the radioactive waste. Advantages of removing Sr(II) and Cs(I) are: stability of vitrified waste, reduction in the need of redundant cooling of the waste solution [2]. Removal treatments frequently used for removal of radionuclides from liquid radioactive waste include chemical preparation, evaporation solvent extraction and ion exchange process [4].

Another toxic metal is thallium. Tl(I) is widely distributed in all environmental media [5]. It is used in many industries like: manufacture of imitation jewelry, thermometers, ceramic semiconductor material, alloys and electronic devices [5]. Thallium compounds are very toxic and are used as insecticides and rodenticides [6]. Its toxic effects are more severe than other metals like mercury, lead, copper and cadmium [6].

### Experimental

Adsorption experiments were carried out in order to determine the equilibrium concentration of the metals on the adsorbent material and to study the influence of the contact time between the metal solution and the solid material.

For this, the adsorbent material was functionalized using the dry method. For 24 h, 5 g magnesium silicate were kept in contact with 0.01 g sodium- $\beta$ -glycerophosphate dissolved in 25 mL ethyl alcohol. It was dried at 323 K for 24 hours. The obtained functionalized adsorbent material was characterized by energy dispersive X-ray analysis (EDX) and scanning electron microscopy (SEM), using a scanning electron microscope Quanta FEG 250, equipped with energy dispersive X-ray quantifier.

The influence of the initial metal (Sr(II), Cs(I), Tl(I)) concentration and of the contact time on the adsorption capacity was investigated. Solutions with different metal concentration (10, 50, 100, 150, 200 mg/L) were prepared through dilution from a stock solution of the concentration 1 g/L. 25 mL of each solution with different concentration were put over 0.1 g adsorbent material and mixed for one hour using a Julabo SW23 mechanical shaker bath at 200 rot/min and 298 K. The samples were filtrated and the metal concentration was analyzed.

For the influence of the contact time samples of 0.1 g adsorbent material were mixed with 25

mL metal solution having the concentration of 10 mg/L. The concentration of the metal in the filtrate was analyzed after 15, 30, 60, 90, 120 minutes of mixing. The metal concentration was analyzed using an inductively coupled plasma mass spectrometry ICP-MS Bruker Aurora M90.

## Results and discussion

### *Characterization of the functionalized material support*

In order to ascertain if the solid support used, magnesium silicate, was successfully functionalized with sodium- $\beta$ -glycerophosphate, the obtained adsorbent material was characterized by energy dispersive X-ray analysis (EDX) and scanning electron microscopy (SEM). Figure 1 and Figure 2 show the morphology and the EDX spectrum of the functionalized material, respectively.

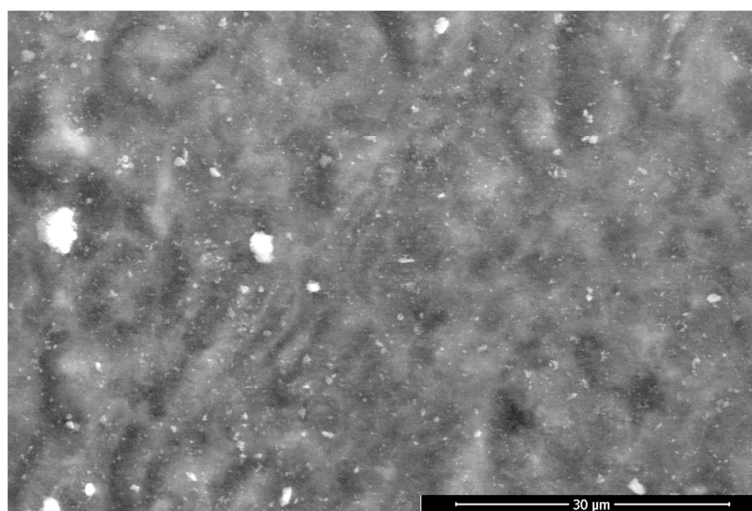


**Figure 1.** SEM image of the obtained material

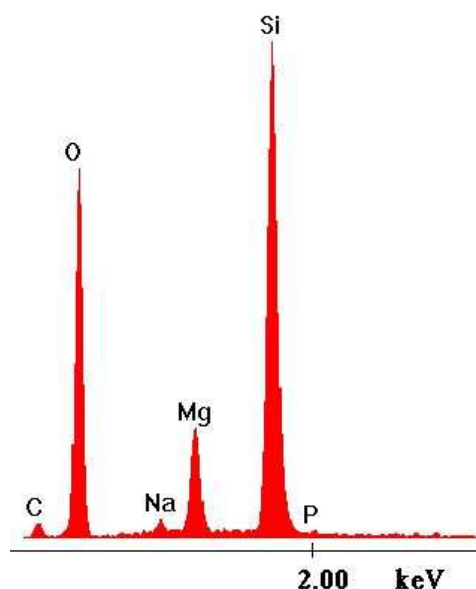


**Figure 2.** EDX spectrum of the obtained material

On the surface of the solid support with spots are to be observed. These are associated to the extractant used for improving the adsorbent properties of the material. Peaks of specific elements of the extractant, like Na, P, C are also visible on the EDX spectrum.

### Influence of the initial metal concentration and contact time

The experimental data regarding the influence of the initial metal concentration and the contact time on the adsorption capacity of the functionalized material were collected and described in Figure 3 and 4, respectively.

The adsorption capacity was calculated from the experimental data using the following equation:

$$q = \frac{(C_0 - C_t)V}{m} \quad (1)$$

where  $C_0$  is the initial metal concentration (mg/L),  $C_t$  the equilibrium concentration of the filtrate at time  $t$  (mg/L),  $V$  is the volume of metal solution (L),  $m$  is the amount of solid support (g).

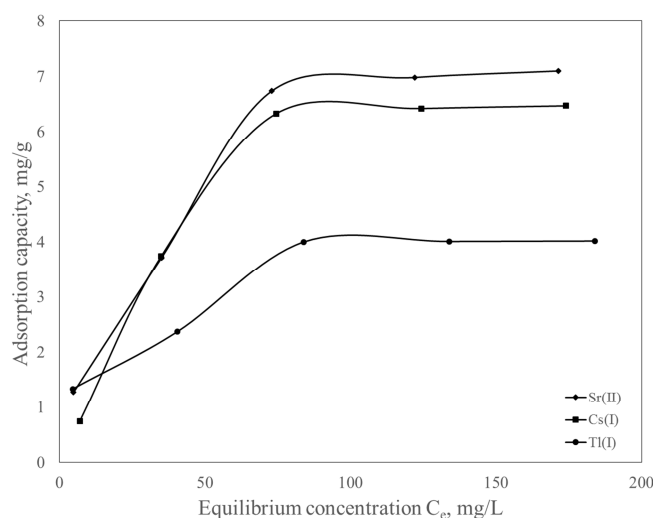


**Figure 3.** Adsorption isotherm of the studied metal ions on the functionalized material

It can be observed from Figure 3 that by increasing the initial concentration the adsorption capacity increases until reaching a constant value. The highest adsorption capacity obtained was for Sr(II) 7 mg/g, then Cs(I) 6.4 mg/g and the lowest for Tl(I) 4 mg/g.

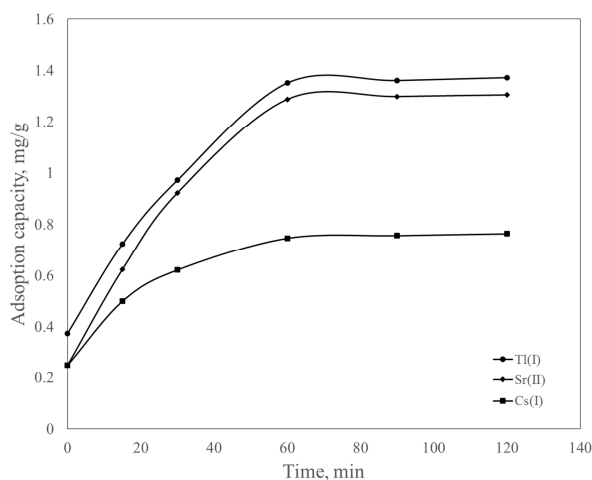


**Figure 4.** Influence of the contact time on the functionalized material

The influence of the contact time was also investigated. It occurs that the adsorption capacity



increases with increase of the contact time of the solid support with the metal ion solution (Figure 4). The equilibrium adsorption capacity is reached after 60 minutes of contact, which means that the adsorption process of the studied metal ions (Sr(II), Cs(I), Tl(I)) for the obtained functionalized material happens relatively quickly.

### **Conclusion**

The metal ions Sr(II), Cs(I), Tl(I) were removed from aqueous solution using the adsorption method. A new adsorbent material was used namely magnesium silicate functionalized with sodium- $\beta$ -glycerophosphate. The SEM and EDX analysis reveal a successfully functionalization of the solid support. High adsorption capacities were obtained for Sr(II) 7 mg/g, then Cs(I) 6.4 mg/g and lower for Tl(I) 4 mg/g. Studying the influence of the contact time between the adsorbent material and the metal ion solution results that the adsorption process of the studied metal ions runs quit quickly, reaching the equilibrium adsorption capacity in 60 minutes.

### **References**

- [1] A. Zhang, W. Wang, Z. Chai, E. Kuraoka, *Eur. Polym. J.* 22 (2008) 3899.
- [2] J.N. Sharma, A. Kumar, V. Kumar, S. Pahan, C. Janardanan, V. Tessi, P.K. Wattal, *Sep. Purif. Technol.* 135 (2014) 176.
- [3] P.K. Mohapatra, D.S. Lakshmi, A. Bhattacharyya, V.K. Manchanda, *J. Hazard. Mater.* 169 (2009) 472
- [4] M.F. Attallah, E.H. Borai, M.A. Hilal, F.A. Shehata, M.M. Abo-Aly, *J. Hazard. Mater.* 195 (2011) 73
- [5] S. Wan, M. Ma, L. Lv, L. Qian, S. Xu, Y. Xue, Z. Ma, *Chem. Eng. J.* 239 (2014) 200.
- [6] T. Sangvanich, V. Sukwarotwat, R.J. Wiacek, R.M. Grudzien, G.E. Fryxell, R.S. Addleman, C. Timchalk, W. Yantasee, *J. Hazard. Mater.* 182 (2010) 225.

## Synthesis and Characterization of some Potential Biologically Active Niclosamide Derivatives

Ioana M.C. Ienaşcu<sup>1,2</sup>, Adina Căta<sup>1\*</sup>, Mariana N. Ştefănuţ<sup>1</sup>, Cristian Tănasie<sup>1</sup>,  
Iuliana M. Popescu<sup>3</sup>

<sup>1</sup> National Institute of Research and Development for Electrochemistry and Condensed Matter, 144 Dr. A. P. Podeanu, 300569, Timișoara, Romania

<sup>2</sup> "Vasile Goldiș" Western University of Arad, Faculty of Medicine, Pharmacy and Dentistry, 86 Liviu Rebreanu, 310045, Arad, Romania

<sup>3</sup> Banat's Agricultural Science University, Faculty of Agriculture, Department of Chemistry and Biochemistry, 119 Calea Aradului, 300645, Timisoara, Romania  
adina.cata@yahoo.com

### Abstract

Compounds with 2-hydroxy-benzanilide core are recognized for their biological effects. Niclosamide, in particular, is authorized for its anti-helminthic properties and, recently, demonstrated additional effects like antitumoral and antiviral ones. Thus, we considered worthwhile to synthesize some niclosamide derivatives, which could possess enhanced biological activity. Starting from 5-chloro-N-(2-chloro-4-nitrophenyl)-2-hydroxybenzamide and methyl/ethyl  $\alpha$ -halogenated acid esters were obtained methyl/ethyl esters. In order to prove the structural identity of the newly synthesized compounds, modern physico-chemical methods (FTIR, <sup>1</sup>H-NMR, <sup>13</sup>C-NMR) were used. The data obtained for the analyzed compounds proved their identity and confirm their structure.

### Introduction

Worldwide, the drug and pharmaceutical products industry is trying to obtain some products, with high biological activity, a broad spectrum of action, minimal toxicity and side effects. Thus, finding new biologically active compounds has been a challenge for researchers, since the incidence of disease and the action spectrum of pathogens was constantly increasing. Salicylanilides and their derivatives proved antifungal, antibacterial, antimycobacterial, analgesic and antiinflammatory effects being used in various pharmaceutical and biochemical fields [1-4].

Niclosamide (5-chloro-N-(2-chloro-4-nitrophenyl)-2-hydroxybenzamide) belongs to the salicylanilides family and appeared on the market in 1960 under the trade name *Bayluscide* (Bayer 73) for treating infections caused by gastrointestinal tapeworm, both in humans and animals [5]. Niclosamide is now an anti-helminthic compound used in human therapy which is approved by FDA [6]. It has an acute oral toxicity in rats (LD<sub>50</sub>) larger than 5 g/kg body weight and a marginal decrease in haemoglobin concentration and erythrocyte count occurred when rats were given niclosamide at 5 g/kg/day for four weeks [7]. Recently, Niclosamide received renewed attention due to its antiviral effects against severe acute respiratory syndrome virus [8] and human rhinovirus [9], anti-neoplastic activity [10] and anti-anthrax toxin effects [11].

Thus, attempting to combine these properties for a better biological activity and fewer side effects, some new Niclosamide derivatives were obtained and characterized.

### Experimental

*Reagents and solvents:* ethyl chloroacetate, methyl chloroacetate, methyl 2-chloro-propionate, 5-chloro-N-(2-chloro-4-nitrophenyl)-2-hydroxybenzamide (Sigma-Aldrich, for synthesis);

absolute ethanol, 2-butanone (Merck, analytical purity); sodium carbonate, magnesium sulfate (Sigma-Aldrich).

**Apparatus:** Melting points are uncorrected and measured Stuart Melting point Apparatus SMP 30. IR spectra ( $\nu_{\max}$  in  $\text{cm}^{-1}$ ) were recorded as KBr pellet, on a Jaskow FTIR-430 instrument. The  $^1\text{H}$ ,  $^{13}\text{C}$ -NMR spectra were recorded in  $\text{DMSO}-d_6$  and  $\text{CDCl}_3$  on a Bruker Avance DRX 400 spectrometer, operating at 400 MHz. Chemical shifts ( $\delta$  values) are expressed in ppm against tetramethylsilane (TMS) as internal standard and coupling constants ( $J$ ) are reported in Hz.

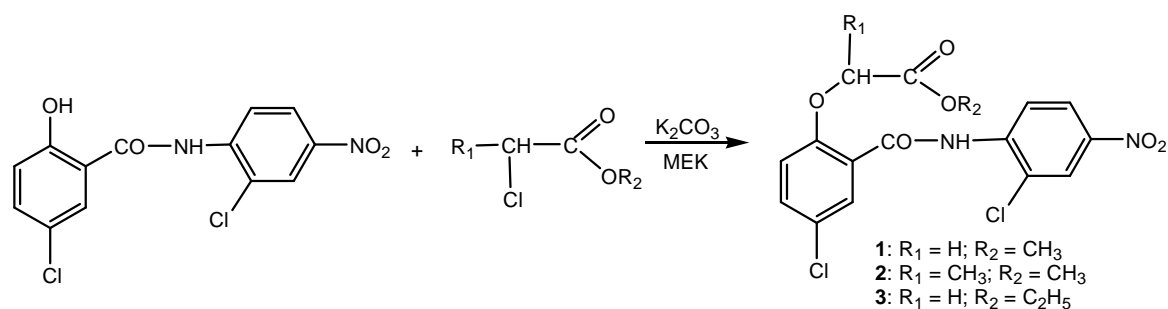
**Synthesis of methyl/ethyl esters of 5-chloro-N-(2-chloro-4-nitrophenyl)-2-hydroxybenzamide** [12]. A mixture of 5-chloro-N-(2-chloro-4-nitrophenyl)-2-hydroxybenzamide and anhydrous  $\text{K}_2\text{CO}_3$  was refluxed in 2-butanone. Ethyl/methylchloro-acetate/propionate was added dropwise. Optimum molar ratio was amide:ester: $\text{K}_2\text{CO}_3 = 1:1:1$ . The mixture was stirred and heated on a steam bath for 5 h. After cooling at room temperature, the mixture was poured into water and shook intensively. The organic phase was dried over  $\text{MgSO}_4$ . After filtration and evaporation of solvent in vacuum, the esters crystallized and were recrystallized from ethanol.

## Results and discussion

The synthesized compounds, 5-chloro-N-(2-chloro-4-nitrophenyl)-2-hydroxybenzamide derivatives, are presented in Table 1. Molecular formula / weight, melting points and yields are also presented in Table 1. The synthesized compounds (**1-3**) are white-yellow or brick-red, crystalline substances. The synthetic route for preparation of the synthesized compounds is outlined in Scheme 1. The final purification was achieved by recrystallization from absolute ethanol. The target compounds were obtained in yields between 63-75%.

**Table 1.** Titled compounds characteristics

No.	Compound name	Molecular formula / weight	M.p. ( $^{\circ}\text{C}$ )	Yield (%)
1	[4-Chloro-2-(2-chloro-4-nitrophenylcarbamoyl)-phenoxy]-acetic acid methyl ester	$\text{C}_{16}\text{H}_{12}\text{Cl}_2\text{N}_2\text{O}_6$ 399.18	187-188	65
2	2-[4-Chloro-2-(2-chloro-4-nitrophenylcarbamoyl)-phenoxy]-propionic acid methyl ester	$\text{C}_{17}\text{H}_{14}\text{Cl}_2\text{N}_2\text{O}_6$ 413.21	284-288	63
3	[4-Chloro-2-(2-chloro-4-nitrophenylcarbamoyl)-phenoxy]-acetic acid ethyl ester	$\text{C}_{17}\text{H}_{14}\text{Cl}_2\text{N}_2\text{O}_6$ 413.21	293-296	75



**Scheme 1.** The synthesis of 5-chloro-N-(2-chloro-4-nitrophenyl)-2-hydroxybenzamide derivatives

The structures of the synthesized compounds were elucidated by IR,  $^1\text{H}$ -NMR and  $^{13}\text{C}$ -NMR analysis. In order to facilitate the NMR spectra interpretation, the numbering of the aromatic rings is presented in Figure 1.

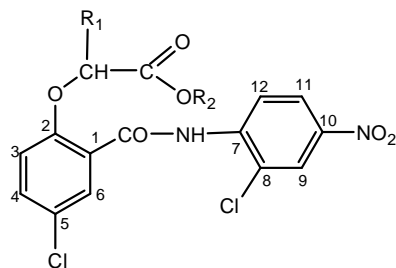


**Figure 1.** Numbering of aromatic rings

The spectral data of the synthesized compounds are listed below.

**[(4-chloro-2-(2-chloro-4-nitro-phenylcarbamoyl)-phenoxy]-acetic acid methyl ester (1)**

IR  $\nu(\text{cm}^{-1})$  KBr pellet: 3317; 3087; 2958; 1735; 1685; 1583; 1548; 1502; 1481; 1400; 1340; 1274; 1205; 1116; 1047; 989; 804; 742;

$^1\text{H}$ -NMR [ $\delta(\text{ppm})$ ]: 3.73 (s, 3H,  $\text{COOCH}_3$ ); 5.22 (s, 2H,  $\text{OCH}_2\text{CO}$ ); 7.34 (d, 1H,  $\text{H}_3$ ,  $J=8.0$ ); 7.65 (dsc, 1H,  $\text{H}_4$ ,  $J=8.0$ ); 7.98 (ssc, 1H,  $\text{H}_6$ ); 8.28 (dsc, 1H,  $\text{H}_{12}$ ,  $J=8.0$ ); 8.39 (ssc, 1H,  $\text{H}_9$ ); 8.64 (d, 1H,  $\text{H}_{11}$ ,  $J=8.0$ ); 10.60 (s, 1H,  $\text{CONH}$ );

$^{13}\text{C}$ -NMR [ $\delta(\text{ppm})$ ]: 51.78 ( $\text{COOCH}_3$ ); 66.06 ( $\text{OCH}_2\text{CO}$ ); 115.96 ( $\text{C}_3$ ); 121.78 ( $\text{C}_1$ ); 122.86 ( $\text{C}_{11}$ ); 123.15 ( $\text{C}_{12}$ ); 123.43 ( $\text{C}_9$ ); 124.36 ( $\text{C}_5$ ); 126.01 ( $\text{C}_8$ ); 130.34 ( $\text{C}_6$ ); 133.21 ( $\text{C}_4$ ); 140.41 ( $\text{C}_7$ ); 143.02 ( $\text{C}_{10}$ ); 154.27 ( $\text{C}_2$ ); 161.70 ( $\text{CONH}$ ); 168.94 ( $\text{COOCH}_3$ );

**2-[4-chloro-2-(2-chloro-4-nitro-phenylcarbamoyl)-phenoxy]-propionic acid methyl ester (2)**

IR  $\nu(\text{cm}^{-1})$  KBr pellet: 3292; 3103; 1745; 1679; 1581; 1544; 1475; 1436; 1402; 1336; 1257; 1193; 1157; 1056; 891; 703;

$^1\text{H}$ -NMR [ $\delta(\text{ppm})$ ]: 1.68 (d, 3H,  $\text{OCH}(\text{CH}_3)\text{COO}$ ); 3.48 (q, 1H,  $\text{OCH}(\text{CH}_3)\text{COO}$ ); 3.69 (s, 3H,  $\text{COOCH}_3$ ); 6.93 (d, 1H,  $\text{H}_3$ ,  $J=8.0$ ); 7.26 (dsc, 1H,  $\text{H}_4$ ,  $J=8.0$ ); 7.86 (ssc, 1H,  $\text{H}_6$ ); 8.17 (dsc, 1H,  $\text{H}_{12}$ ,  $J=8.0$ ); 8.27 (ssc, 1H,  $\text{H}_9$ ); 8.88 (d, 1H,  $\text{H}_{11}$ ,  $J=8.0$ ); 10.26 (s, 1H,  $\text{CONH}$ );

$^{13}\text{C}$ -NMR [ $\delta(\text{ppm})$ ]: 18.12 ( $\text{OCH}(\text{CH}_3)\text{COO}$ ); 55.78 ( $\text{COOCH}_3$ ); 82.20 ( $\text{OCH}(\text{CH}_3)\text{COO}$ ); 114.22 ( $\text{C}_3$ ); 119.09 ( $\text{C}_1$ ); 120.35 ( $\text{C}_{11}$ ); 120.48 ( $\text{C}_{12}$ ); 122.13 ( $\text{C}_9$ ); 123.01 ( $\text{C}_5$ ); 124.23 ( $\text{C}_8$ ); 128.97 ( $\text{C}_6$ ); 132.71 ( $\text{C}_4$ ); 141.26 ( $\text{C}_7$ ); 143.21 ( $\text{C}_{10}$ ); 155.16 ( $\text{C}_2$ ); 161.66 ( $\text{CONH}$ ); 164.60 ( $\text{COOCH}_3$ );

**[4-chloro-2-(2-chloro-4-nitro-phenylcarbamoyl)-phenoxy]-acetic acid ethyl ester (3)**

IR  $\nu(\text{cm}^{-1})$  KBr pellet: 3105; 2904; 1749; 1641; 1600; 1541; 1500; 1473; 1407; 1319; 1242; 1178; 1118; 1045; 889; 825;

$^1\text{H}$ -NMR [ $\delta(\text{ppm})$ ]: 1.19 (t, 3H,  $\text{COOCH}_2\text{CH}_3$ ,  $J=8.0$ ); 4.19 (q, 2H,  $\text{COOCH}_2\text{CH}_3$ ,  $J=8.0$ ); 5.18 (s, 2H,  $\text{OCH}_2\text{COO}$ ); 6.91 (d, 1H,  $\text{H}_3$ ,  $J=8.0$ ); 7.27 (dsc, 1H,  $\text{H}_4$ ,  $J=8.0$ ); 7.87 (ssc, 1H,  $\text{H}_6$ ); 8.18 (dsc, 1H,  $\text{H}_{12}$ ,  $J=8.0$ ); 8.29 (ssc, 1H,  $\text{H}_9$ ); 8.88 (d, 1H,  $\text{H}_{11}$ ,  $J=8.0$ ); 10.60 (s, 1H,  $\text{CONH}$ );

$^{13}\text{C}$ -NMR [ $\delta(\text{ppm})$ ]: 13.87 ( $\text{COOCH}_2\text{CH}_3$ ); 60.83 ( $\text{COOCH}_2\text{CH}_3$ ); 65.27 ( $\text{OCH}_2\text{COO}$ ); 114.23 ( $\text{C}_3$ ); 119.06 ( $\text{C}_1$ ); 119.11 ( $\text{C}_{11}$ ); 120.40 ( $\text{C}_{12}$ ); 122.18 ( $\text{C}_9$ ); 123.00 ( $\text{C}_5$ ); 124.22 ( $\text{C}_8$ ); 128.91 ( $\text{C}_6$ ); 132.67 ( $\text{C}_4$ ); 141.21 ( $\text{C}_7$ ); 143.36 ( $\text{C}_{10}$ ); 155.14 ( $\text{C}_2$ ); 161.51 ( $\text{CONH}$ ); 164.65 ( $\text{COOCH}_2\text{CH}_3$ );

The IR spectral data of the esters show the existence of an ether bond between the phenolic hydroxyl group and the alkyl  $\alpha\text{-C}$  atom of the ester by signals in the range 1200–1260 and 1040–1060  $\text{cm}^{-1}$ . The carbonyl groups from the esters appear in the range 1730–1750  $\text{cm}^{-1}$ . The vibrations of the amide and hydrazide group appear as signals between 3100–3400 and 1640–1690  $\text{cm}^{-1}$ , respectively.

The <sup>1</sup>H-NMR shifts of the methyl protons from the methyl ester were observed in the spectra as singlet between 3.6 and 3.8, whereas the ethyl group from the ethyl ester appears in the range 1.1-4.2 ppm. The proton of the amide group, in all analyzed compounds, was observed as singlet between 10.2 and 10.6 ppm.

The <sup>13</sup>C-NMR signals corresponding to the carbons from the amide group appear in the range 161–162 ppm and those of the aromatic carbons between 114 and 156 ppm.

### Conclusion

Three new compounds, 5-chloro-N-(2-chloro-4-nitrophenyl)-2-hydroxybenzamide derivatives, were synthesized in order to expand the collection of potential biologically active compounds.

The target compounds belonging to esters group were obtained with good yields (>65%) and characterized using modern analytical methods.

All spectral data proved the identity and provided the elemental composition of the analyzed compounds.

### References

- [1]. J. Vinsova, Imramovsky, Ces. Slov. Farm. 53 (2004) 294.
- [2]. I. Ienaşcu, A.X. Lupea, D. Hădărugă, N. Hădărugă, I. Popescu, Rev. Chim. 59(2008) 247.
- [3]. K. Waissner, J. Hladuvkova, J. Kunes, L. Kubicova, V. Klimesova et al., J. Chem. Pap.-Chem. Zvesti 55 (2001) 121.
- [4]. H.H. Fahmy, W. El-Eraky, Arch. Pharm. Res. 24 (2001) 171.
- [5]. S. Sharma, N. Anand, Approaches to design and synthesis of antiparasitic drugs. Pharmacochimistry library v 25, Elsevier, Amsterdam, New York, 1997, pp. 511.
- [6]. J. Ditzel, M. Schwartz, Acta Medica Scandinavica 182 (1967) 663.
- [7]. WHO (1988) Data sheet on pesticides No 63: niclosamide.: Food and Agriculture Organisation: International Programme on Chemical Safety, Inchem. pp. WHO/VBC/DS/88.63.
- [8]. C.J. Wu, J.T. Jan, C.M. Chen, H.P. Hsieh, D.R. Hwang et al. Antimicrob. Agents Chemother., 48 (2004) 2693.
- [9]. A. Jurgeit, R. McDowell, S. Moese, E. Meldrum, R. Schwendener et al., PLoS Pathog. 8 (2012) e1002976.
- [10]. T. Osada, M. Chen, X.Y. Yang, I. Spasojevic, J.B. Vandeusen et al., Cancer Res. 71 (2011) 4172.
- [11]. P.J. Zhu, J.P. Hobson, N. Southall, C. Qiu, C.J. Thomas et al. Bioorg. Med. Chem. 17 (2009) 5139.
- [12]. I.M.C. Ienaşcu, A.X. Lupea, I.M. Popescu, M.A. Pădure, A.D. Zamfir, J. Serb. Chem. Soc., 74 (2009) 847.

## Adsorption Study of Phenol and some Phenol Derivatives on Fe<sub>3</sub>O<sub>4</sub>/C Nanocomposites

Roxana Istrate<sup>1\*</sup>, Cornelia Păcurariu, Robert Ianoş

<sup>1</sup>Politehnica University Timișoara, Faculty of Industrial Chemistry and Environmental Engineering, 6 Pîrvan Blv., RO-300223, Timișoara, Romania  
e-mail: roxana.istrate@upt.ro

### Abstract

Magnetite/carbon nanocomposites, prepared by a simple combustion synthesis technique, were tested for the removal of phenol and of some phenol derivatives: p-chlorophenol (p-CP), 3-aminophenol (3-AP), p-nitrophenol (p-NP), 2,6-dimethylphenol (DMP) and 2,4,6-trimethylphenol (TMP) from aqueous solutions. The effect of different parameters, including the magnetite/carbon ratio, initial concentration of pollutant and the contact time on the removal efficiency was investigated. The adsorption kinetics was described by the pseudo-second-order model and the equilibrium data were well fitted with the Langmuir isotherm in case of phenol, the Sips isotherm in case of 3-aminophenol and the Redlich-Peterson isotherm in case of p-nitrophenol. The good adsorption capacity and easy separation using a magnet, recommend the magnetite/carbon nanocomposites as promising candidates for the removal of phenol and its derivatives from polluted water.

**Keywords:** iron oxides, nanocomposites, adsorption, phenol

### Introduction

Water contamination with aromatic compounds is a usual problem of our days. Among the aromatic compounds which are in wastewater from different industries like: petroleum, paper, paint, resins, pharmaceuticals, phenols and their derivatives are an important category. They were classified like priority pollutants by US Environmental Protection Agency (EPA) and UE because of their toxicity, causing specific taste and odor in drinking water with possible negative effects for biological processes [1]. Repeated exposure to phenols and to their derivatives could cause negative effects to nervous system, digestive system, eyes, heart, lungs, liver, kidney, skin and can cause genetic damages [2].

Throughout time there were developed many techniques for the removal of phenols from wastewater such as: oxidation [3], membrane filtration [4], electrochemical oxidation [5], photocatalytic degradation [6], adsorption [7, 8], ion exchange [9], solvent extraction [10] etc. Among this methods, adsorption is considered by many authors to be a superior technique because of its efficiency, low implementation cost, large availability and simplicity of design [11-16]. However, usual adsorbents have some limitations because of their difficult separation from the solution [17, 18]. Due to these reasons, magnetic nanoparticles have drawn the researchers' attention because of their high adsorption capacity and their effectiveness regarding the separation [19-25].

The aim of this work was to investigate the efficiency of some magnetite/carbon nanocomposites as adsorbents for the removal of phenol and some phenol derivatives: p-chlorophenol (p-CP), 3-aminophenol (3-AP), p-nitrophenol (p-NP), 2,6-dimethylphenol (DMP) and 2,4,6-trimethylphenol (TMP) from aqueous solutions. The effect of different parameters, including the magnetite/carbon ratio, initial concentration of pollutant and the contact time on the removal efficiency was investigated. The kinetics and adsorption isotherm were also evaluated.



## Experimental

### 2.1. Powder preparation

The magnetite/carbon nanocomposites were prepared by the combustion synthesis method as described in our earlier work [26]. The solution resulted from the dissolution of necessary amount of  $\text{Fe}(\text{NO}_3)_3 \cdot 9\text{H}_2\text{O}$  and tartaric acid ( $\text{C}_4\text{H}_6\text{O}_6$ ) in distilled water was mixed with different quantities of carbon in a bottom flask. The flask was placed inside a heating mantle at 400 °C. As the temperature increased, a smoldering combustion reaction occurred between iron nitrate and tartaric acid. The gases evolving from the combustion process were bubbled in a beaker filled with distilled water, to prevent air getting inside the flask.

After 30 minutes a black powder was obtained. The product was washed with distilled water and dried at 70°C for 5 h.

### 2.2. Characterization methods

The nanocomposites characterization by means of phase composition (XRD), FTIR spectroscopy, thermal analysis (TG/DTA), magnetic properties and morphology was reported in our previous work [26].

### 2.3. Adsorption experiments

The experiments of adsorption of phenol, p-chlorophenol (p-CP), 3-aminophenol (3-AP), p-nitrophenol (p-NP), 2,6-dimethylphenol (DMP) and 2,4,6-trimethylphenol (TMP) from aqueous solutions were performed at 25°C, in a thermostated shaker with a shaking speed of 200 rpm, using 1 g L<sup>-1</sup> adsorbent and different initial concentration of pollutants (50 – 300 mgL<sup>-1</sup>). The adsorbent was separated from the aqueous solution using a magnet. The pollutants concentration was measured using a UV – Vis spectrophotometer model UVmini – 1240 SHIMADZU. The absorbance values were measured at 270 nm for phenol, 280 nm for p-CP and 3-AP, 317 nm for p-NP, 217 nm for DMP and 218 nm for TMP.

The amount of pollutant adsorbed,  $q_t$  (mg g<sup>-1</sup>), was calculated according to Eq. (1):

$$q_t = \frac{(C_0 - C_t) \cdot V}{W} \quad (1)$$

where  $C_0$  and  $C_t$  are the concentration of pollutants, initially and, respectively, at any time,  $t$ ,  $V$  is the volume of solution (L) and  $W$  is the mass of adsorbent (g).

The removal efficiency  $R$  (%) was calculated by Eq (2):

$$R = \frac{C_0 - C_e}{C_0} \cdot 100 \quad (2)$$

where  $C_0$  and  $C_e$  (mg L<sup>-1</sup>) are the initial and the equilibrium concentration of pollutants.

## Results and discussion

### 3.1. Characterization of the samples

Some characteristics of the samples are presented in Table 1.

**Table 1.** Characteristics of the prepared samples

Sample symbol	Fe <sub>3</sub> O <sub>4</sub> /carbon mass ratio	Specific surface area S <sub>BET</sub> (m <sup>2</sup> g <sup>-1</sup> )	Micropore area (m <sup>2</sup> g <sup>-1</sup> )	Micropore volume (cm <sup>3</sup> g <sup>-1</sup> )	Particle diameter D <sub>BET</sub> (nm)	Phase composition XRD
M1-C3	1/3	622.4	390.9	0.178	1.85	Fe <sub>3</sub> O <sub>4</sub>
M1-C10	1/10	813.5	505.6	0.234	1.42	Fe <sub>3</sub> O <sub>4</sub>

### 3.2. Adsorption studies

#### Effect of pollutant nature

The studies were effectuated in the following conditions: mass of adsorbent 1 g L<sup>-1</sup>, initial concentration of the pollutant C<sub>0</sub>, 100 mg L<sup>-1</sup>, temperature 25°C, contact time 6 h, shaking speed 200 rpm. The influence of pollutant nature on the adsorption capacity of the adsorbents is presented in Table 2.

**Table 2.** Effect of pollutant nature on the adsorption capacity of adsorbents

Adsorbent	Adsorbed	Solubility at 25°C [g L <sup>-1</sup> ]	pK <sub>a</sub>	R[%]
M1-C3	Phenol	83	9.95	65.2
	p-CP	24	9.42	91.8
	3-AP	35	4.30	75.5
	p-NP	16	7.15	96.9
	DMP	10	10.59	90.3
	TMP	1.2	10.88	95.7
M1-C10	Phenol	83	9.95	73.9
	p-CP	24	9.42	95.0
	3-AP	35	4.30	89.1
	p-NP	16	7.15	98.2
	DMP	10	10.59	97.8
	TMP	1.2	10.88	98.4

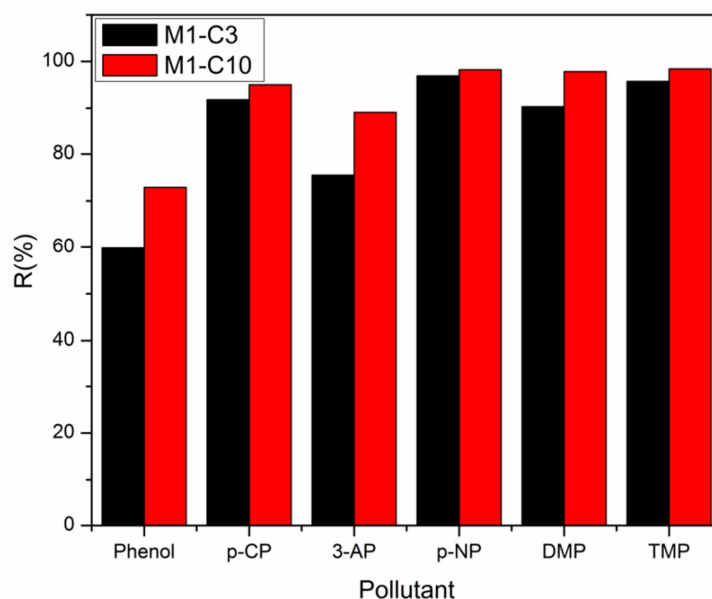
As can be observed, both adsorbents present higher removal efficiency in the case of phenol derivatives as compared to phenol. This behavior was correlated with the solubility and pK<sub>a</sub> values of pollutants, factors that have a significant influence on the adsorption process.

For practically equal pK<sub>a</sub> values, both adsorbents present higher removal efficiency for the less soluble pollutant (phenol compared with p-CP, respectively DMP compared with TMP). The solubility of p-CP is much lower as compared with phenol, while its removal efficiency is much higher. TMP is much less soluble as compared with DMP and its removal efficiency is higher. In case of pollutants with similar solubility, higher removal efficiency can be observed for the pollutant with the smaller pK<sub>a</sub> value.

#### Effect of magnetite/carbon ratio

The effect of magnetite/carbon ratio on the removal efficiency of pollutants is presented in

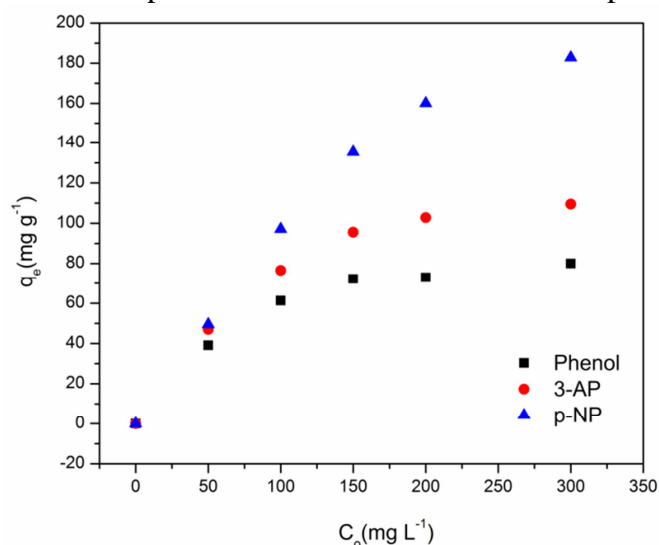
Figure 1.

**Figure 1.** The effect of magnetite/carbon ratio on the removal efficiency of pollutants.

From Table 2 and Fig. 1 it can be observed that the adsorbent M1-C10, with higher carbon content (1/10) presents higher removal efficiency of phenol, respectively of phenol derivatives compared to M1-C3 adsorbent that has a lower content of carbon (1/3). This behavior is correlated with the specific surface area that is higher for M1-C10 adsorbent (813.5 m<sup>2</sup>g<sup>-1</sup>) compared to M1-C3 (622.4 m<sup>2</sup> g<sup>-1</sup>). The significantly increase of carbon content in case of M1-C10 adsorbent does not lead to a spectacular increase of the removal efficiency; therefore is not justified to use an adsorbent with high content of carbon due to higher costs and a lower magnetization which require the use of stronger magnets for phase separation. For these reasons, the following adsorption studies were performed using only M1-C3 as adsorbent and phenol, 3-AP and p-NP as pollutants.

#### *Effect of initial pollutant concentration*

Fig. 2 shows the effect of initial pollutant concentration on the adsorption process.

**Figure 2.** Effect of initial concentration on phenol, 3-AP and p-NP adsorption using M1-C3 adsorbent

In case of phenol, the adsorbed amount at equilibrium continuously increases for initial

concentration between 0-150 mg L<sup>-1</sup> and after that, it remains constant; this behavior can be explained by the saturation of the adsorbent surface with phenol.

In case of p-nitrophenol, it can be observed that the adsorbed amount at equilibrium increases over the entire concentrations range, confirming that the adsorbent M1-C3 shows the highest adsorption capacity for p-nitrophenol, in accordance with the previous results (Fig.1).

#### Effect of contact time

Figure 3 shows the effect of contact time on phenol, p-nitrophenol and 3-aminophenol adsorption onto M1-C3 adsorbent. It can be observed the fast increase of the amount of adsorbed pollutants in the first 20 minutes which can be attributed to the large number of vacant surface sites available at the initial stage of adsorption; then, the adsorption process becomes slower, as the system approaches equilibrium. It can be noticed that the equilibrium was reached faster in case of p-NP (about 30 min.) as compared with 3-AP and phenol (about 240 min).

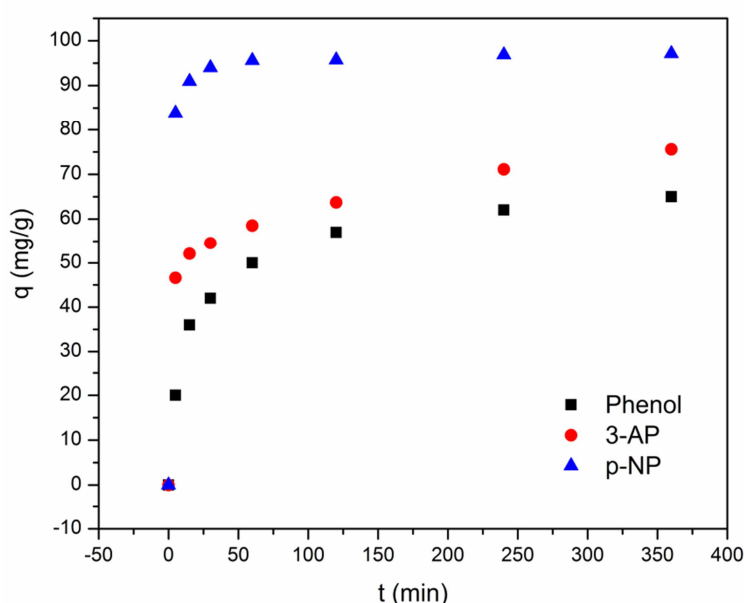


**Figure 3.** Effect of contact time on phenol, 3-AP and p-NP adsorption using M1-C3 adsorbent

#### Adsorption kinetics

The adsorption kinetics of the 3 pollutants onto M1-C3 adsorbent was investigated by fitting the experimental data with the linear form of the pseudo-second-order (Eq. 3).

$$\frac{t}{q_t} = \frac{1}{k_2 q_e^2} + \frac{t}{q_e} \quad (3)$$

where  $k_2$  is the pseudo-second-order rate constant (g mg<sup>-1</sup> min<sup>-1</sup>);  $q_e$  and  $q_t$  are the amount of pollutant adsorbed at equilibrium and at time  $t$  per unit mass of adsorbent, respectively (mg g<sup>-1</sup>).

The results are shown in Fig. 4 and Table 3.

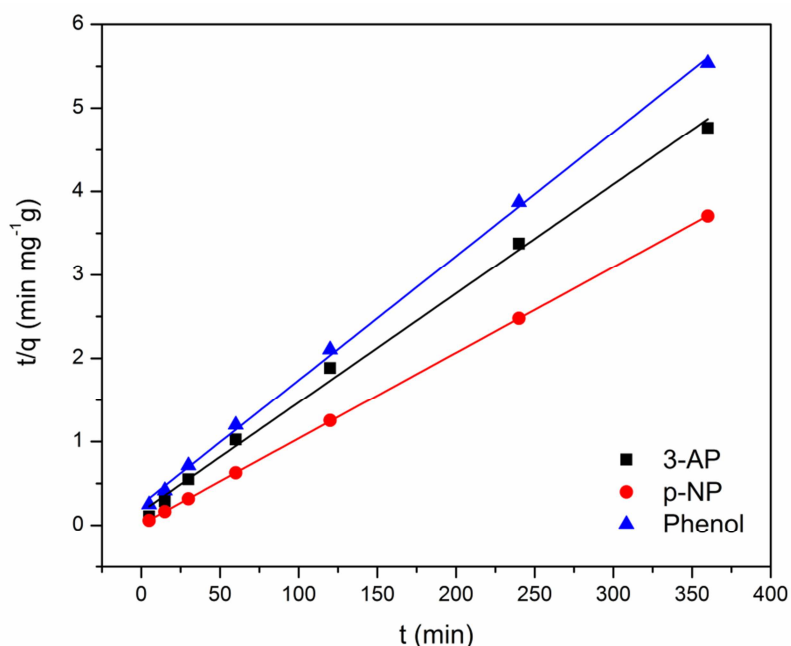


**Figure 4.** Plots of  $t/q=f(t)$  dependencies for the adsorption of phenol, 3-AP and p-NP onto M1-C3 adsorbent

**Table 3.** Kinetics parameters and correlation coefficients for the pseudo-second-order model

Pollutant	Initial concentration $C_0$ (mg L <sup>-1</sup> )	$k_2 \cdot 10^3$ (g mg <sup>-1</sup> min <sup>-1</sup> )	$q_e$ (mg g <sup>-1</sup> )		$R^2$
			Experimental	Calculated	
Phenol	100	0.88	65.2	67.3	0.99878
3-AP	100	1.05	75.6	76.4	0.99575
p-NP	100	8.79	97.1	97.4	0.99999

The correlation coefficients close to unity and experimental values for  $q_e$  very close to the calculated ones indicate that the adsorption kinetics of the 3 pollutants onto M1-C3 adsorbent is described by the pseudo-second-order model.

It can be noticed that, the rate constant in case of p-NP adsorption is about 10 times higher than that of phenol adsorption and about 8 times higher than that of 3-AP adsorption. These results are in full agreement with the shorter time to reach equilibrium in case of p-NP as compared with phenol and 3-AP.

#### Adsorption isotherms

The experimental equilibrium data for the adsorption of the 3 pollutants onto M1-C3 adsorbent were fitted to the Langmuir, Freundlich, Redlich-Peterson and Sips isotherms by plotting  $q_e$  versus  $C_e$  (Figs. 5-7).

The isotherms parameters, calculated by non-linear regression analysis and the correlation coefficients are listed in Table 4.

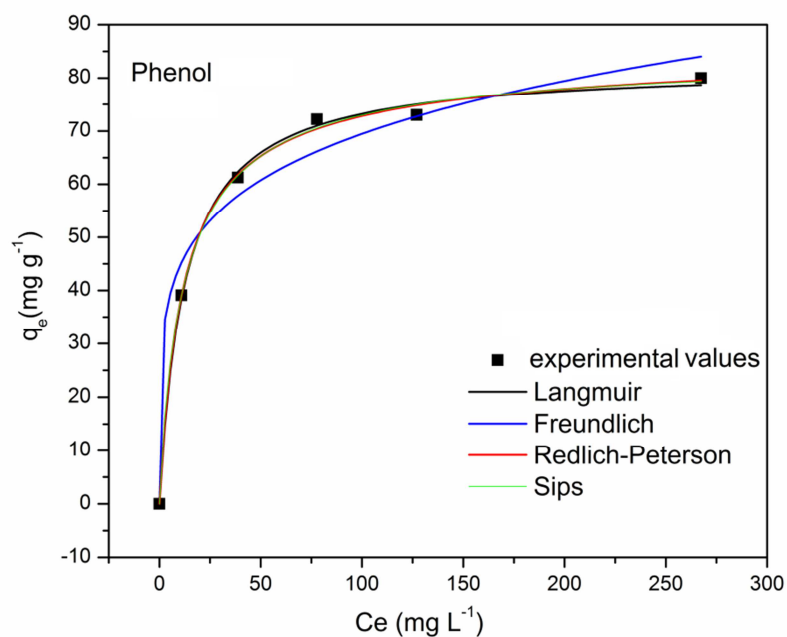


**Figure 5.** Isotherm plots for phenol adsorption onto M1-C3 sorbent.

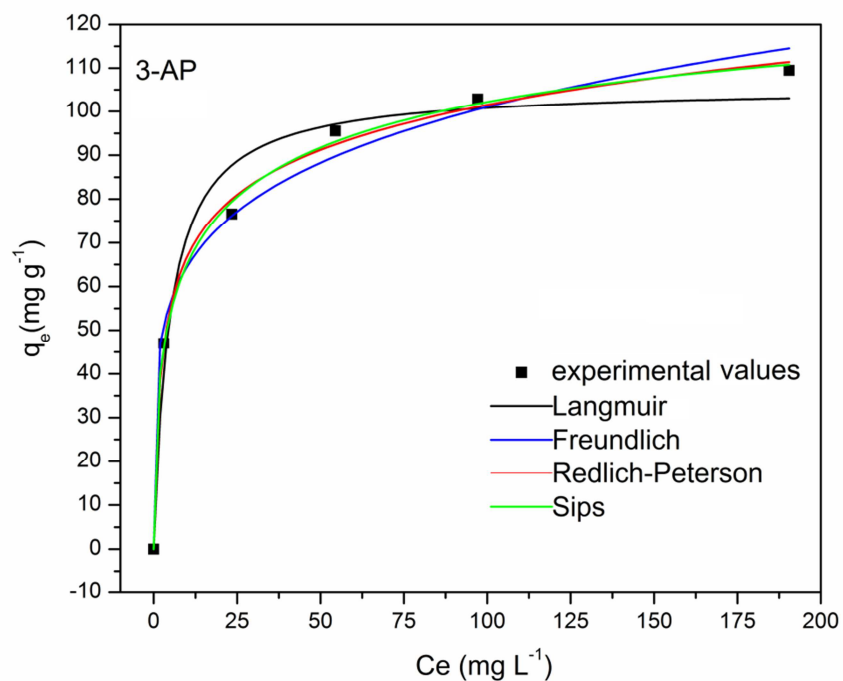


**Figure 6.** Isotherm plots for 3-AP adsorption onto M1-C3 sorbent



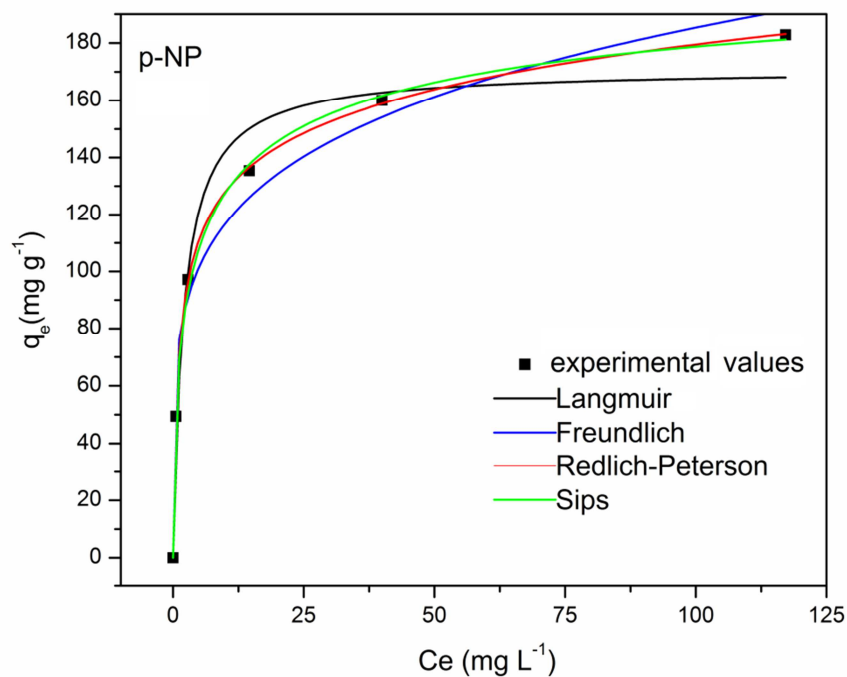


**Figure 7.** Isotherm plots for p-NP adsorption onto M1-C3 sorbent

**Table 4.** The isotherms parameters and correlation coefficients for the adsorption of phenol, 3-AP and p-NP onto M1-C3 adsorbent

		Phenol	3-AP	p-NP
Langmuir	$K_L$ (L mg <sup>-1</sup> )	0.08	0.21	0.49
	$q_m$ (mg g <sup>-1</sup> )	82.34	105.62	170.99
	$R^2$	<b>0.99762</b>	0.96998	0.96831
Freundlich	$K_F$ (((mg <sup>1-(1/n)</sup> L <sup>1/n</sup> )g <sup>-1</sup> ))	28.50	41.20	73.58
	$n$	5.17	5.13	4.98
	$R^2$	0.9718	0.98823	0.97478
Redlich-Peterson	$K_{RP}$ (L g <sup>-1</sup> )	7.32	53.13	183.06
	$\alpha_{RP}$ ((L mg <sup>-1</sup> ) <sup><math>\beta</math></sup> )	0.10	0.94	1.75
	$\beta$	0.97	0.87	0.88
	$R^2$	0.9975	0.99457	<b>0.99978</b>
Sips	$K_S$ (L mg <sup>-1</sup> )	0.10	0.28	0.43
	$q_{mS}$ (mg g <sup>-1</sup> )	84.53	146.75	215.99
	$n$	0.90	0.28	0.52
	$R^2$	0.99737	<b>0.99668</b>	0.99732

As shown in Fig. 5 and Table 4, in case of phenol, the best fit of the experimental data was obtained by the Langmuir isotherm ( $R^2 > 0.99762$ ). The maximum adsorption capacity of M1-C3 adsorbent in case of phenol is  $q_e = 82.34$  mg g<sup>-1</sup>. The adsorption of 3-aminophenol onto M1-C3 adsorbent is described by the Sips isotherm and the adsorption of p-nitrophenol is described by the Redlich-Peterson isotherm. Comparing the maximum adsorption capacity obtained with the Langmuir isotherm, respectively with the Sips isotherm for the 3 pollutants, there was confirmed the increase of the adsorption capacity of M1-C3 adsorbent in the order: phenol < 3-aminophenol < p-nitrophenol.

The values of “n” parameter from Freundlich isotherm, between 4.98 and 5.17, indicate that the adsorption of the 3 pollutants on M1-C3 adsorbent is favored. In the case of phenol adsorption on carbon, the literature data indicate “n” values between 2.793 and 6.821 [27].

## **Conclusion**

The adsorption studies have demonstrated the efficiency of using magnetite/carbon nanocomposites for the removal of phenol and its derivatives from aqueous solutions. It was demonstrated that both studied adsorbents, M1-C3 and M1C10, with different carbon content, show a higher adsorption capacity for pollutants less soluble and with lower pK<sub>a</sub> value.

The increase of carbon content from 1:3 for M1-C3 to 1:10 in case of M1-C10 adsorbent has led to a moderate increase of removal efficiency for both, phenol and its derivatives. This behavior can be explained by the increase of the specific surface area of M1-C10 adsorbent.

The increase of the initial concentration of pollutant determines the increase of adsorbed quantity at equilibrium; the least in case of phenol and the most in case of p-nitrophenol.

The adsorption process is very fast; the contact time to reach equilibrium is about 30 min for p-nitrophenol and approximately 240 min for phenol and 3-aminophenol, in the case of M1-C3 adsorbent.

The kinetics of adsorption process of phenol, 3-aminophenol and p-nitrophenol onto M1-C3 adsorbent is described by the pseudo-second-order model. The rate of adsorption process increases in the order: phenol < 3-aminophenol < p-nitrophenol.

The adsorption process of phenol is described by the Langmuir isotherm, 3-aminophenol by Sips isotherm and p-nitrophenol by Redlich-Peterson isotherm. Comparing the maximum adsorption capacity of obtained with the Langmuir isotherm respectively with the Sips isotherm for the 3 pollutants, it was confirmed the increase of the adsorption capacity of M1-C3 adsorbent in the order: phenol < 3-aminophenol < p-nitrophenol.

In conclusion, the studied magnetite/carbon nanocomposites show both, high adsorption capacity due to the carbon content and easy phase separation using a magnet.

The unique combination between high adsorption capacity, excellent separation capacity and short time to reach equilibrium, that implies low operational costs for the industrial adsorption systems, indicate that the investigated magnetite/carbon nanocomposites are excellent adsorbent materials with great potential for wastewater treatment at industrial scale.

## **Acknowledgements**

This work was partially supported by the strategic grant POSDRU/159/1.5/S/137070 (2014) of the Ministry of National Education, Romania, co-financed by the European Social Fund – Investing in People, within the Sectoral Operational Programme Human Resources Development 2007-2013.

## References

- [1] G. Yanga, L. Tang, Y. Caia, J. Tanga, B. Y. Pangc, Y. Zhoua, Y. Liua, J. Wanga, S. Zhanga, W. Xionga, Chem. Eng. J. 259 (2015) 854 – 864.
- [2] J. Fu, Z. Chen, M. Wang, S. Liu, J. Zhang, R. Han, Q. Xu, Chem. Eng. J. 259 (2015) 53 – 61.
- [3] J. Wu, J. Rudy, J. Spark, Adv. Environ. Res. 4 (2000) 339 – 346.
- [4] D. P. Zagklis, A. I. Vavourakia, M. E. Kornarosa, C. A. Paraskeva, J. Hazard. Mater. 285 (2015) 69 – 76.
- [5] F. Duana, Y. Li, H. Cao, Y. Wanga, J. C. Crittendenc, Y. Zhang, Chemosphere 125 (2015) 205–211.
- [6] Z. F. Guo, R. X. Ma, G. J. Li, Chem. Eng. J. 119 (2006) 55 – 59.
- [7] V. V. Panic, Z. P. Madzarevic, T. Volkov-Husovic, S.J. Velickovic, Chem. Eng. J. 217 (2013) 192 – 204.
- [8] L. Damjanovic, V. Rakic, V. Rac, D.S.A. Auroux, J. Hazard. Mater. 184 (2010) 477 – 484.
- [9] K. Abburi, J. Hazard. Mater. 105 (2003) 143 – 156.
- [10] A. Gomes, L. Fernandes, R. Simoes, Chem. Eng. J. 189 – 190 (2012) 175 -181.
- [11] J. Han, Z. Du, W. Zou, H. Li, C. Zhang, Chem. Eng. J. 262 (2015) 571 – 578.
- [12] A. Turki, C. Guillardb, F. Dappozzeb, Z. Ksibia, G. Berhaultb, H. Kochkara, Appl. Catal. B-Environ. 163 (2015) 404 – 414.
- [13] Ihsanullah, H. A. Asmalya, T. A. Salehb, T. Laouie, V. K. Guptac, M.A. Atieh, J. Mol. Liq. 206 (2015) 176 – 182.
- [14] B. Tanhaei, A. Ayatia, M. Lahtinenb, M. Sillanpää, Chem. Eng. J. 259 (2015) 1 – 10.
- [15] L. Zeng, M. Xie, Q. Zhang, Y. Kang, X. Guo, H. Xiao, Y. Peng, J. Luo, Carbohydr. Polym. 123 (2015) 89 – 98.
- [16] K.L. Ai, Y.L. Liu, C.P. Ruan, L.H. Lu, G.Q. Lu, Adv. Mat. J. 25 (2013) 998 – 1003.
- [17] B. Noroozi, G.A. Sorial, H. Bahrami, M. Arami, J. Hazard. Mater. 139 (2007) 167 – 174.
- [18] Q. Q. Liu, L. Wang, A. G. Xiao, J.G. Gao, W. B. Ding, H.J. Yu, J. Huo, J. Hazard. Mater. 181 (2010) 586 – 592.
- [19] G. Z. Kyzas, K. A. Matisa, J. Mol. Liq. 203 (2015) 159 – 168.
- [20] S. Lia, Y. Gong, Y. Yanga, C. Hea, L. Hua, L. Zhua, L. Suna, D. Shu, Chem. Eng. J. 260 (2015) 231 – 239.
- [21] L.H. Reddy, J.L. Arias, J. Nicolas, P. Couvreur, Chem. Rev. 112 (2012) 5818 – 5878.
- [22] I. Ali, Chem. Rev. 112 (2012) 5073 – 5091.
- [23] S.C.N. Tang, I.M.C. Lo, Water Res. 47 (2013) 2613 – 2632.
- [24] A. H. Lu, E. I. Salabas, F. Schuth, Angew. Chem. Int. Edit. 46 (2007) 1222 – 1244.
- [25] R.D. Ambashta, M. Sillanpaa, J. Hazard. Mater. 180 (2010) 38 – 49.
- [26] R. Ianoş, C. Păcurariu, G. Mihoc, Ceram. Int. 40(8) (2014) 13649 – 13657.
- [27] O. Hamdaoui, E. Naffrechoux, J. Hazard. Mater. 147 (2007) 381–394.

## Electrochemical Oxygen Uptake/Release Process on Ca Doped Y-114 Electrodes in Aqueous Solutions

Victor-Daniel Craia Joldes<sup>\*</sup>, Mircea Laurentiu Dan<sup>\*</sup>, Nicolae Vaszilcsin<sup>\*</sup>, Andrea Kellenberger<sup>\*</sup>, Narcis Mihai Duteanu<sup>\*</sup>

<sup>\*</sup>University Politehnica Timișoara, Faculty of Industrial Chemistry and Environmental Engineering, 300223, Parvan 6, Timisoara, Romania  
e-mail: danycraya@gmail.com

### Abstract

In present study, the electrochemical characterization of  $\text{Y}_{0.5}\text{Ca}_{0.5}\text{BaCo}_4\text{O}_7$  compound in aqueous solution: alkaline ( $1 \text{ mol L}^{-1}$  KOH) and neutral ( $0.5 \text{ mol L}^{-1}$   $\text{Na}_2\text{SO}_4$ ) was followed, correlated with the study of oxygen intake/release process. The use of neutral aqueous solutions is an element of originality in electrochemical studies performed on this family of layered cobalt perovskites.

Electrochemical behavior has been studied by cyclic voltammetry and chrono-electrochemical methods: chronoamperometry and chronocoulometry.

### Introduction

Extended researches carried out on Y-114 perovskite have revealed his electrical and also magnetic properties, and have shown that there is a correlation between compound structure and his properties, especially due to the average cobalt ion valence. Starting from this emerged the idea to replace half of the Y ions amount (in moles) with Ca ions, leading in this way at changes into the average cobalt valence in  $\text{YBaCo}_4\text{O}_7$  perovskite, in order tu study how is affecting electrical and magnetic properties. When the  $\text{Y}_{0.5}\text{Ca}_{0.5}\text{BaCo}_4\text{O}_7$  perovskite was firstly synthesized by M. Valldor was defined as semiconductor material [1]. After first preparation, has been deciphered crystalline structure followed by study of electrical and magnetic properties [1-3].

Average cobalt ions valence modification from +2.25 in  $\text{YBaCo}_4\text{O}_7$  at +2.375 in  $\text{Y}_{0.5}\text{Ca}_{0.5}\text{BaCo}_4\text{O}_7$  explains the electrochemical interest as this compound and justifies the need for future studies. As a consequence of the increase of average cobalt ions valence in studied perovskite it is expected that the maximum oxygen content is decrease from 8.5 in  $\text{YBaCo}_4\text{O}_7$  at 8.25 in  $\text{Y}_{0.5}\text{Ca}_{0.5}\text{BaCo}_4\text{O}_7$  perovskite. Purposes of carried electrochemical tests were to characterize the compound from electrochemical point of view, and also to study sample oxygen uptake/release capacity.

### Experimental

The  $\text{Y}_{0.5}\text{Ca}_{0.5}\text{BaCo}_4\text{O}_7$  compound was obtained using solid state reaction, by mixing the precursors  $\text{Y}_2\text{O}_3$  (Aldrich 99,99%),  $\text{CaCO}_3$  (Aldrich 99,99%),  $\text{BaCO}_3$  (Aldrich 99,99%) and  $\text{CoO}_{1.38}$  (99,99% Normapur) according to the stoichiometric cation ratio. After decarbonation at  $600^\circ\text{C}$  the powder was reground, and fired in air for 48 h at  $1100^\circ\text{C}$  and then removed rapidly from furnace and set ambient temperature. The mixture was then reground and pressed into discs ( $1 \text{ cm}^2$ ) and sintered at  $1100^\circ\text{C}$  for 24 h in air. The structure of obtained  $\text{Y}_{0.5}\text{Ca}_{0.5}\text{BaCo}_4\text{O}_7$  perovskite was checked by X-Ray powder diffraction (Rigaku Ultima IV).

Electrochemical studies were carried out using a BioLogis SP 150 potentiostat/galvanostat equipped with electrochemical impedance spectroscopy module. Electrochemical cell used during experiments was a three electrode one, formed from two counter electrodes placed symmetrically to the working electrode (a disk with the geometric surface of  $0.8 \text{ cm}^2$ ),

and a reference electrode represented by Ag/AgCl electrode. In electrochemical tests were used KOH 1 mol L<sup>-1</sup> and Na<sub>2</sub>SO<sub>4</sub> 0.5 mol L<sup>-1</sup> solutions.

## Results and discussion

Y<sub>0.5</sub>Ca<sub>0.5</sub>BaCo<sub>4</sub>O<sub>7+δ</sub> electrochemical behavior was studied using the cyclic voltammetry recorded in a wide potential range in order to identify all the processes occurring in the electrochemical system: oxidation/reduction reactions, oxygen and hydrogen evolution reactions, followed by further cyclic voltammograms focused on processes which are important for practical applications of these perovskites. Based on previous experiments it can say that the voltammograms shape is influenced by the experimental conditions, and one important parameter is represented by polarization speed [4,5].

In figure 1a there are depicted cyclic voltammograms recorded using KOH 1 mol L<sup>-1</sup> solution at a polarization speed of 100 mV s<sup>-1</sup>, starting from open circuit potential, in a potential range of +1.75 V to -2.0 V vs Ag/AgCl electrode. Using such polarization speed, it can observe on the anodic part of curve the appearance of peaks/plateaus associated with: compound oxidation (1), limiting current (2), and oxygen evolution reaction (3). Also, figure 1b shows cyclic voltammograms recorded in neutral solution (1 mol L<sup>-1</sup> Na<sub>2</sub>SO<sub>4</sub>), on which similar processes deployed on electrode surface can be observed.

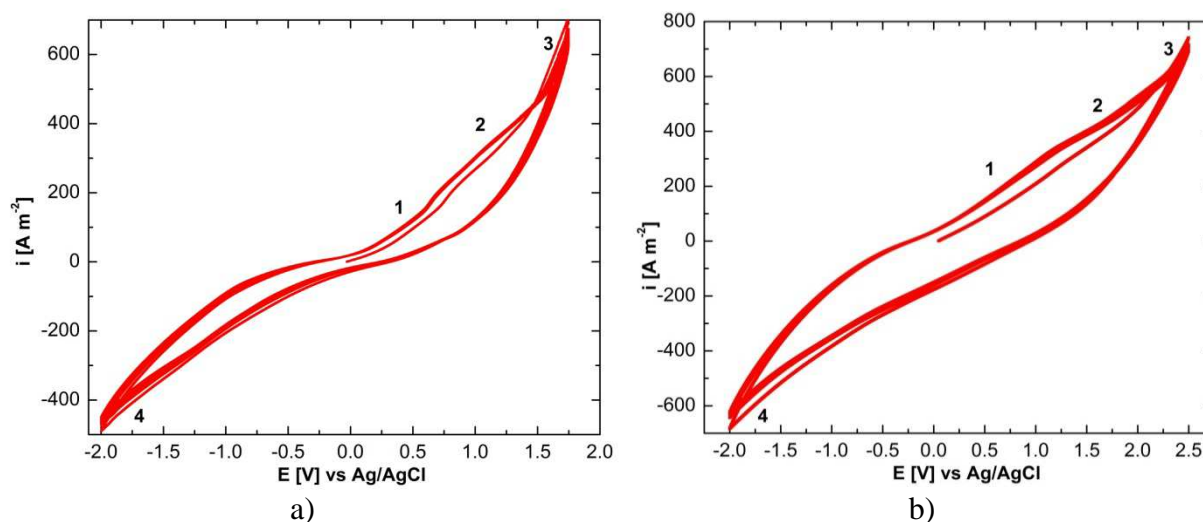


**Figure 1.** Cyclic voltammograms recorded on Y<sub>0.5</sub>Ca<sub>0.5</sub>BaCo<sub>4</sub>O<sub>7</sub> electrodes at 100 mV s<sup>-1</sup>:  
a) 1 mol L<sup>-1</sup> KOH, b) 0.5 mol L<sup>-1</sup> Na<sub>2</sub>SO<sub>4</sub>

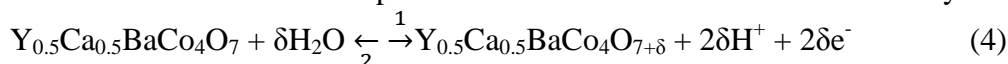
Electrochemical behavior of studied perovskite in alkaline solution can be described by following reaction:



to which are attached two different reactions: anodic oxygen evolution reaction (2) and also cathodic hydrogen evolution reaction (3):



Electrochemical behavior of the compound in neutral solution can be described by:



which describes the oxidation process in the sense 1, and also the cathodic reduction in the sense 2. Similarly, to this global equation the reaction describing the oxygen (5) and hydrogen evolution reactions (6) can be associated:



Chronoamperometric study was the starting point the cyclic voltammograms recorded on perovskite compound in alkaline and neutral solutions. From data depicted in figure 1a, 3 potential values for chronoamperometric studies were chosen: 1-  $E = 0.25$  V vs Ag/AgCl on the compound oxidation plateau, 2 -  $E = 0.65$  V vs Ag/AgCl on the limiting current plateau, and 3 -  $E = 1.0$  V vs Ag/AgCl for the oxygen evolution reaction plateau (figure 2).

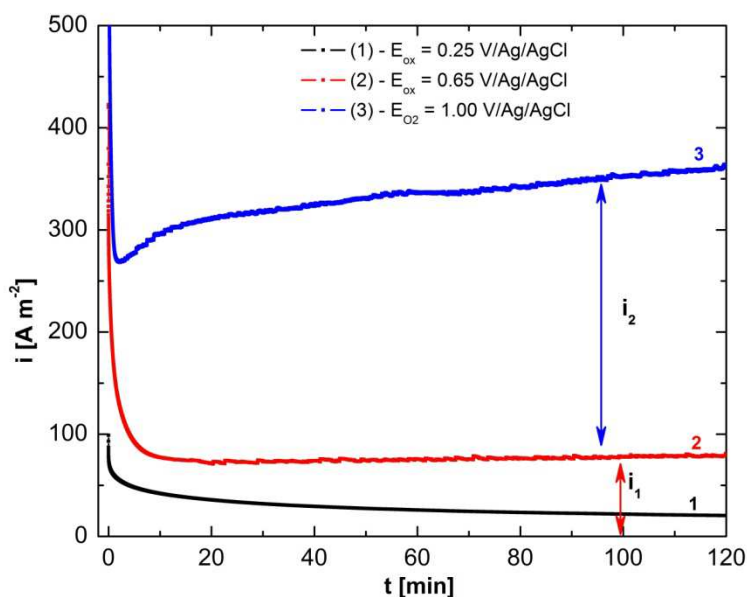


**Figure 2.** Chronoamperometric study on  $\text{Y}_{0.5}\text{Ca}_{0.5}\text{BaCo}_4\text{O}_7$  electrodes in  $1 \text{ mol L}^{-1}$  KOH.

Simultaneously the chronoamperometric curves were recorded in neutral solutions at: 1 -  $0.75$  V vs Ag/AgCl for the perovskite oxidation,  $1.25$  V/Ag/AgCl for limiting current plateau and at  $1.75$  V/Ag/AgCl for oxygen evolution reaction.

In same time, chronocoulometric data were recorded in alkaline and also neutral solutions, when the quantity of electricity used for perovskite oxidation at working potentials was measured. Based on that, using the electrolysis laws, considering that only Co(II) ions oxidation is taking place, it was possible to evaluate the oxygen quantity ( $\delta$ ) inserted in the compound structure as time a function of time. The  $\delta$  values obtained in alkaline and neutral solutions are presented in tables 1 and 2.

**Table 1.** Oxygen content variation ( $\delta$ ) in  $\text{Y}_{0.5}\text{Ca}_{0.5}\text{BaCo}_4\text{O}_{7+\delta}$  during electrochemical oxidation in KOH  $1 \text{ mol L}^{-1}$ :

$E$ [V/Ag/AgCl]	$\delta$			
	$t$ [min]			
	15	30	60	120
0,25	0,022	0,039	0,063	0,097
0,65	0,047	0,080	0,136	0,266



Tabelul 2. Oxygen content variation ( $\delta$ ) in  $Y_{0.5}Ca_{0.5}BaCo_4O_{7+\delta}$  during electrochemical oxidation in  $Na_2SO_4$  0.5 mol  $L^{-1}$ :

$E$ [V/Ag/Ag/Cl]	$\delta$			
	$t$ [min]			
	15	30	60	120
0,75	0,028	0,048	0,064	0,076
1,25	0,028	0,090	0,127	0,175

### Conclusion

Electrochemical oxidation of Co(II) ions at Co(III) ions consists in oxygen atoms insertion into the crystalline network of studied perovskite. Although, in the  $\delta$  values in the case of electrochemical oxidation, in neutral solution are smaller in comparison with the values obtained for alkaline oxidation. Consiquently can conclude the usage of neutral solution represent a viable alternative for  $Y_{0.5}Ca_{0.5}BaCo_4O_{7+\delta}$  oxidation.

### References

- [1] M. Valldor, Solid State Sciences, 8, (2006), 1272–1280.
- [2] W. Schweika, M. Valldor, P. Lemmens, Physical Review Letters, 98, (2007), 067201 .
- [3] J. R. Stewart, G. Ehlers, et al.l, Physical Review B, 83, (2011), 024405 .
- [4] M. Dan, N. Vaszilcsin, A. Kellenberger, N. Duteanu, Journal of Solid State Electrochemistry, 15(6), (2011), 1227-1233.
- [5] M. Dan, N.Vaszilcsin, A. Kellenberger, N. Duteanu, Studia Universitatis Babes-Bolyai, Chemia, 56(1), (2001), 119-126.

## Electrochemical Oxygen Uptake/Release Process over Ca-112 Electrodes in Aqueous Solutions

Mircea Laurentiu Dan<sup>\*</sup>, Nicolae Vaszilcsin<sup>\*</sup>, Andrea Kellenberger<sup>\*</sup>, Narcis Mihai Duteanu<sup>\*</sup>

<sup>\*</sup>University Politehnica Timișoara, Faculty of Industrial Chemistry and Environmental Engineering, 300223, Parvan 6, Timisoara, Romania  
e-mail: mircea.dan@upt.ro

### Abstract

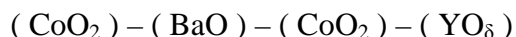
This paper presents the electrochemical study of  $Y^{3+}$  substitution with  $Ca^{2+}$  ions on intake/release of oxygen. These studies were performed using alkaline solution (1 mol L<sup>-1</sup> KOH) and also neutral solution (0.5 mol L<sup>-1</sup> Na<sub>2</sub>SO<sub>4</sub>). All electrochemical behavior presented in this paper has been studied by cyclic voltammetry.

### Introduction

YBaCo<sub>2</sub>O<sub>5+δ</sub> ( $0 \leq \delta \leq 1$ ), named Y-11,2 present a 112 phase which is a structure derived from LnBaCo<sub>2</sub>O<sub>5</sub> perovskites by ordering the rare element and also the barium cations in layers along *c* crystallographic axis, by removing the oxygen ions from yttrium layer.

It is expected, that oxygen carriage inside of YBaCo<sub>2</sub>O<sub>5+δ</sub> compound takes place really easily due to high electrical conductivity of studied perovskite, and also due the high concentration of oxygen vacancies. Based on these considerations it is expected that the studied perovskite can be used as cathode in solid oxide fuel cells.

Crystalline structure of Y-112 perovskite can be regarded as a layered structure formed by consecutive layers:



Different ways of the oxygen arrangement inside of studied compound lead at superstructure formation in which the oxygen atoms are arranged differently into the YO<sub>δ</sub> layer.

In the literature there are presented the substitution and doping possibility of Y-112 perovskites [1]. Until now, in all cases the structural modifications which occurs during Y-112 substitution were studied, and also the influence on the electrical and magnetic properties. Likewise the possibility to replace  $Y^{3+}$  ions with  $Ca^{2+}$  ones was confirmed, there are a small number of studies involving the Y<sub>1-x</sub>Ca<sub>x</sub>BaCo<sub>2</sub>O<sub>5+δ</sub>, where  $0 < \delta \leq 0,5$  [1,2] and only one study for the compound with  $x = 1$  (CaBaCo<sub>2</sub>O<sub>5+δ</sub>) [3]. Aurelio et al. demonstrate in 2013 that  $Ca^{2+}$  ions replace  $Y^{3+}$  ions and not  $Ba^{2+}$  ones inside of the perovskite structure [1]

The present paper describes the influence of  $Y^{3+}$  substitution with  $Ca^{2+}$  ions on to the oxygen intake/release capacity, by studying the compound electrochemical behavior in alkaline and neutral solutions.

### Experimental

CaBaCo<sub>2</sub>O<sub>5</sub> perovskite (Ca-112) was prepared in a similar way with YBaCo<sub>2</sub>O<sub>5</sub> compound by using the solid state synthesis, replacing Y<sub>2</sub>O<sub>3</sub> precursor with CaCO<sub>3</sub> and using a similar thermal treatment as the one used for Y-112 preparation [4].

Electrochemical studies were carried out using a BioLogic SP 150 potentiostat/galvanostat equipped with electrochemical impedance spectroscopy module. During experiments a three electrodes electrochemical cell was used, consisting of two counter electrodes placed symmetrically to the working electrode (a disk with a geometric area of 0.8 cm<sup>2</sup>), and a reference represented by Ag/AgCl electrode. In electrochemical tests

KOH 1 mol L<sup>-1</sup> and Na<sub>2</sub>SO<sub>4</sub> 0.5 mol L<sup>-1</sup> solutions were used.

## Results and discussion

In order to demonstrate the oxygen intake/release affinity the prepared Ca-112 perovskite was firstly studied by thermogravimetric methods, showing that during thermal treatments in air it can accept and also release oxygen from his structure, which can be associated with the modification of average oxidation number of cobalt ions.

Preliminarily, voltammetric studies shown that Ca-112 compound is acting in both solutions (alkaline and also neutral one) as support material, for a long potential range (between +2 and -2 V/Ag/AgCl), when it can be observed only the peaks associated with oxygen and respectively hydrogen evolution reactions (figure 1).

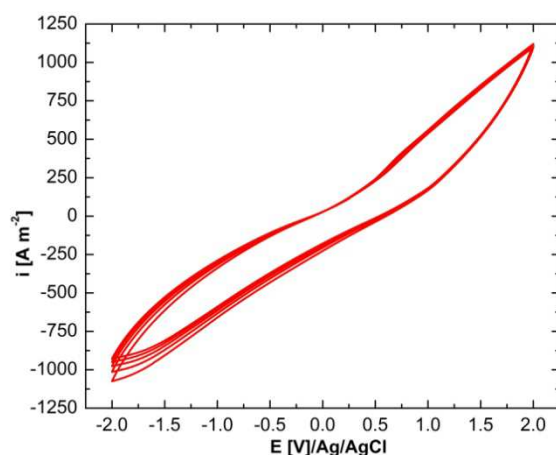


**Figure 1.** Cyclic voltammograms (5 cycles) on Ca-112 in 0.5 mol L<sup>-1</sup> Na<sub>2</sub>SO<sub>4</sub> solution at 100 mV s<sup>-1</sup> scan rate.

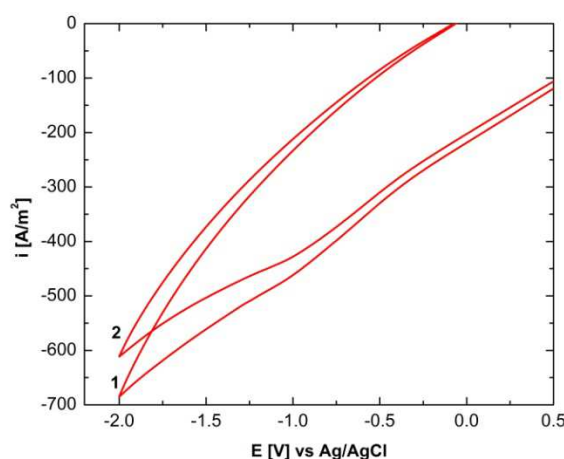


**Figure 2.** Cathodic domain of cyclic voltammograms (2 cycles) on Ca-112 in 0.5 mol L<sup>-1</sup> Na<sub>2</sub>SO<sub>4</sub> solution at 100 mV s<sup>-1</sup> scan rate.

Because the Ca-112 compound is not participant in electrode reactions, it is necessary to activate the electrode surface (figure 2) by cathodic pre-polarization at -1.00 V/Ag/AgCl, when a part of Co<sup>3+</sup> ions are reduced.

After the surface activation at polarization speed of 100 mV s<sup>-1</sup> the separation of peaks corresponding to the electrochemical processes taking place at Ca-112 interface can be observed. On cyclic voltammograms depicted in figure 3a (1 mol L<sup>-1</sup> KOH) and 3b (0.5 mol L<sup>-1</sup> Na<sub>2</sub>SO<sub>4</sub>), recorded for OCP, it can observe that at anodic polarization appear first anodic peak (1) associated with Co(II) ions oxidation  $\text{Co}^{\text{II}} \rightarrow \text{Co}^{\text{III}} + \text{e}^-$  (Co(II) ions are produced in

activation period, followed by a limit current plateau (2), and at more positive potentials the peak (3) associated with oxygen evolution reaction appears.

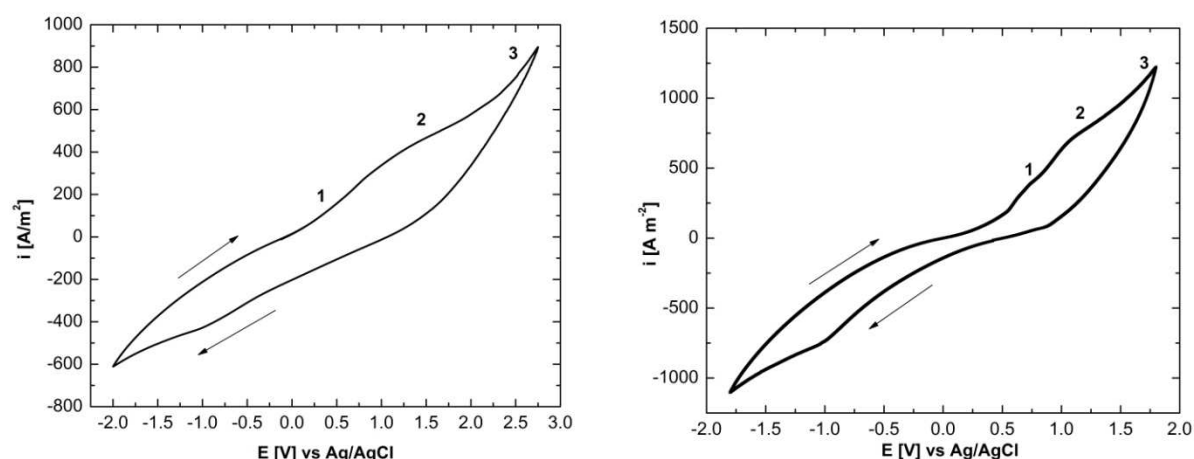


**Figure 3.** Cyclic voltammograms recorder on Ca-112 at  $100 \text{ mV s}^{-1}$ :  
a)  $1 \text{ mol L}^{-1} \text{ KOH}$ , b)  $0.5 \text{ mol L}^{-1} \text{ Na}_2\text{SO}_4$

As effect, the oxidation of Co(II) ions at Co(III) ions supplementary oxygen is inserted into the Ca-112 crystalline structure. Intake/release oxygen ability is a consequence of structural flexibility of 112 stratified perovskites, which allows small distortions without destroying the crystalline structure.

## Conclusion

Based on voltammetric studies it can say that Ca-112 perovskite presents the oxygen intake/release property. Electrochemical oxidation occurs at lowered speed in case of Ca-112 perovskites in comparison with Y-112 one. Ca-112 electrodes require a surface activation stage, which allow the studied compound to be used in all areas where the 112 layered perovskites can be used.

## References

- [1] G. Aurelio, F. Bardelli, R. Junqueira Prado, R. D. Sánchez, M. E. Saleta, G. Garbarino, *Chem. Mater.*, 25 (16), (2013), 3307–3314.
- [2] W. J. Ge, Q. Shao, Y. Z. Ding, X.Y. Lu, *Advanced Materials Research* 830, (2013), 130–134.
- [3] H. Wang, C. Dong, C. Chen, J. Liu, M. Liu, C. Ma, *Recent Developments in Biological, Electronic and Functional Thin Films and Coatings*, 2013.
- [4] M. Dan, N. Vasilcsin, A. Borza, N. Duteanu, *Chem. Bull. "Politehnica" Univ. (Timisoara)*, 55 (2), 2010, 162–166.

## Capsaicin Extract as Corrosion Inhibitor for Carbon Steel in Sodium Chloride Aqueous Solution

Cristian George Vaszilcsin<sup>\*</sup>, Mircea Laurentiu Dan<sup>\*\*</sup>, Andreea Enache<sup>\*\*</sup>

<sup>\*</sup>INCEMC Timișoara, Dr. A. Paunescu Podeanu 144, 300569, Timisoara, Romania

<sup>\*\*</sup>University Politehnica Timișoara, Faculty of Industrial Chemistry and Environmental Engineering, 300223, Parvan 6, Timisoara, Romania  
e-mail: cristi\_vasz@yahoo.com

### Abstract

In this paper are presented preliminary results obtained using capsaicin extract as corrosion inhibitor for carbon steel in sodium chloride aqueous solution. Capsaicin is a chili pepper extract with analgesic properties. The electrochemical behavior of capsaicin in sodium chloride solution was examined by cyclic voltammetry. Further, the inhibitory effect was studied by linear polarization and Tafel method in order to determine the kinetic parameters, providing information about the mechanism of inhibitory effect. The diminution of corrosion rate of carbon steel in the presence of capsaicin can be attributed to the inhibitor molecules adsorption on the sample surface and blocking the active sites, or depositing corrosion products on the metal surface.

### Introduction

Steel is a proven durable and efficient building material. It is cost effective, aesthetically pleasing, sustainable, and strong. However, like all metals, steel corrodes when exposed to the atmosphere. Therefore, it is important to consider corrosion protection methods in constructing projects with exposed steel. Approximately 85% of all steel produced is carbon steel and therefore susceptible to natural oxidation and galvanic corrosion [1]. Corrosion control of steel is an expensive process and industries spend huge amounts to control this problem.

Protection by corrosion inhibitors is one of the well known methods of corrosion protection and one of the most useful in the industry. This method is following stand up due to low cost and practice method [2]. Throughout the ages, plants have been used by human beings for their basic needs such as production of food-stuffs, shelters, clothing, fertilizers, flavors and fragrances, medicines and last but not least, as corrosion inhibitors. The use of natural products as corrosion inhibitors can be traced back to the 1930's when plant extracts of *Chelidonium majus* were used for the first time in H<sub>2</sub>SO<sub>4</sub> pickling baths [2-5].

The active ingredient capsaicin (oleoresin of *Capsicum*) is generally obtained by grinding dried ripe fruits of *Capsicum frutescens* L. (chili peppers) into a fine powder. The extract may be obtained by distillation of the powder in an appropriate solvent, and evaporation of the solvent to yield the liquid oleoresin and associated fatty matter. The fatty matter is removed by decanting or filtration [6].

The diminution of the corrosion rate of carbon steel in the presence of capsaicin or active ingredient of capsaicin can be attributed to the adsorption of inhibitor molecules on the metal surface blocking the active sites or depositing corrosion products.

### Experimental

Electrochemical measurements were conducted using BioLogic SP150 potentiostat/galvanostat in a conventional three-electrode cell systems. The working electrode was carbon steel, the counter electrode was graphite, and a Ag/AgCl acted as the reference electrode. Experiments were performed in 3.5% NaCl solution, to determine the corrosion potential and

corrosion current.

To determine the inhibitor effect of capsaicin on the corrosion rate of carbon steel in sodium chloride aqueous solution in preliminary studies a  $4 \text{ mg L}^{-1}$  concentration has been used. The chemical structures of capsaicin ( $\text{C}_{18}\text{H}_{27}\text{NO}_3$ ) is presented in figure 1 [7].

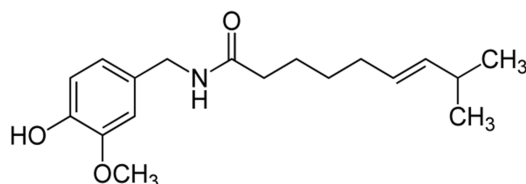
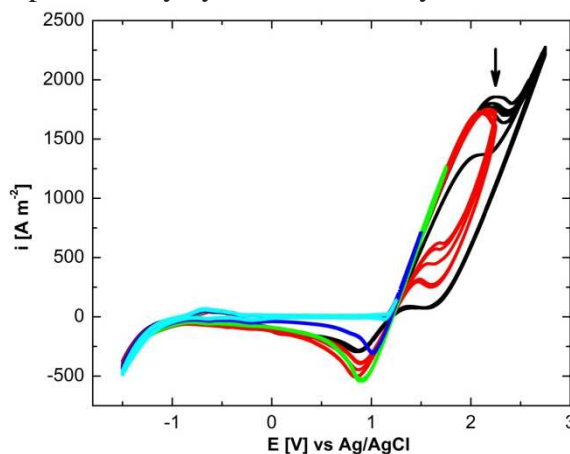


Fig.1. Chemical structures of capsaicin [7].

## Results and discussion

Preliminary information about how capsaicin extract can influence the corrosion process of carbon steel are pointed by its electrochemical behavior on platinum electrode in sodium chloride media emphasised by cyclic voltammetry.



**Figure 1.** Cyclic voltammograms (5 cycles) on Pt electrode in 3.5% NaCl in different fields of potential.

In figure 1 cyclic voltammograms recorded on Pt as working electrode in 3.5% NaCl solution without capsaicin are presented. The base curve obtained in a blank solution presents the characteristics of polarization curves drawn in sodium chloride solutions.

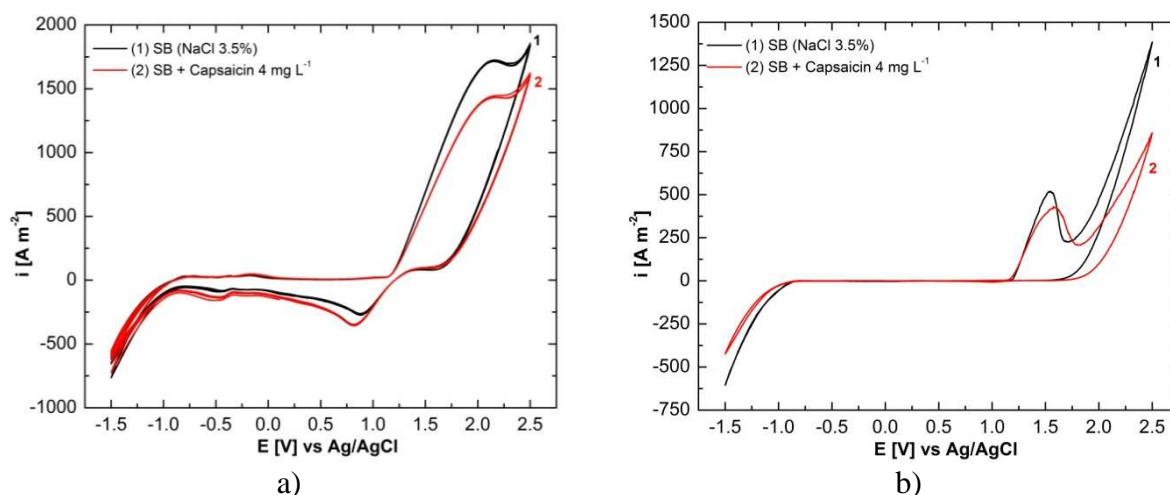


**Figure 2.** Cyclic voltammograms (5 cycles) on Pt electrode in 3.5% NaCl in the absence/presence of  $4 \text{ mg L}^{-1}$  capsaicin, scan rate: a)  $500 \text{ mV s}^{-1}$  and b)  $5 \text{ mV s}^{-1}$ .



In figure 2a ( $dE/dt = 500 \text{ mV s}^{-1}$ ) and 2b ( $dE/dt = 5 \text{ mV s}^{-1}$ ) there are shown cyclic voltammograms recorded on Pt as working electrode, in 3.5% NaCl solutions without and with  $4 \text{ mg L}^{-1}$  capsaicin used in preliminary corrosion tests.

In order to identify how capsaicin extract influences the electrode processes, polarization curves were recorded separately at  $5 \text{ mV s}^{-1}$ , in cathodic domain as well as in anodic one. The obtained voltammograms are presented in figure 3a-b.

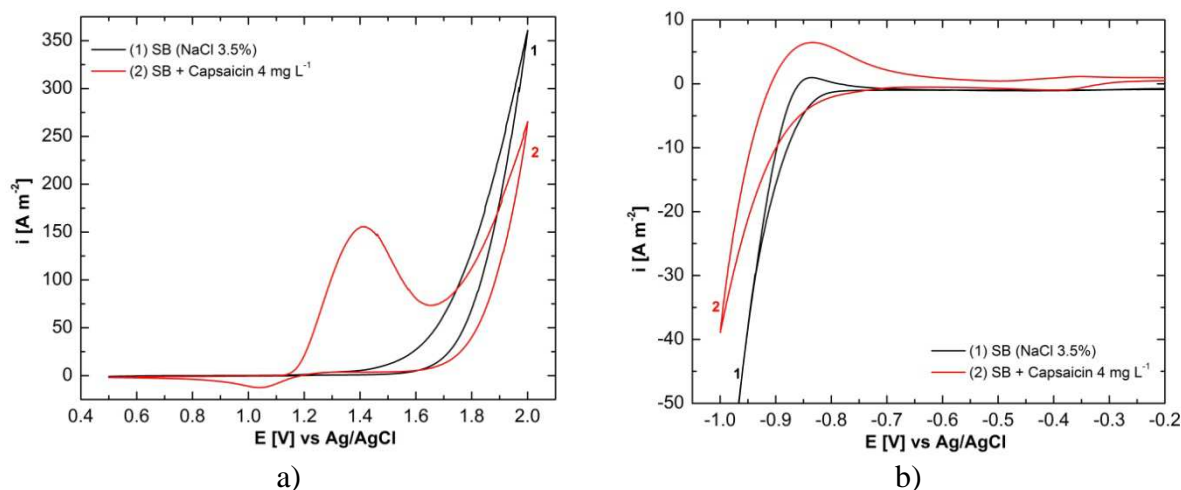


**Figure 3.** Cyclic voltammograms on Pt electrode for anodic (a) and cathodic (b) polarization in 3.5% NaCl in the absence/presence of  $4 \text{ mg L}^{-1}$  capsaicin, scan rate  $5 \text{ mV s}^{-1}$

The manner in which capsaicin acts as corrosion inhibitor for carbon steel in sodium chloride solution and its effect on the corrosion rate can be estimated by Tafel polarization method. The potentiodynamic polarization curves recorded without and with  $4 \text{ mg L}^{-1}$  capsaicin are shown in figure 4.

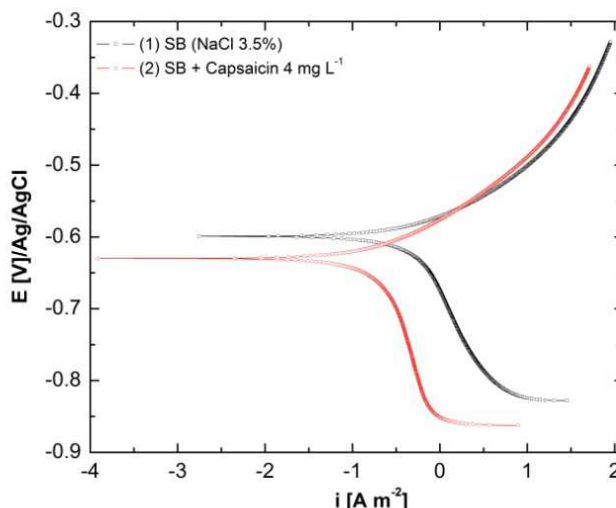


**Figure 4.** Linear polarization curves on carbon steel electrode in 3.5% NaCl in the absence/presence of  $4 \text{ mg L}^{-1}$  capsaicin, scan rate  $1 \text{ mV s}^{-1}$ .

Numerical values of the corrosion current density ( $i_{corr}$ ) variation, corrosion potential ( $E_{cor}$ ), anodic Tafel slope ( $b_a$ ), cathodic Tafel slope ( $b_c$ ) and polarization resistance ( $R_p$ ) were obtained from polarization profiles by extrapolating potentiodynamic curves from figure 4 using BioLogics software and showed in table 1.

Tabel 1. Polarization parameters for the corrosion of carbon steel in 3.5% NaCl in the absence and presence of 4 mg L<sup>-1</sup> capsaicin:

Electrolit	T [K]	$i_{cor}$ [ $\mu\text{A cm}^{-2}$ ]	$E_{cor}$ [mV]	$-b_c$ [mV dec <sup>-1</sup> ]	$b_a$ [mV dec <sup>-1</sup> ]	$R_p$ [ $\Omega$ ]	$v_{cor}$ [mm an <sup>-1</sup> ]	IE [%]
SB (NaCl 3.5%)	298	39.14	-601.1	294.0	77.1	276	1.15	-
SB + 4 mg L <sup>-1</sup> Capsaicin		10.74	-630.0	272.5	74.4	573	0.433	62.94

## Conclusion

Preliminary studies confirm that capsaicin has promising corrosion inhibition properties for carbon steel in aqueous sodium chloride solutions. Capsaicin extract can be added to the list of non-toxic, cheap and effective green corrosion inhibitors from renewable sources.

## Acknowledgements

This work was partially supported by *INCEMC Timisoara* in the frame of *PN 09-34 04 03 Research Program* and by *University Politehnica Timisoara* in the frame of *PhD studies*.

## References

- [1] <http://www.galvanizeit.org/corrosion/>
- [2] M. S. Al-Otaibi, A. M. Al-Mayouf, M. Khan, A. A. Mousa, S. A. Al-Mazroa, H. Z. Alkhatlan, *Arabian Journal of Chemistry*, 7, 2014, 340-346.
- [3] G. Gunasekaran, L. R. Chauhan, *Electrochimica Acta*, 49(25), 2004, 4387–4395.
- [4] A. Y. El-Etre, *Corrosion Science*, 45(11), 2003, 2485–2495.
- [5] A. Y. El-Etre, M. Abdallah, Z. E. El-Tantawy, *Corrosion Science*, 47(2), 2005, 385–395.
- [6] <https://pubchem.ncbi.nlm.nih.gov/compound/Capsaicin#section>
- [7] <https://en.wikipedia.org/wiki/Capsaicin>.
- [8] M. Dan, N. Vaszilcsin, M. Labosel, B. Pancan, *Chem. Bull. "Politehnica" Univ. (Timisoara)*, 59(1), 2014, 13 -18.

## Anodic Oxidation of Sulphite on Graphite Electrode in Alkaline Media

Andreea Enache\*, Mircea Laurentiu Dan, Nicolae Vaszilcsin

*University Politehnica Timișoara, Faculty of Industrial Chemistry and Environmental Engineering, 300223, Parvan 6, Timisoara, Romania*  
*e-mail: enacheandreeafloriana@gmail.com*

This paper presents studies of anodic oxidation of sulfite ions on a graphite electrode in aqueous alkaline solutions. Over the past few years, extensive research has been focused on the use of graphite as electrode material because of its availability, physico-chemical properties, processability and relatively low cost. Graphite electrodes are thermally and mechanically stable, chemically resistant in different solutions (from strongly acidic to strongly basic) and chemically inert [1, 2].

Electrochemical oxidation of graphite during operation of fuel cells has been widely studied [3-6], because electrochemical behavior of graphite has relevant influence on detrimental to the performance and life of fuel cells.

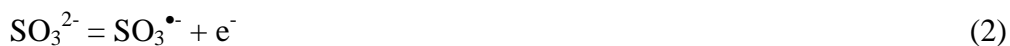
Carbon is oxidised to carbon dioxide at higher potential than  $E^\circ = +0.207 \text{ V}$  (vs. NHE) in accordance with reaction (1). Even if this value means that carbon is unstable to the electrochemical corrosion, slow kinetics of the oxidation reaction ensures good stability of carbon in solid fuel cells [6].



The reaction of sulphite at room temperature has been examined by cyclic and linear voltammetric methods on a graphite electrode. Polarization curves have been plotted in 1M NaOH support electrolyte solution in which have been added different amounts of  $\text{Na}_2\text{SO}_3$  in order to obtain concentrations of  $10^{-1}\text{M}$ ,  $10^{-2}\text{M}$ , respectively  $10^{-3}\text{M}$ . The mechanism of the oxidation reaction was studied by varying the scan rate and the concentration of sulphite in electrolyte solutions.

The sulphite oxidation on graphite electrode occurs in two steps. In the first one, a radical anion  $\text{SO}_3^{\bullet-}$  is formed by losing one electron. Further more oxygen transfer undergoes by losing the second electron. Two sulphite radical can combine and form dithionate, which can then disproportionate into sulphite and sulphate, but the formation of dithionate on the graphite electrode (Equation 4) can be neglected in accordance with the literature [7].

Therefore, anodic oxidation of sulphite ions in alkaline solution on graphite electrode can be expressed by the following equations:



From figure 1, at a potential value of  $+0.3 \text{ V}$  vs. Ag/AgCl, the beginning of the anodic oxidation of sulphite ions can be observed. Due to the evolution of oxygen and possible the oxidation of graphite, gas bubbles are formed on the electrode surface and consequently the oxygen evolution diminished the oxidation of sulphite. Finally the current increased with increasing potential exhibiting the abundantly evolution of oxygen.

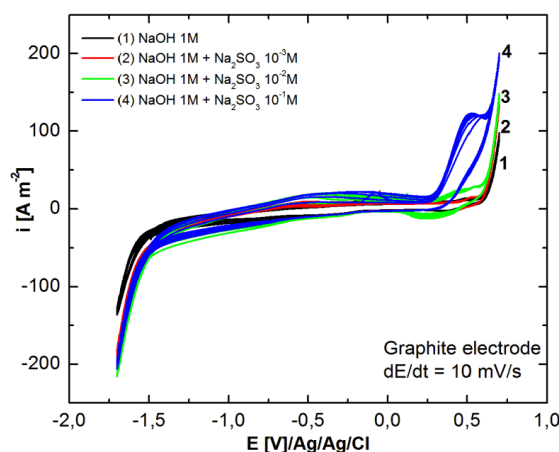


Fig. 1. Cyclic voltammograms (5 cycles) on the graphite electrode  $dE/dt = 10 \text{ mV/s}$  in the alkaline electrolyte with different concentrations of sodium sulfite.

Based on polarization curves resulting from linear voltammetry kinetic parameters ( $I_\alpha$  and  $i_o$ ) for electrochemical oxidation of sulphite to sulphate have been calculated for each electrolyte solution using Tafel method.

### Acknowledgement

This work was partially supported by University *Politehnica* Timisoara in the frame of PhD studies.

### References

- [1] S. Bok, A. Lubguban, Y. Gao, *Journal of the Electrochemical Society* 155(5), (2008), p. 91–95.
- [2] E. Frackowiak, F. Beguin, *Carbon* 39(6), (2001), p. 937–950.
- [3] J. Wang, G. Yin, Y. Shao, S. Zhang, *Journal of Power Sources* 171(2), (2007), p. 331–339.
- [4] K. H. Lim, H. S. Oh, S. E. Jang, Y. J. Ko, *Journal of Power Sources*, 193(2), (2009), p. 575–579.
- [5] C. A. Reiser, L. Bregoli, T. W. Patterson, J. S. Yi, *Electrochemical and Solid-State Letters* 8(6), (2005), p. 273–276.
- [6] Oh H-S, Lee J-H, Kim H., *International Journal of Hydrogen Energy* 37(14), (2012), p. 10844 – 10849.
- [7] J. Lu, D.B. Dreisinger and W.C. Cooper, *Journal of Applied Electrochemistry* 29 (1999), p.1161 - 1170.

## Recycling of Expired Drugs as Additive in a Watts Nickel Electroplating Bath

Delia-Andrada Duca\*, Nicolae Vaszilcsin, Mircea Laurențiu Dan

University Politehnica Timisoara, Faculty of Industrial Chemistry and Environmental Engineering, 300223, Parvan 6, Timisoara, Romania  
e-mail: duca.delia@gmail.com

### Abstract

In this paper are presented studies on the leveling effect of *midazolam* {8 - chloro - 6 - (2 - fluorophenyl) - 1 - methyl - 4H - imidazo[1,5-a][1,4]benzodiazepine}, and *streptomycin* {5 - (2,4 - diguanidino - 3,5,6 - trihydroxy- cyclohexoxy)- 4 -[4,5- dihydroxy - 6 - (hydroxymethyl) - 3 - methylamino- tetrahydropyran - 2 - yl]oxy - 3 - hydroxy - 2 - methyl- tetrahydrofuran - 3 - carbaldehyd}, in a Watts nickel electroplating bath, manifested by the increase of cathode polarization. These drugs were chosen because their pharmaceutical formulation of the commercial product contains only pure compound, without excipients.

### Introduction

Watts nickel bath was discovered over 100 years ago [1] and it is still maintaining actuality and interest for the electrochemists thanks to the anticorrosive efficiency of nickel coatings [2] and ornamental effect [3] as well as due to the possibility of obtaining nanostructures and materials with special proprieties [4]. Nickel coatings are also used as substrate for hydrogen evolution reaction [5,6].

The composition of the deposition bath influences the quality of nickel deposits, such as hardness, internal stress, compactness and brightness, which can be enhanced by adding various agents [7]. Some of the well-known additives are aromatic compounds [8]. The drugs hereinbefore contain only active substance, without any excipients, reason why these studies are based on the use of expired drugs as additives in electrodeposition from Watts bath.

### Experimental

Electrochemical studies were carried out using Biologics SP 150 and AUTOLAB 302N potentiostat/galvanostats, in a three-electrode electrochemical cell, consisting of working electrode (Pt, Cu, or Ni), two graphite rods as counter electrodes and Ag/AgCl as reference electrode ( $E_{Ag/AgCl} = 0,197$  V).

Experiments were performed in 0,5 mol L<sup>-1</sup> Na<sub>2</sub>SO<sub>4</sub>, SB (0,5 mol L<sup>-1</sup> Na<sub>2</sub>SO<sub>4</sub> + 30 g L<sup>-1</sup> H<sub>3</sub>BO<sub>3</sub>) solutions and Watts bath (300 g L<sup>-1</sup> NiSO<sub>4</sub>·6H<sub>2</sub>O + 60 g L<sup>-1</sup> NiCl<sub>2</sub>·6H<sub>2</sub>O + 30 g L<sup>-1</sup> H<sub>3</sub>BO<sub>3</sub>), with different concentrations of additive – midazolam or streptomycin (10<sup>-6</sup> ÷ 10<sup>-3</sup> mol L<sup>-1</sup>).

### Results and discussion

Preliminary information about the electrochemical behavior of midazolam and streptomycin were determined by cyclic voltammetry. It has been observed how expired drugs influence electrode processes.

In these studies, Pt electrode as working electrode was used. The base curve, obtained in blank solution presents the characteristics of polarization curves drawn in 0,5 mol L<sup>-1</sup> Na<sub>2</sub>SO<sub>4</sub>. Further, the electrolyte solution was acidified with 30 g L<sup>-1</sup> H<sub>3</sub>BO<sub>3</sub>, reaching the same pH as in the Watts bath (pH = 3,5 ÷ 4,5).

In figure 1 there are presented cyclic voltammograms recorded with a scan rate of

50 mV s<sup>-1</sup>, on Pt as working electrode, in 0,5 mol L<sup>-1</sup> Na<sub>2</sub>SO<sub>4</sub> (a) and SB (0,5 mol L<sup>-1</sup> Na<sub>2</sub>SO<sub>4</sub> + 30 g L<sup>-1</sup> H<sub>3</sub>BO<sub>3</sub>) (b), without and with 10<sup>-4</sup> mol L<sup>-1</sup> midazolam.

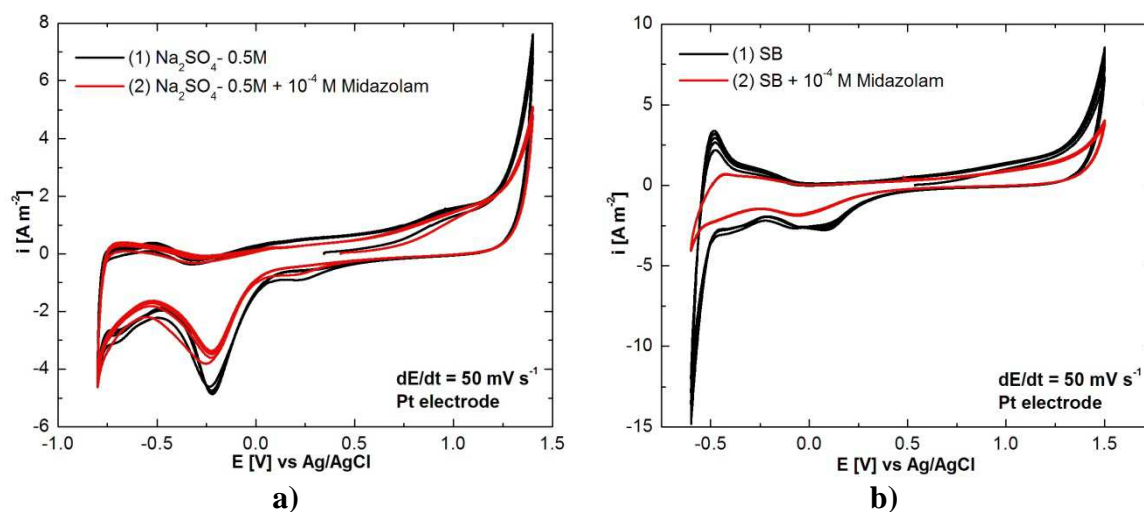


**Fig. 1.** Cyclic voltammograms (5 cycles) on Pt electrode in a) 0,5 mol L<sup>-1</sup> Na<sub>2</sub>SO<sub>4</sub> and b) SB, without and with 10<sup>-4</sup> mol L<sup>-1</sup> midazolam.

From the above figure it can be observed the inhibitory effect of the drug on electrochemical processes.

## Conclusion

Experimental studies presented in this paper shows that both midazolam and streptomycin can be used as leveling additive in nickel Watts bath, manifesting inhibiting effect for the cathodic process of nickel deposition.

## References

- [1] H. Brown, B.B.Knapp, Nickel, in F.A. Lowenheim (Editor), Modern Electroplating, Third Edition, Wiley Interscience Publication, New York, 1974, 287-341.
- [2] S. Hassani, K. Raeissi, M. Azzi, D. Li, M. A. Golozar, J. A. Szpunar, Improving the corrosion and tribocorrosion resistance of Ni-Co nanocrystalline coatings in NaOH solution, Corrosion Science, 51, 2009, 2371-2379.
- [3] T. Sakamoto, K. Azumia, H. Tachikawaa, K. Iokibea, M. Seoa, N. Uchidac, Y. Kagayac, Electrochim. Acta, 55, 2010, 8570-8578.
- [4] E. Rudnik, M. Wojnicki, G. Włoch, Effect of gluconate addition on the electrodeposition of nickel from acidic baths, Surface and Coatings Technology, 207, 2012, 375-388.
- [5] B. Pierozynski, I.M. Kowalski, Hydrogen Evolution Reaction at Pd-Modified Nickel-Coated Carbon Fibre in 0.1 M NaOH Solution, International Journal of Electrochemical Science, 8, 2013, 7938-7947.
- [6] M. Torabi, A. Dolati, A kinetic study on the electrodeposition of nickel nanostructure and its electrocatalytic activity for hydrogen evolution reaction, Journal of Applied Electrochemistry, 40, 2010, 1941-1947.
- [7] Y.D. Gamburg, G. Zangari, Theory and Practice of Metal Electrodeposition, Springer, 2011, ISBN: 978-1-4419-9669-5.
- [8] E.M. Oliveira, G.A. Finazzi, I.A. Carlos, Influence of glycerol, mannitol and sorbitol on electrodeposition of nickel from a Watts bath and on the nickel film morphology, Surface and Coatings Technology, 200, 2006, 5978-5985.



## Corrosion Studies of Copper Electrodes in Acidic Medium in the Presence of N,N-Dimethylaniline

Ágnes Jakab\*, Mircea Laurențiu Dan, Nicolae Vaszilcsin

*Politehnica University of Timișoara, Faculty of Industrial Chemistry and Environmental Engineering, V. Pârvan. No. 6, 300223 Timișoara, Romania  
e-mail: agness.jakab@upt.ro*

### Abstract

In this work, the influence of N,N-dimethylaniline (DMA) as inhibition agent for copper corrosion process has been studied. The electrochemical behaviour of DMA on platinum and copper electrodes in acid solutions has been analyzed by cyclic voltammetry. Inhibitory properties of DMA for copper corrosion protection were studied in 0.5 M H<sub>2</sub>SO<sub>4</sub> solutions in the presence of different concentrations of inhibitor 10<sup>-6</sup> M and 10<sup>-3</sup> M, respectively. The morphology of copper samples obtained in the absence and presence of DMA has been studied by scanning electron microscopy (SEM).

### Introduction

The possibility of the copper corrosion prevention using mostly organic inhibitors has attracted many researchers. The most widely used inhibitors are organic derivatives such as azoles [1,2], amines [3,4], amino acids [5] and many others. The presence of nitrogen heteroatoms in organic compounds like amines improves its action as copper corrosion inhibitor [6]. The aim of this study was to investigate the inhibitory effect of N,N-dimethylaniline (DMA) in 0.5 M H<sub>2</sub>SO<sub>4</sub> at room temperature using cyclic voltammetry and linear polarization.

### Experimental

The chemicals used for this study *i.e.*, sulphuric acid (H<sub>2</sub>SO<sub>4</sub>) and N,N-dimethylaniline (DMA, (CH<sub>3</sub>)<sub>2</sub>NC<sub>6</sub>H<sub>5</sub>) (analytical grade) were purchased from Merck Company (Germany). The distilled water was used for all experiments. Inhibitory properties of DMA for copper corrosion protection were studied in 0.5 M H<sub>2</sub>SO<sub>4</sub> solutions in the presence of different concentrations of inhibitor 10<sup>-6</sup> M and 10<sup>-3</sup> M, respectively. Cyclic voltammetry, linear polarization method (Tafel curves) and scanning electron microscopy (SEM) were carried out to observe the inhibition effect of copper corrosion process.

### Results and discussion

The electrochemical behaviour of DMA on platinum electrode at different scan rates was investigated by cyclic voltammetry measurements. Figure 1 shows cyclic voltamograms recorded in 0.5 M H<sub>2</sub>SO<sub>4</sub> and in the presence of 10<sup>-3</sup> M DMA at different polarization rate between 10 ÷ 500 mV s<sup>-1</sup>.

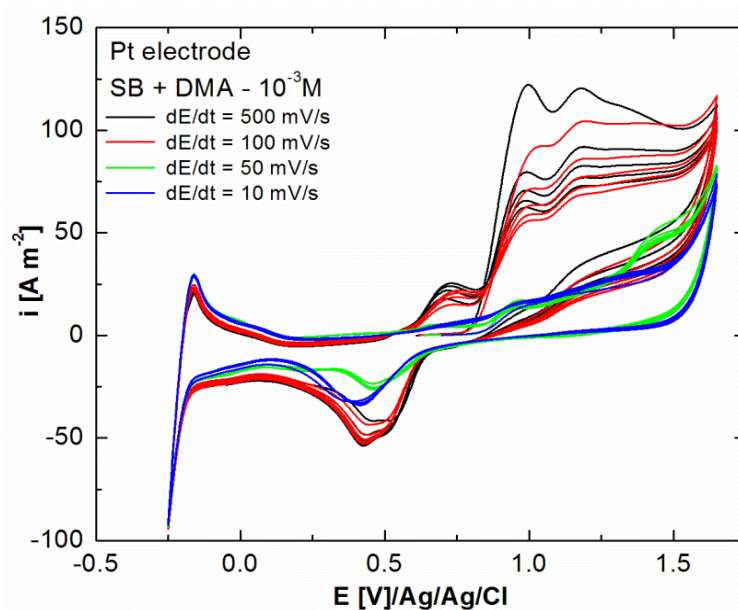


**Figure 1.** Cyclic voltammograms (5 cycles) recorded on Pt in 0.5 M H<sub>2</sub>SO<sub>4</sub> and in the presence of 10<sup>-3</sup> M DMA at different scan rates.

In order to study the DMA influence on the anodic or cathodic process on copper electrode, cyclic voltammograms were recorded in 0.5 M H<sub>2</sub>SO<sub>4</sub> in the absence and presence of 10<sup>-3</sup> M DMA at 500 mV s<sup>-1</sup> polarization rate, which are presented in Figure 2.

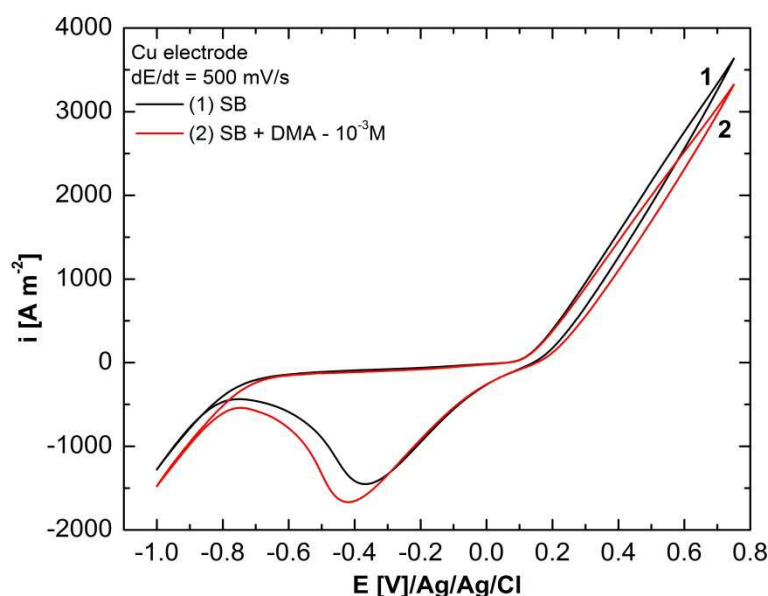


**Figure 2.** Cyclic voltammograms recorded on copper electrode in 0.5 M H<sub>2</sub>SO<sub>4</sub> (1) and in the presence of 10<sup>-3</sup> M DMA (2), scan rate 500 mV s<sup>-1</sup>.

The inhibition effect of different concentrations of DMA on copper corrosion process was studied by Tafel polarization method. Figure 3 shows the Tafel polarization curves recorded on copper electrode in 0.5 M H<sub>2</sub>SO<sub>4</sub> and in the presence of 10<sup>-6</sup> and 10<sup>-3</sup> M DMA at two polarization rates.

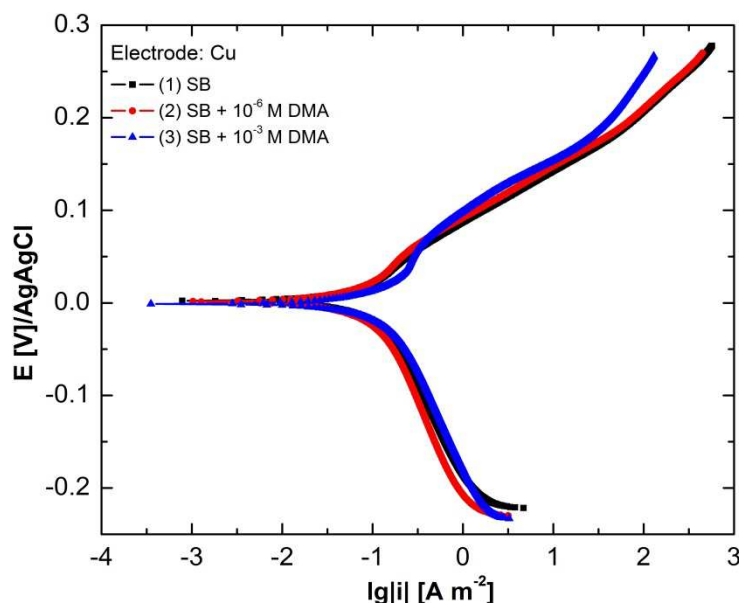


**Figure 3.** Tafel polarization diagrams recorded on copper electrode ( $dE/dt = 2 \text{ mV s}^{-1}$ ) in  $0.5 \text{ M H}_2\text{SO}_4$  without and with different concentrations of DMA.

The obtained polarization parameters, *i.e.*, corrosion current density ( $i_{cor}$ ), corrosion potential ( $E_{cor}$ ), anodic Tafel slope ( $b_a$ ), cathodic Tafel slope ( $b_c$ ), polarization resistance ( $R_p$ ) and corrosion rate ( $v_{cor}$ ) are gathered in Table 1.

**Table 1.** Polarization parameters for the corrosion of copper in  $0.5 \text{ M H}_2\text{SO}_4$  in the absence/presence of different concentrations of DMA.

Inh. conc., M	$i_{cor}$ , $\mu\text{A cm}^{-2}$	$E_{cor}$ , mV	$-b_c$ , $\text{mV dec}^{-1}$	$b_a$ , $\text{mV dec}^{-1}$	$R_p$ , $\Omega$	$v_{cor}$ , $\text{mm year}^{-1}$
BS	7.84	2.01	201.4	64.5	2435	0.36
$10^{-6}$	5.23	1.25	225.1	70.8	3506	0.24
$10^{-3}$	4.75	-5.04	205.4	82.5	4758	0.21

The surface morphology of copper samples was analysed after a corrosive attack in the presence and absence of  $10^{-6} \text{ M DMA}$  during 240 h immersion time. Figure 4 shows SEM images recorded for copper samples.

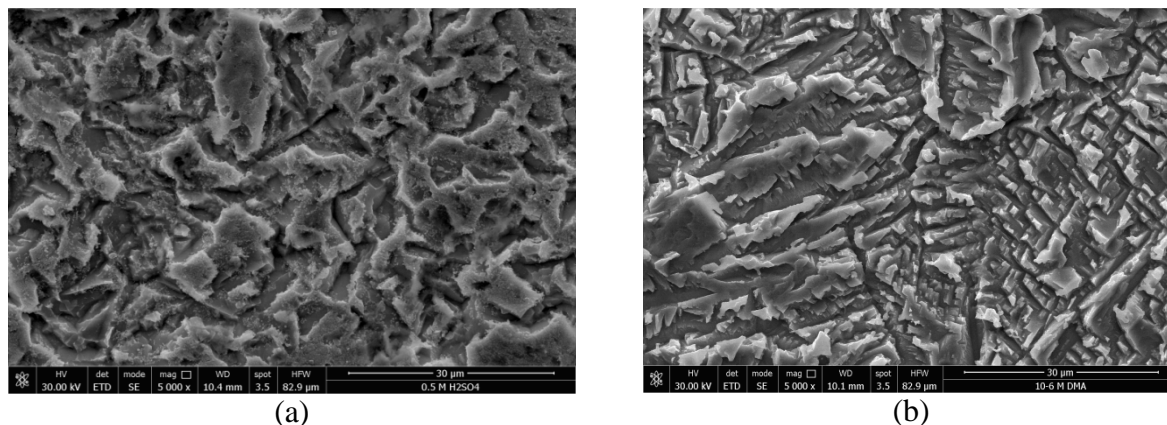


**Figure 4.** SEM images of copper samples after 240 h immersion time in  $0.5 \text{ M H}_2\text{SO}_4$  (a) and  $10^{-6} \text{ M DMA}$  (b).

## **Conclusions**

The obtained results confirm that DMA has promising corrosion inhibition properties for copper in acidic environment. Further studies will be required to determine the weight loss data by gravimetric method in the absence and presence of different amounts of DMA, thereby the inhibition efficiency and surface coverage will be calculated. Also, the inhibition effect of DMA on copper corrosion process at different temperatures (308, 318, 328, 338 K) will be investigated in the future.

## **Acknowledgements**

„This work was partially supported by the strategic grant POSDRU/159/1.5/S/137070 (2014) of the Ministry of National Education, Romania, co-financed by the European Social Fund – Investing in People, within the Sectoral Operational Programme Human Resources Development 2007-2013.”

## **References**

- [1] F. M. Al Kharafi, N. A. Al Awadi, I. M. Ghayad, R. M. Abdullah, M. R. Ibrahim, *Int. J. Electrochem. Sci.*, 6 (2011) 1562-1571,.
- [2] R. Johnson , M. Daroux , E. Yeager and Hatsuo Ishida, *Polymeric Materials for Corrosion Control*, Chapter 23, Vol. 322, 2009, pp. 250–267.
- [3] M.M. Singh, R.B. Rastogi, B.N. Upadhyay, M. Yadav, *Indian J. Chem. Technol.*, 6 (1999) 93-99.
- [4] O.R.M. Khalifa, A.K. Kassab, H.A. Mohamed, S.Y. Ahmed, *J. American Science*, 6(8), 2010.
- [5] D.Q. Zhanga, QR. Caia, X.M. Hea, L.X. Gaob, G.D. Zhuo, *Materials Chemistry and Physics*, 112(2) (2008) 353–358.
- [6] M. Ehteshamzade, T. Shahrabi, M.G. Hosseini, *Appl. Surf. Science*, 252 (2006) 2949–2959.
- [6] M.M. Antonijevic, M.B. Petrovic, *Int. J. Electrochem. Sci.*, 3 (2008) 1 – 28.

## Polyester Resin Coatings as Barrier Against Aggressive Agents. Influence of Volumetric Pigment Concentration

Dorin Jurcau <sup>1</sup>, Nicoleta Plesu<sup>2\*</sup>, Lavinia Macarie <sup>2</sup>

<sup>1</sup>*Elkim Special SRL, str. Constantin cel Mare nr. 21, 300290 Timisoara, Romania*

<sup>2</sup>*Institute of Chemistry of Romanian Academy, Mihai Viteazul Bul.24, 300223-Timisoara, Romania, Tel: +40256491818, Fax: +40256491824,*

*\*email: plesu\_nicole@yahoo.com , nplesu@acad-icht.tm.edu.ro*

### Abstract

In this paper we present experimental results of electrochemical measurements (EIS and anodic polarization) on the performance of polyester copolymers films obtained at the various volumetric pigment content (VPC).

### Introduction

Polymer films could restrain the aggressive action of water and oxygen and act as a barrier against aggressive agents.

The performance of polymer films shows as a barrier against corrosive agents and depends on the polymer structure, the thickness and degree of adhesion to the metal substrate, the nature of metallic substrate [1]. Electrochemical techniques are usually used to evaluate the corrosion behavior of organic coatings. EIS is a non-invasive method and allows the determination of both the dielectric properties of organic coatings and corrosion processes at the interface metal / organic film [3, 4]. The protective properties of the organic film can be increased by use of anticorrosive pigments. The performance of a coating can be evaluated from electrochemical techniques [2].

### Experimental

The protective coatings were obtained from polyester resins with ZnO pigment on iron substrate. Four types of resin are used: R1 fat alkyd; R2 medium alkyd, modified with aromatic polyurethane; R3 medium alkyd, modified with styrene and R4 medium alkyd, modified with aliphatic polyurethane. From each type of resin four formulations are prepared with different volumetric pigment content (**Table 1**).

Properties of the coatings were investigated by electrochemical impedance spectroscopy (EIS) and polarization experiments in 3% NaCl solution.

Before each measurement the iron electrode was carefully polished mechanically with SiC paper and spray with different degrees of diamond abrasive to mirror-surface (glossy).

EIS measurements were performed using FRA AUTOLAB 302N module in the frequency range of 0.1 Hz to 100 kHz and an amplitude AC voltage of 10 mV with. Each spectrum was collected containing 60 points with a logarithmic distribution of 10 points per decade. Experimental electrochemical impedance data were modeled using an equivalent electrical circuit by Levenberg-Marquardt CNLS procedure using the software-Scribner Associates Inc. Zview.

**Table 1.** Characteristic of prepared coatings

No.	Code sample	Resin type	VPC*, %
1	V1	R1 fat alkyd	64.69
2	V2		44.16
3	V3		25.70
4	V4		15.09
5	V5	R2 medium alkyd, modified with aromatic polyurethane	36.89
6	V6		3.3
7	V7		16.58
8	V8		16.22
9	V9	R3 medium alkyd, modified with polystyrene	75.80
10	V10		47.10
11	V11		28.53
12	V12		17.07
13	V13	R3 medium alkyd, modified with aliphatic polyurethane	42.49
14	V14		27.42
15	V15		17.44
16	V16		17.08

\*volumetric pigment content

From the polarization curves  $E_{corr}$  - corrosion potential;  $J_{crt}$  - critical corrosion current density were determined.

### Results and discussion

The Bode and Nyquist diagrams obtained for electrodes coated iron V3, V7, V11 and V15 coatings polyester resins immersed in 3% NaCl solution are shown in **Figure 1**.

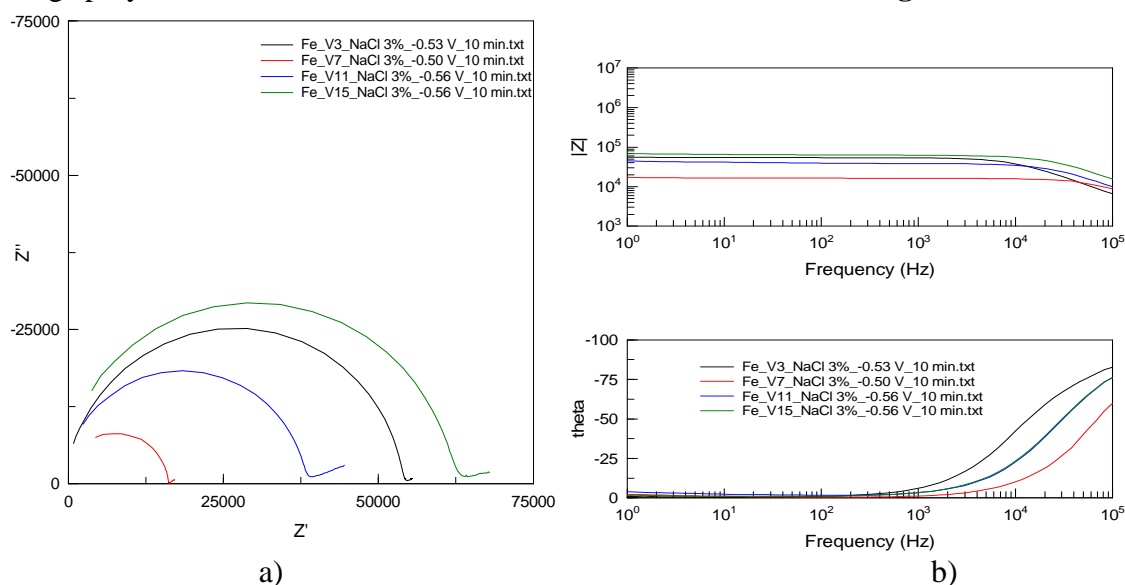


**Figure 1.** a) Nyquist diagram and b) Bode diagram (module of impedance and faze angle) for V3, V7, V11 and V15 coatings at 10 minute minute of immersion in 3% NaCl solution at OCP, V

Impedance spectra analysis revealed the presence of two time constants. A time constant due to the organic layer shaped by capacity -  $C_c$  and resistance of polymer film –  $R_p$  elements, capable to describes the dielectric and barrier properties of organic coating. The second time constant refers to the corrosion reactions and modeling / metal interface of the polymer film



(capacity double layer - Cdl and charge transfer resistance - Rct). Comparing the impedance values of the coatings at the same VPC content, thickness and also exposure time, it was noted that they are dependent on the type of polyester resin.

The polarization resistance values obtained after modeling using equivalent electrical circuit for polymer films are between  $10^4 \sim 10^6 \text{ ohm cm}^{-2}$  and increase in general for the same type of resin with the increase of the volumetric pigment content (VPC %) (**Figure 2**).

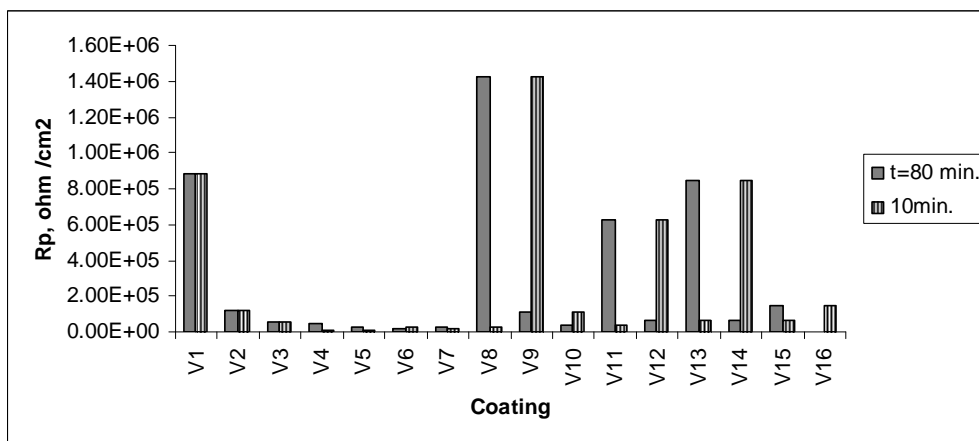


**Figure 2.** Variation of polarization resistance  $R_p$  with resin type for all coating formulation

The polarization resistance of polymer films shows that at a volumetric pigment concentration between 15-65 % it decreases in the order: resin R4 aliphatic polyurethane modified alkyd medium, followed by oil alkyd resin R1, R3 alkyd resin average modified styrene resin, R2 alkyd average modified aromatic polyurethane. For the same pigment concentration (25 %) it was observed that  $R_p$  is the maximum for resin R4, and at a lower concentration of pigment in resin type R3 (15%) allow to obtain a film with a higher  $R_p$  (**Figure 2**).

In time the coating capacitance ( $C_c$ ) coating usually increases due to the water uptake as a result of the capillary action in the micro pore/defect structures. The volume fraction of water absorbed ( $W$ ) can be calculated from coating capacitance ( $C_c$ ) by equation (1) [4].

$$W = \frac{\log[C_t/C_0]}{\log 80} \quad (1)$$

where  $W$  is the volume fraction of the absorbed water,  $C_t$  is the coating capacitance at time  $t$ ,  $C_0$  is the capacitance at  $t = 0$ , and 80 is the dielectric constant of water. In this investigation, the coating capacitance measured after 10 min. of immersion is taken as  $C_0$  and after 80 min. of immersion as  $C_t$ . The water uptake are lower than 0.06 for all coatings and was observed that the fraction of water uptake decrease with decrease of VPC in the formulation for R1 resin. For V7 respectively V15 the  $W$  presents the highest value. For the same VPC (15%),  $W$  is higher for R4 and pointed out that at lower VPC the  $W$  is affected substantially by resin type. R4 resin seems to be the less hydrophobic one. At a higher VPC (25%) the R1 resin is less hydrophobic. From potentiodynamic polarization curves the corrosion currents and corrosion rate were determined (**Figure 3**).

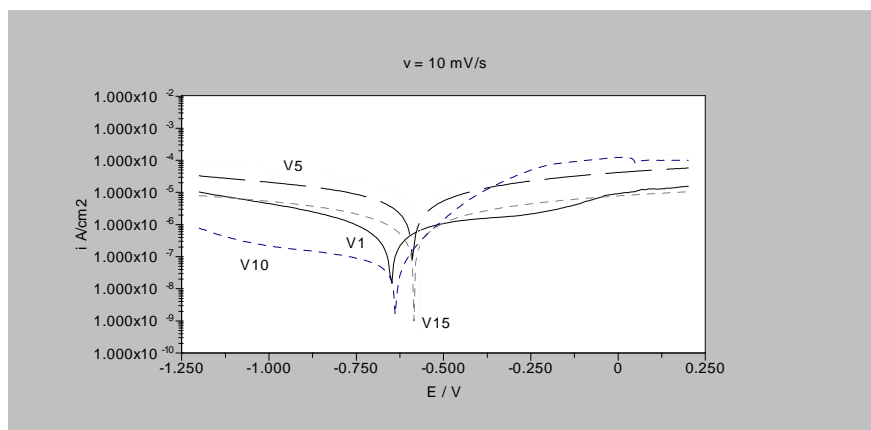


**Figure 3.** Potentiodynamic polarization curves for V1, V5, V10 and V15, scan rate 10 mV/s.

For R1 resin with 25-65 % VPC, R3 resin with 17-75 % VPC and R4 resin 17-47 % corrosion currents are lower. For a volumetric pigment concentration of 15 % and 20 % the lowest corrosion currents was obtained for resins R4. The corrosion rates,  $R_{corr}$  determined from polarization curves for polyester films shows the same behavior observed for  $R_p$  data from EIS (**Figure 4**).

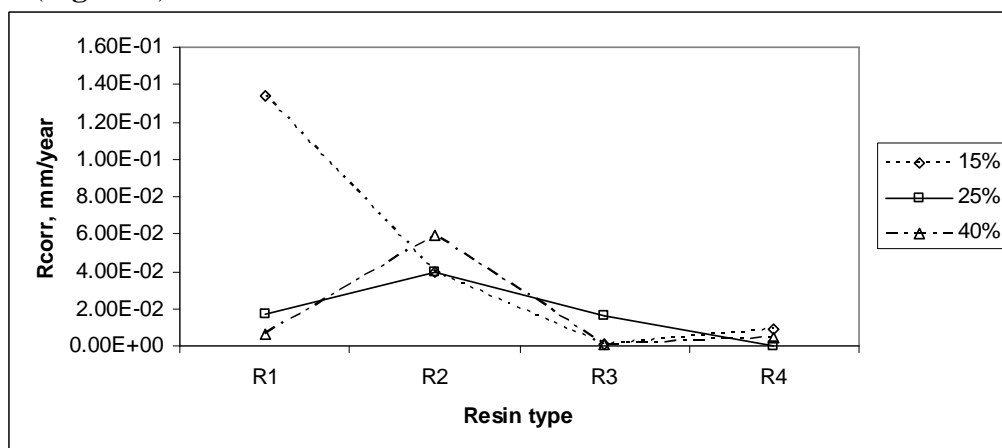


**Figure 4.** Corrosion rates ( $R_{corr}$ ) determined from polarization curve for different VPC

## Conclusion

The corrosion rates decreases in the order: R4, followed by resin R3 and R1 and R2. For the same concentration of pigment, the corrosion rate is lower for films based on resin R4.

## References

- [1]. B.Bieganska, M. Zubielwicz, E. Smieszek, Prog. Org. Coat. 16 (1988) 219–229.
- [2]. L. Derosa, T. Monetta, F. Bellucci, D.B. Mitton, A. Atienza, C. Sinagra, Prog. Org. Coat. 44 (2002)153-159.
- [3]. S. Duval, M. Keddam, M. Sfaira, A. Shiri, H. Takenouti, J. Electrochem. Soc., 149 (2002) B520.
- [4]. S.K. Singh, S.P. Tambe, G. Gunasekaran, V.S. Raja, D. Kumar, Corrosion 21 3(2009) 595.

## Unfired Clayey Pellets as the Adsorbents for Metal Ions Removal from a Waste Printing Developer

Jelena Kiurski <sup>1\*</sup>, Jonjaua Ranogajec <sup>2</sup>, Vesna Kecić <sup>1</sup>, Ivana Oros <sup>1</sup>

<sup>1</sup>University of Novi Sad, Faculty of Technical Sciences, Trg Dositeja Obradovica 6,  
21000 Novi Sad, Serbia

<sup>2</sup>University of Novi Sad, Faculty of Technology, Bulevar Cara Lazara 1,  
21000 Novi Sad, Serbia  
e-mail: kiurski@uns.ac.rs

### Abstract

The paper analyses the application of various forms of unfired clay pellets (whole and half), for the removal of zinc and copper ions from a waste printing developer. The adsorption experiments were performed in batch mode. The textural properties of defined clayey pellets were examined by mercury porosimetry.

Textural characterization showed a significant amount of the small pores in the case of whole pellets in relation to half pellets. The efficiency of the metal ions removal significantly increases with the increase of the adsorbents mass. The removal efficiency varied between 50 and 94%. Considering the adsorption efficiencies, the following order of unfired clay pellets was noticed: whole pellet > half-pellet. The ionic radius of metal ions and the obtained trends of adsorption efficiency show that the selectivity sequence of metal ions on the unfired clay pellets was Zn > Cu.

Therefore, the unfired clayey adsorbents present the promising alternatives for purification of waste printing developers.

### Introduction

Industrial wastewaters are often characterized by considerable heavy metal content and, therefore, it is required to treat them prior disposal into water. The heavy metals, such as lead, copper, cadmium, zinc, silver and nickel are the most common pollutants found in industrial and printing effluents [1, 2]. Adsorption with the clayey minerals is the low-cost promising alternatives for the treatment of heavy metals present in wastewater. There are many advantages of using clay as an adsorbent: cost of clay is relatively low compared to other alternative adsorbents; clay minerals have high specific surface area, excellent physical and chemical stability and other structural and surface properties [3]. Thus, clays can adsorb all kinds of pollutants from large volumes of aqueous solutions. Also, clays are used as barriers to prevent contamination of the subsoil and groundwater by the leaching of landfill containing metals [3, 4].

The aim of this research was to evaluate the adsorption efficiency of different forms of unfired clay pellets for waste printing developer purification.

### Materials and methods

*Printing developer.* The sample of waste printing developer was taken from an offset printing facility in Novi Sad (Serbia).

*Clayey pellets.* The newly designed unfired clayey pellets (whole and half) of diameter size 15 mm were chosen as the adsorbents. The raw clayey mixture consists of natural pozzolanic material, waste glass, surfactant and wooden dust. The material was shaped by extrusion and dried at 105 °C during 24h in laboratory conditions [5].

The textural properties of the unfired clayey pellets were examined by mercury porosimetry [6].

**Methods.** The adsorption experiments were performed in batch mode at standard procedure [6]. In order to reach the adsorption equilibrium waste printing developer were shaken for 30 min (the optimal contact time for defined adsorbent) [7]. The residual concentrations of Zn(II) and Cu(II) ions were determined by Inductively Coupled Plasma Mass Spectrometry method using a PerkinElmer Elan 5000 mass spectrometer.

## Results and discussion

### *Characterization of the unfired clay pellets*

The investigation of textural properties by mercury injection is very suitable for the characterization of porous structures in the range of the pore radius of 0.05  $\mu\text{m}$ . The results of textural characteristics are shown in Figure 1 and Table 1. Based on the obtained results it was observed a monomodal pore radius distribution of the investigated adsorbents, Figure 1.

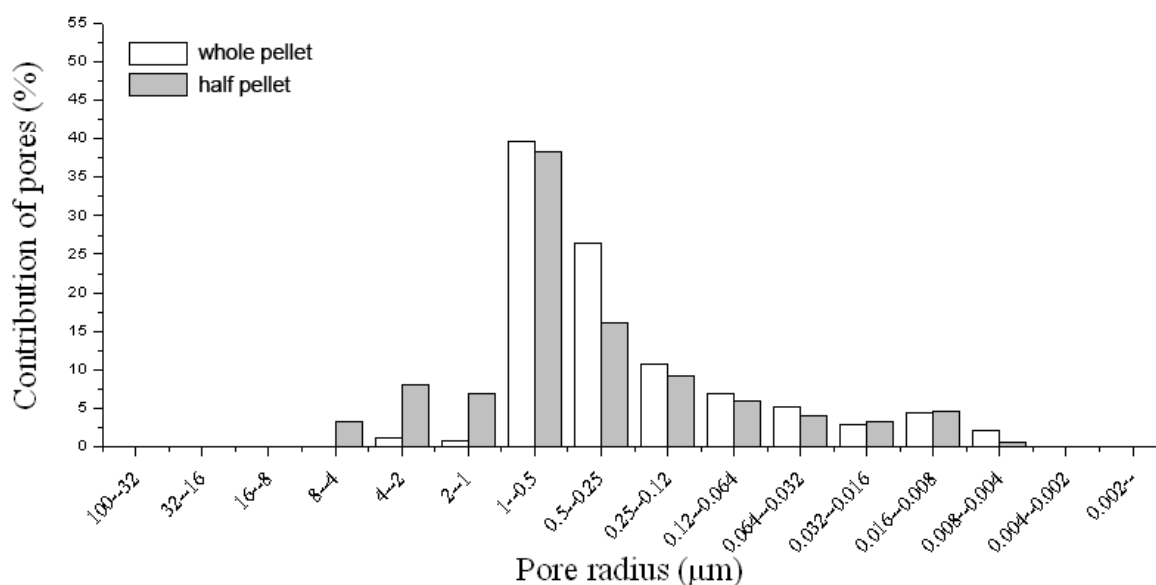


**Figure 1.** Pore size distribution of the unfired clayey pellets

The pore size distribution analysis of the unfired clay pellets (whole and half) indicates the presence of a significant amount of the large pores (pore radius above 1  $\mu\text{m}$ ) in the case of half pellets in relation to whole pellets. Whole pellets are characterized by a slightly larger amount of small pores less than 1  $\mu\text{m}$ , Figure 1. Also, whole pellets showed a higher specific surface area (4.51  $\text{m}^2/\text{g}$ ) in relation to half pellets, Table 1.

**Table 1.** The results of specific surface area

Unfired clay pellet	Specific surface area ( $\text{m}^2/\text{g}$ )
whole	4.51
half	3.85

### *Adsorption efficiency*

The increase of the metal ion adsorption with the usage of clayey materials can be attributed to the increased surface area and the availability of more adsorption sites [8]. Also, the chemical and mechanical stability allow their application in various states and improve the consistency of adsorption relative to less stable materials [8-10].

The influence of unfired pellets forms on the adsorption efficiency, Figure 2a and 2b, indicates that the removal of zinc and copper ions from a waste printing developer increases

with the increase of the adsorbent mass. The maximum adsorption efficiencies of the zinc ion removal by using whole and half pellets were 94.1 and 88.3%, respectively (Figure 2a). Whole and half pellets showed the lower adsorption efficiency (62.4 and 50.4%, respectively) for copper ion removal, Figure 2b. Considering the adsorption efficiencies of used adsorbents the following decrease order was obtained: whole pellet > half pellet.

As whole pellets show a higher surface functionality (specific surface area  $4.51 \text{ m}^2/\text{g}$ , Table 1) a great number of sites is available for the interaction with zinc and copper ion present in a waste printing developer. Beside the availability of the surface sites, the observed trend of adsorption efficiency can also be related to the pore size distribution of whole pellets, Figure 1.

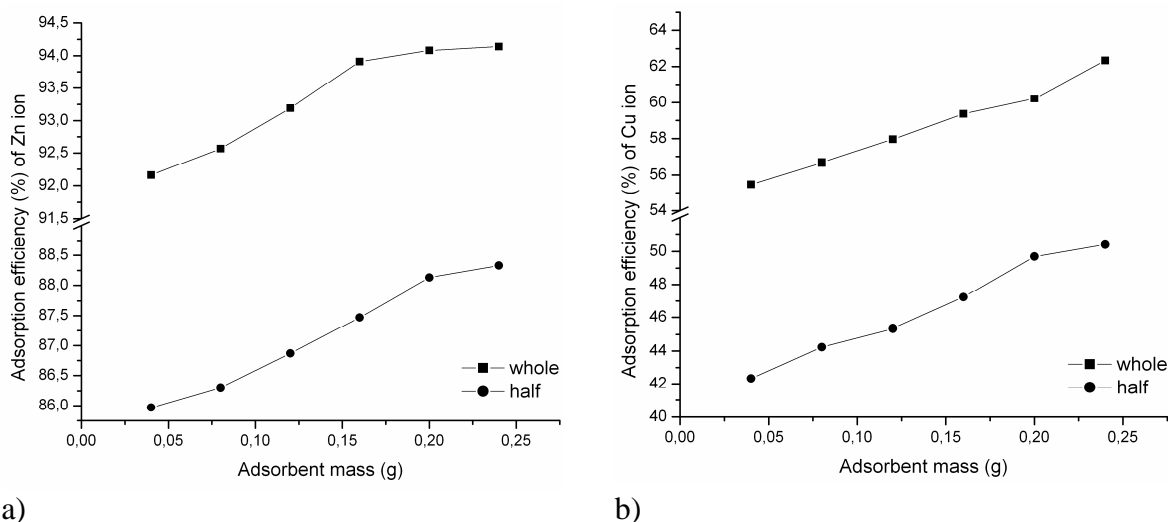


**Figure 2.** Efficiency of zinc (a) and copper (b) ions removal using unfired clay pellets

The trends of adsorption efficiency can also be explained based on the ionic radius of metal ions. The smaller ionic radius of a metal ion means the higher adsorption rate [11]. As  $\text{Zn(II)}$  and  $\text{Cu(II)}$  ions have approximately the same ionic radius it is expected the same removal efficiency. Our study shows that the selectivity sequence of metal ions on the unfired clay pellets is  $\text{Zn} > \text{Cu}$ .

## Conclusions

The adsorption efficiency of the unfired clay pellets (whole and half) was tested in order to remove zinc and copper ions from a waste printing developer. The presence of a significant amount of the small pores (pore radius less than  $1 \mu\text{m}$ ) was observed in the case of whole pellets in relation to half pellets. The maximum adsorption efficiencies of zinc (94%) and copper (62%) ions removal were achieved by using whole pellets. Considering the adsorption efficiencies of used adsorbents the following decrease order was obtained: whole pellet > half pellet. Based on the obtained adsorption efficiency the selectivity sequence of metal ions on the unfired clay pellets was  $\text{Zn} > \text{Cu}$ .

## Acknowledgements

The research is financed by the Ministry of Education, Science and Technological Development of the Republic of Serbia (Projects No. TR 34014 and III 45008).

## List of references

- [1] F. Geyikci, H. Buyukgungor, *Acta Geodyn. Geomater.* 10(3) (171) (2013) 363.

- [2] J.S. Kiurski□, I.B. Oros, N.M. Ralevic, J. Stefanov, Stoch. Env. Res. Risk. A. Online First (2014), DOI 10.1007/s00477-014-1013-1.
- [3] W.J. Chen, L.C. Hsiao, K.K.Y. Chen., Process Biochem. 43 (2008) 488.
- [4] G. Zhao, X. Wu, X. Tan, X. Wang, The Open Colloid Science Journal 4 (2011) 19.
- [5] J. Ranogajec, D. Zorić, O. Rudić, J. Kiurski, International Congress of Energy Efficiency and Energy Related Materials, Kemer, Turkey, 2013, pp. 53.
- [6] J. Kiurski, J. Ranogajec, V. Kecić, O. Rudić, I. Oros, International Conference on Engineering and Applied Sciences Optimization, Kos, Greece, 2014, pp. 2907.
- [7] J. Kiurski, J. Ranogajec, M. Vučinić Vasić, V. Kecić, I. Oros, 12th International Conference on Fundamental and Applied Aspects of Physical Chemistry (Physical Chemistry 2014), Belgrade, Serbia, Vol. III, 2014, pp. 889.
- [8] B. Bedford, Earth and Planetary Materials (2015), pp. 1, Available at: [http://www.academia.edu/6113926/Clays\\_in\\_the\\_removal\\_of\\_heavy\\_metals](http://www.academia.edu/6113926/Clays_in_the_removal_of_heavy_metals) (Accessed 16 March 2015).
- [9] S.M. Abd-Allah, O.M. El Hussaini, R.M. Mahdy, Australian Journal of Basic and Applied Sciences 1(4) (2007) 813.
- [10] N. Karapinar, R. Donat, Desalination 249 (2009) 123.
- [11] J.C. Igwe, A.A. Abia, Eclet. Quím. 32(1) (2007) 33.



## Statistical Interpretation of Carbon Dioxide Emission in the Photocopying Process

Jelena Kiurski<sup>1\*</sup>, Ivana Oros<sup>1</sup>, Vesna Kecić<sup>1</sup>, Snežana Aksentijević<sup>2</sup>

<sup>1</sup>University of Novi Sad, Faculty of Technical Sciences, Trg Dositeja Obradovica 6,  
21000 Novi Sad, Serbia

<sup>2</sup>Business Technical College, Trg Svetog Save 34, 31000 Užice, Serbia  
e-mail: kiurski@uns.ac.rs

### Abstract

The concentration levels of carbon dioxide, monitored in indoor of three photocopying shops in Novi Sad, Serbia, were subjected to two-way ANOVA, in order to investigate statistically significant emission, due to the different sampling points and time intervals. Obtained results pointed out that only selection of time interval significantly affects the emission of carbon dioxide. In addition, the least significant difference test indicated that second time interval has the greatest influence on the CO<sub>2</sub> emission, whereas the CO<sub>2</sub> concentrations of the second time interval were subjected to further cluster analysis. Hierarchical clustering grouped three photocopying shops into four clusters with similar CO<sub>2</sub> concentration levels.

### Introduction

Carbon dioxide (CO<sub>2</sub>) is a natural constituent of the atmosphere, but in increased concentration it can be harmful to human health. Carbon dioxide can be present in occupational environment as a result of people's respiration process, as a product of combustion and as a component of soil gas. Also, it can be produced during the photocopying process, when photocopier or laser printer toner is heated in an inadequate air supply. Further, paper and electricity consumption, as well as human activity during the photocopying process can indirectly contribute to the formation of CO<sub>2</sub> [1]. The importance of controlled carbon dioxide emission is reflected through global warming potential, considering carbon dioxide as a principal greenhouse gas. Since 36% of CO<sub>2</sub> emission is attributable to manufacturing industries, controlled emission is considered as a major requirement and a principal part of environmental maintenance [2].

The present study aims to examine a carbon dioxide emission in three photocopying shops. A two way analysis of variance (ANOVA) with *post hoc* test, as primary statistical methods, was applied in order to investigate the statistically significant differences of pollutant emission. The obtained results served as a basis for further application of cluster analysis, in order to investigate the similarities/dissimilarities between analyzed photocopying shops, in terms of carbon dioxide emission.

### Materials and methods

*Sampling method.* Five day measurements of carbon dioxide were carried out in three photocopying shops located in Novi Sad, Serbia. Air samples were collected and analyzed by using an instrument Aeroqual Series 200 (Aeroqual Limited, New Zealand). Three sampling points A, B and C (A and B – near photocopier machines; C – near the door) were selected based on the CO<sub>2</sub> emission sources. Also, three time intervals were chosen during the day: at the beginning of the working time - from 8 to 10 a.m., during the maximum productivity time - from 13 to 15 p.m. and the end of the working time - from 16 to 18 p.m. [3].

*Two way ANOVA with post hoc test.* The two-way ANOVA is statistical method that examines the influence of two different categorical independent variables on one continuous dependent variable. Obtained results of ANOVA test are interpreted by *F*-value for each factor, which is compared to *F*<sub>critical</sub>, obtained from the table of limit values of *F* distribution

for a certain degrees of freedom. Statistically significant difference exists between observed groups if the value of parameter  $F$  is higher than  $F_{critical}$ , meaning that independent variable has effect on the observed dependent variable [4]. However, the calculated  $F$  value using the ANOVA test does not give an answer to the question whether a statistically significant difference occurs between the mean values of all groups or only between particular groups. Therefore, it is necessary to test the differences between arithmetic means of samples and to determine the correctness of certain alternative hypothesis, which is performed using various *post hoc* tests. The most commonly used *post hoc* test is the least significant differences (LSD) test that compare differences between the absolute values of the examined groups  $|\overline{x_i} - \overline{x_{i+1}}|$  with a critical value, LSD. The difference between two samples is significant if the difference between two sample means is larger than LSD value, and vice versa [4].

**Cluster analysis.** Clustering is one of the most widely used multivariate techniques for exploratory data analysis. The purpose of cluster analysis is to maximize between-group variance and minimize within-group variance by grouping the data objects, based only on information found in the data. In this way, a relationship between the objects is described. Cluster analysis organizes natural groups within the data in such way that each element in the group is similar to each other as possible. At the same time, the groups are dissimilar to other groups [5]. If plotted, geometrically, the objects within the clusters will be close together, while the distance between clusters will be farther apart. If the similarity or homogeneity within a group is greater, the clustering will be better, or more distinct. Cluster analysis is not a statistical technique and the results obtained are justified according to their value in interpreting data and indicating patterns [6].

All the data in ANOVA test and cluster analysis were analyzed using Microsoft Excel 2007 and XLSTAT 2015.1.01.

## Results and discussion

Carbon dioxide emission in the indoor environment may vary depending on the selection of time interval and sampling point, which are identified as factor A and factor B in the present experiment. In order to determine the statistically significant differences in carbon dioxide emissions due to the defined factors, two-way ANOVA without replication was applied on the average CO<sub>2</sub> concentrations in three photocopying shops (Table 1), as primary statistical method in the interpretation of the experimental results. The results of two-way ANOVA are presented in Table 2.

**Table 1.** Average carbon dioxide concentration (ppm)

<b>Photocopying shop 1</b>	1 <sup>st</sup> time interval	2 <sup>nd</sup> time interval	3 <sup>rd</sup> time interval
Sampling point A	1075.16	1186.68	1041.72
Sampling point B	1100.20	1247.88	1053.12
Sampling point C	1097.16	1202.76	1034.96
<b>Photocopying shop 2</b>	1 <sup>st</sup> time interval	2 <sup>nd</sup> time interval	3 <sup>rd</sup> time interval
Sampling point A	911.16	960.84	913.60
Sampling point B	896.72	941.36	913.64
Sampling point C	884.60	940.48	920.80
<b>Photocopying shop 3</b>	1 <sup>st</sup> time interval	2 <sup>nd</sup> time interval	3 <sup>rd</sup> time interval
Sampling point A	874.56	846.28	856.28
Sampling point B	875.96	848.72	864.20
Sampling point C	880.44	844.52	876.56

**Table 2.** Results of two-way ANOVA without replication

	Photocopying shop 1	Photocopying shop 2	Photocopying shop 3
<i>Source of Variation</i>	<i>F-value</i>		
Sampling point	3.69	1.77	1.45
Time interval	101.69	22.21	20.73

The obtained  $F$ -values were compared to the  $F_{critical}$  value of 6.94 for significance level  $\alpha = 0.05$  and the degrees of freedom  $d_f = 2$  and 4. Based on the obtained results,  $F$ -values for factor A - time interval (101.69; 22.21; 20.73) in all photocopying shops were significantly higher than  $F_{critical}$ , in contrast to factor B (sampling point). On that basis, it can be concluded that only selection of time interval significantly affects the emission of carbon dioxide, as opposed to the selection of sampling points. In order to compare statistical differences between time intervals, the least significant difference test is applied. The results are presented in Table 3, where  $x_1$ ,  $x_2$  and  $x_3$  represent the average  $CO_2$  concentration in first, second and third time interval, respectively.

**Table 3.** Results of Least significant difference test

	Photocopying shop 1	Photocopying shop 2	Photocopying shop 3
$ \bar{x}_1 - \bar{x}_2 $	<b>121.60</b>	<b>50.07</b>	<b>30.48</b>
$ \bar{x}_1 - \bar{x}_3 $	47.57	18.52	11.30
$ \bar{x}_2 - \bar{x}_3 $	<b>169.17</b>	<b>31.55</b>	<b>19.18</b>
LSD <sup>a</sup>	62.38	21.06	13.26

<sup>a</sup>least significant difference value

Obtained results of LSD test (Table 3) pointed out that highly significant difference exists between the first and second, as well as between the second and third time interval (bold values), indicating that the second time interval is the most significant in terms of carbon dioxide emission. Based on the obtained results, only the average  $CO_2$  concentrations from second time interval are used for further mathematical processing, applying cluster analysis. Cluster analysis included a hierarchical clustering using the Euclidean distance as a measure of the similarities/disimilarities, as well as Ward's methods of connecting objects. Hierarchical clustering was performed with the aim to group photocopying shops per sampling day, based on the determined carbon dioxide emissions. The result of clustering is presented in a form of dendrogram (Figure 1) which provides a visual representation of analyzed data set grouping (photocopying shop\_sampling day). Four clusters are observed on dendrogram: cluster 1 (1\_1, 2\_3, 2\_5 and 3\_3), cluster 2 (1\_2, 1\_4, 1\_5, 2\_1, 2\_2 and 3\_2), cluster 3 (1\_3) and cluster 4 (2\_4, 3\_1, 3\_4 and 3\_5). In all formed clusters each member is most similar to its adjacent member. It can be observed that cluster 3 corresponds to the photocopying shop 1\_third sampling day, where was the the highest  $CO_2$  emission during the photocopying process. The remaining clusters 1, 2 and 4 grouped the photocopying shops per sampling day based on the similar carbon dioxide emissions.

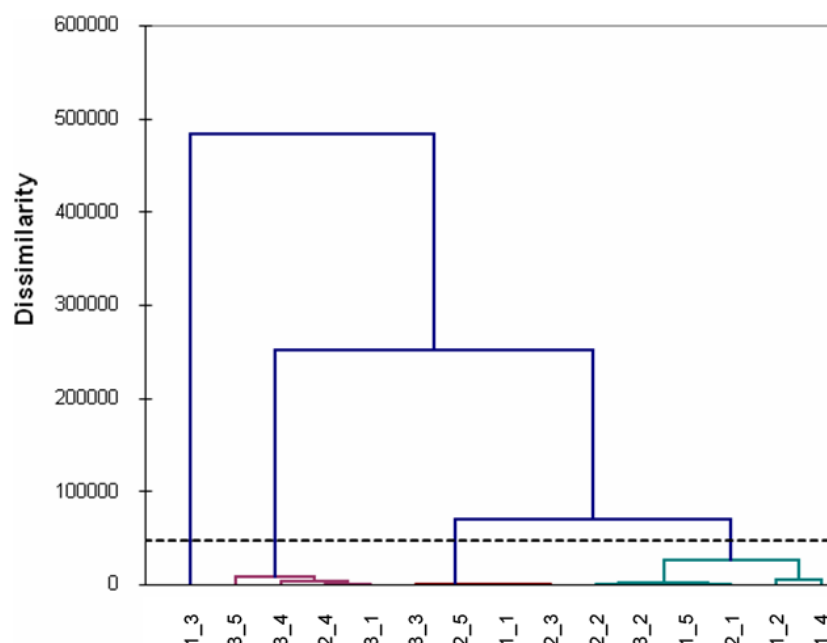


**Figure 1.** Clustering of photocopying shops according to the carbon dioxide emission

### Conclusions

A two way ANOVA with least significant difference test was performed in order to determine the statistically significant emission of carbon dioxide during the photocopying process, due to the different sampling points and time intervals. Given that the results pointed out that second time interval had the greatest influence on carbon dioxide emissions, only the average CO<sub>2</sub> concentrations from this time interval were subjected to cluster analysis. Hierarchical clustering grouped three photocopying shops into four clusters based on similar carbon dioxide emission. Cluster 3 corresponds to photocopying shop 1\_third sampling day with the highest CO<sub>2</sub> emission, which is in a compliance with the obtained results of CO<sub>2</sub> measurement.

### Acknowledgement

The authors acknowledge the financial support of the Ministry of Education, Science and Technological Development of the Republic of Serbia, in the frame of Project applied under No. TR 34014.

### References

- [1] M. Santamouris, A. Synnefa, M. Assimakopoulos, I. Livada, K. Pavlou, M. Papaglas, D. Kolokotsa, V. Assimakopoulos, *Energ. Buildings*. 40 (2008) 1833.
- [2] X. Wang, Z. Duan, L. Wua, D. Yang, J. *Clean. Prod.* 103 (2015) 705.
- [3] J. Kiurski, S. Aksentijević, I. Oros, V. Kecić, 7th International Scientific Conference "Science and Higher Education in Function of Sustainable Development-SED2014", Užice, Serbia, 2014, pp. 16.
- [4] M. Hadži Stojković, in: *Statistics, Descriptive and statistical analysis*, Faculty of Economy, Subotica, University of Novi Sad, 2006. pp. 75. in Serbian
- [5] Yu. Pepelyshev, Ts. Tsogtsaikhan, *Ann. Nucl. Energy*. 83 (2015) 50.
- [6] D.J. Kern, K.E. Culley, *Comput. in Hum. Behav.* 49 (2015) 313.

## Cadmium in Industrial Wastewater

Snežana Aksentijević<sup>1\*</sup>, Jelena Kiurski<sup>2</sup>, Vesna Kecić<sup>2</sup>, Ivana Oros<sup>2</sup>

<sup>1</sup>*Business Technical College, Trg Svetog Save 34, 31000 Užice, Serbia*

<sup>2</sup>*University of Novi Sad, Faculty of Technical Sciences, Trg Dositeja Obradovica 6,  
21000 Novi Sad, Serbia*

*e-mail: sneza.aksentijevic@gmail.com*

### Abstract

The concentration of cadmium in the industrial wastewater discharged from the aluminium and copper metal processing industry was analysed. The samples of water and sediment were taken from the Dragića Stream and the river Đetinja, downstream from the place where the wastewater from the metalworking industry flows into the Dragića Stream. According to the measured metal concentrations in the water and pursuant to the Regulations on Hazardous Substances in Water, issued by the Republic of Serbia, the water from the Dragića Stream belongs to the II class. Based on the obtained results, it was determined that the amount of metals in the water samples taken during the spring/summer season was relatively low, and that cadmium was dominantly present in the sediment.

### Introduction

Cadmium is present in the atmosphere, soil and water, and its increased concentrations can cause serious damage to all living organisms [1]. Although has no essential biological function, its presence has been detected in more than 1,000 species of terrestrial and aquatic flora and fauna [2]. The concentration of cadmium in wastewater is usually low, but since it is a very toxic element, known for its tendency to accumulate in living organisms, it is important to determine even these minimum concentrations. Phosphatic fertilizers are the greatest anthropogenic source of cadmium in Western countries responsible for 58% of the total amount. Atmospheric gasses and sewage sludge contributes with cadmium release of 39 - 41% and 2 - 5%, respectively. The livestock manure contains 0.3 - 1.8 mg/kg Cd in its dry matter [3]. Cadmium is a relatively mobile element in the nature and the Cd<sup>2+</sup> cation is stable at a wide range of pH values. It has a tendency to accompany zinc in the geological material, where the Cd/Zn ratio can range from 1/100 to 1/1000. It is highly toxic for both humans and animals. It tends to accumulate in the organism, most often in kidneys, liver, pancreas, thyroid gland and bones. Cadmium displaces calcium in bones making them brittle. It has been proved to be cancerogenic and mutagenic [4].

### Materials and methods

Eight different sampling localities were selected. The samples were taken from the Dragića Stream to which the wastewater from the metalworking industry is discharged, and downstream the river Đetinja, starting from the place where the Dragića stream joins it. Localities 1 - 4 are on the Dragića Stream, at each 50 meters, starting from the place where the wastewater reaches it. Location 5 is at the place where the Dragića Stream joins the river Đetinja, whereas localities 6 - 8 are downstream the river Đetinja, at each 500 meters. There is arable land at the distance of only a few meters from the bank (localities 6 and 7). Near locality 8, on the right side of the river, is an asphalted local road and, on the left side, there are meadows and agricultural land. At the place where the wastewater is discharged into the Dragića Stream, the water is grey, greasy and smelly. There is a lot of solid waste on the banks, as well as in the water itself (plastic bags, packages, glass, metal and textile products, rotten agricultural products) [5].

*Preparation of water samples.* The handling, storage and preparation of water samples were performed in compliance with the standard EPA 200.7 method [6]. Water samples were placed in plastic containers of 1L, previously washed with the 10% nitric acid solution. Immediately before the sample collection process, the containers were rinsed twice with the water from a certain locality and stored at the temperature of  $-30^{\circ}\text{C}$  until the beginning of the analysis.

*Preparation of sediment samples.* The surface sediment samples were collected into plastic containers of 1L, using the EPA 3050 B method [7]. Collected sample weighed 1-2 g (wet weight) or 1 g (dry weight) and  $10\text{ cm}^3$  of 1:1 nitric acid ( $\text{HNO}_3$ ) was added to it. The sample was heated without boiling at the temperature of  $95^{\circ}\text{C}$  for 10-15 minutes. After the colling,  $5\text{ cm}^3$  of cc  $\text{HNO}_3$  was added to the sample. The same process was being repeated during the period of 30 minutes. The appearance of the brown fume indicated the oxidation of  $\text{HNO}_3$ . Then again  $5\text{ cm}^3$  of cc  $\text{HNO}_3$  was added, until the reaction of the sample with  $\text{HNO}_3$  at the temperature of  $95^{\circ}\text{C}$  during the period of 2 hours was complete. The sample was cooled for 5 minutes.  $2\text{ cm}^3$  of water and  $30\text{ cm}^3$  of hydrogen peroxide ( $\text{H}_2\text{O}_2$ ) were added to it. After heating at the temperature of  $95^{\circ}\text{C}$  for 2 hours, the volume reduced to  $5\text{ cm}^3$ . The purpose of this step was to ensure minimal losses because of the extremely strong reaction.  $10\text{ cm}^3$  of cc  $\text{HCl}$  was added, and the sample was kept for 15 minutes at the temperature of  $95^{\circ}\text{C}$ , after which it was ready for the analysis.

*Sampling methods.* The inductively coupled plasma atomic emission spectrometry (ICP-AES) was used to determine the cadmium concentration in the solution. The ICAP 6500 Duo (Therm Scientific, USA) instrument was used, with the detection limit of 0.09 ppb.

## Results and discussion

The quantity and quality of industrial wastewater can vary widely during a day, even when it comes from the same industrial plant. This is due to the dynamics of wastewater generation during the production process, but also due to the different intensity of operations in an industrial plant. Neither the quality, nor the contamination of wastewater, and therefore the total pollution caused by wastewater, is uniform, especially in the case of discontinual, batch production processes. In the metal processing industry, such as copper and aluminium mills, the quantity of wastewater is relatively small, but it contains very large and specific amounts of toxicants (extreme pH values, the presence of oil, heavy metals, copper, chome, lead, zinc and cadmium, as well as phenol). This can cause the changes in the physical and chemical conditions of the sediment containing such metals, which leads to the resuspension and dissolution of the contaminants adsorbed or coprecipitated in the sediment. The resuspension of a part of the sediment causes the increase in the concentration of heavy metals in the aqueous phase, no matter if these metals are in the suspended, collodal or dissolved form. The cadmium concentrations in the wastewater and sediment samples collected on the Dragića Stream in the spring/summer 2009 (sample localities 1-8) are given in Table 1.



Table 1. Cadmium concentrations in water and sediment

Sampling locality	Concentration of cadmium (mg/L)			
	Water		Sediment	
	spring	summer	spring	summer
1	0.0005	-	0.09	1.60
2	0.0005	0.0001	0.08	1.46
3	0.0009	0.0001	0.32	1.60
4	0.0030	-	0.43	1.02
5	0.0008	0.0001	0.15	1.46
6	0.0005	0.0001	0.65	0.007
7	0.0004	0.0001	0.14	0.02
8	0.0003	0.0001	0.24	0.01

The cadmium concentration in the water ranged from  $1 \cdot 10^{-7}$  mg/L to 0.003 mg/L, and at all sampling localities, it was higher in the spring than in the summer, but did not exceed the maximum allowed concentration (MAC) [8]. The cadmium concentration in the sediment at the first five localities was higher in the summer, ranging from 0.007 mg/kg to 1.6 mg/kg, but not exceeding the MAC [9].

Based on the obtained results regarding the concentrations of metals in the water and sediment, it can be concluded that metal was dominantly present in the sediment. The water flow in the summer was substantially lower than in the spring. The Dragića Steram is directly affected by the industrial wastewater, with a low self-purification potential, which contributes to its poor quality. In the river Đetinja, the exacerbated quality of the sediment was detected. High cadmium concentrations in the samples collected in the summer were probably the result of the pressure coming from diffusion sources, such as the use of phosphate fertilizers in the agriculture, which were made from low quality raw materials. Serbia is known for the production of fertilizers by mixing raw materials and the sulfuric acid. And if there are any harmful admixtures in the raw materials (cadmium, uranium compounds, etc), these will end up in the final product [5].

## Conclusion

The study included examination of industrial wastewater and sediments quality in terms of determination of cadmium concentration in Dragića Stream during the spring/summer 2009. According to the results, the sediment quality was significantly impaired due to the increased cadmium concentration, although it did not exceed the maximum allowed concentration. This leads to the conclusion that the metal concentration in the water was relatively low, compared with the sediment. Analysing these two media separately, cadmium concentration in the spring was higher in the water than in the sediment, at all sampling localities. This was due to the high flow of water in this period of the year, which prevented the precipitation of the analysed metal in the sediment.

The efficient implementation of certain technical and technological measures during the production processes in the metal processing industry could reduce the emission of cadmium and other heavy metals and ensure the protection of the environment from the pollution with heavy metals. Continual monitoring of the mobility of metals in the water/sediment system, together with the obtained result, could make possible to predict the measures necessary for the revitalization of the watercourses of the river Đetinja and Dragića Stream, since the presence of certain metals in the water and sediment has been proved.

## **References**

- [1] M.P. Benavides, S.M. Gallego, M.L. Tomaro, *Brazilian Journal of Plant Physiology*. 17 (2005) 21.
- [2] Š. Goletić, in: *Heavy metals in the environment*, University in Zenica, 2005, pp. 115.
- [3] L. Li, Z. Xi-Bai, B. Ling-Yu, M. Xu-Rong, Y. Jia-Bo, H. Liu-Jie, *Communications in Soil Science and Plant Analysis*. 40 (2009) 2169.
- [4] M. Rodić, M. Vidović, Ž. Mirkov, S. Čupić, 5<sup>th</sup> International Symposium and Exhibition on Environmental Contamination in Central and Eastern Europe, *Symposium Proceedings*, Prague, 2000, manuscript 907
- [5] S. Aksentijević (2011): *Heavy metal distribution model*, Doctoral dissertation
- [6] B. Spence, M. Cassap, (2008) *Environmental Series - US EPA Method 200.7 using the iCAP 6500 Duo ICP*, Thermo Fisher Scientific Inc.
- [7] M. Erdogan, (2009): *Monitoring and Statistical Assessment of EPA Method 3050B*, Available at: <http://www.caslab.com> (Accessed 16 June 2015).
- [8] *Regulations on Hazardous Substances in Water* (1982) ("Official Gazette SRS", no. 31/82)
- [9] *Regulations on Acceptable Concentrations of Hazardous and Harmful Substances in Soil and Water Used for Irrigation and on the Appropriate Research Methods*, (1994) ("Official Gazette RS", no. 23/94)

## Efficient Management in Environmental Protection

Goran B. Andjelic<sup>1</sup>, Vladimir Dj. Djakovic<sup>2</sup>, Nebojsa M. Ralevic<sup>3</sup>, Jelena S. Kiurski<sup>4</sup>

<sup>1</sup>*Educons University, Faculty of Business Economy, Sremska Kamenica, Serbia*

<sup>2</sup>*University of Novi Sad, Faculty of Technical Sciences, Department of Industrial Engineering and Management, Novi Sad, Serbia*

<sup>3</sup>*University of Novi Sad, Faculty of Technical Sciences, Department of Fundamentals Sciences, Novi Sad, Serbia*

<sup>4</sup>*University of Novi Sad, Faculty of Technical Sciences, Department of Graphic Engineering and Design, Novi Sad, Serbia*

*e-mail: goran.andjelic@educons.edu.rs, v\_djakovic@uns.ac.rs, nralevic@uns.ac.rs, kiurski@uns.ac.rs*

### Abstract

The subject of this study is to research, analyse and assess the causal relations between efficient management as a useful and necessary "tool" in the daily operations and the modern aspects of environmental protection in contemporary business conditions. The research objective is to achieve the concrete, practically confirmed knowledge of practical, actually usable relation between efficient management and modern aspects and trends of environmental protection. The study methodology includes descriptive and exploratory techniques, as well as analysis and synthesis. The main research hypothesis is that without an efficient management, the optimum approach to the environmental protection cannot be expected nor can an adequate relation towards environment be ensured. The research results provide actual information about the place, role and significance of efficient management in the contemporary environmental protection.

**Keywords:** environmental protection, management, market environment

### Introduction

The contemporary market milieu constantly increases demands concerning market participants, creating at the same time new, hitherto unidentified challenges which significantly affect the entrepreneurial and market activities. In this sense, one of the key issues of market reality is an attempt to optimize the relationship between the effective and efficient business activities on the one hand, and the market environment, on the other. This relationship comprises the essence of modern business, i.e. a successful attempt at answering the question: "How to operate optimally while maximizing simultaneously available resources, which inevitably imply a dynamic, proactive and responsible approach to environmental issues?" For many years, the answer to this question has been treated as a kind of automatism, i.e. it has been assumed that a responsible entrepreneurship directly implies a protective attitude towards the environment. Practice has repudiated this view, so presently a huge number of challenges are present in the field of environmental protection, which implicitly leads to significant devastation of available resources, with a direct consequence of redefining objects, as well as resources and relations of labour. After all, the global crisis that erupted a few years ago can be viewed through the prism of environmental relations, i.e. as a "habitat" in the broadest sense of the word, its devastation and accordingly, the necessary cost redefinition as a logical disruption consequence of the natural balance established in the environment.

In this sense, the subject of this paper is an attempt to research, analyse and observe causal relations between efficient management as a useful and necessary "tool" and modern aspects

of environmental protection, in the contemporary business environment. The correlation between these important factors, i.e. management as the target-object oriented business process in the present market environment and the modern aspects of environmental protection, is intense and direct, but poorly tested in practice and therefore the specific level of causality between them is not appropriately endorsed. This is exactly what the research has intended to achieve, to respond if the efficient management process as a set of activities connoting the right things accomplished in the right way (i.e. the principle of effectiveness and efficiency) involves a systematic approach towards the environment, in terms of continual dealing with ongoing activities aimed at optimization of used resources and effect maximization of business activities, with the consequential correct attitude towards the environment. This relationship may be represented schematically as follows (*Figure 1*):

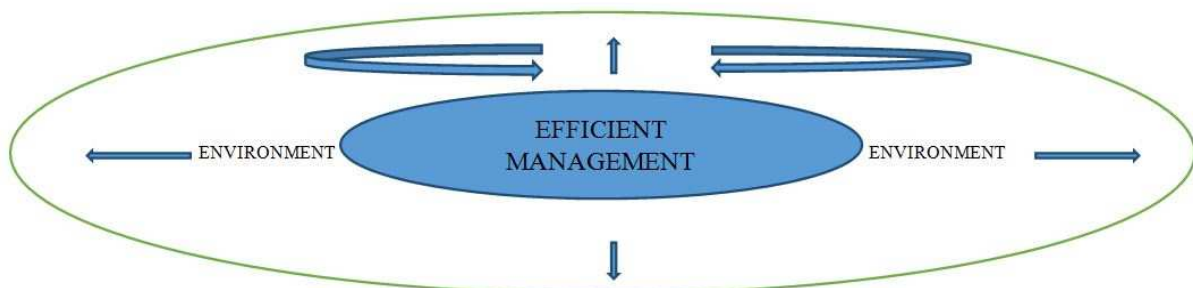


**Figure 1.** Efficient management and environment causality

*Source: the authors*

Only the efficient, cost-oriented management can contribute to the rational use of resources and the appropriate relation towards environmental factors. This fact is imposed by contemporary enterprise as an imperative for successful business.

### **Efficient management - reality or imagination?**

In modern business conditions, especially since the onset of the global crisis, much has been written and said about what can be considered as an efficient management process, and more importantly, how to measure or quantify the efficient management process, and then distinguish the efficient, less efficient and inefficient management process. Many authors have dealt with these issues and their approaches to solving this dilemma are different. Some of them praise purely technocratic optimization of business processes, while the others commend the cash flow optimization. As always, the truth is probably somewhere in the middle. Globally, the competitive advantage is achieved with an adequate attitude towards environmental protection [2]. The issues of environmental protection in small and medium-sized enterprises (SMEs) [1], and policy creation in this area [3], are particularly challenging. The specificity and originality of this work, as well as its logic, lie in the fact that the measure of management efficiency is evaluated through the prism of expenditure of environmental resources and their rational allocation and use, i.e. the achieved level of economic development can be deduced by measuring the degree of environmental protection and preservation. The concrete facts support this thesis. If the achieved level of care and general attitude towards the environment in the Nordic countries (e.g. Norway, Sweden and Finland) is evaluated as well as their level of economic development, it can be unambiguously concluded that the dynamic, intense and high level of economic development does not necessarily imply the accumulated environmental problems.

There exist many challenges in order to achieve efficient management, i.e. the one that can lead to optimal and sustainable growth with efficient use of resources and environmental protection. First, it is necessary to solve the dilemma if efficient management is reality or

imagination in the contemporary business environment. Is it possible to achieve it in practice and, more importantly, keep it? How to characterize the efficient management? Is the emphasis on costs, productivity, time, profitability or something else? It seems that the answer is very simple. In each concrete situation, efficient management has different characteristics. Many research projects have been carried out on this topic and they all share the common view that the only constant common to each form of management is its high flexibility. The efficient management is possible to achieve and maintain in practice, but only as a flexibly directed process that is system-oriented towards problem solving.

**Efficient management - the "cornerstone" of environmental protection policy**

The XXI century will undoubtedly be the century of new approaches and attitudes towards the environment, which will implement in itself the dynamism of change on the one hand and problem-oriented approach in the other. Ultimately, standardization implies the integral approach to solving certain connections and relationships in order to create processes that will enable the efficient and effective proceeding of certain activities. In this sense, the efficient management of the XXI century will necessarily include the essential aspects of the relationship towards the environment, with the control mechanisms that will contribute to its high level of flexibility and proactive attitude towards environmental issues. Experience teaches us that the lack of proactivity towards environmental issues represented the major stumbling block of all previous strategies directed towards comprehensive, systemic attitudes about environmental issues. In future, efficient management should be a starting point and an integral part of strategies intended to protect the environment. The following figure illustrates that specific concept of ordination and subordination (*Figure 2*):

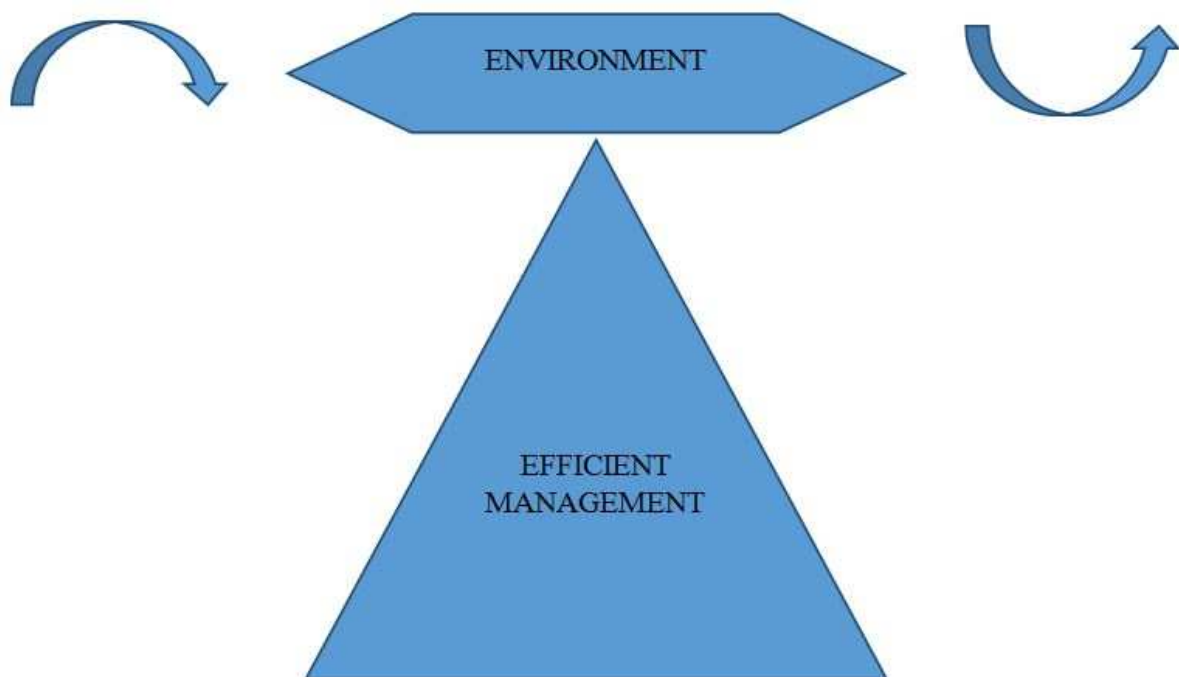


**Figure 2.** Efficient management and environment – future perspective

*Source: the authors*

The level of sensitivity existing between the efficient management and the environment can be best seen in the picture above: the balance is very difficult to achieve and maintain, yet very easy to lose.

## **Conclusions**

Considering the causality of efficient management and the environment through a holistic approach to the research subject, it is evident that it is necessary to establish appropriate baselines and identify the key factors for sustainable development with special emphasis on economic development. Contemporary business conditions are characterized by frequent crisis situations that greatly affect the efficiency of the management process, and thus generate an unfavorable environment and negative approach towards environmental issues. It is essential to adequately formulate, implement and evaluate the strategy of companies in order not to have only maximized yield, i.e. maximized output with minimal input costs as their ultimate starting point, but to take into account all the specificities of environmental protection. Keeping all of the above in mind, the concrete level of causality between efficient management and environmental protection is endorsed, i.e. a rational approach to the optimization of resources spent directly affects the environmental protection. Modern aspects/elements of environmental management must be functionally implemented in specific business activities, thereby taking into account the full complexity of the same. Special attention to environmental protection issues should be given in business on transitional markets, taking into account their imperfections. The aggravating factors of company business in such conditions include the following: inadequate technology in production processes, high costs of introducing ISO standards in business, lack of information and shortage of trained personnel in the field of environmental protection, lack of adequate incentives/subsidies by the state in the environmental protection, implementation and functionality of the legislation issues, identifying and monitoring key parameters of business activities, etc. In given business conditions, the special challenge of efficient management processes is an inadequate understanding of manufacturing costs, i.e. environmental violation due to orientation towards short-term goals of achieving return on business activities. Unwillingness to analyse the situation and circumstances in the modern market environment, in the long term, induces adverse outcomes of business activities in the context of environmental protection. In this regard, it is necessary to achieve continuous growth of flexibility and adaptability as the basis of the efficient management process, taking into account the key determinants of environmental management system.

Further research directions include continuous monitoring of the situation and opportunities in conducting business activities, with a special focus on achieving an appropriate level of efficient management, which will have a starting point in environmental improvement and rehabilitation, i.e. an adequate system of environmental management as a basis for sustainable development.

## **Acknowledgements**

The authors acknowledge the financial support of the Ministry of Education, Science and Technological Development of the Republic of Serbia, within the Project No. TR34014.

## **List of references**

- [1] J.Á. del Brío, B. Junquera, A review of the literature on environmental innovation management in SMEs: implications for public policies, *Technovation*, 23(12), 2003, pp. 939-948.
- [2] M.A. Berry, D.A. Rondinelli, Proactive corporate environmental management: A new industrial revolution, *Acad Manag Exec*, 12(2), 1998, pp. 38-50.
- [3] M.R. Partidario, Strategic environmental assessment: key issues emerging from recent practice, *Environ Impact Asses*, 16(1), 1996, pp. 31-55.



## Anticorrosion Property of Vinylphosphonic acid-co-Diethylvinylphosphonate Copolymers Obtained by UV Curing

Lavinia Macarie, Nicoleta Plesu, Smaranda Iliescu, Gheorghe Ilia, Milica Tara-Lunga-Mihali  
*Institute of Chemistry Timisoara of Romanian Academy, Blv. Mihai Viteazu 24,  
300223 Timisoara, Romania*  
lavi\_mac@yahoo.com

### Abstract

Copolymers of vinylphosphonic acid (VPA) with diethylvinylphosphonate (DEVP) at different molar ratio from 1:1 to 4:1 were synthesized by using ultraviolet light. The polymers are soluble in water. They are investigated as corrosion inhibitors for iron by using impedance spectroscopy. The best result regarding the anticorrosion property was obtained for copolymer VPA:DEVP 1:1, with an inhibition efficiency of 72%.

### Introduction

Vinylphosphonic acid (VPA) homopolymer and its copolymers with various monomers have gained great importance in polymer chemistry due to their special properties given by the presence of phosphonic group [1]. For the beginning, these polymers were used in water treatment process as inhibitors of scale formation [2]. Nowadays, the major applications of copolymers of VPA with different monomers or grafted polyvinylphosphonic acid (PVPA) on other polymers or blends refers to polymer electrolytes membranes for fuel cells [3,4], ion exchange membranes [5], in medical field as component in products for bone reconstruction and tissue engineering [6] and as dental cement[7]. Poly(vinylphosphonic acid) (PVPA) can be synthesized via radical polymerization of vinylphosphonic acid in the presence of initiator [8]. Synthetic copolymers based on dialkylvinyl phosphonates (alkyl=methyl, ethyl, *iso*-propyl) have gained also applicative importance by the presence of phosphonate groups as flame-retardants [9] and anticorrosion agents [10].

The aim of this paper is to study the properties of copolymers of vinylphosphonic acid with diethylvinylphosphonate in aqueous solution as corrosion inhibitors.

The homopolymer of vinylphosphonic acid (VPA) and its copolymers with diethyl vinylphosphonate (DEVP) were prepared by radical polymerization at different molar ratios from 1:1 to 4:1, respectively, by using UV light. The use of UV light to polymerize is an attractive technique from environmental point of view. The photopolymerizable formulations are free of organic solvents, and has the advantages of low energy consumption, low temperature operation (room temperature) and the possibility to coat various substrates (wood, plastics, paper). The obtained polymers were investigated as inhibitors against corrosion for iron surface in neutral aqueous solutions by electrochemical impedance spectroscopy. From the literature data it is known that phosphonic acids and phosphonates, in general, inhibit steel corrosion in neutral and slightly alkaline solutions.[11]

### Experimental

Vinylphosphonic acid (97%) (VPA) was purchased from Aldrich, diethylvinylphosphonate (DEVP) from Merck and photoinitiator Darocure 4265 from BASF.

The iron coins used for measurements against corrosion were previously polished with silicon carbide polishing paper until mirror-like surface was obtained. The iron surface was washed with distilled water and cleaned with ethanol in ultrasound bath.

The photopolymerizable formulations of VPA and VPA with DEVP at different molar ratios (1:1 to 4:1) containing photoinitiator at 3% w/w versus monomers were laid using film applicator (Zehnter) on PTFE plates and exposed to a medium pressure mercury lamp (400W,

Uvitron SUNRAY 400 SM, USA) to obtain cured films. The films were peeled out from PTFE plates and used for subsequent analyses.

Electrochemical experiments were performed by immersing the iron electrode into the 3% sodium chloride aqueous solution with and without PVPA and copolymers VPA:DEVP as corrosion inhibitors (VPA-DEVP 1:1, VPA-DEVP 2:1, VPA-DEVP 3:1 and VPA-DEVP 4:1) and the change of open circuit potential (OCP) was measured from the first moment of iron immersion in the first hour. The polymers were added in a quantity of 50 mg/200 ml solution. The polarization curves were obtained by scanning the potential of iron from -1200 to -200 mV at a scan rate of 1 mV/s. From the Tafel plots the corrosion potential ( $E_{\text{corr}}$ ) and corrosion current density ( $J_{\text{corr}}$ ) were extracted. Based on the  $J_{\text{corr}}$  values the inhibition efficiency ( $IE_p$ ) was calculated using the Equation (1). All measurements were carried out at room temperature.

$$IE_p (\%) = [(J'_{\text{corr}} - J_{\text{corr}})/J'_{\text{corr}}] \times 100 \quad (1)$$

where:  $J_{\text{corr}}$ ,  $J'_{\text{corr}}$  = corrosion current densities in the case of the solution containing inhibitors and the control solution, respectively.

### Results and discussion

The OCP curves for iron electrode in 3% NaCl solution containing (1) 0.0 (control solution), (2) PVPA, (3) VPA-DEVP 1:1, (4) VPA-DEVP 2:1, (5) VPA-DEVP 3:1: and (6) VPA-DEVP 4:1 as inhibitors of corrosion are shown in Figure 1.

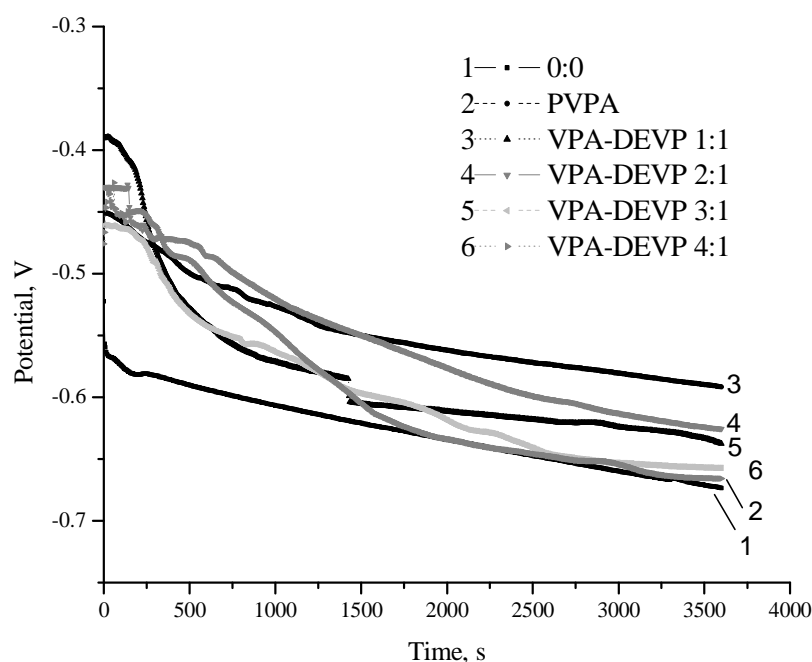


**Figure 1.** OCP curves for iron electrode in 3% NaCl solution containing (1) 0.0, (2) PVPA, (3) VPA-DEVP 1:1, (4) VPA-DEVP 2:1, (5) VPA-DEVP 3:1: and (6) VPA-DEVP 4:1

In the presence of polymers in solution, it can be observed that in the first minutes the potential decreased due to dissolution of iron ions from the surface and oxide formation.

Also, on the surface of electrode it forms a protective layer by the reaction between iron oxide and phosphonic acid and/or phosphonate groups [12]. Therefore, the potential shifted towards the less negative values in time (plots 2-6) and its tendency is to remain almost constant. It

means that the polymer has attached to the surface of iron and in all cases the presence of polymers has prevented the corrosion. The best values of OCP were observed for copolymer VPA:DEVP 1:1 which contains the highest number of phosphonate groups, and could facilitate faster the formation of adherent layer on the metal surface by phosphonate groups. The potentiodynamic polarization curves of iron electrode in 3% NaCl solution in absence and presence of inhibitors are shown in Figure 2.

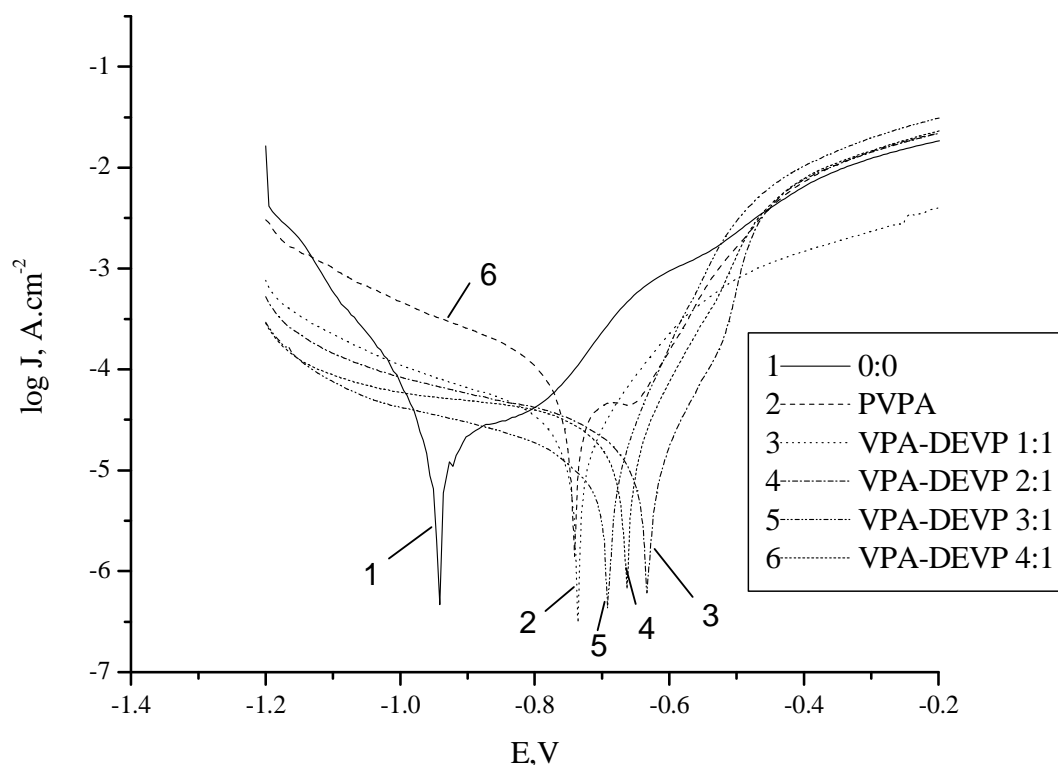


**Figure 2.** Potentiodynamic polarization curves of iron immersed in NaCl solutions for control solution (1) 0.0 and containing (2) PVPA, (3) VPA-DMVP 1:1, (4) VPA-DMVP 2:1, (5) VPA-DMVP 3:1 and (6) VPA-DMVP 4:1 as inhibitors of corrosion

**Table 2.** Corrosion parameters of iron immersed in 3% NaCl solution in the absence and in the presence of inhibitors obtained by potentiodynamic polarization studies.

Sample	$J_{corr}$ , $A/cm^2$	$E_{corr}$ , V	$R_{corr}$ , mm/year	$IE_p$ %
0:0	3.34E-05	-0.942	0.134	-
PVPA	1.58E-05	-0.736	0.119	52.75
VPA:DMVP 1:1	9.07E-06	-0.628	0.0795	72.88
VPA:DMVP 2:1	9.76E-06	-0.685	0.0592	70.82
VPA:DMVP 3:1	1.04E-05	-0.661	0.0907	69.02
VPA:DMVP 4:1	1.18E-05	-0.728	0.159	64.71

The values of the corrosion parameters: corrosion current density  $J_{corr}$  ( $A\ cm^{-2}$ ), corrosion potential  $E_{corr}$  (V), rate of corrosion  $R_{corr}$  (mm/year) and inhibition efficiency of the polymers  $IE_p$  are listed in Table 1. The inhibition efficiency was calculated with Equation 1. The corrosion current density ( $J_{corr}$ ) in case of the control solution is  $3.34 \times 10^{-5}\ A\ cm^{-2}$ . In the presence of the inhibitors the decrease in corrosion current and corrosion rate are observed. The significant reduction in  $J_{corr}$  and  $R_{corr}$  values were observed in the case of

VPA:DMVP 1:1 and 2:1 polymers, which present also good inhibition efficiency. These copolymers have the better ability to anchor to the iron surface and form a more uniform and less porous film.

### Conclusion

The using of UV light to obtain copolymers from vinylphosphonic acid (VPA) and diethylvinylphosphonate (DEVP) was advantageous because DEVP itself does not polymerize by UV light exposure, homopolymer of DEVP is not soluble in water but by copolymerization with VPA were obtained copolymers soluble in water.

Homopolymer of vinylphosphonic acid (PVPA) and copolymers of vinylphosphonic acid (VPA) with diethylvinylphosphonate (DEVP) at different molar ratio from 1:1 to 4:1, respectively, were obtained by polymerization using UV light in the presence of photoinitiator. The polymers were tested as corrosion inhibitors for iron in NaCl aqueous solution and their presence in solution decreased the corrosion current density that means the formation of protective film on iron surface. The presence of phosphonate groups from diethylvinylphosphonate in polymers enhanced the anticorrosion property in comparison with homopolymer of vinylphosphonic acid.

### Acknowledgments

The authors acknowledge for the financial support from Program 2, Project 2.2. of Romanian Academy.

### References

- [1] L. Macarie, G. Ilia, *Progr. Polym. Sci.* (2010), 35, 1078.
- [2] L. W. Becker (Betz Laboratories, Inc.) *US Patent 4 446 046*, 1984.
- [3] S. U. Celik, A. Bozkurt, *Macromol. Chem.Phys.*, (2013) , 214(4), 486.
- [4] B. Bingöl, P. Jannasch, in *Phosphorus-Based Polymers - From Synthesis to Applications*, (Eds: S. Monge, G. David) 1st ed., Royal Society of Chemistry, Cambridge 2014, p. 271.
- [5] B. L. Rivas, E. Pereira, P. Gallegos, D. Homper, K. E. Geckeler, *J. App. Polym. Sci.*, 2004, 92, 2917.
- [6] J. D. Kretlow, M. C. Hacker, L. Klouda, B. B. Ma, A. G. Mikos, *Biomacromolecules*, 2010, 11, 797.
- [7] G. O. Adusei, S. Deb, J. W. Nicholson, *Dent. Mater.*, 2005, 21, 491.
- [8] B. Bingol, W. Meyer, M. Wagner, G. Wegner, *Macromol. Rapid. Commun.*, 2006, 27, 1719.
- [9] H. Vahabi, L. Ferry, C. Longuet, R. Sonnier, C. Negrell-Guirao, G. David, J.-M. Lopez-Cuesta, *Eur. Polym. J.*, 2012, 48, 604.
- [10] T. Sato, M. Hasegawa, M. Seno, T. Hirano, *J. Appl. Polym. Sci.*, 2008, 109, 3746.
- [11] A. Pasternak, I. Felhosi, Z. Paszti, E. Kuzmann, A. Vertes, E. Kalman, E. Niykos, *Electrochim. Acta*, 2010, 55, 804.
- [12] C. Queffelec, M. Petit, P. Janvier, D. A. Knight, B. Bujoli, *Chem. Rev.*, **2012**, 112, 3777.

## Low Cost Production Method of CdS Based Photocatalysts

Radu Banica<sup>1,2</sup>, Petrica A. Linul<sup>1\*</sup>, Andrei Racu<sup>1,3</sup>, Paula Svera<sup>1,2</sup>, Cristina Mosoarca<sup>1</sup>

<sup>1</sup>*Renewable Energies Laboratory – Photovoltaics, National Institute for Research and Development in Electrochemistry and Condensed Matter, Str. Dr. A. Păunescu Podeanu 144, 300569 Timisoara, Romania;*

<sup>2</sup>*University Politehnica Timisoara, 2 Piata Victoriei, 300006 Timisoara, Romania;*

<sup>3</sup>*Institute of Applied Physics of Moldova, ASM, 5 Academiei Str., Chisinau, Moldova;*

Corresponding author: linulpetrica@yahoo.com

In order to produce visible active photocatalysts for water splitting [1] in the presence of sulfide ions, a cheap and environmentally friendly method was developed. Thus, efficient PdS/

Cd<sub>1-x</sub>Zn<sub>x</sub>S type photocatalysts [2] were obtained in a single step by hydrothermally converting cadmium hydroxide originated from Ni-Cd battery wastes in the presence of zinc sulphide. The influence of pH and ultrasonic field on photocatalysis reaction was investigated. The pH was controlled by the addition of NaOH in solution. Photocatalysis experiments were also performed in monochromatic (470 nm) and simulated solar light. The photocatalysts reactivation by hydrothermal treatment was also investigated. The photocatalysts were characterized by X-ray powder diffraction (XRD), transmission electron microscopy (TEM), scanning electron microscopy (SEM), UV-visible spectroscopy, photoluminescence spectroscopy (PL) and energy-dispersive X-ray (EDX).

## References

- [1] Z. Xiong, M. Zheng, C. Zhu, B. Zhang, L. Ma, W. Shen, One-step synthesis of highly efficient three-dimensional Cd<sub>1-x</sub>Zn<sub>x</sub>S photocatalysts for visible light photocatalytic water splitting, *Nanoscale Research Letters*, 2013, 8, 334;
- [2] J. A. Villoria, Rufino M. Navarro Yerga, S. M. Al-Zahrani, Jose Luis G. Fierro, Photocatalytic hydrogen production on Cd<sub>1-x</sub>Zn<sub>x</sub>S solid solutions under visible light: influence of thermal treatment, *Industrial & Engineering Chemistry Research*, 2010, 49, 6854–6861.

## Acknowledgements

This work was supported by a grant of the Romanian Ministry of National Education, project number PN 09-34 02 06.

## Studies Regarding Strontium Adsorption onto Styrene-1% Divinylbenzene Grafted with Phosphonium Groups and Impregnated with Ionic Liquid

Petru Negrea<sup>1</sup>, Lavinia Lupa<sup>1\*</sup>, Adriana Popa<sup>2</sup>, Marcela Stoia<sup>1</sup>

<sup>1</sup>*Politehnica University of Timisoara, Faculty of Industrial Chemistry and Environmental Engineering, 6 Vasile Parvan Blv, 300223, Timisoara, Romania; lavinia.lupa@upt.ro*

<sup>2</sup>*Institute of Chemistry Timisoara of Romanian Academy, Romanian Academy, 24 Mihai Viteazul Blv., 300223 Timisoara, Romania*

### Abstract

The paper presents the studies regarding the strontium ions removal from aqueous solution through adsorption onto a functionalized polymer impregnated with an ionic liquid. As a solid support styrene-1%divinylbenzene grafted with phosphonium groups was used and this was impregnated with 1-ethyl-3-methylimidazolium chloride ionic liquid. The impregnation of the studied ionic liquid onto the studied polymer solid support was realized through ultrasonication. The SEM, and energy dispersive EDX applied to the obtained adsorbents proved the fact that the polymer solid support was impregnated with the studied ionic liquids and also put in evidence the morphology changes of the solid support produced by its impregnation with these ionic liquids. The styrene-1% divinylbenzene functionalised with phosphonium groups and impregnated with 1-ethyl-3-methylimidazolium chloride developed a maximum adsorption capacity in the removal process of  $\text{Sr}^{2+}$  ions from aqueous solution of 1.28 mg  $\text{Sr}^{2+}$ /g of adsorbent. The equilibrium between the adsorbent and adsorbate is achieved in 60 minutes.

### Introduction

The waste aqueous solution containing radionuclides may affect human health and the environment, therefore their treatment received considerable attention worldwide. It was noted that the solvent extraction process is very efficient in the recovery of radionuclides from aqueous solutions as alternative to conventional used methods. [1-4] The volatile organic compounds were substituted by the ionic liquids (ILs) due to their environmental benefits, such as: non-inflammable and non-volatile, good selectivity, sensitivity and reproductibility for metal extraction. [5-7] However, some disadvantages of ILs were found in some liquid-liquid extractions, such as: the use of high concentrations of ionic liquids, decomposition of ionic liquids in water which results in the loss of ionic liquids, high viscosity leading to dissolution and unfavorable diffusion difficulties of separation and recovery and low interface area. Therefore the immobilization of the ionic liquid onto an appropriate solid support is a solution to prevent these disadvantages. The use of ionic liquid impregnated solid support in the removal of radionuclides from aqueous solutions presents a link between the benefits of solvent extraction and solid supports so this application increases selectivity, achieving a high degree of adsorbent-adsorbed interaction and mechanical stability to the solid support. [8-12] The most relevant criteria for the selection of the solid support are surface properties and porosity. Many researchers use macroporous organic polymers as solid support due to their high specific surface area and mechanical stability, suitable for removing toxic elements from dilute solutions due to their high kinetics, ease of regeneration and high adsorption capacity. [13]. The paper presents the studies regarding the strontium ions removal from aqueous solution through adsorption onto a functionalized polymer impregnated with an ionic liquid. As a solid support styrene-1%divinylbenzene grafted with phosphonium groups was used and this was impregnated with 1-ethyl-3-methylimidazolium chloride ionic liquid.



## Experimental

### Obtaining of ionic liquid impregnated polymer

In a 100 mL Erlenmeyer glass were added 5 g of styrene-1%divinylbenzene grafted with phosphonium groups and 0.5 g of 1-ethyl-3-methylimidazolium chloride ionic liquid dissolved in 25 mL of ethanol. The impregnation was done by ultrasound at 30 °C and at 30 minutes working time. The samples obtained were separated by filtration, washed with ethanol and then dried in an oven at 50 °C for 24 hours. The surface morphology of the impregnated material was studied by scanning electron microscopy (SEM) using a Quanta FEG 250 microscope equipped with a EDAX ZAF detector.

### Sr<sup>2+</sup> adsorption onto the ionic liquid impregnated polymer

In order to determine the adsorption capacity of the ionic liquid impregnated polymer this was used as adsorbent materials in the removal process of Sr<sup>2+</sup> ions from aqueous solutions. The Sr<sup>2+</sup> adsorption was achieved by stirring, and for the samples shaking was used a MTA Kutesz shacker with a constant speed of stirring. In order to determine the adsorption capacity of the studied material this was treated with solutions containing different concentrations of Sr<sup>2+</sup> (5, 15, 20, 25 and 30 mg / L). 1 g of the ionic liquid impregnated polymer was treated with 25 ml of Sr<sup>2+</sup> solution. The samples were stirred for 1 hour and after stirring was filtered and the concentration of Sr<sup>2+</sup> was determined by atomic emission spectrometry using an atomic absorption spectrometer Varian 280 SpectrAA with air/acetylene flame.

The adsorption capacity of the ionic liquid impregnated polymer was determined using the following equation:

$$q_e = \frac{(C_0 - C_e) \cdot V}{m}$$

where: C<sub>0</sub> and C<sub>t</sub> are the concentrations of Sr<sup>2+</sup> ions (mg/L) in the initial solution (t=0) and at equilibrium, V is the volume of the solution (L) and m is the mass of adsorbent (g).

It was also determined the dependence of the adsorption capacity of the ionic liquid impregnated polymer a function of stirring time. For this purpose 0.1g of the studied adsorbent was treated with 25 mL of Sr<sup>2+</sup> solution having a concentration of 5 mg/L for different periods of time (range: from 15 to 240 minutes).

## Results and discussion

### Characterization of the ionic liquid impregnated polymer

The morphological structure of the studied adsorbent can be seen from the SEM image presented in Figure 1 a). The EDX spectra is shown in figure 1 b). By SEM and EDX were laid out the presence of the phosphonium and imidazolium groups and the chloride ions on polymeric support. This analyze put in evidence the fact that the studied polymeric support was impregnated with the studied ionic liquid (1-ethyl-3-methylimidazolium chloride).

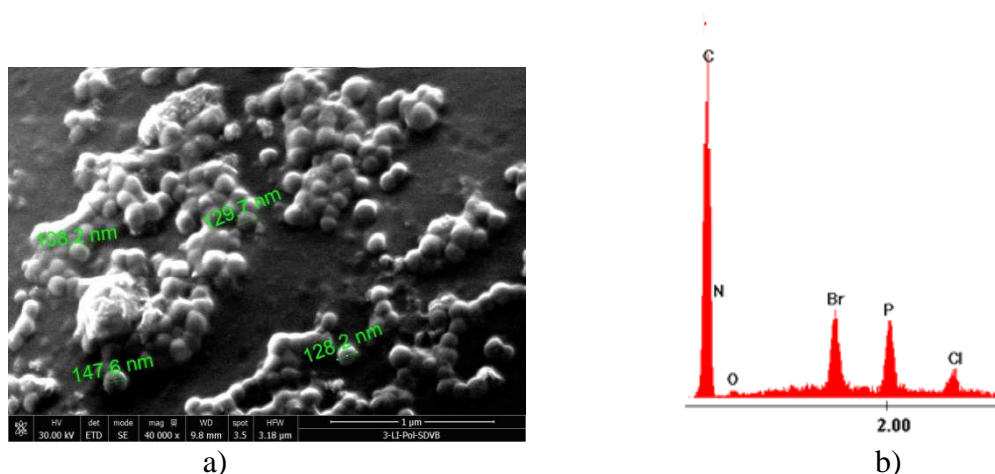


**Figure 1.** SEM image and EDX spectrum of the styrene-1%divinylbenzene grafted with phosphonium groups and impregnated with 1-ethyl-3-methylimidazolium chloride

### Effect of $\text{Sr}^{2+}$ initial concentration on the adsorption process efficiency

The equilibrium isotherm of  $\text{Sr}^{2+}$  adsorption onto the studied material is presented in figure 2. It can be observed that by increasing the initial concentration of the  $\text{Sr}^{2+}$  ions increase the amount of radionuclide adsorbed by 1 g of adsorbent, until it is achieved the equilibrium. The maximum adsorption capacity developed by the styrene-1%divinylbenzene grafted with phosphonium groups and impregnated with 1-ethyl-3-methylimidazolium chloride developed in the removal process of  $\text{Sr}^{2+}$  ions from aqueous solution is 1.28 mg  $\text{Sr}^{2+}$ /g of adsorbent.

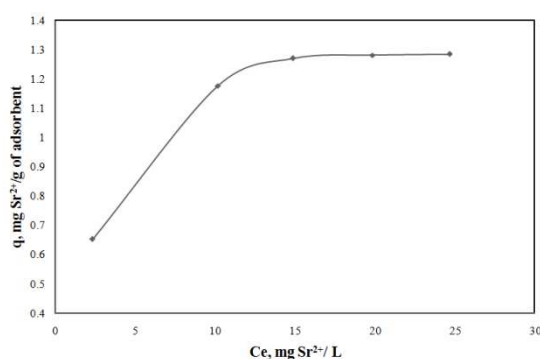


**Figure 2.** Isotherm of  $\text{Sr}^{2+}$  adsorption onto studied adsorbent

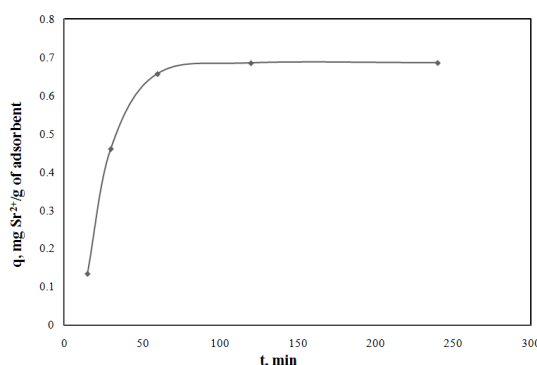


**Figure 3.** Effect of contact time on the adsorption capacity of the studied adsorbent

### Effect of stirring time on the adsorption process efficiency

The experimental data regarding the dependence of the adsorption capacity of the studied adsorbent function of the stirring time are presented in figure 3. It can be notice that the stirring time increasing lead to the increase of the adsorption capacity, untill it reach a constant value. The equilibrium between the adsorbent and adsorbate is achieved in 60 minutes.

### Conclusion

In the present work was studied the removal of  $\text{Sr}^{2+}$  ions from aqueous solutions by adsorption onto styrene-1% divinylbenzene functionalised with phosphonium groups and impregnated with 1-ethyl-3-methylimidazolium chloride. The impregnation of the studied ionic liquid onto the studied polymer solid support was realised through ultrasonication which proved to be an efficient method because is not time consuming, combine the advantages of

the ionic liquids with those of the solid support, is used a smaller amount of the ionic liquid and there is no risk of loss of the extractant in the aqueous phase. The SEM, and energy dispersive EDX applied to the obtained adsorbents proved the fact that the polymer solid support was impregnated with the studied ionic liquids and also put in evidence the morphology changes of the solid support produced by its impregnation with these ionic liquids. From the experimental data it has been found that the adsorption capacity of the studied material increase with the increasing of the initial concentration of  $\text{Sr}^{2+}$  ions and with stirring time increasing. The styrene-1% divinylbenzene functionalised with phosphonium group and impregnated with 1-ethyl-3-methylimidazolium chloride developed a maximum adsorption capacity in the removal process of  $\text{Sr}^{2+}$  ions from aqueous solution of 1.28 mg  $\text{Sr}^{2+}$ /g of adsorbent. The equilibrium between the adsorbent and adsorbate is achieved in 60 minutes.

### Acknowledgements

This work was supported by a grant of the Romanian National Authority for Scientific Research, CNCS – UEFISCDI, project number PN-II-RU-TE-2012-3-0198”.

### References

- [1] A.M. El-Kamash, J. Hazard. Mater. 151 (2008) 432.
- [2] M.M. Abd El-Latif, M.M. Elkady., Desalination 271 (2011) 41.
- [3] M.M.Hamed, M.F. Attallah, F.A. Shehata, Arab J. Nucl. Sci. Appl. 45 (2012) 37.
- [4] A. Hanafi, J. Atom. Molec. Sci. 1 (2010) 292.
- [5] A. Benhamour, M. Baudu, Z. Derriche, J.P. Basly, J. Hazard. Mater. 171, (2009) 1001.
- [6] K. Campos, R. Domingo, T. Vincent, M. Ruiz, A.M. Sastre, E. Guibal, Water Res. 42 (2008) 4019.
- [7] S.D. Cekic, H. Filik, R. Apak, Anal. Chim. Acta. 505 (2004) 15.
- [8] H.T. Huynh, M. Tanak, Ind. Eng. Chem. Res. 42 (2003) 4050.
- [9] A. Negrea, M. Ciopec, L. Lupa, P. Negrea, A. Gabor, AWERProcedia Advances in Applied Sciences, 1 (2013) 241.
- [10] A. Negrea, L. Lupa, M. Ciopec, P. Negrea, I. Hulka, Internat. J. Chem. Eng. Appl. 5(5), (2014) 424.
- [11] L. Lupa, A. Negrea, M. Ciopec, P. Negrea, Molecules 18 (2013) 12845.
- [12] T. Vincent, A. Parodi, E. Guibal, Sep. Purif. Techn. 62 (2008) 470.
- [13] X. Sun, B. Preng, Y. Ji, J. Chen, D. Li, Sep. Purif. Techn. 63 (2008) 61.

## Voltammetric Detection of Drugs Considered as Emerging Pollutant in Water at Carbon Nanofiber Composite Electrode

Magdalena Ardelean<sup>1</sup>, Florica Manea<sup>1\*</sup>, Anamaria Baci<sup>1</sup>, Aniela Pop<sup>1</sup>, Rodica Pode<sup>1</sup>.

<sup>1</sup> "Politehnica" University of Timisoara, Sqr. Victoriei no.2, 300006 Timisoara, Romania, e-mail: florica.manea@upt.ro

### Abstract

In this study, carbon nanofiber-epoxy (CNF) composite electrode was tested using cyclic voltammetry (CV), differential-pulsed voltammetry (DPV) and square-wave voltammetry (SWV) techniques for the quantitative determination of naproxen (NPX), which was chosen the model for the anti-inflammatory drugs as emerging pollutants from water. The best performance in relation with the sensitivity and the detection potential value was obtained by employing DPV, and in relation with the lowest limit of detection and quantification was achieved by SWV under operating conditions of modulation amplitude of 0.2V, step potential of 0.05V and a scan rate of 0.025V.

### Introduction

Naproxen - (2S)-2-(6-methylnaphthalen-2-yl) propanoic acid is a non-steroidal anti-inflammatory drug from the phenylpropanoic acid class, used in the treatment of osteoarthritis, rheumatoid arthritis, degenerative joint disease, ankylosing spondylitis, acute gout and primary dysmenorrhea [1, 2]. This drug belongs to emerging pollutants, which are candidate for the future regulation that requires information about their presence, occurrence, fate and toxicity in the environment.

Various number of studies are directed to drugs, pharmaceuticals and related compounds as emerging pollutants in water, because their presence especial in river water has been reported [3].

One of the most important aspects in order to assess the drugs as emerging pollutants in water is represented by the analytical methods for the quantitative determination of their concentrations. The electrochemical methods should be regarded as feasible alternative due to their simplicity, low-cost, fast and availability for the on-site and in-field detection application. The key for the performance of the electroanalytical method is given by the electrode material and the electrochemical techniques.

Nanostructured carbon based composite electrodes have been reported as very efficient in the electroanalytical detection application [4, 5]. In this study, carbon nanofiber-epoxy composite electrode was tested for the electrochemical detection of naproxen (NPX), which was chosen the model for the drugs as emerging pollutants in water.

### Experimental

Naproxen (NPX) was provided by AC Helcor SRL, Romania. A stock solution of 1mM was prepared by using 0.1 M NaOH solution (Merck, Germany).

#### *Electrochemical measurements*

The electrochemical performance of this electrode was studied by cyclic voltammetry (CV), differential-pulsed voltammetry (DPV), and square-wave voltammetry (SWV). An electrochemical pre-treatment by three repetitive cyclings from 0 V to +1.25 V vs. SCE in

0.09M Na<sub>2</sub>SO<sub>4</sub> and 0.01M H<sub>2</sub>SO<sub>4</sub> supporting electrolyte was performed. All measurements were carried out using an Autolab potentiostat/galvanostat PGSTAT 302 (Eco Chemie, The Netherlands) controlled with GPES 4.9 software and a three-electrode cell, with a saturated calomel electrode as reference electrode, a platinum counter electrode, and the CNF composite working electrode.

## Results and discussion

To develop the voltammetric analytical detection for the quantitative determination of NPX, cyclic voltammograms were recorded on CNF composite electrode in 0.1 M Na<sub>2</sub>SO<sub>4</sub> supporting electrolyte in the presence of various NPX concentrations. The results are presented in Figure 1.

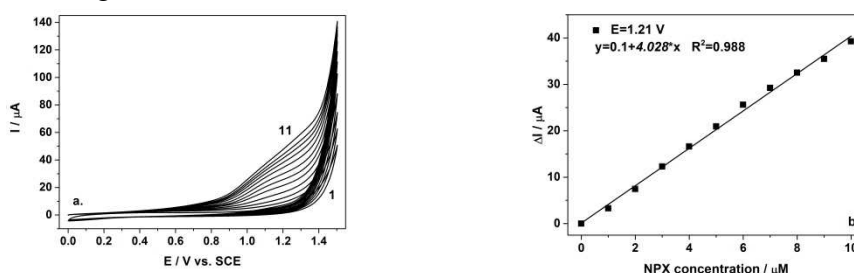


**Figure 1. a.** Cyclic voltammograms recorded on CNF electrode in 0.1 M Na<sub>2</sub>SO<sub>4</sub> supporting electrolyte (curve 1) in the presence of 50 μL 0.1M NaOH (curve 2) and 1-10 μM NPX (curves 3-12), at a potential scan rate: 0.05 Vs<sup>-1</sup> in a potential range: 0 to +1.5 V/SCE; **b.** Calibration plot of the current vs. NPX concentration of the CVs recorded at E= +1.21V/SCE.

The oxidation process of NPX on CNF electrode started at +0.4V/SCE and the peak current slightly increased until +0.9V/SCE, after which, a more pronounced width peak was noticed. Since the stock solution was prepared by using sodium hydroxide, the influence of the hydroxide was studied and no relevant peaks were noticed. As a precaution, before adding the analyte, a 50μL volume of sodium hydroxide was added into supporting electrolyte. Also, it was noticed the lack of the cathodic peak, suggesting the irreversibility of the oxidation process. A good linearity anodic current vs. naproxen concentration was observed, and for the oxidation potential of +1.21 V/SCE, a sensitivity of 4.028 μA/μM was achieved.

For an improvement in relation with the sensitivity and oxidation potential, differential-pulsed voltammetry was employed. Under the optimized conditions previously determined for other drug determination, *i.e.*, a modulation amplitude of 0.2V, step potential of 0.05V and scan rate of 0.025V/s, a good linearity and a better sensitivity were obtained. In Figure 2 are presented the differential-pulsed voltammograms obtained under these conditions for NPX detection on CNF electrode. In this case, the oxidation process started at about +0.45V/SCE and a well-defined peak was noticed at +0.95V/SCE. In comparison with cyclic voltammetry, the oxidation potential shifted to more negative values for DPV (+0.95V/SCE vs. +1.21V/SCE) and an improved sensitivity was reached (9.959μA/μM vs. 4.028 μA/μM).

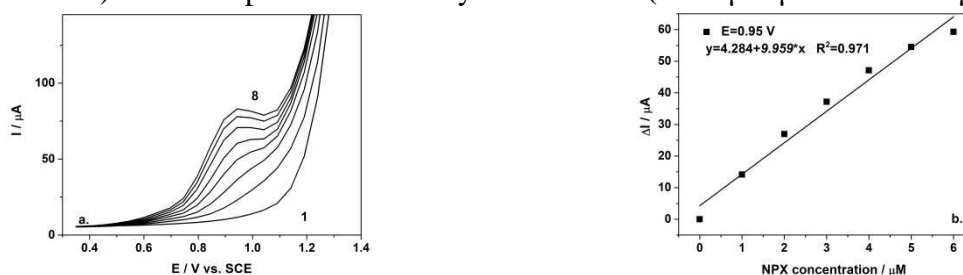


**Figure 2. a.** Differential-pulsed voltammograms recorded on CNF electrode under operating

conditions: modulation amplitude of 0.2V, step potential of 0.05V and potential scan rate of  $0.025 \text{ Vs}^{-1}$  between 0.35 and +1.35V/ SCE in 0.1 M  $\text{Na}_2\text{SO}_4$  supporting electrolyte (curve 1) in the presence of 50  $\mu\text{L}$  0.1M NaOH (curve 2) and 1-6  $\mu\text{M}$  NPX (curves 3-8); **b.** Calibration plot of the current vs. NPX concentration recorded at  $E = +0.95\text{V/SCE}$ .

Square-wave voltammetry was employed also, as advanced pulsed technique, in order to compare with DPV results and to find the best voltammetry technique. Also, previous optimization of operating conditions for SWV technique was achieved for other drug detection.



**Figure 3. a.** Square-wave voltammograms recorded on CNF electrode under operating conditions: modulation amplitude of 0.05V, step potential of 0.005V and a frequency of 10 Hz between 0 and +1.45V/ SCE in 0.1 M  $\text{Na}_2\text{SO}_4$  supporting electrolyte (curve 1) in the presence of 50  $\mu\text{L}$  0.1M NaOH (curve 2) and 1-6 $\mu\text{M}$  NPX (curves 3-8); **b.** Calibration plot of the current vs. NPX concentration recorded at  $E = +1.1\text{V/SCE}$ .

By using modulation amplitude of 0.05V, a step potential of 0.005V and a frequency of 10 Hz, sensitivity of  $4.366 \mu\text{A}/\mu\text{M}$  was reached (Figure 3 b). In comparison with DPV, a slightly shifting to more positive values of oxidation potential was observed (+1.1V/SCE vs. +0.95V/SCE), and also a small decrease of sensitivity ( $4.366 \mu\text{A}/\mu\text{M}$  vs.  $9.959 \mu\text{A}/\mu\text{M}$ ). This decrease of sensitivity value is explained by the use of small values for operating parameters, *e.g.* modulation amplitude of 0.05V for SWV vs. 0.2V for DPV. The sensitivity obtained for SWV is similar with the one obtained for CV.

In Table 1 are gathered all the electroanalytical parameters obtained for naproxen detection in aqueous media on CNF electrode.

**Table 1.** Electroanalytical parameters obtained on CNF electrode for NPX detection

Technique	$E_{\text{ox}} / \text{V}$	Sensitivity ( $\mu\text{A}/\mu\text{M}$ )	Correlation coefficient	RSD (%)	LOD ( $\mu\text{M}$ )	LOQ ( $\mu\text{M}$ )
CV	1.21	4.028	0.988	5.2	0.133	0.444
DPV	0.95	<b>9.959</b>	0.971	4.24	0.146	0.450
SWV	1.1	4.366	0.997	9.01	0.124	0.415

#### 4. Conclusions

Based on the above-presented results, it may be concluded that carbon nanofiber-epoxy composite electrode exhibited the peculiarities for naproxen detection in aqueous media, using voltammetric techniques. The best performance in relation with the sensitivity was obtained by employing DPV under operating conditions of modulation amplitude of 0.2V, step potential of 0.05V and a scan rate of 0.025V. A slight improvement of the lowest limit of detection was achieved using square-wave voltammetry techniques operated at modulation



amplitude of 0.05V, step potential of 0.005V and a frequency of 10 Hz. However, the lowest value of the detection potential and the electroanalytical parameters reclaim the differential-pulsed voltammetry technique the most valuable technique for the detection of naproxen from water on carbon nanofiber composite electrode.

## **References**

- [1] P. Norouzi, F. Dousty, M.R. Ganjali, R. Daneshgar, *Int. J. Electrochem. Sc.* 4 (2009) 1371.
- [2] N. Adhoum, L. Monser, M. Toumi, K. Boujlel, *Anal. Chim. Acta.* 495 (2003) 69.
- [3] A. Nikolaou, Pharmaceuticals and related compounds as emerging pollutants in water: analytical aspects, *Global NEST J.*, 15 (2013) 1.
- [4] A. Remes, A. Pop, F. Manea, S.J. Picken, J. Schoonman, *Sensors.* 12 (2012) 7033.
- [5] S. Motoc, A. Remes, A. Pop, F. Manea, J. Schoonman, *J. Environ. Sci.* 25 (2013) 838.
- [6] M. Ardelean, F. Manea, R. Pode, *Int. J. Pharm. Pharmaceut. Sci.*, 5 (2013) 318.

## **Acknowledgements**

This work was partially supported by the strategic grant POSDRU/159/1.5/S/137070 (2014) of the Ministry of National Education, Romania, co-financed by the European Social Fund – Investing in People, within the Sectoral Operational Programme Human Resources Development 2007-2013 and partially by the PNII-165/2011 and PNII-60/2012.

## Metal Removal from Compost Wastewater Using Algae

Marjana Simonič<sup>\*,a</sup>

<sup>a</sup>University of Maribor/Faculty of Chemistry and Chemical Engineering, Smetanova 17, SI-2000 Maribor, Slovenia. email: marjana.simonic@um.si

### ABSTRACT

The aim of present work was to apply algae for metal removal from compost wastewater. The potential of alginate immobilized *Chlorella* to remove  $\text{Cu}^{2+}$  ions from compost wastewater was investigated in this study. The effect of initial metal concentrations and contact time on biosorption and removal efficiency of tested metals was investigated at original initial pH value of compost wastewater. Firstly, model sample solutions were prepared. We found out that  $\text{Cu}^{2+}$  ions could be removed by using alginate immobilized *Chlorella*.

**Keywords:** algae, compost wastewater, metal removal

### INTRODUCTION

Because of their chemical characteristics, toxic effect and accumulation tendency in human body, heavy metals represent a serious hazard to human health. Several live organisms (e.g. algae, bacteria, fungi) have been investigated for metal sorption from polluted waters. Algae have proven to be very useful for this purpose due to their availability, low costs and the capability to uptake even large quantities of heavy metals. Cells of *Chlorella* were reported to be isolated from soil were highly resistant to heavy metals and were capable of taking up the heavy metal ions such as  $\text{Cd}^{2+}$ ,  $\text{Zn}^{2+}$  and  $\text{Cu}^{2+}$ , respectively [1]. In another research, a series of batch experiments was conducted to compare the ability of several algal species including *Chlorella* in removing nickel and zinc from synthetic wastewater [2]. Physiological and morphological responses of lead or cadmium by *Chlorella* treatment were studied [3].

Different natural immobilisation media, such as alginates, chitosan, and cellulose derivatives have been used for algal cell immobilisation, while alginate is still one of the most frequently used carriers due to its advantages such as very simple preparation, biocompatibility and cost-effective immobilization. Otherwise, the cell immobilization may enhance sorption capacity, offers opportunity for biomass retention within the working environment, easy separation of products from cells and relatively high local cell density. The size of algal beads may also influence the metal removal efficiency of metals as well as other environmental parameters, such as pH and contact time, and initial metal concentration also play a great role in this process [4].

The main objective of this study was to explore the feasibility of alginate immobilized *Chlorella* for removing heavy metal ions  $\text{Cu}^{2+}$  from drinking and compost wastewater samples. The sorption capacities of the sorbent for the above mentioned metals were studied under various initial metal concentrations and different experimental conditions, such as pH and contact time.

## MATERIALS and METHODS

### Samples

Model water sample and compost wastewater were taken for analysis. Model solutions were prepared by dissolving 1 g/L of Cu in drinking water. Adequate solutions were prepared by diluting this standard Cu-solutions. Compost wastewater was taken from the local Industrial composting facility system.

### Analytical methods

The parameters were determined according to the standard methods as seen from Table 1.

Table 1. Analytical methods

Parameter	Unit	Apparatus
pH	-	Iskra pH meter
Conductivity	$\mu\text{S}/\text{cm}$	WTW conductivity meter
Turbidity	NTU	HACH Turbidimeter
Cu	mg/L	AAS

Several analyses were obtained in order to follow the experiment's performance. The samples were filtered through filters (GF-3, Macherey-Nagel) in order to exclude most of the solids present in the water and diluted before analysis if necessary.

The metal content in the solution was determined by an atomic absorption spectrophotometer (AAS, Perkin-Elmer, AAnalyst 400). The calculations for metals were made according to the previously prepared calibration curve. The metal removed by algal beads was determined by subtracting the residual metal concentration from the initial metal concentration in the solution.

### Materials

The cells of *Chlorella* were delivered from the local algal technology center (AlgEn, Slovenia) and cultivated in Bold's Basal growth media at room conditions. After a 10-day cultivation when the microalgae were acclimatised, the algal cells were harvested by centrifugation (at 3500 rpm for 10 min). Immobilised algal beads were prepared by entrapping cells of *Chlorella* in an alginate matrix according to the following steps [5] (Ruiz-Marin): the harvested cells were re-suspended in distilled water to form a concentrated algal suspension, which was then mixed with 4% sodium alginate (Fluka) solution at a 1:1 volume ratio to yield a mixture of 2% algal alginate suspension. The mixture was then dropped into a 2% calcium chloride (Merck) solution using a 25 mL burette. The drops of algal alginate solution gelled into small beads (with cell numbers of around  $6.6 \times 10^5$  cells bead<sup>-1</sup>) upon contact with calcium chloride solution (2%). The solution was stirred to prevent aggregation of the algal cell entrapped in alginate beads. Immobilised algal beads were then stored in a calcium chloride solution for approximately 4 h, rinsed with saline solution (0.85% NaCl) and subsequently with distilled water. The beads were then transferred to the algal growth medium and were incubated under room conditions for 3 days. After short incubation, the beads with immobilised algal cells were removed from the medium and washed twice with saline solution (0.85%) and finally with distilled water. The beads are seen from Figure 1.

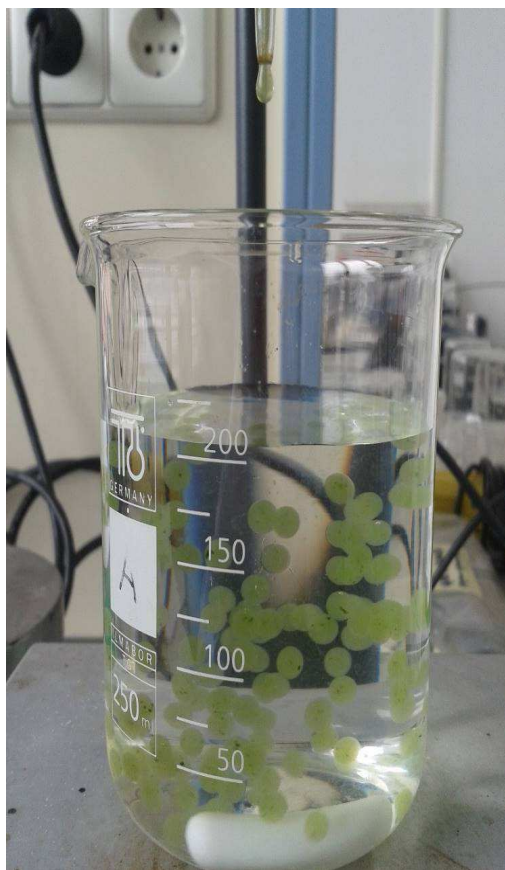


**Figure 1: The alginate beads with algae**

The experiments were performed by *Chlorella* immobilized algal beads placed into glass jars with drinking water. For the experiments with metals, the drinking water was spiked with Cu solutions in adequate concentrations in order to achieve concentrations of 25, 40, 80 or 150 mg/L of Cu ions.

## RESULTS

The pH effect was studied in the range of 3-7 at initial metal concentration of 25 mg/L. The removal capacities of cooper increases with pH up to 5, but it must be considered that at pH values higher than 6 the precipitation effect was observed, more obvious at pH 7. The maximum efficiency for  $\text{Cu}^{2+}$  ions was calculated at 20.24 mg/g (98.86%). This is in accordance with the previous investigations which shown increased metal sorption with increasing pH of the solution [6]. It could be explained by the fact that the increase in the initial solution pH will result in the increase of the dissociation degree of functional groups from sorbent surface, and consequently, the number of electrostatic interactions will increase. The pH was set to 5. The contact time for successful metal removal was tested by using *Chlorella* immobilised algal beads. The contact time was 20, 40, 60, and 180 mins. The initial and equilibrium concentration of Ni was determined. It was found that contact time is around one hour (60 min). The data obtained are presented in Table 2.

Table 2. Influence of contact time in model solution (initial  $c = 25$  mg/L)

t(min)	pH	Cu (%)
20	5	36
40	5	97
60	5	99
180	5	99

In order to study the effect of initial metal concentration on sorption capacity by alginate immobilised *Chlorella*, the experiments with different concentrations of  $\text{Cu}^{2+}$  ions in the sorption medium were performed, wherein the initial metal concentrations were varied in the range of 25–150 mg/L. Results are presented in Figure 2.

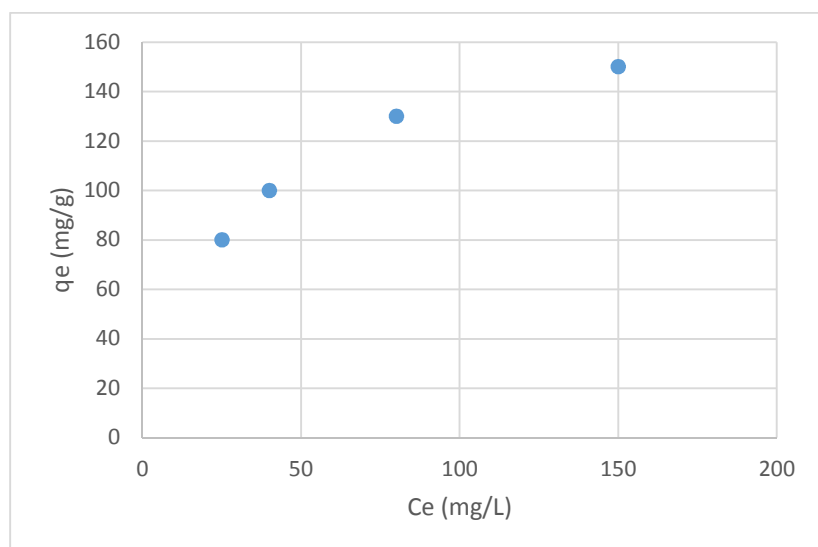


**Figure 2:** The sorption capacity as function of equilibrium concentration for  $\text{Cu}^{2+}$

The sorption capacity of metal ions increased with increase in initial metal concentration, whereby the equilibrium metal concentration also increased. Higher initial concentrations provide the driving force to overcome mass transfer resistance of metal ion between the aqueous solution and solid, thus increasing the metal uptake. In addition, increasing initial metal ion concentrations also increases the number of collisions between metal ions and sorbent, which enhances the sorption process. However, the experimental maximum biosorption capacities obtained in biosorption of  $\text{Cu}^{2+}$  ions by alginate immobilised *Chlorella* cells were found to be 150.07 mg/g.

Table 3 represents the measurement for determining removal efficiency in compost wastewater. The presence of organic compounds has some influence on copper removal since all measured values of Cu-ions were lower compared with model samples. However, pH value 5 is better than higher values. Turbidity was measured at 1000 NTU and conductivity

22 mS/cm. The values are around 1000 times higher as in drinking water samples, which is the reason for the lower efficiency due to hindrance.

Table 3. Determination of Cu removal from compost wastewater

t(min)	pH	Cu (%)
20	5	45,6
20	6	27,9
60	5	68,1
60	6	62,2
180	5	76,3
180	6	64,2

## CONCLUSION

- Alginate immobilised *Chlorella* is efficient for removing  $\text{Cu}^{2+}$  ions from water.
- The capacity by alginate immobilised *Chlorella* cells were found to be 150.07 mg/g  $\text{Cu}^{2+}$  ions.
- In compost wastewater the removal efficiency decrease due to organic compounds content which hinder Cu-ions uptake by alginate beads.

## LIST OF REFERENCES

- [1] Yoshida N., Ikeda R., Okuno T., Identification and characterization of heavy metal-resistant unicellular alga isolated from soil and its potential for phytoremediation, *Bioresource Technology*, 2006, 97, 1843-1849.
- [2] Chong A.M.Y., Wong Y.S., Tam N.F.Y., Performance of different microalgal species in removing nickel and zinc from industrial wastewater, *Chemosphere*, 2000, 41, 251-257.
- [3] Carfagna S., Lanza N., Salbitani G., Basile A., Sorbo S., Vona V., Physiological and morphological responses of Lead or Cadmium exposed *Chlorella sorokiniana* 211-8K (Chlorophyceae), SpringerPlus, 2013, 2.
- [4] Sarı A., Tuzen M., Equilibrium, thermodynamic and kinetic studies on aluminum biosorption from aqueous solution by brown algae (*Padina pavonica*) biomass, *Journal of Hazardous Materials*, 2009, 171, 973-979.
- [5] Ruiz-Marin A., Mendoza-Espinosa L.G., Stephenson T., Growth and heavy metal removal in free and immobilized green algae in batch and semi-continuous cultures treating real wastewater, *Bioresource Technology*, 2010, 101, 58-64.
- [6] Wan Maznah W.O., Al-Fawwaz A.T., Surif M., Biosorption of copper and zinc by immobilised and free algal biomass, and the effects of metal biosorption on the growth and cellular structure of *Chlorella* sp. and *Chlamydomonas* sp. isolated from rivers in Penang, Malaysia, *Journal of Environmental Sciences*, 2012, 24, 1386-1393.



## Fluoride Removal from Aqueous Media by Electrogenerated $\text{Al}(\text{OH})_3$

Monica Ihos\* and Ladislau Andres

National R&D Institute for Industrial Ecology - ECOIND - Timisoara Branch, P-ta Regina Maria Nr.1, Et.2, 300004 Timisoara, Romania, e-mail: monica\_ihos@yahoo.com

### Abstract

The removal of fluoride from aqueous media was carried out by electrocoagulation with aluminium sacrificial anode. The electrogenerated  $\text{Al}(\text{OH})_3$  has high fluoride adsorption capacity. The applied current density was of 10, 30 and 50  $\text{A/m}^2$ , respectively, the initial fluoride concentration was of 5 mg/L and 10 mg/L, respectively and pH of 7. The supporting electrolyte was 0.01 M Na Cl. Concentrations of fluoride in the electrolysed solutions of about 0.20 mg/L were obtained.

### Introduction

Fluoride (F) is widespread in the geologic medium and is released in the groundwater, usually, by the slow dissolution of fluorine-containing rocks. The fluoride is known as one of the contaminants for drinking water that causes serious health concerns and the World Health Organization (WHO) recommendation regarding the limit of the fluoride in drinking water is 1.5 mg/L [1]. The fluoride is an essential element in a narrow range of concentration, between 0.5 and 1 mg/L, but it is harmful for the human health when exceeds 1.5 mg/L.

Groundwater, an important source of drinking water, is also a very important source of fluoride for human intake. Long term ingestion of fluoride rich drinking water causes serious health disorders such as fluorosis, which causes mottling of teeth in mild cases and embrittlement of bones and neurological damage in severe cases [2]. The high concentrations of fluoride can also interfere with carbohydrates, lipids, proteins, vitamins and mineral metabolism [3, 4]. Excess intake of fluoride leads to various diseases such as osteoporosis, arthritis, brittle bones, cancer, infertility, brain damage, Alzheimer syndrome, and thyroid disorder [2].

Because of the harmful effects of fluoride upon human health it is necessary to develop technologies that can effectively remove fluoride from the groundwater used for drinking purposes.

Among the processes studied for fluoride removal from aqueous media, adsorption [5-13], membrane techniques [14-17] and electrochemical processes can be mentioned. The third approach is a versatile and effective method and also a sustainable way to remove the fluoride from aqueous media.

The aim of this paper was to assess the removal of fluoride from aqueous media by using  $\text{Al}(\text{OH})_3$  generated during the electrocoagulation with aluminium sacrificial anode.

### Experimental

Fluoride removal from aqueous media by electrocoagulation was carried out in a plexiglass cell with horizontal electrodes. The sacrificial anode was made of aluminium with an active surface area of 78.4  $\text{cm}^2$ . The cathode was a wire mesh grid made up of 3 mm diameter stainless steel wires. The distance between the electrodes was 5 mm.

Volumes of 500 ml solution were introduced in the cell, and the applied current densities were 10, 30 and 50  $\text{A/m}^2$ , respectively. Electrolysis duration was 60 minutes and samples were taken at every 10 minutes.

Stock solution of 1000 mg/L  $F^-$  was obtained by dissolving the appropriate quantity of NaF (Merck) p.a. in distilled water. Working solution of 5 and 10 mg/L  $F^-$  and pH of 7 were prepared freshly for each experiment by diluting stock solution and adjusting pH with NaOH p.a. The supporting electrolyte was 0.01 M Na Cl.

The fluoride content was determined by using a Thermo Scientific Orion fluoride ion selective electrode. TISAB II solution was used as a buffer to maintain the pH and background ion concentrations.

## Results and discussion

In Table 1 are listed the working conditions during the electrocoagulation and the concentration of  $F^-$  in the electrolysed solutions.

**Table 1.** Working conditions and  $F^-$  concentration;  $pH_{ini}=7$

Time/ min	Current density/ $A/m^2$	*Cell voltage/ V	* $F^-$ conc./ mg/L	* $F^-$ removal efficiency / %	**Cell voltage/ V	** $F^-$ conc./ mg/L	** $F^-$ removal efficiency / %
10	10	1.0	2.32	53.6	1.0	8.57	14.3
20		1.0	2.28	54.4	0.9	7.62	23.8
30		1.1	2.27	54.6	0.9	6.44	35.6
40		1.1	1.96	60.8	0.9	5.11	48.9
50		1.0	1.63	67.4	0.9	3.92	60.8
60		0.9	1.37	72.6	0.9	3.79	62.1
10	30	1.6	2.63	47.4	1.4	5.97	40.3
20		1.5	1.50	70.0	1.4	4.21	57.9
30		1.5	1.12	77.6	1.4	2.66	73.4
40		1.7	0.77	84.6	1.4	1.76	82.4
50		1.7	0.65	87.0	1.4	1.11	88.9
60		1.4	0.54	89.2	1.4	0.65	93.5
10	50	1.9	2.17	56.6	2.0	2.33	76.7
20		1.9	0.80	84.0	2.0	0.82	91.8
30		1.8	0.35	93.0	2.0	0.54	94.6
40		1.8	0.22	95.6	2.0	0.37	96.3
50		1.9	0.19	96.2	1.9	0.22	97.8

\*  $c_{ini}$ : 5 mg/L  $F^-$ ; \*\*  $c_{ini}$ : 10 mg/L  $F^-$

The limit of 1.5 mg/L fluoride recommended by WHO was achieved by applying a current density of 30 and 50  $A/m^2$  whatever the initial concentration of fluoride. The electrolysis time to achieve the recommended limit was higher for 30  $A/m^2$  as the initial concentration of the fluoride increased, but the same at 50  $A/m^2$  for both concentrations. The explanation of this behaviour can follow that one given by Gosh et al. [18]. In the first instances of electrogeneration, aluminium cations contributed to charge neutralization of the pollutant particles as part of a sorption coagulation mechanism, the result was formation of loose aggregates. As the time progresses, further aluminium cation addition resulted in amorphous aluminium hydroxide precipitation that promotes pollutant aggregation. If the current density had remained at 30  $A/m^2$  so the production of the aluminium cation had remained fixed and therefore with the increase in initial fluoride concentration, the complex formation process between the amorphous aluminium hydroxide and fluoride would have been insufficient.

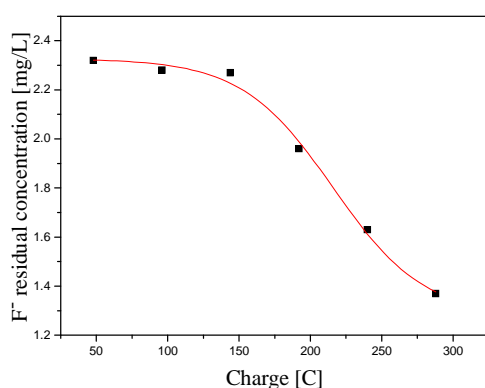


**Figure 1.** Dependence of  $F^-$  residual concentration versus charge;  $c_{ini}$ : 5 mg/L  $F^-$ ,  $pH_{ini}$ : 7, current density: 10 A/m<sup>2</sup>

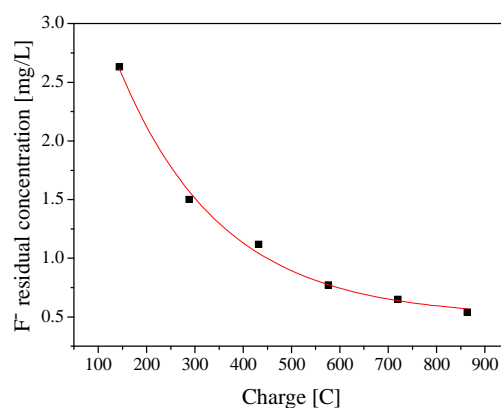


**Figure 2.** Dependence of  $F^-$  residual concentration versus charge;  $c_{ini}$ : 5 mg/L  $F^-$ ,  $pH_{ini}$ : 7, current density: 30 A/m<sup>2</sup>

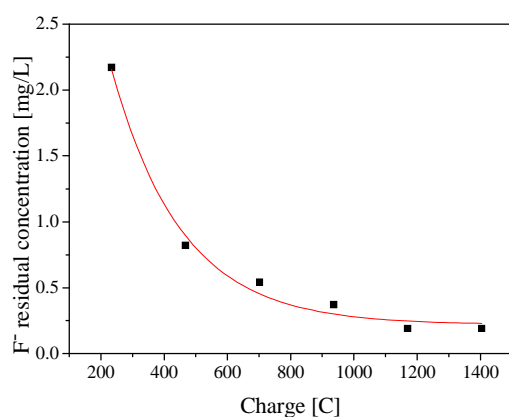


**Figure 3.** Dependence of  $F^-$  residual concentration versus charge;  $c_{ini}$ : 5 mg/L  $F^-$ ,  $pH_{ini}$ : 7, current density: 50 A/m<sup>2</sup>

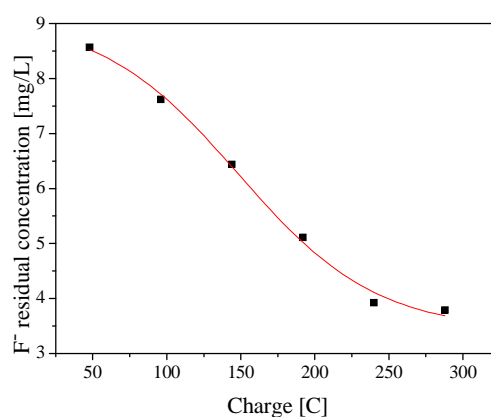


**Figure 4.** Dependence of  $F^-$  residual concentration versus charge;  $c_{ini}$ : 10 mg/L  $F^-$ ,  $pH_{ini}$ : 7, current density: 10 A/m<sup>2</sup>

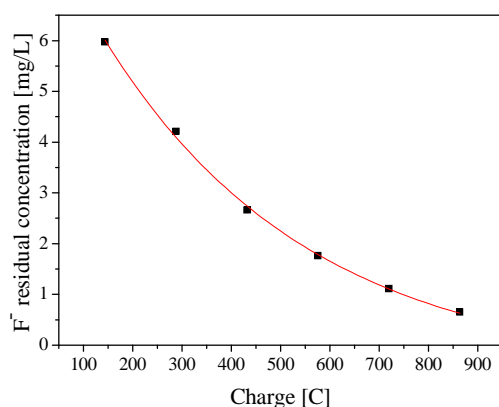


**Figure 5.** Dependence of  $F^-$  residual concentration versus charge;  $c_{ini}$ : 10 mg/L  $F^-$ ,  $pH_{ini}$ : 7, current density: 30 A/m<sup>2</sup>

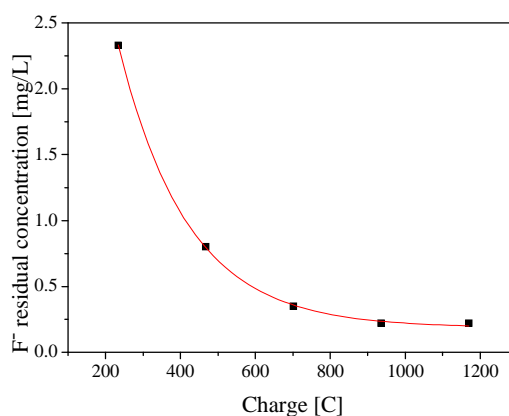


**Figure 6.** Dependence of  $F^-$  residual concentration versus charge;  $c_{ini}$ : 10 mg/L  $F^-$ ,  $pH_{ini}$ : 7, current density: 50 A/m<sup>2</sup>

As it is shown in Figures 1-6, the shapes of the curves for fluoride dependence versus charge are different at 10 A/m<sup>2</sup> from those at 30 and 50 A/m<sup>2</sup> for both concentrations. This finding suggested that the removal process of fluoride by electrocoagulation with aluminium sacrificial anode occurred faster as the applied charge increased when the applied current density was 10 A/m<sup>2</sup>, for both fluoride concentrations. Also for both concentrations and applied current densities of 30 and 50 A/m<sup>2</sup>, the process was faster at the beginning, which was in accordance with the electrocoagulation process progress.

### **Conclusions**

Electrocoagulation with aluminium sacrificial anode was effective in fluoride removal from aqueous media both at fluoride initial concentration of 5 mg/L and 10 mg/L. The fluoride concentration was under 1.5 mg/L, the recommended limit of the fluoride in drinking water by WHO, for an applied current density of 30 A/m<sup>2</sup> and 50 A/m<sup>2</sup>, respectively.

As the electrolysis time increased the removal efficiency of fluoride increased for any applied current density and initial concentration of fluoride. The best results were obtained at 50 A/m<sup>2</sup> and 50 minutes of electrolysis and the fluoride removal efficiency for initial concentration of fluoride of 5 mg/L and 10 mg/L was 96.2% and 97.8%, respectively.

### **Acknowledgements**

This work was financed by Programme Nucleu through the project PN 09-13 03 22.

### **References**

- [1] W.H.O., Guidelines for Drinking Water Quality, fourth edition, 2011.
- [2] A. Bhatnagar, E. Kumar, M. Sillanpaa, Chem. Eng. J. 171 (2011) 811.
- [3] S.K. Swaina, S. Mishrab, T. Patnaikc, R.K. Patel, U. Jhaa, R.K. Deye, Chem. Eng. J. 184 (2012) 72.
- [4] M. Islam, R.K. Patel, Chem. Eng. J. 169 (2011) 68.
- [5] A. Bansiwala, P. Pillewan, R.B. Biniwale, S.S. Rayalu, Micropor. Mesopor. Mat. 129 (2010) 54.
- [6] J. Kang, B. Li, J. Song, D. Li, J. Yang, W. Zhan, D. Liu, Chem. Eng. J. 166 (2011) 765.
- [7] S. Lunge, D. Thakre, S. Kamble, N. Labhsetwar, S. Rayalu, J. Hazard. Mater. 237–238 (2012) 161.
- [8] V. Tomar, S. Prasad, D. Kumar, Microchem. J. 111, (2013) 116.
- [9] J. Wang, W. Xu, L. Chen, Y. Jia, L. Wang, X.-J. Huang, J. Liu, Chem. Eng. J. 231 (2013) 198.
- [10] A. L. Srivastava, P. K. Singh, V. Srivastava, Y. C. Sharma, J. Hazard. Mater. 263 (2013) 342.
- [11] C. Yang, L. Gao, Y. Wang, X. Tian, S. Komarneni, Micropor. Mesopor. Mat. 197 (2014) 156.
- [12] I. Ali, Z. A. AlOthman, M. M. Sanagi, J. Mol. Liq. 211 (2015) 457.
- [13] B.-S. Zhu, Y. Jia, Z. Jin, B. Sun, T. Luo, X.-Y. Yu, L.-T. Kong, X.-J. Huang, J.-H. Liu, Chem. Eng. J. 271 (2015) 240.
- [14] N. Kabay, O. Arar, S. Samatya, U. Yuksel, M. Yuksel, J. Hazard. Mater. 153 (2008) 107.
- [15] F. Elazhar, M. Tahai, A. Achatei, F. Elmidaoui, M. Taky, F. El Hannouni, I. Laaziz, S. Jariri, M. El Amrani, A. Elmidaoui, Desalination 249 (2009) 154.
- [16] D. Dolar, K. Kosutic, B. Vucic, Desalination 265 (2011) 237.
- [17] N. Drouiche, S. Aoudj, H. Lounici, M. Drouiche, T. Ouslimane, N. Ghaffour, Procedia Eng. 33 (2012) 385.
- [18] D. Gosh, C.R. Medhi, M.K. Purkait, Chemosphere 73 (2008) 1393.

## Indium Decorated Silver Nanowires

Radu Banica<sup>1,2</sup>, Cristina Mosoarca<sup>1\*</sup>, Petrica A. Linul<sup>1</sup>, Terezia Nyari<sup>1,2</sup>, Nicolae Vaszilcsin<sup>2</sup>

<sup>1</sup>*Renewable Energies Laboratory – Photovoltaics, National Institute for Research and Development in Electrochemistry and Condensed Matter, Str. Dr. A. Paunescu Podeanu, nr.144, 300569 Timisoara, Romania*

<sup>2</sup>*University Politehnica Timisoara, Piata Victoriei 2, 300006 Timisoara, Romania;*  
*Corresponding author: mosoarca.c@gmail.com*

Metal nanowires have broad applications in energy conversion devices, but also in medicine [1]. Silver nanowires, due to the high electrical conductivity of the metal and good corrosion resistance, are increasingly used in the electronics industry and for the manufacture of flexible electrically conductive electrodes. An important problem existing in the production of these electrodes is the strong adsorption of the polyvinylpyrrolidone (PVP) surfactant on the nanowires surface. The PVP layer leads to an increased contact resistance between the metal nanowires. A number of methods for desorption of the PVP from the nanowires have been investigated [2]. Out of these the thermal treatment and the plasma cleaning have yielded the best results. The first method cannot be applied to the electrodes with inexpensive polymer substrate and the second method involves the use of vacuum and expensive equipment. In order to reduce the contact resistance between nanowires, their decoration with metal nanoparticles having a low melting point may be a solution. In this paper the silver nanowires decoration with indium nanoparticles and the influence of temperature on the alloying process was studied by transmission electron microscopy (TEM) and energy dispersive X-ray analysis (EDX).

### References

- [1] R. M. Silva, J. Xu, C. Saiki, D. S. Anderson, L. M. Franzi, C. D. Vulpe, B. Gilbert, L. S. Van Winkle, K. E. Pinkerton, Short versus long silver nanowires: a comparison of in vivo pulmonary effects post instillation, *Particle and Fibre Toxicology*, 2014, 11, 32-52;
- [2] S. F. Li, H. Y. Zhang, Effect of polyvinylpyrrolidone on the preparation of silver nanowires, *Advanced Materials Research*, 2014, 883, 940-943

### Acknowledgements

This work was supported by a grant of the Romanian Ministry of National Education, CNCS – UEFISCDI, project number PN-II-ID-PCE-2012-4-0398.

## Studies on the Antimicrobial Activity of Aqueous Acids Solutions of Chitosan

Ileana Nichita<sup>1\*</sup>, Adriana Popa<sup>2</sup>, Emil Tirziu<sup>1</sup>, Radu Valentin Gros<sup>1</sup>, Monica Seres<sup>1</sup>,  
Claudia Sala<sup>1</sup>

<sup>1</sup>Banat's University of Agricultural Sciences and Veterinary Medicine "King Michael I of Romania" from Timisoara, Faculty of Veterinary Medicine, 300645, Aradului Street No. 119, Timisoara, Romania

<sup>2</sup>Institute of Chemistry Timisoara of Romanian Academy, Bv. Mihai Viteazu 24, 300119, Timisoara, Romania

\*e-mail: nichita\_ileana@yahoo.com

### Abstract

The paper presents the results of the antimicrobial activity of two aqueous acid solutions of chitosan. Chitosan is a copolymer of glucosamine and N-acetylglucosamine prepared from chitin by deacetylation. It is a natural and non toxic product that tends to be widely-used in medicine and food industry.

The antimicrobial effect was tested against the representative Gram-positive bacteria: *Staphylococcus aureus* and *Bacillus cereus* and Gram-negative bacteria: *Escherichia coli* and *Pseudomonas aeruginosa* and one species of yeast: *Candida albicans* using disc diffusion test. Chitosan had a good antimicrobial action of all tested species. The best antibacterial activity was observed for the acetic acid solution. The acetic acid solution chitosan also present an good antifungal activity. The lactic acid solution of chitosan present antibacterial activity.

**Key words:** chitosan; acid solutions, antimicrobial activity

### Introduction

Chitosan was the subject of various researches during last years [1, 4, 5].

This substance is a copolymer of glucosamine and N acetylglucosamine, prepared by deacetylation from chitin. Being a natural product it considered a non toxic substance. It has a high molecular weight, a poor solubility at neutral pH and a high viscosity in solution [6].

Even the chitosan was considered an important source of bioactive material its use in food, cosmetics and health industry is still limited [6, 7].

Taking in consideration that the antimicrobial activities of chitosan are greatly dependent on its physical characteristics it was considered to investigate the antimicrobial activities of chitosan against two aqueous acid solutions of chitosan. Thset were performed using two Gram-positive bacteria (*Staphylococcus. aureus* - ATCC 25923 and *Bacillus cereus* - ATCC 11778) and two Gram-negative bacteria (*Escherichia coli* - ATCC 25922 and *Pseudomonas aeruginosa* - ATCC 27853), and one specie of yeast of *Candida albicans* - ATCC 10231.

### Experimental

For these tests, were prepared two acid aqueous solutions from chitosan using acetic and lactic acid. The chitosan solution (acetic and lactic) were prepared in 1 % (v/v) acetic solution acid at a concentration of 1% (w/v) and the lactic solution acid at a concentration of 1% (w/v), respectively. These solutions were maintained at 37°C to maintain theirs fluidity.

The antimicrobial activity of these chitosan acid aqueous solutions was tested on four standard bacteria strains (MediMark Europe Company, France): two Gram-positive bacteria – *S. aureus* (ATCC 25923) and *B. cereus* (ATCC 11778) and two Gram-negative bacteria – *E. coli* (ATCC 25922) and *P. aeruginosa* (ATCC 27853), and on a strain of *C. albicans* (ATCC 10231). Standard microbial cultures were maintained in laboratory conditions, at 4°C, in tubes with Mueller-Hinton broth (Oxoid) for bacteria and Sabouraud dextrose broth for yeasts. For



these tests, active cultures (24 h old for bacteria and, respectively, 48 h for yeast) were prepared and all these cultures were diluted 1: 1000. Both aqueous acids solutions of chitosan were subjected to the disc diffusion test [8].

For this methods were prepared discs from filter paper that were sterilized. These discs were impregnated with aqueous acids solutions of chitosan. For the bacterial strains was also tested the Gentamicine inhibition effect and Nystatin for *C. albicans*. Also, discs impregnated only in acid solutions were tested.

Inhibition zones observed after 24 hours of incubation (48 hours for *C. albicans*) were measured, including the diameter of the disc (6 mm). Tests were repeated three times and the results were statistical analyzed using Microsoft Excel application.

## Results and discussion

From both aqueous acids solutions of chitosan that were tested the best results was obtained with the acetic acid solution. The acetic solution of chitosan gave bigger inhibition zones in all bacteria strains tested and also in *C. albicans*. The acetic solution of chitosan were more effective against *Staphylococcus aureus* and *Pseudomonas aeruginosa* (1.56 mm). Against *E. coli* and *B. cereus* the inhibition zone were smaller (1.23 mm) comparatively with the other bacteria strains. It is important to notice the affect of acetic solution of chitosan against *C. albicans* (1.43 mm), that was equal with the same induced by Nystatin.

The lactic acid solution of chitosan inhibit the grow of bacteria strains (0.76 mm for *B. cereus*, 1.06 mm for *Ps. aeuginosa*, 1.13 mm for *S. aureus* and 0.96 mm for *E. coli*) and *C. albicans* (1.23 mm) but much lower than the acetic acid solution.

The Gentamicine inhibition zones were bigger comparatively with those obtained for both aqueous acids solutions of chitosan. The disc impregnated only with the acetic and lactic solution didn't present any antimicrobial activity.

Regarding the antimicrobial action of chitosan there are controversial results. Some authors reported stronger effects of chitosan on Gram-positive bacteria (e.g. *Listeria monocytogenes*, *Bacillus megaterium*, *B. cereus*, *Staphylococcus aureus*, *Lactobacillus plantarum*, *L. brevis*, *L. bulgaris*, etc.) than for Gram-negative bacteria (e.g. *E. coli*, *Pseudomonas fluorescens*, *Salmonella typhymurium*, *Vibrio parahaemolyticus*, etc.) [4].

This aspect was explained by the fact that gram negative bacteria have a higher hydrophilicity than gram- positive bacteria, making them most sensitive to chitosan. This is due to the charge density on the cell surface that is a determinant factor to establish the amount of adsorbed chitosan. More adsorbed chitosan would evidently result in greater changes in the structure and in the permeability of the cell membrane [4]. Allan and Hadwiger, 1974 [2]. have found that 1% solution of chitosan in 1% of acetic acid had completely inhibited growth of *Candida tropicalis*. Quite similar result (the MIC value of 0.6% solution of chitosan in acetic acid) was found also by Balicka – Ramisz and col., 2005 [3].on *Candida albicans*.

## Conclusion

Aqueous acids solutions of chitosan had a good antimicrobial action of all tested species.

The best antibacterial activity was observed for the acetic acid solution.

The acetic acid solution chitosan also present an good antifungal activity.

The lactic acid solution of chitosan present antibacterial activity

## References

1. Acharya, B., Kumar, V., Varadaraj, M. C., Lalitha, R., & Rudrapatnam, N., Characterization of chito-oligosaccharides prepared by chitosanolysis with the aid of papain and pronase, and their bactericidal action against *Bacillus cereus* and *E. coli*.

- Biochemical Journal, 2005, 391, 167-175.
2. Allan C.R., Hadwigar L.A.- Studies on the fungistatic activity of chitosan. *Exp. Mycology* 3, 258, 1974.
  3. Balicka - Ramisz Aleksandra, Wojtasz-Pajak Anna, Pilarczyk Bogumila, Ramisz A., Laurans L., Antibacterial and antifungal activity of chitosan, ISAH - Warsaw, Poland, 2005, 2, 406-408.
  4. Goy R. C., De Britto D., Assis O. B. G., A Review of the Antimicrobial Activity of Chitosan. *Polímeros: Ciência e Tecnologia*, 2009, 19, 3, 241-247.
  5. Kong, M., Chen, X. G., Ke Xing K, Park, H. J., Antimicrobial properties of chitosan and mode of action: A state of the art review. *International Journal of Food Microbiology*, 2010, 144, 1, 51-63.
  6. Li, Q., Dunn, E. J., Grandmaison, E. W., Goosen, M. F. A., Applications and properties of chitosan. *Journal of Bioactive and Compatible Polymers*, 1992, 7(4), 370-397.
  7. Limam, Z., Selmi, S., Sadok, S., El-abed, A., Extraction and characterization of chitin and chitosan from crustacean by-products: biological and physicochemical properties. *African Journal of Biotechnology*, 2011, (4), 640 - 647.
  8. xxx- Clinical Laboratory Standards Institute. 2006. Performance standards for antimicrobial disk susceptibility tests; Approved standard—9th ed. CLSI document M2-A9. 26:1. Clinical Laboratory Standards Institute, Wayne, PA.

## Semi-empirical Proof of Long Bond States as Intermediates in Mass Spectrometry Fragmentation of Aldohexofuranose Derivatives

Mihai-Cosmin Pascariu<sup>1,2,3</sup>, Loreta-Andrea Bozin<sup>1</sup>, Alina Serb<sup>1</sup>,  
Nicolae Dinca<sup>4</sup>, Eugen Sisu<sup>1\*</sup>

<sup>1</sup>Faculty of Medicine, "Victor Babeș" University of Medicine and Pharmacy of Timișoara, 2 Eftimie Murgu Sq., RO-300041, Timișoara, Romania

<sup>2</sup>Faculty of Medicine, Pharmacy and Dental Medicine, "Vasile Goldiș" Western University of Arad, 86 Liviu Rebreanu, RO-310045, Arad, Romania

<sup>3</sup>"Chemeia Semper" Association, 6 Giuseppe Verdi, RO-300493, Timișoara, Romania

<sup>4</sup>"Faculty of Food Engineering, Tourism and Environmental Protection, "Aurel Vlaicu" University of Arad, 2 Elena Drăgoi, RO-310330, Arad, Romania  
e-mail: sisueugen@umft.ro

### Abstract

Following the observation that the  $m/z$  101 peak is usually the base peak in the electron ionization mass spectra of di-*O*-isopropylidenated aldohexofuranose derivatives, quantum chemical calculations were carried out in order to provide a judicious explanation for the preference of these derivatives towards the cleavage of the exocyclic dioxolane moiety. It was also established that geminal electron donor functional groups play an important part in the stabilization of the radical cation generated during the loss of one electron from these compounds (the ionization process). In this paper, by using the PM7 semi-empirical method we show that the radical character is preferentially located between the C4-C5 carbon atoms from the di-*O*-isopropylidenated derivatives, which is why the C4-C5 bond becomes elongated, thus justifying the cleavage that produces the high intensity peak at  $m/z$  101.

### Introduction

Carbohydrates are oxygen-rich compounds, widely spread in nature and, because of their involvement in the fundamental biological processes, with a large pharmaceutical and diagnostic potential. Examples of such compounds can be found in both drugs (e.g., aminoglycosides) and excipients (e.g. biocompatible surfactants, like long chain glycoderivatives) [1].

Among analytical methods, mass spectrometry offers rich and reliable information regarding the structural details of different compounds, including sugars. The parent structure can be reconstructed after analyzing the fragmentation ions. Their abundance is strictly correlated with their stability, and the diverse electronic or steric effects can give strong information for the predominance of a certain fragmentation path over another. When two fragmentation pathways seem to have equal probabilities of taking place, one can invoke molecular mechanics or quantum chemical calculations for deciding which has the highest probability of occurring.

Theoretically predicted structures of alkane radical cations are characterized by a unique valence, the elongated, one-electron bond (long bond). The optimum length calculated for the carbon/carbon bond of the ethane radical cation, for example, is 1.920 Å, and the dissociation energy ( $D$ ) is 43 kcal mol<sup>-1</sup>. More complex alkane radical cations appear to have one such long bond in which the SOMO (single occupied molecular orbital) and the "radical cation character" are rather highly localized. Recognition of such long bond structures has already proved fruitful in both vapor phase (e.g., mass spectrometry) and solution (e.g., cycloaddition) chemistry of radical cations. Theoretical research has further suggested that ground state long bond structures may be found for radical cations of such functionalized organic molecules as

halocarbons, alcohols and ethers, so sugars could also represent promising candidates in this direction [2].

*Ab initio* theoretical studies suggest a unique stabilizing effect of vicinal electron donor substituents on long bond radical cation structures (Figure 1) for which the calculated structural minimum is instead a long bond structure. For example, the 1,2-ethanediamine radical cation long bond (2.030 Å) structure lies 11.2 kcal mol<sup>-1</sup> below the best localized (aminium salt) type structure, with the long bond maintaining substantial bond strength ( $D = 22.6$  kcal mol<sup>-1</sup>), and a similar result is also produced for ethylene glycol (2.048 Å,  $D = 23.6$  kcal mol<sup>-1</sup>) [2].

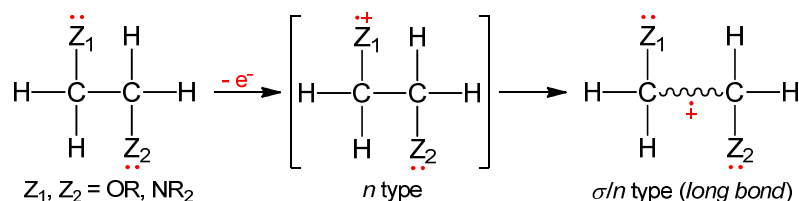


**Figure 1.** Stabilization of radical cations in vicinal groups containing compounds [2]

In this study we investigate the EI-MS (electron ionization mass spectrometry) fragmentation of di-*O*-isopropylidene derivatives of D-glucofuranose, D-galactofuranose and D-mannofuranose (Figure 2). The molecular radical cations were generated from the corresponding neutral molecules during EI-MS experiments conducted in positive ion mode, and were also theoretically analyzed using the PM7 (Parameterized Model 7) semi-empirical quantum chemical method. The findings confirm and explain the mode of cleavage which leads to the abundant  $m/z$  101 ionic fragment in the EI-MS analysis of these sugar acetals (Figure 3). Such sugar derivatives are very useful in organic synthesis as building blocks for a multitude of more complex chiral compounds, including biocompatible and biodegradable surfactants [3].

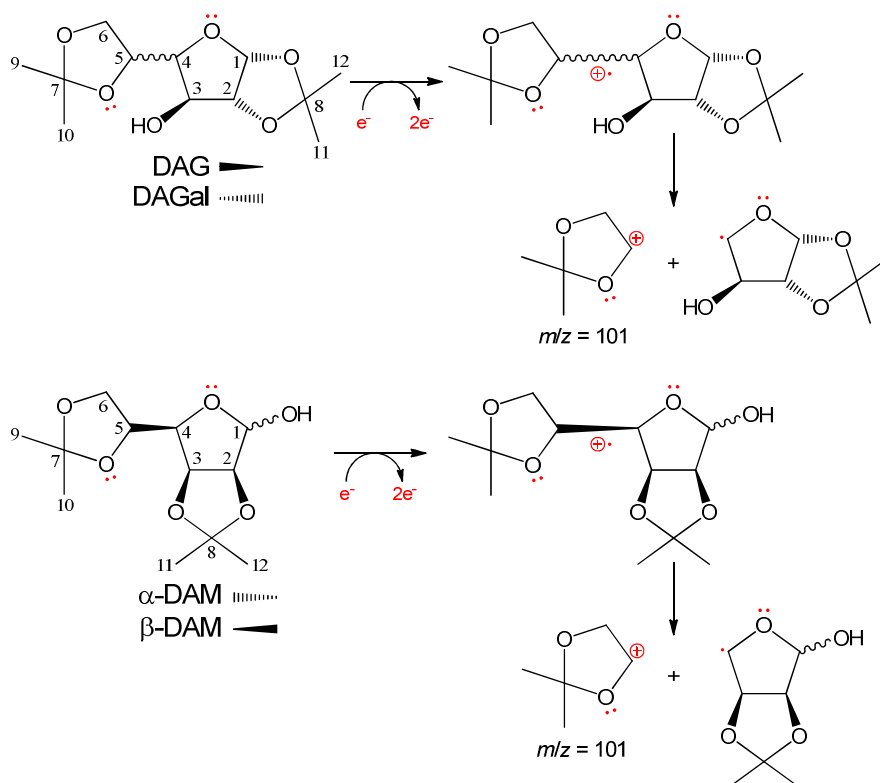


**Figure 2.** Genesis of the 2,2-dimethyl-1,3-dioxolan-4-ylum cation; the true orientation of the wavy bond is given for each family of compounds

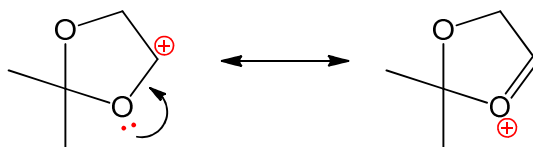


**Figure 3.**  $\alpha$ -Oxy resonance stabilization in 2,2-dimethyl-1,3-dioxolan-4-ylum oxocarbenium ion ( $m/z = 101$ )

## Experimental

The analyzed compounds can be obtained by bis-acetalation of D-glucose, D-mannose or D-galactose with acetone in acidic media. The synthesis of these glycoderivatives and the EI-MS analyses parameters were described in a previous work [3].

All structures were drawn using the *HyperChem* molecular modeling software. After the “Add H & Model Build” command, the starting neutral molecules were pre-optimized with the “MM+” force field (“Polak-Ribière” algorithm, RMS gradient of 0.01 kcal/(Å mol)).

*MOPAC 2012* software was used for PM7 semi-empirical method. The neutral molecules were optimized first, while the radical cations were subsequently obtained from them. Some additional work, like setting the C4-C5 bond length to 2 Å, had to be done. The line of parameters included “GNORM=0.01”, “BONDS”, “AUX”, “GRAPHF” and “PDBOUT”, and also the keyword “OPT” whenever possible. The keyword “SINGLET” was used for neutral molecules, while “CHARGE=+1”, “UHF” and “DOUBLET” were set for radical cations. The data set was obtained by using the “BFGS” algorithm (the “EF” algorithm giving similar results). The resulting structures were analyzed with *Jmol* software.

## Results and discussion

The EI-MS spectra for 1,2:5,6-di-*O*-isopropylidene- $\alpha$ -D-glucofuranose (DAG), 1,2:5,6-di-*O*-isopropylidene- $\alpha$ -D-galactofuranose (DAGal), 2,3:5,6-di-*O*-isopropylidene- $\alpha$ -D-mannofuranose ( $\alpha$ -DAM) and 2,3:5,6-di-*O*-isopropylidene- $\beta$ -D-mannofuranose ( $\beta$ -DAM), taken at 20 eV ionization energy, are given in Figure 4, while the peak intensity values for the  $m/z = 101$  peak are shown in Table 1. As can be seen, this peak, which appears due to the 2,2-dimethyl-1,3-dioxolan-4-ylum cation (Figure 3), has strong intensity, being the base peak in three out of four spectra.

In the case of the radical cations analyzed with the PM7 semi-empirical method, long bonds were observed in the ground state (geometry and heat of formation data given in Table 1), being located for all considered structures between C4 and C5 (where the side 2,2-dimethyl-1,3-dioxolan is connected). It has a length between 2.027 and 2.079 Å (as opposed to 1.528-1.538 Å for the neutral molecule). The O4-C4-C5 and O5-C5-C4 angle values for the radical cations suggest a tendency toward  $sp^2$  geometry with the long bond being almost (but not quite) perpendicular on the plane made by the other three bonds.

**Table 1.** Experimental / calculated parameters (BP = base peak, TIC = total ion current, N = neutral molecule, RC = molecular radical cation)

Compound	Peak intensity (%)		C4-C5 (Å)		O4-C4-C5 (°)		O5-C5-C4 (°)		O4-C4-C5-O5 (°)		$\Delta_f H$ (kcal mol <sup>-1</sup> )	
	To BP	To TIC	N	RC	N	RC	N	RC	N	RC	N	RC
DAG	100.0	18.8	1.538	2.079	104.6	98.7	108.1	99.7	-173.1	165.0	-280.8	-79.7
DAGal	100.0	20.7	1.528	2.027	109.8	102.9	111.0	101.4	66.7	25.3	-278.9	-76.3
$\alpha$ -DAM	86.4	16.7	1.535	2.052	106.8	98.6	106.9	99.9	153.7	171.3	-281.6	-79.2
$\beta$ -DAM	100.0	31.3	1.535	2.051	108.0	99.1	106.7	100.0	139.0	169.3	-278.3	-80.0

The relatively weak long bond, together with the mentioned  $\alpha$ -oxy resonance stabilization (Figure 3), explain very well the high intensity  $m/z$  101 peak.

## Conclusion

The theoretically confirmed long bonds are a strong argument regarding the genesis of the high intensity  $m/z$  101 peak observed in the EI-MS analysis of di-*O*-isopropylidene furanose (glucose, mannose or galactose) derivatives. The results presented in this paper support the utility of such quantum chemical calculations that constitute a strong theoretical background for explaining the experimental data.

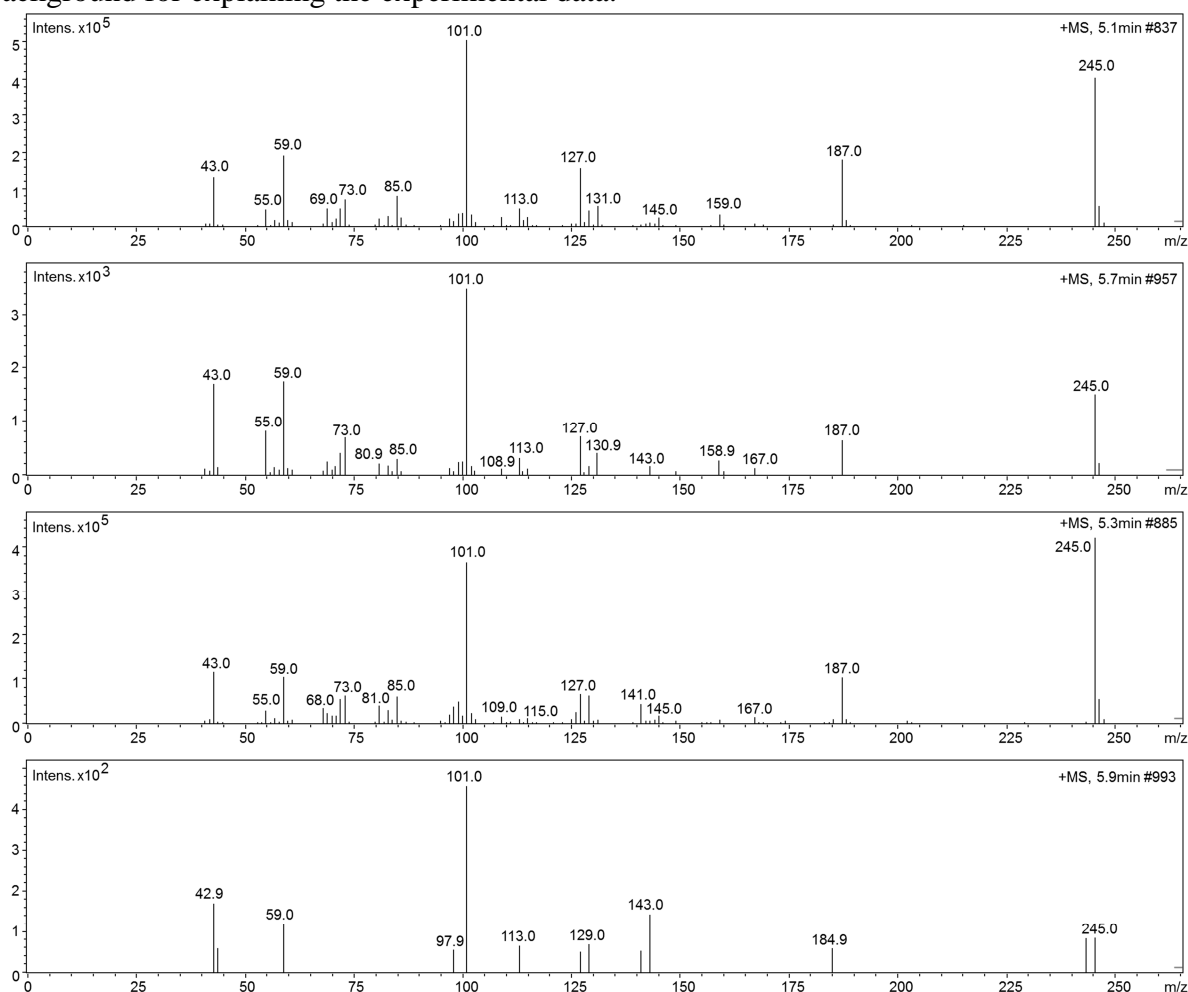


**Figure 4.** EI-MS spectra for (from top to bottom) DAG, DAGal,  $\alpha$ -DAM,  $\beta$ -DAM

## Acknowledgements

This work was supported by the Romanian National Authority for Scientific Research (CNCS-UEFISCDI) through project PN-II-PCCA-2011-142. The research was done in the Center of Genomic Medicine from the “Victor Babeș” University of Medicine and Pharmacy of Timișoara, POSCCE Project ID: 1854, cod SMIS: 48749, contract 677/09.04.2015.

## References

- [1] Carbohydrate-Based Drugs - An Introduction, Drugs and Pharmaceuticals. Current R&D Highlights (Carbohydrate-based Drugs), 33 (2010) 1.
- [2] D.J. Bellville, R.A. Pabon, N.L. Bauld, J. Am. Chem. Soc. 107 (1985) 4978.
- [3] M. Rafailă, M.C. Pascariu, A. Gruia, M. Penescu, V.L. Purcarea, M. Medeleanu, L.M. Rusnac, C.M. Davidescu, Farmacia (Bucharest, Rom.) 61 (2013) 116.



## Oxidic Systems from Some Organometallic Precursors

Mircea Niculescu<sup>1,2</sup>, Mihai-Cosmin Pascariu<sup>2,3,4\*</sup>

<sup>1</sup>University Politehnica Timișoara, Faculty of Industrial Chemistry and Environmental Engineering, 6 Vasile Pârvan Blvd., RO-300223, Timișoara, Romania

<sup>2</sup>“Chemeia Semper” Association, 6 Giuseppe Verdi, RO-300493, Timișoara, Romania

<sup>3</sup>Faculty of Medicine, “Victor Babeș” University of Medicine and Pharmacy of Timișoara, 2 Eftimie Murgu Sq., RO-300041, Timișoara, Romania

<sup>4</sup>Faculty of Medicine, Pharmacy and Dental Medicine, “Vasile Goldiș” Western University of Arad, 86 Liviu Rebreanu, RO-310045, Arad, Romania

e-mail: mihai.cosmin.pascariu@gmail.com

### Abstract

The oxidation of ethylene glycol with Co(II), Ni(II) and Fe(III) nitrates in dilute acid solutions was investigated. The Co(II)/Fe(III) and Ni(II)/Fe(III) heteropolynuclear coordination compounds, having as ligand the oxidation product of ethylene glycol, were both prepared. Under specific working conditions, the oxidation of ethylene glycol to glyoxylic acid takes place, which is coordinated to Ni(II), Co(II) and Fe(III) cations as glyoxylate anion ( $\text{C}_2\text{H}_2\text{O}_4^{2-}$ ), with simultaneous isolation of the corresponding heteropolynuclear coordination compound in both cases. The semi-empirical (PM7) structural investigations of the monomeric units and the thermal analysis (TG, DTG and DSC) of the heteropolynuclear coordination compounds, which are precursors of mixed oxides, are briefly presented.

### Introduction

In our previous papers [1-10], the results of the oxidation of 1,2-ethanediol (ethylene glycol, EG), 1,2-propanediol and 1,3-propanediol with metal nitrates have been described. The complex compounds obtained by this original method contain glyoxylate, oxalate, lactate and 3-hydroxypropionate anions as ligands. The thermal conversion of homo- and heteropolynuclear coordination compounds with carboxylic acid anions as ligands has been carried out, producing metal oxide systems with irreducible structure and properties, which are required by today's technology in different fields: catalysis, electrocatalysis, pigments, electronics, supports for information storage and processing, and also drug industry [11-13]. These coordination compounds undergo thermolysis at relatively low temperatures, giving oxides and gaseous byproducts. The thermal decomposition of solid heteropolynuclear coordination compounds has also been used in the last years for the synthesis of nanoferrites. This method offers the possibility of controlling the composition and microstructure of the final product by selecting suitable ligands. The spinel ferrites and the mixed oxides of spinel type in general show great promise in modern electronic technologies as microwave absorbers, chemical sensors and catalysts, and also in biomedical applications. The fine particle nature of the ferrite, achieved by soft chemistry synthesis methods, is crucial for all these applications [14,15].

This paper shows the results obtained during investigation of EG's oxidation with cobalt(II), nickel(II) and iron(III) nitrates, using an acidic aqueous medium ( $\text{pH} \approx 1 \div 2$ ). The obtained coordination compounds, namely  $[\text{CoFe}_2(\text{C}_2\text{H}_2\text{O}_4)_2(\text{OH}_2)_6\text{O}_2]_n \cdot 1.5n\text{H}_2\text{O}$  and  $[\text{NiFe}_2(\text{C}_2\text{H}_2\text{O}_4)_2(\text{OH}_2)_6\text{O}_2]_n \cdot 1.5n\text{H}_2\text{O}$ , were studied regarding their composition and physical-chemical properties. It was shown that they can also act as precursors for nickel ferrite ( $\text{NiFe}_2\text{O}_4$ ) and cobalt ferrite ( $\text{CoFe}_2\text{O}_4$ ) which can thus be obtained at relatively low temperatures.

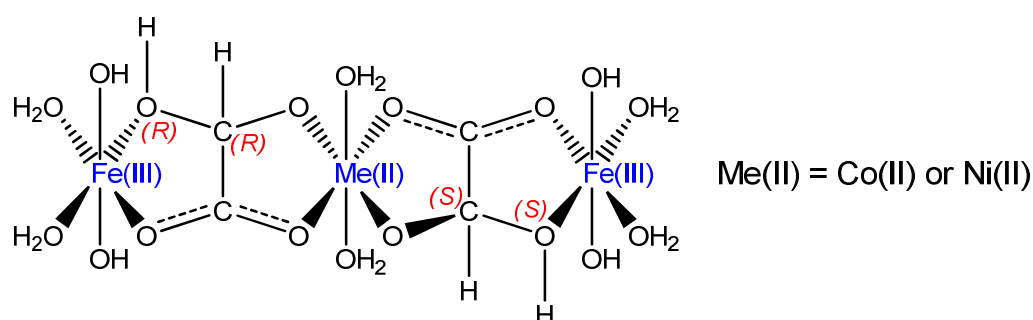
## Experimental

As starting materials,  $\text{Fe}(\text{NO}_3)_3 \cdot 9\text{H}_2\text{O}$ ,  $\text{Ni}(\text{NO}_3)_2 \cdot 6\text{H}_2\text{O}$ ,  $\text{Co}(\text{NO}_3)_2 \cdot 6\text{H}_2\text{O}$ , aqueous nitric acid and EG were employed. The impurities from the reagents are removed in the subsequent purification step of the coordination compound. TG, DTG and DSC curves (in the 25–1000°C range), were registered on a Netzsch Simultaneous TG-DTA/DSC 409PC instrument using a  $10 \text{ K min}^{-1}$  heating rate, in both static air and inert (argon) atmospheres.

Both monomeric structures were drawn using the *HyperChem* molecular modeling software. After the “Add H & Model Build” command, the starting molecules were pre-optimized with the “MM+” force field (“Polak-Ribière” algorithm, RMS gradient of  $0.01 \text{ kcal}/(\text{\AA} \text{ mol})$ ). *MOPAC 2012* software was subsequently used for the PM7 semi-empirical optimization. The line of parameters included “CHARGE=0”, “PM7”, “GNORM=0.01”, “UHF”, “OPT”, “BONDS”, “AUX”, “GRAPHF” and “PDBOUT”. The keyword “SINGLET” was used for the nickel compound, and “DOUBLET” for the cobalt compound. The data sets were obtained by using both the “EF” and the “BFGS” algorithms. The resulting structures were analyzed using the *Jmol* software. PM3 data are also given for comparison.

## Results and discussion

The physical-chemical analyses (electronic spectroscopy, FTIR, XRD) performed have suggested that the monomeric unit should have the following structure for both heteropolynuclear coordination compounds (the *R/S* configurations were randomly chosen for the molecular modeling experiments):



Some parameters obtained through molecular modeling are given in Table 1.

**Table 1.** Heat of formation values for the monomeric units

Structure	$\Delta_f H$ (kcal/mol)		
	PM3	PM7 BFGS	EF
Cobalt compound	-1779.7	-974.7	-977.0
Nickel compound	-1774.6	-1016.9	-1018.5

The molecular models for both monomeric units are shown in Figure 1.

In order to show that  $[\text{CoFe}_2(\text{C}_2\text{H}_2\text{O}_4)_2(\text{OH}_2)_6\text{O}_2]_n \cdot 1.5n\text{H}_2\text{O}$  is decomposed to  $\text{CoFe}_2\text{O}_4$ , the thermal analysis methods were invoked. The obtained TG curves, in air and, respectively, in argon, shown in Figure 2, suggest six steps that take place at the progressive heating of this compound (temperature intervals given for the aerobic decomposition):

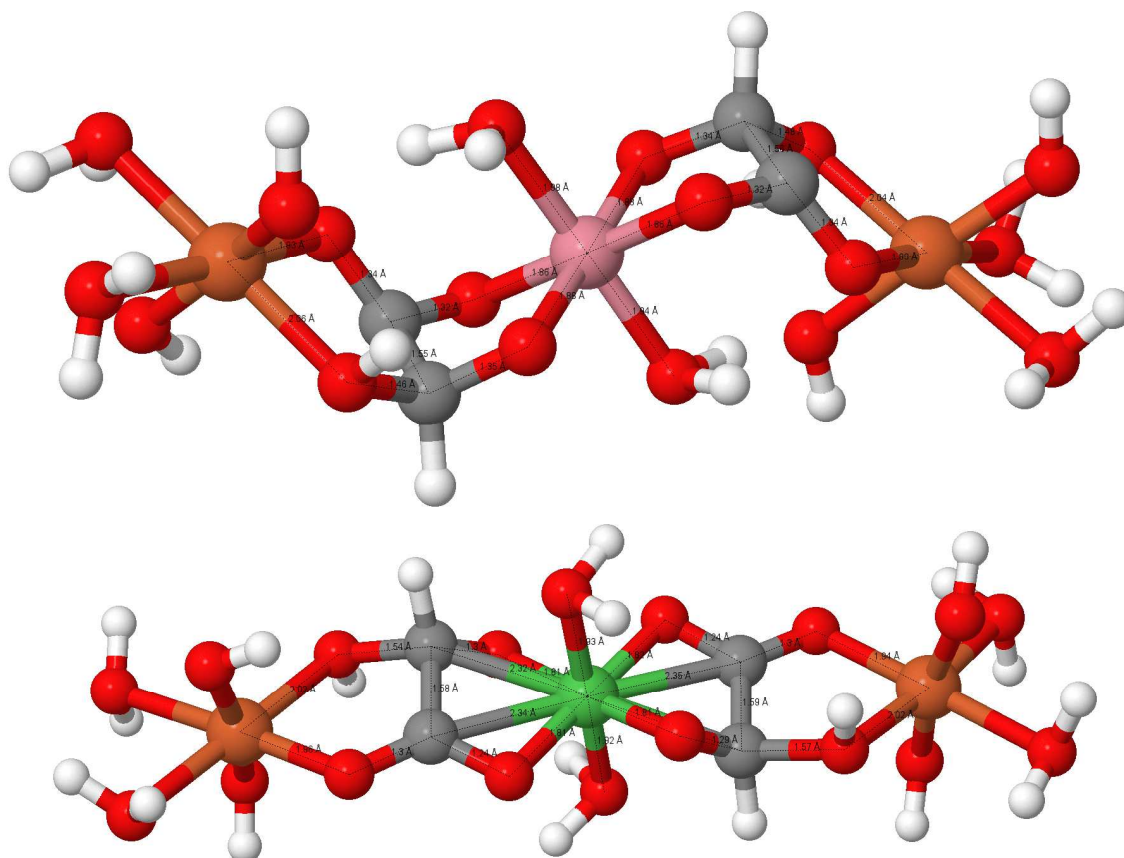


**Figure 1.** Monomeric units (BFGS) of cobalt (left) and nickel (right) coordination compounds

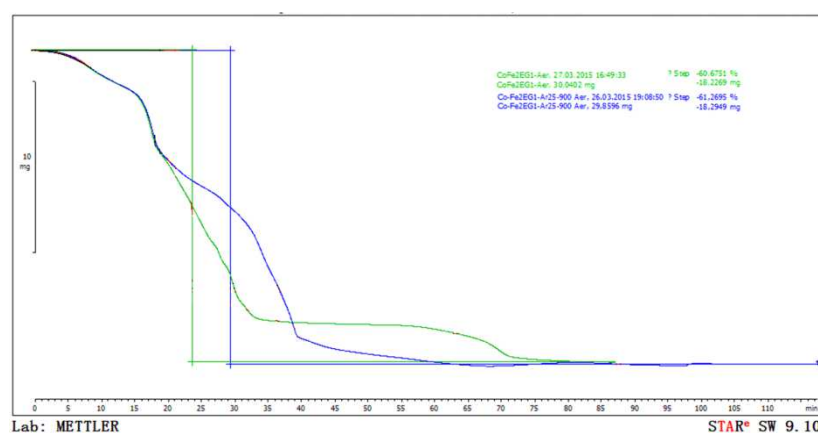
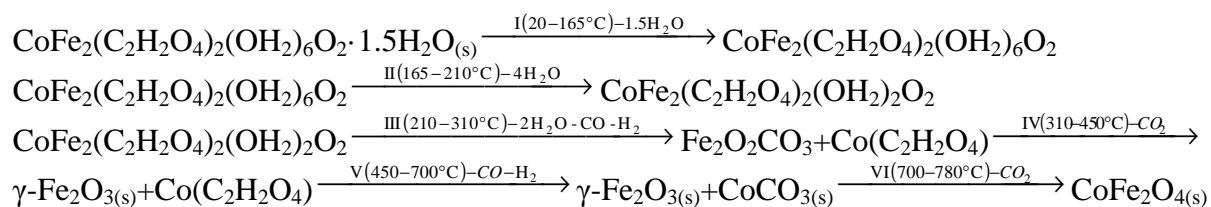
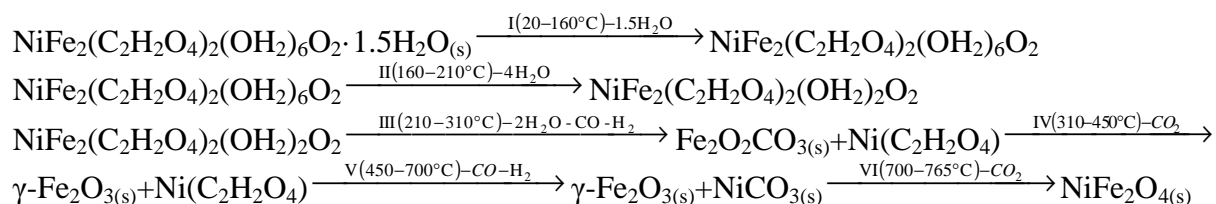


**Figure 2.** TG curves for the decomposition in air (green) and argon (blue) of  $[\text{CoFe}_2(\text{C}_2\text{H}_2\text{O}_4)_2(\text{OH}_2)_6\text{O}_2]_n \cdot 1.5n\text{H}_2\text{O}$

The  $\text{CoFe}_2\text{O}_4$  spinel, obtained at  $780^\circ\text{C}$ , is the final product of the conversion of the  $[\text{CoFe}_2(\text{C}_2\text{H}_2\text{O}_4)_2(\text{OH}_2)_6\text{O}_2]_n \cdot 1.5n\text{H}_2\text{O}$  complex compound,

Similarly, in order to establish the conditions under which the  $[\text{NiFe}_2(\text{C}_2\text{H}_2\text{O}_4)_2(\text{OH}_2)_6\text{O}_2]_n \cdot 1.5n\text{H}_2\text{O}$  complex compound is decomposed to  $\text{NiFe}_2\text{O}_4$ , the thermal analysis methods were also used. The obtained thermograms again suggest six main steps to occur during the aerobic heating of this coordination compound:



The  $\text{NiFe}_2\text{O}_4$  spinel, produced at  $765^\circ\text{C}$ , is the final product of the conversion of the  $[\text{NiFe}_2(\text{C}_2\text{H}_2\text{O}_4)_2(\text{OH}_2)_4\text{O}_2]_n \cdot 1.5n\text{H}_2\text{O}$  coordination compound.

## Conclusion

A new method for the synthesis of coordination compounds having the glyoxylate anion as ligand consists in the oxidation of EG in a diol-water system by nickel nitrate or cobalt nitrate, iron nitrate and nitric acid, with the simultaneous isolation of the corresponding complex compounds in the reaction system. The coordination compounds synthesized by this new method are heteropolynuclear combinations with the formula  $[\text{M}^{\text{II}}\text{Fe}_2(\text{C}_2\text{H}_2\text{O}_4)_2(\text{OH}_2)_6\text{O}_2]_n \cdot 1.5n\text{H}_2\text{O}$  ( $\text{M} = \text{Co}$  or  $\text{Ni}$ ). These compounds were investigated by thermal analysis (TG, DTG and DSC) and quantum chemistry (PM7) methods. The mixed spinels  $\text{M}^{\text{II}}\text{Fe}_2\text{O}_4$  ( $\text{M} = \text{Co}$  or  $\text{Ni}$ ) obtained by thermal decomposition of these heteropolynuclear coordination compounds are the main components of their conversion.

## References

- [1] M. Niculescu, N. Vasilcsin, M. Birzescu, P. Budrueac, E. Segal, J. Therm. Anal. Cal., 63 (2001) 181.
- [2] M. Niculescu, N. Vasilcsin, M. Birzescu, P. Budrueac, E. Segal, J. Therm. Anal. Cal., 65 (2001) 881.
- [3] M. Niculescu, M. Birzescu, E. Şisu, P. Budrueac, Thermochim. Acta, 493 (2009) 1.
- [4] M. Niculescu, R. Dumitru, A. Magda, G. Bandur, E. Şisu, Rev. Chim. (Bucharest), 58 (2007) 932.
- [5] M. Birzescu, M. Niculescu, R. Dumitru, O. Carp, E. Segal, J. Therm. Anal. Cal. 96 (2009) 979.
- [6] M. Niculescu, R. Dumitru, A. Magda and V. Pode, Rev. Chim. (Bucharest), 64 (2013) 271.
- [7] M. Niculescu and P. Budrueac, Rev. Roum. Chim., 58 (2013) 381.
- [8] M. Niculescu, P. Budrueac, I. Ledeti, V. Pode and M. Birzescu, Rev. Roum. Chim., 58 (2013) 387.
- [9] M. Niculescu, D. Roşu, I. Ledeti, M. Milea and P. Budrueac, Rev. Roum. Chim., 58 (2013), 543.
- [10] M. Niculescu, N. Vasilcsin, C.M. Davidescu, P. Negrea, M. Birzescu, P. Budrueac, Rev. Roum. Chim., 48 (2013), 997.
- [11] a) M. Stefanescu, V. Sasca, M. Birzescu, J. Therm. Anal. Cal., 72 (2003) 515.  
b) M. Birzescu, Complex combinations with ethylene glycol and its oxidation products. Ph.D. Thesis, University of Bucharest, 1998.
- [12] M. Brezeanu, E. Safarica, E. Segal, L. Patron, T. Robu, Rev. Roum. Chim., 27 (1982) 137.

- [13] M. Brezeanu, E. Tatu, S. Bocai, O. Brezeanu, E. Segal, L. Patron, *Thermochim. Acta*, 78 (1984) 351.
- [14] J. Haenen, W. Visscher, E. Barendrecht, *J. Electroanal. Chem.* 208 (1986) 273.
- [15] D.P. Lapham, I. Colbeck, J. Schoonman, Y. Kamlag, *Thin Solid Films*, 391 (2001) 17.

## Ecological Survey of Padiş Area, Romania

Mihai-Cosmin Pascariu<sup>1,2,3</sup>, Tiberiu Tulucan<sup>4,5</sup>, Mircea Niculescu<sup>3,6</sup>,  
Iuliana Sebarchievici<sup>7\*</sup>

<sup>1</sup>Faculty of Medicine, "Victor Babeş" University of Medicine and Pharmacy of Timişoara, 2 Eftimie Murgu Sq., RO-300041, Timişoara, Romania

<sup>2</sup>Faculty of Medicine, Pharmacy and Dental Medicine, "Vasile Goldiş" Western University of Arad, 86 Liviu Rebreanu, RO-310045, Arad, Romania

<sup>3</sup>"Chemeia Semper" Association, 6 Giuseppe Verdi, RO-300493, Timişoara, Romania

<sup>4</sup>Izoi - Moneasa Center of Ecological Monitoring, "Vasile Goldiş" Western University of Arad, 94 Revoluției Blvd., RO-310025, Arad, Romania

<sup>5</sup>Romanian Society of Geography, Arad subsidiary, 2B Vasile Conta, RO-310422, Arad, Romania

<sup>6</sup>University Politehnica Timişoara, Faculty of Industrial Chemistry and Environmental Engineering, 6 Vasile Pârvan Blvd., RO-300223, Timişoara, Romania

<sup>7</sup>National Institute for Research&Development in Electrochemistry and Condensed Matter – INCEMC Timişoara, 144 Dr. Aurel Păunescu Podeanu, RO-300569, Timişoara, Romania  
e-mail: iuliana\_p19@yahoo.com

### Abstract

A couple of stream water samples from the Padiş tourist area (Romania) were analyzed using the chemical methods stipulated in the Romanian Pharmacopoeia in order to establish their content of heavy metals and other ions, both cations and anions. Additionally, the samples were investigated using microwave plasma – atomic emission spectrometry (MP-AES) to quantify specific elements, namely aluminium, barium, cobalt, chromium, copper, manganese, molybdenum, nickel, lead, strontium and zinc. The cation levels found were compared with the Romanian and international standards regarding surface and drinking water quality.

### Introduction

The Padiş tourist area is located in the Apuseni Mountains (Western Carpathians, Romania), more precisely in the Bihor Mountains on the west-southwestern slope of Măgura Vânătă Peak (highest altitude: 1641 m). It is placed at the eastern edge of a karst plateau which is developed on an area of about 10 km<sup>2</sup>, at an altitude of around 1300 m, with frequent sinkholes (dolines), uvalas and caves [1].

The hydrographic minibasins are developed on top of the Permo-Mesozoic (sandstones and conglomerates) and the Pannonian Quaternary deposits (sands, gravels and clays). The ponors are located at the lithological contact between the Mesozoic (Anisian) dolomites and the Quaternary deposits, composed of sands, gravels, and clays. The hydrography is characterized by short segments (within 3 km) of epigenous permanent streams (except during extreme drought) which drains the southwestern side of Măgura Vânătă Peak. These streams are focusing towards the many insurgency points (sinkholes) found at the contact between the karstifiable and the non-karstifiable rocks, located in some sinkholes on the plateau (e.g., Trângheşti Ponor). The flow rates are between 1-2 L/s at baseflow and 0.5 m<sup>3</sup>/s at spring floods. The area is wooded with spruce forests (*Picea abies*) and bilberry (*Vaccinium*) which grow on brown acid soils and andosols [1].

Two stream water samples were collected from the Padiş area, one upstream from the main settlement while the other downstream, the two points being separated by a distance of about 1 km. Samples were collected August 2, 2015, at noon. Weather was generally stable



prior and during the sampling, with temperature minima around 8.8°C during the night.

### Experimental

The geographic coordinates and altitudes were established using a Magellan Meridian Platinum Mapping GPS receiver, while air temperature and pressure were recorded with a portable weather station.

The sample temperature, pH, electrical conductivity (EC) and total dissolved solids (TDS) were registered with a portable Hanna HI 98130 Combo pH&EC measuring device. The levels of nitrite and sulfate were estimated *in situ* using Merck test strips (Merckoquant® Nitrit-Test and Merckoquant® Sulfat-Test).

The heavy metal content of solutions may change between sampling and analysis due to adsorption effects on the container walls or by contamination due to extraction of heavy metals already contained in the material of the storage units. To prevent these contaminations thoroughly cleaned plastic recipients were used, taking some special precautions. Thus, the recipients were prepared in the laboratory by protracted soaking with 2M nitric acid followed by rinsing with double distilled water. They were also conditioned *in situ* with several aliquots of the water to be sampled. After completing this protocol a volume of 350 mL of water was collected. Also, to avoid the loss of elements by adsorption on the wall of the storage recipients, the samples were stabilized by acidification to pH~1 by adding 20 mL of 2 mol L<sup>-1</sup> aqueous nitric acid. All glassware needed for analysis was washed with 2 mol L<sup>-1</sup> aqueous nitric acid and thoroughly rinsed with double distilled water just prior of being used [2,3,4].

Preliminary analyses were performed on filtrated samples the day after they were collected according to the general procedures stated by the Romanian Pharmacopoeia (10<sup>th</sup> edition). A blank solution (350 mL double-distilled water with 20 mL 2 mol L<sup>-1</sup> aqueous nitric acid) was also prepared in an identical plastic container and tested for comparison. The following aqueous reagents were used: Nessler's reagent (a mixture of potassium tetraiodomercurate(II), K<sub>2</sub>HgI<sub>4</sub>, and potassium hydroxide, KOH) for ammonium, sodium hypophosphite (NaH<sub>2</sub>PO<sub>2</sub>) in hydrochloric acid (HCl) for arsenic, ammonium oxalate ((NH<sub>4</sub>)<sub>2</sub>C<sub>2</sub>O<sub>4</sub>) for calcium, silver(I) nitrate (AgNO<sub>3</sub>) for chloride, potassium hexacyanoferrate(II) (K<sub>4</sub>[Fe(CN)<sub>6</sub>]) for iron, sodium sulfide (Na<sub>2</sub>S) for heavy metals (e.g., lead) and barium chloride (BaCl<sub>2</sub>) for sulfates. The chemical reactions that use these reagents are stated to have the following detection limits: 0.3 ppm for ammonium, 1 ppm for arsenic, 3.5 ppm for calcium, 0.5 ppm for chlorides, 0.5 ppm for iron, 0.5 ppm for lead and 3 ppm for sulfates [2]. The presence of reducing organic substances was tested using one drop of 0.02 mol L<sup>-1</sup> KMnO<sub>4</sub> and two drops of 98% H<sub>2</sub>SO<sub>4</sub> for 10 mL of sample, followed by heating on the water bath.

For MP-AES an Agilent 4100 with web-integrated Agilent MP Expert software was used. The instrument was adjusted using as calibration standard the provided Wavelength Calibration Concentrate for ICP-OES & MP-AES (Al, As, Ba, Cd, Co, Cr, Cu, Mn, Mo, Ni, Pb, Se, Sr, Zn 50 mg/L, K 500 mg/L). The following wavelengths (in nm) were measured: Al 394.401, Ba 455.403, Co 340.512, Cr 425.433, Cu 324.754, Mn 403.076, Mo 379.825, Ni 305.082, Pb 368.346, Sr 421.552 and Zn 213.857.

### Results and discussion

The surroundings of the sampling sites are illustrated in Figure 1, while the measured sample and environment parameters are given in Tables 1 and 2.



**Figure 1.** The sampling sites for sample 1 (top) and sample 2 (bottom)

**Table 1.** Environment and sample parameters

Parameter	Sample 1	Sample 2
<i>Latitude</i>	46°35'52''N	46°35'49''N
<i>Longitude</i>	022°44'14''E	022°43'50''E
<i>Altitude (m)</i>	1321	1282
<i>Air temperature (°C)</i>	19.6	22.4
<i>Air pressure</i>	657.9	658.8
<i>Sample temperature</i>	12.1	15.5
<i>pH</i>	5.8	5.3
<i>EC (mS/cm)</i>	0.00	0.00
<i>TDS (ppt)</i>	0.00	0.00

**Table 2.** MP-AES cation levels

Sample	Al	Ba	Co	Cr	Cu	Mn	Mo	Ni	Pb	Sr	Zn
<b>1</b>	0.08	0.10	0.00	0.00	0.03	0.04	0.01	0.00	0.00	0.00	0.00
<b>2</b>	0.12	0.10	0.00	0.00	0.05	0.04	0.01	0.00	0.00	0.00	0.01

The ammonium, arsenic, calcium, chloride (also bromide and iodide), iron, heavy metals (i.e., lead), nitrite and sulfate chemical test all gave negative results, an observation also supported by the low conductivity value, which was under the sensibility of the measuring instrument. The only MP-AES detected cations were aluminium, barium, copper

and manganese at low levels, and possibly traces of molybdenum and zinc. A small increase was detected for aluminium and copper in the second sample when compared with the first sample. Also, the pH value dropped by half of a unit, resulting in an increase of acidity for the second sample. The level of reducing organic substances also increased for the second sample.

The pH is below the required minimum value of 6.5 for drinking and surface water, according to both the EU [5] and Romanian [6,7] standards (the WHO [8] standards state no guideline regarding the pH). The measured cation levels are within the imposed limits for drinking water. Also, according to both measured samples, this mountain stream could be included in class I of surface water quality, except for the measured barium and copper levels which place it in class II or III [7].

## **Conclusion**

A negligible increase in the levels of aluminium and copper was observed after the passing of the river through the Padiş settlement. Also, both the acidity and the level of reducing organic substances increase in the same direction, which could relate to natural causes (the acidic soils in the area) or, possibly, to the anthropic activity in the settlement (grazing, logging, and tourism).

## **Acknowledgements**

This work was supported by the Romanian National Authority for Scientific Research (CNCS-UEFISCDI) through project PN-II-PCCA-2011-142. The research was done in the Center of Genomic Medicine from the “Victor Babeş” University of Medicine and Pharmacy of Timișoara, POSCCE Project ID: 1854, cod SMIS: 48749, contract 677/09.04.2015.

## **References**

- [1] M. Măciu, A. Chioreanu, V. Vacaru, G. Posea, M. Ielenicz, M. Pătroescu, I. Velcea, I. Pișota, *Enciclopedia Geografică a României (Romania's Geographic Encyclopedia)*, “Editura Științifică și Enciclopedică” Publisher, București, 1982.
- [2] M.C. Pascariu, A.L. Ciobotaru, T. Tulucan, M.N. Ștefănuț, A. Cătă, I.F. Fițișău, I. Ienașcu, *Jurnal Medical Arădean (Arad Medical Journal)* XVI (2015) 91.
- [3] H. Bradl, C. Kim, U. Kramar, D. Stüben, in: H.B. Bradl (Ed.), *Heavy Metals in the Environment: origin, interaction and remediation*, Elsevier Academic Press, Amsterdam, 2005, pp. 28-164.
- [4] D.O. Ogoyi, C.J. Mwita, E.K. Nguu, P.M. Shiundu, *The Open Environmental Engineering Journal* 4 (2011) 156.
- [5] European Union. 1998. Council Directive 98/83/EC of 3 November 1998 on the quality of water intended for human consumption, downloaded from <http://eur-lex.europa.eu/legal-content/EN/TXT/?uri=URISERV:l28079>, accessed July 12, 2015.
- [6] Romanian Government, Law no. 311 from June 28, 2004, downloaded from [http://www.rowater.ro/dacrisuri/Documente%20Repository/Legislatie/gospodarirea%20apelor/LEGE%20311\\_28.06.2004.pdf](http://www.rowater.ro/dacrisuri/Documente%20Repository/Legislatie/gospodarirea%20apelor/LEGE%20311_28.06.2004.pdf), accessed July 12, 2014. (in Romanian).
- [7] Romanian Government, Order no. 161 from February 16, 2006, downloaded from [http://www.rowater.ro/dacrisuri/Documente%20Repository/Legislatie/gospodarirea%20apelor/ORD.%20161\\_16.02.2006.pdf](http://www.rowater.ro/dacrisuri/Documente%20Repository/Legislatie/gospodarirea%20apelor/ORD.%20161_16.02.2006.pdf), accessed July 12, 2014. (in Romanian).
- [8] World Health Organization. 2011. *Guidelines for Drinking-water Quality*, 4th edition. WHO, 564 p., downloaded from [http://www.who.int/water\\_sanitation\\_health/publications/2011/dwq\\_guidelines/en/](http://www.who.int/water_sanitation_health/publications/2011/dwq_guidelines/en/), accessed July 12, 2015.



## TLC-Densitometric Investigation of Bioactive Components from Mediterranean Algae

Loreta-Andrea Bozin<sup>1#</sup>, Anca Dragomirescu<sup>1#</sup>, Georgeta Simu<sup>1#</sup>,  
Mihai-Cosmin Pascariu<sup>1,2,3</sup>, Alina Serb<sup>1</sup>, Eugen Sisu<sup>1\*</sup>

<sup>1</sup>Faculty of Medicine, "Victor Babeș" University of Medicine and Pharmacy of Timișoara, 2 Eftimie Murgu Sq., RO-300041, Timișoara, Romania

<sup>2</sup>Faculty of Medicine, Pharmacy and Dental Medicine, "Vasile Goldiș" Western University of Arad, 86 Liviu Rebreanu, RO-310045, Arad, Romania

<sup>3</sup>"Chemeia Semper" Association, 6 Giuseppe Verdi, RO-300493, Timișoara, Romania

<sup>#</sup>equal contribution

e-mail: sisueugen@umft.ro

### Abstract

Several photosynthetic pigments from two algae, namely *Padina pavonica* and *Codium fragile*, were extracted in different solvents and subsequently analyzed through TLC. The optimization of the separation parameters led to the choosing of the optimum eluent (hexane/acetone mixture) for polar silica gel plates. The isolated compounds were evaluated through densitometric measurements and by the acquisition of their UV-Vis spectra. While xanthophylls, chlorophyll *a* and pheophytin *a* were the most typical pigments of *Padina pavonica*, chlorophyll *a* and *b*, xanthophyll and  $\beta$ -carotene were the most characteristic pigments for *Codium fragile*.

### Introduction

The algae, omnipresent in seas and oceans, concentrate a wealth of various bioactive substances, which find numerous applications in beauty and health products. Used both internally and externally, they are today a veritable weapon against aging. While strenuous efforts have been made to separate the photosynthetic pigments of phytoplankton, the literature dedicated to those of seaweeds is limited [1–3]. Thus, the present paper aims to expand the knowledge related to the composition and biological roles of the bioactive components of various seaweeds. We selected two species for our study: *Padina pavonica*, a brown algae which is part of the Phaeophyceae class, Dictyotaceae family, and a green algae, *Codium fragile*, from the Bryopsidophyceae class, Codiaceae family. As a reliable and trustworthy analysis method, thin-layer chromatography (TLC) coupled with densitometric analysis was used, through which a multitude of data on the composition of these two algae (including UV-Vis spectra of pure components) were obtained. Some of these constitute the subject of this paper.

### Experimental

Both species of seaweeds were collected from the Tunisian coast in May 2015. They were washed with tap water several times, dried and preserved on ice (-28°C) for further processing. The algae were cut in small pieces, powdered with a blender, and 30 g of dried sample was weighted for each extraction, which was performed for both species with three different solvents, namely methanol, hexane and acetone. Extractions were carried out at room temperature for 24 h under heavy stirring. The extraction mixtures were filtered and the solvent was removed using a rotary evaporator. The evaporated samples were dissolved in a methanol/acetone mixture (1:1 v/v), stirred a couple of minutes, and then placed on the TLC Silica gel 60F<sub>254</sub> plates (10 x 10 cm) from Merck. The plates were eluted in a vertical developing chamber. The densitometric evaluation of the TLC plates was performed using the CAMAG TLC Scanner 3 which is controlled by the winCATS software.

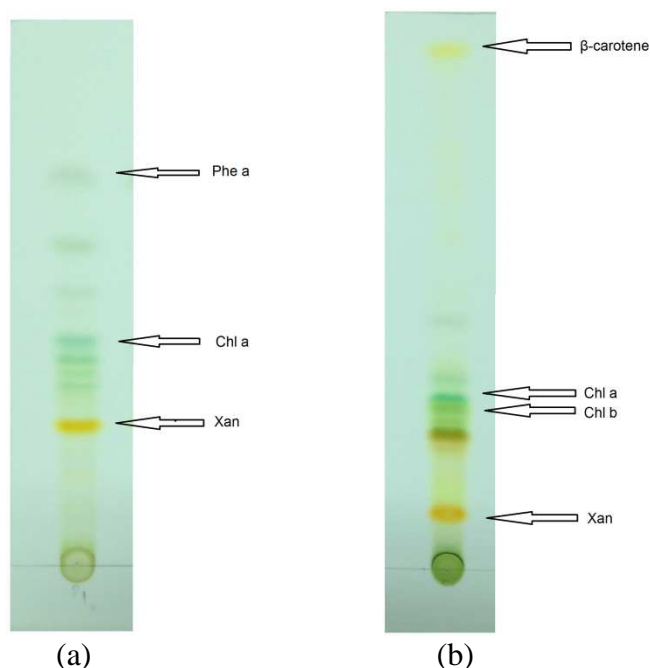
## Results and discussion

Because the dedicated literature contains a scarce amount of experimental data regarding the TLC [5,6] or HPTLC [7,11] separating conditions, in the first stage a study was conducted for determining the optimal eluent which allows the separation of a maximum number of components from these species. The tested eluting systems are shown in Table 1. The most efficient eluent which led to the highest number of separated components was determined to be hexane/acetone 70:30 (v/v).

**Table 1.** Eluents tested for the TLC separation on Silica gel 60F<sub>254</sub> plates

Eluent mixture	% volumes
ethyl acetate : acetone : methanol	60:30:10
ethyl acetate : acetone : methanol	80:10:10
toluene : ethyl acetate : methanol	60:30:10
chloroform : ethyl acetate: methanol	60:30:10
hexane : acetone	65:35
hexane : acetone	70:30

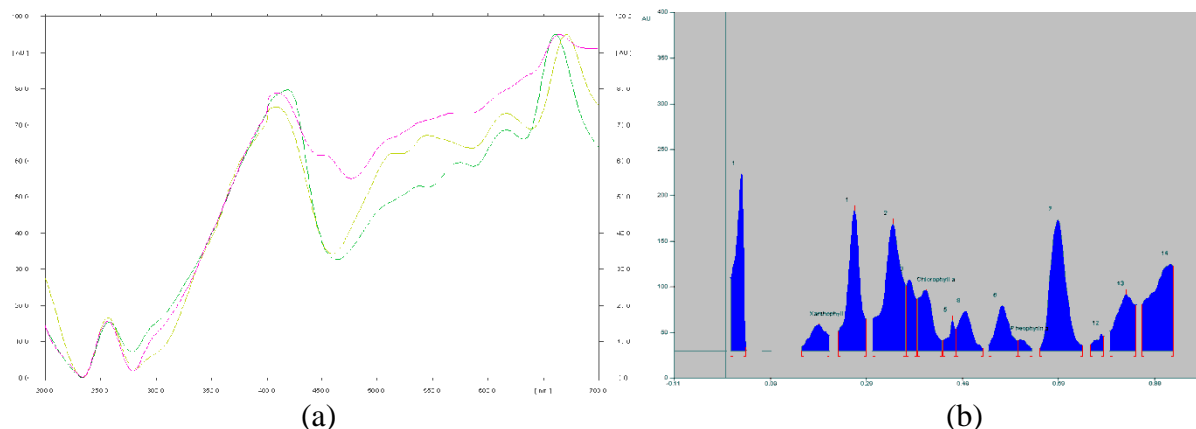
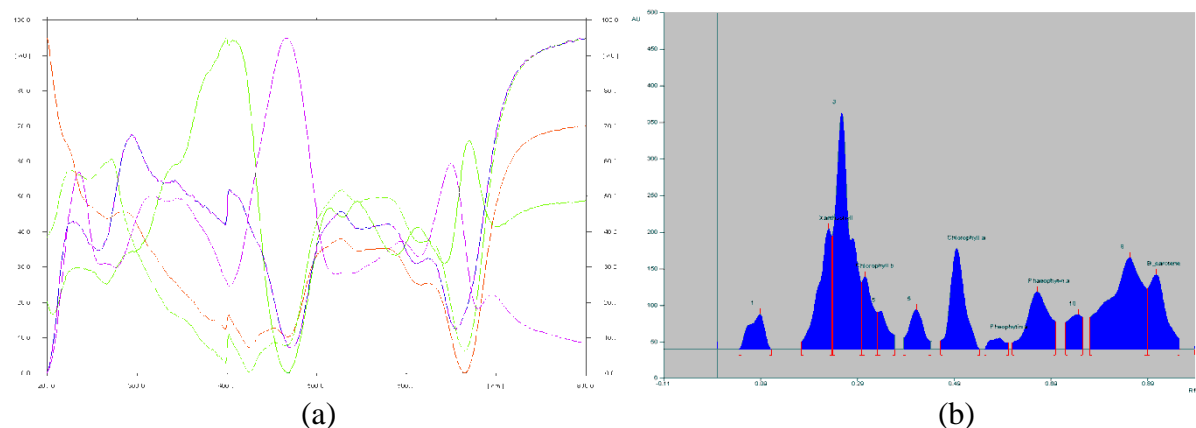
At close inspection of the TLC plates for the methanol extracts (Figure 1), eight peaks are revealed in the case of *Padina pavonica* and nine peaks for *Codium fragile*. Based on the spectral (UV-Vis) characteristics [11], three pigments were identified for *Padina pavonica* (Figure 2A) and four pigments for *Codium fragile* (Figure 3A). The major photosynthetic pigments identified in the two algae, together with their  $R_f$  and the maximum absorbance values, are shown in Table 2. For the quantitative evaluation of the isolated components, the TLC plates were analyzed by densitometry using a 254 nm wavelength UV radiation. The corresponding densitograms are shown in Figures 2B and 3B. Chlorophyll *a* and *b* [4] are characterized by two absorption bands, located in the blue-violet and red region of the spectrum (green photosynthetic pigments), while carotenoids [4,8-10] generally give yellow or orange pigments.



**Figure 1.** TLC plates after elution with hexane/acetone (70:30):  
(a) *Padina pavonica*, and (b) *Codium fragile*

**Table 2.** The major photosynthetic pigments:  $R_f$  and UV-Vis maxima

Substance	$R_f$ (literature)	$R_f$ (determined)	Spectral data (nm)
Chlorophyll <i>a</i>	0.44 [5]	0.42	426, 662
Chlorophyll <i>b</i>	0.32 [5]	0.31	453, 643
Pheophytin <i>a</i>	0.60 [5]	0.58	425, 468, 663
Xanthophyll	0.16 [4]	0.15	421, 667
$\beta$ -carotene	0.91 [4]	0.91	402, 529

**Figure 2.** *Padina pavonica* methanol extract: (a) UV-Vis spectrum of xanthophyll, chlorophyll *a* and pheophytin, and (b) densitogram of all found peaks**Figure 3.** *Codium fragile* methanol extract: (a) UV-Vis spectrum of xanthophyll, chlorophyll *a* and *b*, pheophytin and  $\beta$ -carotene, and (b) densitogram of all found peaks

## Conclusion

Several photosynthetic pigments from two algae, namely *Padina pavonica* and *Codium fragile*, were extracted in various solvents and then analyzed through TLC. The optimization of the separation conditions led to the election of the most favorable eluent (hexane/acetone 70:30) for the silica gel plates. Separated compounds were evaluated through densitometric measurements and UV-Vis spectroscopy [7]. While xanthophylls, chlorophyll *a* and pheophytin *a* were the most typical pigments of *Padina pavonica*, chlorophyll *a* and *b*, xanthophyll and  $\beta$ -carotene were the most characteristic pigments in *Codium fragile*.



## **Acknowledgements**

This work was supported by the Romanian National Authority for Scientific Research (CNCS-UEFISCDI) through project PN-II-PCCA-2011-142.

## **References**

- [1] S.W. Jeffrey, R.F.C. Mantoura, S.W. Wright, *Phytoplankton Pigments in Oceanography: Guidelines to Modern Methods*, UNESCO Publishing, Paris, 1997.
- [2] R.G. Barlow, D.G. Cummings, S.W. Gibb, *Mar. Ecol.: Prog. Ser.* 161 (1997) 303.
- [3] M.M. Hegazi, A. Pérez-Ruzafa, L. Almela, M.E. Candela, *J. Chromatogr. A* 829 (1998) 153.
- [4] L. Jeyanthi Rebecca, S. Sharmila, M.P. Das, C. Seshiah, *J. Chem. Pharm. Res.* 6 (2014) 594.
- [5] H.T. Quach, R.L. Stepper, G.W. Griffin, *J. Chem. Educ.* 81 (2004) 385.
- [6] K. Iriyama, M. Yoshiura, M. Shiraki, S. Yano, S. Saito, *Anal. Biochem.* 106 (1980) 322.
- [7] T. Pocock, M. Król, N.P.A. Huner, *Methods Mol. Biol.* 274 (2004) 137.
- [8] J. Burczyk, *Phytochemistry* 26 (1986) 121.
- [9] J.A. Palermo, E.G. Gros, A.M. Seldes, *Phytochemistry* 30 (1991) 2983.
- [10] F. Shahidi, J.A. Brown, *Crit. Rev. Food Sci. Nutr.* 38 (1998) 1.
- [11] T. Cserhádi, E. Forgács, M. Candeias, L. Vilas-Boas, R. Bronze, I. Spranger, *J. Chromatogr. Sci.* 38 (2000) 145.

# Kazius-Bursi Salmonella Mutagenicity and Carcinogenicity Predicted by the Base of Acute Toxicity in Quantitative SAR (QSAR)-Analysis, by MLR and PNN Applied to 13-Thiophosphonates Pesticides

Alina-Maria Petrescu<sup>1,\*</sup>, Gheorghe Ilia<sup>1,2</sup>

<sup>1</sup> West University of Timisoara, Faculty of Chemistry, Biology, Geography, Dept. of Biology-Chemistry, 16 Pestalozzi Street, 300115 Timisoara, Romania

<sup>2</sup>Institute of Chemistry Timisoara of Romanian Academy, 24 Mihai Viteazu Bvd., 300223, Timisoara, Romania

\*alinapetrescu79@gmail.com

## Abstract

In this paper, the acute toxicity, the carcinogenicity potential, and the **Kazius-Bursi Salmonella mutagenicity** of thirteen compounds were predicted *in silico* technology by ToxPredict software, for *rodent's species*, in a quantitative SAR (QSAR) – analysis. The obtained models demonstrated the dependence of **Kazius –Bursi Salmonella** mutagenicity and carcinogenicity potential with physical-chemical parameters by MLR (multiple linear regression) and PNN (probabilistic neural network).

## Introduction

This approach has its origins in the work of Meyer [1] and Overton [2], from the end of last century and the beginning of our century. Thus, they successfully demonstrated for the first time dependence of bioactivity by physical-chemical parameter, namely, partition coefficient, or lipophilicity by Hansch [3] which is a function of a molecular structure.

Thus, the biological response caused by a bioactive structure with L configuration is determined by its intrinsic activity and its ability to reach a certain receptor, respectively, at a certain site thereof. But if the intrinsic activity of L depends on a number of physicochemical properties and the geometry of molecules, bioactive compound permeability is thought to be the result of a process of passive transport is influenced only by the character of the lipophilic compound.

Therefore, a similar series in which the biological activity must depend, through a simple functional relationship, lipophilicity. And, indeed, was found a linear relationship between biological activity, A, and hydrophobicity, as:

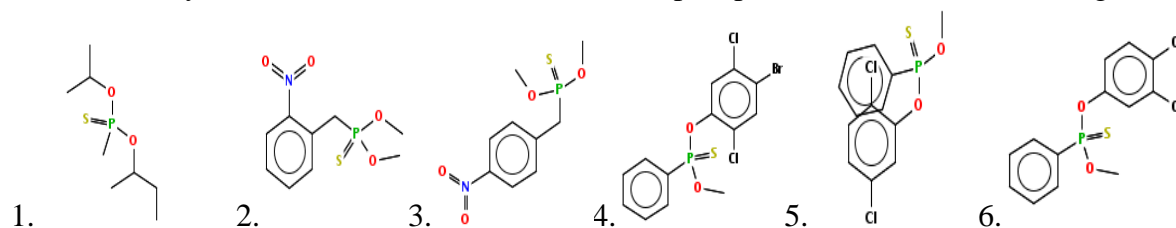
$$A = \log (1 / C) = a_0 + a_1 \cdot \log P \quad (1) \text{ (equation by Hammett, first equation in QSAR)[4]}$$

where C is the molar concentration or dose, which causes a constant biological response, for example; LC50- the concentration required to kill 50% of population that been tested;

and log P represent the logarithmic expression of the partition coefficient between 1-octanol and water, namely hydrophobicity after Hansch [3].

## Experimental

The case study was conducted on a series of 13 thiophosphonates, shown below in figure 1:



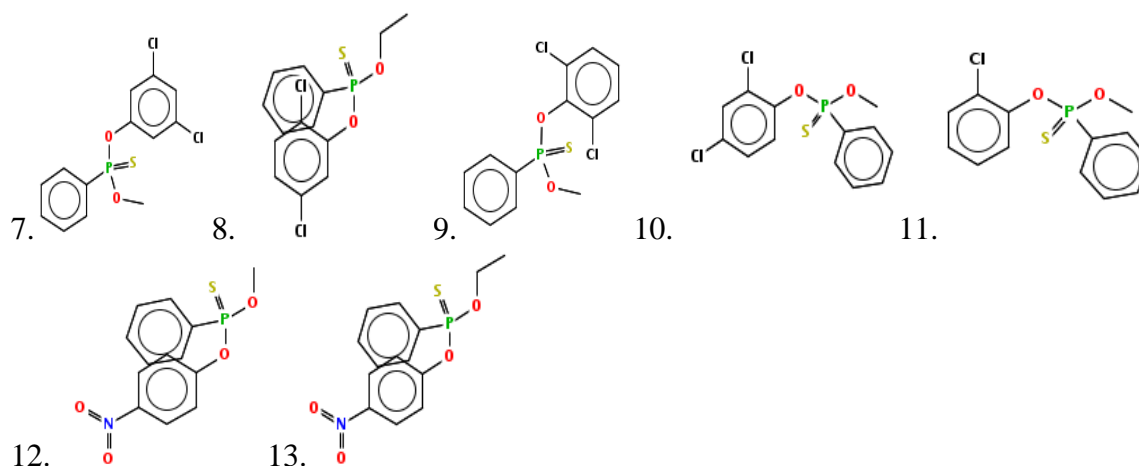


Figure1. Structures of thiophosphonates: **1**: o-butan 2-yl o-propan 2-yl methylphosphonothioate; **2**: AC1LD4KQ ; **3**: AC1LBDMI; **4**: Leptophos; **5**: Debromoleptophos; **6**: BRN 2865560 ; **7**: BRN 2865559; **8**: BRN 2877455; **9**: BRN 2873148 ;**10**. BRN 2871980 ;**11**. BRN 2858294 ; **12**. BRN 2947387; **13**. EPN(O-Ethyl O-(4-nitrophenyl) phenylphosphonothioate) .

The predictions of toxicity, carcinogenicity and mutagenicity were achieved by ToxPredict software [5]. ToxPredict is a web-based interface for predicting toxicity of individual chemicals facilitated by David Gallagher and Barry Hardy[6], and were performed by QSAR modeling, based on the **principle of similarity** between structure and properties, saying that chemicals that have the same structure, generates the same activity [7]. Consequently, biological and toxicological effects of new chemical substances are often derived from existing similar chemical properties. Otherwise, quantitative analysis SAR (QSAR) is based on mathematical algorithms and quantum using physical properties (molecular weight, solubility, melting point, and ionization energy) and chemical properties (such as steric effects, the presence or absence of fragments or functional groups, last orbital energy level: HOMO, and the first orbital energy level: LUMO, and electrophilicity) [8]. The physical chemical properties are obtain by semi-empirical methods, used HyperChem Professional software 7, accessed in 20.08.2015. (Table 2) [9]:

Table 2.The values of the descriptors use in the software ToxPredict

En try	LC50 predicted (mmol)	A=-Log (1/LC 50)	DSS Tox Single CellC all	DSS Tox Multi CellC all	DSS Tox Rat	DSS Tox Mouse	DSST ox MGe	Log P	tPS A	MW	V	HOMO	LUMO
1	0.436	0.36	0.028	0.087	0.068	0.143	0.063	3.37	18.4	210.3	201.1	-9.0929	-1.2433
2.	0.302	0.519	0.046	0.019	0.011	0.0026	0.115	2.90	64.3	261.2	212.5	-9.4326	-1.6643
3.	0.349	0.457	0.067	0.056	0.011	0.052	0.145	2.95	64.3	261.2	212.5	-9.5624	-1.7809
4.	0.179	0.747	0.033	0.020	0.0037	0.0275	0.096	6.81	18.5	412.1	272.2	-9.0344	-1.6017
5.	0.179	0.747	0.033	0.020	0.00368	0.028	0.095	6.07	18.5	333.2	254.3	-9.0545	-1.5044
6.	0.175	0.756	0.015	0.016	0.00368	0.027	0.095	6.07	18.5	333.2	254.3	-9.0023	-1.5207
7.	0.179	0.747	0.055	0.015	0.00367	0.0275	0.124	6.07	18.5	333.2	254.3	-9.2518	-1.5353
8.	0.179	0.747	0.045	0.035	0.00564	0.0275	0.066	6.45	18.5	347.2	271.1	-9.028	-1.4915
9.	0.179	0.747	0.033	0.021	0.00368	0.0275	0.124	6.05	18.5	333.2	254.3	-8.2786	-1.6327
10	0.178	0.749	0.034	0.020	0.00368	0.0275	0.124	6.07	18.5	333.2	254.3	-9.0520	-1.5385
11	0.184	0.735	0.034	0.020	0.00368	0.0277	0.095	5.42	18.5	298.8	240.7	-9.1063	-1.4566
12	0.191	0.719	0.019	0.032	0.419	0.028	0.152	4.75	64.3	309.3	250.5	-9.6330	-1.8934
13	3.6136	0.55	0.017	0.050	0.373	0.027	0.134	5.12	64.3	323.3	267.3	-9.5314	-1.8294

Entry	GPCR ligand	Ion channel	GSK-3	PPAR $\alpha$	Enzyme Inhibitor	Entry	GPCR ligand	Ion channel	GSK-3	PPAR $\alpha$	Enzyme Inhibitor
1	-0.54	-0.37	-1.33	-1.16	0.06	8	-0.13	-0.18	-0.10	-0.03	0.11
2	-0.39	-0.11	-0.87	-0.92	-0.05	9	-0.10	-0.11	-0.11	-0.20	0.12
3	-0.35	-0.02	-0.80	-0.97	0.05	10	-0.12	-0.14	-0.16	-0.24	0.13
4	-0.32	-0.35	-0.31	-0.50	0.1	11	-0.19	-0.16	-0.21	-0.29	0.13
5	-0.12	-0.17	-0.16	-0.20	0.15	12	-0.20	-0.22	-0.17	-0.17	0.04
6	-0.03	-0.19	-0.07	-0.07	0.14	13	-0.21	-0.23	-0.12	-0.02	-0.0
7	-0.02	-0.17	-0.05	-0.08	0.15						

## Results and discussion

**PNN results.** This procedure uses a probabilistic neural network (PNN) [10] to classify cases according to different ligand, and showed Kasius-Bursi Salmonella Mutagenicity based on 5 input variables (biological parameters), like in the Table 3:

Table 3. The values of the descriptors use in the software PNN

Of the 13 cases in the training set, 92.3077 % were correctly classified by the network.

**MLR** (multiple linear regression) results.

Dose response modeling of toxicity pathways involves the integration of mechanism and dosimetric information about the toxicity of a chemical into descriptive mathematical formulas to provide a quantitative model that allows dose extrapolation by MLR.

This response is shown in the Figure 2.

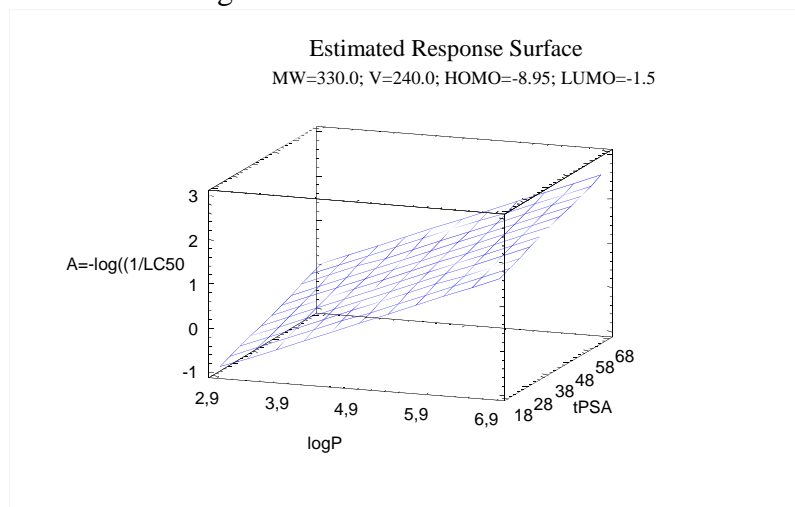


Figure 2. The chart of the estimated response surface of the physico-chemical parameters. We conducted several experiments correlation on quantitative models SAR (QSAR), as predicted data program ToxPredict namely: correlation values quantified according to equation (1) acute toxicity (LC50), the carcinogenicity potential (DSSTox) in mice and rats predicted by a single cell and multi-cell, and mutagenicity potential (DSSToxMGe) to Salmonella, with descriptors of molecular 2D/ 3D obtained through optimization HyperChem: log P (log partition coefficient 1-octanol-water) tPSA (topological area surface), MW (molecular mass) V (molar volume), HOMO and LUMO. The equations (2-4) of the fitted models in MLR, by StatGraphicsCenturion software [10], are:

$$A = -\log(1/LC50) = 3.4575 + 0.6246 \cdot \log P + 0.01939 \cdot tPSA - 0.00063 \cdot MW - 0.020681 \cdot V + 0.06465 \cdot HOMO + 0.5159 \cdot LUMO \quad (2)$$

$R^2 = 0.927121$ ;  $R^2$  (adjusted for d.f.) = 0.854; SEE = 0.05254; MAE = 0.0278, Durbin-Watson statistic = 1.8151 (p = 0.1468)

$$\text{DSSTox} = -1.17072 - 0.1673 \cdot \log P - 0.007 \cdot \text{tPSA} - 0.00021 \cdot \text{MW} + 0.00637 \cdot V - 0.03751 \cdot \text{HOMO} - 0.2901 \cdot \text{LUMO} \quad (3)$$

$R^2=0.849$ ;  $R^2$  (adjusted for d.f.) = 0.698; SEE = 0.01159; MAE= 0.006838; Durbin-Watson statistic = 1.56568 (p = 0.0607)

$$\text{DSSToxMGe} = -0.1538 + 0.0319 \cdot \log P - 0.0006 \cdot \text{tPSA} - 0.0003 \cdot \text{MW} - 0.00159 \cdot V - 0.01693 \cdot \text{HOMO} - 0.2839 \cdot \text{LUMO} \quad (4)$$

$R^2 = 0.9089$ ;  $R^2$  (adjusted for d.f.) = 0.81; SEE= 0.0118091; MSE = 0.00657923; Durbin-Watson statistic = 2.62439 (p = 0.7107)

Where:  $R^2$ -coefficient of the correlation; SEE-standard error of the estimate; MSE-mean error  
The Durbin-Watson (DW) statistic tests the residuals to determine if there is any significant correlation based on the order in which they occur in your data file.

### Conclusion

From ToxPredict software, we obtained the following results: twelve carcinogenic compounds (2÷13), three mutagenic compounds (2, 3, and 13) and eight toxic compounds (4÷12). SAR (QSAR) models were validated in MLR, by  $R^2 = 0.9271$ , for acute toxicity,  $R^2 = 0.849$ , for carcinogenicity potential,  $R^2 = 0.9089$ , for mutagenicity potential, meaning a connection between carcinogenicity potential, mutagenicity, acute toxicity and the physico-chemical properties.

### Acknowledgement

This work was supported by strategic grant POSDRU/159/1.5/S/137750, Project: "Doctoral and Postdoctoral programs support for increased competitiveness in Exact Sciences research" cofinanced by the European Social Fund within the Sectoral Operational Programme Human Resources Development 2007 – 2013. Gainer: "Alexandru Ioan Cuza" University Iasi and West University Timisoara. In addition, I would like to thank to Prof. Dr. Mircea Mracec for giving access to HyperChem software.

### References

- [1] K.H. Meyer, Contributions to the theory of narcosis". *Trans Faraday Societcity* (33) 1062–8(1937).
- [2] C.E.Overton, Studien über die Narkose zugleich ein Beitrag zur all gemeinen, *Pharmakologie*, 1901
- [3] C.Hansch, A.Leo, Exploring QSAR Fundamentals and Applications in Chemistry and Biology, A.C.S, Washington D.C.(1995)
- [4] L.P. Hammett, Louis P, The Effect of Structure upon the Reactions of Organic Compounds. Benzene Derivatives. *Journal of the American Chemical Society*, 59(1), pp. 96-103(1937).
- [5] ToxPredict software, accessed in 30.08.2015, <http://lazar.in-silico.de/predict>
- [6] D. Gallagher, B. Hardy, Collaborative development of predictive toxicology applications, *Journal of Chemoinformatics*, (2010).
- [7] W. Tong, H. Fang, H. Hong, Q. Xie, R. Perkins, J. Anson, D. Sheehan, Regulatory application of SAR/QSAR for priority setting of endocrine disruptors – A perspective, *Pure and Applied Chem*, 75(11-12):2375-2388, (2003)
- [8] A.M.Petrescu, M.V.Putz, G.Ilia, Quantitative Structure-Toxicity Relationships of a Series of Phosphonates, *Environmental Toxicology and Pharmacology*, accepted in 30.08.2015
- [9] HyperChem Profesional software7, accessed in 20.08.2015.
- [10] StatGraphicsCenturion, XVII-X64, software, downloaded and accessed in 02.09.2015.

## Low Cost Production Method of CdS Based Photocatalysts

Radu Banica<sup>1,2</sup>, Petrica A. Linul<sup>1\*</sup>, Andrei Racu<sup>1,3</sup>, Paula Svera<sup>1,2</sup>, Cristina Mosoarca<sup>1</sup>

<sup>1</sup>*Renewable Energies Laboratory – Photovoltaics, National Institute for Research and Development in Electrochemistry and Condensed Matter, Str. Dr. A. Păunescu Podeanu 144, 300569 Timisoara, Romania;*

<sup>2</sup>*University Politehnica Timisoara, 2 Piata Victoriei, 300006 Timisoara, Romania;*

<sup>3</sup>*Institute of Applied Physics of Moldova, ASM, 5 Academiei Str., Chisinau, Moldova;*

Corresponding author: linulpetrica@yahoo.com

In order to produce visible active photocatalysts for water splitting [1] in the presence of sulfide ions, a cheap and environmentally friendly method was developed. Thus, efficient PdS/

Cd<sub>1-x</sub>Zn<sub>x</sub>S type photocatalysts [2] were obtained in a single step by hydrothermally converting cadmium hydroxide originated from Ni-Cd battery wastes in the presence of zinc sulphide. The influence of pH and ultrasonic field on photocatalysis reaction was investigated. The pH was controlled by the addition of NaOH in solution. Photocatalysis experiments were also performed in monochromatic (470 nm) and simulated solar light. The photocatalysts reactivation by hydrothermal treatment was also investigated. The photocatalysts were characterized by X-ray powder diffraction (XRD), transmission electron microscopy (TEM), scanning electron microscopy (SEM), UV-visible spectroscopy, photoluminescence spectroscopy (PL) and energy-dispersive X-ray (EDX).

## References

- [1] Z. Xiong, M. Zheng, C. Zhu, B. Zhang, L. Ma, W. Shen, One-step synthesis of highly efficient three-dimensional Cd<sub>1-x</sub>Zn<sub>x</sub>S photocatalysts for visible light photocatalytic water splitting, *Nanoscale Research Letters*, 2013, 8, 334;
- [2] J. A. Villoria, Rufino M. Navarro Yerga, S. M. Al-Zahrani, Jose Luis G. Fierro, Photocatalytic hydrogen production on Cd<sub>1-x</sub>Zn<sub>x</sub>S solid solutions under visible light: influence of thermal treatment, *Industrial & Engineering Chemistry Research*, 2010, 49, 6854–6861.

## Acknowledgements

This work was supported by a grant of the Romanian Ministry of National Education, project number PN 09-34 02 06.



## Potential Impact of Engineered Nanomaterials Release into Environment

Miljana Prica<sup>1\*</sup>, Savka Adamović<sup>1</sup>, Jelena Radonić<sup>1</sup>, Maja Turk-Sekulić<sup>1</sup>, Milica Velimirović<sup>2</sup>, Jelena Tričković<sup>3</sup>

<sup>1</sup>University of Novi Sad, Faculty of Technical Sciences, Trg Dositeja Obradovića 6, Novi Sad, Serbia

<sup>2</sup>University of Vienna, Department of Environmental Geosciences, Althanstrasse 14 UZAI, 1090 Vienna, Austria

<sup>3</sup>University of Novi Sad, Faculty of Sciences, Trg Dositeja Obradovića 3, Novi Sad, Serbia  
e-mail: miljana@uns.ac.rs

### Abstract

Engineered nanomaterials (ENMs) are defined as a materials with at least one dimension between 1 nm to 100 nm. They have large surface area and specific electronic, optoelectronic, thermal and catalytic properties in comparison to their bulk counterparts, which make them particularly useful. ENMs that are found in different products (paints, cosmetics, medicines, food, sun tan lotions, remediation treatments, etc.) are usually designed to achieve desired properties. Those materials can be released into the environment throughout their entire life cycle and their extensive usage nowadays could led to their accumulation into environment. Over the last twenty years, ENMs have significantly increased in quantity produced, thus their presence in environment could have significant impact. However, understanding the effects that engineered nanomaterials (ENMs) have on environment through these applications is still limited. The aim of this paper is to point out issues releated to release of ENMs into the environment.

**Key words:** engineered nanomaterials, impact, environment, waste

### Introduction

Technologies are constantly changing in a way to provide us a better life, but they also bring new risks. There is a tension between two things: power of science and its capability to avoid consequences, especially in the field of the environment.

The use of engineered nanomaterials (ENMs) has increased during the last years and this will continue in the future. Growth in the usage and development of ENMs has led to their uncontrolled release into different environmental mediums (water, air, soil). ENMs can be released to the environment throughout their entire life cycle [1] and base of that all phases in that process must be monitored.

However, the effects that ENMs have on environment are still not well studied and described. It is likely that, just as the ENMs have influenced science, they will potentially have some effects on environment. Also, these novel materials could pose new challenges to the current waste management strategies either by making them inappropriate or inadequate. The aim of this paper is to point out issues releated to release of ENMs into the environment.

### Discussion

Engineered nanomaterials are identified as a material with at least one dimension between 1 nm to 100 nm. ENMs possess large surface area and they show specific properties (such as electronic, thermal, catalytic, etc.) in comparison to their bulk counterparts. Some of their properties (surface area, biological reactivity, size, durability, tendency to aggregate, hydrophobicity, etc.) may help bonding with different pollutants and facilitate their transport through air, soil and water [2]. ENMs are known to move with significant velocities through

aquifers and soils [3], and may act as carriers for fast transportation of pollutants throughout the environment. For example, polycyclic aromatic hydrocarbons (PAH) [4] can be adsorbed by carbon nanotubes causing an enhancement of the PAH toxicity, and in addition, ENMs have been shown to have affects on the fate, transformation, and transportation of chemical compounds in the environment [5].

ENMs that are found in commercially available products are usually modified in some way: surface and free ENMs are unlikely to be found. Their will most likely be a function of the product matrix and ENM surface characteristics.

The list of most commonly used ENMs consists of fullerenes (e.g., C60), single- and multi-walled carbon nanotubes (SWCNTs and MWCNTs, respectively), nanoclays, and nanoparticles of Ag, Au, TiO<sub>2</sub>, CeO<sub>2</sub>. Due to their properties they can be found in a variety of consumer products such as paints, cosmetics, medicines, food and sun tan lotions, as well as in different applications such as remediation of polluted environments [6]. These ENMs have increased in quantity and volume over the last decades, and their unrestrained release into the environment will probably grow in the following years and decades [7].

Numerous scientific studies have highlighted the influence on science nanomaterials have and exponential growth in nanotechnology [8] but they do not contain enough scientific data on feasible approaches of dealing with nanowaste streams generated at various phases of the nanotechnology-based products and materials life cycle. The insufficiency of scientific publications to address the waste management of nanowaste streams is sign of limited studies in this field and lack of enough verified impacts. However, nanowastes are potentially the most single pathway of introducing ENMs into the environmental systems and because of that this topic certainly deserves scientific attention and further detailed studies. Failure to address these concerns leaves continued uncontrolled release of ENMs into the different environmental mediums that may cause their contamination. In the future, this not only threatens water resources, but, may prove to be impossible to remediate because of: the size of the problems, clean up costs, and insufficiency of adequate technologies for remediation and monitoring tools to identify the contaminated areas.

For example, the cosmetics and personal care sector constitute the largest number of nanoproducts (more than 50%) currently available [9]. Over the last few years the use of ENMs in cosmetics and personal care products has increased for several reasons: ability to absorb and reflect UV light while they remain transparent (e.g. titanium oxide), a excellent antioxidant properties (e.g. C60 fullerene), antibacterial properties (e.g. nanosilver), and anti-aging skin properties (e.g. nanosomes and gold particles). On the other hand, the increased usage of cosmetics will introduce waste streams containing ENMs directly to the aquatic environments (bathing, swimming) or indirectly (sewage systems). This is because of the high concentrations of ENMs in cosmetic products in comparison to other nanoproducts [6]. Also, according to Mueller and Nowack [10] 95% of these nanoscale materials are most likely to end up in water treatment plants. Such data points to potential adverse impacts of nanowaste streams in the environment.

Currently, it has been assumed that the existing waste management technologies have the capability to remove ENMs, but, there are no data available to validate that as this largely remains unknown. Results of Leppard et al. [11] showed that standard wastewater treatment poorly removed ENMs from effluents, nanoparticles being detected in discharges from wastewater treatment plants. The laboratory-scale findings of Westerhoff et al. [12] illustrated the wastewater treatment system inability to remove ENMs from drinking water (low removal efficiencies ranging between 0 and 40%). This implies their potential presence in drinking water, and may pose an exposure pathway to humans [12]. Zhang et al. [13] investigated the dispersion and stability of metal oxide NMs in water as well as their removal through use of

potable water treatment processes. The findings showed that after 24 h of fast aggregation, nanoparticles did not settle out of water efficiently, for example, 20–60% of the initial concentration of 10 mg/l still remained in the settled water. In an aqueous environment containing small concentrations of electrolytes, nanoparticles may be present for a relatively longer time even if they are in an aggregated state [13]. Limbach et al. [14] showed that a significant fraction of the NMs escaped the wastewater plant's clearing system, and up to 6 wt.% of the model compound cerium oxide ( $\text{CeO}_2$ ) was found in the waste stream. This means that current water facilities may face the challenge of removing ENMs as the quantities increases in the future. These findings are important for developing water treatment technologies to remove them from drinking water as well as the effluents. Because research on the efficacy of removing ENMs from wastewater systems has just begun, it is early to draw conclusions on the efficacy of the current waste management systems suitability of dealing with new nanoscale pollutants. As a result, ENMs are likely to pose new challenges to the current waste treatment technologies. One of the problems is reducing waste treatment operational efficacies due to the surface coatings of ENMs.

Also, the use of landfills as a waste disposal is expected to continue into the future and it is likely that products containing ENMs will be placed in landfills at the end of their useful life. This hypothesis has been justified by recent life cycle analyses that suggest over 50% of ENMs produced (worldwide yearly production of 350, 500, and 5000 tones/yr for nano-Ag, carbon nanotubes (CNTs), and  $\text{TiO}_2$ , respectively) will eventually habit in landfills [10].

Current knowledge regarding the long term behavior of nanomaterials in landfill is still limited. Release of ENMs incorporated in commercially-available products is probable mostly for those bound in liquid or gel products (i.e., cosmetics, sunscreens, hair products), wastewater biosolids and in waste streams. After release, they could be easily transferred to the leachate stream. Not enough studies have been conducted evaluating the fate of the ENMs released into the leachate, whether they will aggregate in leachate, or diffuse. Landfill conditions change over time and that may influence ENMs behavior and need to be considered. More over, changes in environmental conditions, such as acidification (acid rain) or changes in the redox potential conditions can favorize mobilisation from the solid to the liquid phase and favour the contamination of surrounding groundwaters. Because of that, it is very important to design laboratory scale experiments that can simulate conditions in landfills. Essentially, degree of leaching from waste is defined by leach resistance. Leaching is known to be a complex phenomenon because many factors may influence the release of specific constituents from a waste over a period of time. These factors include major element chemistry, such as pH value, redox potential, complexation, liquid-to-solid ratio, contact time, etc. Since not enough is known about the chemical species present in these waste forms and their behavior over time, the long-term performance of this waste forms is difficult to predict. Also, leachate limit values have not been established with the particular characteristics and potentially increased toxicity of the nanoform in mind.

One of the wide spread applications of ENMs is also the food packaging. Applications of nanotechnology in fact can provide new food packaging materials with improved mechanical, barrier and antimicrobial properties, together with nano-sensors for tracing and monitoring the condition of food during transport and storage. In particular carbon nanomaterials (CNs) have been attracting a great deal of research interest. Also, carbon nanotubes could be printed on PET and paper to produce chemical sensors to detect  $\text{Cl}_2$  and  $\text{NO}_2$  vapors at sub-ppm concentration levels. These sensors are capable of detecting and differentiating gases and vapors at a ppm concentration level showed the successful implementation of printed CNT-based gas sensors with exceptionally high and immediate sensor response to  $\text{NH}_3$  and  $\text{CO}_2$ . Also, metal nanoparticles such as silver, gold, zinc, or metal oxides have been used in various active packaging applications. Among emerging technologies nanocomposite packages are

predicted to make up a significant portion of the food and beverage packaging market in the near future. But we must have in mind that that every designed package eventually ends up as unwanted waste that must be dealt with at some cost. If the recycling is not resolved, such package can end up at landfills.

### **Conclusion**

Technological development has led to the presence in the waste, of new substances that may influence environment. The majority of monitoring programs and waste treatments are currently based on regulated substances. Currently, questions exist about the potential impacts of materials that are new and not regulated. These materials can be detected in the environment but are not yet included in monitoring programs, and their behavior, fate and ecotoxicological effects are not well understood. Studies that mimic environmentally realistic conditions are necessary to elucidate the real effects of ENMs in the environment. Also, these substances are numerous and widespread in wastes, and conventional waste treatments might be not suitable to deal with them.

### **Acknowledgment.**

The authors acknowledge the support of the Provincial secretariat for science and technological development, Autonomous Province of Vojvodina for participating in ES COST 1205 action and the Ministry of Education, Science and Technological Development, Republic of Serbia (Grant No. TR35015).

### **References**

- [1] F. Gottschalk, B. Nowack, J. Environ. Monit. 13 (2011), 1145.
- [2] A. D. Maynard, R. J. Aitken, Nanotoxicology, 1(1) (2007) 26.
- [3] H. F. Lecoanet, J.-Y. Bottero, M. R. Wiesner, Environ. Sci. Technol. 38(19) (2004), 5164.
- [4] K. Yang, L. Zhu, B. Xing, Environ. Sci. Technol. 40(6) (2006) 1855.
- [5] J. Gao, J.-C. J. Bonzongo, G. Bitton, Y. Li, C.-Y. Wu, Environ. Toxicol. Chem. 27(4) (2008) 808.
- [6] S. Adamović, M. Prica, J. Radonić, J., M. Turk-Sekulić, M., S. Pap, S. (2014). J. Graph. Eng. Des., 5 (2) (2014) 9.
- [7] Musee, N. Environ. Int. 37 (2011) 112.
- [8] P. C. Ke, R. Qiao, J. Phys. Condens. Matter. 19 (2007) 1.
- [9] Woodrow Wilson International Centre for Scholars. A nanotechnology consumer products inventory Project on Emerging Nanotechnologies, 2008.
- [10] N. C. Mueller, B. Nowack, Environ. Sci. Technol. 4 (12) (2008) 4447.
- [11] G. G. Leppard, D. Mavrocordatos, D. Perret, Water Sci. Technol. 50(12) (2003) 1.
- [12] V. H. Grassian (Eds) Nanoscience and Nanotechnology: Environmental and Health Impacts. NJ: John Wiley and Sons, 2008, p. 71 - 90.
- [13] Y. Zhang, Y. Chen, P. Westerhoff, K. Hristovski, C. John, J. C. Crittenden, Water Res. 42 (2008) 2204.
- [14] L. K. Limbach, P. Bereiter, E. Müller, R. Krebs, R. Gälli, W. J. Stark, Environ. Sci. Technol. 42(15) (2008) 5828.

## Effect of Solid Residues from Biogas Plant on Growth and Photosynthetic Characteristics of Cucumber

Marina Putnik-Delić, Ivana Maksimović, Rudolf Kastori, Milica Perišić, Žarko Ilin

*University of Novi Sad, Faculty of Agriculture, 21000 Novi Sad, Serbia  
e-mail: putnikdelic@polj.uns.ac.rs*

### Abstract

Renewable energy sources have an important place in most European countries, with a tendency to increase their share. Biomass deriving from agricultural production is used, besides other purposes, for the production of biogas which is then used to produce electricity or for heating. Solid residues, which remain after the passage of biomass through biogas plant, are still quite voluminous and contain significant amounts of nutrients. In this regard, we studied the effect of solid residues, remained after fermentation, on growth and photosynthesis of cucumber in a semi-controlled conditions. One part of the experiment was done with solid residues as they are, and another part with composted solid residues. Mineral elements were in part supplied by nutrient solution. Significantly higher biomass of cucumber shoots was obtained in the presence of composted solid residues. With increase in amount of added solid residues increased dry weight of cucumber shoots, regardless of additional supply of nutrients through nutrient solution. Similar results were recorded for total leaf area.

### Introduction

The biogas plant is suitable tool not only for exploitation of renewable energy resources but also for designing organic fertilizers by varying anaerobic process parameters like load rate of the reactor, retention time and mechanical treatment before, within and after the anaerobic process (Schäfer et al. 2006). Any biodegradable material of either plant or animal origin can be used for the production of renewable energy (biogas or methane) through anaerobic digestion process (Karki, 2009, Voća et al, 2005). Composition of solid residues from biogas plant as it is and composted solid residues that remained after fermentation of biomass in the biogas plant "Mirotin Energo" Vrbas, show that these residues could be appropriate fertilizer supplements. This is the way to achieve maximum ecological and economic benefits, while at the same time ensuring sustainability and environmental safety (Al Sadi and Lukehurst, 2012). Input streams were: cattle manure, cattle slurry, maize silage, sugar beet chips, sugar beet residue and chicken manure. The quality of biomass supplied to biogas plant, where solid residues are intended for use as fertilizers, is very important since it can affect plant growth. In this regard, the aim of this study was to investigate the effect of various concentrations of solid residue and composted solid residue (remained after fermentation in the biogas plant) on the growth and photosynthetic characteristics of cucumber during vegetative phase, and to identify potential for application of this type of solid residues in vegetable production.

### Material and method

Cucumber seeds, cultivar Tajfun, were sown in the pots ( $V = 750$  ml) containing mixture of agropelrite and various quantities of solid residues and composted solid residues from "Mirotin Energo" biogas plant (Tab. 1). Plants were grown under semi-controlled conditions and watered with respect to evapotranspiration with either  $\frac{1}{2}$  strength Hoagland solution (Hoagland and Arnon (1950); control,  $\frac{1}{2}H$ ),  $\frac{1}{4}$  strength Hoagland solution ( $\frac{1}{4}H$ ) or deionized water (W). One month later plants were analyzed for biomass production of roots and shoots, % of dry matter, total leaf area (by automatic leaf area meter L-3000 (Licor, USA)), and



concentration of photosynthetic pigments (following procedure of Holm, G. (1954) and von Wettstein (1957)).

Tab. 1. Mixtures of agropelrite and solid residues or composted solid residues in which cucumber was grown. Each treatment consisted of 400 ml agropelrite and various amounts of either solid residues (P) or composted solid residues (K). 1/4H and 1/2H denote 1/4 and 1/2 strength Hoagland solution.

Solid residue (g)	Treatment	Composted solid residue (g)	Treatment
0 (control)	1/4H	0 (control)	1/2H
5	1/4H5P	5	W5K
25	1/4H25P	25	W25K
50	1/4H50P	50	W50K
5	W5P	5	1/4H5K
25	W25P	25	1/4H25K
50	W50P	50	1/4H50K

## Results and discussion

Solid residues and composted solid residues from biogas plant affected significantly cucumber growth. Higher proportions of solid residues lead to significant increase in dry weight of cucumber above-ground parts (Fig.1).

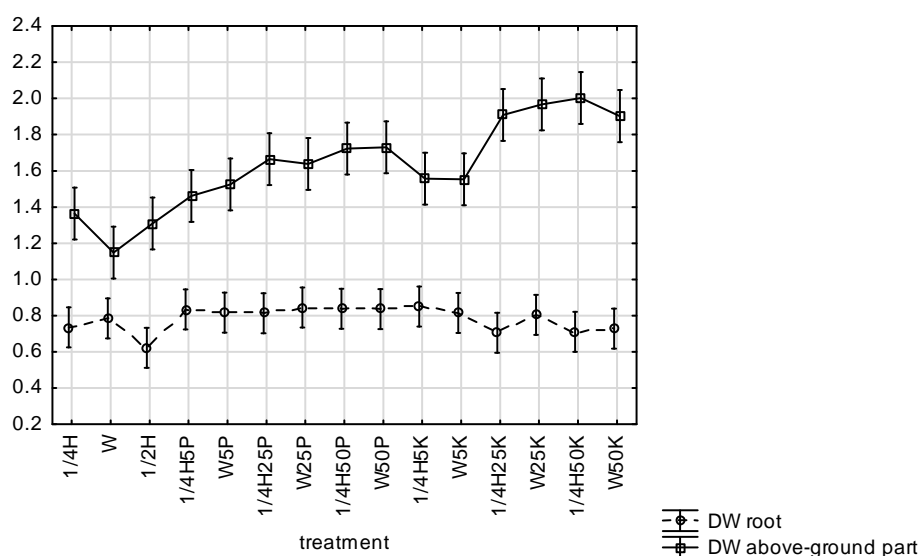
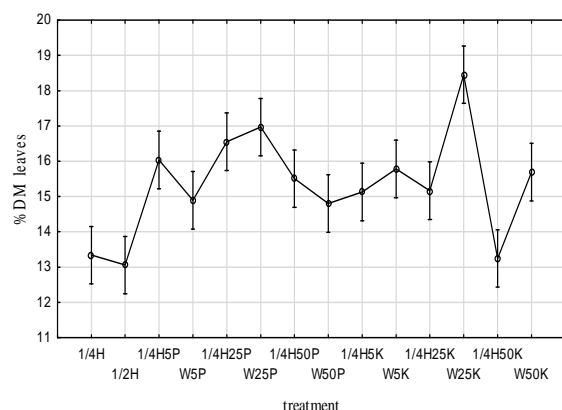


Fig. 1. Effect of solid residues on cucumber dry weight (g/plant). Numbers within labels on the x-axis denote g of solid residues (P) or composted solid residues (K) added to the pot. 1/4H and 1/2H denote 1/4 and 1/2 strength Hoagland solution. Vertical bars denote 0.95 confidence intervals.

Percentage of dry matter increased in comparison to both controls (1/2H and 1/4 H). The highest increase was recorded in leaves under treatment W25K (40% higher % of DW with respect to controls, Fig.2). Total leaf area increased with an increase in the amount of added solid residues. It was the highest in the treatment 1/4H50K: three times higher than the control 1/4H and 1.5 times higher than the control 1/2H (Fig 3).





Numbers within labels on the x-axis denote g of solid residues (P) or composted solid residues (K) added to the pot. 1/4H and 1/2H denote 1/4 and 1/2 strength Hoagland solution. Vertical bars denote 0.95 confidence intervals.

Fig. 2. Effect of solid residues on percentage of dry matter in cucumber leaves.

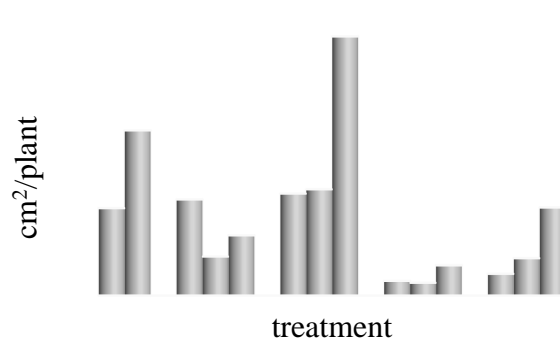


Fig. 3. Effect of solid residues on total leaf area of cucumber

In general, application of solid residues alone, without additional nutrients, resulted in reduced total leaf area, but when applied in combination with (for cucumber) insufficient amount of nutrients deriving from Hoagland solution (1/4H) it exhibited positive effects on cucumber growth (Figures 1, 2, and 3). Similar results were obtained for soybeans where it was shown that application of solid residues from a biogas plant stimulate plant growth, yield and recovery after exposure to stress (Makadi et al., 2012). Qi et al (2005) examined the effect of fermented waste as organic manure in cucumber and tomato production in North China. They found increasing yield (18.4% and 17.8%) of treated cucumber and tomato, respectively.

Concentration of photosynthetic pigments declined with an increase in amount of added solid residues (Fig. 4).

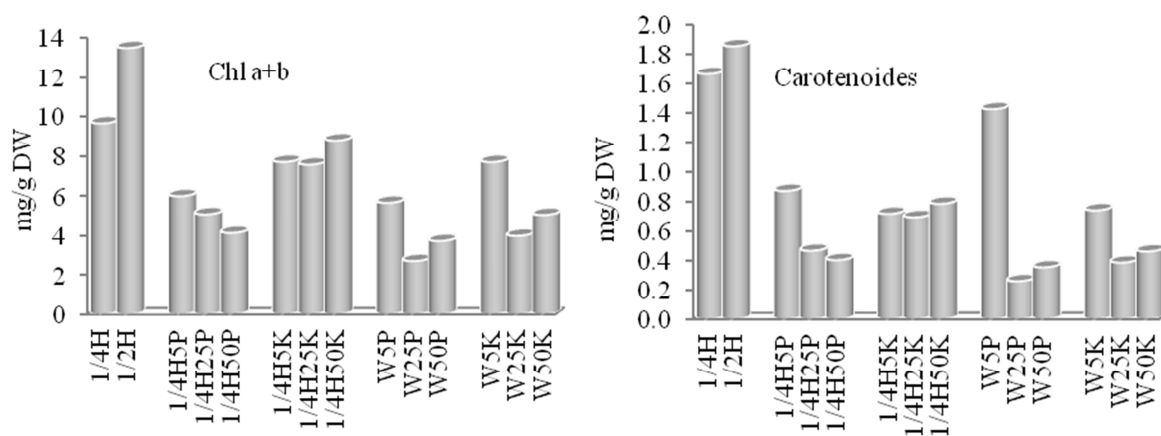


Fig. 4. Effect of solid residues on concentration of photosynthetic pigments

In plants to which was added only water this difference is even more pronounced. In controls (1/4 H and 1/2 H) concentration of chlorophylls was significantly higher (up to 5 times) and carotenoids (up to 7 times) than in plant to which were added solid residues. In spite of reduction in concentrations of photosynthetic pigments, biomass production increased in the presence of solid residues (Fig. 4, Fig. 1). Utilization of solid residues, remained after processing in the biogas plant, as biofertilizers recycles the nutrients and the organic matter, and saves costs to the farmers while enhancing the utilization of their own resources (Al Sadi and Lukehurst, 2012, Liedl, 2006).

### Conclusion

Application of both solid residues as they are and composted solid residues stimulated cucumber growth and this effect was proportional to the amount of applied residues. Percent of dry matter in cucumber leaves increased significantly in the presence of solid residues from biogas plant, regardless of H/W. Concentration of photosynthetic pigments in cucumber declined. Composted residues had better impact on cucumber growth than solid residues that were not subjected to composting prior to application.

### Acknowledgement

Financial support of Ministry of Education, Science and Technological Development of the Republic of Serbia (TR 31036) and Provincial Secretariat for Science and Technological Development APV (No. 114-451-2659) is highly acknowledged.

### References

- [1] T. Al Seadi, C. Lukehurst, Quality management of digestate from biogas plants used as fertilizer. IEA Bioenergy, (2012), 40.
- [2] D. R. Hoagland, D. I. Arnon, The water culture method for growing plants without soil. California Agricultural Experimental Station Circular 347 (1950), 1-32.
- [3] G. Holm, Chlorophyll mutations in barley. *Acta Agriculturae Scandinavica*, 4, (1954), 457.
- [4] A. B. Karki, Biogas as Renewable Energy from Organic Waste. BIOTECHNOLOGY, Vol. X, H. R. Doelle, S. Rokem, M. Beruvic (Eds.), Encyclopedia of life support systems, Eolss Publishers Co. Ltd., Canada, 2009.
- [5] B. E. Liedl, J. Bombardiere, J.M. Chaffield, Fertilizer potential of liquid and solid effluent from thermophilic anaerobic digestion of poultry waste. *Water Science and Technology*, 53 (8), (2006), 6979.
- [6] M. Makádi, A. Tomócsik, V. Orosz, Digestate: A New Nutrient Source. Biogas Edited by Dr. Sunil Kumar, In Tech. (2012), 295-310
- [7] X. Qi, S. Zhang, Y. Wang, R. Wang, Advantages of the integrated pig-biogasvegetable greenhouse system in North China. *Ecological Engineering*, 24, (3), (2005), 175-183.
- [8] W. Schäfer, M. Lehto, F. Teye, Dry anaerobic digestion of organic residues on-farm - a feasibility study. Agrifood Research Reports 77 (2006) 98 p. [www.mtt.fi/met/pdf/met77.pdf](http://www.mtt.fi/met/pdf/met77.pdf)
- [9] N. Voća, T. Krička, T. Ćosić, V. RupiĆ, Ž. Jukić, S. Kalambura Digested residue as a fertilizer after the mesophilic process of anaerobic digestion. *Plant Soil Environ.*, 51 (6), 2005, 262–266.
- [10] D. von Wettstein, Chloropill-letale und submikroskopische formwechsel der plastiden. *Exp. Cell. Res.* 12 (1957), 427-433.

## Effect of strain in Nickel Ferrite thin films

Florina Stefania Rus<sup>1\*</sup>, Andreas Herklotz<sup>2</sup>

<sup>1</sup>National Institute for Research and Development in Electrochemistry and Condensed Matter, Timisoara, Romania

<sup>2</sup>Materials Science and Technology Division, Oak Ridge National Laboratory, Oak Ridge, TN, 37831, USA

e-mail: rusflorinastefania@gmail.com

### Abstract

Nickel ferrite epitaxial thin films grown by PLD technique simultaneously in a series of different thickness varying from 3 to 200 nm on the three (001) orientated substrates SrTiO<sub>3</sub> (STO), MgO and 0.72Pb(Mg<sub>1/3</sub>Nb<sub>2/3</sub>)O<sub>3</sub>–0.28PbTiO<sub>3</sub> (PMN-PT) are studied in this paper. The effects of epitaxial strain on the lattice structure, microstructure and magnetization of nickel ferrite thin films have been studied on several types of single-crystalline substrates with different lattice mismatch. The XRD diffractograms show only (00l) substrate peaks and peaks that can be assigned to the (00l) reflexes of the spinel phase. The films are out-of-plane epitaxial oriented to the substrate. The thinnest films grown on STO and PMN-PT are under a small compressive strain, especially the films on PMN-PT. Here, the strain relaxation is not complete and the strain that is imposed by the substrates is partially maintained. With increasing thickness the strain relaxation of the films proceeds and the strain turns from compressive to tensile. The magnetic properties of a 200 nm nickel ferrite film deposited on STO, MgO and PMN-PT are investigated and correlated with the strain states of the films. The film grown on MgO has the smallest coercive field (980 Oe), whereas the coercive fields of the films grown on STO (2070 Oe) and PMN-PT (2360 Oe) are larger and of about the same magnitude.

### Introduction

Ferrite thin films with spinel structure are potentially interesting and scientifically promising for high frequency devices, where low conductivity and high saturation magnetization are important aspects. The properties of spinel ferrites are of great interest due to its wide implication in magnetic recording media, microwave devices, computer hard disc read/write heads and micro-electromechanical systems and sensors. Among all the ferrites, nickel ferrite (NiFe<sub>2</sub>O<sub>4</sub>) is a ferrimagnetic material used in thin film form efficiently for magnetic cores, opto-magnetic devices, bubble memory devices and vertical recording magnetic materials applications and spintronics [1].

### Experimental

The nickel ferrite target was made of a single phase nickel ferrite powder synthesized by the coprecipitation method. The nickel ferrite thin films were deposited on commercial (001) oriented STO, MgO and PMN-PT substrates using the pulsed laser deposition (PLD) technique. The substrates were ultrasonically washed using acetone and methanol before deposition. A KrF excimer laser (248 nm wavelength and 23 ns pulse width, Lambda Physics) was used for ablating the nickel ferrite target with an energy density of about 4 J/cm<sup>2</sup> and a repetition rate of 10 Hz. The laser beam was focused by optical lenses at an angle of about 45 deg to the rotating target and the substrate was placed at a distance of 4 cm to the target. Before deposition, the chamber was evacuated to 0.08 mbar. The films were deposited at a substrate temperature of 650 °C. After deposition, the films were annealed for 15 min and cooled down to room temperature at an oxygen pressure of about 0.5 bar. The crystallinity

and orientation of the thin films were determined by X-ray diffraction (XRD) analysis using  $\omega$ – $2\theta$  scans, which were performed by Cu radiation (wavelength of 0.154017 nm) using an Panalytical X'Pert MRD diffractometer. Before each XRD analysis, the sample alignment was performed on STO (002) MgO(002) PMN-PT(002) peaks of the substrate in order to avoid the peak shift due to the sample misalignment. The magnetization of thin films was measured for in-plane (magnetic field applied parallel to the film) configurations using a superconductor quantum interference device (SQUID) magnetometer (Quantum Design, MPMS-5 T). The magnetic hysteresis loops (M–H curves) were obtained after subtracting the diamagnetic contribution of the substrate. Atomic force microscopy (AFM) has been employed to investigate the surface of the films. A *DI Nanoscope III* AFM in tapping mode was used for this purpose.

## Results and discussion

The NFO films were grown by on-axis pulsed laser deposition from the  $\text{NiFe}_2\text{O}_4$  target simultaneously on STO, MgO and PMN-PT. The films have been grown in a series of different thickness varying from 3 to 200 nm on the (001) orientated substrates.

In figure 1.a) the reflectivity curves of the films grown on PMN-PT substrates are shown. The thickness of the films is calculated from the distance of the oscillations. The observation of clear thickness fringes is an indication for a good surface roughness of the films.

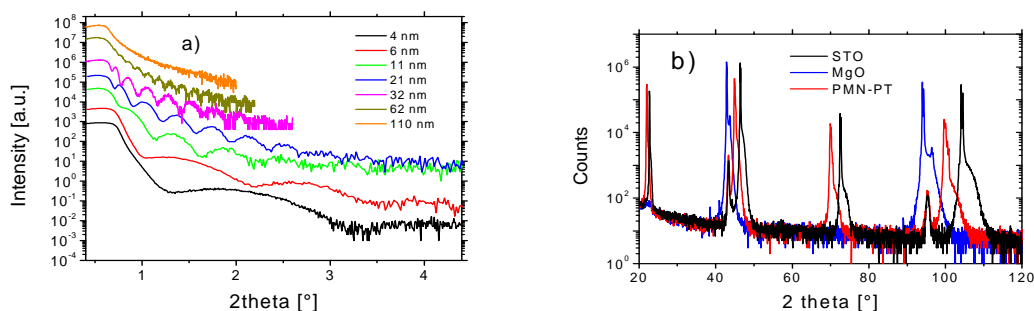


**Figure 1.** a) The reflectivity curves of the films grown on PMN-PT substrates b) X-ray diffraction patterns (Bragg-Brentano  $\theta$ – $2\theta$ ) of the 200 nm films grown on STO, MgO and PMN-PT[1].

Wide angle  $\theta$ – $2\theta$  XRD scans of the films grown on STO, MgO and on PMN-PT have been recorded to investigate the phase-purity and epitaxial nature of the films and are plotted in figure 1.b). The scans show only (001) substrate peaks and peaks that can be assigned to the (001) reflexes of the spinel phase. The films are out-of-plane epitaxial oriented to the substrate. There are no peaks corresponding to other phases or impurities of films.

Reciprocal space maps (RSM) around the (1 1 3) substrate peak and the (2 2 6) film peak were recorded in order to get further information about the strain states of all the films and lattice parameters are presented in Table 1. We find that the peak positions of thick films reveal a  $c$  parameter that almost coincides with the lattice parameter of bulk NFO. This indicates that thick films are essentially strain-relaxed due to the large lattice misfit with STO and PMN-PT (–6.65% and –3.55%). For the thinnest films grown on PMN-PT the peak positions are slightly shifted to the left, i.e. the  $c$  lattice parameter is enhanced. Here the films still take up some partial strain from the substrate and the films are not fully relaxed. The RSM reveal that the films grown on MgO substrate are coherent with the substrate, i.e. the film is strained in-plane to the MgO lattice.

Table 1. In- and out-of-plane lattice parameters of the films [1].

The thickest films of the NFO films all experience a small tensile strain. This tensile strain can be explained by the thermal mismatch between film and substrates [2]. The film on MgO is grown coherent and thus has a quite large tensile strain of about +0.9%. The thinnest films grown on STO on

Sample	Substrate	thickness nm	$a_{\text{substrate}}$ Å	strain %	$c_{\text{film}}$ Å	$a_{\text{film}}$ Å
AH520	STO	22	3.905	-0.053	8.348	8.342
AH517	STO	32	3.905	0.0007	8.346	8.346
AH515	STO	62	3.905	0.120	8.344	8.356
AH516	STO	110	3.905	0.246	8.337	8.348
AH521	STO	200	3.905	0.055	8.341	8.344
AH520	PMN-PT	22	4.022	-0.278	8.389	8.323
AH517	PMN-PT	32	4.022	-0.203	8.376	8.329
AH515	PMN-PT	62	4.022	0.184	8.348	8.362
AH516	PMN-PT	110	4.022	0.218	8.329	8.364
AH521	PMN-PT	200	4.022	0.236	8.324	8.365
AH521	MgO	200	4.212	0.895	8.263	8.421

PMN-PT are under a small compressive strain, especially the films on PMN-PT. Here, the strain relaxation is not complete and the strain that is imposed by the substrates is partially maintained. With increasing thickness the strain relaxation of the films proceeds and the strain turns from compressive to tensile.

## 2 Topography of the Nickel ferrite films

Atomic force microscopy (AFM) was used to investigate the surface of the films. AFM images reveal a film surface that shows a flat film surface but also a large number of droplets. Those droplets are big particles that are formed during the PLD process and are incorporated into the film.

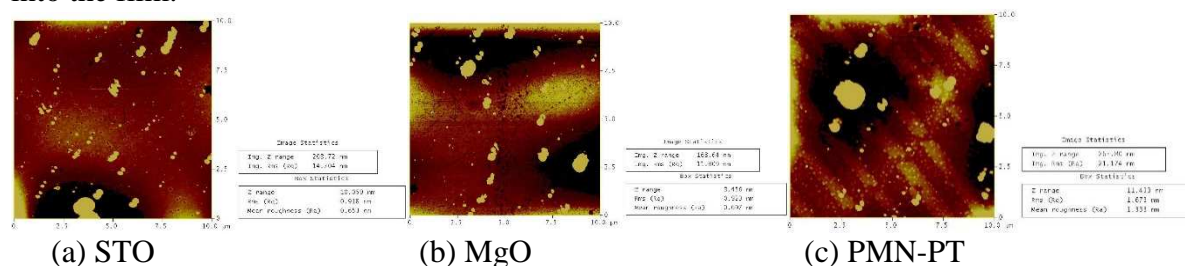
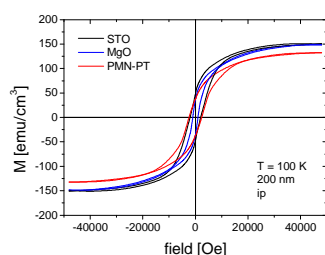


Figure 2: Surface morphology images of 60 nm films of nickel ferrite deposited on a) STO, b) MgO, c) PMN-PT taken by AFM.

## 3 Magnetic properties of the films

The magnetic properties of the N1 films deposited on STO, MgO and PMN-PT are investigated in this part and correlated with the strain states of the films. The 200 nm thick films have been studied since they provide the largest magnetic signal. Fig. 3 shows the in-plane M–H loops at 100K. From the M–H loops the magnetic parameters, such as remanent magnetization  $M_r$ , saturation magnetization  $M_s$  and coercive  $H_c$  are determined. The parameters are listed in table 2. The saturation magnetizations of the films are found to be in the range 130-150 emu/cm<sup>3</sup>. The magnetization of the films is also lower than the bulk value of NFO. This is an experimental observation that was often reported for ferrite spinel films.



Nickel	a [Å]	c [Å]	strain [%]	$M_r$ [emu/cm <sup>3</sup> ]	$M_s$ [emu/cm <sup>3</sup> ]	$M_r/M_s$	$H_c$ [Oe]
PMNPT	8.365	8.324	0.236	37.0	131.5	0.281	2360
S T O	8.344	8.341	0.055	47.8	150.2	0.318	2070
M g O	8.421	8.263	0.895	35.1	149.1	0.235	980

Figure 3 In-plane magnetization versus field (M–H) loops at room temperature of 200 nm nickel ferrite–films grown on an STO, MgO respectively PMN-PT substrates. Table 2 Parameters of in-plane measurement of the 200 nm film [1]

The total magnetic moment per formula unit we calculated using to be  $1.00 \mu_B$  for PMNPT,  $1.153 \mu_B$  for STO and  $1.145 \mu_B$  for MgO. A commonly accepted explanation for the reduced  $M_s$  found films is the presence of anti-phase boundaries (APB) [3]. The film on PMN-PT has the largest lattice mismatch and is thus likely to have the highest concentration of APBs. The lowest saturation magnetization for the film on PMN-PT is in agreement with this picture.

For all films the magnetic hysteresis curve are slim and the ratio  $M_r/M_s$  is small, which indicates that the in-plane measurement is along a magnetic hard axis and that the magnetic anisotropy is out-of-plane. This is in agreement with the tensile strain found in the films. The film on MgO has a significantly lower  $M_r/M_s$  and  $H_c$  than the films on STO and PMN-PT. This means that the film on MgO has the largest out-of-plane anisotropy. It is a result of the pronounced negative magnetostriction in NFO that forces the easy axis to rotate further into the film normal and enhance the anisotropy under increasing tensile strain. The measurements show that epitaxial strain can be used to tailor magnetic properties of NFO films.

## Conclusion

Epitaxial films of nickel ferrite have been grown on single crystalline (001) oriented SrTiO<sub>3</sub> and MgO and PMN-PT substrates. We have observed that thin films grown under compression on STO and PMN-PT. The saturated magnetization we observe to be the smallest for the film grown on PMN-PT. We also find a correlation of epitaxial strain and magnetic anisotropy. The results are in agreement with a strain-driven change of the magnetic anisotropy that is based on the large negative magnetostriction of NFO. The results demonstrate that epitaxial strain can be deployed to tune the magnetic properties of nickel ferrite films. This could potentially be used to produce films with properties designed for specific application.

## Acknowledgements

This work was supported by a grant of the Romanian Ministry of National Education, project number PN 09-34 02 06.



## **References**

- [1] PhD thesis S. F. Rus Nanomateriale oxidice de tipul  $AB_2O_4$  cu aplicatii in senzoristica”, Editura Politehnica, Timisoara, 2014, ISBN: 978-606-554-782-7
- [2] R. Datta et al. / Journal of Crystal Growth 345 (2012) 44–50]
- [3] F. Rigato et al. / Materials Science and Engineering B 144 (2007) 43–48
- [4] N. Wakiya, K. Shinozaki, N. Mizutani, Appl. Phys. Lett. 85 (2004) 1199

## Experimental Study of the Ibuprofene's Interaction with Some Natural Supports

Georgeta-Maria Simu<sup>1\*</sup>, Maria Grad<sup>2</sup>, Sabine Fessi<sup>1</sup>

<sup>1</sup>University of Medicine and Pharmacy „Victor Babeş” de Timișoara, Faculty of Pharmacy, 2 Eftimie Murgu, 300041, Timișoara, Romania

<sup>2</sup>Institute of Chemistry Timișoara of the Romanian Academy, 24 Mihai Viteazul Bv., 300223, Timișoara, Romania  
e-mail: gsimu@yahoo.com

### Abstract

The interaction of ibuprofene with two natural solid supports (orange peel and cotton fibre) was studied at three different temperatures (25, 35 and 45 °C) aiming to establish the best theoretical adsorption model and the corresponding thermodynamic parameters (enthalpy and entropy) of the process. For the investigated systems, the time necessary for attaining the adsorption equilibrium was estimated through a series of preliminary experiments, which indicated periods of time ranging from 195 to 380 minutes. Further, the experimental data resulted from the adsorption process was fitted to the Freundlich and Langmuir classical adsorption models, but also to the Sips and Jossens isotherm models, which were not tested yet in the case of the present studied systems. The obtained results showed that for both investigated systems it was the Sips model which described better the interaction of the model drug with the investigated solid supports.

### Introduction

Different ingredients used in pharmaceutical formulation, or in dosage forms can constitute a source of microbial contamination, or can initiate or participate to some physical or chemical interactions with the active ingredients, and this could generate the degradation of the active pharmaceutical compounds, compromising in some extent their therapeutic effect. Orange peel and cotton are natural ingredients presenting a great deal of interest in the pharmaceutical field, and their interaction with drugs was not thoroughly investigated till present. [1-6]

The interaction between drugs and excipients can be studied considering the adsorption isotherms. Usually, the description of the adsorption isotherms onto different excipients was based on classical Langmuir and Freundlich models, which are models with two parameters. However, in different fields of interest (different organic pollutants) it was found the two-parameter models showed some limits of application, and thus, models based on more parameters have been developed and used in several studies [7-12]. The interest for this kind of models is mainly due to their accuracy, as well as to their wide range of applicability.

### Experimental

Ibuprofene (98%) was supplied by Aldrich Sigma. The cotton was purchased from a local drug store and the orange peel was prepared in our laboratory from Washington Navel oranges (*Citrus sinensis* "Washington Navel").

The UV-VIS spectroscopy study was carried-out with a CECIL CE 7200 spectrophotometer, using two analytical wavelengths, e.g. 265 nm and 273 nm.

The experimental study involved in the first stage the preparation of a series of stock solutions containing Ibuprofene in 0,1 M NaOH aqueous solutions and the measurement of the optical density of the drug solutions at 265 nm and 273 nm. The obtained results were

used in order to obtain the corresponding calibration curves, according to Lambert-Beer law. In the first stage, we investigated the time necessary to reach the adsorption equilibrium. Further, based on these results, we investigated the extent of adsorption of the drug on the specified solid supports. The preliminary experiments were carried-out according to some previous works [7-12], using each time 10 mL of an initial ibuprofene solutions and 0,2 g ( $\pm 0,0001$ ) of solid supports. The mixtures were placed in a shaking bath which was set at different temperatures (ranging from 25, 35 and 40°C ( $\pm 1^\circ\text{C}$ )) and were shaken for different periods of time (12-60 h). At the end, the mixtures were filtered, and the distribution of the drug between solution and support was assessed spectrophotometrically, using the Lambert Beer's plot previously obtained.

The adsorption isotherms of the ibuprofene on the two investigated supports were obtained according to a similar procedure, starting from drug solutions of different concentrations, namely  $1 \times 10^{-5}$  to  $3,2 \times 10^{-4}$  mol/L. Control experiments, in which no drug was added, were performed in parallel, and the filtrate was used as a reference solution. The experiments were performed in triplicate, the values used in the analysis of the adsorption processes representing the average values of the three experiments.

In order to calculate the amount of the adsorbed drug on the solid support, equation (1) was used:

$$[D]_{ad} = ([D]_i - [D]_s) \cdot V / 1000 \cdot m \quad (1)$$

where  $[D]_{ad}$  represents the equilibrium drug concentration on the solid supports (mmol/g),  $[D]_i$  is the initial concentration,  $[D]_s$  the equilibrium concentration of the drug solution (both in mmol/L),  $V$  is the volume of drug solution (L), and  $m$  represents the amount of the solid support (g).

## Results and discussion

In this present work, the investigation of the interaction of Ibuprofene with two natural supports was carried-on as a function of drug concentration and temperature. The sorption isotherms (see Figure 1) were obtained at the three mentioned temperatures, at the optimised condition of shaking time, which were established through preliminary experiments (see Table 1).

**Table 1.** Equilibrium time for the adsorption of Ibuprofen on orange peel and cotton at 25, 35 and 40°C

Solid support	Time [min]	Time [min]	Time [min]
	T= 25 °C	T= 35 °C	T= 45 °C
Orange peel	380	325	270
Coton	335	265	195

As shown in Figure 1, the adsorption of ibuprofene on the two studied solid supports was quite fast in the initial stages, decreasing gradually with the progress of the adsorption process. One could also notice that greater temperatures induced a negative effect onto the adsorption process on both supports. This behavior could suggest that increasing temperature could generate a decrease of the number of accessible sites of the investigated supports. One should also consider that the decreasing sorption associated to the increase of temperature could be explained by the exothermicity of the sorption process, in a similar way with dye-fibre interactions.

The adsorption equilibrium data of Ibuprofen onto the orange peel and cotton were analyzed by non-linear curve fitting analysis, using Origin 6.1 software, in order to fit the experimental data to the considered isotherm models (see equations from Table 2). The principal statistical criteria was the squared multiple regression coefficient ( $R^2$ ) (see Table 3).

The inspection of data depicted in Table 3 indicate that the isotherm model which provided the best representation of the experimental results was the three-parameter model of Sips. This result suggests that the adsorption process of Ibuprofen on both investigated supports occurs after a combined model: Freundlich and Langmuir, involving a diffused adsorption on low drug concentration, and a monomolecular adsorption with a saturation value - at higher concentrations. For this model, the corresponding thermodynamic parameters: saturation value ( $S_f$ ), equilibrium constant ( $K_s$ ) and the value of the parameter  $n$ , were calculated. The obtained results are illustrated in Table 4.

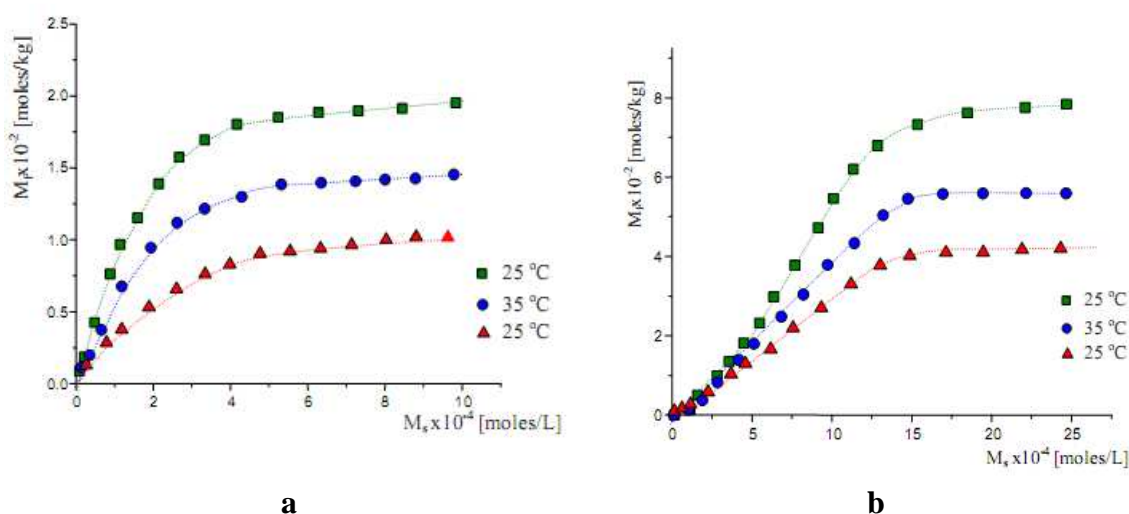


**Figure 1.** Adsorption isotherms of ibuprofen on orange peels (a) and cotton (b) at 25°C, 35°C and 45°C.

**Table 2.** Equations of the theoretical adsorption models

Langmuir	Freundlich	Sips	Jossens
$C_f = \frac{S_f \cdot K_L \cdot C_s}{1 + K_L \cdot C_s}$	$C_f = K_F C_s^{1/n}$	$C_f = \frac{S_f \cdot (K_s \cdot C_s)^{1/n}}{1 + (K_s \cdot C_s)^{1/n}}$	$C_e = \frac{q_e}{H} \exp(F \cdot q_e^p)$

**Table 3.** Statistical parameters for the adsorption process of Ibuprofene on orange peel and cotton at 25, 35 and 40°C

Orange peel								
T [°C]	Langmuir R <sup>2</sup> SE		Freundlich R <sup>2</sup> SE		Sips R <sup>2</sup> SExE <sup>-2</sup>		Jossens R <sup>2</sup> SE	
25 °C	0,96	0,21	0,873	0,685	0,998	1,75	0,969	0,246
35 °C	0,959	0,17	0,872	0,524	0,995	1,65	0,959	0,218
45 °C	0,965	0,11	0,904	0,297	0,996	0,55	0,976	0,119
Cotton								
T [°C]	Langmuir R <sup>2</sup> SE		Freundlich R <sup>2</sup> SE		Sips R <sup>2</sup> SExE <sup>-2</sup>		Jossens R <sup>2</sup> SE	
25 °C	0,973	0,32	0,882	0,656	0,997	1,85	0,971	0,26
35 °C	0,97	0,21	0,87	0,618	0,998	0,85	0,98	0,159
45 °C	0,955	0,12	0,842	0,704	0,998	0,25	0,986	0,157

**Table 4.** Values of Sips's equation parameters

Support	Temperature [°C]	S <sub>f</sub> [mol/kg]	n	K <sub>s</sub> [L/mol]
Orange peel	25	6,879±7,886 E <sup>-2</sup>	0,445±2,235 E <sup>-2</sup>	2610,4±54,6
	35	6,025±0,086 E <sup>-2</sup>	0,448±2,035 E <sup>-2</sup>	2565,78±53,1
	45	5,617±5,986 E <sup>-2</sup>	0,444±0,835 E <sup>-2</sup>	1916,67±29,2
Cotton	25	7,203±7,086 E <sup>-2</sup>	0,283±1,235 E <sup>-2</sup>	1705,67±13,5
	35	6,491±6,386 E <sup>-2</sup>	0,283±1,435 E <sup>-2</sup>	1673,71±12,6
	45	6,584±5,186 E <sup>-2</sup>	0,298±1,235 E <sup>-2</sup>	1606,88±16,3

Further, the thermodynamic parameters of the adsorption process were calculated in order to obtain more information about the effect of temperature onto the adsorption process (see Table 5). The Gibb's free energy ( $\Delta G^0$ ), was calculated according to equation (2) and the corresponding enthalpies ( $\Delta H^0$ ) and entropies ( $\Delta S^0$ ) were computed from van't Hoff equation (3), from the slope and intercept of the linear plot of  $\ln K$  versus  $1/T$ :

$$\Delta G^0 = -RT \ln K_s \quad (2)$$

$$\ln K_s = \frac{\Delta S^0}{R} - \frac{\Delta H^0}{RT} \quad (3)$$

**Table 5.** Thermodynamic parameters for the adsorption of Ibuprofene on orange peel and cotton

Support	Temperature [°C]	$\Delta G^0$ [kJ/mole]	$\Delta H^0$ [kJ/mole]	$\Delta S^0$ [J/mole.K]
Orange peel	25	-18,06	-9,643	83,27
	35	-18,98		
	45	-19,92		
Cotton	25	-18,64	-6,577	41,36
	35	-19,51		
	45	-20,26		

## Conclusion

The adsorption isotherms of Ibuprofene onto two natural supports were studied using two classical isotherm models: Freundlich and Langmuir, as well as two three –parameter isotherm models: Sips and Jossens.

According to the statistical analysis of the obtained results, the Sips model described better the adsorption process in the case of all studied drug-cellulosic supports systems.

The values of the corresponding thermodynamics parameters of the sorption process indicate that the process is spontaneous and exothermic.

## References

- [1] P. Crowley, L. G. Martini, *Pharm Tech Europe* 13(3) (2001) 26.
- [2] S. A. Muratova, N. D. Burkhanova, S.Yagai, G. V. Nikonovich, K. H. Pulatova, S. Rashidova, *Pharm Chem. J.* 36 (2002) 619.
- [3] S. Al-Nimry, S. Assaf, I. Jalal, N. Najib, *Int. J. Pharm.* 149 (1997), 115.
- [4] K. C. Duggan, D. J. Hermanson, J. Musee, J. J. Prusakiewicz, J. L. Scheib, B. D. Carter, S. Banerjee, J. A. Oates, L. J. Marnett, *Nature Chem. Biol.* 7 (2011) 803.
- [5] S. Okada, H. Nakahara, H. Isaka, *Chem.Pharm.Bull.* 35 (1987) 761.
- [6] A. Reem, *Eur. J. Sci. Res.* 40(4) (2010) 580.
- [7]. G. Simu, S. Funar-Timofei, S. Hora, L. Kurunczi, *Mol. Cryst. Liq. Cryst.*, 416 (2004), 97/353.
- [8]. B. Subramanyam, D. Ashutosh, *Int. J. Environ. Res.*, 6(1) (2012), 265.
- [9]. R. J. Sips, *Chem. Phys.* 16 (1948), 490.
- [10]. O. Hamdaoui, E. Naffrechoux, J. Sptil, C. Fachinger, C., *Chem. Eng. J.*, 106(2005), 153.
- [11]. O. Hamdaoui, E. J. Naffrechoux, *Hazard. Mat.*, 147(2007), 401.
- [12]. G. M. Simu, I. V. Ledeti, S. G. Muntean, A. Fuliaş, I. M. Cîtu, C. Şoica, D. Onisei, G. Săvoiu–Balint, *Rev. Chim. (Bucharest)*, 65(6) (2014), 664.



## Toxicological Evaluation of the Organic Phase Resulted from the COSORB Process

Georgeta-Maria Simu<sup>1\*</sup>, Dorina Coricovac<sup>1</sup>, Liliana Cseh<sup>2</sup>, Codruța Șoica<sup>1</sup>, Cristina Dehelean<sup>1</sup>

<sup>1</sup>University of Medicine and Pharmacy „Victor Babeș” de Timișoara, Faculty of Pharmacy, 2 Eftimie Murgu, 300041, Timișoara, Romania

<sup>2</sup>Institute of Chemistry Timișoara of the Romanian Academy, 24 Mihai Viteazul Bv., 300223, Timișoara, Romania  
e-mail: gsimu@yahoo.com

### Abstract

In this work, the toxicological assesment of the organic phase resulted from the COSORB process was performed. For this purpose, an animal model was used to evaluate the effects of the organic phase on skin physiological parameters after topical application to SKH-1 hairless mice. The obtained results revealed that the constituents of the organic phase induce skin toxicity by disturbing the physiological skin parameters status, which represents the first signs of skin pathology.

### Introduction

The COSORB process involves a selective elimination of carbon monoxide by means of complexation/decomplexation of CO on a specific catalyst, in an appropriate aromatic solvent. [1] By this process, it is possible to complexate and recover more then 99% of the CO content [2].

The catalyst is a bimetalic complex of  $Me_I Me_{II} X_n$  type, where  $Me_I$  is often Cu(I), and  $Me_{II}$  is Al(III), X being a halogen, such as chlorine. During the process, the catalyst is involved in several complexation/decomplexation processes, resulting finally in a partially poisoned catalyst due to the accumulation of some sulfures and/or other secondary alkylation or polymerisation products. The disposal of the used catalyst involves several environmental risks, due to its high metal content, and the recovery and subsequent use of these metals presents a great deal of interest. Thus, several processes of Cu and toluene have been developed [3-8]. All of these technologies have advantages and disadvantages, and more or less specific shortcomings, their efficiency being strongly dependent by the type of compound. However, none of the technologies can remove all of the compounds from wastewaters.

Based on these considerations, it seems that the developpement of an unitary technology able to recover all of the usefull materials from the used catalyst should be of great interest. Moreover, the toxicological evaluation of all stages involved in such a technology will bring more added value to this technology.

### Experimental

The analysis of the organic phase was carried-out by means of gas chromatography/ mass spectroscopy (GC/MS), using a Hewlett Packard Gaz Chromatograph HP 6890 associated with a Mass Spectrometer HP 5973. The GC column was of ZB-5MS type, and had a 30m×0.25mm inner diameter and a film thickness of 0,25  $\mu$ m. The stationary phase was a mixture of 95% dimethyl siloxane and 5% phenyl-arylene. The column temperature program was of 6 °/ min, in the temperature range of 50-300°C.

The animals used in the present study were SKH1 hairless male mice (12-14 weeks-old) purchased from Charles River Laboratories, Budapest, Hungary. All experimental procedures were conducted in accordance with the Directive 2010/63/EU on the protection of animals used for scientific purposes. The experimental protocol was approved by the Committee for Ethics Research of the University for Medicine and Pharmacy of Timisoara, Romania. Animals were fed ad libitum and kept under standard conditions: constant temperature of  $22.5 \pm 2^\circ \text{C}$ , humidity  $55 \pm 5\%$  and a 12-h light/dark cycle.

In order to accomplish the present study, the mice were divided in 2 groups (n=5/mice group): group 1 - control group – no interventions were applied; group 2 – the mice were treated with the organic phase solution (100 $\mu\text{l}$ ) which was applied on the dorsal area twice a week for 5 weeks.

For the evaluation of skin response to organic phase effect, we measured several physiological skin parameters (erythema and TEWL – transepidermal water loss) by the means of a non-invasive technique (mexametry and tewametry) using MPA5 System from Courage-Khazaka.

### **Results and discussion**

In this work, the toxicological evaluation of the organic phase resulted from the COSORB process was carried-on, using an animal model.

The content of the organic phase was evaluated by GC/MS and the results are illustrated in Table 1. The percentage composition of the organic phase reveal the presence of 84,46 % toluene (RT = 1,9), 10,1% oxydation products of toluene (RT=21-23 derivatives of bis-(methyl-phenyl) ketone, RT= 28-32 derivatives of trimethyl tritil alcohol), 5,3% xylenes (RT = 3-4) and 0,1% benzene (RT = 1.3).

**Table 1.** The content of the organic phase resulted from the COSORB process

Nr.	Retention time (RT)	Peak area	Area %
1	1,323	59577	0,081
2	1,946	62040506	84,466
3	2,632	196840	0,268
4	2,832	256827	0,35
5	3,021	1320320	1,798
6	3,346	359668	0,49
7	4,318	156802	0,213
8	4,455	165834	0,226
9	21,659	704812	0,96
10	22,407	190586	0,259
11	22,882	543778	0,74
12	23,316	1284443	1,749
13	23,665	124753	0,17
14	28,146	146443	0,199
15	28,734	392714	0,535
16	29,317	393223	0,535
17	29,872	141317	0,192
18	30,083	354484	0,483
19	30,729	1807869	2,461
20	31,369	2215855	3,017
21	31,992	593709	0,808

As it can be seen from the results depicted in Table 1, toluene is the major constituent of the organic phase resulted from the COSORB process, and it is known that this volatile organic compound, affects the central nervous system, as well as the heart, but its noxious effects at skin level are not fully elucidated [9].

Further, the effects of this organic phase were investigated at skin level, after topical application on SKH1 mice, as described in Experimental part. The evaluation of these effects were carried out by means of non-invasive methods, e.g. tewametry and mexametry. The main reason for our choice was the fact that hairless mice represent a great tool for the evaluation of the changes that occur at cutaneous level, changes that can be associated with the application of a toxic or a new drug in the testing phase or after absorption of some substances that possess the capacity to modify skin parameters [10,11].

Moreover, Tewametry and mexametry are established non-invasive methods, used very frequently in the diagnostic of skin pathologies both in humans and in *in vivo* experiments [12, 13].

One of the skin parameters measured in this experiment using a Mexameter probe was the erythema value.

The topical application of the organic phase to the SKH1 mice led to relevant changes regarding the skin parameters evaluated. Our results showed that the application of the test solution induced a significant degree of erythema as compared with the control group (see Figure 1).

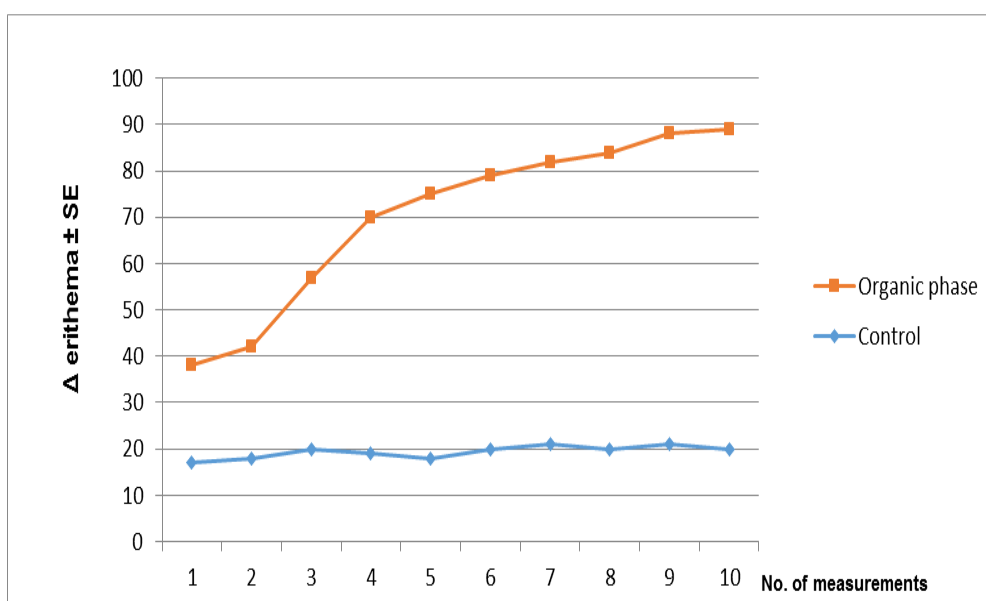


**Figure 1.** Control group and organic phase group - topically applied (data are expressed as differences  $\pm$  SE). The units are arbitrary.

An increase was also observed in the values measured for transepidermal water loss (TEWL) in the group treated with the test solution in comparison with the control group, as illustrated in Figure 2.

TEWL value is considered an index for the estimation of the degree of injury of skin barrier and it measures the rate of skin water loss (it is expressed in  $\text{g}/\text{h}\text{m}^2$ ) [14]. An increased value of TEWL indicates an injury or a skin pathology [15].

Our results showed that the TEWL values were higher in the group that was topically treated with the organic phase what indicates a noxious effect of this solution at cutaneous level.

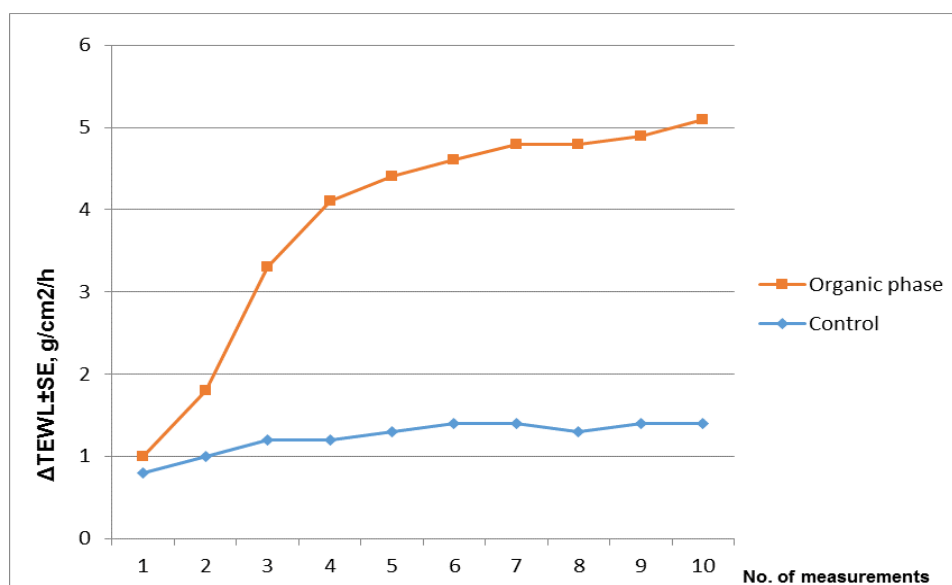


**Figure 2.** Transepidermal water loss (TEWL) evaluation: Control group and Organic phase group - topically applied (data are expressed as differences  $\pm$  SE). The units are arbitrary.

## **Conclusion**

Our preliminary results indicate that the constituents of the organic phase induce skin toxicity by disturbing the physiological skin parameters status, which represents the first signs of skin pathology. Further studies are required in order to elucidate the mechanism involved.

## **Acknowledgements**

This research was supported by a PN-II-PT-PCCA-2013-4-0612 grant, nr. 110/2014 of the Romanian Ministry of Education and Research.

## **References**

- [1] A. Keller, R. Schendel, AICHE Summer Meeting, August 23, 1988.
- [2] F. Rahmani, M. Bayar, M. Haghighi, M. R. Rahimpour, Iranian J. Chem. Eng. 7(3) (2010) 29.
- [3] R. B. Long, H. H. Horowitz, D. W. Savage, US 3754047, 1973.
- [4] D. G. Walker, B. Haase, D. J. Haase, US 3845188, 1974.
- [5] J.R. Sudduth, D. A. Keyworth, US 3960910, 1976.
- [6] D. A. Keyworth, J. R. Sudduth, US 4153669, 1979.
- [7] C. P. Christenson, G. M. McNamee, R. D. Delaune, Method of disposing if spent organic complexing solutions containing couprous halides, US 4249939, 1981.
- [8] I. B. Plecas, S. Dimovic, Bull. Mater. Sci., 27(2) (2004) 175.
- [9] A. Saito, H. Tanaka, H. Usuda, T. Shibata, S. Higashi, H. Yamashita, N. Inagaki, H. Nagai, Environ Toxicol. 26(3) (2011) 224.
- [10] C. Danciu, D. E. Coricovac, C. Soica, V. Dumitrascu, G. Simu, D. Antal, K. Lajos, C. A. Dehelean, F. Borcan, Rev. Chim. (Bucharest) 65(10) (2014) 1195.
- [11] D. Minda, D. Coricovac, I. Pinzaru, C. Dehelean, F. Borcan, D. Muntean, Physiology 25.3 (87) (2015) 25.
- [13] B. Nedelec, N. J. Forget, T. Hurtubise, S. Cimino, F. de Muszka, A. Legault, W. L. Liu, A. de Oliveira, V. Calva, J. A. Correa, Skin Res. Technol. 2015. doi: 10.1111/srt.12256.
- [14] Y. Cheng, Y. Y. Dong, M. X. Dong, C. Wang, N. Su, Y. T. Sun, J. Liu, H. Y. Zheng, A. Schrader, M. Rohr, W. Liu, Skin Res Technol. 14(1) (2008) 45.
- [15] C. Rosado, P. Pinto, L. M. Rodrigues, Int. J. Cosmet. Sci. 27(4) (2015) 237.

## Wastewater Coagulation with Chitosan-Al-Compounds

Masu Smaranda<sup>1\*</sup>, Albulescu Mariana<sup>2,3</sup>

<sup>1</sup>National R & D Institute for Industrial Ecology ECOIND, Branch of Timisoara, 300004, I Regina Maria Square, Timisoara, Romania; e-mail: anda.masu@yahoo.com

<sup>2</sup>West University of Timisoara, Advanced Environmental Research Laboratories, Oituz Street, no.4, 300086, Timisoara, Romania

<sup>3</sup>West University of Timisoara, Faculty of Chemistry, Biology, Geography, Department of Biology-Chemistry, Pestalozzi Street, 16, Timisoara, 300115, ROMANIA

### Abstract

The wastewater containing TPH (total petroleum hydrocarbons), can not be discharged untreated due to the toxic loading. These substances are potential sources of contamination of soil and water. Primary treatments of these waste waters require a coagulation stage. The classical coagulation agents reduce turbidity and partially, the dissolved substances content. In this study, optimized coagulation process was obtained through the use of metal salts and biofloculants. Use of chitosan-Al-compounds has reduced by more than 50% of the dose for Al salts and has produced effective reduction of petroleum products by up to 10% higher.

### Introduction

In recent years the demand for environment-friendly materials in coagulation / flocculation of wastewater is increasing. The biofloculants are materials that seem to be a very good alternative to replace synthetic treatment agents. Until now, the biofloculants were applied as adjuvant in coagulation of wastewaters combined with the following usual coagulating agents: ferric chloride, ferric sulfate, aluminum sulfate, Al polymerized salts. Certain categories of biofloculants were most studied: chitosan, tannin, gums etc. Chitosan is one of the most promising polymer because of its positive charge at acidic pH. It is described as a cationic polyelectrolyte and is expected to coagulate negatively charged suspended particles found in natural waters with increased turbidity. [1-4] Chitosan is a linear copolymer of D-glucosamine and Nacetyl-D-glucosamine produced by the deacetylation of chitin, a major component of the shells of crustaceans such as crab, shrimp, and crawfish. Chitin and chitosan polymers are natural aminopolysaccharides having unique structures, multidimensional properties, highly sophisticated functions and wide ranging applications. [5] Chitosan is insoluble in water or organic solvents, but is soluble in diluted organic acids such as acetic acid, formic acid, etc.. At pH 5 is a cationic polymer chitosan with acidic charge density. In these circumstances it becomes a clotting agent that can remove contaminants in suspended or dissolved state. Wastewater treatment with chitosan facilitate electrostatic interactions between the polymer chains and the negative charges of the anions of metals, organic compounds etc. In this study are reported the results of treatment of wastewater containing TPH with clotting agents based on Al polymerized salts in the absence / presence of a biofloculant, respectively chitosan. Among all the available coagulants, aluminum salts are the most widely used because of their competitive costs, effectiveness and handling. However, the obtained sludge lead to aluminum accumulation in the environment and they are some concerns about the residual aluminum which may be present in the final, treated water [4]. Therefore aluminium dose reduction is important in water coagulation.



## Experimental

In this study, wastewater from petroleum oil extraction unit were collected. Wastewater is pretreated by coagulation process. The coagulation was performed with a stirrer with variable speeds (Phipps & Bird Company USA). The coagulants used were poly-aluminum chloride (PAC) and complex agent chitosan: poly-aluminum chloride in two variants 1.chitosan: Al=0.3 and 2 .chitosan: Al=0.6. The optimal dose (OD) of PAC coagulant in the absence /presence of chitosan was assessed by Jar Test method. Chitosan with average molecular weight was obtained by courtesy of Advanced Environmental Research Laboratories, West University Timisoara. Poly-aluminium chloride, PAC was obtained by reaction of aluminium salts with a base under carefully controlled conditions of ECOIND Laboratory, Branch of Timisoara. They are typically characterized by degree of neutralisation or alkalinity, expressed as "r". "r" is the molar ratio OH: Al = 2.4[6]. Samples of 250 ml for wastewater with TPH were used. The working conditions were: slow stirring for 15 minutes and gravitational sedimentation for 30 minutes. In the supernatant, were analyzed the following conventional parameters: pH using pH-meter model 290A ORION RESEARCH USA, turbidity with Micro 100 Laboratory Turbid meter, Scientific Inc. USA, TOC by TOC Analyzer with Multi N/C 2100 Analytic Jena, Germany. The conventional parameter, the absorbance at 436 nm wave length (A436) and nonconventional parameter, the absorbance at 254 nm wave lengths (A254), was quickly analyzed by UV/VIS spectrophotometer, Specord 205, Analytik Jena, Germany. Total petroleum hydrocarbons were determined according to the Romanian standardized norms by extraction with carbon tetrachloride (SR 7877-1) *i.e.* TPH is extracted from a volume of wastewater at pH=1 corrected with hydrochloric acid,  $d = 1.19 \text{ g} \cdot \text{L}^{-1}$ , (V), by mixing with solvent. The number of extracts was four. Solvent extracts were dried by passing through a filter with anhydrous  $\text{Na}_2\text{SO}_4$  p.a. layer. Then, solvent extracts are placed in capsule, with weight  $m_1$  [g]. The solvent is evaporated and the weight of capsule with TPH residuum, was noted  $m_2$  [g]. The amount of TPH, was calculated with formula:  $\text{TPH } \text{g} \cdot \text{L}^{-1} = [(m_2 - m_1) \text{ V}^{-1} \cdot 1000]$ . Studied waters must have the characteristics required by national norm HG 352/2005 - NTPA 002 to be discharged into the sewerage networks of localities and directly in wastewater treatment plants. Correction of coagulation pH was made with mineral acid/base.

## Results and Discussion

In Table 1 are shown the conventional parameters for untreated/ treated waters, *i.e.*: pH, turbidity, TOC, TPH and the nonconventional parameter - absorbance at  $\lambda = 254\text{nm}$ , PAC optimal dose (OD) and coagulation efficiencies. PAC optimal dose (OD), established by Jar Test, was:  $\text{OD} = 64.0 \text{ mg Al} \cdot \text{L}^{-1}$ . Wastewater shows shocking high content of TPH,  $580.0 \pm 26.5 \text{ mg} \cdot \text{L}^{-1}$ . The loading with organic matter, TOC, was  $145.6 \pm 7.5 \text{ mg C} \cdot \text{L}^{-1}$ . Absorbance A254 was  $2.590 \pm 0.23 \text{ cm}^{-1}$ . The waters are tinted yellow; A436 was  $0.180 \pm 0.018 \text{ cm}^{-1}$ . By using the optimal dose of PAC as coagulation agent in the absence of chitosan, the reduction of TPH was 79.8%, of TOC- 59.8% and of A254 - 63.7%. The use of a coagulation agent based on chitosan and poly-aluminum chloride has reduced dose of Al and increased efficiencies for reducing the organic loading expressed by parameters such as TPH, TOC, at a higher level than those obtained in the absence of chitosan coagulation. In Table 2 are shown the conventional parameters *i.e.*: pH, turbidity, TOC, TPH and the nonconventional parameter - absorbance at  $\lambda = 254\text{nm}$  (A254) and color (A436) of the chitosan: Al optimal dose (OD) treated samples and the coagulation efficiencies, as well. It is seen from Table 2 that the use of chitosan determined the reduction of optimal dose for aluminum by more than 50%. Efficiencies in reduction of organic load when low doses of Al were used are similar or up to 10% higher than the efficiencies obtained when PAC was used as clotting agent, in the absence of chitosan.

**Table 1.** The characterization of untreated / treated wastewater with PAC and coagulation efficiencies. PAC optimal dose for treated samples was  $OD = 64.0 \text{ mg Al} \cdot \text{L}^{-1}$

No	Parameters	Wastewater	Treated water samples	Efficiencies [%]
1	pH	7.53	6.5	
2	Turbidity [ $^{\circ}$ NTU]	$68.3 \pm 5.0$	$12.5 \pm 2.5$	81.7
3	*Absorbance at 436 nm, $A_{436}[\text{cm}^{-1}]$	$0.180 \pm 0.018$	0.034	81.1
4	TPH [ $\text{mg} \cdot \text{L}^{-1}$ ]	$580.0 \pm 26.5$	$117.6 \pm 8.5$	79.8
5	TOC [ $\text{mgC} \cdot \text{L}^{-1}$ ]	$145.6 \pm 7.5$	$58.5 \pm 5.6$	59.8
6	*Absorbance at 254 nm, $A_{254}[\text{cm}^{-1}]$	$2.590 \pm 0.23$	0.94	63.7

\* Samples filtered through filter paper

**Table 2.** The characterization of wastewater samples treated with chitosan : Al at optimal dose (OD) and coagulation efficiencies

No	Parameters	Chitosan:Al = 0.3		Chitosan:Al = 0.6	
		Treated water samples	Efficiencies [%]	Treated water samples	Efficiencies [%]
1	Optimal dose	28.0	-	28.0	-
2	pH	6.5	-	6.5	
3	Turbidity [ $^{\circ}$ NTU]	12.5	81.7	11.5	83.2
4	* $A_{436}[\text{cm}^{-1}]$	0.02	88.9	0.047	73.9
5	TPH [ $\text{mg} \cdot \text{L}^{-1}$ ]	97.9	83.1	68.9	88.1
6	TOC [ $\text{mgC} \cdot \text{L}^{-1}$ ]	57.7	60.4	51.7	64.5
7	* $A_{254}[\text{cm}^{-1}]$	1.15	55.5	1.147	55.7

\* Samples filtered through filter paper

It is seen from Table 2 that the use of coagulation agent chitosan: Al = 0.6 caused a slight increase efficiencies in reduction of TPH and TOC values versus efficiencies obtained using coagulation agent chitosan: Al = 0.3. Figure 1 shows the variations of the  $A_{254}$  in determining the optimal dose of coagulation agent chitosan: Al = 0.6. It is seen from the figure 1 that with increasing dose of Al, from  $14 \text{ mg} \cdot \text{L}^{-1}$  to  $28 \text{ mg} \cdot \text{L}^{-1}$ , decreases the absorbance value from 1.15 to  $1.147 \text{ cm}^{-1}$ . Further increasing the dose of clotting agent, increase of the absorbance  $A_{254}$  was observed, since the organic load increases, perhaps because of higher proportion of chitosan. In Figure 1 it can be seen that the optimal dose of coagulation agent chitosan-Al compounds may be determined in conjunction with the varying spectra of water treated with different doses of coagulating agent. Chitosan: Al optimal dose for wastewater coagulation process was  $28.0 \text{ [mgAl} \cdot \text{L}^{-1}]$ .

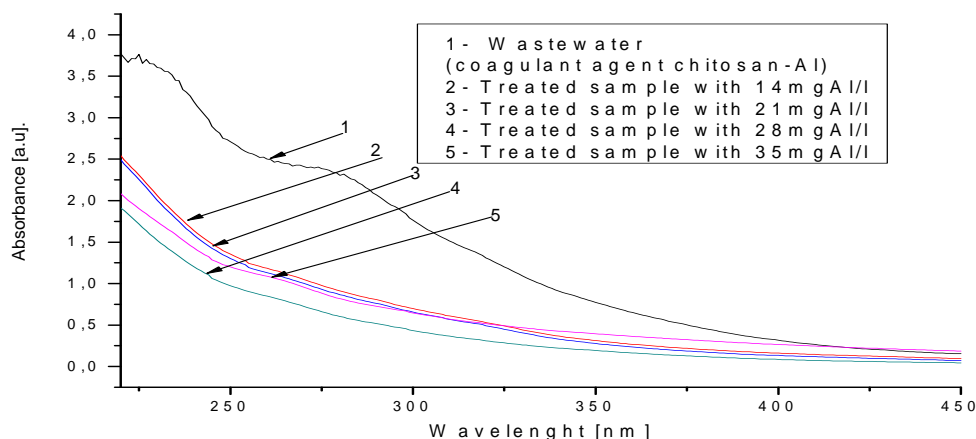


**Figure 1** Selective absorbance spectrum evolution after Jar test application to establish the optimal dose for wastewater treatment with coagulation agent chitosan: Al = 0.6

## Conclusions

The use in the coagulation stage of wastewaters with petroleum hydrocarbons of coagulation agents type chitosan : Al, caused a dose reduction of over 50% for Al and increased efficiencies in reduction of organic load, TPH and TOC. The greatest efficiencies of the coagulation process of water containing TPH were obtained when ratio chitosan: Al = 0.6 was used. At the same time, it must also mention that the use of aluminum in the presence of chitosan, reduces costs and the sludge deposits containing aluminum which depending on quality of it may be considered or not a dangerous deposit for environment.

## References

- [1] M. Ng. A. E. Lian, S. Liu, M. Lim, C. W. K. Chow, D. Wang, M. Drukas, R. Amal, Wat. Res. 46 (2012) 4614.
- [2] F. Renault, B. Sancey, P. M. Badot, G. Crini, Eur. Polym. J. 45 (2009) 1337.
- [3] A. L. Ahmad, S. Sumathi, B. H. Hameed, Chem. Eng. J. 108 (2005) 179.
- [4] R. Bergamasco, Ch. Bouchard, F. Vieira da Silva, M. H. M. Reis, M. R. Fagundes-Klen, Desalination 245 (2009) 205.
- [5] C.K.S. Pillai, W. Paul, C. P. Sharma, Progress in Polymer Science 34 (2009) 641.
- [6] S. Masu., L. Andres, V. Rus, C. Bogatu, D. Botau, D. Cocheci, M. Ilios, L. C. Demetrovici, D. Chira, L. Demetrovici, Process for obtaining of supported materials used for metals immobilization from water, Romanian Patent No. 122630, 2009.

## Oil Polluted Soils Phytoremediation by Grazing Culture

Masu Smaranda\*

National R & D Institute for Industrial Ecology ECOIND.

Branch of Timisoara. 300004. 1 Regina Maria Square. Timisoara. Romania

\*e-mail: andamasu@yahoo.com

### Abstract

Total petroleum hydrocarbon (TPH) polluted soils cannot be used for agricultural, industrial or recreational activities. They are potential sources of contamination of soil, surface water and groundwater. They also directly and indirectly alter the landscape. Phytoremediation of soils polluted with total petroleum hydrocarbon with suitable plants is a technology that requires low cost and traditional plant cultivation strategies. In this study are presented models of phytoremediation of polluted soils with  $79.42 \pm 3.9 \text{ g} \cdot \text{kg}^{-1} \text{ DM}$ . For successful phytoremediation process the TPH polluted soil was fertilized with sewage sludge mixed with varying amounts of fly ash. From the analytical study of the experimental data we could develop the model of phytoremediation by bird's foot trefoil culture (*Lotus corniculatus*). The model applies in the case of oil polluted soil fertilized with a fertilizing agent, *i.e.* sewage sludge, in an amount of 250 g per pot mixed with fly ash in a ratio of 1: 1–5:1 weight parts. The TPH amount lost from polluted soil on a 12-month period was up 88%.

### Introduction

Plants can decrease total petroleum hydrocarbon (TPH) content of polluted soil by absorbing pollutants and translocations them in the plant. In plant tissue pollutants can be seized, metabolized or eliminated through transpiration, etc. The plant development in TPH polluted soil to be promoted by micro- and macro- nutrients added. The necessary nutrients need for plants growth was done by sewage sludge fertilizer. Furthermore sewage sludge in soil inserted microbial dowsy [1, 2]. This stimulates biodegradation of carbon products by specific metabolism of rhizosphere area. Roots are the immediately active plant's parts to access soil different compounds that can also be petroleum hydrocarbons. The roots of the plant act directly on the soil. They break soil aggregates coated with petroleum products and increase soil aeration capacity. The roots of the plant help to increase the bacterial activity in the regions surrounding the root. Plant roots directly contribute to limiting the movement of pollutants, in soils in that they remove water and thus reduce the movement of water with impurities through channels formed among soil aggregates. On the other hand high toxicity of TPH was attenuated by fly ash as temporary adsorbent with high porosity [3.4]. Fly ash is used as fertilizer or amendment to enhance the physico-chemical properties of soil [5.6]. The presence of large amounts of TPH in soil requires the management of these lands. Is welcome selection of plant species for phytoremediation [7]. The strategy for the decontamination of polluted soils with high amounts of TPH in this study comprises the steps of: 1. soil characterization, 2. identifying agricultural works that can be applied in polluted area, in particular soil fertilization, 3. selecting crops tolerant of polluted soil toxicity, *i.e.* grasses, legume, etc.. This study presents the results on phytoremediation of soils polluted with  $79.42 \pm 3.9 \text{ gTPH} \cdot \text{kg}^{-1} \text{ D.M.}$  fertilized with sewage sludge mixed with varying amounts of fly ash. From the comparative study of the experimental data we could elaborate the phytoremediation model by culturing bird's foot trefoil (*Lotus corniculatus*).

## Experimental

TPH polluted soil was taken from the surroundings of an oil field in operation. The soil was cleaned, dried and ground. Petroleum products cause strong adhesion between soil particles forming larger aggregate. After breaking into smaller units of the large aggregate of soil, resulted soil aggregates with sizes between 1-3 cm. Soil contaminated with TPH load of 20% was mixed with unpolluted agricultural soil. Unpolluted agricultural soil was dried, cleaned of various plant residues, pebbles, etc., crushed and homogenized. Agricultural soil screening was performed by sieve with a mesh size of 1 mm. The TPH polluted soil with a large amount of 20% was mixed with unpolluted agricultural soil. Mixing was performed in proportion of polluted soil: unpolluted soil of 1:2 wt.: wt. The amount of TPH in the soil mixture resulting from mixing the polluted soil with unpolluted soil was  $79.42 \pm 3.9 \text{ gTPH} \cdot \text{kg}^{-1} \text{ D.M.}$  The experimental study included experimental variants of soil contaminated with an amount of  $79.42 \pm 3.9 \text{ g gTPH} \cdot \text{kg}^{-1} \text{ D.M.}$  untreated / treated by fertilizing with sewage sludge in amount of 250g per vegetation pot. As a temporary agent of adsorption of TPH from the soil were used different amounts of fly ash 50, 25, and 500 g fly ash per pot, respectively. The experimental study variants were: **P** - uncultivated polluted soil; **PB** - cultivated polluted soil fertilized with sewage sludge; **PB 1** - polluted soil fertilized with sewage sludge mixed with fly ash 50g per pot and cultivated with plant; **BC** - polluted soil fertilized with sewage sludge mixed with fly ash 250 g per pot and cultivated with plant and **PB 3** - polluted soil fertilized with sewage sludge mixed with 500 g fly ash per pot and cultivated with plant. The plant species used in phytoremediation process was the bird's foot trefoil (*Lotus corniculatus*). Characteristics fertilizer sewage sludge used were: moisture 88.6%, organic matter content of 33.4%, 0.55% total nitrogen, phosphorus 0.37% and pH = 6.5. The experiment was carried out in pots with 6.5 kg of untreated/treated polluted soil. Cultures were performed in triplicates each, a total of 15 pots. The experimental unit was placed during the study outdoors. In the cold winter pots were covered with straw. The method of TPH content of polluted soil analysis was presented by Masu et al. [8].

## Results and discussion

Table 1 describes the evolution of the crop monitored for 12 months. The initial concentration of TPH in soil was  $79.42 \pm 3.9 \text{ gTPH} \cdot \text{kg}^{-1} \text{ D.M.}$  It is noted from Table 1 that the bird's foot trefoil plants sprout late on the experimental variant treated with sewage sludge in fly ash absence. There is a two weeks delay compared to the other plants in the experimental variants. Plants develop with difficulty. They form a small number of offshoots. Plants suffer during growth showing such as yellowing and drying of leaves gradually.

**Table 1** Vegetation cover degree of the experimental variants seeded with bird's foot trefoil during the monitored period of 12 months. (3 replicates for each experimental variant, total of 15 variants)

Experimental variants	P*	PB	PC3	BC	PB1
Plant sprouting		3-4 week	2 week	2 week	2 week
Plant cover degree during the first year [%]		5-10	15-18	25-35	25-35
Number of offshoots		1-2	1-3	2-3	2-3
Plant cover degree during the second year [%]		**	80-85	85-95	80-90
Number of offshoots			3-4	5-6	5-6

\* P uncultivated polluted soil; \*\* PB polluted soil fertilized with sewage sludge. The plants dried in winter.

During the cold winter plants on this experimental variant dried. In comparison, the plants on the variants fertilized with sewage sludge mixed with fly ash sprouted in larger numbers. Plants gradually occupied up to 35% of the sown surface in the first year. The plants were more vigorous. They showed a greater number of offshoots than the ones grown in the absence of fly ash fertilized variant. The plants endure during winter. In the second year of culture, plants grown on variants fertilized with sewage sludge mixed with fly ash will continue to develop. They will form a double number of offshoots compared to the first year. Moreover, they will cover up to 80- 95% of the sown area. Table 2 shows the variations in the content of petroleum products after 2, 4, 9 and 12 months of vegetation respectively in all the studied soil experimental variants: cultivated and uncultivated plants. From Table 2 it is observed that in the monitored period of 12 months from the polluted soil TPH content decreases by  $23.0 \pm 2.8 \text{ gTPH} \cdot \text{kg}^{-1} \text{ D.M.}$  The decrease is due to volatilization phenomena of some oil components. From the polluted soil fertilized with sewage sludge in the absence of fly ash, TPH content decreases by  $37.5 \pm 2.0 \text{ gTPH} \cdot \text{kg}^{-1} \text{ D.M.}$  The decrease is due to volatilization phenomena of TPH and metabolic phenomena performed by the biological heritage of the sewage sludge. The polluted soil fertilized with sewage sludge and fly ash, cultivated with bird's foot trefoil, the content of TPH decreased by  $68.5\text{-}70.0 \text{ gTPH} \cdot \text{kg}^{-1} \text{ D.M.}$  The addition of sewage sludge mixture and fly ash in a ratio with 1:1–5:1 weight parts decreased the most the TPH content. The efficiency of TPH reduction in soil during the period of 12 months was up 88%. The addition of fly ash in larger quantities did not determine the expected plant growth efficiencies on the variants and the advanced reduction of TPH content.



**Table 2** Variation of TPH content from the experimental variants of soil studied and cultivated with bird's foot trefoil on the monitored period (initial concentration  $79.42 \pm 3.9$  gTPH·kg<sup>-1</sup> D.M.). 3 replicates for each experimental variant, total of 15 variants)

No	Vegetation period	Experimental variants/ TPH content in soils g·kg <sup>-1</sup> D.M.				
		P*	PB**	PC3	BC	PB1
1	2 months of vegetation	68.8±5.8	64.8±5.2	74.±6.8	55.3±5.0	64.6±5.2
2	4 months of vegetation	59.5±5.4	52.0±4.8	58.4±5.7	29.5±3.8	47.3±4.8.
3	9 months of vegetation	55.5±5.5	46.0±4.7	47.2±4.8	14.4±2.6	28.5±3.3
4	12 months of vegetation	55.5±5.	42.0±4.3	11.6±1.8	9.44±1.5	9.97±1.0

\* P uncultivated polluted soil; \*\* PB polluted soil fertilized with sludge. The plants dried in winter.

It can be seen a reduced decrease of TPH in soil in winter when the plant metabolism and that of soil biocenosis was slower. The analysis of the experimental data presented in Table 1 and 2 is seen that in the variants fertilized with sewage sludge mixed with fly ash bird's foot trefoil crops gradually develop occupying the sown areas. They develop normally under the conditions specific to the climate in the west part of the country. In conclusion it was possible to develop a model of phytoremediation of the polluted soils with  $79.42 \pm 3.9$  gTPH·kg<sup>-1</sup> D.M. by bird's foot trefoil (*Lotus corniculatus*) culture. To form and maintain a layer of plants is needed a treatment of the TPH polluted soil with fertilizer agent, *i.e.* sewage sludge in an amount of 250g per pot mixed with fly ash in a ratio of 1:1—5:1 wt. :wt. parts. In Figure 1 are shown the bird's foot trefoil cultures formed on the experimental variants in pots after 12 month of vegetation.



**Figure 1.** In pots experimental variants from *Lotus corniculatus* after 12 months

## Conclusions

Bird's foot trefoil cultures have developed on soils contaminated with  $79.42 \pm 3.9$  gTPH·kg<sup>-1</sup> D.M. gradually occupying the sown areas. In the 12 months of monitoring the crop the areas occupied reached 80-95%. For the application of the phytoremediation process with bird's foot trefoil plants of soil contaminated with TPH was necessary fertilization with a fertilizer agent *i.e.* sewage sludge. For culture maintain was necessary sewage sludge mixing fly ash in

1:1–5:1 wt.: wt. The process of phytoremediation for soils contaminated with  $79.42 \pm 3.9$  gTPH·kg<sup>-1</sup> D.M. by bird's foot trefoil (*Lotus corniculatus*) culture for an appropriate treatment of soil can render these soils back to the agricultural circuit. Soil TPH loss was up to 70 gTPH·kg<sup>-1</sup> D.M. for 12 monitored months. Furthermore efficiencies reduction of soil TPH planted with bird's foot trefoil were up 88%.

## References

- [1] L. Kim, K. R. Owens, J. Environ. Manage. 91(2010) 791.
- [2] C Ram, R.E. Mastro, Earth Sci. Rev. 128(2014) 52.
- [3] V.C. Panday, N.Singh, Agric. Ecosyst. Environ. 136 (2010)16.
- [4] Z.T. Yao, X.S. Ji, P.K. Starker, J.H. Tang. L.Q. Ge. M.S. Xia. Y.Q. Xi, Earth Sci. Rev. 141 (2015) 105.
- [5] P. Kishor, A.K.. Ghosh, D. Kumar, Asian Journal of Agricultural Research 4 (2010) 1.
- [6] S. Raj, S. Mohan, International Journal of Emerging Technology and Advanced Engineering 4 (2014) 709.
- [7] J. Bilski, K. McLean, E. McLean, F. Soumaila, M. Lander, Int. J. Environ. Sci. Te. 1(2011) 2028.
- [8] S. Mășu, A. A. Marin, D. Popescu, F. Morariu, Phytoremediation TPH polluted soil with common flax, Proceedings of the 20<sup>th</sup> International Symposium on Analytical and Environmental Problems, Szeged Hungary (2014) 270.

## Oil Wastewater Coagulation with Industrial Waste Iron Coagulant

Smaranda Mășu\*, Ladislau Andres

*National R & D Institute for Industrial Ecology ECOIND, Branch of Timisoara, 1 Regina Maria, Square, 300004, Timisoara, Romania;  
e-mail: andamasu@yahoo.com*

### Abstract

The study presents the results obtained during the coagulation of water with high content of oil compounds assessment as total petroleum hydrocarbon (TPH). Coagulation was carried out with a complex coagulation agent based on iron salts obtained from industrial waste. The control parameters of coagulation: turbidity, organic carbon (TOC), TPH, chemical oxygen demand (COD) in treated water samples with the optimal dose of coagulation agent based on iron salts obtained from industrial waste are similar to the residual values of the parameters determined in samples treated with the optimal dose of ferric chloride. The results obtained for the coagulation of oil wastewaters with optimal doses with different coagulation agents are supported also by the UV spectra. The advantage of the complex coagulation agent obtained from industrial waste was that it can be used for some wastewater in lower doses, by 25%, vs. ferric chloride.

### Introduction

Oil compounds assessment as total petroleum hydrocarbon (TPH) ending up in the environment through contaminated water can cause many changes, degradation, and depreciation thereof. TPH wastewater contains organic load varying from a few hundred to thousands of  $\text{mgO}_2 \cdot \text{L}^{-1}$ , expressed by COD parameter. The pH of the wastewater is usually neutral [1-3]. One of the typical processes used as a primary treatment for this wastewater types is coagulation-flocculation process. Literature data on the quantities of pollutants removed by coagulation of wastewaters containing TPH are very different. In recent years the demand for recyclable material, environment friendly, increased in the treatment of waste water [1, 4, 5]. Studies done on total petroleum hydrocarbon wastewater resulting from the oil industry report the use of aluminum salts (alum, poly aluminum chloride.etc.), iron salts (ferric chloride or sulfate), etc., as coagulants [2, 6]. The studies consider the selection of optimal pH, and the coagulant dosage required to obtain the best possible performance in the process of coagulation. Coagulation pH was controlled and then adjusted with mineral base or acid. Coagulation studies are conducted in the pH domain 5.5 to 8.5. The optimal dose established was of tens  $\text{mg} \cdot \text{L}^{-1}$  of metal to several hundred metal  $\text{mg} \cdot \text{L}^{-1}$ . The efficiency of the removal of the color was in the range 86-91.3%, when using aluminum salts *i.e.* poly aluminum chloride, poly-aluminum zinc silicate chloride compared to the reduction efficiency due to the ferric chloride, which was 74-79%. The removal of the COD was performed with yields of 67-72%. The removal of suspensions was of 71.0-98.9% [2, 6]. In the present study were studied comparative total petroleum hydrocarbon wastewaters treatment with complex coagulation agent based on iron salts obtained from industrial waste vs. ferric chloride coagulant agent.

## Experimental

Were studied wastewater input taken from the zone of the effluent wastewater from oil extraction scaffolding. Wastewaters containing TPH studied are apparent water color yellow-brown / brown and real shades of yellow. Wastewaters strong smell of petroleum products. They were in the range 33.5-72.5<sup>0</sup>NTU turbidity. Wastewaters studied exhibit a pH in the range of 7.16-7.91. Wastewaters presents high loads of TPH. Total petroleum hydrocarbon are in the range 95.9-526.0 mg TPH·L<sup>-1</sup>. Organic load expressed by the TOC was in the range of 32.76-99.34 mg C·L<sup>-1</sup>. Organic load expressed by the COD does not express correctly the organic load. Wastewater COD values are in the range of 161.3-515.35.0 mg O<sub>2</sub>·L<sup>-1</sup>. It is known that the oxidation of organic compounds with dichromate in strongly acidic medium (COD parameter) does not oxidize the aromatic substances probably heavily loaded in the studied wastewaters. Therefore by the low values of COD the organic load of these wastewaters cannot be properly assessed. The spectra drawn in the UV-VIS were performed on the filtered water. These waters show a range of absorption at 240-260 nm. A<sub>254</sub> is specific absorbance at 254nm wavelength. Studied wastewater presents A<sub>254</sub> range from 1.031 to 2.230 absorbance units (cm<sup>-1</sup>). Coagulating agents used were: ferric chloride produced by Chimopar S. A. Bucharest and a complex coagulant based on iron salts obtained from industrial wastes in the absence/presence of aid coagulant: indigenous tuff originated from Zalau Quarry, Romania. Indigenous volcanic tuff contains 72% clinoptylolite. Coagulation was performed with a stirrer equipped with variable speeds (Phipps & Bird Company, USA). The optimal dose of the coagulation agents, in the absence / presence of coagulation aids for maximum pollutant removal, was done by Jar Test. The coagulation pH of the wastewater investigated was 7.0, corrected with hydrochloric acid or sodium hydroxide. In the supernatant separated from the treated water samples, conventional parameters were analyzed according to the standardized norms: pH determined by pH-meter model 290A ORION RESEARCH USA, turbidity with Micro 100 Laboratory Turbid meter, Scientific Inc. USA; COD by hot K dichromate oxidation in strongly acidic medium; TOC by TOC Analyzer with Multi N/C 2100 Analytic Jena, Germany. The absorbance – the unconventional parameter, at 254 nm wave length, A<sub>245</sub>, was analyzed by UV VIS spectrophotometer, Specord 205, Analytic Jena, Germany. Total petroleum hydrocarbons were determined according to the Romanian standardized norms by extraction with carbon tetrachloride (SR 7877-1) *i.e.* TPH is extracted from a volume, (V), of wastewater at pH=1 corrected with hydrochloric acid,  $d = 1.19 \text{ g} \cdot \text{L}^{-1}$ , by mixing with solvent. Extracts number is four. Solvent extracts dried by passing through a filter with anhydrous Na<sub>2</sub>SO<sub>4</sub> p.a. layer. Then solvent extracts are placed in capsule, with  $m_1$  [g]. The solvent is evaporated and weigh the capsule with TPH residuum with  $m_2$  [g]. Calculate the amount of TPH,  $\text{TPH g} \cdot \text{L}^{-1} = (m_2 - m_1) \cdot V^{-1} \cdot 1000$ . Studied waters must have the characteristics required by national norm GD 352/2005 - NTPA 002 to be discharged into the sewerage networks of localities *i.e.* solvent extraction compounds = 30mg·L<sup>-1</sup>[7].

## Results and Discussion

Table 1 shows an example of determining the optimal dose of ferric chloride for the a randomly selected wastewater with TPH content, by Jar Test method. As can be seen from Table 1 water samples treated with ferric chloride remain colored in yellow, probably because some of the components of the petroleum hydrocarbon in the water are not removed using ferric chloride as a coagulating agent. There is the likelihood that iron forms yellow chelates during coagulation thus giving the final color of the treated water. Optimal doses for ferric chloride for the studied wastewaters were between 12.0-24.0 mg Fe · L<sup>-1</sup>. Efficiencies of the

coagulation process for the range of coagulation dosage 8.04-24.0 mg Fe  $\cdot$  L<sup>-1</sup>, were 30.5 to 38.1% for the organic load expressed by parameter TOC, 67.1-73.4% for total petroleum hydrocarbon, and for turbidity of 64.1 to 76.1%. For COD, coagulation efficiencies were of 40.0 to 41.0%. Minimal dose to strongly reduce turbidity was at 12.06 mg Fe  $\cdot$  L<sup>-1</sup>, see Table 1. For higher doses than 24.1 mg Fe  $\cdot$  L<sup>-1</sup>, the colloidal system of the wastewater recovers.

**Table 1.** Optimal dose of ferric chloride coagulant for wastewater studied, at pH = 7.0;  
Wastewater characteristics: TPH = 95.9mg  $\cdot$  L<sup>-1</sup>, TOC = 32.76 mg C  $\cdot$  L<sup>-1</sup>, COD = 161.3mgO<sub>2</sub>  $\cdot$  L<sup>-1</sup>, A254 = 1.031 cm<sup>-1</sup>

No	Parameters	Treated samples					
		1	2	3	4	5	6
1	Dose[mg Fe $\cdot$ L <sup>-1</sup> ]	4.0	8.04	<b>12.06</b>	16.08	24.1	28.0
2	Color	Yellow	Yellow	<b>Yellow</b>	Yellow	Yellow	-
3	Residual turbidity [NTU]	F	12.0	<b>8,0</b>	8,2	8,2	23.0
4	Reduction efficiency [%]	51.6	64.1	<b>76.1</b>	75.5	75.5	31.8
5	COD[mgO <sub>2</sub> $\cdot$ L <sup>-1</sup> ]	-	139.5	<b>95.34</b>	96.7	-	-
6	Reduction efficiency [%]		13.5	<b>41.0</b>	40.0	-	-
7	TPH [mg $\cdot$ L <sup>-1</sup> ]	67.2	31.3	<b>29.9</b>	26.8	25.5	-
8	Reduction efficiency [%]	30.7	67.1	<b>68.1</b>	72.1	73.4	-
9	TOC [mg C $\cdot$ L <sup>-1</sup> ]	29.7	21.33.	<b>22.6</b>	22.86	20.3	-
10	Reduction efficiency [%]	12.2	34.8	<b>31.1</b>	30.5	38.1	-

Table 2 presents the results obtained when determining the TPH wastewater optimal dose of complex coagulant based on iron salts obtained from industrial waste in the absence/presence of the coagulation aid: volcanic indigenous tuff.

**Table 2.** Optimal dose of complex coagulation agent based on iron salts obtained from industrial waste in the absence/presence of the coagulation aid: volcanic indigenous tuff.  
Coagulation pH = 7.0.

No.	Parameters	Treated samples				
		1	2	3	4	5
1	Dose [mg Fe $\cdot$ L <sup>-1</sup> ]	3.0	6.0	<b>9.0</b>	15.0	<b>9.0 and aid tuff 0.5 g/l</b>
2	Color	Yellow	Yellow	<b>Colorless</b>	-	<b>Colorless</b>
3	Residual Turbidity [NTU]	16.2	15.2.0	<b>12.5</b>	11.0	<b>12.5</b>
4	Reduction efficiency [%]	51.6	54.6	<b>62.6</b>	67.1	<b>62.6</b>
5.	COD[mgO <sub>2</sub> $\cdot$ L <sup>-1</sup> ]	-		<b>109.0</b>	109.0	<b>103.6</b>
6	Reduction efficiency [%]			<b>32.8</b>	<b>32.8</b>	<b>35.7</b>
7	TPH [mg $\cdot$ L <sup>-1</sup> ]		41.3	<b>27.9</b>	26.8	<b>19.1</b>
8	Reduction efficiency [%]		56.9	<b>70.9</b>	72.0	<b>79.6</b>
9	TOC [mg C $\cdot$ L <sup>-1</sup> ]	29.7	28.1	<b>18.6</b>	22.86	<b>12.9</b>
10	Reduction efficiency [%]	9.5	14.6	<b>43.2</b>	30.5	<b>60.4</b>

The optimal dose of complex coagulant based on iron salts obtained from industrial waste was 9.0 mg Fe  $\cdot$  L<sup>-1</sup>. The advantage of the complex coagulant based on iron salts from industrial waste was that it required reduced optimal doses by 25% vs. the optimal doses of ferric



chloride. Residual values of turbidity, TOC, TPH and COD in the water samples treated with the optimal dose complex coagulant based on iron salts obtained from industrial wastes are similar with the residual values of parameters determined in samples treated with the optimal dose of ferric chloride. Aid coagulant addition to the optimal dose of the coagulation with complex coagulant determined lower residual values for parameters TOC and TPH. Indigenous volcanic tuff addition to the optimal dose of coagulation with complex coagulant from industrial wastes caused an increase in the reduction efficiency of TPH from 70.9% to 79.6% and for TOC from 43.2% to 60.4%. These results are further confirmed by UV spectra shown in Figure 1. Figure 1 shows that treating the wastewater with the optimal dose of complex coagulation agent from industrial wastes in the absence of indigenous tuff determines  $0.56 \text{ cm}^{-1}$  for A254 and in the presence of tuff  $0.46 \text{ cm}^{-1}$ .

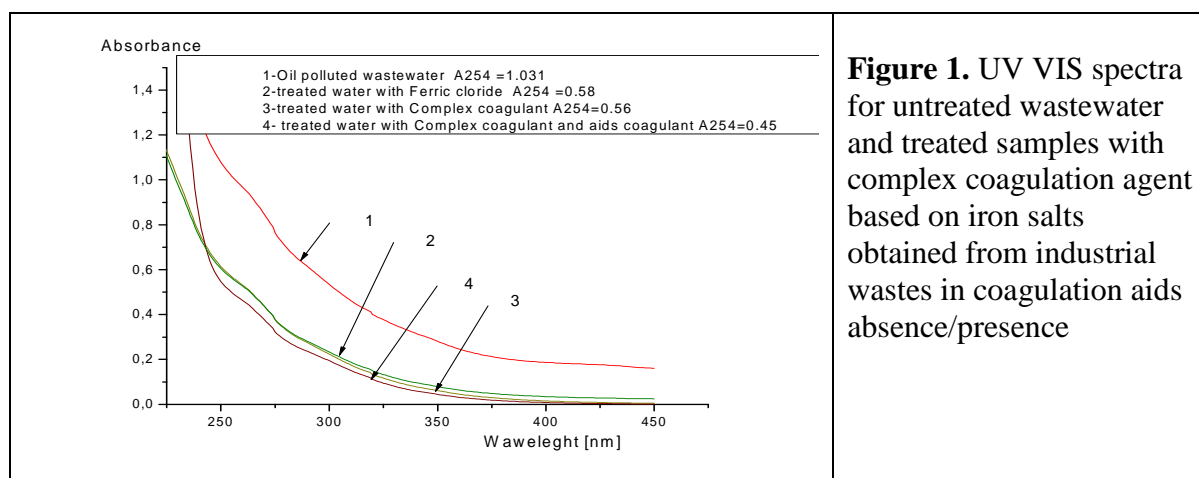


**Figure 1.** UV VIS spectra for untreated wastewater and treated samples with complex coagulation agent based on iron salts obtained from industrial wastes in coagulation aids absence/presence

## Conclusions

The study compared the efficiencies of removing total petroleum hydrocarbon from wastewater obtained in the coagulation stage performed using a complex coagulation agent based on iron salts obtained from industrial wastes and a classic agent the ferric chloride showed that: 1. The residual values of the turbidity, TOC, TPH and COD in water treated samples with the optimal dose of complex coagulation agent are similar to the residual values of the parameters determined in samples treated with the optimal dose of ferric chloride, 2. The addition of tuff to the optimal dose of complex coagulation agent caused lower residual values for the parameters TOC and TPH, 3. The efficiencies of the process of coagulation with various coagulating agents used are supported also by UV spectra, 4. The advantage of complex coagulation agent based on iron salts obtained from industrial wastes was that it required reduced optimal dose by 25%, vs. the optimal doses of ferric chloride.

## References

- [1] F. R. Ahmadun, A. Pendashteh, L. C. Abdulah, D. R. A. Biak, S. S. Madaienii, Z. Z. Abidin, J of Hazard. Mater., 170 (2009) 530.
- [2] H. Farajnezhad, P. Gharbani, International Journal of Research and Reviews in Applied Sciences 13 (2012) 306.
- [3] V. Rajakovic, G. Aleksic, M. Radetic, L. Rajakovici, J. Hazard. Mater. 143 (2007) 494.
- [4] C.E. Santo, V.J.P. Vilar, C.M.S. Botelho., A. Bhatnagar, E. Kumar, R.A.R. Boaventura, Chem. Eng. J. 183 (2012) 117.
- [5] S. Verma, B. Prasad, I. M. Mishra, J. Hazard. Mater. 178 (2010) 1055.



- [6] J. Sanaa, G. Adewale, W. H. Shadi, J. Environ. Sci. 37 (2015) 15.
- [7] National norm HG 352/2005 NTPA 002 Amending and supplementing Government Decision no 188/2002 to approving the rules on the condition of discharging wastewater into the aquatic environment Romania Monitor Official Bucharest, (2005) 378.

## Simultaneous Determination of Mesotrione and Nicosulfuron in OD Formulations

Sanja Lazić, Dragana Šunjka\*, Jovana Bajčić, Slavica Vuković

*Faculty of Agriculture, University of Novi Sad, 21214 Novi Sad, Trg Dositeja Obradovića 8, Serbia*

*e-mail: draganas@polj.uns.ac.rs*

### Abstract

In this study an isocratic high-performance liquid chromatographic method with diode array detection was developed for simultaneous determination of mesotrione and nicosulfuron active ingredients content in pesticide products formulated as oil dispersion (OD). For the analysis, LC system an Agilent Technologies 1100 was used. Good separation was achieved on a Zorbax SB-C18 column using a mobile phase consisting of 0.1% CH<sub>3</sub>COOH/acetonitrile (75:25), at a flow rate of 0.9 ml/minute and UV detection at 245 nm. Column temperature was 40 °C, injected volume was 1 µl. Retention times for nicosulfuron and mesotrione were 3.009 min and 4.363 min, respectively. Validation of the method was performed according to IAEA guidelines. The obtained results showed that the linear coefficients were 0.9999 for both analyzed herbicides in the mixture. The repeatability of the method expressed as relative standard deviations (%RSDr) was 0.33% for mesotrione and 0.18% for nicosulfuron. The accuracy of the proposed method was determined from recovery experiments. The obtained results for mesotrione and nicosulfuron were 100.5-102.9% and 99.3-103.9%, respectively, proved to be acceptable. Precision of the method expressed as %RSD was 0.38% for mesotrione and 0.99% for nicosulfuron and are lower than the values calculated by the Horwitz equation.

### Introduction

For the successful pest control, use of pesticide products of known quality is essential. Recommended methods for active ingredients content in pesticide products are collaboratively tested and published by Association of Official Analytical Chemists (AOAC) and Collaborative International Pesticides Analytical Council (CIPAC). Shortage of the available standard methods for certain active ingredients in pesticide products of different formulations conditions the development of the appropriate methods in a laboratory. This refers especially to more frequent use of one or more active ingredients combinations, matters in the formulated product, and to the lack of the methods for simultaneous determination of their content.

Positive experiences on nicosulfuron (the herbicide from sulfonylurea group) and mesotrione (the herbicide belonging to the group of triketones) compatibility and efficiency led to formulation of the products in combination of these two active ingredients. Determination of nicosulfuron by CIPAC MT 709 method refers to the determination of technical matter purity and to the pesticide products formulated as water dispersible granules (WG). It is based on the use of the reverse-phase high-performance liquid chromatography with the application of detectors with a variety of photosensitive diodes [1].

For the analysis of mesotrione, as well as for the simultaneous determination of these two active ingredients in oil dispersion pesticide formulations (OD), corresponding methods are not available.

The objective of this work has been the development of a simple and fast HPLC-DAD procedure which could be applied to the routine quality control analysis of pesticide formulated product (OD) containing mesotrione and nicosulfuron as active ingredients.

### Experimental

Stock solutions of each active ingredient were prepared by diluting appropriate amount of analytical standards mesotrione (99.9%, Dr Ehrenstorfer, Germany) and nicosulfuron (97%, Dr Ehrenstorfer, Germany) in acetonitrile. Final concentration was ~ 1.0 mg/ml. Working standard solutions were prepared by diluting mixture of stock solution in acetonitrile, in concentration ranged between 0.04-0.27 mg/ml for mesotrione and 0.03-0.25 mg/ml for nicosulfuron.

As the certified referent material for the accuracy determination was not available, samples with a known content of the studied active ingredients were enriched by the known quantity of mesotrione and nicosulfuron analytical standards. The appropriate quantity of a sample was weighted into volumetric flask (25 ml), dissolved in acetonitrile and fortified with standards mixture of mesotrione (0.07, 0.14 and 0.27 mg/ml) and nicosulfuron (0.06, 0.12 and 0.25 mg/ml). All solutions were filtered through membrane filter of 0.45 µm and analyzed by HPLC-DAD.

### Results and discussion

#### HPLC analysis

To achieve adequate separation factor value and sensitivity of the method it is necessary to select the appropriate column, the detector wavelength of the detector, the mobile phase, volume of injection and column temperature. For the analysis of mesotrione and nicosulfuron, HPLC system an Agilent Technologies 1100 was used. The best determination was achieved on a Zorbax SB-C18 column using a mobile phase consisting of 0.1% CH<sub>3</sub>COOH/acetonitrile (75:25), at a flow rate of 0.9 ml/minute and UV detection at 245 nm. Column temperature was 40 °C, injected volume was 1 µl. Qualitative HPLC analysis of a certain ingredient presence was carried out on the basis of retention times, while the quantitative ones were based on the size of the analytical signal. Chromatogram of mesotrione and nicosulfuron standard mixture and sample are presented in Figure 1. Retention times of mesotrione and nicosulfuron were established at 4.330 min and 3.000 min, respectively.

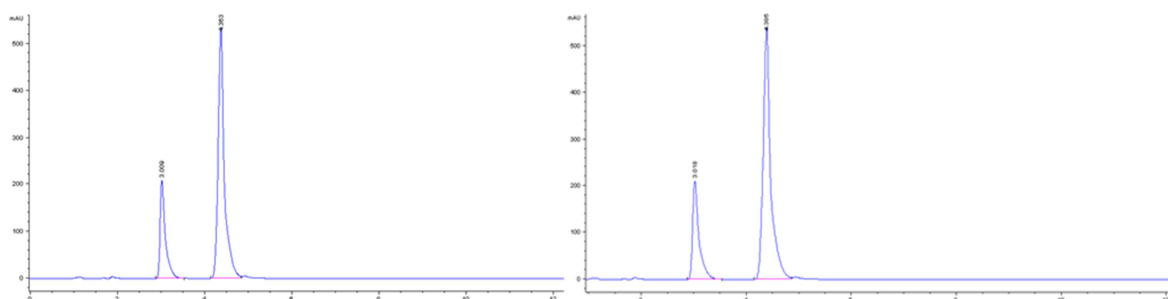


**Figure 1.** The chromatogram of nicosulfuron and mesotrione in standards solution and In OD formulation sample

Component identification was achieved on the basis of  $R_t$  and also by comparison of UV-VIS spectrum of unknown peak with the spectrum of the referent standard [2]. Figure 2 presents spectra of mesotrione and nicosulfuron from analytical standards and sample solution. On y-axis are given values of the current signal detector (mAU), while on the x-axis are wavelength values (nm).

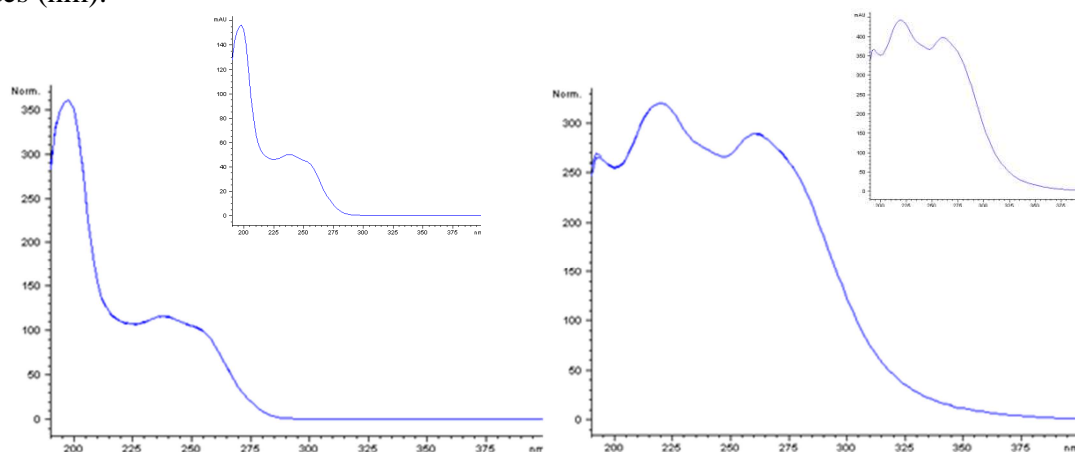


**Figure 2.** UV spectra of nicosulfuron and mesotrione peak from the standards and the sample

#### Validation of the method

According to IAEA guidelines, validation was performed checking the following analytical performance parameters - linearity of detector response, repeatability of injections, precision of the method and accuracy, as well as by determination of Horwitz's limit.

The linearity was established by the scope of the analytical method and it is presented by the regression equation. The linearity of detector response was determined at five levels of concentrations in triplicate, by injecting 1  $\mu$ L of the standard mixture. Calibration curve was defined as dependence of the peak area from concentration and expressed by regression equation with correlation coefficient ( $R^2$ ) (Table 1).

**Table 1.** Linearity parameters

	Active ingredient	
	Mesotrione	Nicosulfuron
concentration range (mg/ml)	0.04-0.27	0.03-0.25
regression equation	$y=55.72x-71.91$	$y=45.86x-43.57$
correlation coefficient ( $R^2$ )	0.9996	0.9999

The obtained values suggest high susceptibility of mesotrione and nicosulfuron determination by this method.

Repeatability of mesotrione and nicosulfuron determination was checked by injecting of the standard solution of these ingredients in concentrations of 0.16 and 0.12 mg/ml of mesotrione and nicosulfuron five times, respectively. The repeatability of the method expressed as relative standard deviations was 0.33% and 0.18%.

The precision of the method is defined by repeatability. In order to check the repeatability of determination 1  $\mu$ l of investigated sample with 0.369 mg/ml of mesotrione and 0.147 mg/ml of nicosulfuron were injected 5 times. The obtained RSDs values for mesotrione and

nicosulfuron were 0.38% and 0.99% respectively. This result suggests good precision of the method for determination of mesotrione and nicosulfuron [2].

According to SANCO 3030/99, the assessment of the method precision is based on Horwitz's limit. Horwitz's equations aroused from numerous inter-laboratory studies conducted by AOAC during several years lasting period, and represent exponential dependence between in laboratory determined relative standard deviation  $RSD_r$  and concentration  $C$ .

The value of Horwitz's limit is calculated by the equation:

$$\%RSD_r = 2^{(1-0.5 \log C)} \times 0.67$$

The obtained relative standard deviation for the repeatability of mesotrione and nicosulfuron determination for the peak areas (1.97% and 5.32%) were significantly under modified values of Horwitz's limit for inter-laboratory repeatability of formulated products determination with active ingredient content of 7.56% and 3.24%, respectively. These results suggest good reproducibility of mesotrione and nicosulfuron determination.

The recoveries of the three fortification levels for mesotrione and nicosulfuron were 100.5-102.9% and 99.3-103.9% respectively. The acceptable values of accuracy for the active ingredients determination in pesticide formulations with a content of less than 10% [2], as well as high accordance between the values obtained in the process and the actual value (102.7% and 102.2%), confirm accuracy of the applied method for determination of mesotrione and nicosulfuron in products of OD formulation.

## **Conclusion**

The method established in this study enables new, simple, selective and accurate routine HPLC analysis of the herbicides mesotrione and nicosulfuron in the OD (oil dispersion) pesticide formulation. This method fully meets the standards of HPLC pesticide analysis in formulations, according to IAEA-TECDOC-1612. Finally, developed method was applied for the determination of mesotrione and nicosulfuron content in a pesticide product. The obtained results of active ingredients are within the permissible deviations [3].

## **References**

- [1] W. Dobrat, A. Martijn (Eds.), Nicosulfuron 709/TC/M, CIPAC Handbook M, Collaborative International Pesticides Analytical Council Ltd.,UK, 2009, pp. 22-128.
- [2] IAEA-TECDOC-1612 (2009). Quality control of pesticide products. International Atomic Energy Agency.
- [3] FAO (2010). Manual on development and use of FAO and WHO specifications for pesticides.

## Effects of the precursors on the photocatalytic water splitting activity of ZnS/CdS compounds

Paula Svera<sup>\*1,2</sup>, Andrei V. Racu<sup>1,3</sup>, Cristina Mosoarca<sup>1</sup>, Daniel Ursu<sup>1,2</sup>,  
Petrica Linul<sup>1</sup>, Radu Baies<sup>1,2</sup>, Radu Banica<sup>1,2</sup>

<sup>1</sup>*Renewable Energies Laboratory – Photovoltaics, National Institute for Research and Development in Electrochemistry and Condensed Matter, 144 Dr. A. Paunescu Podeanu Str., 300569 Timisoara, Romania;*

<sup>2</sup>*University Politehnica Timisoara, 2 Piata Victoriei, 300006 Timisoara, Romania;*

<sup>3</sup>*Institute of Applied Physics of Moldova, ASM, 5 Academiei Str., Chisinau, Moldova;*

Corresponding author: radu.banica@yahoo.com

CdS-based calcogenic photocatalysts show the highest efficiency of hydrogen production by photocatalysis reaction in aqueous solution medium containing sulfide ions [1]. The work aim was to understand the influence of the ZnS precursor crystallinity on the formation of heterostructured PdS/ZnS/Cd<sub>1-x</sub>Zn<sub>x</sub>S photocatalysts and also the influence of the synthesis temperature and time on photocatalysts activity. Particularly, Cd<sub>1-x</sub>Zn<sub>x</sub>S type photocatalysts can be obtained by various techniques including hydrothermal method. We use hydrothermal technique due to the fact that this method allows the obtaining of high crystallinity and large surface area photocatalysts [2]. Photocatalyst's morphology and its compositional homogeneity was determined by SEM, TEM/EDX, crystallinity by XRD and the optical properties of the material by UV-VIS and photoluminescence spectroscopies. Photocatalytic reactions were conducted at room temperature under visible light irradiation. It was observed that the precursor's crystallinity has greater impact on the photocatalytic performance than the synthesis temperature and the reaction time. This confirm that the efficiency of hydrogen production can be influenced and improved by controlling of crystalinity of photocatalysts.

### References:

- [1] Q. Chen, C. Suo, S. Zhang, Y. Wang, *Effect of PdS on photocatalytic hydrogen evolution of nanostructured CdS under visible light irradiation*, International Journal of Photoenergy, 2013, vol. 2013, pg. 1-5
- [2] Z. Xiong, M. Zheng, C. Zhu, B. Zhang, L. Ma, W. Shen, *One-step synthesis of highly efficient three-dimensional Cd<sub>1-x</sub>Zn<sub>x</sub>S photocatalysts for visible light photocatalytic water splitting*, Nanoscale Research Letters, 2013, 8:334, pg. 1-6

### Acknowledgments:

This work was carried out through the Partnerships in priority areas - PN II program, developed with the support of MEN - UEFISCDI, project no. PN-II-PT-PCCA-2013-4-1708.



## As(V) Adsorption using $\text{MFe}_2\text{O}_4$ ( $\text{M}=\text{Cd}^{2+}$ , $\text{Ni}^{2+}$ ) Ferrite Nanoparticles

Raluca Vodă<sup>1\*</sup>, Mihaela Ciopec<sup>1</sup>, Adina Negrea<sup>1</sup>, Lavinia Lupa<sup>1</sup>, Petru Negrea<sup>1</sup>,  
Corneliu M. Davidescu<sup>1</sup>

<sup>1</sup>University Politehnica Timisoara, Faculty for Industrial Chemistry and Environmental Engineering, Bv. Parvan no. 6, Timisoara, RO-300223, Romania  
raluca.voda@upt.ro

### Abstract

The paper present the possibilities of arsenic removal from aqueous solutions using as adsorbent  $\text{MFe}_2\text{O}_4$  ( $\text{M}=\text{Cd}^{2+}$ ,  $\text{Ni}^{2+}$ ) ferrite nanoparticles due to the affinity of arsenic towards iron ions. The ferrites were obtained after a heating treatment of the cadmium respectively nickel ferrioxalate coordination compounds, as precursors, at 500°C. From the two studied adsorbent material the nickel ferrite developed a higher maximum adsorption capacity (132  $\mu\text{g As(V)/g}$  of ferrite) than the cadmium ferrite (109  $\mu\text{g As(V)/g}$  of ferrite) in the removal process of As(V) from aqueous solutions. In both cases the equilibrium between the adsorbent and adsorbate was achieved in 60 minutes.

**Keywords:** ferrite, adsorption, oxalate, arsenic

### Introduction

The main source of drinking water for many countries in the world is the ground water. These waters in most of the cases contain as a natural fond a concentration of arsenic higher than the maximum acceptable concentration by the World Health organization (WHO) of 10  $\mu\text{g/L}$  [1, 2]. The presence of arsenic in drinking water has serious adverse effects on human health and other living organisms [3-5], therefore the development of an adequate removal process of arsenic from drinking water is an issue relevant to almost all countries. From the many techniques studied for the arsenic removal from drinking water, adsorption proved to be the most efficient due to its simplicity and feasibility even for low arsenic concentrations [2, 4, 5]. Because it was proved that the iron compounds present a high affinity for arsenic, these were intensive studied as possible adsorbents materials for arsenic removal from aqueous solutions [6-9]. In this paper we studied and compared the performance of two nanoferrites used as adsorbent material in the removal process of arsenic form aqueous solutions. The ferrites have the advantages that are reusable adsorbents because these can be efficient and economic separated from solutions due to their ferromagnetic or supermagnetic properties [10-15].

### Experimental

For the synthesis of  $\text{MFe}_2\text{O}_4$  ( $\text{M}=\text{Cd}^{2+}$ ,  $\text{Ni}^{2+}$ ) was used the thermal decomposition of cadmium respectively nickel ferrioxalate precursors, it represents an efficient route of various ferrites synthesis [16]. The oxides were obtained after heating treatment of the precursor at 500°C for one hour, with a heating rate of 5°C/min. The SEM images were recorded using a Quanta FEG 250 microscope, equipped with an EDAX ZAF quantifier.

The obtained ferrites were used in the removal process of As(V) from aqueous solutions. In order to compare their adsorption performance in the removal process of As(V) from aqueous solutions, the dependence of the adsorption capacity function of S:L ratio, stirring time and As(V) initial concentration was determined. The adsorption performance of the studied material was expressed as arsenic metal uptake ( $\mu\text{g/g}$ ) eq.1. [1-5]:

$$q_e = \frac{(C_0 - C_e) \cdot V}{m} \quad (1)$$

where:  $C_0$  and  $C_e$  are the concentrations of arsenate ( $\mu\text{g/L}$ ) in the solution, initially ( $t=0$ ) and at equilibrium, respectively,  $V$  is the volume of the solution and  $m$  is the mass of adsorbent.

For the study of the S:L influence various quantities of ferrites (0.05, 0.1, 0.2, 0.3, 0.4 and 0.5 g) were treated with 25 mL of As(V) aqueous solutions containing a concentrations of 100  $\mu\text{g/L}$ . The samples were shaken for 1 hour (using a Julabo SW 23 shaker), and after the time elapsed were filtrated and in the resulted solutions was determined the residual concentration of As(V) through atomic absorption spectrometry using a Varian SpectrAA 110 atomic absorption spectrometer with a Varian VGA 77 hydride generation system. When the effect of the initial As(III) concentration (range: 100 – 700  $\mu\text{g/L}$ ) was studied, in each experiments 0.1 g of adsorbent was suspended in 25 mL of As(V) solutions. To study the effect of contact time on adsorption, the experiments were carried out with samples of 0.1 g studied materials in 25 mL of 100  $\mu\text{g/L}$  As(V) solutions. The suspensions were stirred for various periods of time: 15, 30, 45, 60, 90 and 120 (min).

### Results and discussion

The size of the nanoparticles evaluated from SEM images (Fig. 1) was found to be in the range of 20-50 nm, almost homogeneous as shape and size. The nickel ferrite present a higher porosity than the cadmium ferrite. This may conduce to a higher adsorption capacity in the removal process of As(V) from aqueous solutions. Qualitative and quantitative EDX analyses showed a high purity and suitable stoichiometry of the investigated ferrites.

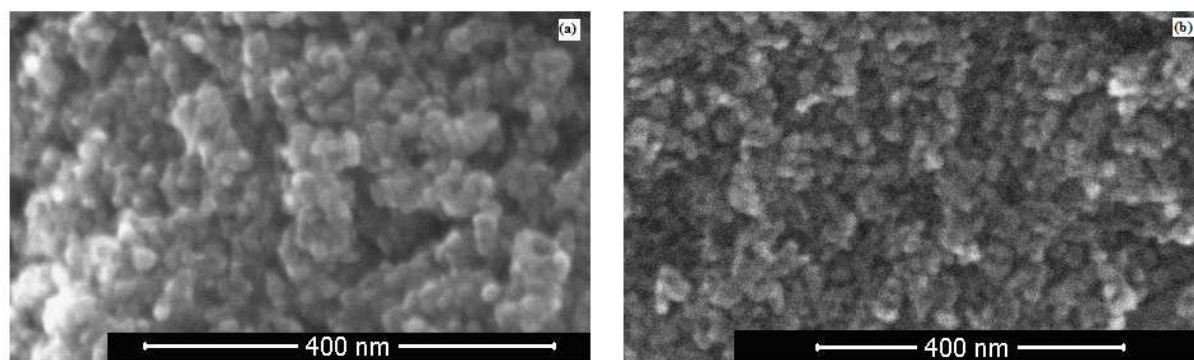


**Figure 1.** SEM images of  $\text{MFe}_2\text{O}_4$  ferrites: (a)  $\text{CdFe}_2\text{O}_4$  and (b)  $\text{NiFe}_2\text{O}_4$

The influence of the S:L ratio upon the adsorption performance of the studied ferrites is presented in figure 2.

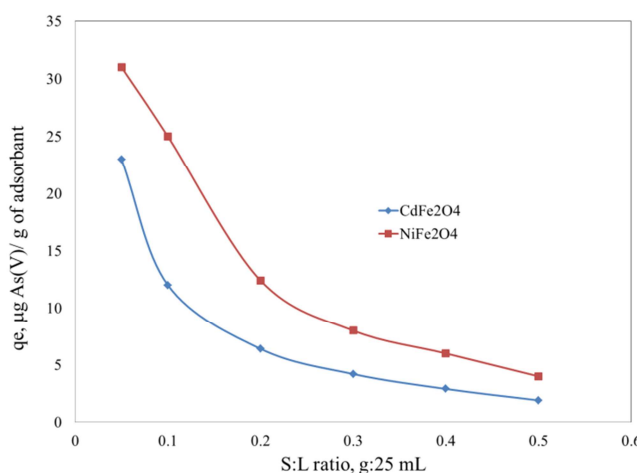


**Figure 2.** S:L influence on the adsorption process

It can be observed that a higher quantity of adsorbent material lead to the degreasing of the adsorption capacity, because the adsorbent capacity is related to the amount of adsorbent. Therefore in order to obtain both maximum values for removal degree but also for adsorption capacity for the future experiments a S:L ratio of 0.1 g of ferrites compounds : 25 mL of As(V) solution was used.

The experimental data regarding the dependence of As(V) uptake function of the As(V) equilibrium concentration are presented in figure 3.

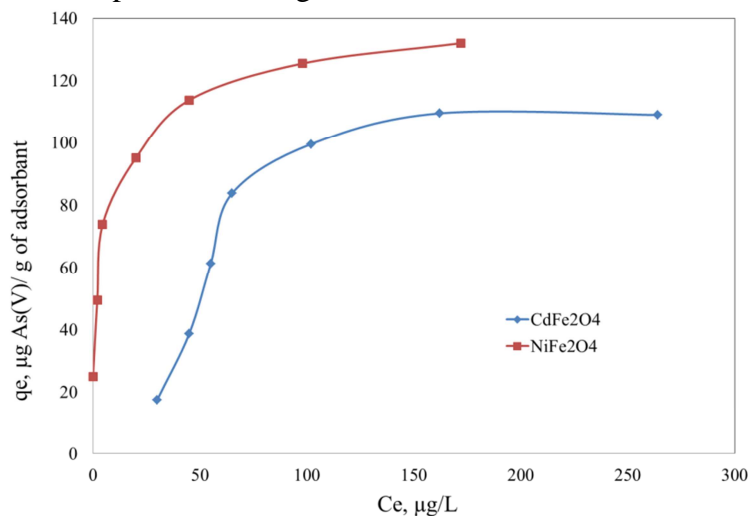


**Figure 3.** As(V) initial concentration influence on the adsorption process

The adsorption capacity of studied ferrites in the removal process of As(V) increased with increasing equilibrium concentration of As(V), and then it approached a constant value at higher equilibrium concentrations. It can be observed that the nickel ferrite developed a higher maximum adsorption capacity (132 µg As(V)/g of ferrite) than the cadmium ferrite (109 µg As(V)/g of ferrite) in the removal process of As(V) from aqueous solutions. This is in accordance with the conclusion raised from the SEM analysis.

The As(V) adsorption behavior onto studied ferrites was studied by the variation of the equilibrium time in the range of 15 - 120 min. The adsorption capacity of the As(V) as a function of contact time is plotted in figure 4. It can be observed that the adsorption capacity of As(V) increase with the stirring time increasing for the both studied ferrite. The highest

amount of As(V) uptake occurs in the first 60 minutes.

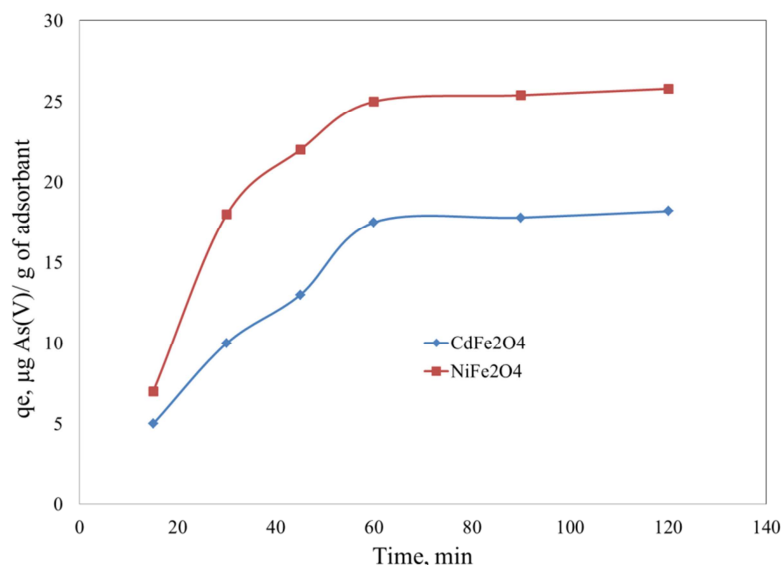


**Figure 4.** Stirring time influence on the adsorption process

### Conclusion

MFe<sub>2</sub>O<sub>4</sub> (M=Cd<sup>2+</sup>, Ni<sup>2+</sup>) ferrite nanoparticles were obtained by thermolysis of oxalate coordination compounds at 500°C. The SEM and EDX analysis a high purity and suitable stoichiometry of the investigated ferrites. The results showed that MFe<sub>2</sub>O<sub>4</sub> (M=Cd<sup>2+</sup>, Ni<sup>2+</sup>) ferrite nanoparticles can be used with good results as adsorbent material in the removal process of As(V) from aqueous solutions. The use of these materials present the advantages compared with other adsorbents that present a very good efficiency, can be easily removed from the aqueous solutions and can be regenerated. From the two studied adsorbent material the nickel ferrite developed a higher maximum adsorption capacity (132 µg As(V)/g of ferrite) than the cadmium ferrite (109 µg As(V)/g of ferrite) in the removal process of As(V) from aqueous solutions. In both cases the equilibrium between the adsorbent and adsorbate was achieved in 60 minutes.

### Acknowledgements

„This work was partially supported by the strategic grant POSDRU/159/1.5/S/137070 (2014) of the Ministry of National Education, Romania, co-financed by the European Social Fund – Investing in People, within the Sectoral Operational Programme Human Resources Development 2007-2013”.

### References

- [1] K. Banerjee, G.L. Amy, M. Prevost, S. Nour, M. Jekel, P.M. Gallagher, C.D. Blumenschein, *Wat. Res.* 42 (2008) 3371.
- [2] S.K. Maji, A. Pal, T. Pal, *J. Hazard. Mater.* 151 (2008) 811.
- [3] A. Maiti, J.K. Basu, S. De, *Ind. Eng. Chem. Res.* 49 (2010) 4873.
- [4] D. Borah, S. Satokawa, S. Kato, T. Kojima, *J. Colloid Inter. Sci.* 319 (2008) 53.
- [5] D. Borah, S. Satokawa, S. Kato, T. Kojima, *J. Hazard. Mater.* 162 (2009) 1269.
- [6] Y. Jeong, M. Fan, S. Singh, C.L. Chuang, B. Saha, J.H. van Leeuwen, *Chem. Eng. Proc.* 46 (2007) 1030.
- [7] J.C. Hsu, C.J. Lin, C.H. Liao, S.T. Chen, *J. Hazard. Mater.* 153 (2008) 817.

- [8] P. Mondal, C.B. Majumder, B. Mohanty, J. Hazard. Mater. 150 (2008) 695.
- [9] A. Ramesh, H. Hasegawa, T. Maki, K. Ueda, Sep. Purif. Technol. 56 (2007) 90.
- [10] S.X. Zhang, H.Y. Niu, Y.Q. Cai, Y.L. Shi, Chem. Eng. J. 158(3) (2010) 599.
- [11] J.G. Parsons, M.L. Lopez, J.R. Peralta-Videa, J.L. Gardea-Torresdey, Microchem. J. 91 (2009) 100.
- [12] J. Hu, I.M.C. Lo, G. Chen, Sep. Purif. Technol. 56 (2007) 249.
- [13] Z. Gao, F.M. Cui, S.Z. Zeng, L.M. Guo, J.L. Shi, Microporous and Mesoporous Mater. 132(1/2) (2010) 188.
- [14] X.-yu Hou, J. Feng, X.-han Liu, M.-lin Zhang, Chem. Res. Chinese Universities 27(4) (2011) 543.
- [15] J.T. Mayo, C. Yavuz, S. Yean, L. Cong, H. Shipley, W. Yu, J. Falkner, A. Kan, M. Tomson, V.L. Colvin, Sci. Technol. Adv. Mater. 8 (2007) 71.
- [16] R. Dumitru, F. Papa, I. Balint, D.C. Culita, C. Munteanu, N. Stanica, A. Ianculescu, L. Diamandescu, O. Carp, Appl. Catal. A Gen. 467 (2013) 178.

## Humán Szérum Tokoferol- és Ubikinonszintek Bioanalitikai Vizsgálata

Bajtai Attila<sup>1\*</sup>, Veres Gábor<sup>1,3</sup>, Szpisjak László<sup>1</sup>, Ilisz István<sup>2</sup>, Klivényi Péter<sup>1</sup>, Vécsei László<sup>1,3</sup>, Zádori Dénes<sup>1‡</sup>

<sup>1</sup>Szegedi Tudományegyetem, Általános Orvostudományi Kar, Szent-Györgyi Albert Klinikai Központ, Neurológiai Klinika, Semmelweis u. 6, 6725 Szeged

<sup>2</sup>Szegedi Tudományegyetem, Természettudományi és Informatikai Kar, Szervetlen és Analitikai Kémiai Tanszék, Dóm tér 7, 6720 Szeged

<sup>3</sup>MTA-SZTE Idegtudományi Kutatócsoport, Semmelweis u. 6, 6725 Szeged

### Abstract

The vitamin E group of compounds and ubiquinone are widely known substances with antioxidant properties. However, the setup of high-performance liquid chromatography (HPLC) methods for the detection of these molecules in human serum are often difficult. We report here a reversed-phase HPLC method using diode array detection and a single C18 column separation kept at 25 °C with an isocratic system of acetonitrile, tetrahydrofuran, methanol, ammonium acetate and water at a flow-rate of 2.1 mL/min. This method resolves 3 tocopherols ( $\alpha$ ,  $\gamma$ ,  $\delta$ ) and ubiquinone from human serum within 17 minutes with the application of tocol as an internal standard. We conclude that our procedure provides an adequate sample preparation and separation of the 3 examined tocopherols ( $\alpha$ ,  $\gamma$ ,  $\delta$ ). Although the developed method has been proven to be efficient, accurate and inexpensive, further improvements in the quantitative assessment of ubiquinone are necessary.

### Bevezetés

A tokoferolok (E-vitamin) antioxidáns sajátága jól ismert és ennek köszönhetően hatásos védelmet nyújtanak az oxidatív stressz ellen többek között az artériák, kapillárisok, vérben található lipidek és az idegszövet esetén [1]. Az ubikinon, más néven koenzim Q10, minden sejtben és membránban megtalálható molekula. A légzési lánc egyetlen olyan elektron átvivője, amely nem kötődik kovalens kötéssel fehérjéhez, ezért a mitokondrium belső membránjában viszonylag szabadon mozoghat. A légzési láncban betöltött szerepe mellett zsírban oldódó antioxidánsként nélkülözhetetlen a jelenléte főként a lipidek védelméhez a szervezetben kialakuló oxidatív stressz ellen [2].

Számos neurológiai kórkép kialakulásában, lefolyásában az antioxidáns rendszer nem megfelelő működése kóroki szereppel bírhat. Erre példa az ataxia izolált E-vitamin hiánnyal (ataxia with vitamin E deficiency, AVED), mely esetén az  $\alpha$ -tokoferol transzport zavart a májsejtekben [3], így a szervezetben kialakuló alacsony koncentrációja miatt nem képes a megfelelő antioxidáns védelem biztosítására. Ezért e kórképek esetén a vérben található tokoferolok pontos mennyiségének ismerete az egyéb felszívódási zavarok kizárása esetén, például AVED vonatkozásában diagnosztikus szereppel bírhat.

Célunk egy olyan bioanalitikai metodika kidolgozása és validálása volt, mellyel tokoferolok ( $\alpha$ -,  $\gamma$ -,  $\delta$ -tokoferol) és az ubikinon mennyiségét gyorsan és megbízhatóan mérhetjük humán szérum mintákban.

### Metodika

A humán szérum minták sárga kupakos vérvételi csőben kerültek levételre, melyek szeparáló gélt tartalmaznak, amely centrifugálást követően stabil határt képez a szérum és a vérsejtek között. Fél óra véralvadást követően 10 percig 3500 fordulat/perc sebességgel 4 °C-



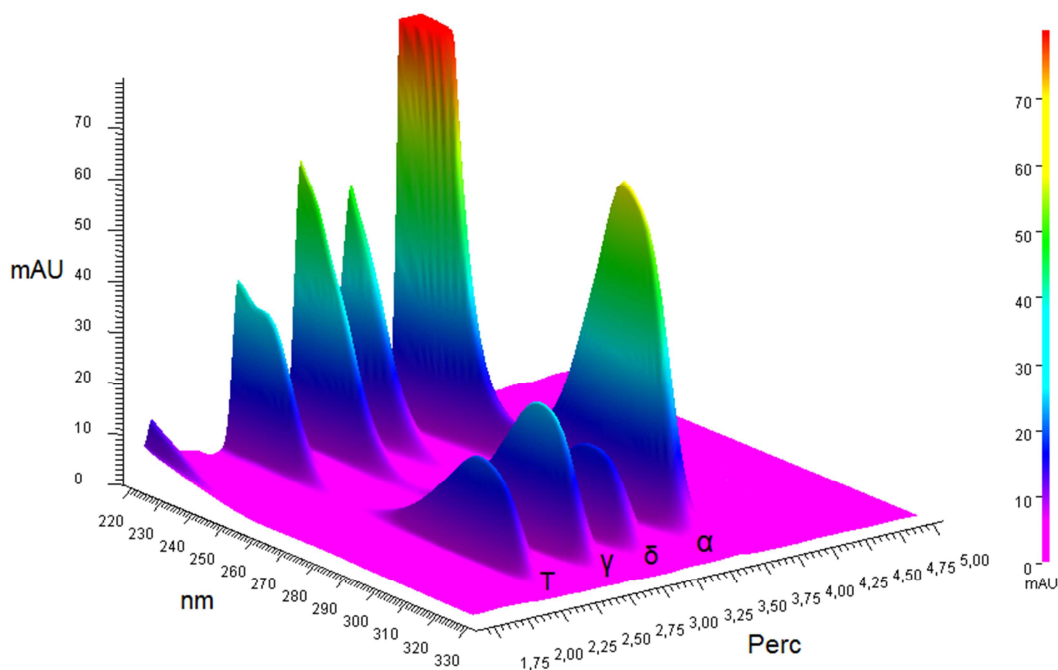
on hűtve lettek centrifugálva. A centrifugálás után a felső folyadékfázist kinyertük és azonnal stabilizáltuk 2,2 mL-es Eppendorf csövekbe 200  $\mu$ L-es részletekben szétosztva: 200  $\mu$ L 85 mM-os aszkorbinsav vizes oldat, majd 400  $\mu$ L 1,13 mM-os BHT-s etanol oldat hozzáadását követően 10 másodperc vortex kevertetéssel. Az így kapott oldatot tekintettük a továbbiakban a tényleges mintának, amely  $-80^{\circ}\text{C}$ -on hónapokig változatlan állapotban tárolható.

Ezt követően a mintákhoz 600  $\mu$ L 1,13 mM koncentrációban BHT-t és rac-tocolt 10  $\mu$ M-ban tartalmazó hexán oldatot adtunk. Pontosan 1 percen keresztül kevertettük vortex segítségével az oldatokat. Ezután a hexános és etanolos fázist elválasztandó 3000 fordulat/perc-es sebességgel 5 percig centrifugáltunk. A centrifugálást követően a felső, hexános fázisból 450  $\mu$ L-t bepároltunk  $\text{N}_2$  gázzal hozzávetőlegesen 15 perc alatt. Ezután a visszamaradt komponenseket 28,57 V/V% EtOH, 28,57 V/V% dioxán, 42,86 V/V% ACN elegyben oldottuk és 10 másodpercig vortexszel homogenizáltuk, így injektálásra és elválasztásra kész állapotba hozva a mintákat.

Az elválasztáshoz Alltech Prevail C18 (150x4,6 mm; 5  $\mu$ m) oszlopot használtunk  $25^{\circ}\text{C}$ -os hőmérsékleten termosztálva. A kolonna védelme érdekében előtét kolonnát használtunk: Security Guard C18 (4x3 mm).

A mobilfázis összetétele: 66,54 V/V% acetonitril, 21,40 V/V% tetrahidrofuran, 6,61 V/V% metanol, 2,72 V/V% ammónium-acetát 1 vegyes százalékos oldata, 2,72 V/V% desztillált víz. A mobilfázist minden mérés előtt frissen készítettük és az elkészítését követően kerámiaszűrőn 0,45  $\mu$ m-es pórusméretű hidrofób PVDF membránszűrőn vízsugárszivattyú segítségével szűrtük. A mobilfázis áramlási sebessége 2,1 mL/perc volt. Minden mintából 50  $\mu$ L térfogatot injektáltunk a mérések során.

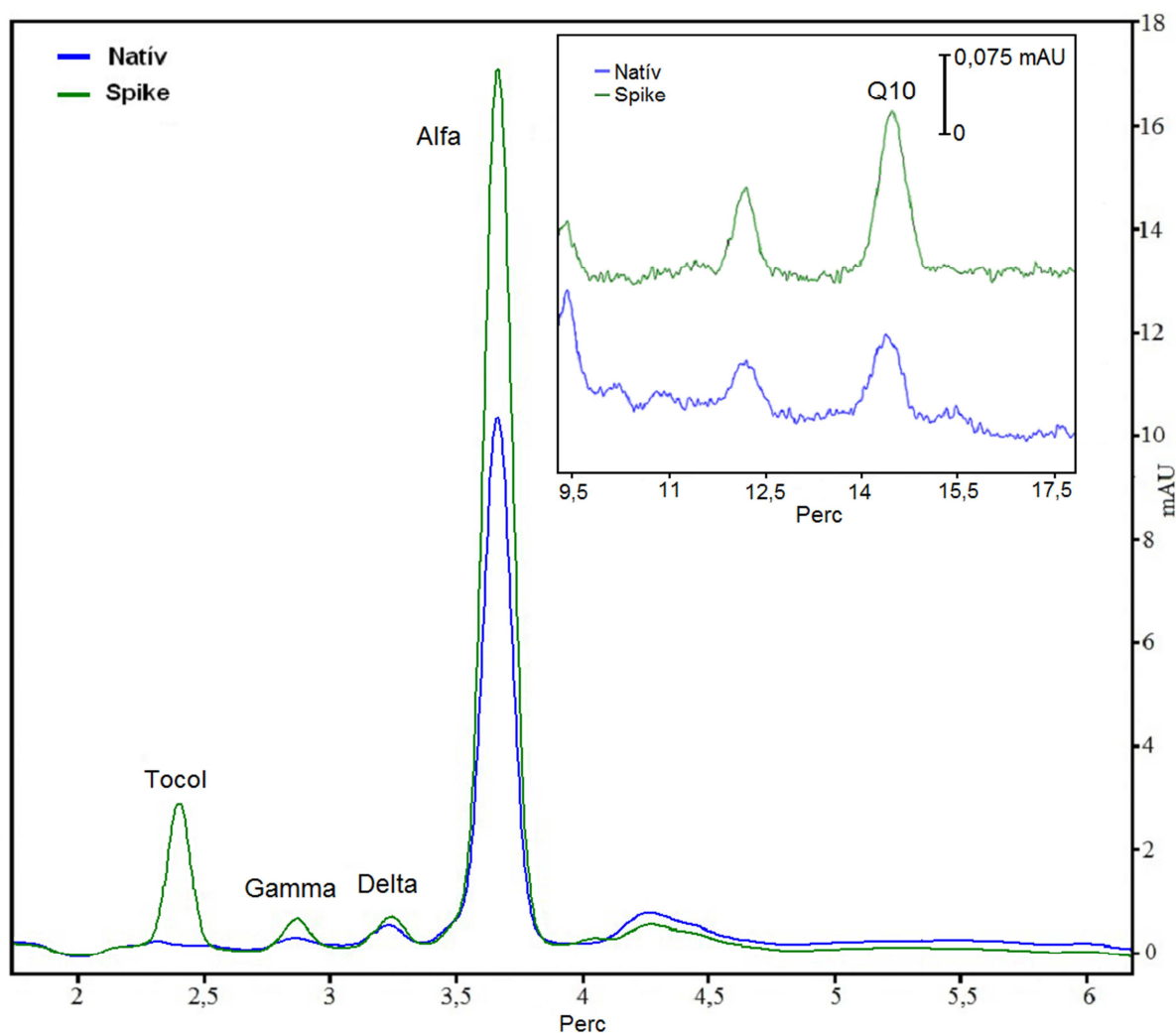
Az analit koncentrációk méréséhez Agilent 1260 diódasoros detektorral meghatároztuk az optimális mérési hullámhosszokat. Ehhez rögzítettük 190 és 800 nm hullámhossz tartományban az abszorbanciát az idő függvényében megnövelt analit tartalmú szérum minta mérése közben. Ennek egy részletét mutatja be az 1. ábra.



1. Ábra: Humán szérum minta kromatogram részlete a hullámhossz függvényében, T: tocol;  $\alpha$ ,  $\gamma$ ,  $\delta$ :  $\alpha$ -,  $\gamma$ -,  $\delta$ -tokoferol

## Eredmények és értékelésük

Az elválasztandó komponensek szelektivitásának meghatározására a biológiai mátrixot hat különböző forrásból származó humán szérum minta összekeverésével alkottuk. A mérendő komponensek azonosításához ismert koncentrációjú analit addíciójával mért mintákat hasonlítottunk össze az azonos eredeti összetételű addíció nélküli (vak) oldatokkal, ezt mutatja be a 2. ábra.



2. Ábra: Humán szérum minta kromatogram részlete 292 nm-en tocol,  $\alpha$ -,  $\gamma$ -,  $\delta$ -tokoferol oldatokkal spikeolva, a kis ábrán az ubikinon oldattal spikeolt kromatogram részlet látható 276 nm-en

A precizitás meghatározása során hat párhuzamos mérést végeztünk, melyek eredményeiből számított relatív standard deviációkat az 1. táblázat tartalmazza. Nem biológiai mátrixok esetén a precizitás értéke 5% alatt kell, hogy maradjon, míg biológiai minták esetén 15%-os relatív standard deviáció az általánosan elfogadott érték. A belső standardot nem validáltuk, mivel abból a nekünk megfelelő mennyiséget használtunk minden méréshez.

A mérendő anyag visszanyerhetőségének vizsgálata során a biológiai mátrixhoz ismert, két különböző koncentrációban hozzáadtuk a vizsgált anyagokat és 3 párhuzamos méréssel megállapítottuk az analitok koncentrációt. A hozzáadott analitokat tartalmazó oldatok koncentrációiból levontuk a vak oldatban mért analitok koncentrációit. A kapott

eredményt összehasonlítottuk az elvárt ismert koncentrációkkal, amit százalékosan adtunk meg. A visszanyerésnek nem kell 100%-nak lennie, de legyen konzisztens, pontos és reprodukálható.

Az ubikinon esetén a mérés precizitása és a kalibrációs egyenes  $R^2$  értéke további fejlesztést tesz indokolttá.

Eredmények					
	$\alpha$ -tokoferol	$\delta$ -tokoferol	$\gamma$ -tokoferol	Q10	tocol
Mérési hullámhossz (nm)	292	297	297	276	297
Retenció idő (perc)	3,7	3,3	2,9	15,5	2,3
Standardsor tartománya ( $\mu$ M)	0 - 40	0 - 6	0 - 6	0 - 2,4	0 - 24
Kalibrációs egyenes $R^2$	0,9934	0,9985	0,9996	0,9840	0,9999
Precizitás - RSD%	4,066	2,949	15,187	20,134	-
Visszamérhetőség %	87,7 - 104,5	95,4 - 108,4	116,2 - 123,8	106,7 - 116,9	-

1. Táblázat: Az elválasztott komponensek és validálásuk adatai

## Összefoglalás

Sikerült megfelelő mintaelőkészítést tartalmazó analitikai eljárást kidolgoznunk humán szérum minták  $\alpha$ -,  $\delta$ -,  $\gamma$ -tokoferol belső standard melletti koncentráció-meghatározására. Az ubikinon koncentráció megbízható meghatározására további fejlesztések szükségesek. Az eredményeink a szakirodalmi adatokkal összhangban vannak [4]. Metodikánk nemcsak a kutatások során, hanem a későbbiekben akár a mindennapi orvosi diagnosztikában is jól hasznosítható eredményekkel szolgálhat.

## Köszönetnyilvánítás

A kutatást a Nemzeti Agykutatási Program - KTIA\_13\_NAP-a-III/9 és az MTA-SZTE Idegtudományi kutatócsoport támogatta.

## Referenciák

- [1]Hacquebard M., Carpentier Y. A., Current Opinion in Clinical Nutrition & Metabolic Care, 2005;8:133-138.
- [2]Bentinger M., Brismar K., Dallner G., Mitochondrion, 2007;7S:S41-S50.
- [3]Eggermont E., European Journal of Pediatrics, 2006;165:429-434.
- [4]Lai J. F., Franke A. A., Journal of Chromatography B, 2013;931:23-41.

## Különleges Mézek Összehasonlító Vizsgálata

Szigeti Ferenc<sup>1</sup>, Stefanovits-Bányai Éva<sup>2</sup>, Soós Anita<sup>1</sup>

<sup>1</sup> Budapesti Corvinus Egyetem, Élelmiszertudományi Kar, Gabona- és Iparinövény  
Technológia Tanszék, 1118 Budapest, Villányi u. 29-43. Hungary

<sup>2</sup> Budapesti Corvinus Egyetem Élelmiszertudományi Kar, Alkalmazott Kémia Tanszék, 1118  
Budapest, Villányi u. 29-43. Hungary  
e-mail: anita.soos@uni-corvinus.hu

### Abstract

Our work aimed to compare the most important characteristics of unifloral honeys and their parent plants; these were water content, conductivity, acidity, antioxidant capacity by FRAP method as well as total phenol content.

We found that antioxidant capacity and total phenol content were in close correlation in case of yellow sweet clover and hawthorn; such relationship, however, was not detectable in the case of honeys.

We further found that conductivity of yellow sweet clover, tilia and hawthorn honeys comply with the food safety regulations, but fennel showed values higher than acceptable.

We could conclude that biologically active materials are only partially present in the honeys, since during the formation of various types of honey new active materials may appear.

### Bevezetés

A méz az egyik ősidők óta használt édesipari termékünk, az emberiség több mint 10000 éve fogyasztja és használja fel különböző betegségek gyógyítására is élvezeti értéke mellett.

Miután az emberek egyre inkább térnek vissza a szintetikus gyógyszerekkel való kezelések helyett, vagy mellette a természetes alapú orvosláshoz, ezért egyre nagyobb figyelem irányul például a méz, mint természetes alapanyag felé. Kialakult egy újfajta tudomány, az apiterápia, melyben a kutatók és az orvosok a méhészeti termékekben próbálják megtalálni a különféle gyógyhatású anyagokat a különböző betegségekre. Ezen feltevések alapját a mézben előforduló értékes beltartalmi komponensek képezik.

A mézek kedvező tulajdonságainak kialakítása számos fizikai és kémia paraméter együttesen járul hozzá. A mézek fizikai tisztasága mellett fontos a színe [1], a megfelelő nedvességtartalma [2], sűrűsége, viszkozitása [3], elektromos vezetőképessége [4], fajhője [5], a kristályosodásra való hajlama [6], stb.

A mézek fizikai jellemzői mellett talán a legfontosabb a bennük előforduló értékes komponensek sokasága, és azok ismerete. Elsőként kell kiemelni a mézekben megtalálható igen gazdag szénhidráttartalmat. A glükóz és fruktóz mellett számos di – és oligoszacharid is megtalálható bennük (szacharóz, melezitóz, maltóz, turanóz, izomaltóz, panóz, trehalóz és cellobióz és raffinóz, stb) de előfordulnak enzimatis tevékenység során keletkezettek is [7].

Nem lehet említés nélkül hagyni a HMF-t (hidroximetil-furfurol), a mézben előforduló mono-, és diszacharidok, elsősorban a gyümölcscukornak a bomlástermékét, a Maillard-reakció egyik intermediér vegyületét sem [8], mely karcinogén, mutagén és toxikus tulajdonságokkal rendelkezik.

Ismert, hogy a mézek illat és aromaanyagainak kialakításához hozzájárulnak/meghatározók a mézek alapját adó növények terméseinek, virágainak jellegzetes aromakomponensei [9, 10, 11].

A mézben található fehérjetartalom az állati (méhek garatváladéka) illetve növényi forrásból (virágpor, nektár) származik [5], gazdag aminosavtartalmából (mind a 20 féle aminosav) kiemelendő a prolin [12].

Említést érdemel a méz nektáreredetű ásványi elem tartalma [13], és az ismerten úgy szint alacsony vitamintartalma [14]. Kiemelendő a mézek antimikrobiális, antibakteriális hatásért felelős, antioxidáns tulajdonságainak kialakításában szerepet játszó polifenolos vegyületekben való gazdagsága [15] és meg kell említeni az anyagcserében szerepet játszó kolin [16] előfordulását is.

Előkísérleteinkben a célkitűzésünk az volt, hogy néhány különleges méz fizikai és beltartalmi jellemzése mellett az antioxidáns kapacitásukat összehasonlítsuk és összefüggéseket keressünk a mézek és a mézek alapját képező növények teáinak antioxidáns kapacitásai között.

### **Anyag és módszer**

Kísérletünk alapanyagának somkóró (üllői bio), hárs (Bertók Méhészet Bt., galagonya (Ásotthalmi Bivalyos Tanya Kft.) és édeskömény (Hungary Honey Kft.) mézeket használtunk, míg a mézek alapját képező gyógynövényeket, galagonya-, és a hársfavirágzatot, somkóró szárát és az édeskömény magtermését (csak ez állt rendelkezésünkre) kereskedelmi forgalomból szereztük be.

Mintaelőkészítés: a mézek esetében 5g/20 ml-es koncentrációjú vizes oldat készült, míg a gyógynövényekből 1g/100 ml-es 100 °C-os vizes (24 órás áztatás), illetve 20%-os etanolos kivonatot készítettünk (72 órás áztatás).

A vezetőképességet a Magyar Élelmiszerkönyv 1-3-2001/110 számú Méz című előírásban előírt követelmény szerint mértük, milliSiemens per centiméterben.

A nedvességtartalom meghatározása az AOAC Official methods 925.45 Moisture in sugars szabványának megfelelően történt, a szárazanyag %-ában kifejezve.

A savfokot az MSZ 6943/3-80 szerint határoztuk meg.

Az összes polifenoltartalmat Singleton és Rossi [17], módszerével határoztuk meg, az eredményeket  $\mu\text{MGS(galluszsav)/l}$ -ben adtuk meg.

Az antioxidáns kapacitást Benzie és Strain [18] módszerével határoztuk meg és az eredményeket  $\mu\text{MAS(aszkorbinsav)/l}$ -ben adtuk meg.

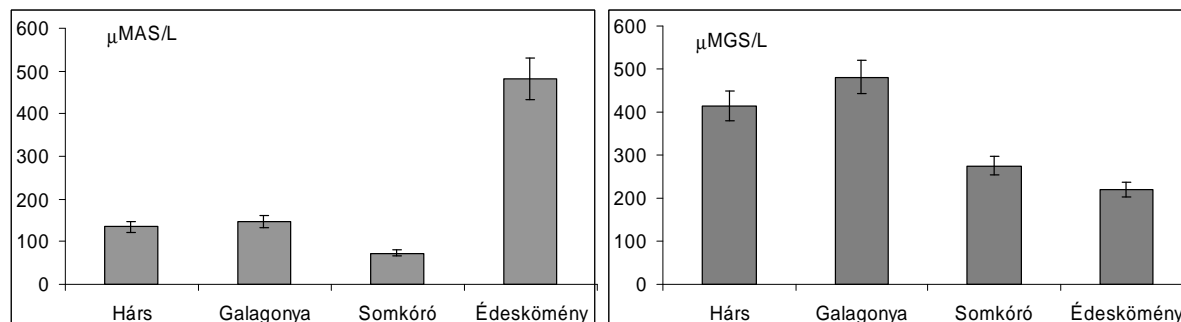
### **Eredmények és értékelésük**

Az elektromos vezetőképesség mérés során a hársméz értéke volt a legnagyobb (átlag:1,18 mS/cm; szórás:0,08), a megengedett vezetőképessége legfeljebb 0,8 mS/cm lehet. A galagonya-, édeskömény-, és somkóróméz mindegyike a határérték alatt volt, a legkisebb értéke a galagonyaméznek volt (átlag:0,2; szórás:0,0014). A nedvességtartalom esetében az édesköményméz nedvességtartalma volt a legnagyobb (átlag:22,79; szórás:0,14), a somkóró mézé volt a legkisebb (átlag:18,3;szórás:0,16), míg a hárs- és a galagonyaméz közel azonos értéket mutattak. A vizsgálataink szerint az édesköményméz savtartalma számottevően nagyobb, mint a többi mézé (átlag:7,8; szórás:0,15), ami az ízében is kifejezésre jutott, legkisebb értéke a somkóróméznek volt (átlag:1,47; szórás:0,1), míg a hárs-és a galagonyaméz közel azonos értékekkel szerepeltek.

A mézek vizes kivonatának vizsgálata során (1. ábra) az összes antioxidáns kapacitást és az összes polifenoltartalmat határoztuk meg.

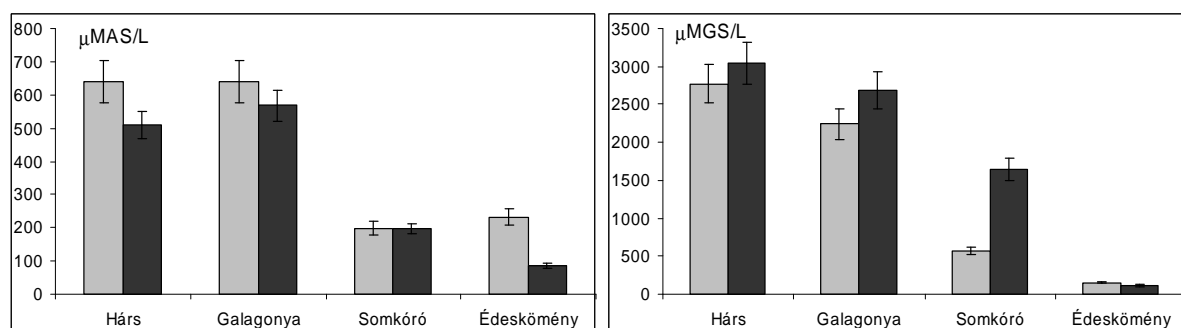
Az egyes mézek vizes oldatainak vizsgálata során a legnagyobb antioxidáns kapacitást az édeskömény méz mutatta, míg a többinél közel azonos értékeket mértünk. A polifenolos vegyületek vizsgálata során a hárs és a galagonyamézek tartalmaztak több polifenolos

komponenst, a somkóró és az édeskömény mézek jelentősen szegényebbek voltak a ezen vegyületekben. Feltételezhető, hogy az édeskömény kimagasló antioxidáns kapacitása nem ezen komponenseknek az eredménye.



**1. ábra.** A különböző mézek antioxidáns- ( $\mu\text{MAS/L}$ ) és polifenoltartalma ( $\mu\text{MGAS/L}$ )

Megvizsgáltuk a mézek alapjául szolgáló növényi minták vizes és alkoholos kivonatának azonos komponenseit. Meg kell jegyezni, hogy a mézek alapjául a virágporok ugyan a kiindulási pontok, de sajnos minden esetben nem tudtuk ezeket beszerezni, így más növényi részeket voltunk kénytelenek használni. Ezért az előkísérleteink eredményei ezen hibákkal terheltek, de a későbbiek számára informatívak lehetnek (2. ábra).



**2. ábra.** A vizes és alkoholos kivonatok antioxidáns kapacitásai ( $\mu\text{MAS/L}$ ) és összes polifenoltartalmai ( $\mu\text{MGAS/L}$ ) (világos-vizes, fekete-alkoholos kivonat)

A vizes és alkoholos növényi kivonatok vizsgálata során szinte két nagy csoportra lehet osztani mind az antioxidáns kapacitás, mind a polifenolos komponensek eredményeit. Mindkét esetben a jobb eredményeket a hárs és a galagonya képezte, míg a második csoportba a somkóró és az édeskömény növényi kivonatok kerültek. Feltételezhető, hogy a forró vizes kioldás eredményesebb az antioxidáns kapacitás szempontjából, mint az alkoholos, vagyis nem biztos, hogy csak a polifenolos komponensek tehetők felelőssé ezen antioxidáns kapacitásért. A polifenolos komponensek vizsgálatakor a meglévő két csoport elkülönítése mellett megállapítható, hogy szinte mindegyik növény esetében nagyobb az alkohol által kivonható polifenolos vegyületek mennyisége.



Míg a mézek esetében egyik méznél sem mutatott statisztikailag szignifikánsan szoros kapcsolatot az összes polifenoltartalom és az antioxidáns kapacitás, addig ez a kivonatoknál igen szoros volt.

### Következtetések

Néhány különleges méz fizikai és kémiai paramétereinek vizsgálata során a vezetőképesség vizsgálatakor az egyes mézek között jelentős eltérések nem voltak kimutathatók. A kristályosodásra hajlamos hárs méz vezetőképessége a szabványban megengedett feletti értéket mutatott, míg a többi méz a szabványérték alatt szerepelt. A savtartalom vizsgálatánál az édesköménny savas íze az eredményekben is megjelent. Ahhoz, hogy a mézek antioxidáns kapacitását jobban tudjuk jellemezni, a polifenolos komponensek vizsgálata mellett célszerű más, a gyakorlatban elterjedt módszerekkel is megmérve is összehasonlítani az egyes mézeket. Meg kell jegyezni, hogy teljes biztonsággal ezek ismeretében sem tudunk egyértelmű választ kapni. Célszerű és kívánatos lenne a mézek alapját képező virágpollenek elemzése is hasonló paraméterek alapján, ami közelebb vihet az egyes mézek jobb megismeréséhez.

### Felhasznált irodalom

- [1] L.A. Boughediri, E.N. Arena, et al., 2011. Quality Evaluation of Some Honey from the Central Region of Algeria. *Jordan Journal of Biological Sciences* 4(4): 243-248.
- [2] M. Kashanijedat, M. Ramzi, et al., 2015. Modeling of rheological behavior of honey using genetic algorithm-artificial neural network and adaptive neuro-fuzzy inference system. *Food Bioscience* 9: 60-67
- [3] D. Weihs, I. Cohen, 2010. Rheology and microrheology of natural and reduced-calorie Israeli honeys as a model for high-viscosity Newtonian liquids. *Journal of Food Engineering* 100: 366-371.
- [4] P. Buera, B. Elizalde, 2007. Pattern of pH and electrical conductivity upon honey dilution as a complementary tool for discriminating geographical origin of honeys. *Food Chemistry* 101:695-703.
- [5] Czipa N. 2010. Különböző mézek összehasonlító vizsgálata és a gyártmánykialakítás hatása a minőségre. Debrecen. Doktori értekezés.
- [6] L. Bulacio, H. Lucero, et al., 2004. Effect of honey high-temperature short-time heating on parameters related to quality, crystallisation phenomena and fungal inhibition. *Lebensm.-Wiss. u.-Technol.* 37: 669-678.
- [7] M.T. Batista, P.B. Andrade, et al., 2001. Determination of sugar composition on Portuguese Heather honeys by HPLC/RI. Porto. Portugália.
- [8] A. Assia, L. Ali, 2015. Enzymes activities, hydroxymethylfurfural content and pollen spectrum of some Algerian honey. *African Journal of Agricultural Research*, 10(7): 613-622.
- [9], Szél Zs. 2006. A selyemkóróméz kémiai vizsgálata és összehasonlítása az akácmézzel. Budapest. Doktori értekezés.
- [10] J. Sanz, A.C. Soria, et al., 2008. Some aspects of dynamic headspace analysis of volatile components in honey. *Food Research International* 41: 838-848.
- [11] E. Anklam, 1998. A review of the analytical methods to determine the geographical and botanical origin of honey. *Food Chemistry*, 63(4): 549-562.
- [12] M.D. Cabezudo, I. Hermosin, 2003. Free amino acid composition and botanical origin of honey. *Food Chemistry* 83: 263-268.
- [13] A. Terrab, R.A. Recamales, et al., 2004. Characterisation of Spanish thyme honeys by their physicochemical characteristics and mineral contents. *Food Chemistry* 88: 537-542.

- [14] A. Panzanelli, M. Ciulu, et al., 2011. RP-HPLC determination of water-soluble vitamins in honey. *Talanta* 83: 924–929.
- [15] A. Salminen, N. Piippo, et al., 2015. Quercetin alleviates 4-hydroxynonenal-induced cytotoxicity and inflammation in ARPE-19 cells. *Exp Eye Res.* 132: 208-215.
- [16] Frank, R. 2006. *A csodálatos méz.* Cser Kiadó. Budapest.
- [17] V.L. Singleton J.A. Rossi 1965. Colorimetry of total phenolics with phosphomolybdic-phosphotungstic acid reagents. *Am. J. Enol Vitic* 16. 144-158.
- [18] I.F.F. Benzie, J.J. Strain, 1996. The ferric reducing ability of plasma (FRAP) as a measure of "antioxidant power": The FRAP assay. *Analytical Biochemistry*, (239): 70-76.

## Noise Measurements and Noise Distribution in the City of Szeged

Zsolt I. Benkő<sup>1\*</sup>

<sup>1</sup>Department of technology, University of Szeged, H-6725 Szeged, Boldogasszony sgt. 6,  
Hungary  
e-mail: bzs@jgypk.u-szeged.hu

### Abstract

Measurements were carried out on different picked points of Szeged to achieve a noise distribution of the city. Careful measurements were carried out to obtain the environmental noise load values caused by traffic. The noise distribution data were taken in 2012 and the measurements were repeated on the same locations in 2015, too.

### Introduction

Our most important senses are sight and hearing. Almost all the information is acquired through them. 83% percent of the information is taken through sight and 11% through the hearing. The modern era brought a lot of mechanization and automation. More and more people live in big, crowded cities. The current environment – comparing to the original, natural environment – is noisy. This noise can be even harmful to the hearing. It is necessary to check from time to time that our environment is still within the healthy limits.

The normal hearing ranges from 20 Hz frequency to 20000 Hz.[1]

The hearing is logarithmic. The industrial tools for noise measurements are based on sound pressure level and the data are given in decibel (dB).[2] The sound pressure level is given by Eq.1:

$$L_p = 20 \log_{10} \left( \frac{\Delta p}{p_0} \right) \text{ dB} \quad (1)$$

where  $\Delta p$  is the sound pressure fluctuation, and  $p_0$  is the reference pressure fluctuation value (audition threshold);  $p_0 = 20 \mu\text{Pa}$ .

Table 1 contains some common examples

L(SPL) (dB)	<i>phenomenon</i>
0	audition threshold; mosquito at 3 m
10	human breathing at 3 m
30	theatrical stillness
40	living area at night; stillness of nature
60	office
70	street traffic at 5 m
90	noise in factory
100	jackhammer at 1 m; disco inside
120	train horn at 10 m
130	pain threshold

**Table 1.** Sound pressure level examples

It is worth noting that 85 dB or higher sound pressure level over long-term exposure can cause hearing damage. The hearing damage is cumulative throughout the entire life.

The auditory sensation strongly depends on the frequency of the sound: at the same sound pressure level a 200 Hz sound feel much weaker than a 1000 Hz sound. The equal loudness curves are measured first by Harvey Fletcher and Wilden A. Munson in 1933. The measurements were repeated in the 2000-2003 period.[3][4][5]

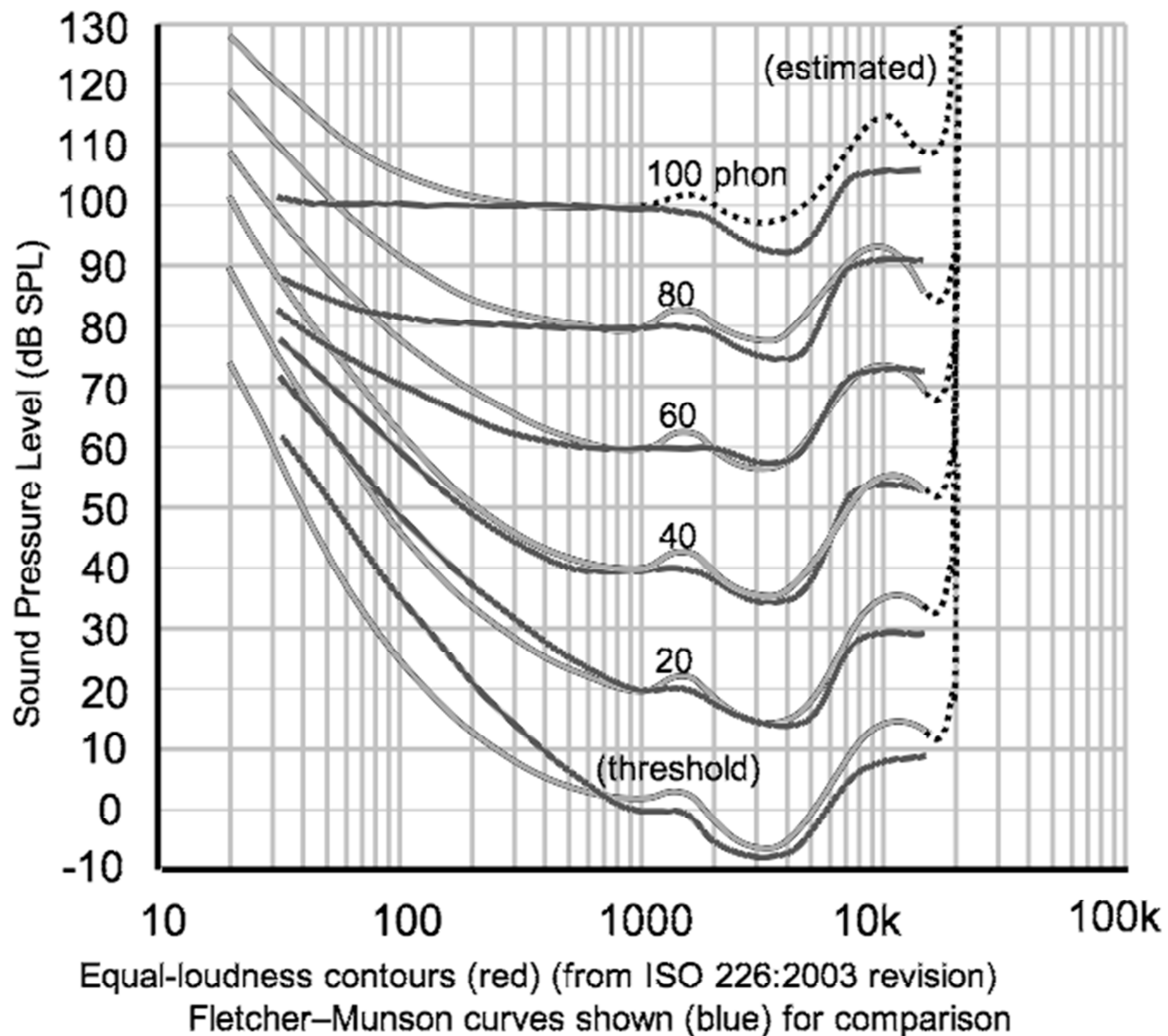


**Figure 1.** Fletcher-Munson curves (dark) and ISO226:2003 (light) [6]

The industrial noise meters use weighting curves to show similar responses to the human hearing. The A-weighting is used for auditory purposes. The C-weighting is almost flat; that can be used as the real physical sound pressure.[7]

Though +6 dB means twice the power, the human perception does not work this way. What is heard two times louder is +10 dB more.[8][9]

### Experimental

The noise level was measured in a school in the corridor in a break. It was in the range of 75-85 dB with using A-weighting and C-weighting as well. That means that the noise caused by children is at the most sensitive frequency of hearing. This value can lead to the teachers' loss of hearing.

The noises of different vehicles were measured from the pavement of a road by using A and C weighting as well. The much larger C values show that the vehicles have a big amount of low frequency emission, too.

vehicle	A-weighting (dB)	C-weighting (dB)
car	65-70	80-85
trolley/truck	70-75	85-90
tram	73-77	88-92
motorcycle	75-85	90-100

**Table 2.** Typical noise levels of vehicles

Different locations were chosen to achieve a noise distribution of the city of Szeged.

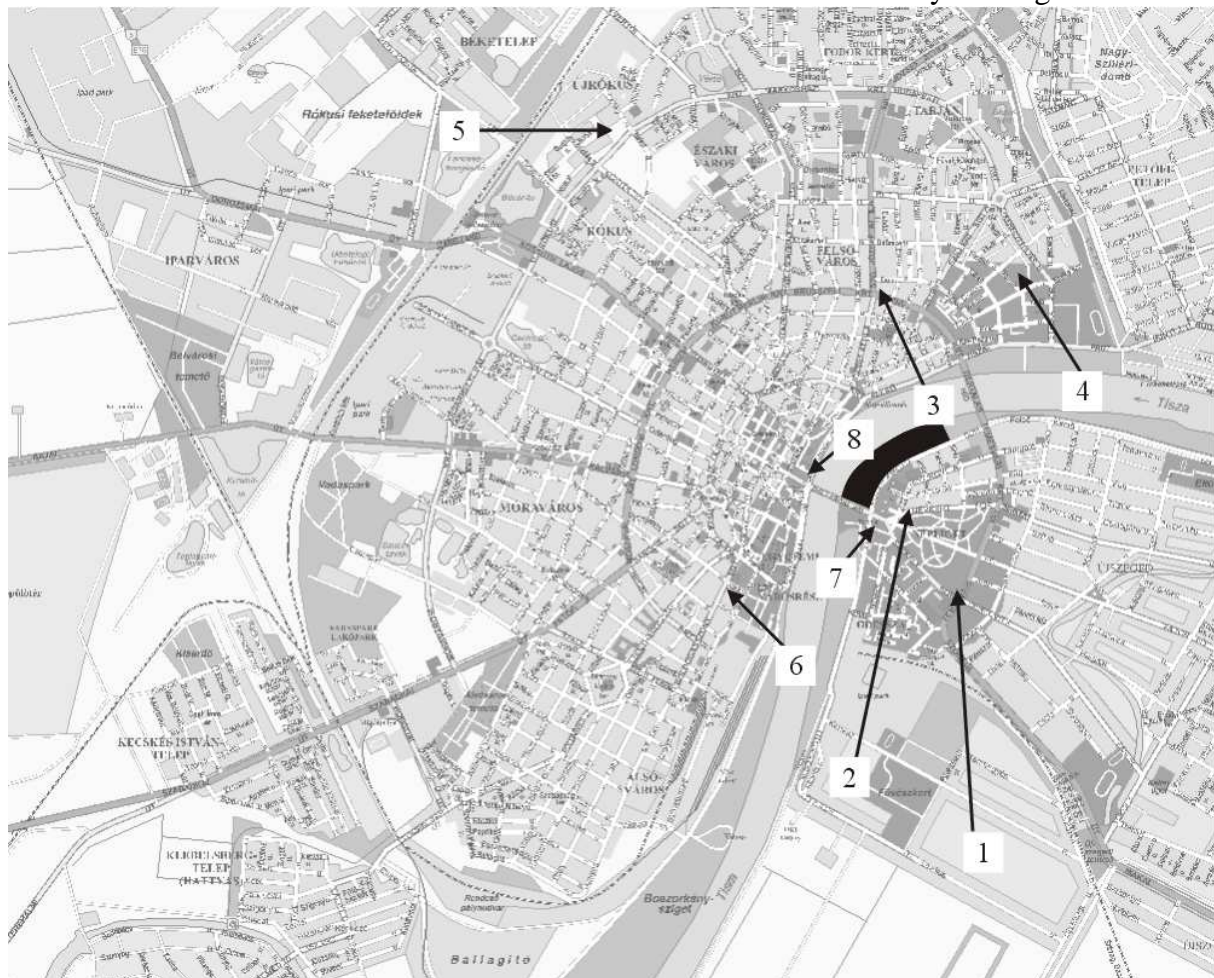


**Figure 2.** Locations of measuring in Szeged

number	location (GPS)
1	intersection of Székely sor and Temesvári krt. (46° 14.728' N ; 020° 09.842' E)
2	close to the bridge (46° 14.991' N ; 020° 09.605' E)
3	intersection of Római krt. and József Attila sgt. (46° 15.696' N ; 020° 09.479' E)
4	council block, Csaba u. 43 (46° 15.732' N ; 020° 10.116' E)
5	school at Rókusi krt. near Tesco (46° 16.253' N ; 020° 08.290' E)
6	school at Boldogasszony sgt. 8 (46° 14.759' N ; 020° 09.738' E)



7	parking area at the bridge (46° 14.933' N ; 020° 09.410' E)
8	museum garden (46° 15.124' N ; 020° 09.162' E)

## Results and discussion

The measured values are shown in the next table. The A-weighting curve was used.

<i>location</i>	<i>workday morning (7h-8h) dB</i>	<i>workday daytime (12h-15h) dB</i>	<i>workday evening (20h-22h) dB</i>	<i>Sunday daytime (9h-12h) dB</i>
1 (2012)	61.9 ± 5.2	55.5 ± 7.1	52.9 ± 6.8	54.9 ± 7.7
1 (2015)	64.6 ± 6.0	58.0 ± 8.0	52.2 ± 7.7	56.9 ± 8.0
2 (2012)	59.2 ± 7.3	57.4 ± 7.8	54.9 ± 8.1	54.4 ± 8.3
2 (2015)	60.7 ± 8.5	56.9 ± 9.9	55.6 ± 7.1	59.8 ± 9.2
3 (2012)	64.4 ± 3.4	63.4 ± 4.3	60.0 ± 4.9	61.1 ± 4.1
3 (2015)	67.5 ± 2.7	65.1 ± 4.0	60.1 ± 5.0	66.4 ± 6.3
4 (2012)	43.4 ± 2.1	50.0 ± 3.5	42.9 ± 2.9	41.6 ± 4.4
4 (2015)	44.6 ± 2.1	35.3 ± 2.7	42.1 ± 4.1	45.4 ± 3.0
5 (2012)	57.5 ± 2.9	49.3 ± 2.5	51.4 ± 3.2	50.3 ± 3.5
5 (2015)	52.1 ± 3.3	51.0 ± 3.3	49.0 ± 3.2	49.3 ± 3.6
6 (2012)	64.0 ± 3.4	59.6 ± 6.2	51.9 ± 8.3	57.9 ± 8.3
6 (2015)	62.9 ± 4.7	63.8 ± 4.6	60.2 ± 4.0	55.8 ± 9.1

**Table 3.** Noise levels at the picked locations

A measurement was carried out to check the noise levels of the Youth Days of Szeged (black area in the map) in 2012 and 2015, too. The samples were taken in the timeframe of 22h-24h.

<i>location</i>	<i>YDS in 2012 (dB)</i>	<i>YDS in 2015 (dB)</i>
1	54.2 ± 6.1	53.8 ± 7.2
2	59.0 ± 4.1	60.6 ± 4.4
7	59.7 ± 2.4	64.2 ± 2.3
8	64.9 ± 2.5	61.3 ± 2.3

**Table 4.** Noise levels around the area of the Youth Days of Szeged

The results show that Szeged has a quiet acoustical environment.

The Youth Days of Szeged kept the sound levels well within the legal limits.

The measurements do not show significant changes from 2012 to 2015. The acoustical load of traffic is quite acceptable in the city of Szeged and the city has a very good structure to present really quiet living areas.

## References

- [1] Tóth Dezső: Multimédia mikroszámítógépes környezetben, LSI Oktatóközpont, ISBN: 963 577 168 1, 54-55. o.
- [2] Thompson, A. and Taylor, B. N. sec 8.7, "Logarithmic quantities and units: level, neper, bel", Guide for the Use of the International System of Units (SI) 2008 Edition, NIST Special Publication 811, 2nd printing (November 2008)
- [3] Suzuki, Yôiti, et al. "Precise and full-range determination of two-dimensional equal loudness contours." Tohoku University, Japan (2003)
- [4] <http://www.mp3-tech.org/programmer/docs/IS-01Y-E.pdf>



- [5] ISO 226:2003
- [6] [http://en.flossmanuals.net/csound/ch008\\_c-intensities/\\_book/csound/static/Fletcher-Munson.png](http://en.flossmanuals.net/csound/ch008_c-intensities/_book/csound/static/Fletcher-Munson.png)
- [7] <http://en.wikipedia.org/wiki/A-weighting>
- [8] Stanley Smith Stevens: A scale for the measurement of the psychological magnitude: loudness. See: Psychological Review. 43, Nr. 5, APA Journals, 1936, pp. 405-416
- [9] <https://en.wikipedia.org/wiki/Sone>

## **Lipidomic Approach to Identify Patterns in Phospholipid Profiles in Atherosclerosis in ApoE Deficient Mice Infected with Chlamydia Pneumoniae**

**Nóra Kovács<sup>1</sup>, Ildikó Lantos<sup>2</sup>, Valéria Endrész<sup>2</sup>, Róbert Berkecz<sup>1</sup>**

<sup>1</sup> Department of Medical Chemistry, University of Szeged, H-6720, 8 Dóm tér, Szeged, Hungary, E-Mail: berkecz.robert@med.u-szeged.hu

<sup>2</sup> Department of Medical Microbiology and Immunobiology, University of Szeged, H-6720, 10 Dóm tér, Szeged, Hungary

Atherosclerosis is a sustained process in humans, therefore using animal models where more rapid changes helps for the study of this process. Apolipoprotein E knock out (apoE-KO) mice show impaired clearing of plasma lipoproteins and they develop atherosclerosis in a short time. Substantial evidence supports an association between atherosclerosis and infection with Chlamydia pneumoniae (CP).

Glycerophospholipids (PLs) as a major class of lipid. Changing of the level of PLs in tissue are associated with some disease such as Alzheimer's, Farber disease, Niemann-Pick disease, Gaucher disease. In addition the bioactive lysophospholipids and related sphingolipids (SM) contribute to the progression of different cancers.

According to chemical composition the main classes of PLs are the following, phosphatidylcholine (PC), phosphatidylethanolamine (PE), phosphatidylinositol (PI), phosphatidylserine (PS), phosphatidylglycerol (PG) and phosphatidic acid (PA) where the phosphate group is not derivatised.

Analysis of membrane PLs is challenging both in an identification and quantification point of view for analytical chemist because of the wide range distribution of PLs in tissues and the diverse behavior of different PL classes during the separation and detection process. Amphipathic property of PLs gives opportunity to use different LC techniques such as hydrophilic interaction chromatography (HILIC) as a novel chromatographic separation technique where the separation mechanism is based on variant polarity of head group of PLs.

The primary aim of this research is development of HILIC separation method and combining it with mass spectrometric measurement for qualitative and quantitative analysis of PLs from mouse plasma. The second goal is the application of the developed analytical method for PL profiling of plasma PLs in apoE knockout mice were infected with CP.

## Brain Phospholipid Profiling in a Mouse Model of Anxiety Disorder

**Róbert Berkecz<sup>1</sup>, Sára Zsigrai<sup>1</sup>, Viktor Szegedi<sup>2</sup>**

<sup>1</sup> *Department of Medical Chemistry, University of Szeged, H-6720, 8 Dóm tér, Szeged, Hungary, E-Mail: berkecz.robert@med.u-szeged.hu*

<sup>2</sup> *Institute of Biochemistry, Biological Research Center, Hungarian Academy of Sciences, H-6726, Temesvári krt. 62, Szeged, Hungary*

Nowadays lipidomics is a rapidly expanding research field thanks to the important biomolecular attributions of the lipids. Glycerophospholipids (PLs) are the major component of biological membranes and play a key role in a variety of biological processes including membrane trafficking and signal transduction.

Here we introduce an analytical method for comprehensive phospholipid (PL) analysis of biological samples using hydrophilic-interaction liquid chromatography coupled with electrospray ionization-mass spectrometry (LC-MS). Chromatographic and mass spectrometric parameters were optimized to enable a separation of main PL classes. The developed LC-MS method was applied for the characterization of mouse brain PLs, and resulted in the identification of PL species showing significant differences between in high anxiety-related behavioral phenotype (AX) and low anxiety-related behavioral phenotype (nAX) mouse model.

## Microbial Degradation of Hydrophobic Compounds under Various Environmental Conditions

Attila Bodor<sup>1,2\*</sup>, Krisztián Laczi<sup>1,2</sup>, Ágnes Kis<sup>2,3</sup>, Sándor Mészáros<sup>1</sup>, Nikolett Rácz<sup>1</sup>,  
Gábor Rákhely<sup>1,2,3</sup>, Katalin Perei<sup>1,2</sup>

<sup>1</sup>Department of Biotechnology, University of Szeged, H-6726 Szeged, Közép fasor 52, Hungary

<sup>2</sup>Institute of Environmental Sciences, University of Szeged, H-6726 Szeged, Közép fasor 52, Hungary

<sup>3</sup>Institute of Biophysics, Biological Research Centre, Hungarian Academy of Sciences, H-6726 Szeged, Temesvári krt. 62, Hungary  
e-mail: perei.katalin@brc.mta.hu

### Abstract

Human activities related to industry, agriculture and increasing human population have a great impact on the environment and easily lead to pollution jeopardizing natural habitats and ecosystems. Oil and its derivatives from inadequate disposal and accidental spills are among the most common pollutants. Microbial degradation of these hydrophobic, organic compounds is a topic currently generating a great number of studies in environmental protection. The aim of this study is the comparison of two *Rhodococcus* strains isolated from soil and aqueous phase regarding the biodegradation efficacy in various environmental niches: minimal media, salted water and potting soil. Being aware of the changes of enzymes activity affected by various environmental conditions, we will be able to apply the most adequate microbial strains in bioremediation processes.

### Introduction

Oil and oil-related pollutants from industrial activities and accidental spills are among the most recent environmental problems that humankind must cope with [1]. Biodegradation of hydrophobic compounds is in the focus of attention [2] and seems to be a very promising process. Applying bioremediation methods, various microorganisms and their microbial pathways can be exploited in environmental protection [3]. *Rhodococci*, which are ubiquitous, aerobic, Gram+ rods, belonging to the *Nocardiaceae* family of the order *Actinomycetales*, have the ability to utilize hydrocarbons as sole carbon and energy source [4].

### Experimental

Several bacterial strains were isolated in our laboratory from oil-contaminated soil and even from dead oil. One of them was identified as a *Rhodococcus* sp. MK1. This isolate was compared to a *Rhodococcus erythropolis* PR4 strain (NBRC 100887, NITE) regarding oil degradation efficiency. This strain was isolated from sea water [5] and its whole genome was sequenced.

Since one of the strains was originated in soil and the other one in aqueous phase, the degradation activity might depend on these environmental conditions. The degradation experiments were performed in various niches: minimal medium, artificial sea water and potting soil. Contamination was modelled with hexadecane that was used as a sole carbon and energy source. Respiration and hydrocarbon consumption were monitored, carbon and oxygen balance were determined to compare the bacterial strains to each other concerning the efficiency of oil biodegradation.

## Results and discussion

Based on the respiratory activity of bacterial cells, oxygen consumption in aqueous samples inoculated with *Rhodococcus erythropolis* PR4 was higher than those which were inoculated with *Rhodococcus sp.* MK1 (Figure 1.).

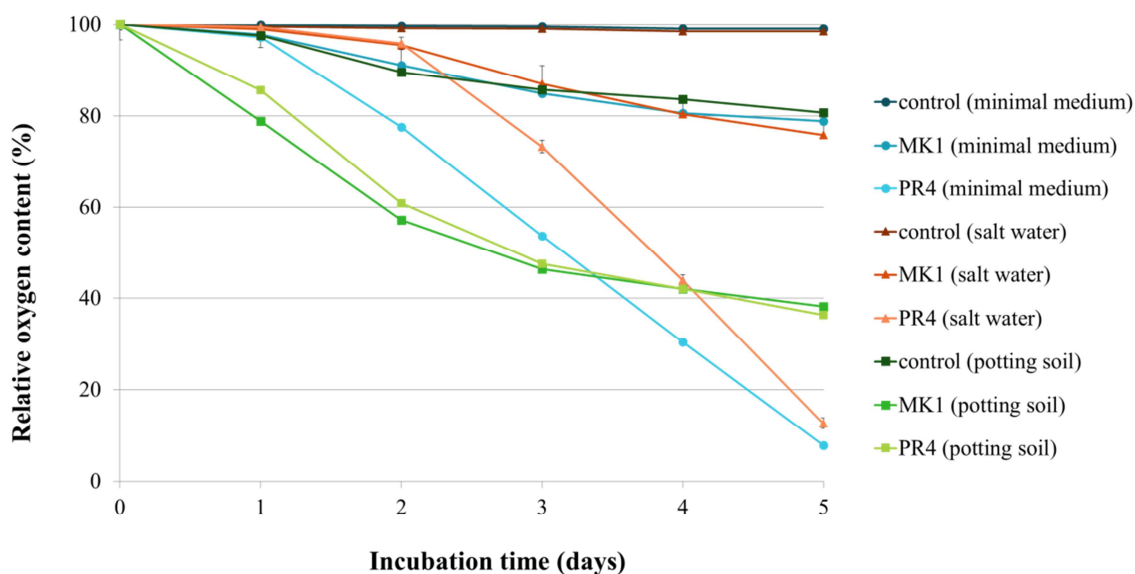


**Figure 1.** Changes in relative oxygen contents under variuos conditions

Biodegradation of hexadecane was most intensive in potting soil for both strains, but *Rhodococcus erythropolis* PR4 appeared to be more potent in water-based niches. The rate of hydrocarbon biodegradation showed a slight decrease under high salinity conditions compared to the activity in minimal medium (Figure 2).

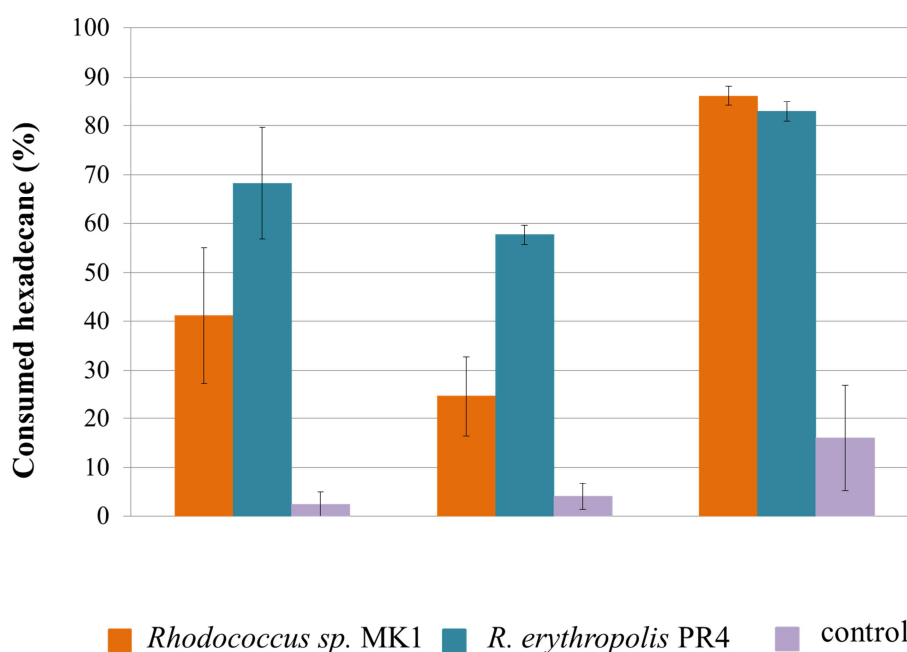


**Figure 2.** Consumed n-hexadecane in 5 days of incubation

During the hexadecane biodegradation process, hexadecane is converted by monooxygenases into hexadecanol, then into an aldehyde and further into a carboxylic acid. Carbon and oxygen balance can be estimated using the values of oxygen consumption, carbon dioxide production and hexadecane consumption. Based on these data, the results suggested that hexadecane was mainly utilized for biomass production (Figure 3).

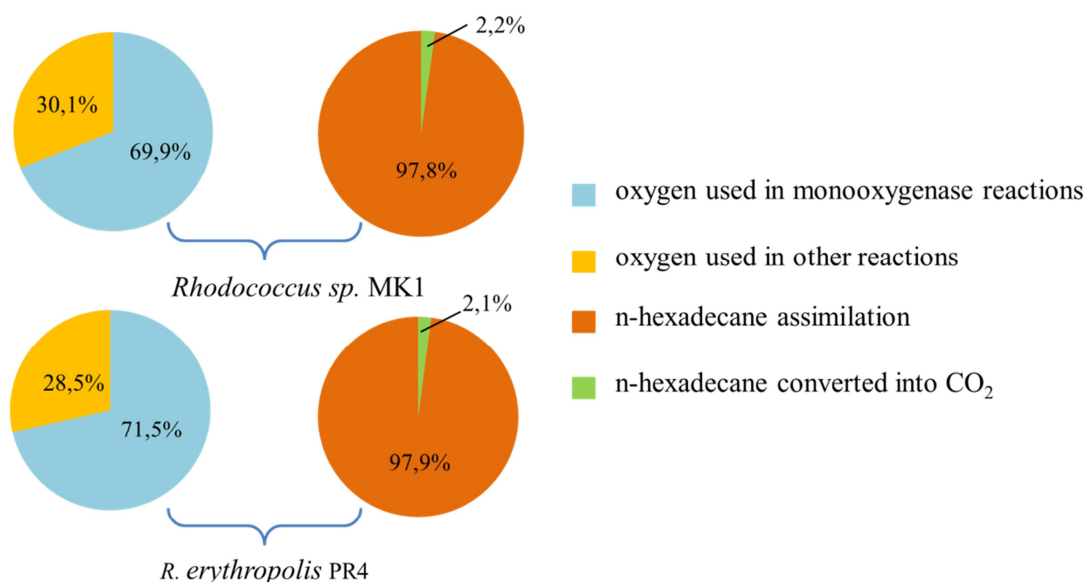


**Figure 3.** Carbon and oxygen balance of the hexadecane biodegradation in potting soil



## Conclusion

Our experiments demonstrate that both of the *Rhodococcus* strains are able to utilize hydrocarbons as sole energy source under various conditions that makes them effective microbial tools for environmental remediation processes like *in situ* bioremediation (even in sea water e.g. the Gulf of Mexico). Better performance in potting soil suggests the presence of biofilm on the surface of the soil particles which might have beneficial effect for bacterial cells.

## Acknowledgements

This research was realized in the frames of TÁMOP 4.2.4. A/2-11-1-2012-0001 „National Excellence Program – Elaborating and operating an inland student and researcher personal support system convergence program” The project was subsidized by the European Union and co-financed by the European Social Fund. The presentation is supported by the European Union and co-financed by the European Social Fund (grant agreement no. TÁMOP-4.1.1.C-12/1/KONV-2012-0012) and by the Norway Grant (grant agreement no. HU09-0044-A1-2013).

## References

- [1] Committee on the Effects of the *Deepwater Horizon* Mississippi Canyon-252 Oil Spill on Ecosystem Services in the Gulf of Mexico; Ocean Studies Board; Division on Earth and Life Studies; National Research Council, An Ecosystem Services Approach to Assessing the Impacts of the *Deepwater Horizon* Oil Spill in the Gulf of Mexico. The National Academies Press, Washington (DC), 2013. p. 3.
- [2] E.Z. Ron, E. Rosenberg, Curr. Opin. Biotechnol. (2014) 27:191-194
- [3] M. Vidali, Pure Appl. Chem. (2001) 73.7:1163-1172
- [4] C.C.C.R. de Carvalho, L.Y. Wick, H.J. Heipieper, Appl. Microbiol. Biotechnol. (2009) 82:311-320
- [5] H.M. Alvarez, Central Metabolism of Species of the Genus *Rhodococcus*. In: Biology of *Rhodococcus*. Springer Berlin Heidelberg, 2010. p. 91-108.

## Antibacterial Effects of Sour Cherry and Sea Buckthorn

Diána Furulyás<sup>1</sup>, Szabolcs Keszti<sup>2</sup>, Tekla Engelhardt<sup>2</sup>, Csilla Mohácsi-Farkas<sup>2</sup>, Éva Stefanovits-Bányai<sup>3</sup>, Hegedűs Attila<sup>4</sup>, Papp Nóra<sup>3</sup>, Mónika Stégerne-Máté<sup>1</sup>

<sup>1</sup>Department of Food Preservation, Corvinus University of Budapest, Faculty of food Science

<sup>2</sup>Department of Microbiology and Biotechnology, Corvinus University of Budapest, Faculty of food Science

<sup>3</sup>Department of Applied Chemistry, Corvinus University of Budapest, Faculty of food Science

<sup>4</sup>Department of Genetics and Plant Breeding, Corvinus University of Budapest, Faculty of Horticultural Science

e-mail: diana.furulyas@uni-corvinus.hu

### Abstract

The aim of the study is to examine the anti-microbial effect of those plant species, which, based on our previous results, significantly inhibit the growth of microorganisms.

The cultivars of the chosen sea buckthorn and sour cherry species, originated in Hungarian growing regions, and they are rich in polyphenolic and anthocyanin compounds. The antioxidant capacity was determined by FRAP (Ferric Reducing Ability of Plasma), total polyphenol content (TPC) and TEAC (Trolox Equivalent Antioxidant Capacity) assays.

In this study, antimicrobial effect was tested on the strains of two bacteria (*E. coli*, *S. aureus*). The degree of inhibition was measured by rapid methods: impedance technique (RABIT, Don Whitley Scientific Ltd., UK). The antimicrobial effect was compared with analytical results.

The results of our measurement show that due to the high antioxidant capacity of sea buckthorn; have higher antimicrobial effect against chosen bacteria. Anti-microbial efficiency of sour cherry was significantly less than effect of sea buckthorn, but it reached greatly inhibition of microorganisms. Further researches these fruits can serve as a raw material for new, natural origin, and effective antimicrobial agents in a food industry which can use as bio-preservatives.

### Bevezetés

A XXI. században a fogyasztók egyre inkább olyan termékeket keresnek, melyeket kevésbé szélsőséges kezelésekkel és hozzáadott adalékanyagoktól mentes technológiával állítanak elő. Ennek érdekében egyre több kutatás folyik természetes adalékanyagok kifejlesztésére [1; 3; 4; 5; 7; 11].

A homoktövis latin néven *Hippophae rhamnoides* L., az ezüsfafélék (*Elaeagnaceae*) családjába tartozik, felhasználása széles körben elterjedt magas C-vitamin, és antioxidáns tartalma miatt, de jelentős a karotinoidok és egyéb vitamin (B-, E-, F-), aminosav (cisztein, lecitin, fenilalanin), illetve mikroelem tartalma is. Használják gyógyászati, kozmetikai és étkezési célokra egyaránt [6].

A meggy (*Prunus cerasus* L.) a *Rosaceae* család, *Prunoideae* alcsaládjába tartozó gyümölcs, mely úgyszintén számos értékes komponenst tartalmaz, köztük polifenolokat, antocianint, vitaminokat és ásványi anyagokat [9; 12; 13]

A homoktövis bogyós terméséről már köztudott, hogy nagymértékű antimikrobás hatékonysággal rendelkezik, azonban a meggy terméséről már kevésbé elterjedt ez a tény. Míg a homoktövis savanykás, markáns íze miatt kevesebb élelmiszerhez adható hozzá a termék ízének befolyásolása nélkül, a meggy íze és kedveltségi szintje lehetővé teszi szélesebb körű felhasználását.

Célunk megvizsgálni, illetve összehasonlítani a homoktövis és a meggy termésének antimikrobás hatékonyságát és mindezt összevetni antioxidáns kapacitásuk mértékével.

### Anyagok és módszerek

A gyümölcsök (homoktövis - *Hippophae rhamnoides* L., meggy - *Prunus cerasus* L) mindegyike hazánk termőterületeiről származó nagy antioxidáns kapacitással rendelkező fajták, melyeket több, Magyarországon elterjedt fajta közül előzetes vizsgálatokat követően választottuk ki: a Jászapátiból származó "Pető1" homoktövist, „Pipacs 1” meggyet.

A termések mikroba gátló hatását kétféle mikroorganizmussal szemben vizsgáltuk: *Escherichia coli* (6739), *Staphylococcus aureus* (ATCC 6538), melyek a Budapesti Corvinus Egyetem Mikrobiológiai és Biotechnológiai Tanszékén fenntartott törzsek.

A vizsgálatokat megelőzően a gyümölcsöket azonos mintaelőkészítési módszernek vetettük alá. Gyümölcsök aprítását követően liofilizáltuk a mintákat, majd vizes extrakcióval 80mg/ml-es oldatokat készítettünk. A mintákat egy órán keresztül ultrahangos fürdőbe helyeztük, majd szűrővatta segítségével átszűrtük. A mintákon elvégzett vizsgálatok a következők voltak:

- **Vasredukálóképességen alapuló antioxidáns kapacitás** meghatározását (**FRAP**) Benzie és Strain [2] által kidolgozott módszerrel mértük. A minta antioxidáns kapacitását aszkorbinsav ekvivalensben határoztuk meg (mM AS/100g).
- **Összes polifenol tartalmat (TPC)** Singleton és Rossi [10] módszere alapján határoztuk meg. Az eredményeket mM galluszsav/100g mértékegységben kaptuk meg (mM GS/100 g).
- **Troloxra vonatkoztatott antioxidáns kapacitás (TEAC)** meghatározását Miller és munkatársainak [8] módszere alapján végeztük el. (mM trolox ekvivalens /L mértékegységben megadva, mM TS/L)
- **Antimikrobás mérés:** A Budapesti Corvinus Egyetem Mikrobiológiai és Biotechnológiai Tanszékén elhelyezett RABIT (Rapid Automated Bacterial Impedance Technique) műszer impedancia mérésén alapuló technológia, mely a mikroorganizmusok szaporodása által bekövetkezett ellenállás- vagy vezetőképesség változását detektálja. A mérésekhez steril, elektródákkal ellátott RABIT-csővekbe 2-2 ml Don Whitley táplevest adagoltunk, melybe 700 µl baktérium szuszpenziót és 300 µl gyümölcs extraktumot tartalmazó minta került. A méréseknél pozitív kontrollként csak táplevest és baktérium szuszpenziót tartalmazó, negatív kontrollként pedig csak táplevest tartalmazó mintát alkalmaztunk. A mérési időintervallum 24 óra volt, a mintamérés 6 percenként automatikusan történt. Az inkubálási hőmérséklet 37°C volt. A kiértékelést a vezetőképességi görbékről leolvasható detekciós időkkal (TTD), illetve a görbék alatti területek (TE) segítségével elemeztük. Az integrálszámításokat R-project 3.2.1 programmal számítottuk.

### Eredmények és értékelés

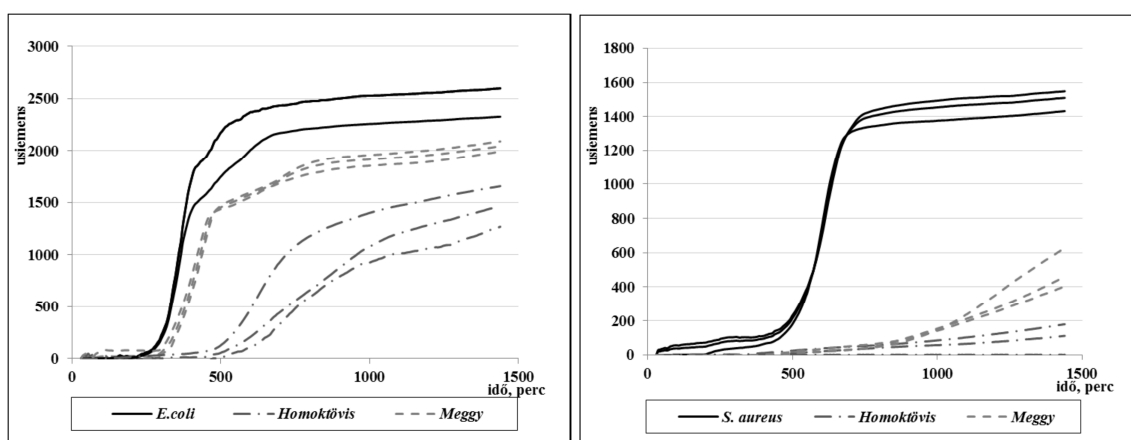
Az antioxidáns kapacitás (AOC) eredményeinek átlagértékeit az 1. táblázatban foglaltuk össze. A homoktövis vasredukálóképességen alapuló antioxidáns kapacitása (FRAP) nagyobb, mint tízszerese a meggy mintának. Az összes polifenol tartalomnál ez az arány már kisebb, de még mindig szignifikáns mértékű. A legkisebb eltérést a troloxra vonatkoztatott antioxidáns kapacitásnál mértük, de még itt is közel kétszerese a homoktövis AOC értéke a meggy mintának.

	FRAP mM AS/L	TPC mM GS/L	TEAC mM trolox ekvivalens/L
<b>Homoktövis</b>	242,37	305,81	130,89
<b>Meggy</b>	21,54	40,59	66,13

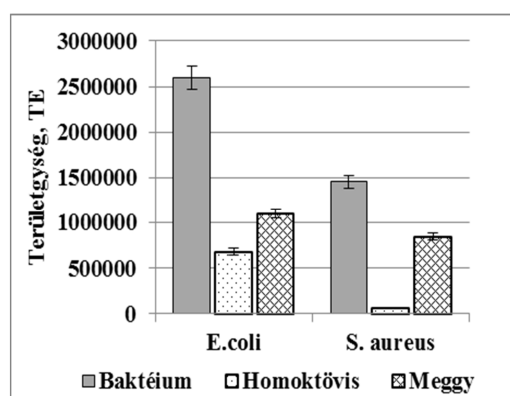
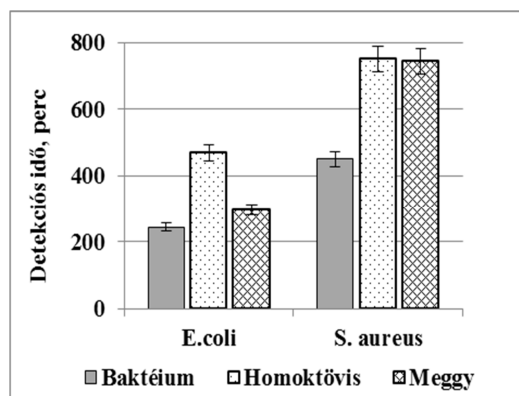
**1. táblázat:** Antioxidáns mérések átlageredményei mM/L-ben

Az antimikrobás mérések során kapott vezetőképességi görbéket az idő függvényében ábrázoltuk (1. ábra), ahol a pozitív kontrollként alkalmazott, csak baktérium szuszpenziót tartalmazó minták (—), a homoktövis hozzáadásával készült minták (— • — • —), valamint a meggy hozzáadásával készült minták (- - - -) vezetőképességi görbáját láthatjuk. A görbe kezdeti (lag) szakasza a baktériumok adott körülményekhez való adaptációját jelzi, majd ezt követi a hirtelen emelkedő exponenciális szakasz, ahol a mikroba szaporodása eléri a maximális sebességét. Ennek kezdeti pontja adja meg a detekciós időt (TTD). A görbe harmadik szakasza a stacioner fázis, ahol a mikroorganizmus szaporodási sebessége állandósul.

Az 1. ábrán megfigyelhető, hogy a baktériumok szaporodása közben bekövetkező elektromos vezetőképesség legnagyobb mértékű csökkenését a homoktövis minta hozzáadásával értük el. Azonban a meggy is jelentős gátlást mutatott. Mindkét növény esetében a *S.aureus* baktériummal szemben erősebb tendenciát mutat a jelcsökkenés mértéke.



**1. ábra:** RABIT műszer által detektált vezetőképességi görbék



**2. ábra:** Vezetőképeségi görbék detekciós idejének átlagértékei (perc)

**3. ábra** Vezetőképeségi görbék alatti területek átlagértékei (TE)

A 2. ábra a görbék detekciós idejének átlagértékeit jeleníti meg. A detekciós idő fordítottan arányos a baktérium szaporodásának mértékével. Mindkét gyümölcsextraktum hozzáadása szignifikánsan növelte a detekciós időket.

A 3. ábrán mutatjuk be a vezetőképeségi görbék területességét, amely egyenesen arányos a baktériumok sejtszámával. Itt is az látszódik, hogy a homoktövis a meggyénél nagyobb mértékben gátolta a baktériumok szaporodását.

**Következtetés**

Az antimikrobás mérési eredmények azt mutatták, hogy a minták jelentős mértékű gátlást fejtettek ki mindkét mikroorganizmussal szemben. A homoktövis mindkét baktérium esetében nagyobb mértékű szaporodásgátlást ért el, mint a meggy minta. A *S.aureus* törzzsel szemben erősebb gátlást tapasztaltunk mindkét gyümölcs hozzáadása esetében.

Az analitikai eredményeket összevetve az impedimetriás gyorsmódszerrel mért eredményekkel egyértelmű korreláció mutatkozik az antioxidáns kapacitás és az antimikrobás hatás között. A homoktövis nagyobb mértékű antioxidáns kapacitásának következtében lényegesen erősebb szaporodás gátlást tudott elérni a mikroorganizmusoknál, azonban a meggy antimikrobás hatása is jelentős, így javasolható az élelmiszeriparban természetes tartósítószerként történő felhasználásának további vizsgálata.

**Köszönetnyilvánítás**

Köszönettel tartozom az OTKA K84290 támogatásáért.

**Irodalomjegyzék**

- [1] R. Arora, S. Mundra, A. Yadav, R.B. Srivastava, T. Stodban, Antimicrobial activity of seed, pomace and leaf extracts of sea buckthorn (*Hippophae rhamnoides* L.) against foodborne and food spoilage pathogens, African Journal of Biotechnology (2012) 11(45):10424-10430.
- [2] Benzie, I.I.F., Strain, J.J. 1966. The ferric reducing ability of plasma (FRAP) as a measuring of "antioxidant power": The FRAP assay. Analytical Biochemistry 239, 70-76.
- [3] G.W. Gould, Overview, In New Methods of Food Preservation. Blackie Academic & Professional (1995) Glasgow, XV-XIX
- [4] G.W. Gould, Industry perspectives on the use of natural antimicrobials and inhibitors for food applications, Journal of Food Protection (1996) 82–86.
- [5] A. Hegedűs, A csonthéjas gyümölcsök antioxidáns hatásában megnyilvánuló genetikai variabilitás jellemzése, Doktori (Ph.D) értekezés, Budapesti Corvinus Egyetem (2013) Budapest
- [6] L. Hornok (szerk), Gyógynövények termesztése és feldolgozása. Második átdolgozott kiadás, Budapest, Mezőgazdasági Kiadó (1990) 161-164.
- [7] T.E. Michel, G. Destandaua, F. Le, M.E. Lucchesi, C. Elfakir, Antimicrobial, antioxidant and phytochemical investigations of sea buckthorn (*Hippophaë rhamnoides* L.) leaf, stem, root and seed. Food Chemistry, (2012) 131(3):754-760.
- [8] Miller, N.J., Rice-evans, C., Davies, M.J., Gopinathan, V., Milner, A. 1993. A novel method for measuring antioxidant capacity and its application to monitoring the antioxidant status in premature neonates, Clinical Science, 84, 407-412.
- [9] N. Papp, B. Szilvássy, Z. Szabó, J. Nyéki, É. Stefanovits-Bányai, A. Hegedűs, Antioxidant capacity, total phenolics and mineral element contents in fruits of Hungarian sour cherry cultivars, International Journal of Horticultural Science (2008) 14 (1–2):59–64.

- [10] Singleton, V.L., Rossi, J.A., 1965. Colorimetry of total phenolics with phosphomolybdic-phosphotungstic acid reagents. *American Journal of Enology and Viticulture*, 16, 144–158.
- [11] G. Tarnavölgyi, Az élelmiszeradalékanyagok szakmai és fogyasztói megítélése. Kaposvári Egyetem, Doktori (Ph.D) értekezés (2008) Kaposvár
- [12] Zs. Veres, M. G. Fári Antioxidánsok a mezőgazdaságban. Debreceni Egyetem, Agrártudományi közlemények (2004) 195–200.
- [13] Zs. Veres, I. Holb, J. Nyéki, Z. Szabó, M. G. Fári, Total anthocyanine content and antioxidant density of some Hungarian sour cherry varieties. *International Journal of Horticultural Science* (2005) 11 (2):109–113.



## Possibilities of Complex Food-Processing of Quince

Diána Furulyás<sup>1</sup>, Orsolya Nagy<sup>1</sup>, Nóra Papp<sup>2</sup>, Éva Stefanovits-Bányai<sup>2</sup>, Mónika Stéger-Máté<sup>1</sup>

<sup>1</sup>Department of Food Preservation, Corvinus University of Budapest, H-1118 Budapest, Villányi Street 29-43, Hungary

<sup>2</sup>Department of Applied Chemistry, Corvinus University of Budapest, H-1118 Budapest, Villányi Street 29-43, Hungary  
e-mail: diana.furulyas@uni-corvinus.hu

### Abstract

The food industry generate large amount of such by-products, which may also contain unused, valuable components. In this research the possibilities of complex food industry usability were investigated for three species of quince (*Cydonia oblonga* Mill.) (“Angersi, Bereczki, Konstantinápolyi”). The nutritional characteristics of quince skin, pulp and ovary were compared. We measured the nutritional properties: dry matter content, pectin and acid content, polyphenol and flavonoid content. Moreover the rheological properties were investigated. The results were analyzed with statistics method.

The results of dry content are not significant, but between samples of quince parts the pectin and acid content have significant difference. It was largest amount of polyphenol in the pulp of quince, and the most of flavonoid content were measured in the skin of quince. Concluding from the rheological properties ‘Angersi’ species are suggested to use as jam, quince jelly or natural texturing, while ‘Konstantinápolyi’ species are recommended to use for the production of fiber juices or syrups. Because of their high pectin content, the skin and ovary suitable to use as production of pectin or natural texturing. Due to high antioxidant capacity of skin and ovary may use at manufacture of natural antimicrobial agents, dietary supplements or functional food.

### Bevezetés

A birsalma (*Cydonia oblonga* Mill.) táplálkozás élettani szempontból kiemelkedik a többi gyümölcs közül, alacsony zsírtartalma, és gazdag ásványi anyag, cukor, rost és szerves savtartalmának köszönhetően. Egészségvédő hatása, magas antioxidáns kapacitásával köthető össze. Mindemelllett, gyulladáscsökkentő, antikarcinogén, antimikrobiális és antiallergén tulajdonságaik révén átfogó védelmet nyújtanak a humán szervezetnek [1; 2; 3; 8; 10; 12; 6].

Az almástermésűekben, köztük a birsalmában is, az értékes komponensek eltérő mennyiségben vannak jelen a gyümölcsök különböző részeiben. Főként a héj, a magház és a velő részekre vonatkozóan. A gyümölcsvelő egy natúr félkésztermék, ami a gyümölcshúst áttört, pépes formában tartalmazza, mag- és héjmentesen. A gyümölcs nem ehető részeinek eltávolításával, valamint gyümölcshús passzírozással és homogenizálással állítják elő. Ezt nem önmagában, de számos gyümölcskészítmény alapanyagaként hasznosítják, valamint különböző élelmiszeripari termék fontos alkotójaként is felhasználják [5]. A birsalma savas ízének és kemény állományának köszönhetően nyersen ritkán fogyasztják. A gyümölcsvelő főként lekvár, birsalmasajt, befőtt, szörp, illetve szeszesital gyártásának alapanyagaként szolgál, azonban a birsalma termésének héj és magház része is tartalmaz értékes komponenseket, melyeket az iparban nem hasznosítanak [3; 7; 9].

Tanulmányunk célja, megvizsgálni három különböző birsalmafajtának élelmiszeripari szempontból jelentős beltartalmi paramétereinek eloszlását a gyümölcs különböző (héj, velő,

magház) részeiben.

### Anyagok és módszerek

A mérések során három különböző fajtájú, Magyarországon termesztett birsalma komplex élelmiszeripari feldolgozási lehetőségeit vizsgáltuk („Angersi, Bereczki, Konstantinápolyi”). Kutatásunk a termések beltartalmi jellemzőire irányultak, melyek befolyásolják a termék élelmiszeripari felhasználását.

A mintaelőkészítés az összes mintánál azonos módon történt. Minden termés esetében mosás, hámozás és darabolást követően elkülönítettük a héjat, a velőt és a magházat, majd 75°C-on hőkezeltük és 90 másodpercig botmixer segítségével daráltuk. A vizsgált paraméterek a következők voltak:

- A **vízoldható szárazanyagtartalom** (refrakció%) meghatározását a Codex Alimentarius 558/93 előírásai alapján, ATAGO DBX-55 típusú digitális refraktométerrel végeztük.
- A **pektintartalom** meghatározását Kyriakidis és Psoma [4] módszerének megfelelően, kénsavas-karbazolos kinyerést követően az abszorbanciát 525 nm-en mértük.
- Az **összes savtartalmat** lúgos titrálással, az MSZ 3619-1983 szabványának megfelelően határoztuk meg. Az összes savtartalmat citromsavban kifejezve adtuk meg.
- A **polifenol tartalom** (TPC) meghatározása Singleton és Rossi módszerével [11] történt. Az eredményeket mg/kg friss mintára vonatkoztatva adtuk meg.
- Az **összes flavonoid** (TPC) tartalom mérését Woisky és Salatino [13] módszere alapján végeztük. Az eredményt mg/ml adtuk meg.
- **Reológiai mérést** Physica MCR 51, Anton-Paar reométerrel, BM12 QC mérőrendszerrel végeztük. A minták folyásgörbéjét szobahőmérsékleten (20°C), 0,3-70 1/sec-os tartományban növekvő deformációsebesség mellett vettük fel. Kiértékeléshez Rheoplus v32 szoftvert használtunk. Az adatokra Herschel-Bulkley modellt illesztettünk. A folyáshatár ismeretével meghatározhatóvá vált, milyen élelmiszeripari célra javasolt felhasználni az adott birsalmafajtákat.

A mérések alkalmával minden esetben három párhuzamos mérést végeztünk. Az eredményeket IBM SPSS Statistics szoftver segítségével, több szempontos varianciaanalízissel elemeztük.

### Eredmények és értékelés

Az analitikai mérési eredmények átlagértékeit az 1. táblázat tartalmazza.

	Szárazanyag	Pektin	Savtartalom	Polifenol	Flavonoid
	Ref. (%)	g/100g	(m/m) %	mg/kg	mg/ml
„Angersi” héj	14,5	0,43	0,34	158,9	0,07
„Angersi” velő	14,8	0,33	0,61	162,7	0,036
„Angersi” magház	16,2	0,44	0,39	242,9	0,04
„Bereczki” héj	15,8	0,39	0,51	37,7	0,05
„Bereczki” velő	13	0,41	0,52	71,7	0,022
„Bereczki” magház	14,9	0,52	0,5	205,1	0,026
„Konstantinápolyi” héj	14,6	0,44	0,29	86,5	0,059
„Konstantinápolyi” velő	13	0,38	0,35	109,9	0,029
„Konstantinápolyi” magház	14,7	0,42	0,33	124,3	0,032

1. táblázat Beltartalmi jellemzők mérési átlageredményeinek összefoglalása

A vízoldható szárazanyag tartalom mérési eredményeinél a birs fajták között elhanyagolható

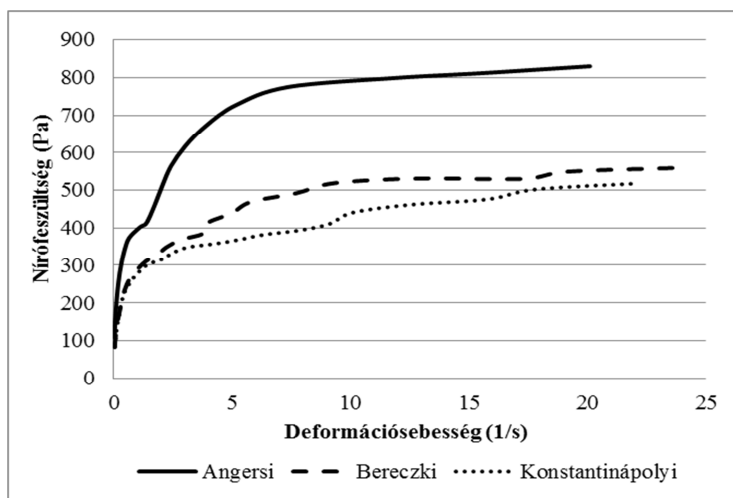
mértékű volt az eltérés. A legnagyobb szárazanyag tartalommal az „Angersi” minta magháza (16,2%) rendelkezett, a legalacsonyabb szárazanyag tartalmat pedig a „Bereczki” és a „Konstantinápolyi” birselő (13,0%) tartalmazta.

A pektintartalom mérési eredményi azt mutatták, hogy a birsfajták magháza rendelkezik a legnagyobb pektintartalommal, ezt követi a héjhoz tartozó értékek, végül a legalacsonyabb pektin tartalmat a gyümölcsök húzában mértük. A fajták közül szignifikánsan kiemelkedő pektin tartalommal a „Bereczki” fajta rendelkezett, ezt követte a „Konstantinápolyi”, végül az „Angersi”.

A legnagyobb savtartalommal minden fajta esetében a gyümölcselő rendelkezett. A birs fajták tekintetében pedig a legnagyobb savtartalmat a „Bereczki” mintánál mértünk, ahol a savtartalom a birs minden részében meghaladta a 0,5 %-ot (m/m).

A birs minták összes polifenol tartalma 37,7 mg/kg és 242 mg/kg között változott. Mindegyik fajtánál szignifikáns mértékben a magház tartalmazta a legtöbb polifenolt, míg a legalacsonyabb értéket a birs fajták héjában mértük. A legmagasabb polifenol mennyiséget az „Angersi” fajtánál tapasztaltuk. A „Bereczki” birsfajta a minták közül a legkevesebb polifenol tartalommal rendelkezett.

A flavonoid tartalom vizsgálatánál a minták esetében 0,022 mg/ml és 0,07 mg/ml közötti értékeket mértünk. A polifenollal ellentétben, a legmagasabb flavonoid tartalmat a birs minták héja tartalmazta, ezt a magház értékek követték, majd a legkisebb eredményt a gyümölcselőlől készült mintákban mértük.



1. ábra Birsalma minták folyásgörbéje

A minták nyírófeszültség görbéjének felvétele, és folyáshatárának meghatározása megmutatja mekkora nyírófeszültség hatására kezd az anyag folyni. Az „Angersi” birs folyáshatár értéke a legmagasabb (528,69 Pa). A „Bereczki” (262,64Pa) és a „Konstantinápolyi” (394,22 Pa) mintánál pedig a mért értékek szignifikánsan nem tértek el egymástól.

## Következtetés

A reológiai eredményekből látszik, hogy a legnagyobb folyáshatárral bíró „Angersi” velő elsősorban lekvárok, birsalmasajtók, valamint magas pektintartalmának köszönhetően természetes állománykialakítóként javasolt felhasználni. Ezzel ellentétben a „Konstantinápolyi” birsfajtából gyártott velő rostos levek, vagy szörpök gyártásához lehetne

ideális.

A nagyobb pektintartalommal rendelkező héj és magház az élelmiszeriparban a préselési, passzírozási folyamat melléktermékeként keletkezik, további felhasználása javasolt pektingyártásra, vagy szárított törköly formájában természetes állománykialakítónak.

A birsalma egyes részeinek magas polifenol, illetve flavonoid tartalma miatt, alkalmasak természetes antimikrobás anyagok kinyerésére, étrend kiegészítők gyártására, valamint funkcionális termékek előállítására. A birsalma törköly további felhasználása egyben csökkentené a birsalma feldolgozás következtében keletkezett melléktermékek mennyiségét.

### Köszönetnyilvánítás

Köszönettel tartozunk az OTKA K84290 támogatásáért.

### Irodaljegyzék

- [1] A. Borhidi, A zárwatermők fejlődéstörténeti rendszertana. Nemzeti Tankönyvkiadó, Budapest, 1998
- [2] Y. Hamauzu, T. Inno, C. Kume, M. Irie, K. Hiramatsu, Antioxidant and antiulcerative properties of phenolics from Chinese quince, quince, and apple fruits. J. Agric. Food Chem. (2006) 54, 765–772.
- [3] S. Fattouch, P. Caboni, V. Coroneo, C. Tuberoso, A. Angioni, S. Dessi, N. Marzouki, P. Cabras, Antimicrobial activity of Tunisian quince (*Cydonia oblonga* Miller) pulp and peel polyphenolic extracts. J. Agric. Food Chem. (2007) 55, 963–969
- [4] N. B. Kyriakidis, E. Posma Hydrocolloid interferences in the determination of pectin by the carbazol method, Journal of AOAC International, (2001) 84:1947-1949.
- [5] J. Ott, Aszeptikus technológia, Kertészeti és Élelmiszeripari Egyetem, Budapest, 1990
- [6] J. Podani, A szárazföldi növények evolúciója és rendszertana Vezérvonal egy nem is olyan könnyű tárgy tanulásához, ELTE Eötvös Kiadó, Budapest, 2007
- [7] I. Rodríguez-Guisado, F. Hernández, P. Melgarejo, P. Legua, R. Martínez, J.J. Martínez Chemical, morphological and organoleptical characterisation of five Spanish quince tree clones (*Cydonia oblonga* Miller). Sci. Hortic. (2009) 122, 491–496
- [8] F. Shinomiya, Y. Hamauzu, T. Kawahara, Anti-allergic effect of a hot extract of quince (*Cydonia oblonga*). Biosci. Biotechnol. Biochem. (2009) 73, 1773–1778.
- [9] B.M. Silva, P.B. Andrade, C.R. Martins, M.R. Seabra, A.M. Ferreira Principal component analysis as tool of characterization of quince (*Cydonia oblonga* Miller) jam, Elsevier Ltd., Porto (2004)
- [10] T. Simon, A magyarországi edényes flóra határozója. Harasztok-virágos növények, Nemzeti Tankönyvkiadó, 1992
- [11] V.L. Singleton, J.A. Rossi, Colorimetry of total phenolics with phosphomolibdicphosphotungstic acid reagents. Am. J. Enol. Viticult., (1965) 161: pp. 144-158.
- [12] T.G. Tutin, V.H. Valentine, S.m. Walters, D.A. Webb Flora Europea. II. kötet Rosaceae to Umbelliferae. Nyolcadik kiadás, Cambridge University Press, Cambridge, USA, 2001
- [13] R.G. Woisky, A. Salatino, Analysis of propolis: some parameters and procedures for chemical quality control. Journal of agricultural research. vol. (1998) 37, pp. 99-105

## The Environmental and Biological Risks of Extreme Low Doses of Chlorobenzenes

Ibolya Budai<sup>1,2</sup>, Dóra Hopenthaler<sup>1,2</sup>, Zsolt Molnár<sup>1</sup>, Marianna Radács<sup>1</sup>, Márta Gálfi<sup>1</sup>

<sup>1</sup>*Institute of Applied Natural Science, Faculty of Education, University of Szeged Hungary  
Department of Environmental Biology and Education, Juhász Gyula Faculty of Education,  
University of Szeged*

<sup>2</sup>*Faculty of Science and Informatics, University of Szeged*

*e-mail: ibolya29budai@gmail.com*

### Abstract

Several environmental chemicals and pesticides have been found to alter neuroendocrine communication and behaviour in exposed biological systems. The aim of this study was to demonstrate the effects of the ubiquitous chlorobenzenes on the behavioural elements of Wistar rats. For this reason rats (n=50 in each group) were treated with a mixture of 0.1 and 1.0 µg/kg each of hexachlorobenzene and 1,2,4-trichlorobenzene via a gastric tube for 30, 60 and 90 days. At the endpoints of the experiment the behavioural elements of rats were detected and tissue samples were taken for chlorobenzene analysis in gas-chromatography. It was found that the anxiety-related behavioural elements were altered and chlorobenzenes were present in different tissues.

### Introduction

Persistent interaction evolves among living creatures and their environment, this connection maintains the equilibrium of the biotic and abiotic systems. Results were born with the activity of mankind, which have altered the local environments of the territories of Earth. The procedure was induced by the applied chemicals and the purposes of their use, basic biological and ecological problems of chemical application in agriculture and horticulture, namely by the chemisation. These chemicals are xenobiotics. One group of special interest is the persistent organic pollutants (POPs). One group of the heterogeneous POPs can interfere with the endocrine communication that called endocrine disruptor agents (EDCs). EDCs are proved to have an effect on homeostasis and/or its regulation [1] [2]. The toxicity of POPs results their hazardous nature, in combination with high chemical and biological stability, and a high degree of lipophilicity. Various benzene derivatives such as alkylbenzenes and chlorobenzenes, however, continue to be used as chemical intermediates, solvents, pesticides in spite of incomplete knowledge of their chronic toxicity. Several of the chlorinated benzenes are known to be porphyrogenic, carcinogenic, mutagenic in animals and humans, in rats anxiety, aggression [3] [4] and in fish predator avoidance and social behaviours are developed [5] by EDCs.

EDCs can affect sexual and reproductive behaviours. For example exposed female mosquitofish displayed male reproductive behaviour and males showed more aggressive courtship behaviour [6] [7]. Sexual and reproductive behaviour of birds and mammals were also altered by the exposition of POPs. Porter et al. [8] indicated that adult male mice exposed to a mixture of aldicarb, atrazine showed significantly more aggressive behaviour compared to the control groups.

Our aim was to present contemporary research in connection with the complex environmental strains and their effects on the equilibrium process of living organisms. We also wanted to demonstrate the effects of chronic exposure to extremely low (legally often negligible) doses

of a chlorobenzene mixture on the behavior of male Wistar rats and to investigate the organic accumulation of chlorobenzenes in rats.

### Experimental

Adult Wistar male rats were (weighing 120-250 g, aged 4-6 weeks at the beginning of the research,  $n=50$ ) exposed daily with a mixture of 0.1 (D1) and 1.0 (D2)  $\mu\text{g/kg}$  each of hexachlorobenzene and 1,2,4-trichlorobenzene via a gastric tube for 30, 60 and 90 days. After ClB treatment, aggression/anxiety-related behavioral elements were detected in open field and elevated plus maze tests. The animal care and research protocols were in full accordance with the guidelines of University of Szeged, Hungary. During the research period, rats were kept under controlled parameters. Control groups were set up: stress control ( $n=50$ , gastrostomy tube insertion group) and absolute control ( $n=50$ , untreated group). To compare the means of treatment doses (0.1 and 1.0  $\mu\text{g/b.w. kg}$ ) to the controls during 30, 60 and 90 days long treatments two-way ANOVA were run.

At the end of the experiment certain tissues (endocrine, immune, neuronal and reproductive) were removed for chlorobenzene analysis. After the specific extraction the ClB levels were measured by gas-chromatography (Hewlett-Pacard 5890 Series II. gas-chromatograph).

### Results and discussion

Our experiments revealed statistical differences between treated and untreated groups. As shown in Figure 1. after ClB treatment the anxiety related-behavioural elements altered significantly depending on the dose and the duration of exposure. In Figure 2 anxiety-related elements, the total distance moved and the mean velocity of the movement were decreased in open-field tests following 30, 60 or 90-day ClB treatment.

**Figure 1.** Anxiety related behaviour measured in elevated plus maze test after ClB treatment (means  $\pm$  S.E.M., A:  $p < 0.001$ ,  $n=50$ )

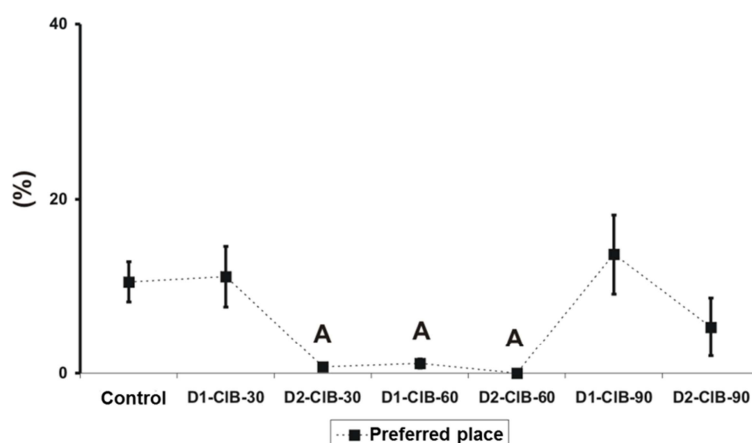
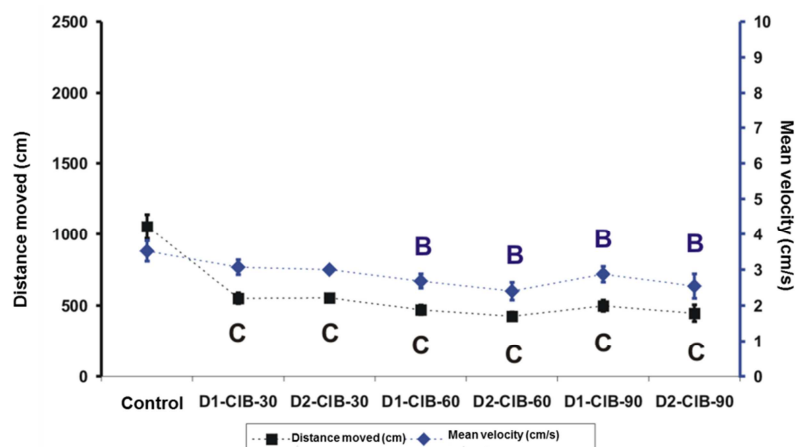




**Figure 2.** The locomotive behaviour after ClB treatment measured in open field test (means  $\pm$  S.E.M., B, C:  $p < 0.001$ ,  $n = 50$ )



In Table 1., it is showed that the ClB is present in the different types (endocrine, immune and neuro) of tissue both in the treated and groups.

**Table 1.** Determination of ClB content in different tissue types after 0.1  $\mu\text{g}/\text{b.w.kg}$  doses of ClB exposition (pg/g tissue;  $n = 50$ )

Tissue type	Control	30 days	60 days	90 days
Adipose tissue of abdomen	<0.001	0.048	0.113	0.321
Liver	<0.001	0.011	0.087	0.101
Brain	<0.001	<0.001	0.015	0.027
Bone marrow	<0.001	0.025	0.063	0.131
Adrenal cortex	<0.001	0.031	0.087	0.151

It is generally accepted that POP/EDCs may alter a wide variety of behavior, including sexual and reproductive behavior, communication, dominance, aggression and cognitive elements such as attention, learning and memory. The mechanisms are still often unclear, or the attempts to explain them involve known target hormones (usually steroids and/or thyroids) at the level of synthesis, storage, release, transport, clearance, receptor, or receptor recognition) within the relevant brain areas.

## Conclusion

In conclusion, the subtoxic and chronic exposures to extremely low doses of endocrine disruptor chlorobenzenes affect the anxiety-related behavioural elements of Wistar rats. The ratio of accumulated ClB depends on the modulation of the homeostatic status and the reserved ClB volume. Since the living organisms are threatened by several types of environmental loads it was essential to use combined types of ClBs. According to our findings obtained in an experimental model, the ubiquitous POPs and EDCs exposure agents can generate systematic alterations in the homeostasis of biological systems even in extremely low doses, when acting on the long term.

### **Acknowledgements**

This study was supported by TÁMOP-4.2.2.D-15/1/KONV-2015-0010, TÁMOP-4.2.6-15/1-2015-0002

### **References**

- [1] Colborn T, S. vomSaal F, Soto MA. Developmental effects of endocrine-disrupting chemicals in wildlife and humans. *Environ Health Perspect* (1993);101: 378-384.
- [2] M. Weselak, T. E. Arbuckle and W. Foster, Pesticide exposures and developmental outcomes: the epidemiological evidence. *J Toxicol Environ Health B Crit. Rev.* 10, (2007) 41-80
- [3] G. Nagyeri, Z. Valkusz, M. Radacs, T. Ocsko, P. Hausinger, M. Laszlo, F. A. Laszlo, A. Juhasz, J. Julesz, M. Galfi: Behavioral and endocrine effects of chronic exposure to low doses of chlorobenzenes in Wistar rats. *Neurotoxicology and Teratology*, (2012) 34, 9-19
- [4] Bigsby R, Chapin ER, Daston PG, Davis JB, Gorski J, Gray LE, Howdeshell KL, Zoeller RT, S. vom Saal F. Evaluating the effects of endocrine disruptors on endocrine function during development. *Environ Health Perspect* (1999); 107: 613-618.
- [5] B. M. Jenssen, Endocrine-disrupting chemicals and climate change: A worst-case combination for arctic marine mammals and seabirds? *Environ Health Perspect* (2006). 114 Suppl. 1, 76-80.
- [6] S. M. Zala and D J . Penn, Abnormal behaviours induced by chemical pollution: a review of the evidence and new challenges. *Animal Behaviour*, (2004), 68, 649-664
- [7] De Bleecker JL, De Reuck JL, Willems JL. Neurological aspects of organophosphate poisoning. *ClinNeurolNeurosurg* (1992); 94: 93-103.
- [8] Porter, W. P., Jaeger, J. W. & Carlson, I. H. Endocrine, immune, and behavioural effects of aldicarb (carbamate), atrazine (triazine) and nitrate (fertilizer) mixtures at groundwater concentrations. *Toxicology and Industrial Health*, (1999) 15, 133-150.

## The Effect of the Plasma Sampling Depth and the Flow Rate of the Aerosol Dilution Gas on the Performance of Single Particle Inductively Coupled Plasma Mass Spectrometry (SP-ICP-MS) Measurements

Ildikó Kálomista, Albert Kéri\*, Gábor Galbács

*Department of Inorganic and Analytical Chemistry,  
University of Szeged, H-6720 Szeged, Dóm tér 7, Hungary  
e-mail: galbx@chem.u-szeged.hu*

### Abstract

Single Particle Inductively Coupled Plasma Mass Spectroscopy is a modern technique available for the characterization of nanoparticles. Optimization of the measurement conditions can increase the potential of the technique, especially with regards to the minimum detectable particle size (typically ca. 15 nm). To this end, in this work we explored the effects of changing the (interface) sampling depth and the on-line aerosol dilution by the High Matrix Introduction (HMI) function on an Agilent 7700X ICP-MS.

### Introduction

Inductively coupled plasma-mass spectroscopy (ICP-MS) is one of the most prominent techniques of modern analytical chemistry that allows us to detect metals as well as several non-metals in ultra trace analytical concentrations. The effective and robust inductively coupled plasma ion source combined with the selective and highly-sensitive detector of mass spectrometry result in ng/L or attogram limits of detection.

A few decades ago the idea surfaced that ICP-MS may be utilized to measure (characterize) single nanoparticles [1]. As an advantage of this method, the single particle inductively coupled plasma spectroscopy (SP-ICP-MS), we can mention that the measurements can be executed in solution phase (sol form) that makes the sample preparation simpler. The traditional nanoparticle analyzing techniques, e.g. scanning electron microscopy (SEM), transmission electron microscopy (TEM), and the dynamic light scattering (DLS) are often time consuming and impractical [2]. In our experience, SP-ICP-MS can indeed detect nanoparticles at a low concentration (even  $10^3$ - $10^4$ /mL) that is typical for environmental samples [3] and can provide size and number concentration, as well as compositional information within a short time (5-60 minutes).

In ICP-MS spectrometry, it is practical to optimize the main experimental parameters in order to achieve the best performance. One of these settings is the interface sampling depth, that determines the depth within the central analytical channel in the plasma from where ions are extracted by the interface. According to the zone model [4], there is an optimum zone (highest concentration of ions) in the central channel where the concentration of the singly charged ions of the isotope is at maximum. This optimum sampling depth changes with the element and also with the setting of relevant other instrumental parameters (e.g. plasma RF power, carrier gas flow rate, etc.). ICP-MS manufacturer Agilent Technologies equips 7700-range instruments with a High Matrix Introduction (HMI) function. Originally, this function was developed for the handling of concentrated sample matrices (up to ca. 2.5%, as opposed to ca. 0.2% with regular ICP-MS instruments). This HMI option operates by adding an extra tangential Ar gas to the aerosol carrier flow, thereby enabling on-line aerosol dilution. This can also be helpful, when analysing nanosols.

At present, our research group actively investigates the possibilities for increasing the performance of SP-ICP-MS analyses and for eliminating spectral interferences [5]. Within these activities, the present report describes the results of our latest investigations dealing with the tuning of the interface sampling depth and the HMI gas flow rate. To our knowledge, no such previous reports have been published.

## Experimental

The experimental instrument was an Agilent 7700X type ICP-MS with an Agilent I-AS autosampler. The sample uptake rate was 400  $\mu\text{L}/\text{min}$  performed by a MicroMist nebulizer. During the SP-ICP-MS experiments, the data acquisition software was used in Time Resolved Analysis (TRA) mode with an integration time of 6 ms and measurement time of 100 seconds. All measurements were performed at  $^{197}\text{Au}$ .

Agilent technologies Multi-Element Standard 3 was used to prepare Au solutions in different concentrations. Gold nano sols were prepared from PELCO NanoXact 40 and 60 nm Au nano sol standards (Ted Pella Inc., USA) stabilized with tannic acid. High purity deionized water (Millipore Elix Advantage 3+ Synergy, USA) was used during sol preparation. The particle concentration was  $5 \cdot 10^4/\text{mL}$ . To ensure the homogeneity of the sols and to avoid the aggregation of the nano particles we applied ultrasonic treatment with an Ultrasonik 300 Instrument (Ney, USA).

## Results and discussion

A calibrating series was prepared from the gold stock a solution to produce solutions of 0, 1, 5 and 10 ppb concentration. We observed that for solutions, the intensity of the signals increased with the decrease of the sampling depth. The sampling depth difference of 14 mm (between 6 and 20 mm) resulted in about one full order of magnitude change. We determined the sensitivity that belongs to each sampling depth value and it was found that the highest sensitivity was featured by the lowest value of sampling depth (6 mm). As can be seen in Figure 1, with the increase of the sampling depth the sensitivity decreases.

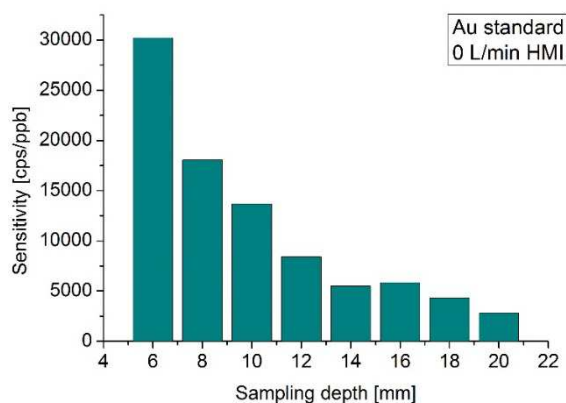


**Figure 1.** Sensitivity values in function of sampling depth

For nano sols (both the 40 nm and 60 nm Au particles) we observed the same tendency: with the decrease of the sampling depth the nano particle signal increased. About 6 times higher signals could be achieved by adjusting the sampling depth between 6 and 20 mm. The histograms in Figure 2. illustrate our observations (please note that the counts on the abscissa are related to the particle size and hence the signal). It can also be observed that the histogram peaks become significantly broader at lower sampling depth values, which can decrease the

dynamic size range of SP-ICP-MS measurements. On the other hand, the number of detection events is fairly constant in the range of 6 to 20 mm, which allows one to perform accurate particle number concentration measurements.

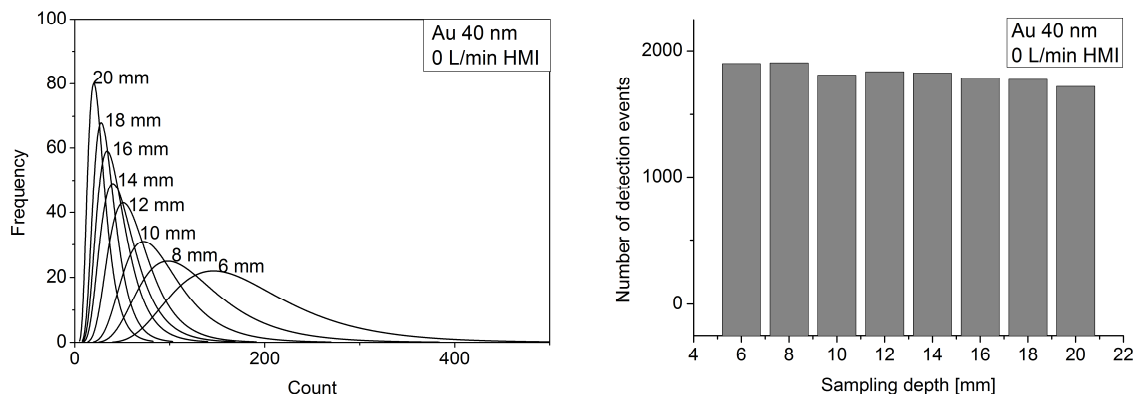


**Figure 2.** The signal histograms (left) and the number of detection events (right) for a 40 nm Au sol recorded with different sampling depth values

The observation of the effects of HMI was also performed by using both standard solutions and the nano sols. We also performed a cross-optimization by varying the sampling depth too. We investigated the effects of three settings of the HMI flow: 0, 0.5 L/min and 1.0 L/min. The experiments were executed first with the Au solution. Figure 3. shows the results for the example of the 10 ppb solution. The case of no HMI flow was already discussed. Setting 0.5 L/min HMI we found that the signal intensity decreased. Moreover, the intensity maximum moved to the 16 mm sampling depth value for all concentrations respectively (not shown in Figure 3). Using the aerosol dilution causes the flow rate to increase, which in turn results in a shift of the optimum sampling depth. A further increase in the HMI flow to 1.0 L/min was found to suppress the signal even more and the optimum sampling depth shifted to an even higher value (20 mm). These changes were experienced for all concentration and can be explained the same way as in the case of 0.5 L/min HMI. The overall suppression effect of HMI flow on the signal was several orders of magnitude.

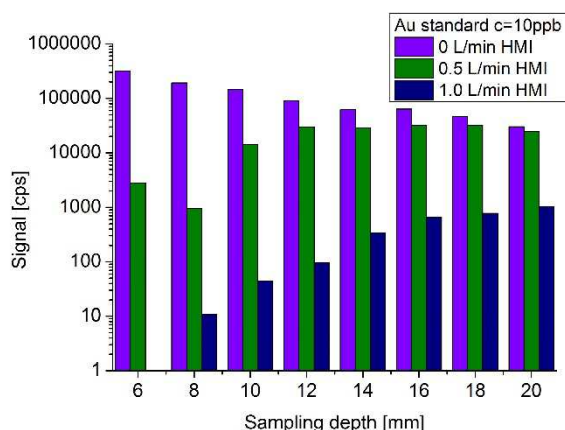


**Figure 3.** The variation of the signal of 10 ppb Au solution as a function of HMI flow rate and the sampling depth

The signal from nano particles were only investigated for the HMI flow equals 0.5 L/min case, as with higher HMI settings for all depth values and even for this one at lower (6-12 mm) depth values, the nanoparticle signal was so low that it could not be separated from the background signal in the histograms. The peak of the nano particles was most separable from the background at 16 mm sampling depth; at higher depths the background and particle signals started fusing together again. This is demonstrated in Figure 4.

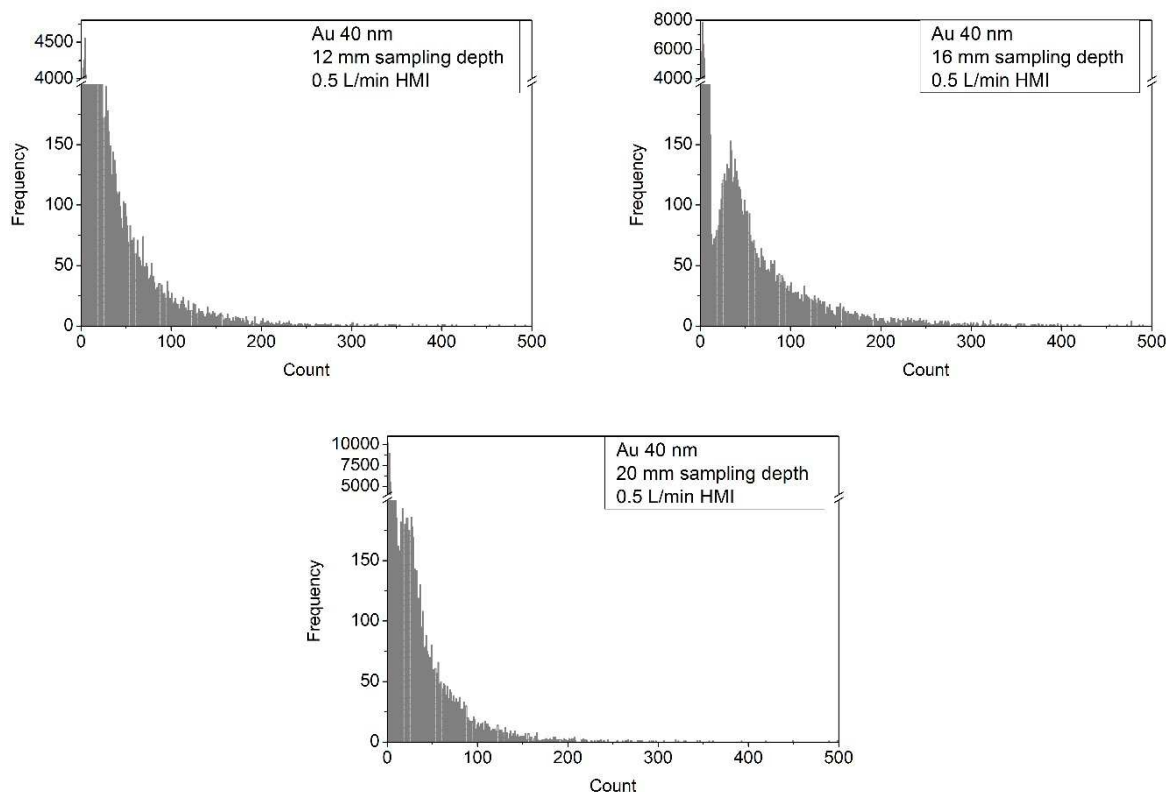


**Figure 4.** The effect of changing the sampling depth on signal histograms as obtained for a 40 nm gold sol with the indicated HMI and sampling depth settings

## Conclusions

According to our expectations, the HMI flow and the sampling depth have a substantial influence on the performance of SP-ICP-MS measurements. It was established that by the optimization of sampling depth, a factor of 6 signal increase (or decrease) can be realized. Upwards from 6 mm sampling depth, the number of detection events were fairly constant, but the histogram peaks became narrower. Thus, this optimization can be used to find conditions under which the best size detection limits can be achieved within the lowest possible measurement time. Using the HMI flow was found to greatly reduce the signals, which may be useful for the on-line dilution of nano sol samples, but it must be accompanied by a concurrent optimization of the sampling depth, as HMI shifts the sampling depth optimum towards significantly higher values.

## References

- [1] C. Degueldre, P.-Y. Favarger, Coll. Surf. 62 (2003) 137.



- [2] H.E. Pace, N.J. Rogers, C. Jarolimek, V.A. Coleman, E.P. Gray, C.P. Higgins, J.F. Ranville, *Env. Sci. Tech.* 4 (2012) 12272.
- [3] H.E. Pace, N.J. Rogers, C. Jarolimek, V.A. Coleman, C.P. Higgins, J.F. Ranville, *Anal. Chem.* 83 (2011) 9361.
- [4] F. Vanhaecke, R. Dams, J. Anal. At. Spectrom. 8 (1993) 433.
- [5] I. Kálomista, A. Metzinger, G. Galbács, EWCPs (February 22-26, 2015) NP5-PO03

## Discriminant Analysis of Coal Samples by Laser Induced Breakdown Spectroscopy

Dávid Palásti<sup>\*1</sup>, Anikó Metzinger<sup>1</sup>, Róbert Rajkó<sup>2</sup>, Tibor Ajtai<sup>3</sup>,  
Éva Kovács-Széles<sup>4</sup>, Gábor Galbács<sup>1</sup>

<sup>1</sup>Department of Inorganic and Analytical Chemistry, University of Szeged,  
6720 Szeged, Dóm square 7., E-mail: galbx@chem.u-szeged.hu

<sup>2</sup>Department of Process Engineering, University of Szeged,  
6725 Szeged, Moszkvai boulevard 5-7.

<sup>3</sup>Department of Optics and Quantum Electronics, University of Szeged,  
6720 Szeged, Dóm square 9.

<sup>4</sup>Nuclear Security Department, Centre for Energy Research, Hungarian Academy of Sciences,  
1121 Budapest, Konkoly-Thege Miklós way 29-33.

### Abstract

The quick analysis of coal samples is fundamental in many industrial processes to optimize the operation and minimize the pollution emission, for soot is one of the main pollutants generated in coal combustion. LIBS is a technique that has a great potential for real-time analysis of coal and soot samples. In particular, we have investigated here the applicability of LIBS to the discrimination of coal and soot aerosols of different origins.

### Introduction

Laser induced breakdown spectroscopy (LIBS) is a modern, versatile atomic spectroscopy technique, which is becoming increasingly popular in recent years both in quantitative and qualitative applications. The advantages of LIBS analysis include that it is fast, needs practically no sample preparation, samples of any size and phase can be analyzed, it is virtually non-destructive, and it can be applied also in the field using compact/portable LIBS devices or remotely [1].

The objective of the present research was to assess the information content of LIBS spectra of bulk carbon samples and of aerosols (soot, carbonaceous aerosols) generated from these coal samples by laser ablation. In particular, the LIBS analysis can potentially reveal the elemental composition (contaminants) of the samples and can be the basis of sample discrimination due to their varying trace element content (coal types and aerosol sources may be classified based on the obtained LIBS spectra). The technique builds on the phenomenon of laser induced breakdown, namely that if the energy density of a pulsed laser beam focused on the sample, an ablation and plasma formation will occur in the focal spot of the beam. The analytical information about the elemental composition of the sample then can be gained from the emission spectroscopic observation of this microplasma.

Different types of coal are extensively used as fuels and industrial raw materials. Combustion of coal is one of the main sources of energy, but it generates ash soot aerosol which is one of the main antropogenous air pollutant. Thus the examination of these samples requires newer and newer chemical and physical techniques [2].

The goals of this research were exploring the chemical and physical attributes that can be measured by the LIBS investigation of carbonaceous samples (graphite, anthracite, lignite and other coal types) and their aerosols. In the present study, six different coal samples, obtained from local depots, were analyzed.

## Experimental

The samples studied originated from different locations and have different caloric values. The six samples studied were identified as „Graphite”, „Anthracite”, „Czech brown coal”, „Polish brown coal”, „Lignite” and „Pécs-vasasi brown coal”.

For the purposes of LIBS measurements, a special, windowed sample cell was fabricated, in which the application of a selected standing or flowing gas environment was also allowed. The samples were machined to a specific shape and size before analysis: disks of 23 mm in diameter and ca. 5 mm in thickness were made and used both in bulk and aerosol measurements. We recorded all spectra in grade 4.5 purity nitrogen.

An Applied Photonics LIBScan 25+ Nd:YAG laser was employed for plasma generation (50 mJ pulse energy, ca. 10 ns pulse length), focusing the laser beam into the cell through the top window. The plasma emission was collected from the side by quartz lenses and 200  $\mu\text{m}$  diameter solarization resistant fiber optic cables and detected by an Avantes AvaSpec FT2048 CCD spectrometer in the 190-880 nm UV-Vis spectral range. The start of the spectral data collection was triggered by a fast photodiode observing the plasma initiated by the laser.

The carbonaceous aerosol was generated in a KrF laser based ablation setup. The laser worked at 248 nm with 18 ns long impulses. The energy density of the focused beam was  $2.5 \text{ J/cm}^2$  and the repetition rate was ca. 1 Hz. The concentration of the aerosol generated from graphite was found to be ca.  $10^7\text{-}10^8 \text{ m}^{-3}$  and the mode of particle distribution was at around 150 nm [3].

Discriminant analysis is an upcoming research direction in LIBS spectroscopy. This is due to the realization that LIBS spectra are line-rich and very characteristic (“fingerprint-like”) of the sample. In novel, related works, chemometric (statistical) methods are used to discriminate the LIBS spectra of samples, which can be made automatic and the efficiency of recognition can be also raised. The simple chemometric methods are based on calculating a Q similarity index which’s value the higher the more the two spectra similar. Q can be defined and calculated in various ways. It is common to count from the linear correlation (LC) of the spectra [4], but the methods based on the sum of squared differences (SSD) and overlapping integral (OI) are also widespread [5]. Advanced chemometric methods can also be employed. For example, our research group earlier successfully used Multivariate Curve Resolution Alternating Least Squares (MCR-ALS), Discriminant Analysis (DA) and Classification Tree (CT) methods to discriminate paper and ink types. In the present study, we also employed these methods, a brief description of which can be found in [6], to discriminate coal sample types.

## Results and discussion

The spectra of bulk coal samples contained intensive, characteristic atomic lines (Ca, Na, N, C), but some molecular lines ( $\text{C}_2$ , CN) also appeared. This is illustrated in **Fig 1**. The elemental composition was different at different points of the samples due to inhomogeneity, but the inter-sample differences were found larger than intra-sample differences.

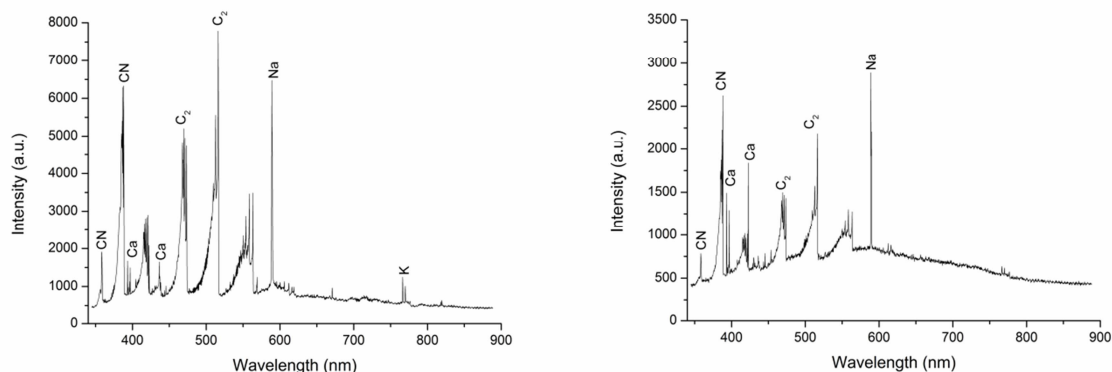


**Fig 1.** LIBS spectra of the bulk anthracite (left) and Polish brown coal (left) samples

In the case of coal aerosols, not all laser pulses hit a particle during LIBS analysis, therefore a pre-processing of spectral data is needed - only those spectra which contain carbon spectral lines above a certain intensity are retained. We also found that the relative frequency of plasma generation was different for different samples. For example, the relative number of successful shots with “anthracite” aerosol was 2%, whereas it was 80% with lignite. This difference may be explained by different breakdown thresholds or by different particle concentrations. Aerosol spectra collected were also found to be less intensive and had worse peak to noise ratio than those of bulk samples. They were also found to be less characteristic. Two aerosol spectra can be seen in **Fig. 2**.

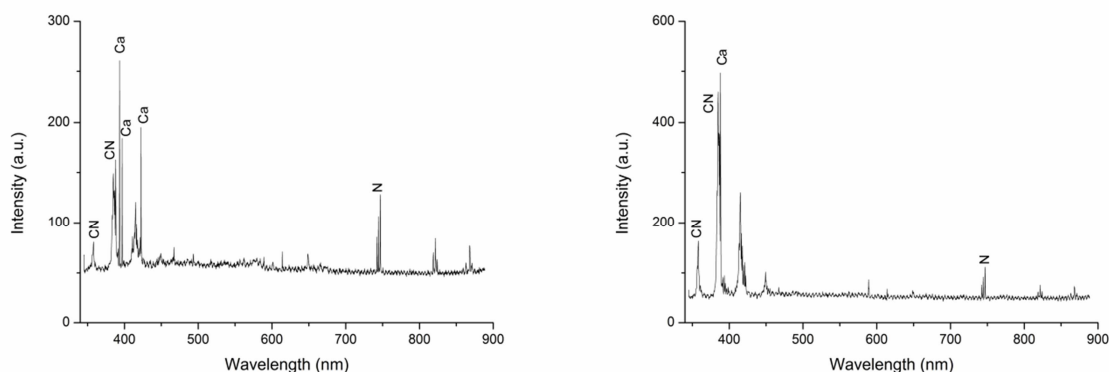


**Fig 2.** LIBS spectra of anthracite (left) and Polish brown coal (left) aerosol

Due to the above characteristics, the discrimination of bulk coal samples is relatively easy. We successfully identified the samples by all three simple and two advanced statistical methods alluded to above. We found the best discrimination results with the linear correlation method, calculated on the full UV-Vis spectra (**Fig. 3**). The combined MCR-ALS/CT method was also found to be efficient (**Fig. 4**).

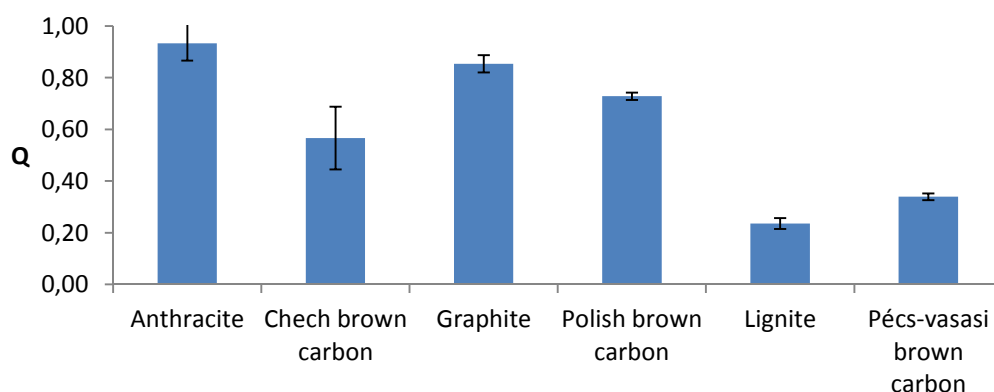


**Fig 3.** Discrimination results for the LC method, based on UV-Vis spectra and anthracite reference.  $Q=1$  means complete similarity, whereas  $Q=0$  complete dissimilarity

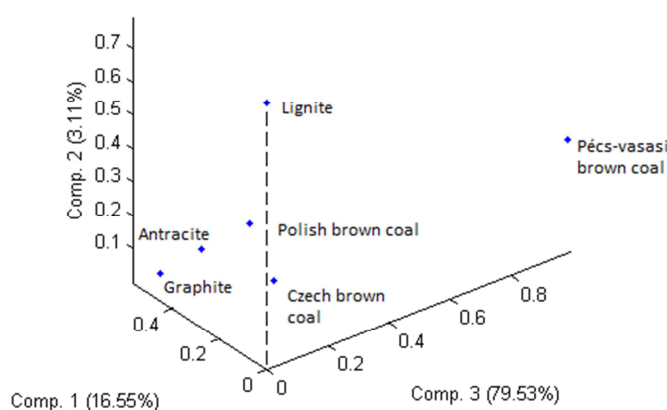


**Fig. 4.** Discrimination of coal samples according to MCR-ALS method, based on their UV-Vis spectra

We found that simple numerical methods are not capable of sufficiently discriminate different soot aerosol types. This is probably mainly caused by the poor S/N ratio in the spectra, which for this reason, also are highly similar to each other.

On the other hand, more advanced chemometric methods, such as MCR-ALS/CT were found to be powerful enough to efficiently discriminate aerosol spectra. In fact, it was even possible to create a model, which is able to describe both the bulk and the aerosol samples. The results of the assignment are shown in **Fig. 5.** below.

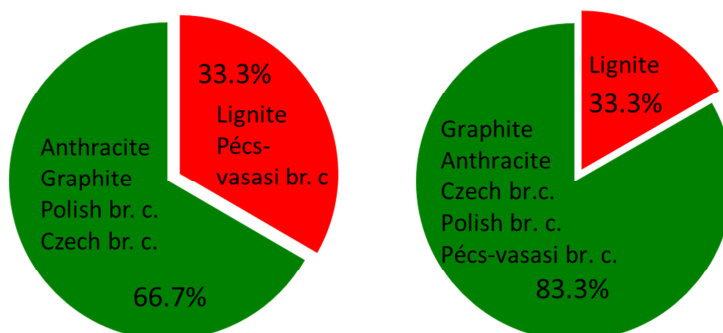


**Fig. 5.** Results of discrimination of bulk (left) and aerosol (right) samples according to the CT method, and based on visible range spectral data

### Conclusion

We successfully created an experimental system, in which we could measure bulk coal and soot aerosol samples by LIBS spectroscopy, in a nitrogen atmosphere. Simple and advanced chemometric techniques were successfully employed to discriminate different bulk coal samples from each other, as well as to identify the source coal type of soot aerosol samples. The aerosol analysis was performed on about aerosols having ca.  $10^8 \text{ m}^{-3}$  particle concentration and about 150 nm average particle size.

### References

- [1] W. Miziolek, V. Palleschi, Israel Schechter: Laser-induced breakdown spectroscopy (LIBS), Chapter 5, Cambridge University Press, 2006.
- [2] S. K. Stattheesh, K. K. Moorthy, Atmos. Environ., 39 (2005) 2089.
- [3] T. Ajtai, N. Utry, M. Pintér, G. Kiss-Albert, R. Puskás, Cs. Tápai, et al., Atmos. Meas. Tech., 8 (2015) 1207.
- [4] A. L. Edward: An introduction to linear regression and correlation, W. H. Freeman and Company, 1976.
- [5] G. Galbács, N. Jedlinszki, A. Metzinger, Microchem. J. 107 (2013) 17.
- [6] A. Metzinger, R. Rajkó, G. Galbács, Spectrochim. Acta B 94-95 (2014) 48.



## Enantioseparation of Amino Alcohol Analogs Possessing 1,2,3,4-Tetrahydroisoquinoline Skeleton and its Derivatives Using Polysaccharide-based Chiral Stationary Phases

Nóra Grecsó<sup>1,2\*</sup>, Gyula Lajkó<sup>1,2</sup>, Tímea Orosz<sup>1</sup>, László Schönstein<sup>2</sup>,  
Ferenc Fülöp<sup>2</sup>, Antal Péter<sup>1</sup>, István Ilisz<sup>1</sup>

<sup>1</sup>Department of Inorganic and Analytical Chemistry, University of Szeged, Dóm tér 7, H-6720 Szeged, Hungary

<sup>2</sup>Institute of Pharmaceutical Chemistry, University of Szeged, Eötvös utca 6, H-6720 Szeged, Hungary

### Abstract

The stereoisomers of 1,2,3,4-tetrahydroisoquinoline amino alcohol analogues were directly separated on modified cellulose based chiral stationary phases. The effects of the mobile phase composition, the structure of the analytes and temperature on the separations were investigated. Experiments were performed at constant mobile phase compositions with varying temperature in order to calculate thermodynamic parameters from plots of  $\ln \alpha$  versus  $1/T$ . Some mechanistic aspects of the chiral recognition process are discussed with respect to the structures of the analytes.

### Introduction

One of the most interesting challenges of the modern analytical chemistry is the separation of chiral compounds. In living organisms the bioorganic molecules, such as amino acids, enzymes, nucleic acids, sugars and proteins, have been of great interest because these molecules are chiral. Problems related to the presence of chirality may cause great anxiety to the modern pharmaceutical industry in several cases [1,2]. In the chirally stereoselective living systems, the enantiomers of a racemic drug are essentially involved in different biological processes, like absorption, secretion, metabolism, allosteric control, protein binding, receptor-ligand interactions and others. One of the enantiomers, the so-called eutomer is often belongs to the optimum therapeutic effects, while the other isomer (distomer) is inactive, but in its presence even the eutomer effect can be prevented in some cases; in worst cases some unwanted (or even toxic) effects can also be induced. So it is understandable that issues of chirality have become of especial importance in the drug safety [3]. To control the chiral purity of starting materials and products, well reproducible, reliable, accurate analytical methods with high sensitivity and stereoselectivity are needed in the industrial and pharmaceutical research. One of the most frequently applied techniques is chiral high-performance liquid chromatography (HPLC).

For its potential biological activity the 1,2,3,4-tetrahydroisoquinoline (Tiq) skeleton is very useful in pharmaceuticals and drug research. The antitussive nescapin and the antitumour agent trabectedin contain the enantiomerically pure Tiq skeleton.

The stereoisomers of 1,2,3,4-tetrahydroisoquinoline amino alcohol analogues and derivatives thereof were separated in normal-phase mode on chiral stationary phases based on preprepared silica coated with

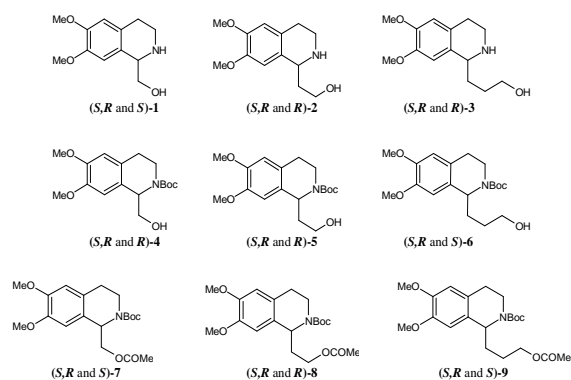


Figure 1. The structures of the studied analytes

cellulose *tris*-(3,5-dimethylphenyl carbamate), cellulose *tris*-(3-chloro-4-methylphenyl carbamate), cellulose *tris*-(4-methylbenzoate) or cellulose *tris*-(4-chloro-3-methylphenyl carbamate). The structures of the investigated analytes are shown in Figure 1.

### Experimental

The analytical measurements were made on a Waters Breeze system consisting of a 1525 binary pump, a 487 dual-channel absorbance detector, a 717 plus autosampler and Empower 2 data manager software (Waters Chromatography, Milford, MA, USA). As alternative, a Waters HPLC system consisting of an M-600 low-pressure gradient pump, an M-2996 photodiode-array detector and an Empower 2 Chromatography Manager data system (Waters Chromatography, Milford, MA, USA) was employed. Both systems were equipped with a Rheodyne Model 7125 injector (Cotati, CA, USA) with a 20- $\mu$ l loop. For thermostating of the columns, a Spark Mistral column thermostat with a temperature adjustment precision of  $\pm 0.1$  °C (Spark Holland, Emmen, The Netherlands) was used.

The polysaccharide-based chiral selectors were cellulose *tris*-(3,5-dimethylphenyl carbamate) (Lux Cellulose-1; 3  $\mu$ m), cellulose *tris*-(3-chloro-4-methylphenyl carbamate) (Lux Cellulose-2; 5  $\mu$ m), cellulose *tris*-(4-methylbenzoate) (Lux Cellulose-3; 5  $\mu$ m) and cellulose *tris*-(4-chloro-3-methylphenyl carbamate) (Lux Cellulose-4; 5  $\mu$ m), packed into 250 x 4.6 mm I.D columns (Phenomenex, Torrance, CA, USA).

*n*-Heptane, *n*-hexane, methanol (MeOH), ethanol (EtOH), *n*-propanol (PrOH), propan-2-ol (2-PrOH), 1-butanol (BuOH) and *t*-butanol (*t*-BuOH) of HPLC grade were purchased from VWR International (Arlington Heights, IL, USA), while other reagents of analytical reagent grade were from Sigma-Aldrich (St. Louis, MO, USA).

Before use, all eluents were degassed in an ultrasonic bath, and helium gas was purged through them during the HPLC analyses. Stock solutions of analytes (1 mg ml<sup>-1</sup>) were prepared by dissolution in the mobile phase.

### Results and discussion

For comparison of the performances of the four polysaccharide-based columns, separations were carried out with the same mobile phase, *n*-heptane/IPA/DEA=90/10/0.1 (v/v/v), on Cellulose-1, Cellulose-2, Cellulose-3 and Cellulose-4. Cellulose-3 seemed to be the least effective in the separation of this set of enantiomeric analytes. Although  $k_1$  was generally higher on the Cellulose-4 CSP than on the Cellulose-2,  $\alpha$  and  $R_S$  values obtained on the Cellulose-2 CSP in most cases were higher. It seems that protected amino alcohol analogues possessing a Tiq skeleton fit sterically better into the cavity of cellulose *tris*-(4-chloro-3-methylphenyl carbamate), but the difference in the strength of complex formation for the two stereoisomers is higher in the cavity of *tris*-(3-chloro-4-methylphenyl carbamate) and therefore higher  $\alpha$  and  $R_S$  values were observed.

The enantioresolution of this set of Tiq analogues on the four polysaccharide-based CSPs with mobile phases of *n*-hexane containing different alcohols (EtOH, PrOH, 2-PrOH, BuOH or *t*-BuOH) and 0.1% amines [ethylamine (EA), diethylamine (DEA), triethylamine (TEA), propylamine (PRA)] as mobile-phase additives was evaluated.

The retention factors depended strongly on the alcohol content of the mobile phase. Typical normal-phase behaviour was observed at ambient temperature on the cellulose-based columns: decrease of the IPA content resulted in larger  $k$  and in most cases larger  $\alpha$  and  $R_S$  values. The nature of the alcoholic modifier influenced the retention. For analytes **1** and **4** on the Cellulose-1 column, in response to the application of EtOH, PrOH, 2-PrOH, BuOH or *t*-BuOH in the same molar concentration (0.13 M), with a few exceptions  $k_I$  decreased slightly in the sequence EtOH – PrOH – BuOH and increased in the presence of 2-PrOH or *t*-BuOH (Figure 2). It seems that solvation of the analytes in a mobile phase containing an alcohol with a branched side-chain was less favorable, resulting in increased  $k_I$ . The nature of the alcohol modifier influenced the enantioselectivity and resolution, *i.e.* the ratio of the non-chiral and chiral interactions between the CSP and the analytes depended on the nature (and also the concentration) of the alcohol. The selectivity increased slightly with increasing alcohol carbon number (an exception was BuOH), but the application of BuOH and *t*-BuOH was disadvantageous because of their high viscosity. The changes caused in the CSP structure by the different alcohols may affect the chiral selectivity of the CSP, depending on the size and structure of the analyte. The influence of the nature of the alcohol on the resolution was also investigated. When separation occurred, alcohols with bulky and branched side-chains, such as 2-PrOH and *t*-BuOH, sometimes resulted in higher  $R_S$ . In most cases, the use of 2-PrOH led to high enantioselectivity and resolution and most of the experiments were therefore carried out in the presence of IPA as alcohol modifier.

On polysaccharide-based CSPs, a base additive together with an alcohol in the *n*-hexane mobile-phase system is frequently applied to improve the peak shape and selectivity. The effects of base additives on the enantioseparations of **1-9** on Cellulose-1 and Cellulose-2 columns were investigated in the presence of 0.1 v/v% of EA, DEA, TEA or PRA in the *n*-hexane/2-PrOH (90/10 v/v) mobile-phase system. The nature of the base additives usually exerted a slight effect on the chromatographic parameters, as depicted for **6** and **9** in Figure 3.

In order to investigate the effects of temperature on the chromatographic parameters, a variable-temperature study was carried out on Cellulose-1, Cellulose-2 and Cellulose-4 columns for **4** and **7**, usually over the temperature range 10–50 °C, with the mobile-phases (i): *n*-hexane/EtOH/DEA = 93/7/0.1 (v/v/v), (ii): *n*-hexane/2-PrOH/DEA = 90/10/0.1 (v/v/v), (iii): *n*-hexane/2-PrOH/DEA = 80/20/0.1 (v/v/v), and (iv): *n*-hexane/BuOH/DEA = 88/12/0.1 (v/v/v). All of the recorded values decreased with increasing temperature, together with the separation factor,  $\alpha$ , and the resolution,  $R_S$ , while on Cellulose-1 for **4** with all three applied mobile phases and on Cellulose-2 for **7** at certain cases increases in  $\alpha$  and  $R_S$  were observed (not presented).

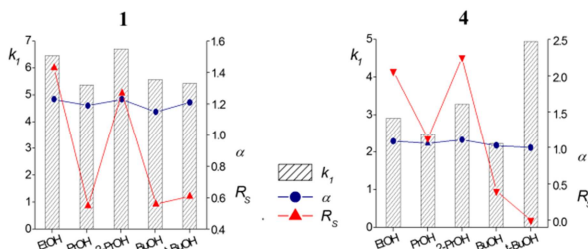


Figure 2. Effects of nature of alcohol additives

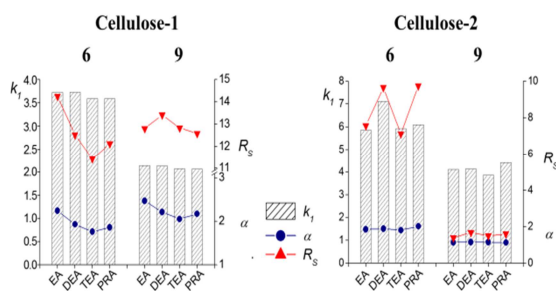


Figure 3. Effects of nature of base additives

To shed light on the effects of temperature on the separations, chromatographic data were accumulated from which van't Hoff plots were constructed based on the application of equation 1.

$$\ln \alpha = -\frac{\Delta(\Delta H^\circ)}{RT} + \frac{\Delta(\Delta S^\circ)}{R} \quad (1)$$

The  $\Delta(\Delta H^\circ)$  values range from -9.3 to 0.9 kJ mol<sup>-1</sup>. The interactions of **4** with Cellulose-2 in mobile phase (ii) were characterized by the highest negative  $\Delta(\Delta H^\circ)$  value, while **4** on Cellulose-1 in mobile phase (iv) exhibited the highest positive  $\Delta(\Delta H^\circ)$ .  $\Delta(\Delta S^\circ)$  ranged from -22.7 to 4.0 J mol<sup>-1</sup> K<sup>-1</sup>. Under conditions where  $\Delta(\Delta H^\circ)$  was negative,  $\Delta(\Delta S^\circ)$  was also negative and the largest positive  $\Delta(\Delta H^\circ)$  was accompanied by the largest positive  $\Delta(\Delta S^\circ)$ . The  $\Delta(\Delta S^\circ)$  values are governed by the difference in the number of degrees of freedom between the stereoisomers on the CSP, and mainly by the numbers of solvent molecules released from the chiral selector and the analyte when the analyte is associated with the CSP. For **4** on Cellulose-1 in mobile phases (i), (ii) and (iv) and for **7** on Cellulose-2 in mobile phase (i) above temperature  $T_{iso}$ , both  $\Delta(\Delta H^\circ)$  and  $\Delta(\Delta S^\circ)$  were positive, indicating an entropically driven separation. When the selectivity increased with increasing temperature,  $\Delta(\Delta H^\circ)$  and  $\Delta(\Delta S^\circ)$  were positive. In these cases, the change in the adsorption enthalpy with increasing temperature had a positive effect on the enantioselectivity. On the other hand, the positive  $\Delta(\Delta S^\circ)$  compensated the positive  $\Delta(\Delta H^\circ)$  and resulted in a negative  $\Delta(\Delta G^\circ)$ .

Comparison of the effects of the three additives (EtOH, 2-PrOH and 1-BuOH) on the thermodynamic parameters revealed that the application of 2-PrOH ensured the largest - $\Delta(\Delta H^\circ)$  and - $\Delta(\Delta S^\circ)$  values on both Cellulose-1 and Cellulose-2. Solvation of the selectors is probably favorable, with the application of 2-PrOH leading to better separation.

The thermodynamic parameter - $\Delta(\Delta G^\circ)_{298}$  suggests that Cellulose-2 with the mobile phase *n*-hexane/2-PrOH/DEA=90/10/0.1 (v/v/v) induces highly efficient binding to the selector, as reflected by the large - $\Delta(\Delta G^\circ)$  values.

From the  $-T\Delta(\Delta S^\circ)$  data for some analytes, the positive  $\Delta(\Delta S^\circ)$  on both CSPs compensated for the positive  $\Delta(\Delta H^\circ)$  and resulted in a negative  $\Delta(\Delta G^\circ)$  value (Table 3). For these analytes in this temperature range, enantioresolution is entropically driven, and the selectivity increases with increasing temperature.

The data were used to calculate the temperature  $T_{iso}$  at which the enantioselectivity balance out. In most cases,  $T_{iso}$  was considerably higher than room temperature; enthalpically driven enantioseparation was obtained. When  $T_{iso}$  was obtained at lower than ambient temperature, positive  $\Delta(\Delta H^\circ)$  and  $\Delta(\Delta S^\circ)$  were observed and the selectivity increased with increasing temperature. These enantioseparations were entropically driven.

## Conclusion

The stereoisomers of some Tiq analogues were separated on CSPs containing the chiral selectors of cellulose *tris*-(3,5-dimethylphenyl carbamate) (Cellulose-1), cellulose *tris*-(3-chloro-4-methylphenyl carbamate) (Cellulose-2), cellulose *tris*-(4-methylbenzoate) (Cellulose-3) and cellulose *tris*-(4-chloro-3-methylphenyl carbamate) (Cellulose-4). The chromatographic parameters depended on the mobile-phase composition, the nature and concentrations of the mobile-phase additives and temperature. Baseline resolution was achieved in all cases; the polysaccharide-based CSPs have a complementary character which leads to successful resolution.

### **Acknowledgements**

This work was supported by Hungarian National Science Foundation grant K 108847.

### **References**

- [1] S. Lam and G. Malikin, *Chirality*, **4** (1992) 395.
- [2] I.W. Wainer (Editor), *Drug Stereochemistry Analytical Methods and Pharmacology*, Marcel Dekker, Inc., New York, New York, 1993.
- [3] M.R. Islam, J.G. Mahdi, I.D. Bowen, *Drug Safety* **3** (1997) 149.

## The effects of chlorobenzenes with the combination of extreme low electromagnetic field

Dóra Hopenthaler<sup>1,2</sup>, Ibolya Budai<sup>1,2</sup>, Zsolt Molnár<sup>1</sup>, Marianna Radács<sup>1</sup>, Márta Gálfi<sup>1</sup>

<sup>1</sup>*Institute of Applied Natural Science, Faculty of Education, University of Szeged Hungary  
Department of Environmental Biology and Education, Juhász Gyula Faculty of Education,  
University of Szeged*

<sup>2</sup>*Faculty of Science and Informatics, University of Szeged  
e-mail: dodika91@gmail.com*

### Abstract

Conditions of the evolution (physical, chemical and biological factors) determined the emergence and the survival of the earthly life. Natural conditions have been transformed by the presence of the society, change its contact networks. Accordingly, evolution takes place deterministically to the new condition.

There are some physical expositions which are not researched because of its low energy. Electromagnetic field is a very significant and it is caused by the electrical equipments.

### Introduction

The natural and anthropogenic electromagnetic fields are parts of the environment, in which the living systems have been constantly exposed the effects of it. It is intriguing and likely important to investigate how the changes of natural background affect the adaptation. Electromagnetic field (EMF) effects on organisms have been rise, which was largely due to the technological advances [1, 2].

Trichlorobenzene (TCB) and hexachlorobenzene (HCB) are the derivatives of benzene. TCB is colorless liquid or solid, soluble in organic solvents, insoluble in water. HCB is a white, crystalline substance. TCB is used for insulating material, exchanger, component of synthetic oils and lubricants and insecticide [3]. HCB have been manufactured since the 1930's. Initially it was used as fungicide for the treatment of cereal. However, HCB measured in the nature originate from the accumulation of the HCB previously dropped [4, 5, 6].

Capacitors are for storing elementary charges, two conductive elements which are separated from each other with insulating material. In case of cells, there are great similarities with the capacitors' technical design. Biological systems can also be "capacitors", lipid bilayer is the insulator, plasma components are the leaders, and they are all sensitive for the changes of EMF [7].

It is known, that there is electric potential difference between the inner and outer surfaces of cell membrane, caused by the potassium, sodium and chloride ions.

The EMF effects can cause changes at about 2-5 eV. Radio and microwaves can modify the vibrational states of molecules, and also generate heat. Non-thermal effects can change the electrical properties of the cells with the modification of the membrane potential [8].

In our research methods we have created different types of cell models, and test them at standard conditions, which are essentials for the living organisms. Monolayer cell cultures will be able to show the consequences of EMF effects through function changes [9, 10].

In this present research, we aimed to study the effects of the extremely low intermittent EMF on cellular biological systems. Furthermore, we are looking for some standardized test method, through which we can follow the effects.

Because of this in this study, we would like to develop a method for study and follow the



effects of extremely low dose of intermittent electromagnetic fields and the subtoxic effects of chlorobenzenes (CIB).

### Experimental

*In vitro* monolayer cell culture models from Wistar rats' pituitary and liver were made to investigate the electromagnetic exposure.

Control systems were set up. Samples for absolute control was not exposed to any test step (A(C)), n=10. We moved in experimental steps our stress control samples (S(C)), n=10. For investigate the electromagnetic field exposition, an ineffective head at negative control (- (K)) was used, n=10. In case of positive control an instrument with a capable of inducing exposition was used in zero position (+ (C)), n=10.

Changes in cell transformation can show the initiating action of DNA of cell cultures after chemical induction. Benz-c-acridine (1mg/mL, 24 h) was used as a certified dedifferentiated agent. We followed the DNA and the protein production of the cell cultures.

For test the function ability of the cell cultures we used proven differentiation crocin+retinoic acid (CRA) (1:1, 1 µg/mL, 5 days).

We test our standardised *in vitro* model system to search the effects of the extremely low dose intermittent electromagnetic energy. (50µT,  $\nu$  = 60 Hz, for 5 days, /times of 6 hours for 20 minutes/)

In this, adenohypophysis (ADH), neurohypophysis (NH), hepatocyte (HEP) monolayer confluent cell cultures were treated (chemical /CIB: chlorobenzene mix / hexachlorobenzene: 2,4,6-trichlorobenzoene = 1:1/0,1µg/g protein; t=6 h, or physical EMF: 50µT,  $\nu$  = 60 Hz, for 5 days, /times of 6 hours for 20 minutes, n=10).

During investigations we measured the <sup>3</sup>H-Thymidine incorporation and protein content of cell cultures with modified Lowry method and a Pierce BCA protein Assay Kit (Thermo Fisher Scientific Inc., Rockford, IL, USA).

### Results

Our results were described in two different graphs. It is shown in Figure 1 how the <sup>3</sup>H-Thymidine incorporation of the cell cultures was changed after physical and/or chemical expositions compared to absolute control. Protein production of the samples was shown in Figure 2.

There was not any notable difference between the control samples. For benz-c-acridine exposition there was a clear rise in DNA and protein production, which proves the operability of the model system.

Effects of CIB for DNA and protein production of various cell types did not show significant difference. We experienced similar to this, when the cell cultures were exposed to physical exposition.

There was negligible difference when we expose the cell cultures to at first, physical and then chemical effects. Conversely (chemical then physical), there was significant difference.

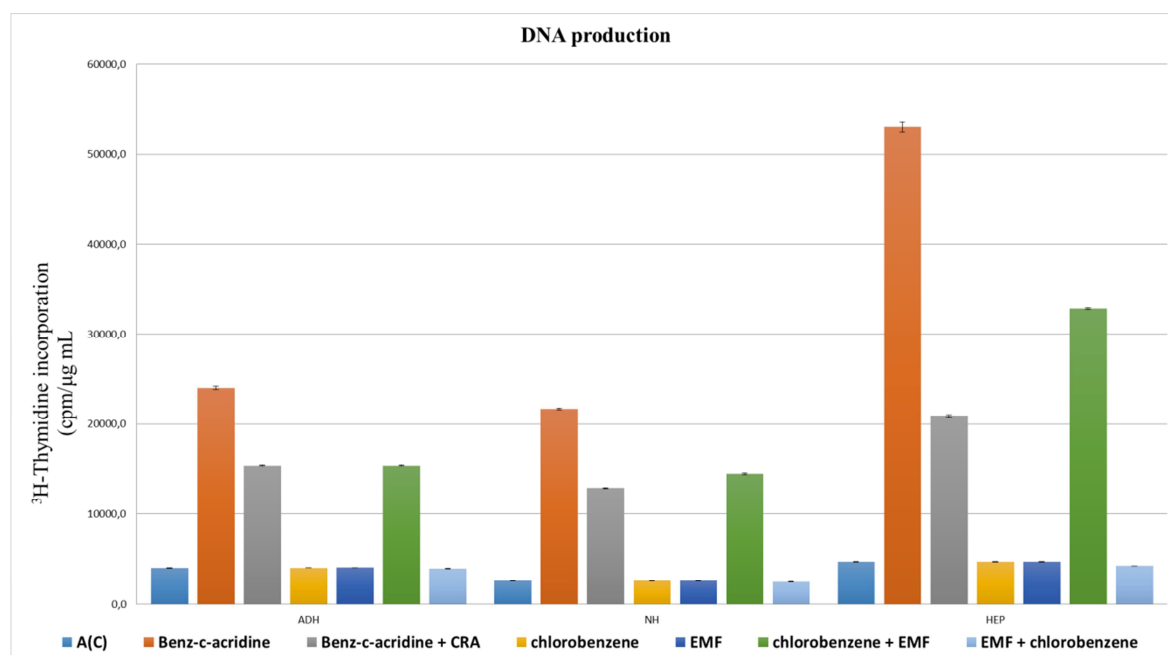


Figure 1

The effects of chlorobenzenes and/or electromagnetic field (EMF) on DNA production of the different types of cell cultures ( $n=10$ , means  $\pm$  SEM )

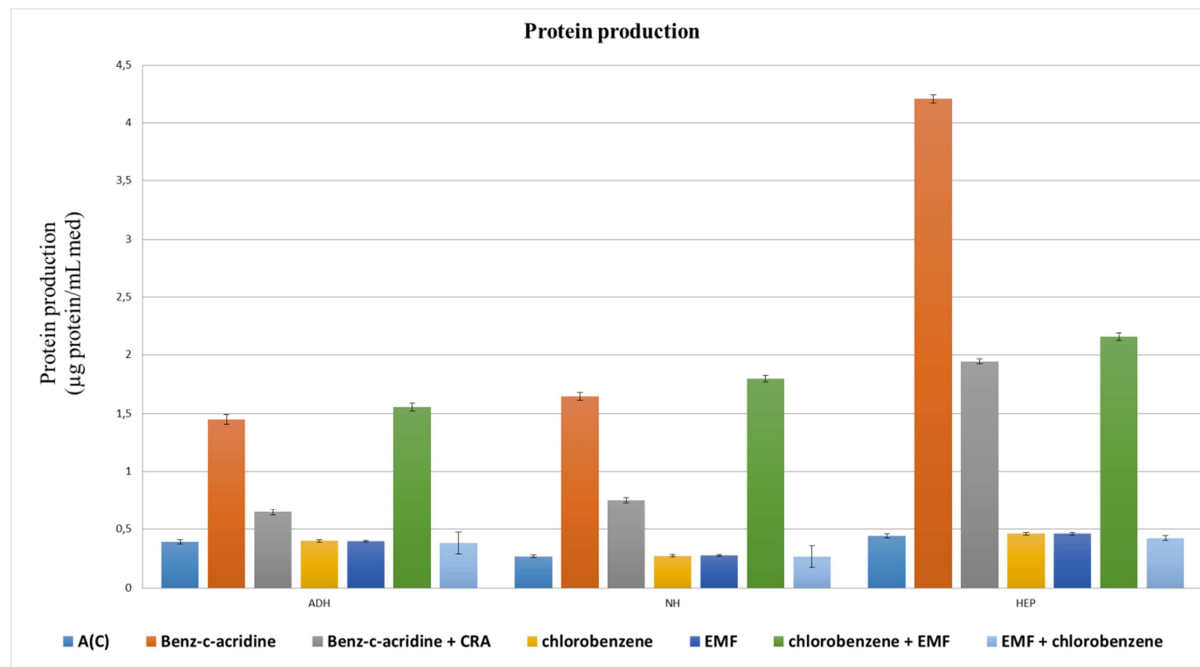


Figure 2

The effects of chlorobenzenes and/or electromagnetic field (EMF) on protein production of the different types of cell cultures ( $n=10$ , means  $\pm$  SEM)

## **Conclusion**

According to our results, we can state that the EMF exposure can cause large deviations on those cells, which was previously been exposed to an initiating effect by the ClB. The promoter effect of EMF can be considered. The physiological elements were modulated by these chronic, but extremely low doses of environmental loads (ClB with the combinations of EMF).

## **Acknowledgements**

This study was supported by TÁMOP-4.2.2.D-15/1/KONV-2015-0010, TÁMOP-4.2.6-15/1-2015-0002

## **References**

- [1] WHO – Extremely low electromagnetic fields; Environmental health criteria pp: 238, 2007
- [2] L. Zombory – Élet a sugárözönben; Magyar Tudomány, No: 8, pp: 989 , 2002
- [3] R. E. Bailey Global hexachlorobenzene emissions. Chemosphere 43, 167-182, 2001
- [4] Balint G. A.- Galfi M- Rimanoczka Á- Falkay G- Juhász.: On a possible new intracellular signal-system in rat gastric mucosa. Journal of Physiology 95 243–245. 2001
- [5] D. Adjarov, E. Ivanov, D. Keremidchiev Gamma-Glutamyl-Transferase Transferase - A Sensitive Marker in Experimental Hexachlorobenzene Intoxication. Toxicology 23, 73-77, 1982
- [6] J. L. Barber, A. J. Sweetman, D. Wijk, K. C. Jones Hexachlorobenzene in the global environment: emissions, levels, distribution, trends and processes. Sci Total Environ 349, 1-44, 2005
- [7] E. Kovács, B. Paripás – Fizika II.; Ed: Miskolci Egyetem Földtudományi Kar, 2011
- [8] J.Toldi – Communication Among Neurons; Our Age issue, No: 4; pp: 57-64, 2012
- [9] A. Zamanian, C. Hardiman – Electromagnetic radiation and human health; High frequency electronics No: 7; pp: 1-26, 2005
- [10] WHO – IPCS/OECD Key generic terms used in chemical hazard/risk assessment; IPCS risk assessment terminology, 2004

## Possible Neurotoxicity of Titanium Dioxide Nanoparticles in a Subacute Rat Model

Tamara Horváth<sup>1</sup>, Tünde Vezér<sup>1</sup>, András Papp<sup>1</sup>

<sup>1</sup>*Department of Public Health, University of Szeged Faculty of Medicine, Szeged, H-67210  
Szeged, Dóm tér 10, Hungary  
e-mail: horvath.tamara@med.u-szeged.hu*

### Abstract

Titanium dioxide nanoparticles (TiO<sub>2</sub> NPs) have many industrial applications and also appear in various consumers' goods including foods and medicines. This widespread application raises the question of a potential occupational, environmental and/or intentional human exposure and health hazard. Motility of NPs within the organism and surface reactivity of TiO<sub>2</sub> NPs suggests, among others, potential nervous system toxicity. In the present work, rats were intratracheally exposed to TiO<sub>2</sub> NPs and functional changes in the nervous system were examined using electrophysiological, behavioural and biochemical methods. The results verified to some extent the neurotoxicity of nano-titanium but also underlined the need for further investigations.

### Introduction

Thanks to the recent advances in nanosciences and nanotechnology, more and more industrial processes and products involve the presence of NPs, that is particles with <100 nm typical diameter. Beside research applications NPs have had their entry in the fields of health care, energy production, agriculture and environmental protection [1] and are being released in the environment [2]. The physical, chemical and biological properties of nanoparticulate substances differ from those seen in other physical states, leading to biological, and hence, toxicological, interactions not seen with more conventional materials, which also means novel health risks [3].

Particles of TiO<sub>2</sub> – in the micrometer, and newly, nanometer, range – have been used in paints, various coatings, plastics, food (E171), toothpastes, skin care products and in sunscreens as radiation blocking agent [4]. The anatase form of TiO<sub>2</sub> has photocatalytic properties in UV light, it is applied as a sterilizer and deodorant, and as additive in paints and building materials to reduce the level of air pollutants [5].

This broad and growing range of application raises questions about possible health risks involved. Today, chemical safety is a primary requirement so toxicological evaluation of novel materials should precede their application or at least go in parallel [4, 5]. Contradictory findings are found in the literature on the absorption and migration, including penetration to the brain, of TiO<sub>2</sub> NPs after pulmonary, dermal, oral etc. exposure. That nervous system effects can be expected, is indicated by the oxidative stress generating potency of TiO<sub>2</sub> NPs, and by biochemical, histological and functional alterations observed mostly in mice [4].

In the present work, rats were exposed to nano-TiO<sub>2</sub> by the intratracheal route, and functional alterations of the nervous system were detected by electrophysiological and behavioral methods. The aims were determining the suitable dose range and testing the applicability of the methodological approach proven in toxicological work with other metal oxide NPs [6].

## **Experimental**

Young adult SPF Wistar rats were used, obtained from Toxi-Coop Ltd. (Hungary). The animals (with  $170 \pm 20$ g body weight at start) were kept in polypropylene cages (3-4 rats/cage) under GLP-equivalent conditions. The rats had free access to fresh water throughout the experiment. Based on previous data, the daily food ration (rat chow) was 30g/animal. (Ssniff R/M-Z+H rat chow, Toxi-Coop Ltd., Hungary). The animals' body weight was measured daily.

The rats were randomly distributed to 5 groups of 10 rats each based on their performance in preliminary spontaneous exploratory activity test. Rats in the control group (C) were totally untreated while vehicle control rats (VC) received a 1% solution of HEC (hydroxyethyl cellulose) in phosphate-buffered saline by intratracheal instillation (see [6]). Treated rats received TiO<sub>2</sub> nanoparticles (NPs) suspended in the HEC-containing vehicle and instilled, the doses were 1 mg/kg body weight (low dose, group L), 3 mg/kg (medium dose, M), and 10mg/kg (high dose, H). The TiO<sub>2</sub> NPs were spherical with <50 nm diameter. Treatment was done every day during a 28 days period, between 8:00 and 10:00 a.m.

The rats' spontaneous exploratory activity was tested, at start and after the last treatment day, in an open field (OF) box (Conducta 1.0 System, Experimetria Ltd., Hungary). The animals were, one by one, placed into the centre of the box, and 16 motility parameters – ambulation distance, time and count; local activity time and count; vertical activity (rearing) time and count; immobility time and count – were measured in one 10 min session.

On the day following the final OF session, the rats were prepared for electrophysiological recording in urethane anesthesia (1000 mg/kg b.w. ip). The skull was opened over the left hemisphere, and silver electrodes were placed on the the primary somatosensory (SS) visual (VIS) and auditory (AUD) areas. Spontaneous electrical activity was recorded from these sites simultaneously for 6 min, and the relative spectral power of the frequency bands was determined. Then, sensory stimuli were applied to obtain sensory evoked potentials (EPs, for details see [6]) Fifty stimuli of each modality per rat were applied. For VIS and AUD stimulation, 1 Hz frequency was applied, and for SS stimulation 1, 2 and 10 Hz. The 50 EPs were averaged and onset latency was measured. To see changes in peripheral nerves, the tail nerve was electrically stimulated at the tail base (3-4 V; 0.05 ms) and the nerve action potentials were recorded 50 mm more distally. Conduction velocity was calculated from the response latency, and refractory period, from the extra latency of the second action potential obtained by double stimulation. The complete recording and evaluation was performed by the software NEUROSYS 1.11 (Experimetria Ltd., Hungary).

After that, the rats were sacrificed by an overdose of urethane, were dissected and organs were weighed. Relative organ weights were calculated to 1/100 body weight. From each group, samples of 3 randomly chosen rats were kept for metal level determination, and of another 3, for biochemical measurements.

From the functional, biochemical and general toxicological data, group means were calculated and checked for normality by the Kolmogorov-Smirnov test. The main statistical test used was parametric one-way ANOVA or non-parametric Kruskal-Wallis method. Post hoc analysis of group differences was done by Tukey test and the paired Mann-Whitney U test with Holm correction. SPSS 17.0 (IBM Corporation, U.S.A.) was used.

## **Results and Discussion**

The general toxicity on TiO<sub>2</sub> NP exposure was detected by means of changes in body weight gain and organ weights. The effect of treatment was seen, both in the vehicle control group (VC) and the TiO<sub>2</sub> NP-treated groups, from the 2<sup>nd</sup> week on. By the end of the treatment

period, the total weight gain over the 6 weeks was significantly lower in the groups receiving the two higher doses of nano-TiO<sub>2</sub> (Table 1).

The relative weight of the lungs increased significantly vs. C and VC in the groups M and L. Relative brain weight decreased significantly in groups M and H vs. C. For both organs, the maximal change was seen in group M.

**Table 1.** Body weight gain (g) of the control and nano-TiO<sub>2</sub> treated rats over the 6 weeks treatment. Mean±SD, n=10. \*: p<0.05 vs. C.

Groups	C	VC	L	M	H
Body weight gain	213.6±34.9	177.4±43.4	187.7±37.2	142.2±16.5*	165.2±26.6*

Out of the electrophysiological parameters investigated, the band spectrum of the ECoG was shifted slightly to higher frequencies in the nano-TiO<sub>2</sub> treated groups but this was below significance. The changes in EP latency were, however, significant. As seen in Fig. 1, latency increased also in VC vs. C but the changes in the treated groups were mostly significant vs., both controls. It is also conspicuous that, similar to body weight gain, the biggest change of SS and VIS EP latency was seen with the medium dose (group M) not the high dose (H). This was somewhat in parallel with the Ti levels of the tissue samples (Table 2).

In the tail nerve, the conduction velocity was significantly reduced but the length of relative refractory period changed less markedly (Fig. 2.)

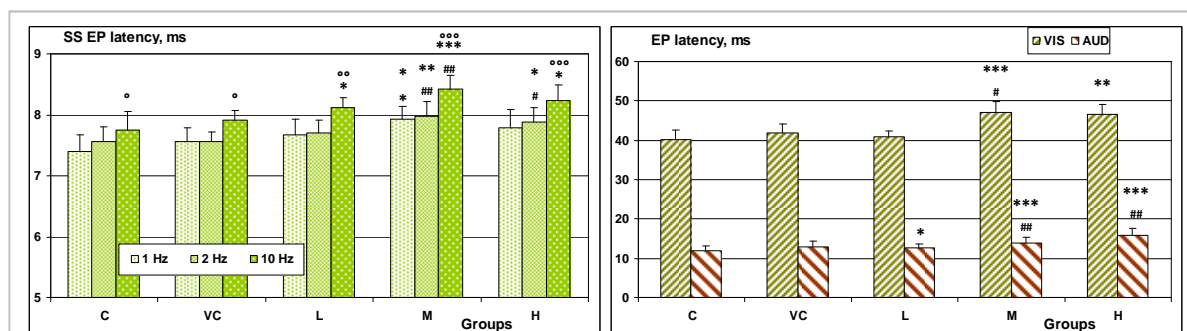


**Figure 1.** Latency of the somatosensory EP (at various frequencies, left) and the visual and auditory EP (right) after 6 weeks nano-TiO<sub>2</sub> treatment. Mean+SD, n=10. \*, \*\*, \*\*\*: p<0.05, 0.01, 0.001 vs. C.; #, ##, ###: p<0.05, 0.01 vs. VC; °, °°, °°°: p<0.05, 0.01, 0.001 vs. 1 Hz stimulation within the same group.

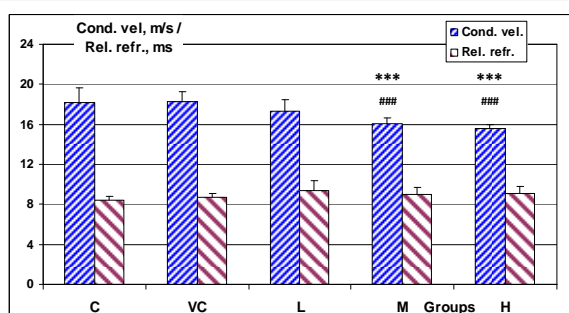


**Figure 2.** Conduction velocity and relative refractory period of the tail nerve after 6 weeks nano-TiO<sub>2</sub> treatment. Mean+SD, n=10. \*\*\*: p<0.001 vs. C.; ###: p<0.001 vs. VC



In the OF activity, the treated rats tended to spend more time in the corner zones of the field than those without nano-TiO<sub>2</sub> exposure although the difference between group C and VC was not negligible. Activity in the first minute, showing immediate reaction of the rat on the novel environment, also showed the preference of treated rats to the corners, indicating increased level of anxiety (Fig. 3). The tissue Ti levels (Table 2) and the relative organ weights (not shown) indicated that most of the nano-TiO<sub>2</sub> remained in the lungs and that the amount reaching other organs had the same non-linear dose dependence seen also in several functional alterations, pointing to a causative role of the NPs.

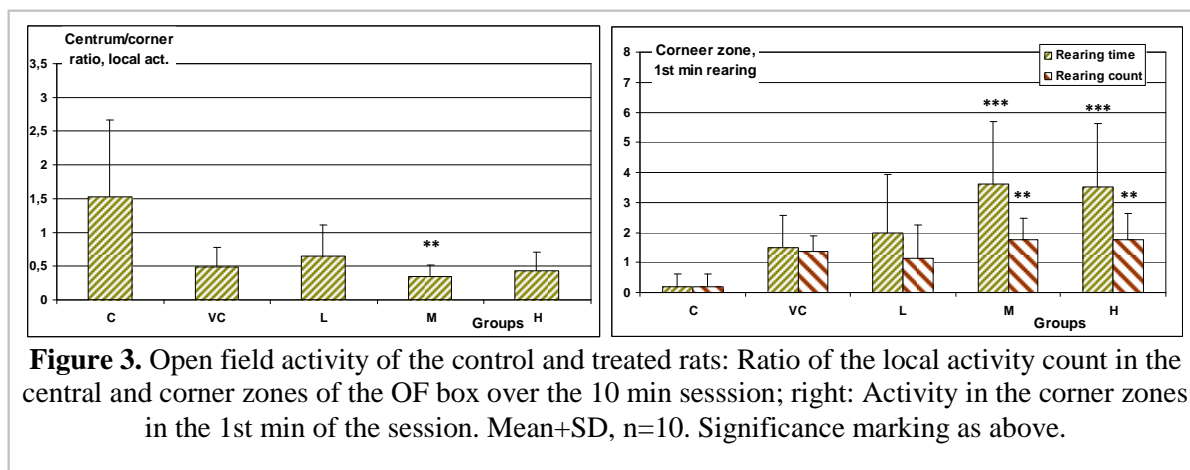


**Figure 3.** Open field activity of the control and treated rats: Ratio of the local activity count in the central and corner zones of the OF box over the 10 min session; right: Activity in the corner zones in the 1st min of the session. Mean+SD, n=10. Significance marking as above.

**Table 2.** Ti levels ( $\mu\text{g/kg}$  wet tissue) of various organs (Mean $\pm$ SD, n=3)

Groups	Lungs	Blood	Liver	Brain
VC	1.494 $\pm$ 0.925	1.543 $\pm$ 0.941	3.953 $\pm$ 3.306	2.846 $\pm$ 1.619
L	43.232 $\pm$ 6.146	3.169 $\pm$ 1.852	1.263 $\pm$ 0.455	2.916 $\pm$ 2.126
M	42.314 $\pm$ 6.467	3.486 $\pm$ 2.160	2.680 $\pm$ 2.959	6.235 $\pm$ 3.188
H	81.488 $\pm$ 4.261	1.000 $\pm$ 0.000	1.691 $\pm$ 1.196	1.241 $\pm$ 0.418

The intensity of thiobarbiturate reaction, as a measure of oxidative damage of lipids, was dependent on Ti dose in the lungs and liver, but not in the brain. This contradicts to the functional alterations and metal levels and argues more for an indirect mechanism of action.

## Conclusion

It was possible to detect functional neurotoxicity of TiO<sub>2</sub> NP given to the rats. The results, however, raise questions to be answered in further experiments such as the dose dependence and the relationship of neuro-functional and biochemical changes to the external and internal nano-TiO<sub>2</sub> dose.

## Acknowledgements

The authors are thankful to Prof. Zoltán Kónya and coworkers (Department of Applied and Environmental Chemistry) for providing the NPs; to Prof. Gábor Galbács and coworkers (Department of Inorganic and Analytical Chemistry) for Ti level determination; and to Dr. Mónika Kiricsi and coworkers (Department of Biochemistry and Molecular Biology) for biochemical measurements.

## **References**

- [1] C. Buzea, I. I. Pacheco, K. Robbie, *Biointerphases* 2 (2007) MR17.
- [2] A. A. Keller, S. McFerran, A. Lazareva, S. Suh, *J. Nanopart. Res.* 15 (2013) 1692.
- [3] W. G. Kreyling, M. Semmler-Behnke, W. Möller, *J. Nanopart. Res.* 8 (2006) 543.
- [5] J. Chen, C. Poon, *Building and Environment* 44 (2009) 1899.
- [4] M. Czajka, K. Sawicki, K. Sikorska et al., *Toxicol. in Vitro* 29 (2015) 1042.
- [5] Regulation (EC) No 1907/2006 of the European Parliament and of the Council, *Official Journal* L396 (2006) 1.
- [6] G. Oszlanczi, E. Horváth, A. Szabó et al., *Acta Biol. Szeged.* 54 (2010) 165.

## Examination of the Photocatalytic Activity of Differently Shaped Bismuth Tungstate Microcrystals

Zsolt Kása<sup>1\*</sup>, Kata Saszet<sup>2</sup>, Zsolt Pap<sup>1,2,3</sup>, Gábor Kovács<sup>2,3</sup>, András Dombi<sup>1</sup>, Klára Hernádi<sup>1,4</sup>, Lucian Baia<sup>3</sup>, Virginia Danciu<sup>2</sup>

<sup>1</sup>Research Group of Environmental Chemistry, University of Szeged, Szeged, HUNGARY

<sup>2</sup>Faculty of Chemistry and Chemical Engineering, University of Babeş-Bolyai, Cluj-Napoca, ROMANIA

<sup>3</sup>Faculty of Physics, University of Babeş-Bolyai, Cluj-Napoca, ROMANIA

<sup>4</sup>Applied and Environmental Chemistry Department, University of Szeged, Szeged, HUNGARY

e-mail: kasa.zsolt@chem.u-szeged.hu

### Abstract

In this study, Bi<sub>2</sub>WO<sub>6</sub> photocatalysts with different morphologies were obtained by a one-step hydrothermal method. The resulted 3D structures (e.g. “flowers”) (d ≈ 2 µm) consisted from individual nanoplates. The synthesis procedure involved acetic acid, a surfactant (Triton X-100) and a shaping agent, such as urea, thiourea and glycine. The effect of these compounds were also investigated in-detail. The crystallization was performed using the well-known hydrothermal method. The above mentioned morphological changes significantly influenced the photocatalytic activity, which was evaluated successfully by the degradation of Rhodamine B (RhB) under UV irradiation.

### Introduction

Nowadays semiconductor photocatalysis is an intensively studied research field due to its potential in solar energy conversion and degradation of organic pollutants. The most studied semiconductor in photocatalysis is titanium dioxide, because it is photostable, biologically inert, and it can be produced cheaply [1]. Besides, the industry already uses titania in several applications. Its major drawback is that UV light is required for excitation. An emerging alternative is bismuth tungstate, which is active under visible light ( $\lambda > 400\text{nm}$ ) [2]. This property can be an advantage, because the major component (38 – 40 %) of the sunlight's emission spectrum is in the visible range, while the UV light is just 3-5 % of the full spectrum [3]. The activity of the photocatalysts can be maximized by shape-tailoring with appropriate chemical reagents, such as in case of titanium dioxide, where F<sup>-</sup> ions are applied for the stabilization of reactiva crystallographic planes [4]. Therefore, if the shape is changing, then the physical and chemical properties of the chosen material is also changing. This means that the photocatalytic activity is also influenced. In our preliminary experiments octyl phenol ethoxylate (Triton X-100), was used, while the influence of the hydrothermal treatment time was investigated. It was found that the hydrothermal treatment time significantly influenced the morphology of the Bi<sub>2</sub>WO<sub>6</sub>, together with the observed photocatalytic activity [5].

## Experimental

### Controllable synthesis of $\text{Bi}_2\text{WO}_6$ microflowers

$\text{Bi}_2(\text{NO}_3)_3 \cdot 5 \text{H}_2\text{O}$  (5 mmol) was dissolved in 43 mL 36 % acetic acid (transparent solution, A). After that,  $\text{Na}_2\text{WO}_4 \cdot 2 \text{H}_2\text{O}$  (2.5 mmol), Triton X-100 (1.25 mmol) and thiourea (1.25 mmol) were dissolved in 68.8 mL distilled water (transparent solution, B). The solution B was added dropwise into solution A, under continuous stirring. The solution containing the amorphous precipitate was transferred into a Teflon-lined stainless steel autoclave. The temperature was adjusted and maintained at 180 °C for 15 h, and cooled down to room temperature without the usage of a supplementary cooling agent. The gained powder was collected and washed five times with ethanol and deionized water. After that, the catalysts were dried at 40 °C for 12 h [5]. The synthesis strategy is listed in Table 1, where the different shape-directing agents were listed.

Sample name	Used materials	
TU	thiourea	triton X-100
TU-TRX	thiourea	×
U	urea	triton X-100
U-TRX	urea	×
G	glycine	triton X-100
G-TRX	glycine	×
TRX	×	triton X-100

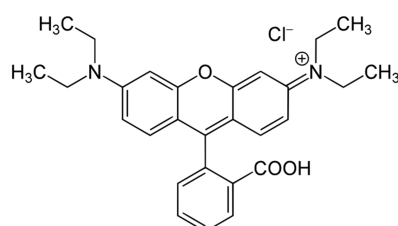
Table 1. Used ashaping agents and the samples' nomenclature

### Characterization

The obtained microcrystals were analyzed using scanning electron microscopy (SEM), and X-Ray diffraction (XRD), while the optical features were followed by diffuse reflection spectrometry (DRS).

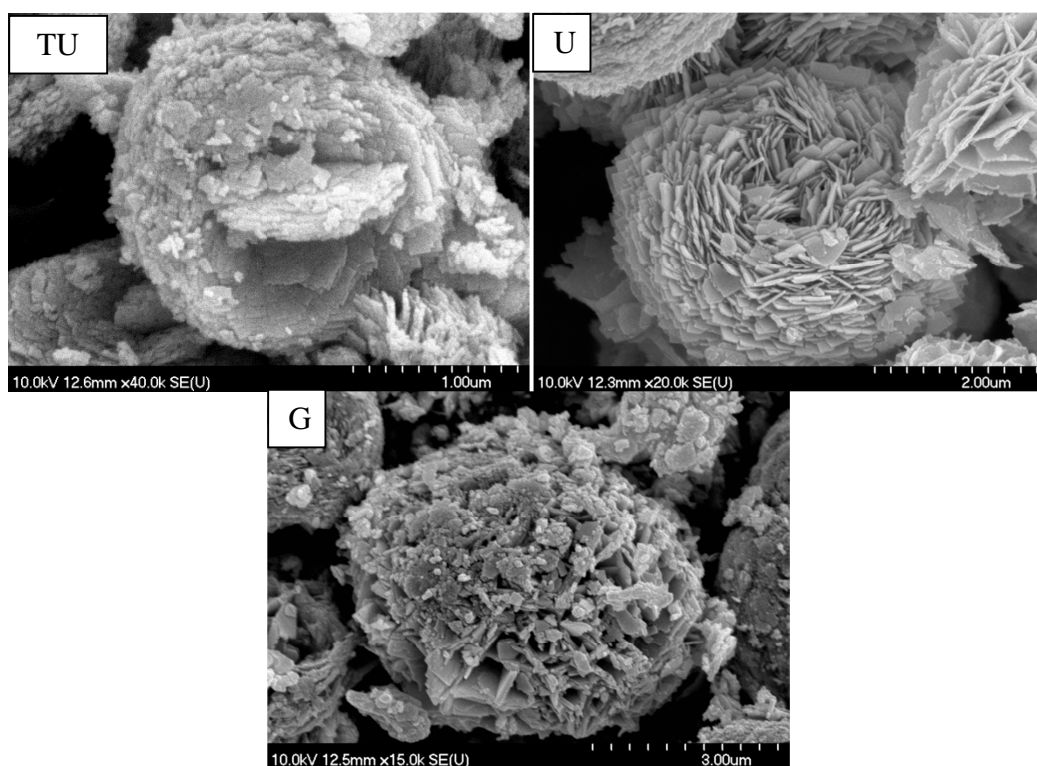
### Photocatalytic activity tests

The photocatalytic activity tests of the samples were carried out by the photodegradation of a Rhodamine B (RhB) at 25 °C.  $6 \times 6 \text{ W}$  fluorescent UV lamps were used as a light source ( $\lambda_{\text{max}} = 365 \text{ nm}$ ). The experiments of RhB degradation were performed as follows: 0.1 g  $\text{Bi}_2\text{WO}_6$  was added to 100 mL RhB solution (initial concentration:  $5 \cdot 10^{-5} \text{ M}$ ). Before the UV illumination, the suspension was stirred for 30 minutes in the dark. After the lamp was switched on, in every 30 minutes, 2 mL suspension was collected and centrifuged. The concentration of Rhodamine B were determined by UV-Vis spectroscopy (detection wavelength = 553 nm).



**Figure 1.** The structure of Rhodamine B**Results and discussion**

The results show, that the used shaping agents (Triton X-100, urea, thiourea and glycine) influenced the microcrystals' shapes. As shown in the Figure 2, if the thiourea was changed to urea or glycine, completely different microstructures were formed (not "flower-like" structure). But all samples' shapes were spherical, with a diameter about 2-3  $\mu\text{m}$ . The TU sample has a flower-like structure, while the U sample is similar to a rose, and the G sample does not show any specific shape. Nevertheless, the G sample has the best photocatalytic degradation capacity. Furthermore, if the Triton X-100 was not involved the synthesis, the "flower-like" shape remained. This leads to the conclusion that the main shape controlling reagents are the thiourea and glycine. Nevertheless, all the samples had a secondary structure which consisted from thin sheets.

**Figure 2.** SEM micrographs

The main diffraction peaks the samples can be identified as an orthorhombic crystal structure. The G and G-TRX samples contain a small amount of  $\text{WO}_3$  (Figure 3/a.). Furthermore, on the diffuse reflectance spectra is clearly visible, that the G and the G-TRX samples show an additional electron transition band (530 nm), besides the one observed at 410 nm.(Figure 3/b)

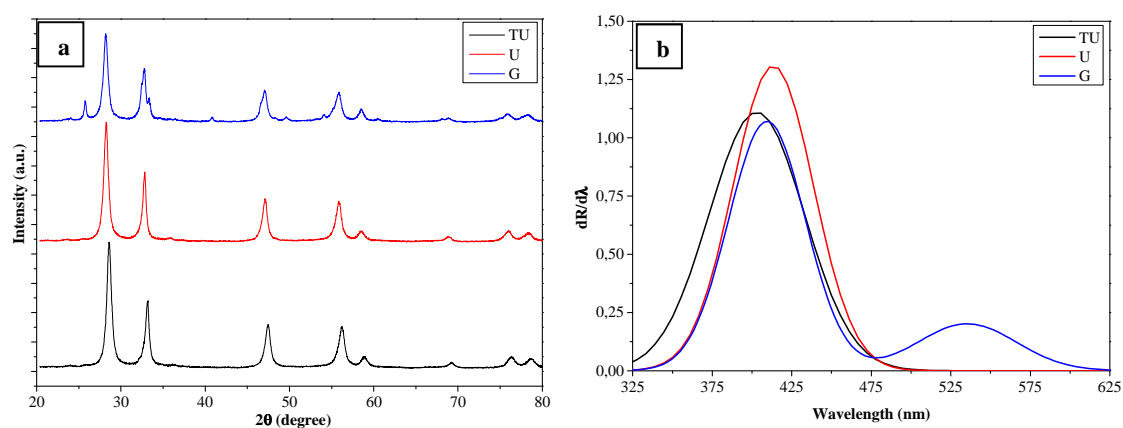


**Figure 3.** X-ray diffractogram (a) and diffuse reflectance spectra (b)

Finally, the photocatalytic degradation capabilities of the obtained materials were tested for Rhodamine B under UV light irradiation. The decomposition curves are shown in Figure 4.

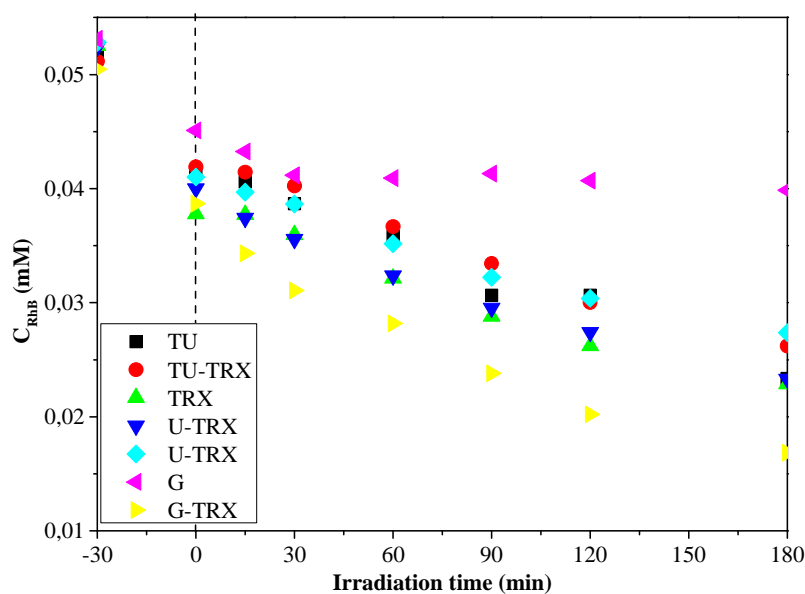


**Figure 4.** Photocatalytic degradation of RhB

## Conclusion

In summary, differently shaped  $\text{Bi}_2\text{WO}_6$  photocatalysts were successfully synthesized with one-step hydrothermal method. The shaping agents (urea, thiourea and glycine) are the most important in the formation of bismuth tungstate, while the surfactant serves as a size controlling agent. Moreover, the  $\text{Bi}_2\text{WO}_6$  microflowers showed high photocatalytic activity for Rhodamine B degradation under UV light irradiation.



## **Acknowledgements**

The financial support was provided by the Campus Hungary Programme (TÁMOP-4.2.4.A/2-11/1-2012-0001) and the Swiss Contribution (SH/7/2/20).

## **References**

- [1] W. Guo, F. Zhang, C. Lin, Z. L. Wang: Adv. Mater. **2012** 4761
- [2] S. Malato, J. Blanco, A.R. Fernandez-Alba, A. Agüera, Chemosphere, **2000** 403
- [3] L. Zhang and Y. Zhu, Catal. Sci. & Technol., **2012**. 694
- [4] K. Vajda, Zs. Kása, A. Dombi, Z. Németh, G. Kovács, V. Danciu, T. Radu, C. Ghica, L. Baia, K. Hernádi and Zs. Pap, Nanoscale, **2015**. 5776
- [5] H. Jinyun, W. Weimin, Z. Linlang, Z. Zhengguang, F. Zhengyi and X. Zhe, J. of Mater. Sci. Ed., **2013**. 231

**Reaction of Biofilms (Cyanobacterial, Diatom and Green Algae) from Lake Balaton and River Danube to Herbicide Preparation ROUNDUP and its Components (Glyphosate, POEA)**

**Szandra Klátyik<sup>1,2</sup>, Angéla Földi<sup>3</sup>, Éva Ács<sup>3,4</sup>, Tamás Cséffán<sup>1</sup>, Gyula Pasaréti<sup>1</sup>, Mária Mörtl<sup>1</sup>, Eszter Takács<sup>1</sup>, Péter Bohus<sup>5</sup>, András Székács<sup>1</sup>, Béla Darvas<sup>1,3\*</sup>**

<sup>1</sup>Agro-Environmental Research Institute, National Agricultural Research and Innovation Centre, H-1022 Budapest, Herman O. u. 15, Hungary; <sup>2</sup>Szent István University, Doctoral School of Biological Sciences, Páter Károly u. 1. H-2100, Gödöllő, Hungary; <sup>3</sup>Eötvös Loránd University, Doctoral School of Environmental Sciences, Pázmány Péter sétány 1/A, H-1117, Budapest, Hungary; <sup>4</sup>Danube Research Institute, Centre for Ecological Research, H-1113 Budapest, Karolina út 29, Hungary; <sup>5</sup>Lamberti SpA, 21041 Albizzate, via Piave 18, Italy  
\*e-mail: b.darvas@cfri.hu

**Abstract**

The behavior of biofilms developing during 6 weeks on sheets of glass fixed to AKK-1<sup>®</sup> type carrier buoy in River Danube (Green Island, Budapest) and in Lake Balaton (Tihany Bay) in spring time was investigated in aquaria exposed to *glyphosate* at concentrations of 100 and 1000 µg/l for 6 and 4 weeks, respectively. The effects of adjuvant *POEA* and formulated herbicide ROUNDUP<sup>®</sup> at *glyphosate* equivalent concentrations were also tested. Sensitivities of biofilms from River Danube and Lake Balaton were different under laboratory conditions. No adverse effects of *POEA* were determined on the well-estimable biofilm originated from River Danube, while *glyphosate* caused a 30% decrease in 10 weeks. Realignment of biofilms was typical, the initial ratio of diatom (Bacillariophyceae) and cyanobacteria (*Cyanobacteria*) decreased, and these species were replaced by a filamentous green alga (*Chlorophyta*) population.

**Introduction**

Pesticides applied in chemical plant protection contain various additives, beside their active ingredient(s) [1]. Additives have been considered as inert/inactive components. Authorization requires simplified risk assessment (RA) for additives compared to RA of the active ingredients [2], even though several studies proved the toxicity not only of the leading herbicide active ingredient *glyphosate*, but also of polyethoxylated tallowamines (*POEA*) applied as adjuvants in *glyphosate*-based formulations [3-6]. Biofilms developing on stone surfaces in water media play an important role in the biogeochemical cycles of water ecosystems. A significant part of biofilm communities constitute of photoautotrophic benthic species [7-8], thus, effects of herbicides on these algae deserve special attention.

**Experimental**

The natural biofilms were grown on glass substrates fixed to AKK-1<sup>®</sup> type carrier buoy (Cséffán, Darvas and Pasaréti) placed in River Danube (Green Island – 47.481641, 19.057645) and in Lake Balaton (Tihany Bay – 46.914190, 17.892916) between early May and mid-June of 2015 for 6 weeks. The AKK-1<sup>®</sup> buoy includes four algal deposition units (containing no metal or plastic elements) with 6 glass sheets in each unit. After the 6-week developing period, the glass substrates were placed under laboratory conditions into eight aquaria containing water from the original location of the buoy. Water in the aquaria was slowly stirred (oxygen dissolution), temperature-controlled (22±2°C) and illuminated (L:D =

15:9, daily light program 6-9 hrs 400 lux, 9-18 hrs 2000 lux, 18-21 hrs 400 lux; XiLong White T8<sup>®</sup>). Five biofilm substrates with blasted and smooth surface sides were placed into each aquarium (the sixth substrate was used for analytical and microscopic evaluations). The water in the aquaria was changed weekly, with water of unchanged quality from the original locations, where the biofilm developed, and with treatment concentrations applied. During the first 6 weeks the aquaria were treated with *glyphosate* at 100 µg/l and with adjuvant *POEA* or with formulation ROUNDUP<sup>®</sup> (*glyphosate* isopropylamine salt) at *glyphosate*-equivalent concentrations, except for the untreated control. After the 6<sup>th</sup> week the concentration of the *glyphosate*-equivalent treatments was increased to 1000 µg/l. Although the detected *glyphosate* content in Hungarian surface waters (1 ng/ml) is much below our evaluation level [9], mean *glyphosate* concentration in runoff was ~140 µg/l (max. 180-233 µg/l) in USA [10], moreover, the value can exceed it (~5 mg/l) in some cases [11]. The quantity of the diatom (*Bacillariophyceae*), cyanobacteria (*Cyanobacteria*) and green algae (*Chlorophyta*) species in the untreated and treated units was determined with a BBE MOLDAENKE BENTOTORCH<sup>®</sup> algae torch instrument. Beside investigation of biofilm composition, weekly degradation of *glyphosate* was determined daily in water samples of River Danube and Lake Balaton, and in cleaned drinking water (CLEARWATER<sup>®</sup>). The initial concentration of *glyphosate* was 100 µg/l. *Glyphosate* concentration of water samples were measured by HPLC after derivatization. Grubbs-test (XLSTAT<sup>®</sup>) was applied to eliminate outliers. Effects of treatments were statistically analyzed by ANOVA and Tukey, Spjotvoll/Stoline *post hoc* tests (STATISTICA<sup>®</sup>). Effectivity was determined by the Henderson-Tilton formula.

## Results & Discussion

No significant differences (ANOVA) were seen between cyanobacterial and diatom biofilms formed either on the sand blasted or on the smooth surface sides of the glass substrates fixed on the AKK-1<sup>®</sup> buoy in the case of River Danube and Lake Balaton during the 6-week exposition period (data not shown). Results indicated no significant differences prior treatment between the quantity of cyanobacterial and diatom biofilm from River Danube and the cyanobacterial biofilm from Lake Balaton, on either sides of the glass substrate (Figs 1, 3-4). In the case of quantity of diatom biofilm from Lake Balaton, the control unit was significantly lower (Fig 2), than the units treated with *glyphosate* and ROUNDUP<sup>®</sup>.

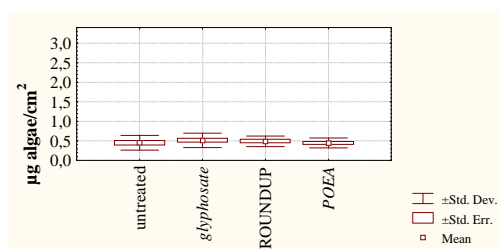


Fig. 1 Cyanobacterial biofilm originated from Lake Balaton, before treatment

Different capitals mean significant differences between groups

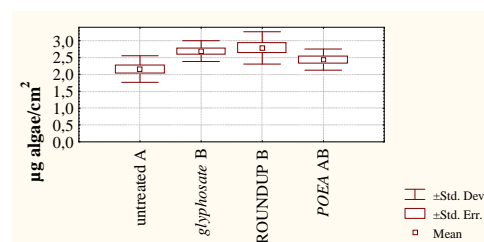


Fig. 2 Diatom biofilm originated from Lake Balaton, before treatment

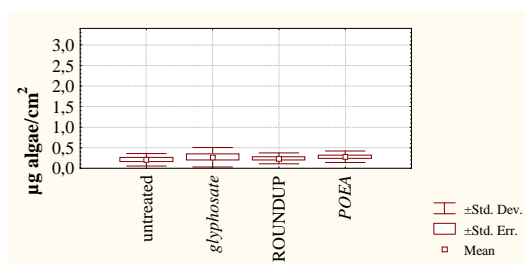


Fig. 3 Cyanobacterial biofilm originated from River Danube, before treatment

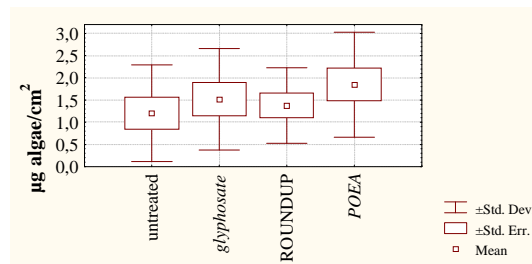


Fig. 4 Diatom biofilm originated from River Danube, before treatment

The untreated control units from River Danube grew from 1.9 to 5.5  $\mu\text{g}/\text{cm}^2$  in 10 weeks (Figs 5-6), while those from Lake Balaton degraded from 2.6 to 1.5  $\mu\text{g}/\text{cm}^2$  (Figs 7-8). The composition of the developing biofilms in the case of River Danube was 12-14% cyanobacterial and 86-88% diatoms, while corresponding values in Lake Balaton were 16-17% cyanobacterial and 83-84% diatoms. *POEA* occurred not to affect the formation of the algal communities. The efficiency of *glyphosate* was 30% at 100  $\mu\text{g}/\text{l}$  for cyanobacterial algae species, while 39% for diatoms in River Danube. In contrast to the active ingredient, *ROUNDUP*<sup>®</sup> showed a substantially lower efficiency. The value of efficiency did not further increase at the level of 1000  $\mu\text{g}/\text{l}$  *glyphosate* (data not shown), presumably due to pre-selection at lower doses. However, during the entire 10-week period of the investigation (exposition: 6 weeks at 100  $\mu\text{g}/\text{l}$  and 4 weeks at 1000  $\mu\text{g}/\text{l}$ ), the composition of the algal community was changed to 17% cyanobacterial, 60% diatom and 23% green algae species. Statistical analysis of the apparently more sensitive biofilms from Lake Balaton was feasible only in the first 2 weeks of the experiments. The efficiency of the 100  $\mu\text{g}/\text{ml}$  *glyphosate*-equivalent *ROUNDUP*<sup>®</sup> treatment was 31% for cyanobacterial algae and 20% for diatoms. From the 4<sup>th</sup> week filamentous algae species were replacing *glyphosate*-sensitive algal communities (Figs 9-10).

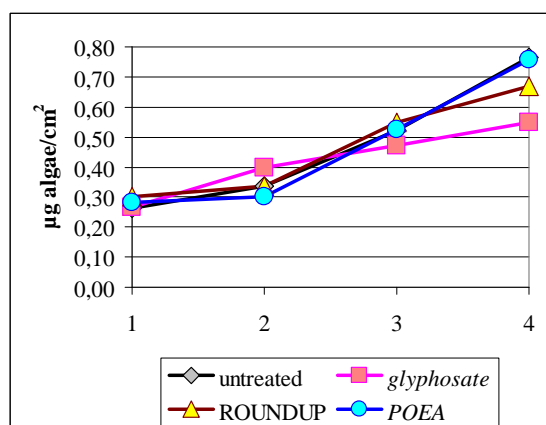


Fig. 5 Cyanobacterial biofilm originated from River Danube after 100  $\mu\text{g}/\text{l}$  *glyphosate*-equivalent treatment

Notes: 1 – June 17, 2 – July 1, 3 – July 15, 4 – July 29

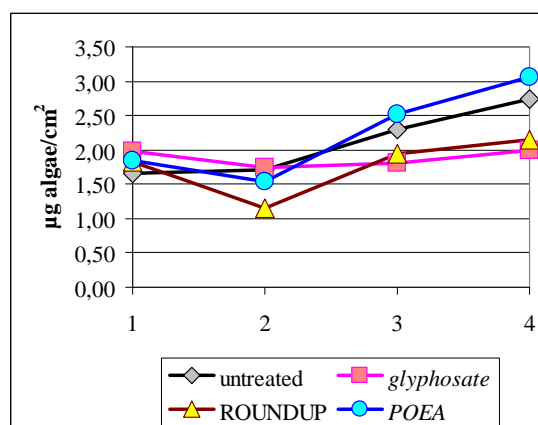


Fig. 6 Diatom biofilm originated from River Danube after 100  $\mu\text{g}/\text{l}$  *glyphosate*-equivalent treatment

Notes: 1 – June 17, 2 – July 1, 3 – July 15, 4 – July 29

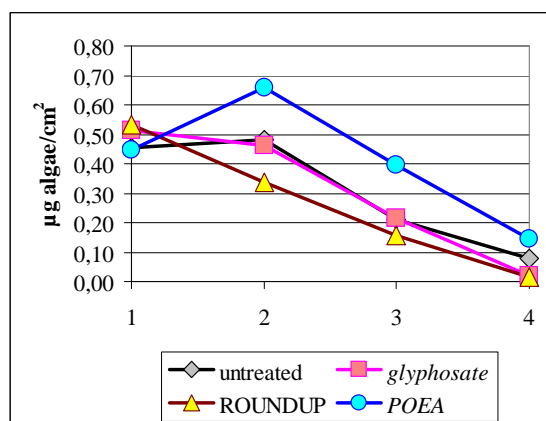


Fig. 7 Cyanobacterial biofilm originated from Lake Balaton after 100 µg/l *glyphosate*-equivalent treatment

Notes: 1 – June 17, 2 – July 1, 3 – July 15, 4 – July 29

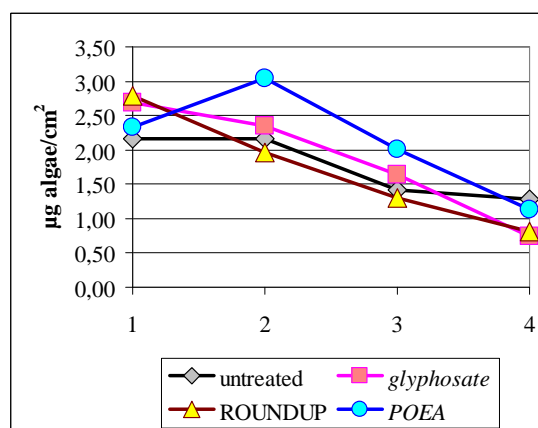


Fig. 8 Diatom biofilm originated from Lake Balaton after 100 µg/ml *glyphosate*-equivalent treatment

Notes: 1 – June 17, 2 – July 1, 3 – July 15, 4 – July 29

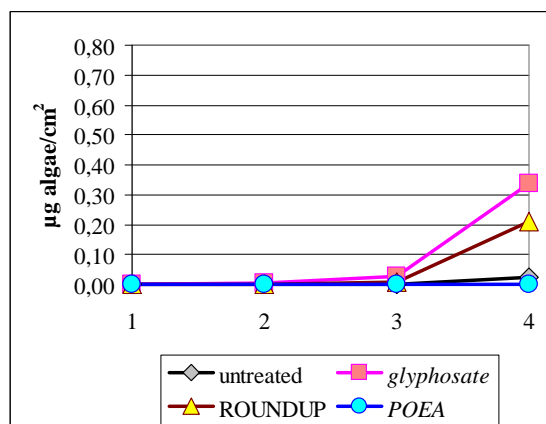


Fig. 9 Green algal biofilm originated from River Danube after 100 µg/l *glyphosate*-equivalent treatment

Notes: 1 – June 17, 2 – July 1, 3 – July 15, 4 – July 29

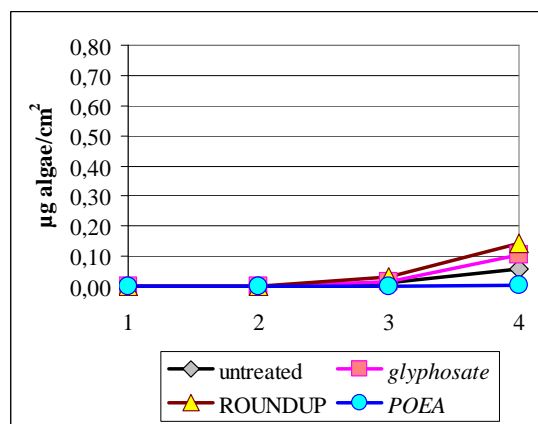


Fig. 10 Green algal biofilm originated from Lake Balaton after 100 µg/ml *glyphosate*-equivalent treatment

Notes: 1 – June 17, 2 – July 1, 3 – July 15, 4 – July 2

## Conclusions

In 6 weeks, homogeneous biofilms were formed on the glass substrates fixed to the AKK-1<sup>®</sup> carrier buoy, and mainly consisted of diatom algae species. Under laboratory conditions (water changed weekly with the same quality as at the original location of the buoy) the biofilms from River Danube adapted well, and the untreated control units continuously thrived. In contrast the biofilm from Lake Balaton (with rich invertebrate fauna including arthropods and worm species) gradually perished within 10 weeks. Identification of the algae species in the various communities with light- and electron microscopy is in progress.

The worldwide detectable water pollution by *glyphosate* can modify the structure of the algal community in biofilms. In biofilms originated from River Danube the filamentous green algae species were integrated into the place of *glyphosate*-sensitive cyanobacterial and diatom algae species. Individual toxicity of surfactant *POEA* was not detectable.

### Acknowledgements

Research was carried out within projects *K109865* by the Hungarian Scientific Research Fund (OTKA) and *AD 002* by the Ministry of Agriculture. The authors thank Gyula Záray *DSc*, Pál Hofmann (Eötvös Loránd University, Green Island), János Győri *PhD*, Géza Dobos (Balaton Limnological Institute, Centre for Ecological Research, HAS, Tihany) for the outplacement of the buoy and Balázs Magyarósy, Dániel Takács and Judit Juracsek for technical support.

### References

- [1] T. Katagi, *Rev. Environ. Contam. Toxicol.* 194 (2008) 71-177.
- [2] European Parliament and Council, *Offic. J. Eur. Comm. L* 104 (2004) 1-35.
- [3] M.T.K. Tsui, L.M. Chu, *Chemosphere*. 52 (2003) 1189-1197.
- [4] I. Székács, Á. Fejes, Sz. Klátyik, E. Takács, D. Patkó, J. Pomóthy, M. Mörtl, R. Horváth, E. Madarász, B. Darvas, A. Székács, *Internat. J. Biol., Vet. Food Engineer.* 87 (2014) 213-218.
- [5] R. Mesnage, N. Defrage, J.S. Vendômois, G.E. Séralini, *Biomed. Res. Int.* (2014) 179691
- [6] J.M. Brausch, P.N. Smith, *Arch. Environ. Contamin. Toxicol.* 52 (2007) 217-221.
- [7] W.G. Characklis, K.C. Marshall (Eds.), *Biofilms*, John Wiley & Sons, New York (1990) p. 135.
- [8] K. Kröpfel, P. Vladár, K. Szabó, É. Ács, A.K. Borsodi, Sz. Szikora, S. Caroli, Gy. Záray, *Environ. Poll.* 144 (2006) 626-631.
- [9] M. Mörtl, Gy. Németh, J. Juracsek, B. Darvas, L. Kamp, F. Rubio, A. Székács, *Microchem. J.* 107 (2013) 143-151.
- [10] E.A. Warnemuende, J.P. Patterson, D.R. Smith, C.-H. Huang, *Soil Till. Res.* 95 (2007) 19-26.
- [11] W.M. Edwards, G.B. Triplett, R.M. Kramer, *J. Environ. Qual.* 9 (1980) 661-665.



## Waste Water Treatment by Iron Nanoparticles Prepared by Pulsed Electrochemical Deposition

Éva Fazakas, Mátyás –Karácsony Zsuzsanna, Mónika Furkó

Bay Zoltán Nonprofit Ltd. for Applied Research, 1116 Budapest, Fehérvári út 130., Hungary  
Corresponding author: [eva.fazakas@bayzoltan.hu](mailto:eva.fazakas@bayzoltan.hu)

### Abstract

Recent industrial and urban activities have led to elevated concentrations of a wide range of contaminants in groundwater and wastewater, which affect the health of millions of people worldwide. In recent years, the use of zero-valent iron (ZVI) for the treatment of toxic contaminants in groundwater and wastewater has received wide attention and encouraging treatment efficiencies have been documented. In the present work, nanoscale iron was prepared by pulse electrodeposition of nano iron by chemical reduction of iron chloride and iron sulfate. Our research focuses on iron nanoparticles preparation and its use for wastewater treatment.

### Introduction

Various technologies are currently available to remove arsenic from waste water, such as ion exchange [1], coagulation (coprecipitation) [2], reverse osmosis [3], bioremediation [4], and adsorption [6]. Adsorption is a common practice for arsenic removal from waste water due to technological and cost advantages. Because of their high affinity for arsenite (As(III)) and arsenate (As(V)), elemental iron and iron (hydr)oxides are widely applied as the adsorbents for arsenic removal [5], [6] and [7]. Nano iron powders have been used in permeable reactive barriers for intercepting arsenic plumes in contaminated groundwater [8] or added to household filters for arsenic removal in developing nations [9]. Nanoscale iron (NSI) was recently reported as an ideal candidate for *in situ* remediation of arsenic contaminated groundwater [10] and [11]. It can also be a promising material for arsenic removal from wastewater because of its large active surface area and high arsenic adsorption capacity.

All described properties of Fe (iron) nanoparticles can be even used for decomposition of pollutants contained in the waste water, mainly for treatment of industrial sewage and hutch water. The usage of nanoiron can represent a significant qualitative step in the classical technologies of water treatment including drinking water. NSI can be also used for a reduction of the content of heavy metals, nitrates and phosphates in the drinking water.

Nanotechnology has widespread application potential and offers also the possibility of an efficient removal of pollutants and germs in the area of wastewater treatment. The objectives of this study were to prepare NSI by pulse electrodeposition and to test its performance for efficient removal of pollutants from the wastewater. Electrochemical deposition is a cost effective, competitive method, which allows control over composition and microstructure of the powder.

## Experimental

### Synthesis of nano-iron powder

Iron nanoparticles were produced by pulse electrodeposition. In pulse electrodeposition a D.C. current is applied for a short period time,  $t_{on}$ , that is followed by a period of time when no current is applied,  $t_{off}$ . Typical values for  $t_{on}$ , and  $t_{off}$  are between 5 and 200 ms and between 1 and 10 ms respectively. Through the use of a high current density as well as some grain growth inhibitors, such as saccharine, it is possible to increase the nucleation rate and reduce grain growth.

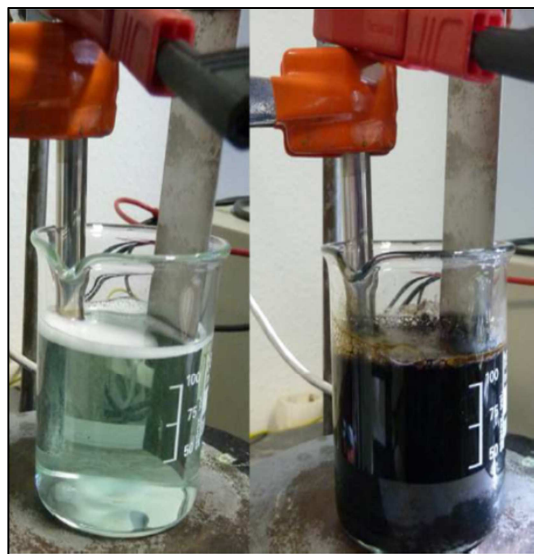


Fig1. Pulse electrodeposition of nano iron.

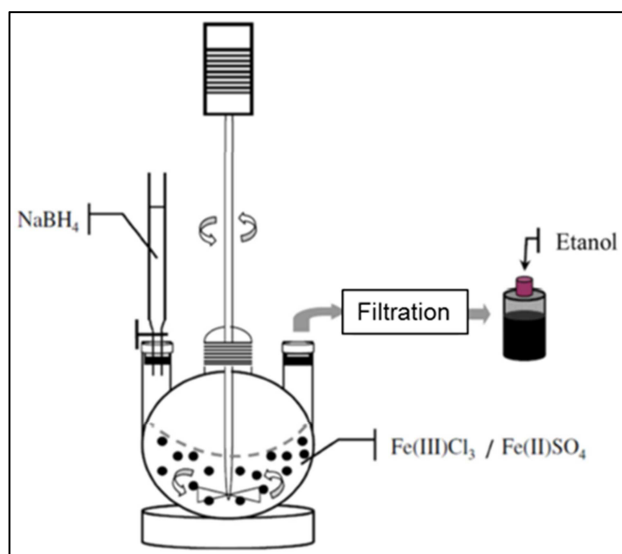
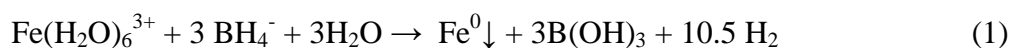


Fig. 2. Schematic figure of nano iron preparation.



The structure of the materials prepared was investigated using X-ray powder diffraction using Co  $K_\alpha$  radiation and with a highresolution SEM from JEOLJSM-5600LV.

As mentioned, the bath composition for the Fe electrodeposition was composed mainly of:

Composition	$\text{g} \cdot \text{dm}^{-3}$
boric acid	30,9
L-ascorbic acid	17,6
ammonium sulfate	39,6
Na (II) sulfate	2
magnesium sulfate·7H <sub>2</sub> O	123,24 (0,5M)
iron (II) -chloride·4H <sub>2</sub> O	49,7
iron (II) -sulfate·7H <sub>2</sub> O	208,5

Sacharin  $0.3 \text{ g} \cdot \text{dm}^{-3}$  and magnesium sulfate ( $\text{MgSO}_4$ ) between 0 and 0.5M was added as a grain refining agent. The temperature of the solution was  $25^\circ\text{C}$  and the pH varied from 3.5 to 6.0. Pulse current was between 10 and 20mA. All cases deposition were made on titanium cathode in order to facilitate their removal from the substrate which allows to perform experiments on self supported samples. One should also mention that the more additives are added to the solutions the larger is the contamination problem of the samples. For this reason, most of the experiments were done with the lowest amount of additive as possible.

## Results and discussion

Pulse current electrodeposition of nano-Fe was carried out to investigate the effect of  $\text{MgSO}_4$  on the microstructure and the reactivity of the electrodeposited films. Electrodeposition without in  $\text{MgSO}_4$  electrolyte gave smaller grain size than with it.

XRD results in Fig.3. demonstrated that no other component were present within the Fe1 and Fe2 samples. We used  $\text{MgSO}_4$  as a grain refining agent. From the X-ray diffractogram was calculated the grain size of the NSI using Debye-Scherrer equation:

$$\tau = \frac{K \cdot \lambda_{\text{Co}}}{\beta \cdot \cos \theta} \quad (3)$$

where,  $\tau$  is the grain size;  $K$  is a dimensionless shape factor, with a value 0.9,  $\lambda_{\text{Co}}$  is the X-ray wavelength ( $1.788897 \text{ \AA}$ );  $\beta$  is the line broadening at half and  $\theta$  is the Bragg angle.

From the calculation turns out that the Fe1 grain size is about 11 nm and in the case of Fe2 samples it was 7-8 nm.

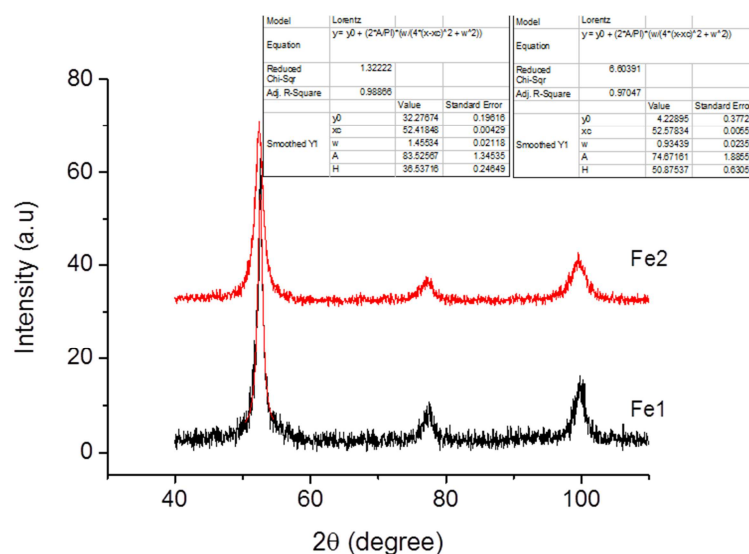


Fig.3. X-ray diffractogram of the NSI samples prepared without and with added  $\text{MgSO}_4$ .

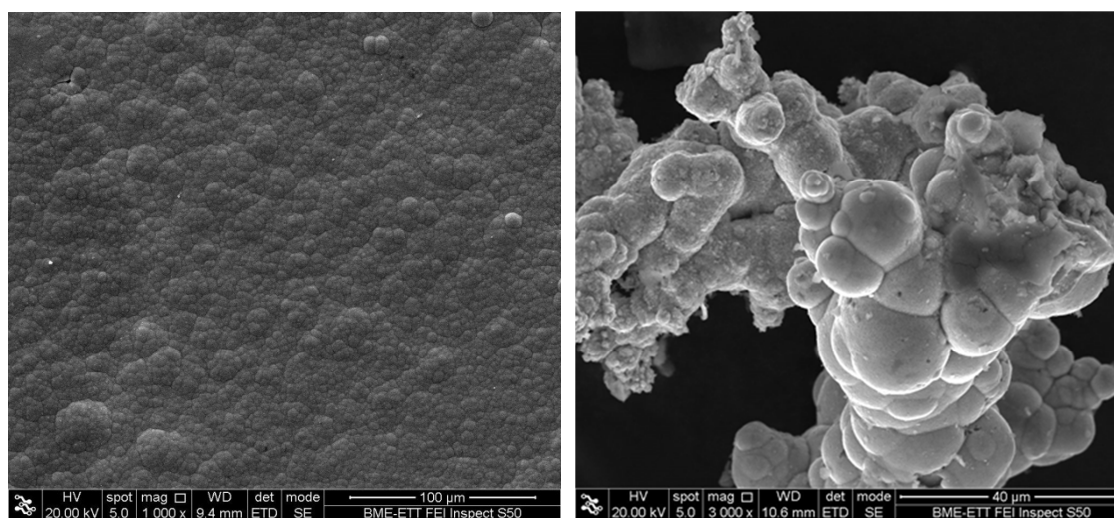


Fig.4. SEM results of the nano-scale Fe1 powder without added  $\text{MgSO}_4$ .

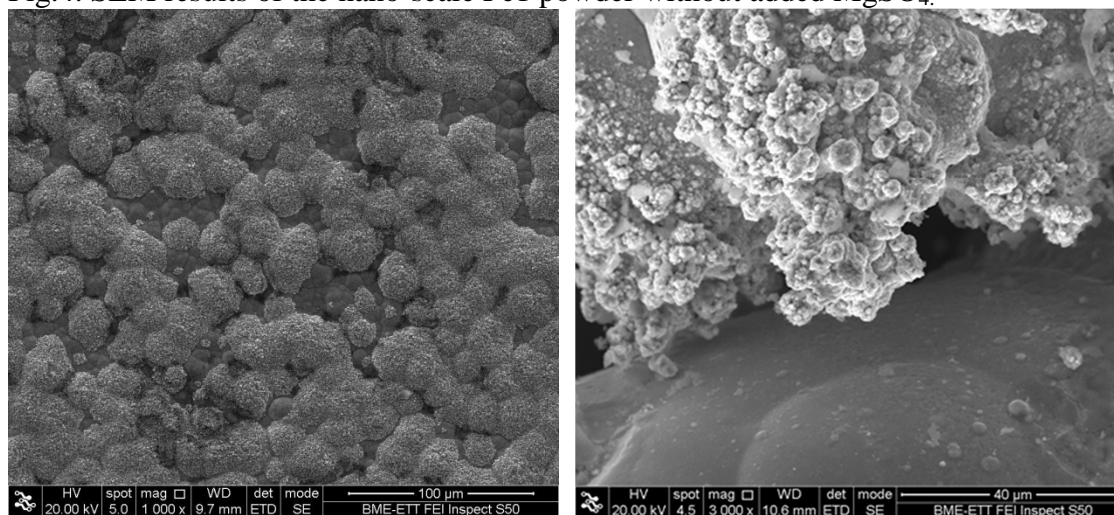


Fig. 5. SEM results of the nano-scale Fe2 powder with added  $\text{MgSO}_4$ .

The surface morphology of the nano-Fe was characterized with SEM (scanning electron microscope). The surface morphology changed as rough surface, where the concentration of  $\text{MgSO}_4$  increased. The reactivity of active surface of nano-Fe increasing as a function of decreasing of grain size in presence of  $\text{MgSO}_4$ .

### Conclusion

There is an increasing interest in the use of NSI for the removal of contaminants from groundwater and wastewater. NSI has been successfully applied for the remediation/treatment of groundwater and wastewater contaminated with chlorinated organic compounds, nitroaromatic compounds, arsenic, heavy metals, nitrate, dyes, and phenol. The review shows that there is a need for more detailed systematic studies on contaminants removal mechanism and also some technical improvements in utilizing NSI.

### Acknowledgement

This work was supported by TÉT\_13\_DST Indo-Hungarian (KTIA-DST) R & D & I Cooperation Programme with identification number of TÉT\_13\_DST-1-2013-0004.

## **References**

- [1] J. Kim, M.M. Benjamin, *Water Res.* 38 (2004) 2053–2062.
- [2] A. Zouboulis, I. Katsoyiannis, *Sep. Sci. Technol.* 37 (2002) 2859–2873.
- [3] R.Y. Ning, Arsenic removal by reverse osmosis, *Desalination* 143 (2002) 237–241.
- [4] T.M. Gihring, G.K. Druschel, R.B. Mccleskey, R.J. Hamers, J.F. Banfield, *Environ. Sci. Technol.* 35 (2001) 3857–3862.
- [5] Q.L. Zhang, Y.C. Lin, X. Chen, N.Y. Gao, *J. Hazard. Mater.* 148 (2007) 671–678.
- [6] X. Guo, F. Chen, *Environ. Sci. Technol.* 39 (2005) 6808–6818.
- [7] W. Driehaus, M. Jekel, U. Hildebrandt, *J. Water SRT Aquat.* 47 (1998) 30–35.
- [8] X.H. Guan, J. Wang, C.C. Chusuei, *J. Hazard. Mater.* 156 (2008) 178–185.
- [9] S. Bang, G.P. Korfiatis, X. Meng, *J. Hazard. Mater.* 121 (2005) 61–67.
- [10] O.X. Leupin, S.J. Hug, *Water Res.* 39 (2005) 1729–1740.
- [11] S.R. Kanel, B. Manning, L. Charlet, H. Choi, *Environ. Sci. Technol.* 39 (2005) 1291–1298.



## Hydroxyl Radical Reaction with Monuron

Viktória Mile<sup>1</sup>, Ildikó Harsányi<sup>1</sup>, Krisztina Kovács<sup>1</sup>, Tamás Földes<sup>2</sup>, Imre Pápai<sup>2</sup>,  
Erzsébet Takács<sup>1</sup>, László Wojnárovits<sup>1</sup>

<sup>1</sup>*Institute for Energy Security and Environmental Safety, Centre for Energy Research,  
Hungarian Academy of Sciences, Budapest, Hungary*

<sup>2</sup>*Institute of Organic Chemistry, Research Centre for Natural Sciences, Hungarian Academy  
of Sciences, Budapest, Hungary  
e-mail: mile.viktoria@energia.mta.hu*

### Abstract

On the example of monuron, aromatic ring hydroxylation reactions were studied by Density Functional Theory calculations. In order to model the aqueous media the Solvation Model Density technique was used. Based on the relatively low activation energies of hydroxyl radical additions to *ipso*-, *ortho*- and *meta*-positions of the benzene ring (19-42 kJ mol<sup>-1</sup>) and also the Gibbs free energies ((-16)-(-41) kJ mol<sup>-1</sup>) of reactions, hydroxyl radical addition to any of these positions may take place. However, according to the calculations the *ortho*-addition is preferred in agreement with the experimental results. In these reactions hydroxycyclohexadienyl type radicals form. The first step in the mechanism of *para*-reaction is OH/Cl substitution without cyclohexadienyl type intermediate. The results of theoretical calculations here are also in agreement with the experimental results which show that the hydroxyl radical reaction with monuron in 40% results in Cl elimination.

### Introduction

In Advanced Oxidation Processes hydroxyl radicals are the reactive intermediates which induce the decomposition of toxic organic compounds present in water matrices. Previously, the degradation of monuron (3-(4-chlorophenyl)-1,1-dimethylurea) herbicide in dilute aqueous solution (1×10<sup>-4</sup> mol/dm<sup>3</sup>) was studied in our laboratory. Based on the experimental results, the main process is the reaction between monuron and •OH forming hydroxycyclohexadienyl radical.

### Experimental

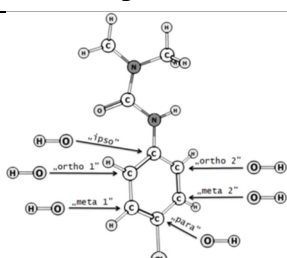
The calculations were performed by using Density Functional Theory (DFT) [1]. Becke's three parameter hybrid functional was used with the Lee-Yang-Parr correlation one, generally known as B3LYP [2] The standard 6-311G++(d,p) [3-4] basis set was applied for optimizing the structure, which contains diffuse [5] and polarization [6] functions to improve the description of the hydrogen bonds because of presence of urea-group. In order to model the aqueous media we applied the Solvation Model Density (SMD) technique [7]. First, the optimized geometry of the isolated compounds was determined, then the complexes were put together manually from the two optimized geometries. To determine the structures of the transition state and the product, the bond length between C (given position) and •OH was changed in equidistant steps and at each point a constrained geometry optimization was carried out. The structure at the maximum of the energy curve is probably very close to the real transition state and the geometry at energies minima correspond to addition complex. In all cases, the nature of the extrema was verified through frequency calculations. The electronic energy was refined by single-point energy calculations at the B3LYP/6-



311++G(3df,3pd) level [3-4]. All energies are reported at 298.25 K. The calculations were performed with the Gaussian program package [8].

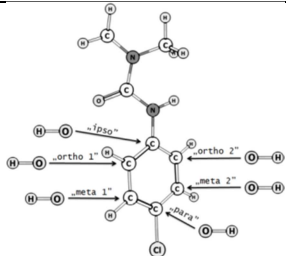
## Results and discussion

The Gibbs energies of the reactions ( $\Delta_r G$ ) and activation energies ( $E_a$ ) of the aromatic ring hydroxylation are collected in Table 1 and Table 2. The data in Table 1 were obtained without water model (i.e. gas phase)) and Table 2 shows the data with using SMD water model. Both using water model and without the applied water model  $\Delta_r G$  is significantly different in case of *para*-reaction than in the other reactions. The *meta* addition path is energetically less favourable than the *ipso*- and the *ortho1*- and the *ortho2*-hydroxylation due to the effect of electron donating groups. The Gibbs free energies of the reactions are somewhat higher in presence of water except for *para* reaction where the energy is lower due to solvation energy of chlorine.

Possible positions of attack.	Position	$\Delta_r G / \text{kJmol}^{-1}$	$E_a / \text{kJmol}^{-1}$	$d_1 / \text{\AA}$	$d_2 / \text{\AA}$
	<i>ipso</i>	-30.15	42.27	2.006	1.417
	<i>ortho 1</i>	-35.46	31.51	2.002	1.436
	<i>ortho 2</i>	-40.32	16.06	2.117	1.456
	<i>meta 1</i>	-19.21	38.76	2.000	1.445
	<i>meta 2</i>	-20.78	32.05	2.024	1.448
	<i>para</i>	-155.91	39.49	2.069	1.259

**Table 1.** Thermodynamic and structural properties of hydroxyl radical reactions with the aromatic ring of monuron at 298.25 K in gas phase (without applied water model):  $\Delta_r G$  Gibbs free energy,  $E_a$  activation energy,  $d_1$  and  $d_2$  C-•O distances in the transition state and in the product, respectively.

Activation energies without using water model are between 30-42  $\text{kJ mol}^{-1}$  except for *ortho2* reaction, where the activation energy of hydroxylation is significantly lower. In aqueous media  $E_a$ 's are somewhat lower (20-30  $\text{kJ mol}^{-1}$ ). In the applied SMD at the transition state of *ortho 2* has not been found yet. Further calculations are in progress in order to find the TS or prove this reaction is barrierless.

Possible positions of attack.	Position	$\Delta_r G / \text{kJmol}^{-1}$	$E_a / \text{kJmol}^{-1}$	$d_1 / \text{\AA}$	$d_2 / \text{\AA}$
	<i>ipso</i>	in progress	29.70	2.025	in progress
	<i>ortho 1</i>	-30.31	19.55	2.076	1.457
	<i>ortho 2</i>	-36.53	in progress		1.462
	<i>meta 1</i>	-18.93	30.03	2.076	1.461
	<i>meta 2</i>	-16.10	29.92	2.118	1.462
	<i>para</i>	-179.64	27.59	2.152	1.318

**Table 2.** Thermodynamic and structural properties of hydroxyl radical reactions with the aromatic ring of monuron at 298.25 K in aqueous media (using SMD water model):  $\Delta_r G$

Gibbs free energy,  $E_a$  activation energy,  $d_1$  and  $d_2$  C-•O distances in the transition state and in the product, respectively.

The distance of  $C_{\text{ring}}-\text{O}_{\text{radical}}$  of transition state of *ortho*2-hydroxycyclohexadienyl radical differs from the other cases in gas phase. This process has lower activation energy. In the products of *ortho*1-cases the  $C_{\text{ring}}-\text{O}_{\text{radical}}$  lengths are somewhat shorter because of developed hydrogen bond both in water and in gas phase. The effect of hydrogen bond in TS can be observed just in *ipso*-reaction in aqueous medium. The C-•O bond lengths in cyclohexadienyl radicals and in their TS are shorter in gas phase than in aqueous medium.

In the *para*-case, the reason of the different value of  $\Delta_r G$ , is the changer of reaction mechanism from radical addition to dechlorination reaction. It is worth to mention that the bond lengths of  $C_{\text{ring}}-\text{O}_{\text{radical}}$  of end product of *para* reaction are significantly different. Without using water model the end product is phenoxy type radical, i.e. the released chlorine atom tear down the hydrogen atom from the •OH radical. In the applied water model (after the Cl/OH substitution) the hydroxylated molecule is stabilized by solvation. The attack of the •OH radical to *para*-position is shown in Figure 1. Experiments suggest that the phenoxy radicals are created during the attack of the •OH radical in aqueous medium. In order to better understand the exact mechanism further calculations are necessary paying special attention to the effects of water.

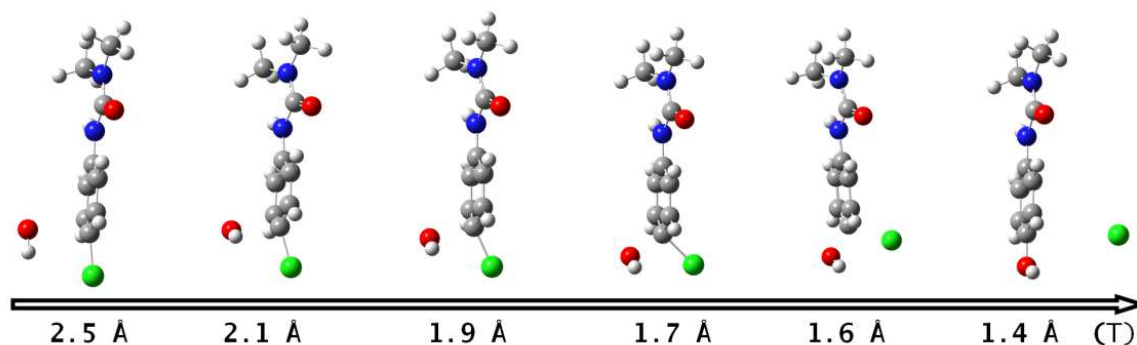


**Figure 1.** Conformational changes during hydroxyl radical reaction in *para* case. In the lower part of the figure the  $C_{\text{ring}}-\text{O}_{\text{radical}}$  distances are shown in Å units.

## Conclusion

The aromatic ring hydroxylations were studied by quantum chemical calculations. In the *ipso*-, *ortho*- and *meta*-reaction simple addition with cyclohexadienyl type radical formation takes place. In case of *para* hydroxylation reaction OH/Cl substitution occurs without cyclohexadienyl type intermediate. Solvation plays a very important role in determining the directions of reactions.

## Acknowledgements

The authors thank Hungarian Science Foundation (OTKA, NK 105802), the Swiss-Hungarian project (No SH7/2/14) and International Atomic Energy Agency (Contract No. 16485 and HUN8008) for the support.

## References

- [1] R. G. Parr és W. Yang, *Density-functional theory of atoms and molecules* (Oxford Univ. Press, Oxford, 1989)
- [2] D. Becke, J. "A new mixing of Hartree-Fock and local density-functional theories" *Chem. Phys.* **98**, 5648 (1993).
- [3] A. D. McLean és G. S. Chandler, *J. Chem. Phys.*, **72** (1980) 5639
- [4] R. Krishnan, J. S. Binkley, R. Seeger, és J. A. Pople, *J. Chem. Phys.*, **72** (1980) 650
- [5] M. J. Frisch, J. A. Pople, és J. S. Binkley, *J. Chem. Phys.*, **80** (1984) 3265
- [6] T. Clark, J. Chandrasekhar, G. W. Spitznagel, és P. v. R. Schleyer, *J. Comp. Chem.*, **4** (1983) 294
- [7] A. V. Marenich, C. J. Cramer, and D. G. Truhlar, "Universal solvation model based on solute electron density and a continuum model of the solvent defined by the bulk dielectric constant and atomic surface tensions," *J. Phys. Chem. B*, **113** (2009) 6378-96.
- [8] Gaussian 09, Revision A.02,  
M. J. Frisch, G. W. Trucks, H. B. Schlegel, G. E. Scuseria, M. A. Robb, J. R. Cheeseman, G. Scalmani, V. Barone, B. Mennucci, G. A. Petersson, H. Nakatsuji, M. Caricato, X. Li, H. P. Hratchian, A. F. Izmaylov, J. Bloino, G. Zheng, J. L. Sonnenberg, M. Hada, M. Ehara, K. Toyota, R. Fukuda, J. Hasegawa, M. Ishida, T. Nakajima, Y. Honda, O. Kitao, H. Nakai, T. Vreven, J. A. Montgomery, Jr., J. E. Peralta, F. Ogliaro, M. Bearpark, J. J. Heyd, E. Brothers, K. N. Kudin, V. N. Staroverov, R. Kobayashi, J. Normand, K. Raghavachari, A. Rendell, J. C. Burant, S. S. Iyengar, J. Tomasi, M. Cossi, N. Rega, J. M. Millam, M. Klene, J. E. Knox, J. B. Cross, V. Bakken, C. Adamo, J. Jaramillo, R. Gomperts, R. E. Stratmann, O. Yazyev, A. J. Austin, R. Cammi, C. Pomelli, J. W. Ochterski, R. L. Martin, K. Morokuma, V. G. Zakrzewski, G. A. Voth, P. Salvador, J. J. Dannenberg, S. Dapprich, A. D. Daniels, O. Farkas, J. B. Foresman, J. V. Ortiz, J. Cioslowski, and D. J. Fox, Gaussian, Inc., Wallingford CT, 2009.

## Effect of Salinity Stress on Ion Accumulation and on the Photosynthetic Activity of a New Energy Plant, *Phalaris arundinacea* Cultivars

Péter Poór<sup>1\*</sup>, Attila Ördög<sup>1</sup>, Barnabás Wodala<sup>1</sup>, Péter Borbély<sup>1</sup>, Ionel Samfira<sup>2</sup>, Monica Butnariu<sup>2</sup>, Dóra Hegedűs<sup>1</sup>, Katalin Szabó<sup>1</sup>, Attila Pécsváradi, Irma Tari<sup>1</sup>:

<sup>1</sup>Department of Plant Biology, University of Szeged, 6726 Szeged, Közép fasor 52, Hungary<sub>1</sub>

<sup>2</sup>Banat University of Agricultural Sciences and Veterinary Medicine "Regele Mihai I al Romaniei", Calea Aradului 119, Timișoara 300645, Romania<sub>2</sub>

e-mail: poorpeti@bio.u-szeged.hu

### Abstract

Reed canarygrass (*Phalaris arundinacea*) is a good candidate for bioenergy production in Northern and Middle Europe. The crop is well-adapted to cold and drought stress but its resistance to high salinity has not been revealed in details. In this study the effects of 75 and 150 mM NaCl treatments were investigated on the ion accumulation, water potential changes and photosynthetic activity of three Romanian reed canarygrass genotypes, Tardin, Romanesti diverse and Timpuriu. Since cv. Tardin was able to maintain high K<sup>+</sup> level and relatively low Na<sup>+</sup> concentration in leaf tissues, high stomatal conductance and net CO<sub>2</sub> fixation rate under salt stress and as it could maintain the water potential of tissues at control level, this genotype can be defined as salt tolerant. Salt stress induced significant Na<sup>+</sup> accumulation, very low K<sup>+</sup>/Na<sup>+</sup> ratio, and severe reduction in stomatal conductance and photosynthetic activity in the leaf tissues of Timpuriu cultivar, which proved to be sensitive to high salinity.

### Introduction

Renewable energy is an important source of energy that reduces the dependence on fossil fuels and emission of greenhouse gases, thus, the use of biofuel feedstock has a great economic impact. There has been increasing interest in the use of perennial grasses as energy crops in Europe since the mid-1980s. The characteristics which make perennial grasses attractive for biomass production are their high yield potential, the high contents of lignin and cellulose of their biomass, and their generally anticipated positive environmental impact [1]. Among those indigenous grasses, which are characterized by regionally high biomass yields and which seem to offer good bioenergy characteristics, reed canarygrass (*Phalaris arundinacea*) was found to be a suitable candidate for Northern Europe [2]. Reed canarygrass belongs to the subfamily Pooideae of the Gramineae family. It is native to the temperate regions of Europe, including Middle Europe. Reed canarygrass displays a number of advantages, which can be exploited in Northern part of Europe. It is already adapted to short vegetation periods and low temperatures, seed establishment is possible, the biomass has good combustion quality and the plant has broad genetic variability [3].

*Phalaris arundinacea* is a perennial C3 species growing to 1.5-3 m at a fast rate. It can be cultivated in sandy, loamy and clay soils of broad pH range. Plants have a running root system and form an impenetrable ground cover [4].

Reed canarygrass is one of the main species used in the reed bed system for the water purification treatment of grey water and for pollution control of sewage effluent from municipal and industrial sources. It is one of the best grass species for poorly drained soils and tolerates flooding better than other cool-season grasses. Even though it naturally grows in wet places, it is nevertheless more drought resistant than many other grass species [3].

The content of major elements in reed canarygrass tissues shows considerable differences between different locations and genotypes. Moreover, photosynthetic activity and biomass production of various lines may also show considerable differences. The aim of our work was to reveal these differences after salt stress in photosynthetic activity, biomass production (biomass per one cm<sup>2</sup> leaf area) and ion accumulation of reed canarygrass lines originated in Romania.

## Experimental

The salt stress response of three *Phalaris arundinacea* cultivars, Tardin, Timpuriu and Romanesti diverse was investigated in our experiments. The plants were grown in 2.5 kg soil (Bioland Tőzegfeldolgozó Kft., Biatorbágy, Hungary) containing N (20 to 500 mg L<sup>-1</sup>), P<sub>2</sub>O<sub>5</sub> (200 to 500 mg L<sup>-1</sup>); K<sub>2</sub>O (300 to 600 mg L<sup>-1</sup>), white peat (50%, m/v), black peat (50% m/v), and CaCO<sub>3</sub> (2 kg m<sup>-3</sup>) at pH 7.0. The environmental conditions in the greenhouse were 12/12 h day/night cycle, 25/20 °C day/night temperature, 200 µmol m<sup>-2</sup> s<sup>-1</sup> light intensity and 55 to 60% relative humidity. After 12 weeks of pre-culture, the soil was irrigated two times a week with 300 mL of 75 and 150 mM NaCl (stressed plants) for 6 weeks and the control plants received the same irrigation with distilled water. Water potential of the tissues was measured with pressure chamber and the macroelements in plant samples were determined with XSeries II ICP-MS (Thermo Scientific, Bremen, Germany). Net photosynthetic rate (A, µmol fixed CO<sub>2</sub> m<sup>-2</sup> s<sup>-1</sup>) and stomatal conductance were measured on fully expanded leaves using a portable photosynthesis system (LI-6400, LI-COR, Inc.; Lincoln, NE), as described by Poór et al. [5].

## Results and discussion

Salinity is one of the major abiotic stresses, which reduces plant growth and productivity and can cause programmed cell death in the plant tissues by inducing strong ionic-, osmotic and oxidative stress [6]. Production of reactive oxygen species (ROS) and the failure of ROS-scavenging mechanisms caused by supraoptimal salt concentrations induce a decline in the photosynthetic activity and other biochemical reactions in the tissues, which lead to the degradation of proteins, lipids and DNA and to the decrease of the biomass [7; 8]. Salt tolerant genotypes are able to cope with the ionic stress caused by excess of Na<sup>+</sup> by activating Na<sup>+</sup> exclusion from the cytoplasm.

The K<sup>+</sup> and Na<sup>+</sup> content as well as K<sup>+</sup>/Na<sup>+</sup> ratios were very similar values in the control leaves of the three cultivars. The plants were able to maintain potassium contents but accumulated significantly more sodium when they were exposed to salt stress. However, high salinity evoked by 150 mM NaCl resulted in much higher accumulation of Na<sup>+</sup> in the leaf tissues, than medium salt stress, which was exceptionally high in cv. Timpuriu. This led to the reduction in K<sup>+</sup>/Na<sup>+</sup> ratios under increasing salt stress, but Timpuriu had the lowest ratio among the three genotypes (Table 1).

**Table 1.** Changes in the intracellular K<sup>+</sup> and Na<sup>+</sup> contents and the ratio of K<sup>+</sup>/Na<sup>+</sup> in the leaves of different *Phalaris* cultivars after exposure to 75 or 150 mM NaCl for six weeks.

Elements (mg gDW <sup>-1</sup> )	Treatments								
	Control			75 mM NaCl			150 mM NaCl		
	Tardin	Romanesti diverse	Timpuriu	Tardin	Romanesti diverse	Timpuriu	Tardin	Romanesti diverse	Timpuriu
K <sup>+</sup>	82.7 ± 4.7	76.1 ± 1.4	76.6 ± 2.6	98.1 ± 0.8*	65.0 ± 0.1***	77.0 ± 2.9 <sup>ns</sup>	70.8 ± 5.4*	87.9 ± 0.9*	74.5 ± 0.8 <sup>ns</sup>
Na <sup>+</sup>	1.7 ± 0.2	1.4 ± 0.0	1.7 ± 0.2	38.8 ± 0.2***	26.0 ± 0.2***	35.0 ± 3.8***	59.0 ± 4.5***	32.5 ± 0.0***	111.3 ± 1.1***
K <sup>+</sup> /Na <sup>+</sup>	48.3 ± 4.7	52.7 ± 0.7	46.6 ± 7.2	3.2 ± 0.7**	2.4 ± 0.0**	2.2 ± 0.1**	1.1 ± 0.0***	1.8 ± 0.8***	0.6 ± 0.0***

Results are the average  $\pm$  SE (n=5). \*, \*\*, \*\*\* indicate significance levels compared to the untreated control at  $P < 0.05$ , 0.01, 0.001, respectively in each time point (Student's t test; ns: not significant).

High salinity induces osmotic stress and a decrease in water potential ( $\Psi_w$ ) of treated tissues [9]. While cvs Tardin and Romanesti diverse could maintain  $\Psi_w$  under salt stress, Timpuriu exhibited a significant decline under high salinity, triggered by 150 mM NaCl (Fig 1A). Increasing salt concentrations induced the closure of stomata and resulted in significant decrease in stomatal conductance, which was most pronounced in Timpuriu cultivar (Fig 1C). Net  $\text{CO}_2$  fixation rate, which is a best indicator of biomass production [10], declined significantly in plants exposed to salt stress. Since control plants displayed different basic activities, the decline in the photosynthetic rate was less pronounced in cv Romanesti diverse and most severe in Timpuriu genotype (Fig 1D). As a result, specific leaf area was maintained during salt stress in Tardin genotype while the other two genotypes showed reduction in these parameters under salt stress (Fig 1B).

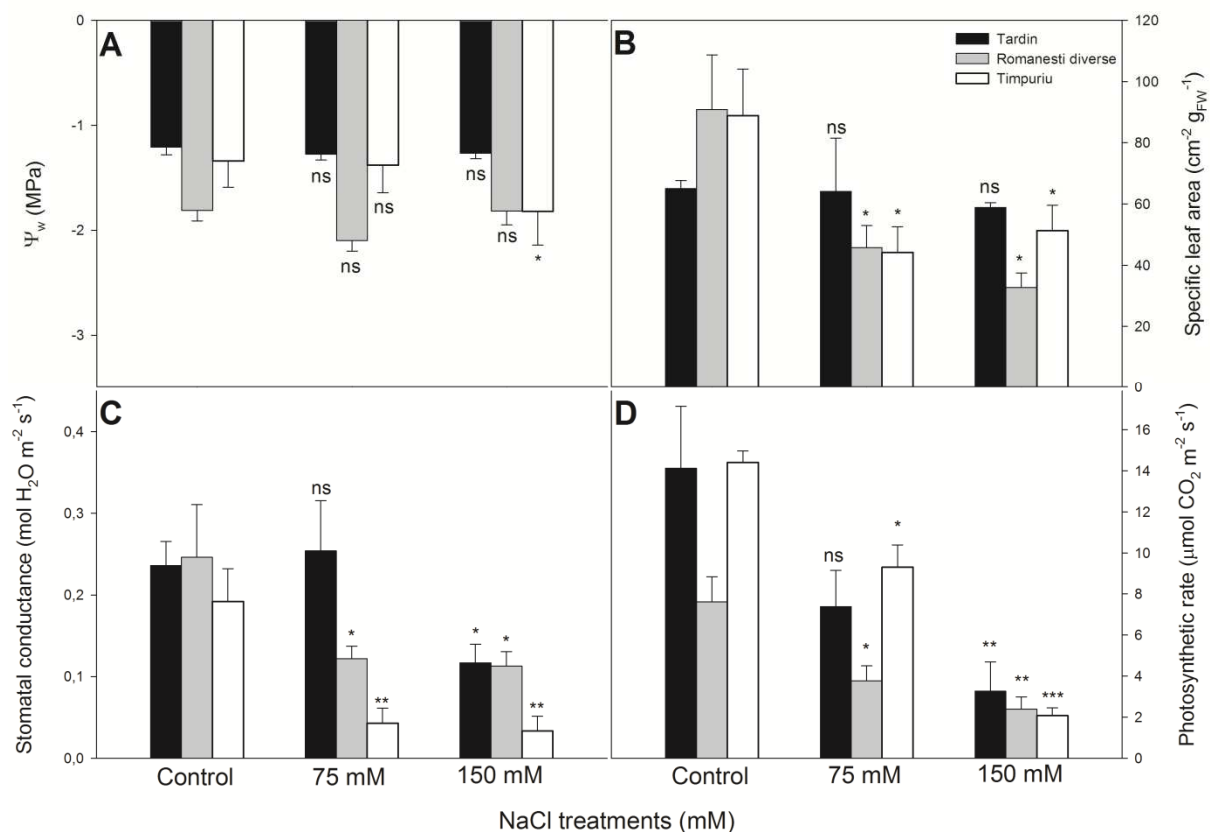


**Figure 1.** Changes in water potential (A), specific leaf area (B), stomatal conductance (C) and photosynthetic rate (D) in the leaf of different *Phalaris* cultivars after exposure to 75 or 150 mM NaCl for six weeks. Results are the average  $\pm$  SE (n=5). \*, \*\*, \*\*\* indicate significance levels compared to the untreated control at  $P < 0.05$ , 0.01, 0.001, respectively in each time point (Student's t test; ns: not significant).

## Conclusion

Salt stress resulted in higher  $\text{Na}^+$  levels and lower  $\text{K}^+/\text{Na}^+$  ratio in the leaf tissues of reed canarygrass genotypes, these parameters of Timpuriu cultivar overtopped the changes observed in cvs Tardin and Romanesti diverse.



On the basis of the photosynthetic parameters, stomatal conductance, water potential and specific leaf area changes we can conclude that cv. Tardin proved to be most tolerant to salinity stress among the three genotypes of reed canarygrass, while cv. Timpuriu was the most sensitive cultivar.

### Acknowledgements

This work was supported by the projects named “TÁMOP-4.2.2.D-15/1/KONV-2015-0010 „Távérzékelési és zöldenergia témájú célzott komplex alapkutatási programok előkészítése, hálózatosodás és felkészülés nemzetközi programokban és kezdeményezésekben való részvételre” financed by the European Union and co-financed by the European Regional Fund (www.nfu.hu, www.okmt.hu). We thank Etelka Kozma Bécs and Erzsébet Porkoláb for their excellent technical assistance. We also thank Professor Ionel Samfira, Timișoara, Romania for providing reed canarygrass lines.

### References

- [1] Tari, I., Laskay, G., Takacs, Z., Poor, P. (2013). Response of Sorghum to abiotic stresses: a review. *Journal of Agronomy and Crop Science*, 199(4), 264-274.
- [2] Andersson, B. (2000). Prospects for breeding and supply of plant material. In: Bioenergy Workshop Report: Renewable Energy and Sustainable Agriculture “The Impact of Perennial Grass Research”. Brussels: European Commission, 2000. p. 50–52.
- [3] Lewandowski, I., Scurlock, J. M., Lindvall, E., Christou, M. (2003). The development and current status of perennial rhizomatous grasses as energy crops in the US and Europe. *Biomass and Bioenergy*, 25(4), 335-361.
- [4] Lyons, K.E., Randall, J., Robison, M., Morisawa, T., Rice, B., Team, G.I.S. (2010). *Phalaris arundinacea*. J. Randall, M. Robinson, T. Morisawa and B. Rice. Element Stewardship Abstracts. Global Species Invasive Team, The Nature Conservancy. See websites: <http://www.invasive.org/gist/esadocs/documnts/phaaru.pbf> and [http://wiki.bugwood.org/Phalaris\\_arundinacea](http://wiki.bugwood.org/Phalaris_arundinacea).
- [5] Poór, P., Ördög, A., Wodala, B., Tari, I. (2015). Effect of EDTA-assisted copper uptake on photosynthetic activity and biomass production of sweet sorghum. *Cereal Research Communications*, 43(4), DOI: 10.1556/0806.43.2015.028
- [6] Munns, R., Tester, M. (2008). Mechanisms of salinity tolerance. *Annual Reviews of Plant Biology* 59, 651-681.
- [7] Chaves, M. M., Flexas, J., Pinheiro, C. (2009). Photosynthesis under drought and salt stress: regulation mechanisms from whole plant to cell. *Annals of Botany*, 103(4), 551-560.
- [8] Cong, L. L., Zhang, X. Q., Li, Y. X., Cheng, K. K., Zhang, Y. W. (2012). Response of Reed Canary Grass to Salt Stress during Seed Germination and Vegetative Stage. In *Advanced Materials Research* (Vol. 518, pp. 5355-5362).
- [9] Zhu, J. K. (2001). Plant salt tolerance. *Trends in Plant Science*, 6(2), 66-71.
- [10] Zhou, X., Ge, Z.M., Kellomäki S., Wang, K.Y., Peltola, H., Martikainen, P. (2011). Effects of elevated CO<sub>2</sub> and temperature on leaf characteristics, photosynthesis and carbon storage in aboveground biomass of a boreal bioenergy crop (*Phalaris arundinacea* L.) under varying water regimes. *GCB Bioenergy*, 3(3), 223-234.

## Determination of Volatile Metabolite Markers Using HS-SPME-GC-MS Technique Illékony Anyagcseremarkerek Meghatározása HS-SPME-GC-MS Technikával

Loretta Juhász<sup>1</sup>, Dalma Radványi<sup>1\*</sup>, Zsuzsa Jókai<sup>1</sup>, Péter Fodor<sup>1</sup>

<sup>1</sup>Department of Applied Chemistry, Corvinus University of Budapest, H-1118 Budapest,  
Villányi út 29-43., Hungary  
e-mail: dalma.radvanyi@uni-corvinus.hu (radvanyi.dalma@gmail.com)

### Abstract

In our study, headspace solid-phase microextraction coupled with gas chromatography–mass spectrometry (HS-SPME-GC-MS) technique was used to analyse microbial volatile organic compounds (MVOC's) of a mushroom disease-related microorganism: *Trichoderma aggressivum*. Its volatile metabolite markers were monitored and then identified. To make reliable identification results, different manual correction steps were implemented into the evaluation process (depending on the compound intensity or on the rate of compound coelution). Identification steps were the follows: background subtraction then manual deconvolution. In some cases, compounds' molecular ion appeared on the mass spectra, which molecular ion's  $m/z$  value was also used for the identification. Moreover retention index (RI) of the evaluated compound was also calculated then compared to the RI values found in the literature and WebBooks.

### Bevezetés

A gázkromatográfia széles körben alkalmazott módszer a komplex illékony és fél-illékony minták elemzésére. Az élelmiszerminták gázkromatográfiás méréséhez történő előkészítés általában hosszú és munkagényes folyamat, magába foglalva a homogenizálást, többszöri extrakciót, centrifugálást és egyéb előkészítési műveleteket. Az elmúlt 15-20 évben ezért megnövekedett az igény a gyorsabb GC-s módszerekre. Ezen igények és az egyre inkább elterjedő oldószermentes vizsgálatokra való törekvés hívta életre a HS-SPME-GC-MS (Gőztér analízis szilárd fázisú mikroextrakció gázkromatográfia és tömegspektrométeres analízátor kapcsolt rendszer) kapcsolt rendszer működtetését.

A gőztér analízishez használt SPME eszköz kifejlesztése Arthur és Pawliszyn nevéhez fűződik [1]. A mintavételhez egy kvarcüveg szál külsejét vonják be a megfelelő állófázissal (szorbens réteggel). A vizsgálandó komponens extrahálása és koncentrációja közvetlenül erre a szálbevonatra történik. Ezt követően a GC injektorában megtörténik a deszorpció, és az extrahált komponensek elválasztásra kerülnek. A technika nagy előnye, hogy oldószermentes, alkalmazásával idő és költség takarítható meg azáltal, hogy direkt mintavétellel mérhetőek az illékony komponensek a gőztérből [2, 3].

Kezdetben a SPME mintavételi módszert illékony szerves vegyületek (VOCs) meghatározására használták környezeti mintákból. Ma már a technikát a biogyógyászat területén, az élelmiszerelemzésben, továbbá kevésbé illékony vegyületek meghatározására is alkalmazzák [3]. Számos kutatás irányult már különböző mikrobiális illékony vegyületek (MVOCs) vizsgálatára is [5,6]. Kluger és társai [7] szintén vizsgáltak fonalas gombafajok által termelt MVOC vegyületeket HS-SPME-GC-MS technikával. A kiértékelés és vegyület azonosítás során a komponens LTPRI (lineáris hőmérsékletprogram mellett számolt retenciós index) értékeit és a tömegspektrum vizsgálatát vették alapul. Az LTPRI meghatározásához alkán homológ sort használtak, majd ennek segítségével számolták ki az egyes

komponensekhez tartozó retenciós index értékeket, melyeket később az irodalomban lévő értékekkel vetettek össze. A komponensek tömegspektrumának vizsgálatához AMDIS kiértékelő programot használtak, mely segítségével elvégezték a dekonvolúciót, így egy zavaró fragmesektől mentes tömegspektrumhoz jutottak, majd az adott komponenszt azonosították.

### Célkitűzés

A gombatermesztésben a csiperke és más termesztett gombafajok zöldpenészes megbetegedésért felelős *Trichoderma aggressivum* kórokozó illékony anyagcseretermékeinek (MVOCs) vizsgálatát tűztük ki célul. A mikroorganizmus minél közelebbi megismerése érdekében célunk volt a gomba illékony anyagcseretermékeinek feltérképezése HS-SPME-GC-MS technikával, valamint adatbank segítségével a megjelenő komponensek azonosítása, ezáltal a kórokozó jelenlétének indikálása.

### Anyagok és módszerek

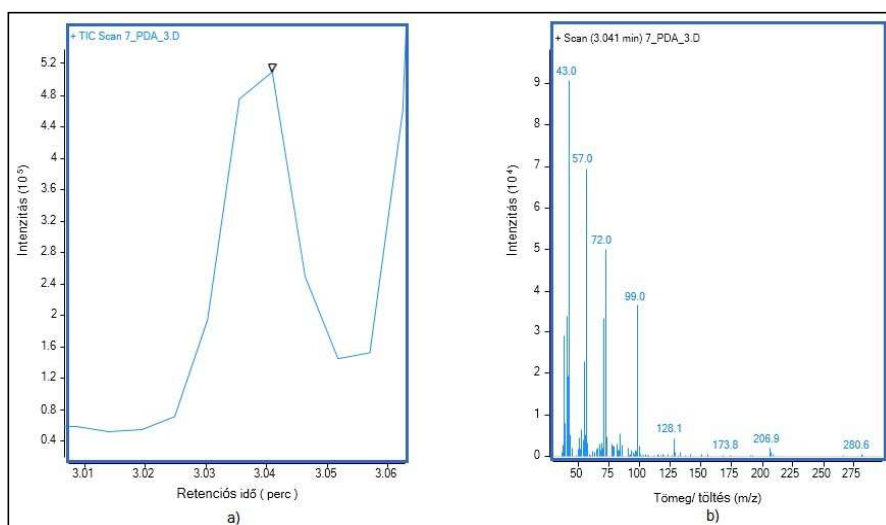
*Trichoderma aggressivum* spóra szuszpenzióból készítettünk leoltást PDA táptalajokra ( $2,4 \cdot 10^8$  spóra/ 500  $\mu$ L) 20 ml-es üvegcsébe, melyeket a leoltást követően légmentesen lezártunk. Ezután 24 °C-on 7 napon keresztül növekedett a penész, melyet naponta monitoroztunk. A méréseket három párhuzamosban és kontroll minta vizsgálatával végeztük.

Az extrakció 65  $\mu$ m Stable Flex<sup>TM</sup> PDMS/DVB bevonatú szállal történt napi egyszeri 15 perces mintavétellel majd 4 percig tartó deszorpcióval (250 °C). Agilent 6890 típusú gázkromatográf és 5975 C MSD típusú tömegspektrométer kapcsolt analitikai rendszert használtunk optimált paraméterek között [8]. Agilent Enhanced MSD ChemStation szoftvert alkalmaztunk a GC-MS paramétereinek felügyeléséhez. A kromatogramok teljeskörű kiértékelése (dekonvolúció, háttérkorrekció, integrálás...) Agilent Enhanced Data Analysis és Agilent MassHunter Qualitative Analysis B.06.00 szoftverek segítségével, míg az egyes komponensek azonosítása NIST (NIST 2011, Wiley 10<sup>th</sup> edition) könyvtár segítségével történt tömegspektrumuk alapján.

### Eredmények

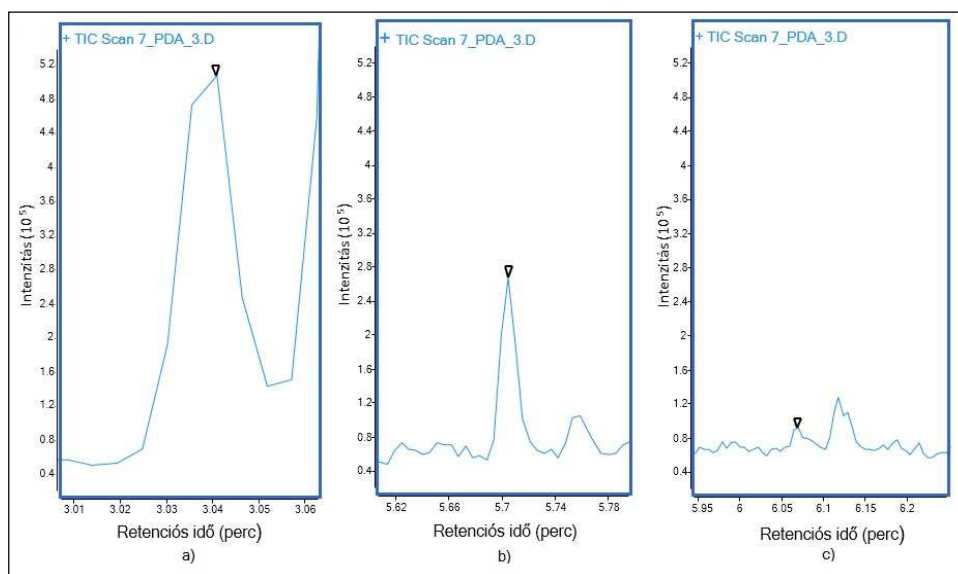
#### 1) Egyértelmű azonosítás

Az azonosítás során talált kellően nagy intenzitású csúcsok ( $4 \cdot 10^5$  intenzitás értéknél nagyobb) esetében a csúcs a háttértől kellőképp elvált, az alig zavart. Az adatbank (NIST) segítségével nagy találati eredménnyel jól azonosíthatóak ezek a komponensek. Ilyen egyértelmű vegyületként azonosítottuk az oktanont, 3,04 perc retenciós időnél és 93,46%-os találati átlaggal. (1.ábra a)



1. ábra: Azonosított oktanon csúcs (a) és tömegspektruma (b)

Az ilyen karakterisztikus csúcsok akár automatikus kiértékelő szoftverek segítségével is azonosíthatók (például: MassHunter Unknown Analysis, MassHunter Quantitative Analysis, Metbolite Detector), köszönhetően az intenzív tömegspektrumnak (1. ábra b). Méréseink során azonban a komponensek nagy része közepes ( $1,2 \cdot 10^5$  és  $3 \cdot 10^5$  közé eső intenzitás érték), illetve kis (közel alapvonalban lévő) intenzitású volt, ami igen nehezítette az azonosítást (2. ábra a) b) c)).



2. ábra: Nagy (a), közepes (b) és kis (c) intenzitású komponensek

## 2) Eredményes azonosítás egyszeri háttérkorrekcióval

Kisebbségi intenzitású csúcsok (2. ábra b) esetében az azonosítást a háttér kivonás segítségével végeztük. Ez esetben a háttér (zaj) spektruma kivonható az adott komponens tömegspektrumából, így egy háttérzajtól mentes, tiszta komponens tömegspektrumot kapunk. E módszerrel történő azonosítás során a 70 % fölötti találatlallal megjelenő vegyületeket elfogadtuk.

### 3) Kis intenzitású csúcsok több lépéses azonosítása

Az alapzajtól alig elkülöníthető, kis intenzitású, de egyértelműen komponens jelenlétét jelző csúcsok azonosítását több oldalról kellett megközelítenünk. Vizsgáltuk önmagában a komponens tömegspektrumát (itt háttérzavarás előfordulhat), illetve ugyanezen komponens háttérmentes tömegspektrumát is. A kis intenzitású komponensek esetében azonban sokszor hibát követhetünk el az alapzaj (háttér) kivonásával. A hibát az okozhatja, hogy a kiértékelő szoftver a kis intenzitás miatt a komponensből származó fragmens ion  $m/z$  értékét is háttérként azonosíthatja és kivonja, melyekkel fals eredményekhez juthatunk.

Fontos tehát megnéznünk az eredeti, illetve a háttérmentes tömegspektrumot és a kettőt összevetni. Kisebb mértékű átfedésben érkező, koeluálódó komponensek esetén is hasonló, többlépéses visszaellenőrzéses, manuális eljárást végeztünk.

A kisebb találati százalékkal azonosítani vélt komponens esetében segíthet a molekula tömegének figyelembevétele. Az ionizációt követően ugyanis van esély arra, hogy a molekulából történő egy elektronvesztéssel keletkező molekulaion is megjelenik, melynek tömege (az elektron elhanyagolható tömege miatt) megegyezik a molekuláéval. Ami még segítségünkre lehet, az az adott komponens NIST könyvtárban vagy Webbook-ban található retenciós indexe (RI). A könyvtárban fellelhető és az általunk számolt retenciós index összevethető, ami információval szolgálhat az azonosításra vonatkozóan. Végül támpontként szolgálhat a szakirodalom ismerete is, ott esetleg találunk utalást arra nézve, hogy az általunk azonosítottként vélt komponens valóban jellemző-e az adott penészgombára.

### **Összefoglalás**

Összességében elmondható, hogy a HS-SPME-GC-MS kapcsolt technika alkalmas mikrobiológiai illékony vegyületek meghatározására. A vizsgálatok során *Trichoderma aggressivum* faj illékony anyagcseretermékeit monitoroztuk hét napon keresztül és azonosítottuk a megjelenő csúcsokat. Az azonosítás az egyértelmű és nagy intenzitást adó vegyületek esetében nem jelentett gondot, adatbázis alkalmazásával könnyedén végrehajtottuk a feladatot.

A kisebb, alacsony intenzitású komponensek azonosítását több oldalról közelítettük meg: a háttér kivonásával illetve a háttér kivonása nélkül. Az eredmény biztosítása érdekében RI indexeket mértünk, melyeket irodalmi adatokkal hasonlítottunk össze.

Összességében elmondható, hogy az automatikus kiértékelő szoftver kizárólagos használata a kis intenzitású komponensek esetében nem vezet eredményre. A háttér kivonásával, esetleg retenciós indexek figyelembevételével, manuális értékeléssel azonban helytálló eredmény születhet.

### **Köszönetnyilvánítás**

A szerzők szeretnék megköszönni a segítséget Geösel Andrásnak, aki a penész leoltásában és előkészítésében segített.

### **Irodalomjegyzék**

- [1] Arthur, C.L., Pawliszyn, J. 1990. Solid Phase Microextraction with Thermal Desorption Using Fused Silica OpticalFibers. *Analytical Chemistry*. 62:2145-2148.
- [2] Koning, S.D., Janssen, H.G., Brinkman, U.A.Th. 2009. Modern Methods of Sample Preparation for GC Analysis. *Chromatographia*. 69(1):33-78.

- [3] Kataoka, H., Lord, H.L., Pawliszyn, J. 2000. Applications of solid-phase microextraction in food analysis. *Journal of Chromatography A*. 880:35–62.
- [5] Malheiro, R., Pinho, P.G., Soares, S. et. al. 2013. Volatile biomarkers for wild mushrooms species discrimination. *Food Research International*. 54:186–194.
- [6] Pinho, P.G., Ribeiro, B., Gonçalves R.F. et. al. 2008. Correlation between the Pattern Volatiles and the Overall Aroma of Wild Edible Mushrooms. *Journal of Agricultural and Food Chemistry*. 56(5):1704–1712.
- [7] Kluger, B., Zeilinger, S., Wiesenberger, G., Schöffbeck, D., Schuhmacher, R. 2013. Detection and identification of fungal microbial volatile organic compounds by HS-SPME-GC-MS. In Gupta, V.K., Tuohy, M., Ayyachamy, M., Turner, K.M., O. Donovan A. (Eds): *Laboratory Protocols in Fungal Biology: Current Methods in Fungal Biology*, Springer ISBN: 978-1-4614-2355-3, pp. 455-466.
- [8] Radványi D, Gere A, Jókai Zs, Fodor P (2015) Rapid evaluation technique to differentiate mushroom disease-related moulds by detecting microbial volatile organic compounds using HS-SPME-GC-MS., *Analytical and Bioanalytical Chemistry* 407:537–545, DOI 10.1007/s00216-014-8302-x



## Ionization Techniques of Volatile Compounds CI vs. EI

Dalma Radványi<sup>1\*</sup>, Zsuzsa Jókai<sup>1</sup>, Péter Fodor<sup>1</sup>

<sup>1</sup>Department of Applied Chemistry, Corvinus University of Budapest, H-1118 Budapest, Villányi út 29-43., Hungary

e-mail: dalma.radvanyi@uni-corvinus.hu (radvanyi.dalma@gmail.com)

### Abstract

Different ionization modes were used in this study to identify unknown compounds. EI (electron impact) ionization was used at 70 eV energy level to create comparable mass spectra, therefore compound identification was done using NIST mass library. CI (chemical ionization), as a softer ionization, was used to avoid the hard fragmentation of molecules. Using CI, molecular ion can be found on the mass spectra, which molecular ion gives more information about the component. In our study lower EI energy level was used to create similar mass spectra as CI, so molecular ions were also prepared. The applied lower EI energy level warrants the undamaged molecule and can give more information about the analyzed molecule as well as CI. In untargeted analysis, it is very important to extract as much information about the component as possible to determine the molecule structure and identify it.

### Introduction

Determination of volatile fungal metabolites usually is done using gas chromatography (GC) coupled with mass spectrometry (MS) methods. Solid-phase micro extraction (SPME) fibers are used worldwide to collect the volatile compounds from the headspace (HS) (1, 2, 3). It seems that the above mentioned coupled technique has enough high sensitive detection capabilities, however the identification often cannot be really completed, we can still find only chemical classes (for example terpenoids, sesquiterpenes, unidentified diterpenes...) (2). According to a usual workflow the fungal VOCs are detected and identified using single quadropole MS data in electron ionisation (EI) mode (3) and applying a similar evaluation process to identify EI spectra. In EI mode, ions are formed when a 70 eV beam of electrons hits the sample molecules in the gas phase so many fragment ions create. These ions can be used for determining the structure of the molecules; therefore we can use the generated spectrum to compare library spectra and identify the compounds. Unfortunately, some compounds will completely fragment and not give molecular ions. In these cases there is an alternate method, which gives a softer ionization process. This method is the chemical ionization (CI) mode. Untargeted analysis requires as much information about the molecules as possible to get better opportunity to identify the found component.

### Experimental

#### Samples

Different mould samples were inoculated on PDA substrata in 20 mL HS-vials. These microorganisms were measured using HS-SPME-GC EI/CI qTOF MS in EI and CI mode.

Different tomato volatiles were sampled from 20 mL HS-vials and analyzed by HS-

SPME-GC-MS. Only EI mode was used but EI energy level was modified.

#### Equipment

EI measures: An Agilent 6890 Gas Chromatograph coupled with a 5975 C MSDMass Spectrometer was used with a non-polar HP-5MS ((5 %-phenyl)-methylpolysiloxane; 30 m, 0.25 mm i.d., 0.25  $\mu$ m film, Agilent Technologies) column. Optimised oven temperature program was used [4]. During the procedures, inlet temperature was held constant at 250 °C. Hydrogen was used as carrier gas with a constant 1.2 mL/min flow to accelerate the separation on the column. The MS source temperature was set to 230 °C and the quadrupole temperature was held at 150 °C. Positive electron ionisation (EI+) was used, with an electron energy level of 70 eV. After the energy level was decreased until it reached 5 eV (the minimum E level of mass spectrometer). The MS was tuned using perfluorotributylamine (PFTB) every day before the measurements. Agilent Enhanced MSD ChemStation software handled the GC and MS parameters.

EI and CI measures: Agilent 7890B GC and Agilent 7200 EI/CI qTOF MS coupled analytical system were used to analyse the emitted compounds. HP-5MS capillary column (the same as in EI measures) and 5 m long pre-column was equipped without stationary phase. Helium was used as a carrier gas with 1.3 ml/min (pre-column 1.2 ml/min) gas flow. Oven temperature program was set according to Stoppacher and his co-worker (Stoppacher et al., 2010), but we supplemented the program after the last step, thus the following oven temperature program was achieved: 40 °C (hold 2 min), 10 °C/min to 200 °C, 25 °C/min to 260 °C (hold 5 min), 25 °C/min to 300 °C (hold 5 min).

EI TOF MS parameters: electron impact ionization (EI) at 70 eV, ion source 230 °C, quadrupole 150 °C, acquisition parameters: m/z range: 40-700, rate: 3.33 spectra/sec, transfer line to MS 280 °C.

CI TOF MS parameters: chemical ionization (CI) with 20% methane (gas flow 5 ml/min) at 160 eV, emission voltage: 10  $\mu$ A, ion source 150 °C, quadrupole 150 °C, acquisition parameters: m/z range: 50-700, rate: 3.33 spectra/sec, transfer line to MS 280 °C.

Agilent Enhanced Data Analysis, Agilent MassHunter Qualitative Analysis B.07.00 and Agilent MassHunter Quantitative Analysis B.06.00 software were used for evaluation and comparison of the chromatograms. Mass Frontier software was used to fragment the compounds based on their molecule structure. The collected compounds were identified using NIST Mass Spectral Search Program (NIST 2011, Wiley 10<sup>th</sup> edition) and the calculated retention index was compared with literature values (NIST Chemistry WebBook).

#### Results and discussion

As a first step, samples were measured in EI mode using 70 eV energy level. The obtained compound's mass spectra were compared with reference mass spectra (NIST library); hence the identification step was done. To ensure the reliability of the result, different ionization modes were used. In the case of mould samples, beyerene compound was found at 19.44 min. Fig. 1. shows the results of EI and CI ionization. Using CI, molecular ion ( $[M+H]^+$ ) was clearly found at 273.2578 m/z value and the mass accuracy was less than 0.5 ppm (TOF MS has higher resolution so mass accuracy is appropriate). Quasi molecular ion group ( $[M-H]^+$ ,  $[M]^+$ ,  $[M+H]^+$ ) can also

found on the mass spectra which gives information about the molecule mass, in this case: 273.2578 m/z.

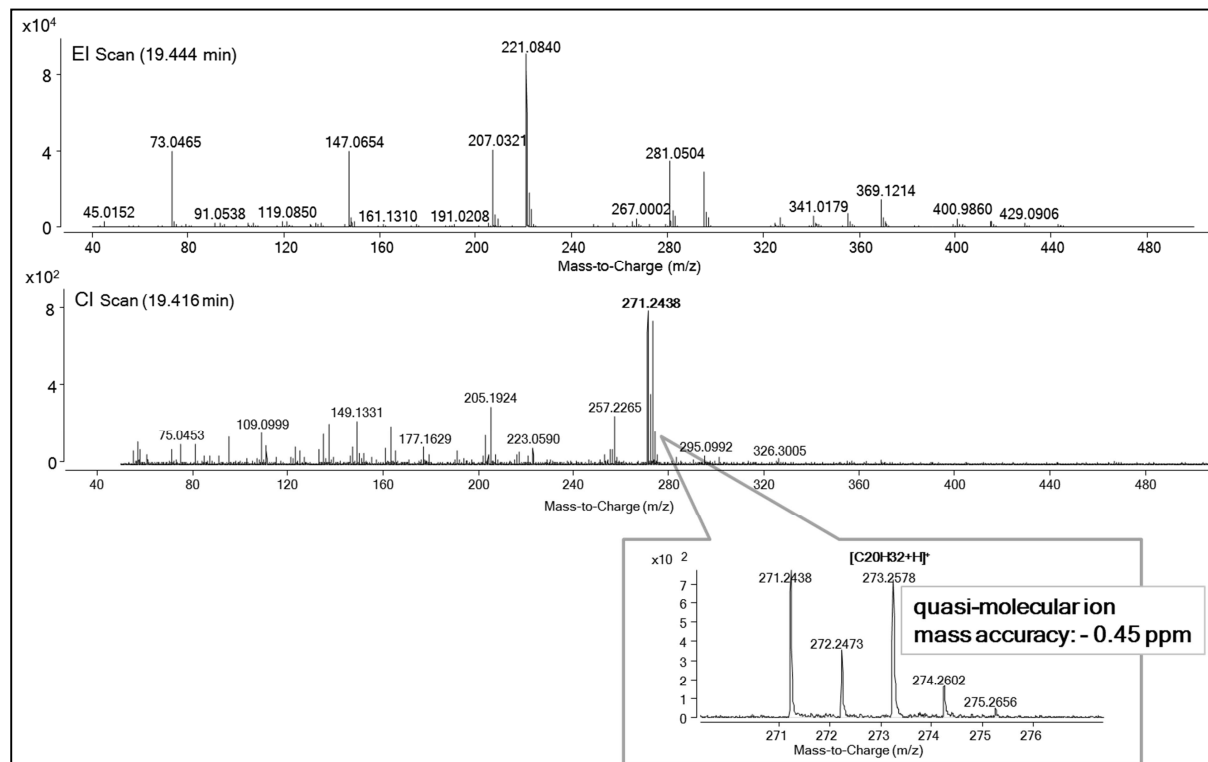


**Figure 1.** Example of EI vs CI mass spectra using TOF MS (mould sample). Mass spectra of beyerene: molecular weight: 272.247, molecular formula: C<sub>20</sub>H<sub>32</sub>, RI: 1898.4, ID: 85,2%

Using CI ionization, molecule identification could be more accurate because ionization is softer than in the case of EI; the molecule ion did not break into fragments. We can also avoid the fragmentation of molecular ion in EI mode due to decreasing EI energy level. Seven ionization energy levels were used in this experiment (70 eV, 60 eV, 50 eV, 40 eV, 20 eV, 10 eV, 5 eV). According to the results, the highest compound intensity was found at 60 eV energy level. Until 10 eV energy level, the fragmentation is very similar as it was at 70 eV. Using 5 eV ionization energy level, the molecular ions ( $M^+$ ) appeared in the case of most compounds. After that we were able to compare the identified compound mass (identification step was done by NIST library using 70 eV) with the molecular ion mass which was created at 5 eV energy level. Fig 2. shows the experiment results and the clearly identified molecular ion.

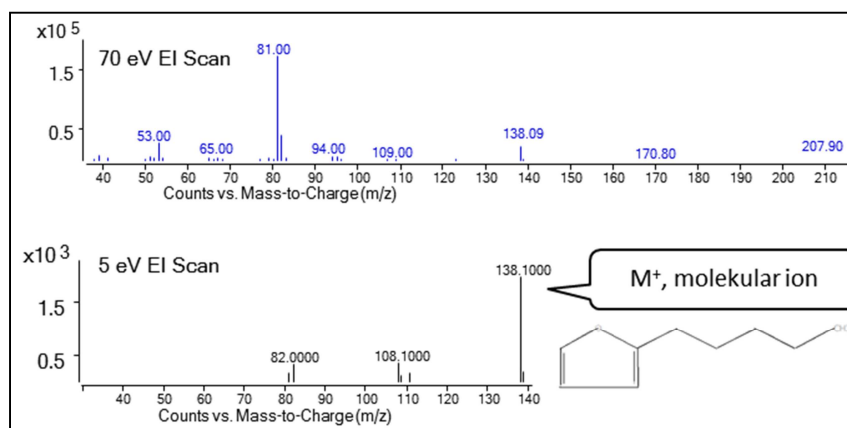


**Figure 2.** Example of decreased energy level of EI ionization using quadrupole MS (tomato sample). Mass spectra of furan, 2-pentyl-: molecular weight: 138.104, molecular formula: C<sub>9</sub>H<sub>14</sub>O, RI:1040, ID: 93.9%

Using softer EI ionization similar results were obtained as in the case of CI. Our EI method is also included the advance of CI mode, keeping the advances of EI, for example it is more widespread, easier to use and more understable than the CI.

## Conclusion

In the case of decreased energy level of electron ionization, similar clear mass spectra can be reached as in the case of CI. Furthermore, molecular ion can be also found in 5eV energy level EI mass spectra. Using this ionization technique, more information can be evaluated from the analyzed molecule, which is beneficial, because untargeted analysis requires as much information about the molecules as possible to get better opportunity to identify the found, unknown component.

## Acknowledgements

Dalma Radványi thanks the ERASMUS the opportunity to travel BOKU University, Vienna. EI/CI qTOF MS measures were done at BOKU. The authors would also thank the tomato samples for László Csambalik and the mould samples for András Geösel. Moreover, authors thank the helping hands of Ferenc Lovász during the measurments.

## References

1. Stoppacher N, Kluger B, Zeilinger S, Krska R, Schuhmacher R (2010) Identification and profiling of volatile metabolites of the biocontrol fungus *Trichoderma atroviride* by HS-SPME-GC-MS. *Journal of Microbiological Methods* 81(2):187-193.
2. Polizzi V, Adams A, Malysheva SV, Saeger SD, Peteghem CV, Moretti A, Picco AM, Kimpe ND (2012) Identification of volatile markers for indoor fungal growth and chemotaxonomic classification of *Aspergillus* species. *Fungal Biology* 116(9): 941-953
3. Kluger B, Zeilinger S, Wiesenberger G, Schöfbeck D, Schuhmacher R (2013) Detection and Identification of Fungal Microbial Volatile Organic Compounds by HS-SPME-GC-MS In book: *Laboratory Protocols in Fungal Biology*, Chapter: 42, Publisher: SpringerLink, Editors:

Gupta, V.K., Tuohy, M.G., Ayyachamy, M, Turner, K.M., O'Donovan, A, pp.455-466, DOI: 10.1007/978-1-4614-2356-0\_42

4. Radványi D, Gere A, Jókai Zs, Fodor P (2015) Rapid evaluation technique to differentiate mushroom disease-related moulds by detecting microbial volatile organic compounds using HS-SPME-GC-MS., *Analytical and Bioanalytical Chemistry* 407:537–545, DOI 10.1007/s00216-014-8302-x

## The Effect of the Simultaneous Presence of Four Non-Steroidal Anti-Inflammatory Drugs During the Vacuum Ultraviolet Photolysis

**Georgina Rózsa<sup>1,2</sup>, Eszter Arany<sup>1</sup>, Zsuzsanna Kozmér<sup>1,2</sup>,  
Tünde Alapi<sup>1,2</sup>, András Dombi<sup>1</sup>**

<sup>1</sup>Research Group of Environmental Chemistry, University of Szeged, H-6720 Szeged,  
Dóm tér 7, Hungary

<sup>2</sup>Department of Inorganic and Analytical Chemistry, University of Szeged, H-6720 Szeged, Dóm  
tér 7, Hungary  
e-mail: rozsa.georgina@chem.u-szeged.hu

### Abstract

Non-steroidal anti-inflammatory drugs (NSAIDs) are somewhat recently recognized pollutants, which are widely used by the society. Their sources in natural waters are the domestic and industrial effluents. Moreover, their possible interference with the water cycle and concurrent effects on the human health system has been implicated.

Advanced oxidation processes (AOPs) could help to solve this problem as alternative methods, which are based on the generation of reactive radicals to induce the transformation of organic contaminants beside biological methods, which are often ineffective for this purpose. Vacuum ultraviolet (VUV) photolysis is a suitable method among AOPs to study the effects of different parameters on the radical set and on the degradation of organic contaminants, since the generated radical set is well-known.

In this study, we aimed to investigate the simultaneous determination of pharmaceuticals (four non-steroidal anti-inflammatory drugs), namely ibuprofen, ketoprofen, naproxen and diclofenac. In this work we examined the degradation of compounds simultaneously, as wastewaters generally are multi-component solutions, where the components can effect the rate of decomposition of each other due to the competition for the reactive radicals. The pairing of the binary compounds in solution were ibuprofen+naproxen and ketoprofen+diclofenac, in order to be able to separate them by liquid chromatography. The results show that under the applied conditions (photon flux and initial concentration) the rates of the simultaneous degradation were slightly lower than in cases of one-component solutions because of the competition of the pharmaceuticals for the reactive species as we expected, however the influence of the competition was minor.

### Introduction

Chemicals, such as pesticides, pharmaceutical products are continually being released into the environment in increasing amounts causing concerns as they are non-biodegradable and also being hazardous to living organisms, including humans. Traditional treatment processes are not designed to remove these compounds [1]. Consequently, the development of efficient processes is needed in order to remove them from wastewaters and drinking water.

During this work the simultaneous VUV photolytic degradation of NSAIDs were examined. These compounds are non-sterane arylcarboxylic acids containing phenyl groups.



Ibuprofen ((*RS*)-2-(4-(2-methylpropyl)phenyl)propanoic acid), ketoprofen ((*RS*)-2-(3-benzoylphenyl) propanoic acid), naproxen ((*RS*)-2-(6-methoxynaphthalen-2-yl)acetic acid) and diclofenac (2-(2-(2,6-dichlorophenylamino)phenyl) acetic acid) (Fig. 1) are pharmaceuticals with analgesic, anti-pyretic and anti-inflammatory properties. Their annual production surpasses several kilotonnes, which has led to environmental concentrations from ppt to ppb levels to be found [2, 3].

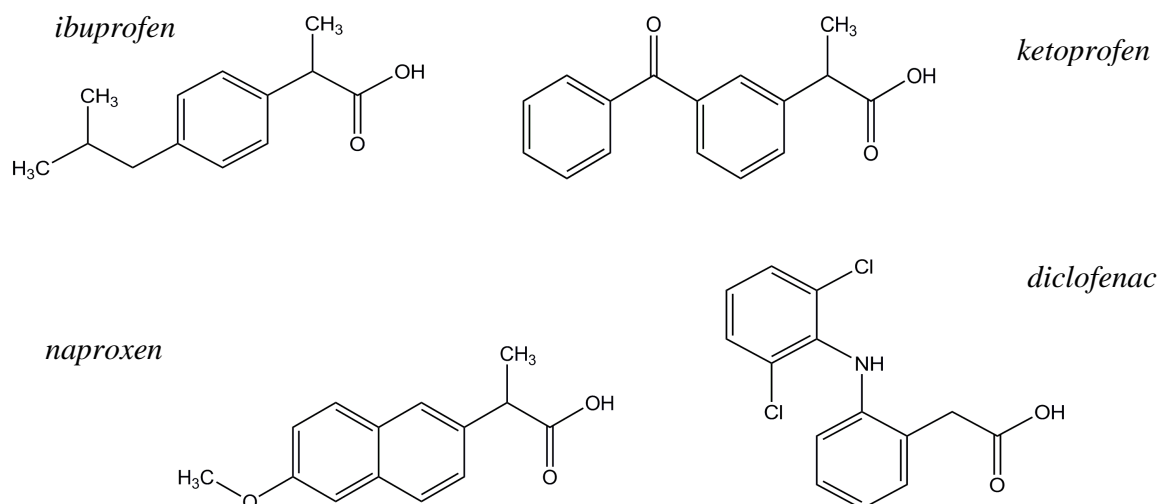
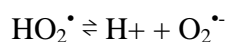
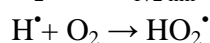
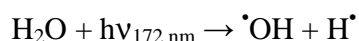


**Fig. 1:** The chemical structure of NSAIDs examined

During VUV photolysis, the homolysis of  $\text{H}_2\text{O}$  molecule takes place initiated by high-energy VUV photons generated by xenon excimer lamps emitting radiation at wavelengths shorter than 200 nm [4]. The primary radicals generated are mainly hydroxyl radicals ( $\cdot\text{OH}$ ) and hydrogen radicals ( $\text{H}\cdot$ ). In  $\text{O}_2$ -saturated solutions the radical set contains  $\cdot\text{OH}$  in elevated concentration and hydroperoxyl radicals/superoxide radical anions ( $\text{HO}_2\cdot/\text{O}_2^{\cdot-}$ ) because  $\text{H}\cdot$  is trapped by molecular oxygen.



$$\Phi_{\cdot\text{OH}}^{172\text{ nm}} = 0.42 \text{ [5]}$$

$$k = 2.1 \times 10^{10} \text{ L mol}^{-1} \text{ s}^{-1} \text{ [6]}$$

$$\text{pK}_a = 4.8 \text{ [7]}$$

The aim of this study was to compare the simultaneous degradation of NSAIDs with the case when only one compound is present in the system.

## Experimental

### Reactor configurations

In this study, the experiments were performed in the apparatus containing a 20 W xenon excimer lamp (Radium Xeradex<sup>TM</sup>) emitting at  $172 \pm 14$  nm of wavelength. 250 ml aqueous solutions were circulated by a peristaltic pump between the reactor and reservoir tanks (both thermostated at  $25 \pm 0.5$  °C) at  $375 \text{ ml min}^{-1}$  flow rate. To investigate the influence of oxygen,  $\text{O}_2$  gas (99.995 % purity) was bubbled through the solutions starting 15 minutes before and until the end of the

irradiation. The  $c_0$  values of NSAIDs were  $0.5 \times 10^{-4}$  mol L $^{-1}$  in individually, thus the total initial concentration of NSAIDs in the combined solutions were  $1.0 \times 10^{-4}$  mol L $^{-1}$ .

### Analytical methods

Ibuprofen and naproxen were purchased from Fluka, ketoprofen and diclofenac were purchased from Sigma-Aldrich. The purity of acetylsalicylic acids was >98% in each case.

The samples were analyzed by an Agilent 1100 HPLC equipment (using an LiChroCART® C18 reverse-phase column) with a diode array detector. In our case acetonitrile and 1% aqueous acetic acid were used in 1:1 ratio as eluent at a flow rate of 0.8 ml min $^{-1}$ . The wavelengths of quantification were 220 nm in the case of ibuprofen, 256 nm in the case of ketoprofen, 230 nm in the case of naproxen and 280 nm in the case of diclofenac.

### Results and discussion

The results show that the rate of degradation of NSAIDs decreased when the compounds applied were present simultaneously compared with the one-component cases (*Fig. 2a and b*).

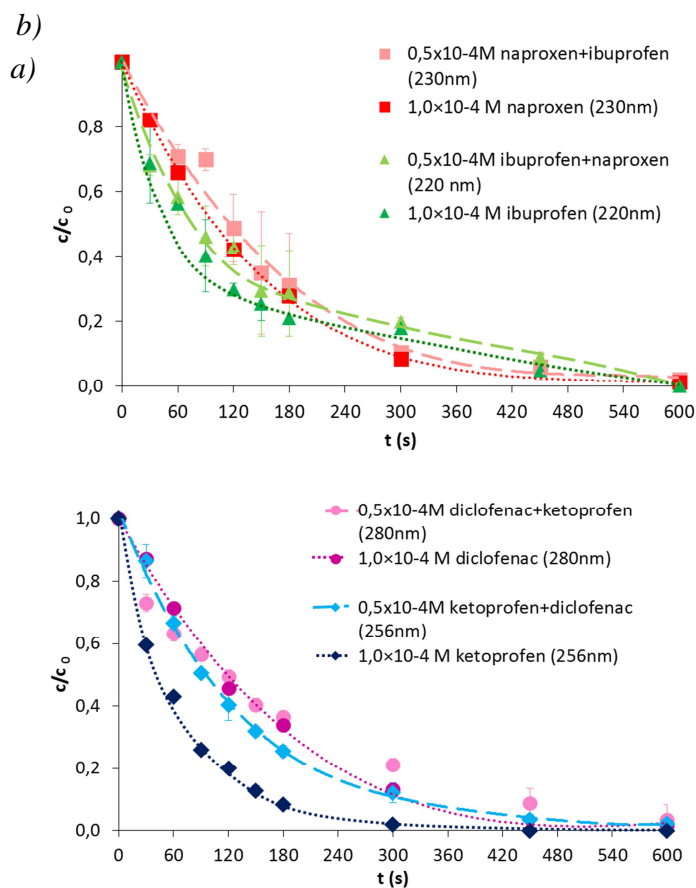


**Fig. 2:** The kinetic curves of NSAIDs in the presence of dissolved oxygen during vacuum ultraviolet photolysis

**Table 1:** Reaction rate constants of  $\cdot\text{OH}$  radical with NSAIDs

	$k(\text{substance} + \cdot\text{OH})(\times 10^9 \text{ mol}^{-1} \text{ dm}^3 \text{ s}^{-1})$
Ibuprofen	6.05
Naproxen	5.50
Ketoprofen	5.05
Diclofenac	8.85

This phenomena can be explained by the completion of NSAIDs mainly for the hydroxyl radical. Regarding the rate constants of reactions of NSAIDs with  $\cdot\text{OH}$ , in case of ibuprofen and naproxen this values are similar, thus the degrees of the reduction of degradation rates were similar also (*Fig. 2a*).

However, in cases of ketoprofen and diclofenac, the second one has one order of magnitude higher reaction rate constant with  $\cdot\text{OH}$  (*Table 1*). This means that diclofenac competes with ketoprofen for the radicals successfully, which results that the ketoprofen decomposes with significantly lower rate in the presence of the second contaminant than in the absence of that (*Fig. 2b*).

### Conclusion

- The effect of simultaneous presence of NSAIDs on their VUV photolysis was investigated.
- The rates of transformation of NSAIDs were lower in solutions that contained simultaneously two contaminants than in one-component solutions.
- Diclofenac reacts more effectively with  $\cdot\text{OH}$  than ketoprofen, thus during their simultaneous VUV-irradiation the transformation rate of ketoprofen decreased significantly.

### References

- [1] T.H. Yu, A.Y. C.Lin, S.K. Lateef, C.F. Lina, and P.Y. Yang, *Chemosphere* 77 (2009)175-181.
- [2] H.R. Buser, T. Poiger, and M.D. Muller, *Environmental Science & Technology* (1999)2529-2535.
- [3] L.H.M.L.M. Santos, A.N. Araújo, A. Fachini, A. Pena, C. Delerue-Matos, and M.C.B.S. M., *J Hazard Mater* 175 (2010)45-95.
- [4] T. Oppenländer and R. Schwarzwaldler, *J. Adv. Oxid. Technol.* 5 (2002)155-163.
- [5] G. Heit, A. Neuner, P.Y. Saugy, and A.M. Braun, *J. Phys. Chem. A* 102 (1998)5551-5561.
- [6] G.V. Buxton, C.L. Greenstock, W.P. Helman, and A.B. Ross, *J. Phys. Chem. Ref. Data* 17 (1988)513-886.
- [7] B.H.J. Bielski, D.E. Cabelli, R.L. Arudi, and A.B. Ross, *J. Phys. Chem. Ref. Data* 14 (1985)1041-1100.

## Functionalized Hematite Photoelectrode for Solar Water Splitting

Krisztina Schrantz<sup>1,2</sup>, Pradeep P. Wyss<sup>3</sup>, Debajeet K. Bora<sup>1</sup>, Elena Rhozkova<sup>4</sup>,  
Julian Ihssen<sup>5</sup>, Artur Braun<sup>1</sup>

<sup>1</sup>*Empa, Swiss Federal Laboratories for Materials Science and Technology, Laboratory for High Performance Ceramics, Überlandstrasse 129, CH-8600 Dübendorf, Switzerland*

<sup>2</sup>*Department of Inorganic and Analytical Chemistry, University of Szeged, H-6720 Szeged, Dóm tér 7, Hungary*

<sup>3</sup>*FHNW – University of Applied Sciences Northwestern Switzerland, School of Life Sciences and Institute for Chemistry and Bioanalytics, Grünenstrasse 40, CH-4132 Muttenz, Switzerland*

<sup>4</sup>*Nano Bio Interfaces, Center for Nanoscale Materials, Argonne National Laboratory, 9700 South Cass Avenue, Argonne, IL, 60439, USA*

<sup>5</sup>*Empa, Swiss Federal Laboratories for Materials Science and Technology, Laboratory for Biomaterials, Lerchenfeldstrasse 5, CH-9014, St. Gallen, Switzerland  
e-mail: sranc@chem.u-szeged.hu*

### Abstract

We show how the enzymatic polymerization of tyrosine with tyrosinase can be exploited for the immobilization of the light harvesting protein C-phycocyanin on the surface of hematite. This results in the in situ formation of the organic semiconductor melanin which stabilizes the protein strains on the semiconductor surface and increases the photocurrent by a factor of two in environmentally benign conditions. The PC-melanin coating on the hematite exhibits a self-similar, comb-like fractal pattern, pointing to the possibility to control the orientation of the chromophore for optimal light harvesting. Operating this bio-hybrid photoelectrochemical cell in environmentally benign environment could extend its lifetime compared with those used in strongly alkaline electrolyte and enhance the acceptance of the PEC cells in the society.

### Introduction

The use of solar energy to satisfy the increasing energy demand has been pointed out by Ciamician about 100 years ago [1]. Yet, 40 years after the pioneering photoelectrochemical water splitting on titanium oxide by Honda and Fujishima (1972), high conversion efficiencies in photoelectrochemical (PEC) cells are missing [2,3]. Hematite ( $\alpha\text{-Fe}_2\text{O}_3$ ) satisfies many requirements for a good photocatalyst and is thus a prospective photoanode material for PEC water splitting [4]. However, the conduction band of hematite is below the electrochemical water reduction potential and therefore needs a small bias voltage in a PEC cell. Its short hole diffusion length is believed to be the most probable cause for the low efficiency [5]. The performance of pristine hematite can be improved by increasing the semiconductor - electrolyte interface area via nanostructuring [6], cation doping [7], or by surface functionalization with proteins [11], which can enhance electron injection into the conduction band.

Artificial photosynthesis mimics the natural photosynthesis, a process that converts sunlight, water, and carbon dioxide into oxygen and carbohydrates. Various approaches [8-10] have been made to combine semiconductor electrodes with natural light harvesting motifs to mimic photosynthesis. The aim is to build a device for converting the energy from sunlight in the chemical bonds of a fuel. In the prokaryotic cyanobacteria and eukaryotic red algae, light

harvesting is performed by phycobiliproteins [11]. The phycobilisomes are the macromolecular complexes of these proteins [12] and act as light absorbing antennas. Their main components are phycoerythrin (PE), phycocyanin (PC) and allophycocyanin (APC), having different chromophores. The chromophore in PC is a linear tetrapyrrole called phycocyanobilin (PCB), absorbing between 590 - 610 nm [13]. An absorbed photon can initiate electron excitation and transfer. The energy is funneled to the reaction center and converted into chemical energy in photosystem II [14,15].

We present here a stable protein functionalized hematite photoanode assembly synthesized by enzymatic polymerization of melanin. The basic idea behind tyrosinase-catalyzed melanin formation in the context of PEC is on one hand, to integrate PC in a polymer structure of melanin, so as to have a mechanically and biologically stable protein coating on hematite. On the other hand, due to the semiconducting properties of melanin itself [16], to maintain or enhance the water splitting performance of the bio-functionalized hematite.

## Experimental

**Precursor synthesis and hematite film deposition.** An FTO glass slide (12 x 30 x 2 mm, TEC-8 from Hartford Glass Inc.) was dip coated with the precursor [6] using DipMaster<sup>TM</sup>-50 (Chemat Technology Inc., USA) and annealed for 30 min at 500°C. Dip coating and annealing were repeated three more times to obtain four layers of hematite with approximate 550 micrometer film thickness.

**Electrochemical measurements.** Linear voltammetry [17] in dark and under illumination was conducted using a photoelectrochemical cell and a potentiostat (*VoltaLab80 PGZ 402*). The hematite film sample was connected as the working electrode in a three electrode configuration. A platinum plate was set as counter electrode and an Ag/AgCl (with sat. KCl) electrode was used as the reference electrode. The electrodes were immersed in 1 mol L<sup>-1</sup> KOH (pH 14) or PBS, 0.05 mol L<sup>-1</sup> sodium phosphate, 0.15 mol L<sup>-1</sup> NaCl, pH 7.2), respectively. Simulated sunlight was provided by a *1 Sun Oriel Lamp* from *L.O.T. – Oriel AG*, corresponding to AM 1.5 global standard solar spectrum. The applied bias potential was 600 mV and 1000 mV in case of KOH and PBS electrolytes, respectively.

**Gas chromatography.** GC-2014 (Shimadzu) with TCD detector and Hayesep D 10' column was used to measure H<sub>2</sub>. Temperatures of the injector, column and detector were 60, 38 and 140 °C, respectively. The generated H<sub>2</sub> was recirculated with Ar carrier gas using a pump at 0.1 bar overpressure, enabling the online monitoring of H<sub>2</sub> evolution. 10 µL samples of the headspace were injected after selected reaction times. The evolved H<sub>2</sub> was quantified based on calibration with 50, 100 and 500 ppm standard H<sub>2</sub> in Ar.

**Protein immobilization.** For the cross-linking of proteins with the photoanode, the pristine hematite film was first conditioned with agarose and then activated with 1,1-carbonyldiimidazol (CDI) [8]. This conjugate [18] can react directly with primary amine groups on the surface of PC, or indirectly, involving enzymatic reactions such as with the subsequently formed melanin. These activated electrodes were then treated in two different ways to obtain melanin (A) and melanin-PC (B) coated surfaces.

**A: Melanin synthesis with tyrosinase from L-tyrosine**

0.1 mg mL<sup>-1</sup> L-tyrosine solution in PBS was prepared. 5 µL of the tyrosinase stock solution (10 mg mL<sup>-1</sup>) was added to 1 mL L-tyrosine solution. The activated hematite surface was covered with 200 µL of this solution for 1h.

**B: Enzymatic cross linking of PC with tyrosinase in presence of L-tyrosine**

0.1 mg mL<sup>-1</sup> L-tyrosine solution in PBS was prepared. 1 mg PC was added to 5 mL of this L-tyrosine solution. 5 µL of the tyrosinase stock solution (10 mg mL<sup>-1</sup>) was added to 1 mL L-tyrosine-PC solution. The activated hematite surface was covered with 200 µL of this solution and incubated for 1h at room temperature.

**Results and discussion**

Pristine hematite films are built from nanoparticles with average size of 50 nm and have a highly porous morphology. X-ray diffraction on the pristine film showed the typical Bragg reflections for hematite, the (104) and the (110). The photocurrent densities of the hematite electrodes for every level of processing in alkaline and neutral electrolytes are compared in Figure 1. The photocurrent density of the pristine hematite was 275 µA cm<sup>-2</sup> at 500 mV in the standard 1 mol L<sup>-1</sup> KOH electrolyte (Fig. 1, left panel), and 160 µA cm<sup>-2</sup> at 900 mV in 0.05 mol L<sup>-1</sup> phosphate buffer solution (PBS) (Fig. 1, right panel). Coating the pristine hematite with melanin only yields a slightly increased photocurrent of 300 µA cm<sup>-2</sup> in KOH, whereas in PBS the photocurrent is slightly decreased to 140 µA cm<sup>-2</sup>. In alkaline electrolyte the photocurrent density of the hematite further functionalized with both melanin and PC differs not significantly from the only melanin coated and pristine hematite. However, in PBS, the melanin-PC functionalized hematite yields a photocurrent density of 450 µA cm<sup>-2</sup>. This is more than double enhancement compared to the pristine electrode in PBS, and still a 50% enhancement when compared to the electrode measured in strongly alkaline standard electrolyte.

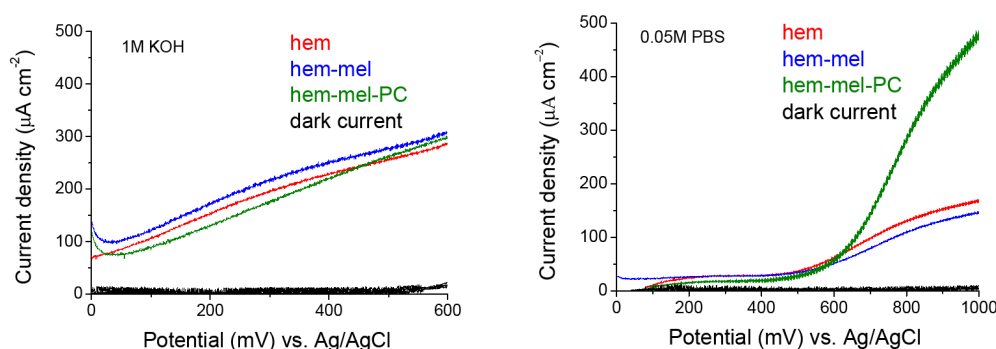


**Figure 1.** Current density of the pristine hematite (—), melanin coated hematite (—) and melanin-PC coated hematite films (—) recorded in 1 mol L<sup>-1</sup> KOH (left panel) and 0.05 mol L<sup>-1</sup> PBS (right panel). The black curves show the dark current density.

The striking difference in the photocurrent density for the differently functionalized films is paralleled by the evolution of H<sub>2</sub> as monitored with gas chromatography (GC). After 20 min of chronoamperometry the calculated H<sub>2</sub> concentration produced by the PC-melanin coated hematite was about three times more than produced on the pristine hematite. This corresponded to the aforementioned photocurrent density enhancement.



Note that the photoanode in fact evolves  $O_2$  from water splitting, whereas the  $H_2$  is evolved at the counter electrode.

We have shown recently that the combination of adsorption and cross linking of PC to hematite photoanodes results in a doubling of the photocurrent density in  $1 \text{ mol L}^{-1}$  KOH electrolyte [8]. There, the chromophores remain active even in strongly alkaline conditions as high as  $\text{pH} \sim 14$ , when attached to a hematite support. This situation cannot be the case in the present work because melanin can be dissolved in KOH [10], hence it could likely cause disintegration of the protein network. Even when the chromophores remain intact in the alkaline electrolyte, the dissolution of the melanin disrupts the attachment of the PC to the hematite. Consequently, charge transfer between PC and hematite is not warranted anymore. However, when we chose PBS as electrolyte, enzymatic melanin-PC coating allowed for an enhancement in photocurrent density by a factor of almost 3. Equal important to the increase of the photocurrent density is that this hybrid photoanode works in  $\text{pH}$  neutral electrolyte. This shows that water splitting devices can be fabricated and used also in a protein friendly, and thus in a generally more benign environment [19]. For the acceptance of a solar energy conversion system in public areas, environmentally benign components, i.e. phosphate buffer rather than concentrated KOH, are more likely to be accepted.

The electron micrographs in Figure 2 provide a visual impression of the morphology of the melanin-PC coated (right panel) and melanin coated (left panel) hematite surface. Most interesting, the organic layer from melanin and PC has arranged in a regular, self-similar pattern with a comb-like architecture on the hematite. The comb branches are aggregates from globular primary particles of around 200 nm diameter. The aggregate branches range from 500 nm to 5  $\mu\text{m}$  in length. The reason behind the high structural organization could be due to the PC-melanin polymer assembly.

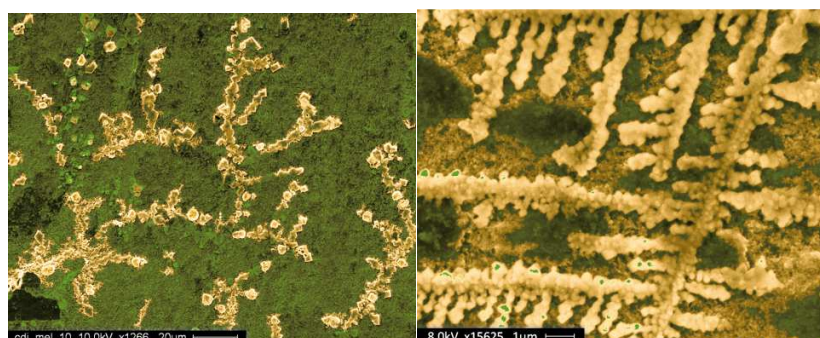


**Figure 2.** SEM micrographs of PC-melanin (left panel) and melanin-only (right panel) coated hematite films surfaces with 2 different magnifications.

Hematite films functionalized with only melanin are shown in left panel of Figure 2. Melanin chain organizes in a different pattern when PC is not present, in contrast to hematite co-functionalized with melanin and PC. In particular, melanin arranges in more random bow-like branches, where the branches consist of chain of nanoparticles similar in morphology obtained by earlier study [20]. Highly organized structures formed only in the presence of PC, and may

potentially be responsible for the high increase of the photocurrent due to optimized orientation of the chromophores [21,22].

## Conclusion

In this work we show how enzymatic formation of melanin can immobilize the cyanobacterial light harvesting protein PC on the surface of hematite and in this way enhance the efficiency of the photoanode. Upon addition of tyrosinase to a PC-L-tyrosine mixture on hematite surfaces, a melanin-PC network is formed which is cross-linked to the hematite, causing an increase in photoelectrochemical performance by a factor of two. Melanin-PC coating shows a fractal structure which might contribute to the observed photoelectrochemical efficiency. At this point it remains open whether this fractal structure is functional or coincidental. Enhanced H<sub>2</sub> production rates were observed for lab-scale PEC cell with melanin-PC coated hematite photoanode. A technological and societal benefit of the demonstrated system is its operability under benign conditions at neutral pH.

## Acknowledgements

Funding for this research was provided by the Swiss Federal Office of Energy project No. 100411, the Seventh Framework Program grant No. 227179 (NanoPEC), the SNF R'Equip No. 206021-121306 and IZKOZ2 - 133944, the Swiss State Secretariat for Education and Research project Sciex 10.013 (Nanobio-Interfaces for Photocatalytic Solar Hydrogen).

## References

- [1] C. Ciamician, *Science*, 1912, **36**, 385–394.
- [2] A. Fujishima and K. Honda, *Nature*, 1972, **238**, 37 – 38.
- [3] S. D. Tilley, M. Cornuz, K. Sivula, and M. Grätzel, *Angewandte Chemie (International ed. in English)*, 2010, **49**, 6405–8.
- [4] J. H. Kennedy and K. W. Frese, *J. Electrochem. Soc.*, 1978, **125**, 709–714.
- [5] R. Nakamura, K. Kamiya, and K. Hashimoto, *Chemical Physics Letters*, 2010, **498**, 307–311.
- [6] D. K. Bora, A. Braun, R. Erni, G. Fortunato, T. Graule, and E. C. Constable, *Chemistry of Materials*, 2011, **23**, 2051–2061.
- [7] S. Saremi-Yarahmadi, K. G. U. Wijayantha, A. A. Tahir, and B. Vaidhyanathan, *J. Phys. Chem. C*, 2009, 4768–4778.
- [8] D. K. Bora, E. A. Rozhkova, K. Schrantz, P. P. Wyss, A. Braun, T. Graule, and E. C. Constable, *Advanced Functional Materials*, 2012, **22**, 490–502.
- [9] A. Kathiravan and R. Renganathan, *Journal of colloid and interface science*, 2009, **335**, 196–202.
- [10] F. Bernsmann, B. Frisch, C. Ringwald, and V. Ball, *Journal of colloid and interface science*, 2010, **344**, 54–60.
- [11] Govindjee and D. Shevela, *Frontiers in plant science*, 2011, **2**, 28.
- [12] R. Dna, D. A. Bryant, V. L. Stirewalta, M. Glauser, G. Frank, W. Sidlet, and H. Zuber, *Gene*, 1991, **107**, 91–99.
- [13] R. J. Buehler, R. C. Pierce, L. Friedman, and H. W. Siegelman, *The Journal of Biological Chemistry*, 1976, **251**, 2405–2411.
- [14] D. Frackowiak, *Biophysics*, 1978, **27**, 161–167.

- [15] M. Yang, R. Agarwal, and G. R. Fleming, *Journal of Photochemistry and Photobiology A: Chemistry*, 2001, **142**, 107–119.
- [16] V. Capozzi, G. Perna, P. Carmone, A. Gallone, M. Lastella, E. Mezzenga, G. Quartucci, M. Ambrico, V. Augelli, P. F. Biagi, T. Ligonzo, A. Minafra, L. Schiavulli, M. Pallara, and R. Cicero, *Thin Solid Films*, 2006, **511-512**, 362–366.
- [17] M. Dincă, Y. Surendranath, and D. G. Nocera, *Proceedings of the National Academy of Sciences of the United States of America*, 2010, **107**, 10337–41.
- [18] K.-Y. Ju, Y. Lee, S. Lee, S. B. Park, and J.-K. Lee, *Biomacromolecules*, 2011, **12**, 625–32.
- [19] T. S. Balaban, *Accounts of chemical research*, 2005, **38**, 612–23.
- [20] M. Sun, *International Journal of Quantum Chemistry*, 2006, **106**, 1020–1026.
- [21] Z. Chen, T. F. Jaramillo, T. G. Deutsch, A. Kleiman-Shwarscstein, A. J. Forman, N. Gaillard, R. Garland, K. Takanabe, C. Heske, M. Sunkara, E. W. McFarland, K. Domen, E. L. Miller, J. a. Turner, and H. N. Dinh, *Journal of Materials Research*, 2011, **25**, 3–16.
- [22] G. S. Bethell, J. S. Ayers, and W. S. Hancock, *The Journal of Biological Chemistry*, 1979, **254**, 2572–2574.

## Hol Jobb: a Fitotronban vagy a Konyhában?

Schvéder Eszter<sup>1</sup>, Dudás Zsolt<sup>2</sup>, Stefanovits-Bányai Éva<sup>3</sup>, Firtha Ferenc<sup>1</sup>,  
Papp Nóra<sup>3</sup>

<sup>1</sup>BCE, Élelmiszertudományi Kar, Fizika-Automatika Tanszék, Budapest

<sup>2</sup>ELTE, Informatikai Kar, Programozási Nyelvek és Fordítóprogramok Tanszék, Budapest

<sup>3</sup>BCE, Élelmiszertudományi Kar, Alkalmazott Kémia Tanszék, Budapest

### Abstract

Sprouts are rich in vitamins and minerals, what was known to the ancients. Because of this health-conscious customers prefer this kind of consumer's goods in the organic food store. Germination known several advantages, such as low cost of the seeds, the short duration of the germination, and because of the costumer can garminate at home at any time, in any season without special horticultural knowledge. The goal of our research is to investigate controlled sprouts and those affected by the natural environment, and measure the antioxidant capacity, content of chlorophyll and carotene. We found, that sprouts from our propagator had higher antioxidant capacity compared to the conventional method, the chlorophyll and carotene content increased with the temperature.

### Összefoglalás

A növényi csíra ásványi anyagokban és vitaminokban gazdag, ami már az ókorban is ismert volt. Így az erre specializálódott üzletekben, például a bioboltokban egyre inkább keresett fogyasztási cikké kezd válni az egészségtudatos fogyasztók körében. A csíráztatásnak számos előnye ismert, mint például a csíragok alacsony ára, a csíráztatás rövid időtartama, illetve, hogy a fogyasztó maga csíráztathat otthoni kontrollált és ellenőrzött körülmények között bármely évszakban, speciális kertészeti ismeretek nélkül. A munkánk célja az volt, hogy megvizsgáljuk a szabályozott és a természetes környezeti hatásoknak kitett csíranövények antioxidáns kapacitását, valamint a karotin- és a klorofilltartalmát. Azt tapasztaltuk, hogy az általunk épített csíráztatóban a csíranövények antioxidáns kapacitása a hagyományos módszerhez képest magasabb volt, a klorofill- és karotintartalma a hőfok emelkedésével nőtt.

### Bevezetés

Az egészséges táplálkozással foglalkozó szakemberek a múlt század utolsó évtizedeiben kezdtek el egyre nagyobb figyelmet fordítani a csírák biológiai értékeinek meghatározására [1]. Azóta számos kutatás jelent meg a csírák emberi szervezetre kifejtett jótékony hatásairól [2]. A csírák fontos enzimeket, fehérjéket, szénhidrátokat, vitaminokat (A-, B-, C-, E-, K vitamin), ásványi anyagokat (például Zn, Fe, K, Ca Mg, Cu) és tápanyagokat tartalmaznak, valamint a magokhoz hasonlóan megnő bennük a többszörösen telítetlen zsírsavak és a szabad aminosavak aránya [3]. Mivel a növényt fejlődésének kezdeti stádiumában fogyasztjuk, így tápanyagsűrűségük igen nagy, ezért magasabb tápértékkel bírnak [4]. A csíranövénynek flavonoid-tartalma különböző és a csírák fejlődése során tartalmuk folyamatosan változik. Általában az első négy napban a növények flavonoid-tartalma nő, majd a negyedik nap után csökken, de hosszabb csíráztatás során újból elkezd nőni [5]. A kutatások során azt is megállapították, hogy a növények flavonoid tartalma összefüggésben van a környezettel szembeni védekezőképességével [5]. A csírázás során az antinutritív anyagok (tannin, pentozán, fitinsav) mennyisége csökken, ezáltal a csírák emészthetőbbé válnak. A keményítő-tartalom is lecsökken, ami a megnövekedett amiláz

aktivitásnak köszönhető, így a di- és monoszacharidok mennyisége megnő [6]. A fehérjetartalom, aminosavak, zsírsavak mennyisége jelentősen nem változik a csíráztatás során [7]. A csíráztatást követően a növényekből számos jótékony hatással bíró fitokémiai komponens, mint például antioxidáns és glükozinolát mutatható ki [8]. Ezek közül néhány egészségvédő fitokémikália nagyobb koncentrációban van jelen a csírában, mint a kifejlődött növényben [9]. Munkánk során célul tűztük ki, egy hétköznapi fogyasztóknak szánt, általános csíráztatási célokra kialakított automatizált csíráztató berendezés elkészítését. A növények számára kontrollált körülményeket kialakítva megvizsgáltuk, hogy tapasztalunk-e jelentős változást azok antioxidáns kapacitásában, valamint karotin- és klorofilltartalmában.

## Anyagok és módszerek

**A fitotron nagyobb fizikai és szoftveres részei:** A különböző alkatrészeket egy számítógépen (Raspberry Pi) futó Erlang programozási nyelven megírt szoftver vezérelte. A természetes fény mellett a csírák megvilágítását 6:1 arányban nagy teljesítményű piros és kék ledes fényforrások [10] adták. A hőmérsékletet egy hőmérő modul által szolgáltatott adatok alapján Peltier elemmel szabályozta a rendszer. A vizet egy szobaszőkőkút szivattyú pumpálta a fitotronban lévő csírákra a hagyományos csíráztatásnál is alkalmazott gyakorisággal (naponta kétszer).

**Nyersanyag:** A kereskedelmi forgalomban kapható búzamagok (*Triticum aestivum* L.) és retekmagok (*Raphanus sativus* L.) voltak.

**Minta-előkészítés:** A különböző csíraminták antioxidáns kapacitásának, karotin-, és klorofilltartalmának összehasonlításához két párhuzamos mintát csíráztattunk az általunk épített fitotronban eltérő hőmérsékleteken (25°C, 30°C, 35°C-on), melynek célja a növényi stressz hatás vizsgálata volt. Ezzel párhuzamosan otthoni körülmények között is folytattunk csíráztatást, kitéve ezzel a növényt a csírázást befolyásoló környezeti paraméterek folyamatos változásának.

**TPC- Összes polifenoltartalom meghatározása Folin-Ciocalteu reagenssel:** A vizsgált minták összes polifenol-tartalmát  $\lambda=760$  nm-en Folin-Ciocalteu reagenssel segítségével határoztuk meg [11]. A galluszsavra vonatkoztatott polifenol- tartalmat mmol galluszsav-ekvivalens/g szárazanyag-tartalomra vonatkoztatva (GSE/g szárazanyag) adtuk meg.

**Összes antioxidáns kapacitás meghatározása FRAP (Ferric Reducing Antioxidant Power) módszerrel:** A módszer segítségével a  $\text{Fe}^{2+}$ - TPTZ-t tartalmazó oldat kék színének erősségéből spektrofotometriás úton ( $\lambda=593$  nm) mérhető a mintában levő vegyületek redukáló képessége [12]. Az eredményeket mmol aszkorbinsav-ekvivalens /g szárazanyag- tartalomra vonatkoztatva (ASE/g szárazanyag) adtuk meg.

**Összes antioxidáns kapacitás meghatározása TEAC (Trolox Equivalent Antioxidant Capacity) módszerrel:** Spektrofotometriás úton 734 nm-en megmérhetük az antioxidáns hatású vegyületek következtében létrejövő színváltozást [13]. Kalibrációs sztenderdnek Trolox oldatot használtunk. Az eredményeket mmol Trolox-ekvivalens /g szárazanyag- tartalomra vonatkoztatva (TE/g szárazanyag) adtuk meg.

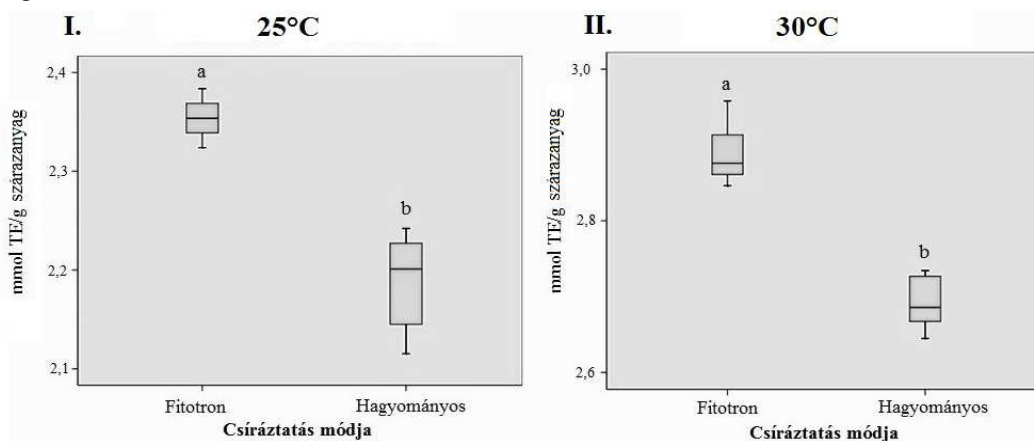
**Karotin- és klorofilltartalom mérése:** A csíra levelek karotinod- és klorofill tartalmának meghatározása során a mintákat először egy 80 tömegszázalékos acetone oldattal kiextraháltuk, majd a szeparációt követően a minta abszorbanciáját spektrofotometriás módszerrel a klorofill A és klorofill B esetében 644 nm és 663 nm hullámhosszon [14], míg a karotinoidoknál 480 nm-en fotometráltuk [15].



## Eredmények és kiértékelésük

Egyik kísérleti célunk volt a különböző módokon és hőmérsékleteken csíráztatott növények antioxidáns kapacitásának, valamint karotin- és klorofilltartalmának meghatározása. A csírák antioxidáns kapacitását minden esetben mindhárom mérőmódszerrel megmértük. Az eredmények hasonlósága miatt csak az általunk kiválasztott mérőmódszerek segítségével szemléltettük. A szignifikánsan eltérő csoportokat az ábrákon is eltérő betűkkel jeleztük.

Megvizsgáltuk, hogy van-e különbség a csíráztatási módok között, eltérő hőmérsékleten, különböző csírafajtánál. A hagyományos módon és a fitotronban csíráztatott retek- és búzamatot csak 25°C-on és 30°C-on tudtuk összehasonlítani, mivel ezek a hőmérséklet értékek mindkét mérőmódszer esetén megegyeztek. Tehát mikor a fitotronban 25°C és 30°C-os csíráztatást folytattunk az otthoni napi átlagos hőmérséklet is 25°C és 30°C körül volt. Megvizsgáltuk, hogy a csíráztatás módjától függően tapasztalható-e jelentős antioxidáns kapacitás eltérés. Mivel mindkét csírafajtánál ugyanazt a tendenciát tapasztaltuk, ezért az 1. ábrán a búzacsíra példáján keresztül TEAC mérőmódszerrel szemléltettük a mérőmódszerek közti különbséget.

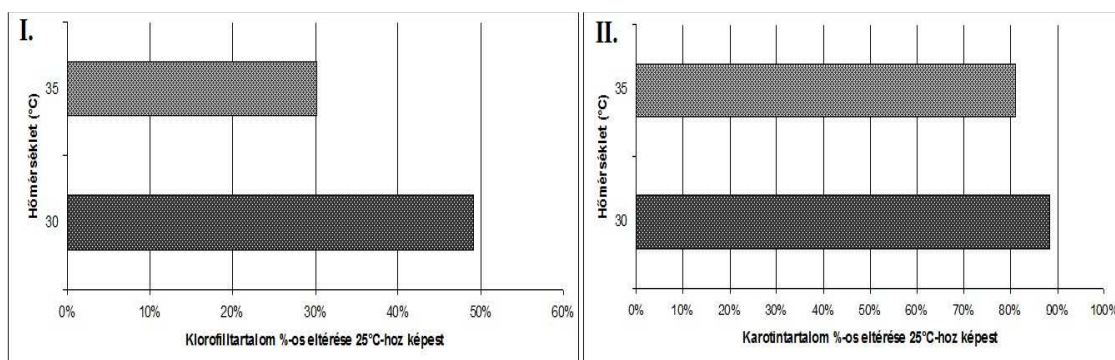


**1. ábra: Eltérő hőmérsékleten, valamint fitotronban és hagyományos módon csíráztatott búza (I., II.) antioxidáns kapacitásának meghatározása TEAC módszerrel.**

Az eredményeket kiértékelve mindkét csírafajtánál és hőmérséklet értéknél ugyanazt tapasztaltuk. A búza- és a retekcsíra antioxidáns kapacitása 25°C-on és a 30°C-on is szignifikánsan nagyobb volt a fitotronban, mint a hagyományos csíráztatási mód esetében. A hagyományos módon csíráztatott növények szórás értékei is sokkal nagyobbak voltak a fitotronban kifejlődött növényekénél, mely az additív stressz hatással van összefüggésben.

Mivel a kapott eredmények azt igazolták, hogy a fitotronban csíráztatott búza és retek antioxidáns kapacitása nagyobb volt, ezért további vizsgálatokat végeztünk arra vonatkozóan, hogy az eltérő hőmérséklet értékeken hogyan változik a búzacsíra karotin- és klorofilltartalma a különböző hőmérsékleteken (2. ábra). Azt tapasztaltuk, hogy a 25°C-os csíráztatási hőmérséklethez viszonyítva 30°C-on és 35°C-on nőtt a növények karotin- és klorofilltartalma. A búzacsíra klorofilltartalma 30°C-on volt a legnagyobb, míg 35°C-on az eltérés már sokkal kisebb volt. A karotintartalom mérési eredménye ugyanazt a tendenciát mutatja, mint amit a klorofilltartalomnál láthatunk.





**2. ábra: Fitotronban csíráztatott búza klorofill- (I.) és karotintartalmának(II.) százalékos eltérése 25°C-hoz képest különböző hőmérséklet értékeken.**

### Következtetések

Előkísérletünk alapján jobb eredményt értünk el a csírák antioxidáns kapacitását illetően a házilag elkészített kontrollált környezeti paramétereket biztosító fitotronban, mint a hagyományos csíráztatás során. Továbbá megállapítottuk, hogy a fitotronban csíráztatott növények karotin- és a klorofilltartalma a 25°C-os csíráztatási hőmérséklethez képest 30°C-on volt a legnagyobb.

### Köszönetnyilvánítás

A kémiai mérések költségét az OTKA K84290 támogatta.

### Felhasznált irodalom

- [1] Penas, E., Gomez, R., Frias, J., Vidal-Valverde, C. (2008). Application of high-pressure on alfalfa (*Medicago sativa*) and mung bean (*Vigna radiata*) seeds to enhance the microbiological safety of their sprouts. *Food Control*. 19. 698-705.
- [2] Shapiro, T.A., Fahey, J.W., Wade, K.L., Stephenson, K.K., Talalay, P. (2001). Chemoprotective glucosinolates and isothiocyanates of broccoli sprouts: metabolism and excretion in humans. *Cancer Epidemiology Biomarkers and Prevention*. 10. 501-508.
- [3] Márton, M., Csapó, J. (2010): The role of sprouts in human nutrition. *Acta Agraria Kaposváriensis*, 14 (1): 31-55.
- [4] Finley, J.W. (2005). Proposed criteria for assessing the efficacy of cancer reduction by plant foods enriched in carotenoids, glucosinolates, polyphenols and selenocompounds. *Annals of Botany*. 95. 1075-1096.
- [5] Sousa, C., Lopes, G., Pereira, D.M., Taveira, M., Valentão, P., Seabra, R.M., Pereira, J.A., Baptista, P., Ferreres, F., Andrade, P.B. Screening of antioxidant compounds during sprouting of *Brassica oleracea* L. var. costata DC. 2007. *Combinatorial Chemistry & High Throughput Screening* 10:377-386.
- [6] Mwikya, S.M., Camp, J.V., Rodriguez, R., Huyghebaert, A., Effects of sprouting on nutrient and antinutrient composition of kidney beans 2001. *European Food Research and Technology* 212:188-191.
- [7] Danilcenko, H., Taraseviciene, Z., Jariene, E., Gajewski, M., Szymczak, P., Seroczynska A. (2006): Vegetables seeds – nutritional aspects in response to germination time. *Vegetables Crops Research Bulletin* 65: 39-48.
- [8] Sangronis, E., Machado, C.J. (2007). Influence of germination on the nutritional quality of

*Phaseolus vulgaris* and *Cajanus cajan*. LWT. 40. 116-120.

[9] Fernández-Orozco, R., Piskula, M.K., Zielinski, H., Kozłowska, H., Frias, J., Vidal-Valverde, C. (2006). Germination as a process to improve the antioxidant capacity of *Lupinus angustifolius* L. var. Zapaton. European Food Research and Technology. 223. 495-502.

[10] <http://kertlap.hu/szobanovenyek-megvilagitasa/>, 2015

[11] Singleton, V. L. Rossi, J. A. (1965): Colorimetry of total phenolics with phosphomolibdic-phosphotungstic acid reagents. Am. J. Enol. Vit., 161. 144-158.

[12] Benzie, I.I.F., Strain, J.J. (1996): The ferric reducing ability of plasma (FRAP) as a measuring of „antioxidant power”. The FRAP assay. Annal.Biocem., 239:70-76.

[13] Miller, N. J., Rice, Evans C., Davies, M. J., Gopinathan, V., Milner, A. (1993): A novel method for measuring antioxidant capacity and its application to monitoring the antioxidant status in premature neonates. Clinical Science, 84: 407-412.

[14] Arnon, D. I. (1949): Copper enzymes in isolated chloroplasts. Polyphenoloxidase in *Beta vulgaris*. Plant Physiol., 24: 1-15.

[15] Lichtenthaler H.K. (1987): Chlorophylls and carotenoids: pigments of photosynthetic membranes.- Methods Enzymol. 148: 350-382.

## Módszerfejlesztés Szintetikus Kannabinoidok Kimutatására Vizeletből

### Method Development for Determination of Some New Synthetic Cannabinoid Drugs from Urine

Sija Éva<sup>1\*</sup>, Berkecz Róbert<sup>2</sup>, Janáky Tamás<sup>2</sup>, Kereszty Éva<sup>1</sup>, Varga Tibor<sup>1</sup>, Institóris László<sup>1</sup>

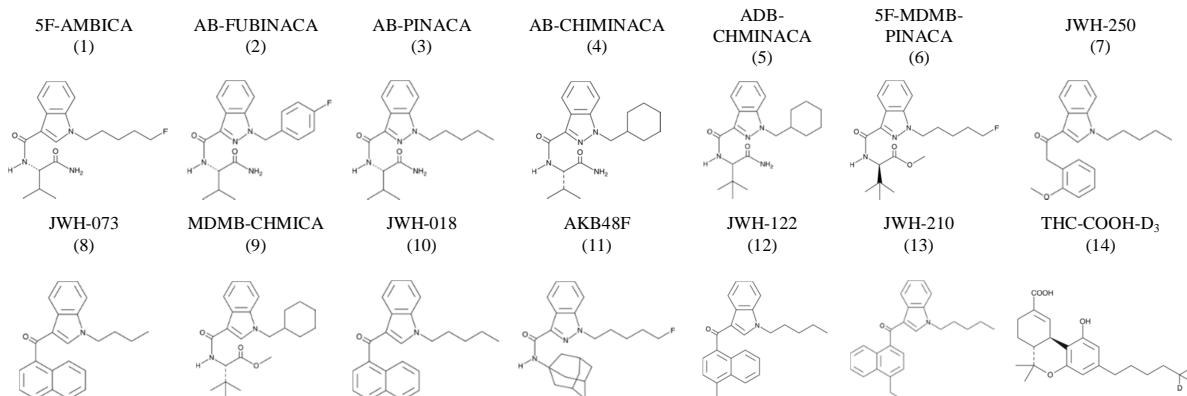
<sup>1</sup>Igazságügyi Orvostani Intézet, Szegedi Tudományegyetem, H-6724 Szeged, Kossuth Lajos sgt. 40, Hungary

<sup>2</sup>Orvosi Vegytani Intézet, Szegedi Tudományegyetem, H-6720 Szeged, Dóm tér 8, Hungary  
e-mail: sija.eva@med.u-szeged.hu

#### Abstract

The continuously increasing number of synthetic cannabinoids requires continuous method development for their determination in biological fluids.

The aim of this work was to develop a reversed-phase liquid chromatography-tandem mass spectrometry (LC-MS/MS) method for the analysis of 13 synthetic cannabinoids (5F-AMBICA, AB-FUBINACA, AB-PINACA, AB-CHMINACA, ADB-CHMINACA, 5F-MDMB-PINACA, JWH-250, JWH-073, MDMB-CHMICA, JWH-078, AKB-48F, JWH-122, JWH-210) in human urine samples.



For sample preparation two types of beta-glucuronidases were tried for glucuronide hydrolysis as it was unknown whether the substances are present in free or glucuronide form. The optimal enzyme concentration was 500 U/mL of *Helix Pomatia*. *E. Coli* glucuronidase or *Helix Pomatia* when it was applied in higher concentration resulted in a lower area under curve (AUC) for more substances related to the samples without enzymatic treatment.

#### Bevezetés

A kannabisz sokak számára egyet jelent a „füvezéssel”. Azonban tudatmódosító szerként való felhasználásán kívül a gyógyászatban is nagy jelentőségű. Az 1990-es évek elején számos tudományos kutatás folyt, melyek eredményeként felfedezték a szervezet belső kannabinoid

rendszerét. A receptorok két fajtája közül a CB1 receptor többnyire a központi idegrendszerben helyezkedik el – ehhez köthető a kannabisz hatóanyagának, a tetrahidrokannabinolnak (THC) pszichoaktív hatása is –, a CB2 receptorok pedig inkább az immunrendszer sejtjein találhatók. Ezek alapvető életfolyamatokat szabályoznak, rendellenességük gyulladásos folyamatokhoz és autoimmun zavarokhoz vezet [1]. Ezekhez a kannabinoid receptorokhoz kötődni képes hatóanyagokat nevezzük kannabinoidoknak. Az elmúlt 25 évben nagyszámú (több ezer) szintetikus kannabinoidot állítottak elő, a cél elsősorban pszichoaktív hatás nélküli, a CB2 receptorhoz szelektíven kötő hatóanyagok kifejlesztése volt. Az irodalomban számtalan példát olvashatunk szintetikus kannabinoidok előállításáról, állatkísérletek eredményeiről valamint a CB1 és CB2 receptorokhoz való kölcsönhatásukról [2]. Az előállított szintetikus kannabinoidok azonban sokszor jóval nagyobb pszichoaktív hatással rendelkeznek, mint maga a THC [3]. Mindez a fekete piac melegágyává vált, és nap mint nap kerülnek a drogpiacon az illegális laboratóriumok újabb és újabb termékei. A szintetikus kannabinoidokat különböző oldószerben oldják majd főként növényi törmelék felületére impregnálják. „Filléres” áruk miatt rendkívül népszerűek a tinédzserek körében. Sokszor csak néhány hónapig vannak jelen a fekete piacon, törvényi szabályozásuk után eltűnnek. Emiatt anyagcseréjükéről és kiválasztásukról nagyon keveset, olykor semmit nem tudunk. Ezek a szerek a szervezetbe kerülve már ng/ml-es koncentráció alatt is hatásosak. Egyes esetekben azt feltételezik, a metabolit lehet felelős a pszichoaktív hatásért. Kromatográfiai vizsgálatokhoz analitikai tisztaságú standardok beszerzése a nagy számuk, a gyorsan és kiszámíthatatlanul változó piac miatt rendkívül nehézkes. Sokszor a hatóságok által lefoglalt és azonosított standardok használatára kell támaszkodunk. Ezen okok miatt szintetikus kannabinoidok biológiai mintákból való kimutatása igazi kihívás.

Munkánk célja olyan módszer kifejlesztése volt, amely alkalmas a szintetikus kannabinoidok biológiai mintákból LC-MS/MS-sel történő kimutatására. Mivel a vegyületek egy része glükuronid formában választódik ki a vizeletbe, a minták béta-glükuronidáz enzimmel való kezelése elkerülhetetlen. Ezért megvizsgáltuk, hogy a béta-glükuronidáz típusa és mennyisége hogyan befolyásolja a mérési eredményeket. A minta-előkészítés során más laboratóriumokból származó, általuk már lemerített, illetve spike-olt negatív vizeletmintákhoz különböző mennyiségű *E. Coli*-ból és *Helix Pomatia*-ból (HP) származó béta-glükuronidázt adtunk, a mérési eredményeket enzimmel nem kezelt, spike-olt mintákkal hasonlítottuk össze.

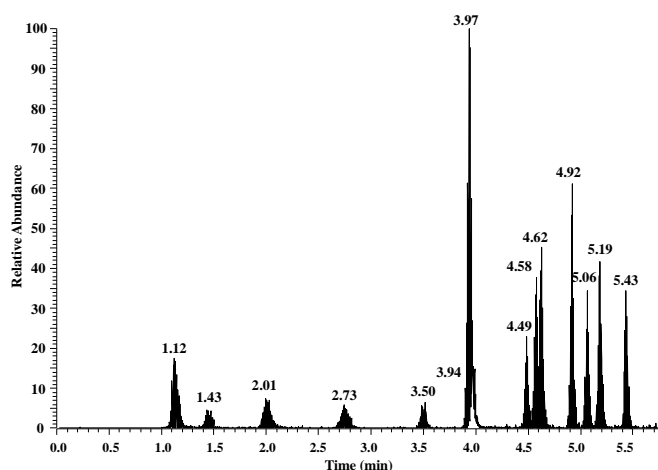
### Kísérleti körülmények

A mintaelőkészítés során 1 ml vizeletmintához 10 µl belső standardot (10 µg/ml THC-COOH-D<sub>3</sub>-oldat), béta-glükuronidázt (*Helix Pomatia* esetében 400 µl 0,1 mólos ecetsav/nátrium-acetát-pufferben, pH=5,0; *E. Coli* esetében 0,075 M-os, pH=6,8 foszforsav/nátrium-hidrogén-foszfát-pufferben) adtunk, és a mintákat 25 °C-on, egy éjszakán át inkubáltuk. A mintákhoz ezt követően 1,5 ml acetonitrilt és 400 mg ammónium-szulfátot adtunk majd. 1 perces vortexelés és centrifugálás (2500 rpm, 5 perc) után a felső fázisból 1,1 ml-t bepárló csőben nitrogén árammal (50 °C, 15 perc) szárazra pároltunk. A maradékot 100 µl ACN:H<sub>2</sub>O elegyben oldottuk és LC-MS/MS-sel (Agilent 1100 HPLC rendszer, Thermo Finnigan TSQ 700 MS, Phenomenex Kinetex C18-as oszlop 100 x 2,1 mm átmérő, 2,6 mikrométer szemcseméret, gradiens elúció: 0,1 % hangyasav-víz és 0,1 % hangyasav-ACN elegye) analizáltuk.

### Eredmények és értékelésük

Az 1. ábrán egy spike-olt negatív vizelet tipikus kromatogramja látható. A vegyületek

azonosítása a standard vegyületek retenciós idejével, atömegspektrumában megjelenő jellegzetes ionokkal, valamint azok arányának összehasonlításával történik. A vegyületek retenciós idejét és MRM átmeneteit a 1. táblázatban foglaltuk össze. Mennyiségi meghatározásuk előzetesen felvett kalibrációs görbék segítségével történt.

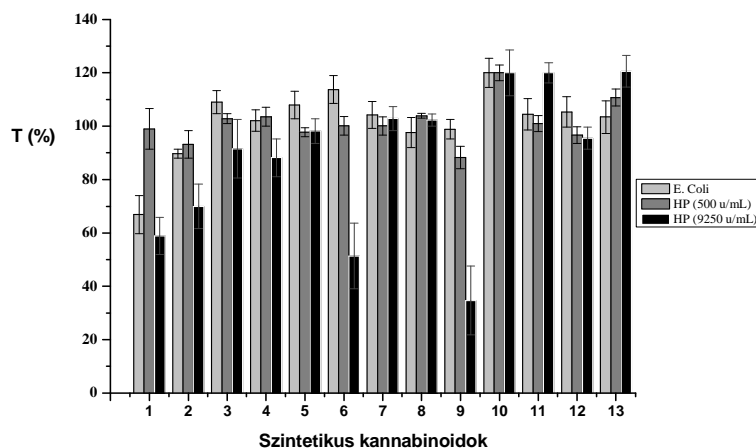


1. Ábra HP-val kezelt, spike-olt vizelet minta TIC kromatogramja

1. Táblázat: A vizsgált szintetikus kannabinoidok legfontosabb kromatográfiás paraméterei (\*belső standard)

	Komponens	MRM-átmenetek	RT (perc)		Komponens	MRM-átmenetek	RT (perc)
1	5F-AMBICA	348.0; 232.0; 144.0	1.12	8	JWH-073	328.0; 155.0; 127.0	4.58
2	AB-FUBINACA	369.0; 253.0; 109.0	1.43	9	MDMB-CHMICA	385.0; 240.0; 144.0	4.62
3	AB-PINACA	331.0; 215.0; 286.0	2.01	10	JWH-018	342.0; 155.0; 214.0	4.92
4	AB-CHMINACA	357.0; 241.0; 312.0	2.73	11	AKB48F	384.0; 135.0; 93.0	5.06
5	ADB-CHMINACA	371.0; 241.0; 326.0	3.5	12	JWH-122	356.0; 169.0; 141.0	5.19
6	5F-MDMB-PINACA	378.0; 233.0; 318.0	3.94	13	JWH-210	370.0; 183.0; 214.0	5.43
7	JWH-250	336.0; 121.0; 91.0	4.49	14	THC-COOH D <sub>3</sub> *	348.0; 330.0; 302.0	3.97

Célunk az volt, hogy a már meglévő eljárást hatékonyabbá tegyük, és megállapítsuk hogyan hat a különböző enzimes kezelés a szintetikus kannabinoidok kimutatására.



**2. Ábra** Enzimkezelés hatása szintetikus kannabinoidok görbe alatti területére

A 2. ábrán a különböző enzimes kezelésnek kitett minták kromatogramja alapján nyert görbék csúcs alatti területeinek változását mutatjuk be. Referenciaként (100%) az enzimet nem tartalmazó acetát-puffer-oldattal kezelt vizeletminták szolgáltak. Ha összehasonlítjuk, hogyan változik a kapott kromatogramokon az egyes anyagok görbe alatti területe különböző enzimes kezelés hatására spike-olt vizeletekben, láthatjuk, hogy a nagyobb koncentrációban alkalmazott HP béta-glükuronidáz enzim hatására több esetben is szignifikánsan csökkent a görbe alatti terület a kontroll mintákhoz képest. MDMB-CHMICA, 5F-MDMB-PINACA és 5F-AMBICA esetében a visszanyerés 60%-nál kevesebb volt. Ennek a jelenségnek több oka is lehet. Elképzelhető, hogy a nagy enzimkoncentráció az inkubálási idő alatt a molekulák degradációját okozta. A másik ok lehet, hogy az enzimfehérjék felületére a drogmolekulák adszorbeálódtak, mely szintén okozhatta a visszanyerés hatékonyságának csökkenését. Ehhez fontos megjegyeznünk, hogy a törzsoldatként használt HP enzim-koncentrátum nem homogén oldat, hanem inkább szuszpenzióhoz hasonlítható. Az 500 U/ml-es koncentrációban alkalmazott enzimes kezelés E. Coli, és HP-ból nyert béta-glükuronidáz enzim esetében sem csökkentette jelentős mértékben a görbe alatti területeket. A legtöbb esetben az enzimes kezelés nélküli visszanyerésekhez hasonló eredményeket kaptunk. (Ez alól az 5F-AMBICA jelent kivételt E. Coli enzimes kezelés hatására, ahol a csúcs alatti terület ~ 60 %-ra csökkent).

Vizsgálataink során lehetőségünk nyílt arra, hogy más laboratóriumból származó, pozitív vizeletmintákkal is dolgozzunk. A pozitív minták vizsgálatakor E.Coli béta-glükuronidáz enzimes mintaelőkészítést alkalmaztunk. A mérési eredményeket a 2. táblázatban mutatjuk be.

**2. Táblázat:** Pozitív vizeletminták E. Coli enzimes kezelés során nyert görbe alatti területének %-os aránya

Anyagok	Csúcssterület %
5F-AMBICA	52.9
ADB-CHMINACA	167
MDMB-CHMICA	89.9

A számolt csúcssterület 5F-AMBICA és MDMB-CHMICA esetében hasonló volt a spike-olt mintáknál kapott eredményekhez. ADB-CHMINACA esetében azonban a csúcssterületre az enzimmel nem kezelt mintákhoz hasonlítva jóval nagyobb értéket kaptunk. Az kísérlet eredményeiből arra következtetünk, hogy az 5F-AMBICA és MDMB-CHMICA nem glükuronid



formában, hanem az ADB-CHMINACA glükuronidált formában jelent meg a vizeletben, melynek kimutatását az enzim jelenléte segítette.

### **Konklúzió**

Eredményeink szerint a glükuronidot képező származékok legmagasabb koncentrációit az 500 U/ml Helix Pomatia enzimmel végzett kezelést követően mértük. Ennél nagyobb koncentrációknál, vagy E. Coli enzim alkalmazásakor egyes esetekben a kimutatás hatékonysága csökkent.

A módszert jelenleg 16 származék meghatározása (5F-AMBICA, AB-FUBINACA, AB-PINACA, AB-CHMINACA, ADB-CHMINACA, MDMB-CHMICA, 5F-MDMB-PINACA, 5F-AMB, ADB-PINACA, AKB-48F, PB-22, JWH-250, JWH-073, JWH-018, JWH-122 és JWH-210) alkalmazzuk; a más laboratóriumokból származó pozitív minták ismételt mérése jól igazolja a módszer megfelelőségét.

### **Köszönetnyilvánítás**

A szerzők szeretnék kifejezni köszönetüket Vannai Mariannak (Igazságügyi és Biztosítás-orvostani Intézet, SOTE), Dobos Adriennek és Hídvégi Elődnek (ISZKI OITI) módszerfejlesztésben való nélkülözhetetlen segítségükért.

### **Irodalomjegyzék**

- [1] A.C. Howlett, Prostaglandins Other Lipid Mediat. 68–69 (2002) 619.
- [2] J.W. Huffman, G. Zengin, M. Wu, J. Lu, G. Hynd, K. Bushell, A.L.S. Thompson, S. Bushell, C. Tartal, D.P. Hurst, P.H. Reggio, D.E. Selley, M.P. Cassidy, J.L. Wiley, B.R. Martin, Bioorganic & Medicinal Chemistry, 13 (2005) 89.
- [3] M.S. Castaneto, D.A. Gorelick, N.A. Desrosiers, R.L. Hartman, S. Pirard, M.A. Huestis, Drug and Alcohol Dependence, 144 (2014) 12.

## Identification of By-products Formed During the Oxidative Transformation of Phenylurea Pesticides

Gergő Simon<sup>1,2\*</sup>, Virág Farkas<sup>1,2</sup>, András Dombi<sup>1</sup>, Klára Hernádi<sup>1</sup>, Tünde Alapi<sup>1,2</sup>

<sup>1</sup>Research Group of Environmental Chemistry, University of Szeged, H-6720 Szeged, Rerrich Béla tér 1, Hungary

<sup>2</sup>Department of Inorganic and Analytical Chemistry, University of Szeged, H-6720 Szeged, Dóm tér 7, Hungary

e-mail: gsimon@chem.u-szeged.hu

### Abstract

The goal of this study was to identify the by-products that form during the oxidative degradation of five phenylurea pesticides. Four advanced oxidation processes were used including photolysis, ozonation, heterogeneous photocatalysis, and the combination of photolysis with ozonation. After concentrating the by-products using solid phase extraction, our samples were analyzed by mass spectrometry. We have managed to identify the main products for each pesticide and process, from which we could determine that the main reactions during the application of AOPs were the dehalogenisation and hydroxylation of the aromatic ring, as well as the terminal demethylation and the oxidation of the methyl groups.

### Introduction

Organic contaminants, such as pesticides, pharmaceuticals, etc. have become a major concern regarding the environment due to their persistence and low biodegradability that can lead to accumulation in soils and waters.<sup>[1]</sup> A large number of these contaminants have presumed or proven negative health effects (carcinogens, endocrine disruptors). Phenylurea herbicides are one such type of chemicals that are widely used for weed control, mostly in non-agricultural areas, and their high half-life in soils<sup>[2]</sup> causes them to wash into waters, even appearing in drinking water. Another problem is that regular water treatment methods often are ineffective in the removal of these contaminants. Therefore applicable methods are being developed based on advanced oxidation processes (AOPs) that are capable of the degradation of organic matter by forming highly reactive radicals. These methods include photolysis by ultraviolet light, ozonation, heterogeneous photocatalysis, Fenton-reaction, which can be effective themselves, but also can be further improved by their combination<sup>[3]</sup>, resulting in higher radical concentrations or different reaction pathways. This also means that the various processes will result in different by-products that can be identified using mass spectrometry. This information is essential for the development of analytical processes for these compounds and their metabolites.

### Materials and methods

Four phenylurea pesticides were used for our experiments, as presented on **Figure. 1**.

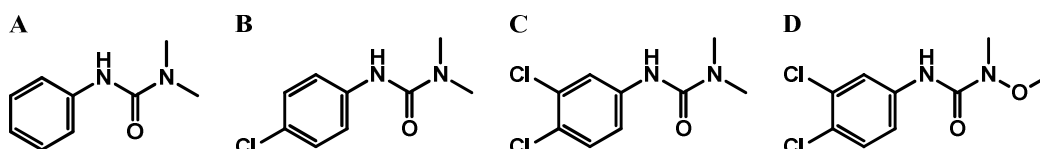


**Figure 1.** Molecular formulae of the pesticides: A: fenuron; B: monuron; C: diuron; D: linuron. During the experiments 500 cm<sup>3</sup> of aqueous pesticide solutions ( $c_0 = 3.7 \times 10^{-5} \text{ mol dm}^{-3}$ ) were circulated with a peristaltic pump between the stirred reservoir and reactor tanks, both were thermostated at  $25 \pm 0.1^\circ \text{C}$ . The solutions were bubbled with air (in case of photolysis and photocatalysis) or oxygen (in case of ozonation and the combined UV/ozone method) 10 minutes before and throughout the measurements.

Three low-pressure mercury vapour lamps with identical parameters (15 W, 227 mm arc length, 307 mm length and 20.5 mm external diameter) were used, emitting at differing wavelengths: standard UV (254 nm), UV/VUV (185 and 254 nm) and fluorescent lamp (with maximum emitted photon flux at 365 nm). Each process was executed by the selection of the light source and the material of the envelope (quartz or glass) covering it. The measurements were initiated by switching the lamp on.

Process	Lamp	Envelope
Photolysis	254 nm	quartz
Ozonation	185/254 nm	perforated glass
Photolysis and ozonation	185/254 nm	perforated quartz
Heterogeneous photocatalysis	365 nm	quartz

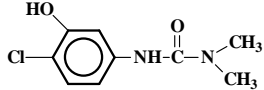
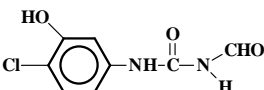
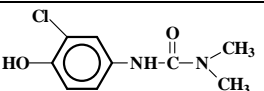
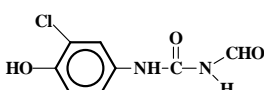
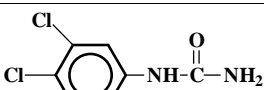
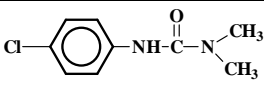
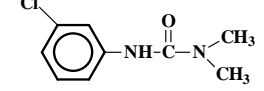
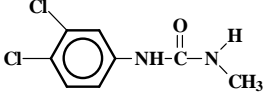
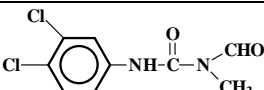
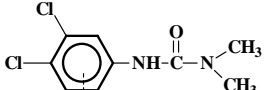
UV-vis spectrometry was performed using an Agilent 8453 spectrophotometer, while high-performance liquid chromatographic measurements were made utilizing an Agilent 1100 modular HPLC system equipped with a diode-array detector. The mobile phase consisted of acetonitrile and water (60:40 %V/V) for diuron and linuron, also methanol and water (60:40 %V/V) for fenuron and monuron. For isoproturon gradient elution was used according to Kovalczuk et al.[4] The separation of compounds was achieved on a LiChroCART® C-18 column (250 mm  $\times$  4 mm, 5  $\mu\text{m}$ ) at  $25^\circ \text{C}$  temperature with an injection volume of 20  $\mu\text{L}$ . The mass spectrometric measurements were performed on an Agilent G1956A quadrupole mass spectrometer.

## Results

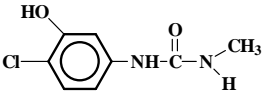
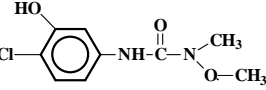
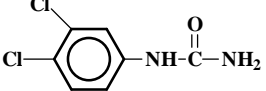
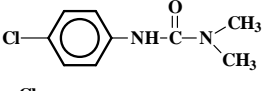
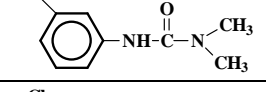
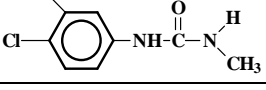
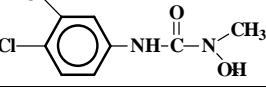
From the degradation curves of the target compounds, the initial rates of transformation can be obtained, which serves as the basis of the comparison of the processes. Furthermore, the time required to transform 50 % the parent compound can also be calculated, which is important in the identification of the by-products, the reason being that at this point most of them are present in the solutions.

Mass spectrometric measurements were made both with the original and the concentrated samples. The identified by-products are shown in the following tables (**Tables 1-4**). The tables contain the products' retention times, molecular weight, number of chlorine atoms, the suggested formulae, and the processes during which each of them were detected. The results indicate that during the oxidative transformation of these compounds the hydroxylation and dehalogenisation of the aromatic ring, the oxidation of the methyl groups, and terminal demethylation are the primary reactions in all cases.

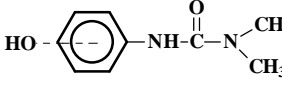
**Table 1.** By-products formed during the oxidative transformation of diuron  
(○: detected without enrichment by SPE, ●: detected after enrichment by SPE)

Retention time (min)	M	Cl	Suggested formula	UV photolysis (UV)	Ozonation (O <sub>3</sub> )	Combined method (UV/O <sub>3</sub> )	Het. Photocat. (TiO <sub>2</sub> )
2.78	213	0		○			○
3.09	213	0		○		○	○
3.24	214	1	 	○●	●	●	●
3.39	214	1	 	●	●	●	●
4.06	204	2		○●	○●	○●	○●
4.51	198	1	 	●	○●	●	
5.06	218	2		○●	○●	○●	○●
5.58	203	2		○	●	○●	○●
8.22	246	2		○●	○	●	○●
9.08	248	2		●	●	●	●
9.38	232	2	possible diuron contamination	●	●	●	●

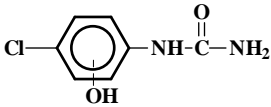
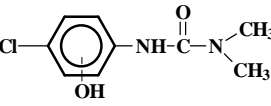
**Table 2.** By-products formed during the oxidative transformation of linuron  
(○: detected without enrichment by SPE, ●: detected after enrichment by SPE)

Retention time (min)	M	Cl	Suggested formula	UV photolysis (UV)	Ozonation (O <sub>3</sub> )	Combined method (UV/O <sub>3</sub> )	Het. Photocat. (TiO <sub>2</sub> )
2.46	200	1		○●		○●	●
3.13	230	1		●		●○	
3.22	204	2		○●	○●	○●	○●
3.58	198	1	 		●		●
4.04	218	2		○●	●	○●	○●
4.55	234	2			●		●
4.64	203	2					●
4.86	232	2		●	●	●	●
5.90	203	2		●	●	●	●
11.20	280	2		●	●		

**Table 3.** By-products formed during the oxidative transformation of fenuron (○: detected without enrichment by SPE, ●: detected after enrichment by SPE)

Retention time (min)	M	Suggested formula	UV photolysis (UV)	Ozonation (O <sub>3</sub> )	Combined method (UV/O <sub>3</sub> )	Het. Photocat. (TiO <sub>2</sub> )
2.61	186		○●	○●	○●	○●
3.33	180		○●	○●	○●	○●
4.00	186		○●	○	○●	○●
4.85	164			○●	●	●

**Table 4.** By-products formed during the oxidative transformation of monuron  
(○: detected without enrichment by SPE, ●: detected after enrichment by SPE)

Retention time (min)	M	Cl	Suggested formula	UV photolysis (UV)	Ozonation (O <sub>3</sub> )	Combined method (UV/O <sub>3</sub> )	Het. Photocat. (TiO <sub>2</sub> )
2.59	202	0		○●	○●	○●	○●
3.58	235	0		○●	○●	○●	○●
4.88	153	1		●		●	●
5.63	214	1				●	●
5.99	198	1	possible isomers of monuron				●
7.58	198	1				●	●
9.54	198	1			○●	○●	
11.09	220	1		●	●	●	

We have identified the most by-products for diuron, followed by linuron, while we could identify only 2 and 1 products for monuron and fenuron, respectively. In the case of monuron we have found several products with the same mass, which we consider to be contamination in the initial compound.

### Conclusions

- We have successfully identified the main products of the oxidative transformation of four phenylurea herbicides
- The main reaction pathways have been found to be the dehalogenation and hydroxylation of the aromatic ring, and also the demethylation and oxidation of the methyl groups

### References

- [1] Barbash, J.E., Thelin, G. P., Kolpin, D. W., Gilliom, R. J., J. Environ. Qual., 2001. 30(3): p. 831-45.
- [2] Katsumata, H., Kaneco, S., Suzuki, T., Ohta, K., Yobiko, Y., Chem. Eng. J., 2005. 108(3): p. 269-276.
- [3] Hoigne, J., The Handbook of Environmental Chemistry, 1998.
- [4] Kovalczuk, T., J. Poustka, and J. Hajslova, Czech J. Food Sci., 2006. 26(2): p. 146-152.



## Antioxidáns Hatású Vegyületek Koncentrációjának Változása Pirosribiszke-Lé Membránszeparációval Történő Besűrítése Során

Dóra Schenk<sup>1</sup>, Diána Furulyás<sup>2</sup>, Nóra Papp<sup>3</sup>, Szilvia Bánvölgyi<sup>1\*</sup>, István Kiss<sup>4</sup>, Éva Stefanovits-Bányai<sup>3</sup>, Gyula Vatai<sup>1</sup>

<sup>1</sup>Budapesti Corvinus Egyetem, Élelmiszeripari Műveletek és Gépek Tanszék, 1118 Budapest, Ménesi út 44.

<sup>2</sup>Budapesti Corvinus Egyetem, Konzervtechnológiai Tanszék, 1118 Budapest, Villányi út 29-43.

<sup>3</sup>Budapesti Corvinus Egyetem, Alkalmazott Kémia Tanszék, 1118 Budapest, Villányi út 29-43.

<sup>4</sup>Fitomark Kft., 3934 Tolcsva, Arany János u. 16/a.

### Összefoglalás

A piros ribiszke (*Ribes rubrum* L.) a bogyós gyümölcsök többségéhez hasonlóan pozitív táplálkozás-élettani hatásokkal bíró, és színét biztosító antioxidáns hatású vegyületeket tartalmaz. A különböző feldolgozási módok hatása az egyes vegyületek koncentrációjára manapság az élelmiszeripar számára egyre fontosabb. A kísérletek során három különböző módszerrel - FRAP, TPC és antocianin méréssel - vizsgáltuk a gyümölcslé jellemző antioxidáns hatású vegyületek koncentrációjának változását a besűrítés egyes lépcsői után. A besűrítést 3 lépcsőben végeztük: mikroszűréssel (MF) való tükrösítés után fordított ozmózissal (RO) készítettünk egy fél-sűrítmenyt, melyet ozmotikus desztillációval (OD) végsűrítettünk. A mérés minden lépését kéméletes hőfokon, 25 °C-on végeztük. A besűrítés végére a sűrítmeny szárazanyag-tartalma 70 Brix% fölé emelkedett. A polifenol és antioxidáns kapacitás tartalom nem változott jelentősen az OD sűrítés alatt, míg a színanyagok koncentrációja közel négyszeresére emelkedett.

### Bevezetés

Az ember számára mindig is a zöldségek és főként a gyümölcsök jelentették az elsődleges vitaminforrást. Az információs forradalomnak és a szigorú szabályozásoknak köszönhetően a mai fogyasztó az interneten, vagy akár a termék csomagolásáról pillanatok alatt információt szerezhet a termék összetételéről, tápanyag- és vitamintartalmáról. A kialakuló fogyasztói tudatosság egyre jobban elvárja a termékek tápanyagokkal szemben kéméletes és minél kevésbé környezetterhelő gyártástechnológiáját.

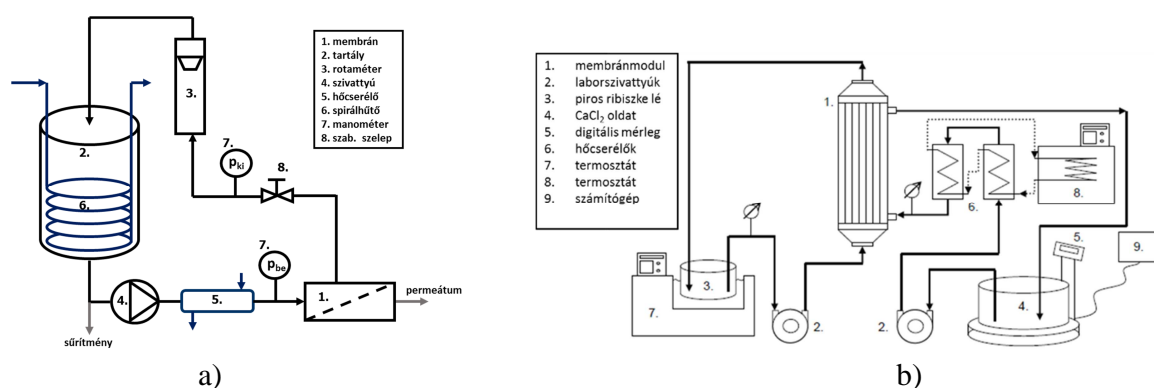
Újfajta szempontot jelent a kutatásoknál, hogy kiderült, a növényi termékek bizonyos kémiai komponensei kedvező élettani hatással (pl. antioxidáns hatás) rendelkeznek, melyek szerepet játszhatnak az emberi szervezetre káros folyamatok, megbetegedések megelőzésében, kivédésében. Az aktív oxigénformák káros hatása bizonyított mind az ateroszklerózis (érelmeszesedés), a diabetes mellitus (cukorbetegség), a gyulladásos folyamatok és a daganatos megbetegedések kapcsán [1, 2].

Választásunk azért esett a piros ribiszkére, mert a fogyasztók számára kellemesebb érzékszervi tulajdonságokkal, ízzel és illattal rendelkezik a fekete ribiszkével ellentétben. A termesztési viszonyokra is kevésbé érzékeny, hazai termesztésének több évszázados hagyománya van [3, 4]. Kísérleteinkben membránszűréssel végeztük a pirosribiszke-lé előszűrését és besűrítését. Célunk az volt, hogy a piros ribiszke értékes komponenseit megőrizzük a besűrítés alatt, amelyre alkalmas a membrántechnika. A hagyományos technikákkal szemben a membránszeparáció előnye, hogy alacsony hőmérsékleten megvalósítható, így elkerülhető a vitaminok és értékes

komponensek sérülése, elbomlása [5]. A technika emellett környezetkímélő, mert nincs szükség kémiai segédanyag használatára, valamint a sűrítés során keletkező szűrlet (permeátum) víz tisztaságú, amely csatornába engedhető vagy visszaforgatható [6].

## Anyagok és módszerek

A mérések során használt piros ribiszke lé a Fitomark Kft.-től (Tolcsva) került beszerzésre. A bogyózúást követően Pektopol PT 400 pektinbontó enzimet adagoltak a gyümölcshez, mely növeli a préselés léhozamát, és megkönnyíti az előszűrési műveletet. Ezután szorbittal tartósították a gyümölcslevet, a felhasználásig fagyaszttva tárolták.



1. ábra: Mérőberendezések működési vázlata: a) MF és RO; b) OD

Az előszűrést – a lében lévő lebegő anyagok eltávolítását – Pall gyártmányú, 200 nm pórusméretű, 0,125 m<sup>2</sup> aktív szűrőfelületű kerámia csöves MF membránnal végeztük. Az így kapott tükrösített pirosribiszke-levet sűrítettük be TRISEP gyártmányú 91 % sóvisszatartású, poliamid RO lapmembránnal, melynek szűrőfelülete 0,18 m<sup>2</sup>. A OD végsűrítés négyszeres mennyiségű telített CaCl<sub>2</sub> sóoldattal került kivitelezésre. A mérőberendezések működési vázlatát mutatja az 1. ábra. A hőmérséklet állandó értéken (25 °C) tartását spirálhűtővel és beépített hőcserélővel valósítottuk meg.

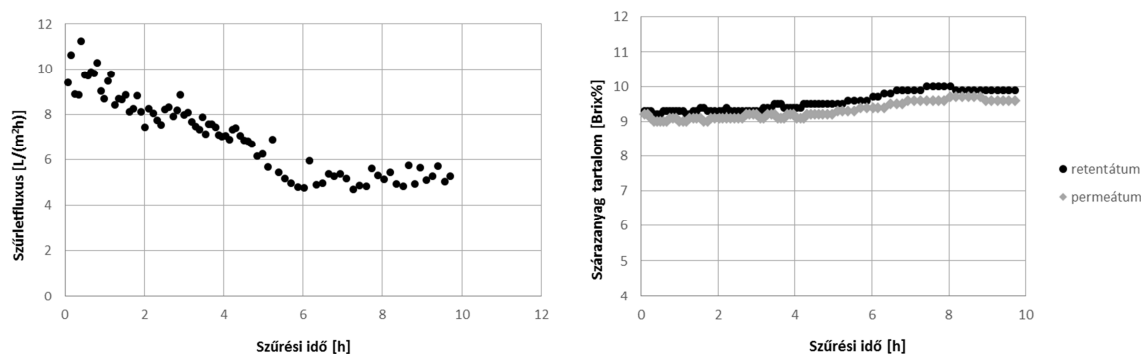
A besűrítési folyamatok alatt a szárazanyag-tartalmat kézi Atago PAL-α digitális refraktométerrel követtük. Az összes polifenol-tartalmat (TPC) spektrofotometriásan (λ=760 nm) határoztuk meg Folin-Ciocalteu reagenssel. A FRAP mérést Benzie és Strain módosított spektrofotometriás (λ=593 nm) módszerével mértük. Az összes monomer antocianin tartalmat szintén spektrofotometriás módszerrel határoztuk meg pH=1 és pH=4,5 pufferoldatok segítségével (λ=520 és 700 nm) [7].

## Eredmények

### Mikroszűrés

A mikroszűrést a pirosribiszke lé tükrösítésére alkalmaztuk. Ezáltal kiszűrhetők a lebegő anyagok a léből, megkönnyítve a következő lépést, a besűrítést. A mérés 10 órát vett igénybe, 13,8 liter kiindulási mennyiséggel dolgoztunk. A 2. ábra mutatja a szűrés közben bekövetkező szűrletfluxus és szárazanyag-tartalom változását. A szűrletfluxus a kezdeti 12 L/(m<sup>2</sup>h) értékről 6

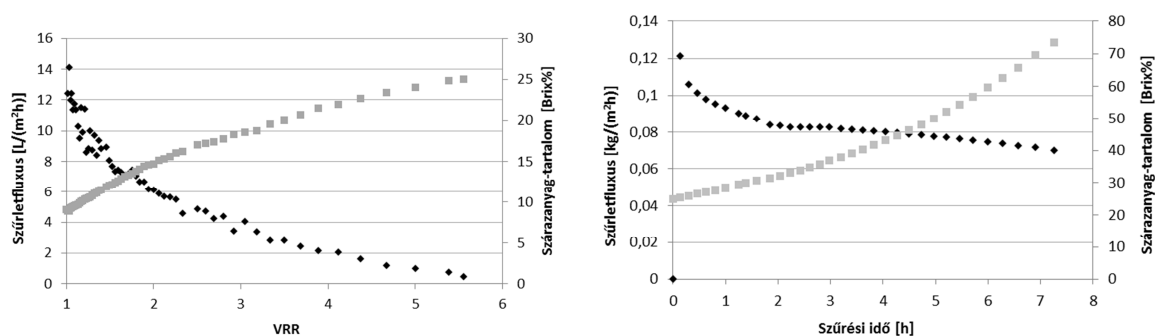
$L/(m^2h)$  értékre csökkent a szűrés alatt, mely a membrán eltömődésével és a koncentráció polarizációval magyarázható. A keletkező szűrlet szárazanyag-tartalma 9,6 °Brix volt, amely nem változott lényegesen.



**2. ábra:** A szűrletfluxus és a szárazanyag-tartalom változása pirosribiszke-lé előszűrése (MF) során ( $Q_{rec}=200$  L/h,  $\Delta p_{TM}=4$  bar,  $T=25$  °C)

### Fordított ozmózis és ozmotikus desztilláció

A mikroszűrt, tükrösített levet fordított ozmózzissal 25 Brix% szárazanyag-tartalomig sűrítettük be, majd ozmotikus desztillációval ezt tovább növeltük 73 Brix%-ig. A 3. ábra mutatja a besűrítések alatti szűrletfluxus és szárazanyag-tartalom változásait.



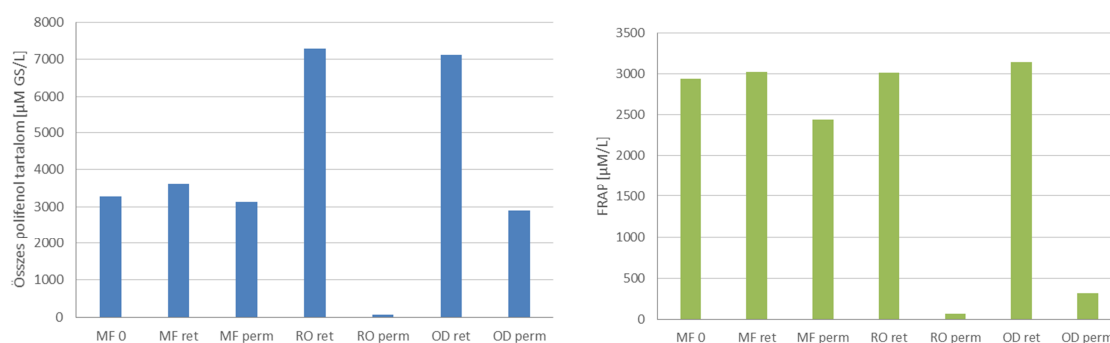
**3. ábra:** A szűrletfluxus és a szárazanyag-tartalom változása pirosribiszke-lé elősűrítése (RO) ( $Q_{rec}=400$  L/h,  $\Delta p_{TM}=48$  bar,  $T=25$  °C) és végsűrítése (OD) során

Az RO esetén a szűrletfluxus csökkenését a membrán eltömődése és a koncentráció polarizáció okozza, valamint az, hogy a besűrítés alatt folyamatosan nő a gyümölcsle szárazanyag-tartalma, ezért folyamatosan nő az oldat ozmózis nyomása is. Emiatt a hajtóerő folyamatosan csökken; ezért a besűrítés végére a szűrletfluxus értéke megközelítette a nulla értéket. OD esetén is a szárazanyag-tartalom növekedése és a hajtóerő csökkenése idézi elő a szűrletfluxus csökkenését.

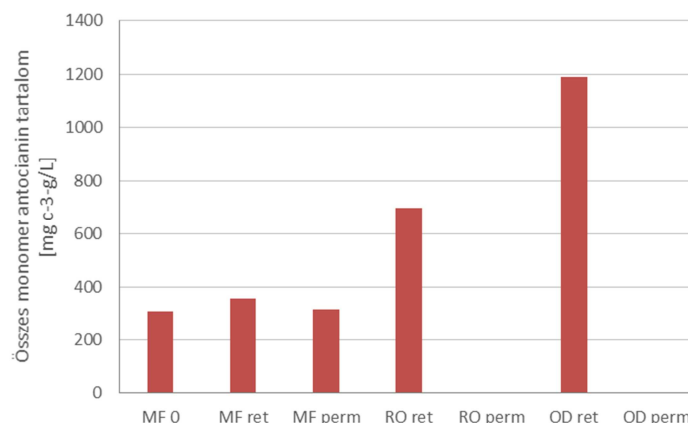
### Értékes komponensek koncentrációjának változása

A 4. és 5. ábrán a pirosribiszke-lé értékes komponenseinek változása látható a besűrítési folyamatok alatt. Az összes polifenol tartalom RO sűrítés során több, mint a kétszeresére

növekedett, mely megfelel az elvárásainknak. Ezzel szemben OD-val történő sűrítésnél sem a összes polifenol, sem az antioxidáns kapacitás értéke nem növekedett, mely háttérében valamilyen kémiai folyamat valószínűsíthető. Az antocianin tartalom változása a várt eredményt hozta. RO esetén kétszeresére, OD sűrítéssel az eredeti koncentráció négyszeresét sikerült elérni.



4. ábra: Összes polifenol és antioxidáns kapacitás (FRAP) változása a besűrítések alatt



5. ábra: Monomer antocianin tartalom változása a besűrítések alatt

## Összefoglalás

Kísérleteinkben a pirosribiszke-lé előszűrhetőségét és besűríthetőségét vizsgáltuk mikroszűrés, fordított ozmózis és ozmotikus desztilláció alkalmazásával. Tekintettel arra, hogy magasabb hőmérsékleten sérülnek az értékes anyagok és az aromakomponensek, ezért a kísérleteket alacsony hőmérsékleten végeztük (25 °C). A sűrítmény szárazanyag-tartalma RO esetén elérte a 25 Brix%-ot, ami megfelelt elvárásainknak. A sűrítményt továbbbsűrítve ozmotikus desztillációval elértük a 70 Brix%-ot is, amely megfelel az ipari elvárásoknak. Az összes polifenol és antioxidáns kapacitás koncentrációja nem az elvárásnak megfelelően alakult, az OD sűrítményekben nem tapasztaltunk növekedést. Ezzel ellentétben a színanyagok koncentrációja az elvárásnak megfelelően közel négyszeresére növekedett a végsűrítményben.

## Irodalomjegyzék

- [1] K. Yamagata, M. Tagami, Y. Yamori, Nutr 31 (2015) 28-37

- [2] M.J. Kruger, N. Davies, K.H. Myburgh, S. Lecour, Food Res. Int. 59 (2014) 41-52
- [3] A. Pongráczy, Ribiszke, Mezőgazdasági Kiadó, Budapest, 1972, pp. 19-21, 25.
- [4] J. Papp, A. Pongráczy, Szeder, ribiszke, köszméte, különleges gyümölcsök, Mezőgazda Kiadó, Budapest, 1999, pp. 52-55.
- [5] B.B. Mikkelsen, L. Poll, J. of Food Science 67 (2002) 3447-3455
- [6] H. Strathmann, L. Giorno, E. Drioli, An introduction to Membrane Science and Technology, Consiglio Nazionale delle Ricerche, Roma, 2006.
- [7] A. Hegedűs, É. Stefanovits-Bányai, Természetes antioxidáns források: A GYÜMÖLCS, Debreceni Egyetem, AGTC, Kertészettudományi Intézet, 2012, pp. 127-133.

## Soil Herbicides Efficacy in Pumpkins

Meseldzija Maja<sup>1</sup>, Brdar-Jokanovic Milka<sup>2</sup>, Ljevnaic-Masic Branka<sup>1</sup>, Bursic Vojislava<sup>1</sup>,  
Medic Jelena<sup>1</sup>

University of Novi Sad, Faculty of Agriculture, Trg Dositeja Obradovica 8, 21 000 Novi Sad,  
Serbia

Institute of Field and Vegetable Crops, 21 000 Novi Sad, Serbia

E-mail: maja@polj.uns.ac.rs

### ABSTRACT

Pumpkins competitiveness to weeds is variable and depending on the stage of development. Weeds that occur in pumpkin crops are related flora with other row crops. In order to study the soil herbicide efficacy in pumpkin crops, *Cucurbita pepo* L., variety Olivia, testing was conducted on the experimental field at the Backi Petrovac locality, at the Institute for Alternative Culture, during 2015. The experiment was set according to EPPO/OEPP standards (2012), in the aim to determine the efficacy and phytotoxicity of the herbicide, applied in various quantities and combinations. Weed control was done by applying the herbicide linuron in an amount of 2 and 2.5 l ha<sup>-1</sup> and s-metolachlor (1.2 and 1.5 l ha<sup>-1</sup>). It was determined 15 weed species established in the pumpkin crop. Temporal phytotoxicity was determined in variants with s-metolachlor application in the quantity of 1.5 l ha<sup>-1</sup>.

### INTRODUCTION

As an intercrop, pumpkins were grown in the former Yugoslavia at around 335 000 ha, mostly in the central Serbia, and were mainly intended for animal feed (Popovic, 2000). Today, the only raised for the production of seed from which oil is obtained. Areas that cover the 2000-3000 ha have a tendency of growth (Berenji, 2010). Oil pumpkin is produced on 45,500 ha of arable land (Kapaun, 2002). At the world level, production of pumpkin was 17 million tons in 2002, according to FAO data, while the same year the total production of all species of the genus *Cucurbita* was 156 million tons, exceeding the production of tomatoes. Today, most pumpkins grown in the US, Mexico, India and China. The economically most important weeds, and the weeds more difficult to suppress are the perennial broadleaved weeds, although some annual weeds can be a problem. Main weeds, a large number and cover the weed community made *Ambrosia artemisiifolia* L., *Amaranthus retroflexus* L., *Datura stramonium* L., *Abutilon theophrasti* Medic., *Chenopodium album* L., *Cirsium arvense* L., *Echinochloa crus-galli* L., *Solanum nigrum* L., *Sorghum halepense* (L.) Pers., *Xanthium strumarium* L. (Besek et al., 2012). Successful production of the pumpkin can be achieved only by integrating measures that ensure clean crop in the period from emergence until the conclusion of rows and simultaneously eliminate and minimize the negative impacts later germinated weeds (Berenji, 2010). The widest application for weed control is a combination of preparation based on s-metolachlor (Dual Gold 960 EC-1-1.4 l ha<sup>-1</sup>) and linuron (Afalon 1 l ha<sup>-1</sup>). They are effective in broadleaf weed control in pumpkin crops (Ostojic and Baric, 2002).



## MATERIALS and METHODS

In order to study the efficacy of herbicides on pumpkin crops, *Cucurbita pepo* L., variety Olivia, testing was conducted on the experimental field at the Backi Petrovac locality, Institute for Alternative Culture in 2015. The experiment was set according to EPPO / OEPP standard (2012) to determine the efficacy and phytotoxicity of the herbicide in various quantities and combinations. Weed control is done by applying the herbicide linuron (Afalon) in an amount of 2 and 2.5 l ha<sup>-1</sup> and S-metolachlor (Dual Gold) in quantities of 1.2 and 1.5 l ha<sup>-1</sup>, and the combination linuron+s-metolachlor (1 + 1 l ha<sup>-1</sup>). The experiment was a randomized block design, with the basic plot of 25m<sup>2</sup> with four replications (EPPO Standards, 2012). Besides the variant with herbicides in the experiment included an untreated control plot. The herbicides were applied 7<sup>th</sup> May 2015, after planting and before the emergence of the crop (preemergence). Assess the effectiveness of the herbicide were carried out according to EPPO/OEPP methods of identifying and counting the dominant weed species after treatment. Efficiency coefficient (Ef.) was calculated according to the Dodel (Janjic, 2005) and evaluations were made 19 (Ef1) and 40 (Ef2) days after treatment (table 1).

## RESULTS

In experimental pots, it was found and determined 15 weed species: *Abutilon theophrasti* Medik., *Amaranthus retroflexus* L., *Ambrosia artemisiifolia* L., *Chenopodium album* L., *Convolvulus arvensis* L., *Cynodon dactylon* Pers., *Datura stramonium* L., *Fumaria officinalis* L., *Hibiscus trionum* L., *Lamium purpureum* L., *Myosotis arvensis* (L.) Hill., *Polygonum aviculare* L., *Solanum nigrum* L., *Sorghum halepense* (L) Pers. and *Xanthium strumarium* L. The following annual broadleaves weeds were dominated: *Abutilon theophrasti* Medik., *Amaranthus retroflexus* L., *Ambrosia artemisiifolia* L., *Chenopodium album* L., *Datura stramonium* L., *Fumaria officinalis* L., *Hibiscus trionum* L., *Lamium purpureum* L., *Myosotis arvensis* (L.) Hill., *Polygonum aviculare* L., *Solanum nigrum* L., *Xanthium strumarium* L. The perennial broadleaf species *Convolvulus arvensis* L. and perennial grassweeds *Cynodon dactylon* Pers. and *Sorghum halepense* (L) Pers. were established also (table 1).

Tested preparations Afalon (linuron) and Dual Gold (s-metolachlor) had a high efficiency on a broadleaf weed species *Abutilon theophrasti* Medik., *Amaranthus retroflexus* L., *Ambrosia artemisiifolia* L., *Datura stramonium* L., *Fumaria officinalis* L., *Hibiscus trionum* L., *Lamium purpureum* L., *Myosotis arvensis* (L.) Hill., *Polygonum aviculare* L.

During the second assessment, all applied combinations had a low effect on the perennial grass weeds *Cynodon dactylon* Pers. and *Sorghum halepense* (L) Pers., as well as on the *Xanthium strumarium* L., which was also found during the first assessment. The overall effectiveness of the herbicide during the second evaluation was 78.33 to 88.08%.

Herbicide phytotoxicity was performed according to a European Weed Research Society scale (Janjic, 1985). Temporal phytotoxicity was determined during the application Dual Gold in quantity of 1.5 l ha<sup>-1</sup> (table 2). According to the literature, s-metolachlor can be phytotoxic at the soils with low content of humus (with values below 1% of humus) and soils with a pH below 5.5. In terms of time after treatment due to the unfavorable conditions for development (cold and too wet or dry weather) can occur plant injuries (Sekulic and Jelcic, 2013).

Weed species	Afaion (linuron) 2 l/ha		Afaion (linuron) 2,5 l/ha		Dual Gold (s-metolachlor) 1,2 l/ha		Dual Gold (s-metolachlor) 1.5 l/ha		Afaion + Dual Gold (linuron+s- metolachlor) 1+1 l/ha	
	Ef1	Ef2	Ef1	Ef2	Ef1	Ef2	Ef1	Ef2	Ef1	Ef2
<i>Abutilon theophrasti</i> Medik.	100	100	100	100	100	50,00	100	100	100	100
<i>Amaranthus retroflexus</i> L.	93,33	90,47	100	98,80	80,00	91,66	86,66	95,23	93,33	92,85
<i>Ambrosia artemisiifolia</i> L.	100	100	100	100	100	100	100	100	100	100
<i>Chenopodium album</i> L.	100	88,00	100	100	88,88	92,00	100	100	100	96,00
<i>Convolvulus arvensis</i> L.	100	33,33	100	33,33	20,00	33,33	100	33,33	100	33,33
<i>Cynodon dactylon</i> Pers.	68,42	71,42	10,52	71,42	73,68	85,71	47,36	85,71	68,42	85,71
<i>Datura stramonium</i> L.	100	100	100	100	100	100	100	100	100	100
<i>Fumaria officinalis</i> L.	100	100	100	100	100	100	100	100	100	100
<i>Hibiscus trionum</i> L.	100	100	100	100	100	100	100	100	100	80,00
<i>Lamium purpureum</i> L.	100	100	100	100	100	100	100	100	100	100
<i>Myosotis arvensis</i> (L.) Hill.	100	100	100	100	100	100	100	100	100	100
<i>Polygonum aviculare</i> L.	66,66	100	66,66	100	100	100	100	100	100	100
<i>Solanum nigrum</i> L.	75,00	80,00	75,00	100	75,00	80,00	100	100	100	100
<i>Sorghum halepense</i> (L.) Pers.	27,84	53,12	60,75	87,50	69,62	84,37	53,16	90,62	40,50	96,87
<i>Xanthium strumarium</i> L.	50,00	61,53	66,66	69,23	66,66	53,84	66,66	61,53	66,66	69,23
Total efficacy	48,78	78,33	58,53	88,08	65,85	84,11	59,14	88,44	56,09	88,44

Table 2. Evaluation of herbicide phytotoxicity

No.	Preparations	Amount (l ha <sup>-1</sup> )	First evaluation	Second evaluation
1	Afaion (linuron)	2	1	1
2	Afaion (linuron)	2,5	1	1
3	Dual Gold (s-metolachlor)	1,2	1	1
4	Dual Gold (s-metolachlor)	1,5	2	2
5	Afaion + Dual Gold (linuron+s-metolachlor)	1+1	1	1
6	CONTROL (untreated)	-	-	-

## CONCLUSIONS

- In a field trial was identified and determined 15 weed species, dominated by broadleaf weed species, with the presence of perennial weeds (*Convolvulus arvensis* L., *Cynodon dactylon* Pers. and *Sorghum halepense* (L) Pers.)
- Herbicide combination linuron and s-metolachlor had the highest overall efficiency (88.44%) on the present weed species
- all applied herbicides had a low effect on the perennial grass weeds *Cynodon dactylon* Pers. and *Sorghum halepense* (L) Pers., as well as on the broadleaf species *Xanthium strumarium* L.
- Temporal phytotoxicity was determined during the application of s-metolachlor in higher quantity of 1.5 l ha<sup>-1</sup>

## LIST OF REFERENCES

- Besek, Z., Balicevic, R., Ivezić, M., Raspundić, E., Ravlić, M. (2012). Primjena kemijskih mjera u suzbijanju korova u uljnoj bundevi (*Cucurbita pepo* L. var *oleifera* Pietsch). *Poljoprivreda*, 18: (1), 30-35.
- Berenji, J. (2010): Uljana tikva i njena proizvodnja. Institut za ratarstvo i povrtarstvo, Novi Sad, 7-63.
- EPPO/OEPP Standards (2012). Guidelines for the efficacy evaluation of plant protection products. Phytotoxicity assessment. 31-37.
- EPPO/OEPP Standards (2012). Guidelines for the efficacy evaluation of plant protection products. Weed control between crops. 77-81.
- Janjić, V. (2005). Fitofarmacija, Drustvo za zaštitu bilja Srbije, Beograd.
- Kapaun F. (2002). Die Lage am Markt. In Pfannhauser, V.W. (Ed.), Neues von Kürbis- kern und Kürbiskernöl. Tagungsband., Analyticum, Grambach bei Graz, 35-40.
- Ostojic, Z., Barić, K. (2002). Opcenito o korovnoj flori i suzbijanju korova u povrcu. *Glasilo biljne zaštite*, 6: 317 – 324.
- Popović, M. (2000). Lubenica, dinja, muskatna tikva. Mala poljoprivredna biblioteka, Nolit.
- Sekulić J., Jelić S. (2013). Sredstva za zaštitu bilja u prometu u Srbiji, Drustvo za zaštitu bilja Srbije, Biljni lekar.

## Ground Beetles as Bioregulators of Harmful Insect Populations on Arable Land

Aleksandra Popović<sup>1</sup>, Miloš Petrović<sup>1</sup>, Jovana Šućur<sup>1</sup>, Aleksandra Petrović<sup>1</sup>, Vojislava Bursić<sup>1</sup>,  
Ivana Ivanović<sup>1</sup>

University of Novi Sad, Faculty of Agriculture, 8 Trg Dositeja Obradovića Street, 21000 Novi  
Sad, Serbia

e-mail: popovica@polj.uns.ac.rs

### ABSTRACT

Ground beetles are the typical polyphagous predators, very important for the maintenance of agroecosystems and other ecosystems, therefore often the subject of research. The aim of this study is to determine the adults of the family of ground beetles. Moreover, the dominance and degree of faunal similarity of ground beetles were observed. During research in the fields of wheat, maize and sugar beet on the territory of Vojvodina on the fields of Bečej and Rimski Šančevi, using the method of "Barber traps" a total of 1,519 individuals of the ground beetles family were collected. The dominant species in the three above-mentioned crops and at all three sites were predators in the genera of *Pterostichus* spp., *Harpalus* spp. and *Anchomenus* spp. Furthermore, based on the obtained results it can be concluded that the composition of ground beetles is dependent on the ruling biotic and abiotic factors, and the combination of these factors creates a specific micro climate conditions, thus the characteristic fauna.

### AIMS AND BACKGROUND

Ground beetles belong to the cosmopolitan group of insects, with over 40,000 species worldwide, out of which 2,700 species are registered in Europe. On the territory of Serbia, a total of 520 species of ground beetles were recorded<sup>2,3</sup>. Ground beetles are important biological control agents in agroecosystems. Members of ground beetles family as predators can significantly reduce the population of harmful species<sup>6,7</sup>. Considering that the agricultural land is covered with vegetation in some parts only a few months during the year, the seasonal activity of ground beetles involves their removal from agricultural areas to adjacent habitats for food and shelter. One very important reservoir of ground beetles is the vegetation on the edge areas of arable land. The edges of the fields affect the increase in population of ground beetles by providing shelter and places to overwinter. The edges of the fields with a well-developed plant cover and stable micro habitats such as hedges indicate an increased rate of overwintering in relation to the open-air habitats within an agricultural land<sup>7</sup>. Given the economic importance of this family, as well as its degree of exploration, the main objective of this study was to investigate the qualitative and quantitative composition of species in the family of ground beetles in the crops of wheat, sugar beet and maize.

### EXPERIMENTAL

The experiment was set up in chernozem soil in the crops of wheat, maize and sugar beet during in the experimental field of the Institute for wheat, maize and sugar beet in Rimski Šančevi (GPS coordinate: N45 40 6.015 E19 5 3.376) and in the experimental fields of Bečej (GPS: N45 37 0 E20 1 59.999). Through the year of research, experimental plots with different plant species observed were located at the distance of 1-2 km within an experimental field. A total of 60 pitfall traps, i.e. Barber traps, were set in maize, wheat and sugar beet, ten in each plant species, at the

distance of 20 m in the same row of each field. The "Barber traps" were placed during the period of vegetation.

All numerical data obtained after processing the samples are expressed by appropriate quantitative and qualitative indicators. In order to describe quantitative structure, the term active dominance was used, which is calculated according to the procedure applied by Heydemann:

$$D (\%) = \frac{\text{No. of individuals of a given species}}{\text{The total no. of individuals of a given habitat}} \times 100$$

D - Active dominance of individuals of a given species

## RESULTS AND DISCUSSION

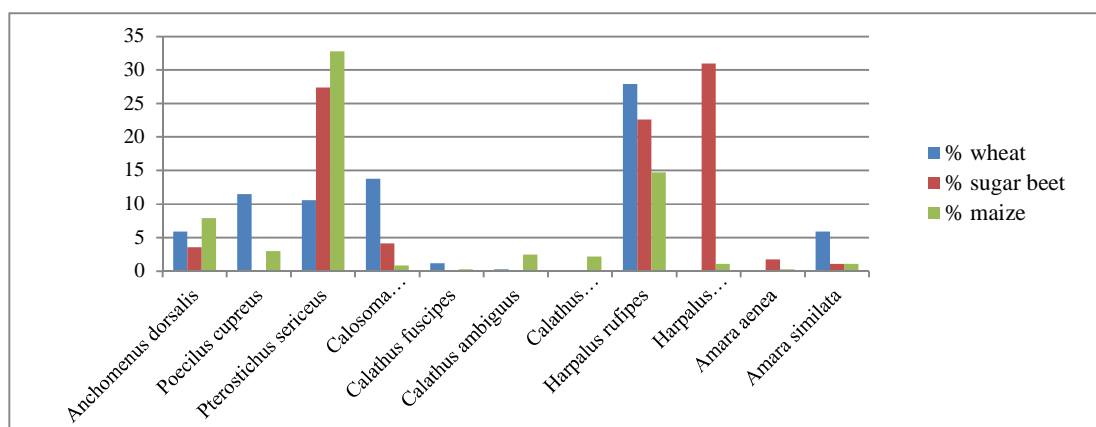
According to the research of numerous authors in entomofaunal fields of wheat, sugar beet, maize, sunflower and alfalfa, beetles representatives are very numerous, even dominant in the total registered macroentomofauna<sup>6</sup>.

During research, ground beetles were distinguished as a very important group of predators. In the crops of wheat, maize and sugar beet in the experimental fields of Becej and Rimski Sancevi, using the method of "Barber traps", a total number of 1,159 individuals of ground beetle family were collected and classified into 51 species. During the growing period of vegetation in the experimental fields of Becej in all three crops a total number of 869 individuals were collected, while the smaller number of individuals was recorded in the fields of Rimski Šančevi, that is 650 individuals, where also the number of insecticide treatments was greater.

The composition of the ground beetle fauna in a habitat depends primarily on the agrotechnical measures, cultivated crops, and much of the agroprotective belts, which were very scarce and rare in the observed sites, yet play an important role in maintaining the population of ground beetles and other insects. As part of an agricultural land, the edge parts of plots are very important for biodiversity. Agroprotective belts enable biodiversity in agricultural areas in several ways: they are important for species that inhabit arable land, they are their shelter during and after the agricultural practices, and can also serve as places for overwintering or summer diapause<sup>5</sup>, or provide an alternative source of food.

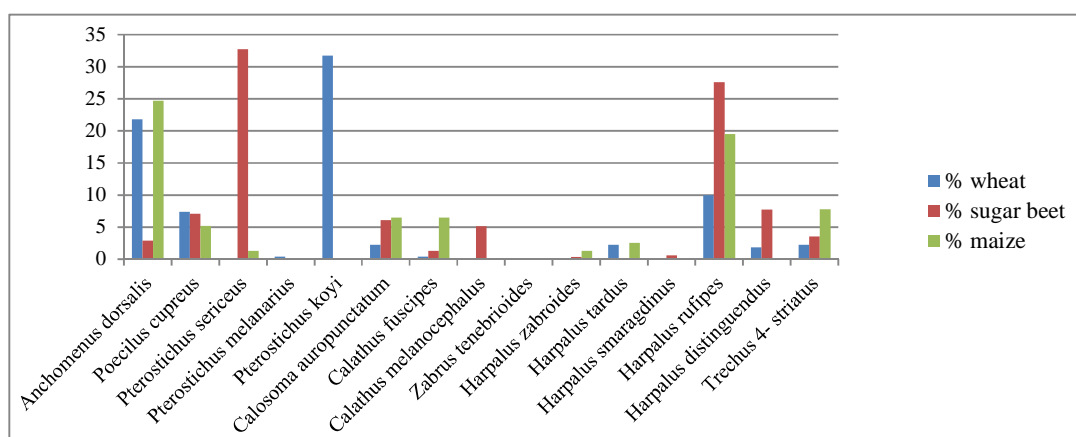
In order to determine the dominant species, in the total insect material collected, the concept of an active dominance has been introduced, as stated in the experimental section. On the researching fields of Becej, the dominant species in all three plant crops were *Pterostichus sericeus* and *Harpalus rufipes*; *Anchomenus dorsalis* species was dominant in wheat and maize, while in sugar beet it belonged to the subdominant species. Individuals belonging to *Poecilus cupreus* species were dominated in wheat, subdominant in corn whereas in sugar beet they were not recorded. The number of individuals belonging to *Calosoma auropunctatum* was largest i.e. dominant in wheat, subdominant in sugar beet and recedent in maize. Furthermore, the subdominant maize species were, in addition to the above-mentioned, *Calathus ambiguus*, *Calathus melanocephalus*, *Harpalus distinguendus* which dominated in sugar beet. All other species, belonged to the groups of recedent and subrecedent species (Figure 1).

Figure 1. Active dominance of ground beetles in three different plant crops in the experimental fields of Becej



In the experimental fields of Rimski Sancevi in 2010, dominant species were *Anchomenus dorsalis*, *Poecilus cupreus* in the crops of wheat and maize, and *Harpalus rufipes* in all three crops, then *Calosoma auropunctatum* in the crops of sugar beet and maize. In much larger number, in sugar beet crop were found individuals belonging to species *Pterostichus sericeus*, but also *Pterostichus koyi* in wheat, and *Trechus 4 - striatus* in maize (Figure 2).

Figure 2. Active dominance of ground beetles in three different plant crops in the experimental fields of Rimski Šančevi





Similar studies were also carried out in Eastern Lithuania and 41 species of ground beetles were collected in the fields of wheat<sup>1</sup>. On the territory of Hungary the following species were present *Anisodactylus signatus*, *Harpalus pubescens*, *Anchomenus dorsalis*, *H. distinguendus*, *Poecilus cupreus*, *Pterostichus sericeus* and *Zabrus tenebrioides*, which also coincides with the species that were found at our sites. Then, species belonging to gender *Bembidion*, according to research of many authors, are very widespread and numerous both in wheat and sugar beet, alfalfa, cabbage, carrots and grassy areas, while in our samples only single individuals of *Bembidion properans* species were recorded in wheat and sugar beet<sup>4</sup>.

When it comes to a diet regime of ground beetles, we can analyse the diet of the dominant species in order to partially understand their vital role as bioregulators. Divided ground beetles between phytophagous, predators and omnivores. According to this division, among recorded dominant species during the study, only *Z. tenebrioides* species belongs to phytophagous species, while the group of predators, which is far more numerous, includes: *P. vulgaris*, *A. dorsalis*, *P. cupreus*, *P. sericeus*, *P. punctulatus*, *P. koyi*, *C. auropunctatum*, *Calathus ambiguus*, *Trechus quadristriatus*, *Brachynus crepitans* while *Harpalus rufipes*, *Harpalus distinguendus* belong to omnivores. When it comes to the last group of ground beetles, omnivores, some authors believe that this group of insects is very important because of its abundance and that they should be considered harmful, while increasing number of authors, however, argues that they do insignificant damage, and are more significant as predators<sup>5</sup>.

## CONCLUSIONS

Based on the presented results it can be concluded that in the collected material almost all species belong to beneficial insects, i.e. predators or omnivores, with the exception of *Z. tenebrioides* species, which indicates the important role of this group of insects in the abundance regulation of pest species that inhabit a variety of plant crops on arable land. We can conclude that agroprotective belt, which consists of a thick hedge and crop residues instead of grassy edge parts of arable land, provides the shelter to insects during winter and vegetation period. Also, preservation of ground beetle habitat and application of appropriate cultural practices can improve natural regulation of harmful insects which also reduces their need for chemical control.

## REFERENCES

- [1] Bukejs, A., Balalaikins, M., (2008): Ground Beetles (Coleoptera: Carabidae) of Wheat Agroecosystem in Latvia. Acta Zoologica Lituanica. Volume 18, Issue 2.
- [2] Ćurčić, S.B. (2000): On the diversity of some ground beetles (Coleoptera: Carabidae: Carabidae and Harpalinae) in Serbia. Archive of Biological Science (Belgrade) 52(4):219–226.
- [3] Ćurčić, S.B., Brajković, M.M., Ćurčić, B.P.M., (2007): The Carabidae of Serbia. Faculty of Biology, Faculty of Life Sciences, University of Vienna & UNESCO MAB Committee of Serbia; Belgrade-Vienna; Vol.11, pp. 1085
- [4] Kennedy, P. (1994): The distribution and movement of ground beetles in relation to set-aside arable land. In: Desender K, Dufrene M, Loreau M, Cuff ML, Maelfait J-P, (eds.) Ground Beetles: Ecology and Evolution. Kluwer Academic, Dordrecht, pp. 439-444.
- [5] Maudsley, M.J. (2000): A review of the ecology and conservation of hedgerow invertebrates in Britain. J Environ Manage 60, 65-76.
- [6] Popović, A., Štrbac, P. (2011): Occurrence and fauna composition of ground beetles in wheat fields. Journal of Central European Agriculture. Vol. 11 (2011), No. 4 (423-432)

[7] Popovic, A. (2014): Fauna of carabid beetles (Coleoptera; Carabidae) in defferent agro-ecological conditions of Vojvodina. Faculty of Agriculture, Novi Sad. Doctoral thesis, UC 631.95 (043.3), pp 1-123.